Protein quality control and tubulin signature in inherited cardiomyopathies

Dorsch, Larissa Maria

2021

document version
Publisher's PDF, also known as Version of record

Protein quality control and tubulin signature in inherited cardiomyopathies

Larissa M. Dorsch

The work presented in this thesis was performed at the Amsterdam UMC, Vrije Universiteit, Department of Physiology, Amsterdam Cardiovascular Sciences Research Institute, Amsterdam, The Netherlands.

Cover design: Tabitha Müller
Layout: Larissa M. Dorsch
Printing: Ridderprint | www.ridderprint.nl

ISBN: 978-94-6416-691-0

VRIJE UNIVERSITEIT

Protein quality control and tubulin signature in inherited cardiomyopathies

ACADEMISCH PROEFSCHRIFT

ter verkrijging van de graad Doctor
aan de Vrije Universiteit Amsterdam,
op gezag van de rector magnificus
prof.dr. V. Subramaniam,
in het openbaar te verdedigen
ten overstaan van de promotiecommissie
van de Faculteit der Geneeskunde
op donderdag 9 september 2021 om 11.45 uur
in de aula van de universiteit,
De Boelelaan 1105

door

Larissa Maria Dorsch
geboren te Bad Friedrichshall, Duitsland

promotoren:	prof.dr. J. van der Velden prof.dr. B.J.J.M. Brundel
copromotor:	dr. D.W.D. Kuster

voorzitter promotiecommissie:	prof.dr. C.A.C. Ottenheijm
overige leden promotiecommissie:	prof.dr. D.J.G.M. Duncker prof.dr. A.C. van Rossum prof.dr. N.M.S. de Groot dr. P.A. van der Zwaag dr. H.H.W. Silljé

The research described in this thesis was supported by a grant of the Dutch Heart Foundation (CVON2014-40 DOSIS). Financial support by the Dutch Heart Foundation for the publication of this thesis is gratefully acknowledged.

If you don't risk it, you won't get the biscuit.

TABLE OF CONTENTS

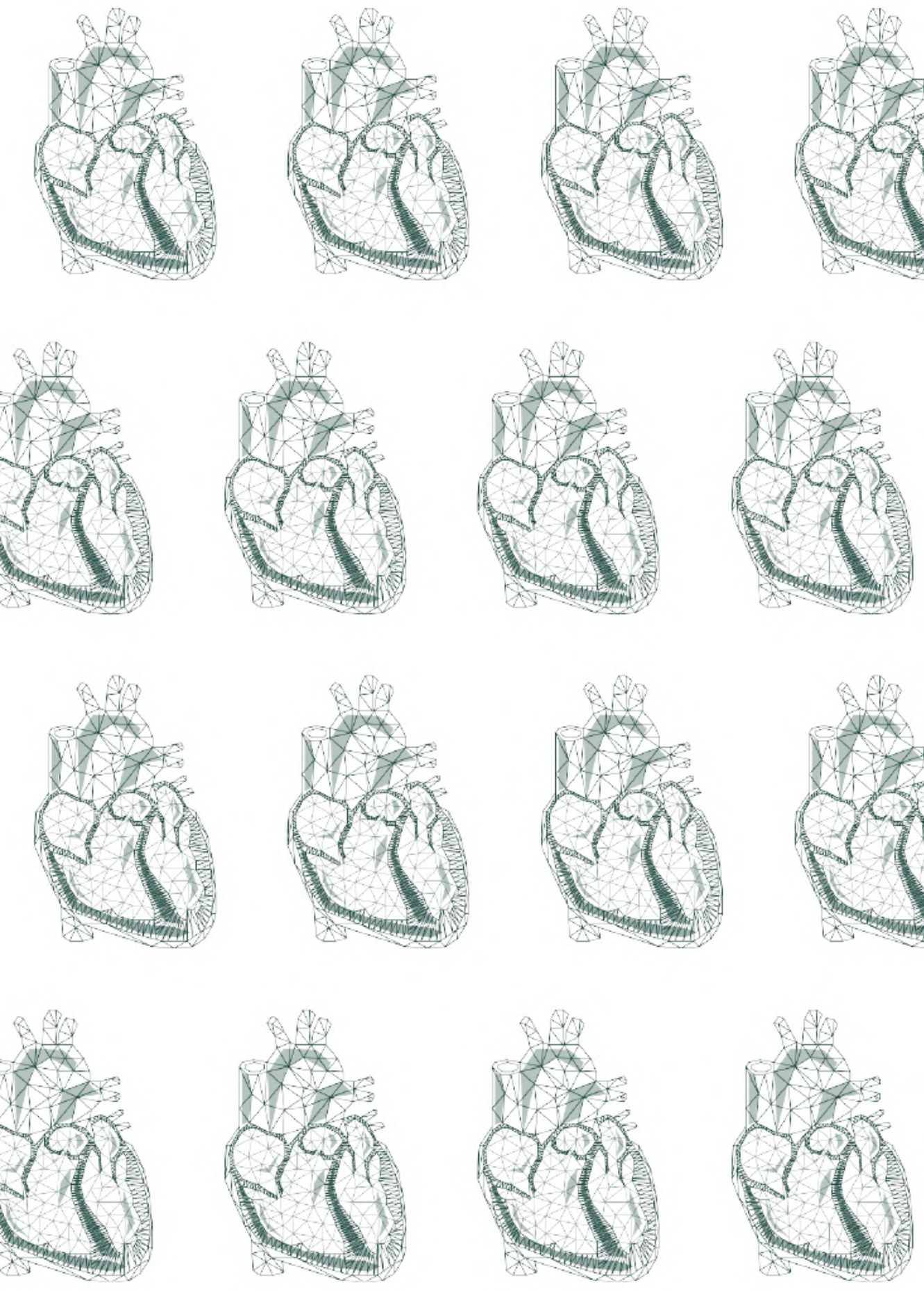

PART

GENERAL INTRODUCTION AND THESIS OUTLINE

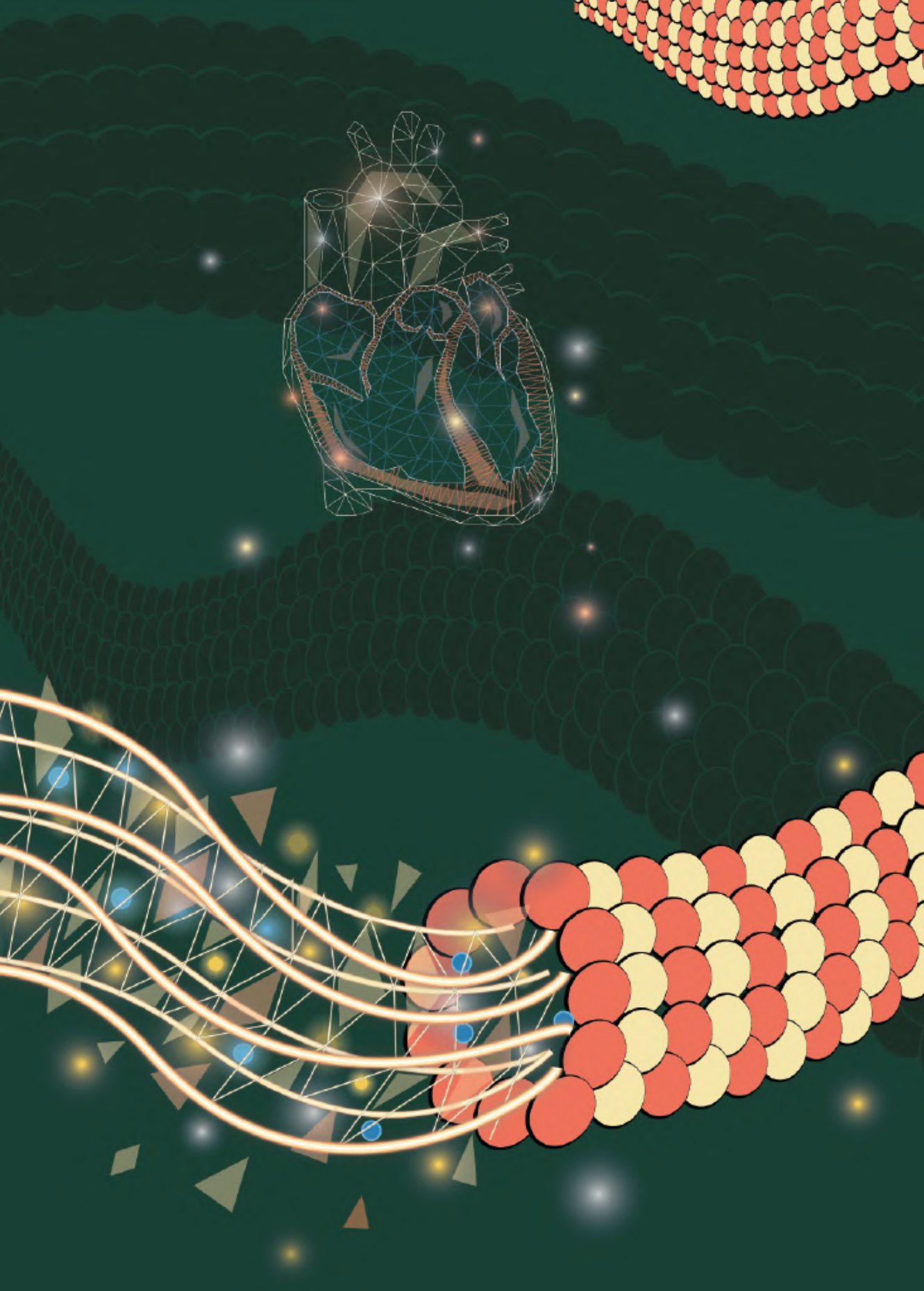

Chapter 1

Strength of patient cohorts and biobanks for cardiomyopathy research

R.A. de Boer, L.L.A.M. Nijenkamp, H.H.W. Silljé, T.R. Eijgenraam, R. Parbhudayal, B. van Driel, R. Huurman, M. Michels, J. Pei, M. Harakalova, F.H.M. van Lint, M. Jansen, A.F. Baas, F.W. Asselbergs, J.P. van Tintelen, B.J.J.M. Brundel, **L.M. Dorsch**, M. Schuldt, D.W.D. Kuster, J. van der Velden (DOSIS consortium)

Adjusted based on the publication in the Neth Heart J 28, 50–56 (2020).

ABSTRACT

In 2011 the Netherlands Heart Foundation initiated consortium funding (CVON, Cardiovasculair Onderzoek Nederland) to stimulate collaboration between clinical and basic (preclinical) researchers on specific areas of research. One of those areas involves genetic heart diseases, which are frequently caused by pathogenic variants in genes that encode sarcomere proteins. In 2014, the DOSIS (**D**eterminants **o**f **s**usceptibility **i**n inherited cardiomyopathy: towards novel therapeutic approache**s**) consortium was initiated, focusing their research on secondary disease hits involved in the initiation and progression of cardiomyopathies. This thesis describes several main findings of the work performed in the DOSIS consortium. This chapter introduces the clinical genetic phenotypes and provides an introduction to the work described in this thesis.

INTRODUCTION

Inherited cardiomyopathies, caused by pathogenic variants in genes encoding proteins that regulate cardiomyocyte contractility, are a major cause of morbidity and mortality. In 50–60% of familial hypertrophic cardiomyopathy (HCM) and 30–40% of dilated cardiomyopathy (DCM), a pathogenic gene variant can be identified. The most common genes that are affected in HCM are *MYH7*, *MYBPC3* and *TNNT2*, which encode the thick filament proteins myosin heavy chain, cardiac myosin-binding protein C (cMyBP-C), and the thin filament protein troponin T. Tropomyosin (TPM1) variants are observed in DCM, HCM and restrictive cardiomyopathy (RCM) patients (**Chapter 2**). In DCM the titin (*TTN*) gene, which encodes the giant myofilament protein titin, is the most frequently affected gene (~15–20% of all gene variants);[1] in particular gene variants that lead to *TTN* truncation have been shown to be pathogenic.[2] In addition, in the Netherlands, a founder mutation in the *PLN* gene, which encodes the calcium-handling protein phospholamban, was identified in 2012 as a now well-known cause of DCM and arrhythmogenic cardiomyopathy.[3,4] Figure 1.1 depicts a cardiomyocyte to illustrate the affected proteins involved in cardiomyopathies. Upon activation of a cardiomyocyte, calcium enters the cell via the L-type calcium channel, which subsequently releases calcium from the intracellular calcium store, the sarcoplasmic reticulum. Calcium binds to the troponin complex, which induces a conformational change of troponin-tropomyosin, and thereby releases binding sites for myosin heads on the thin actin filament. Binding of myosin to actin (so-called cross-bridge) results in force development. The kinetics of cross-bridge cycling is regulated by cMyBP C, and the giant protein titin, encoded by *TTN* and linked with DCM, underlies passive stiffness of sarcomeres.[5]

In past years the number of genes in genetic diagnostic panels has increased with the hope to identify a disease-causing variant in a larger group of patients and their family members. However, recent studies conclude that the additional benefit of screening large numbers of genes is disappointingly low and of marginal clinical utility[7,8] Numerous new *TTN* gene variants have been identified, mainly because of its large size. A study in three European cardiogenic centres showed that missense and non-frameshifting insertions/deletions variants are most likely benign, as reference populations showed comparable frequencies of these rare *TTN* variants.[9] The current panels thus rather increase the number of variants with unknown significance, which are likely benign, though they may have a modifier role in disease. Cardiomyopathy patients with a suspected genetic aetiology should be referred for genetic screening. For HCM this includes patients with asymmetric left ventricular hypertrophy, not explained by abnormal loading conditions, with or without a clear family history. For DCM this includes patients with non-ischemic DCM, not fully explained by other aetiological factors. Young age of onset and familial occurrence are important parameters that hint towards a genetic aetiology. However, late onset in seemingly sporadic cases does not exclude a genetic origin due to the reduced penetrance and variable disease expression. All HCM and DCM patients in whom genetic screening was performed can be added to the biobanks, including their relatives (asymptomatic mutation carriers).

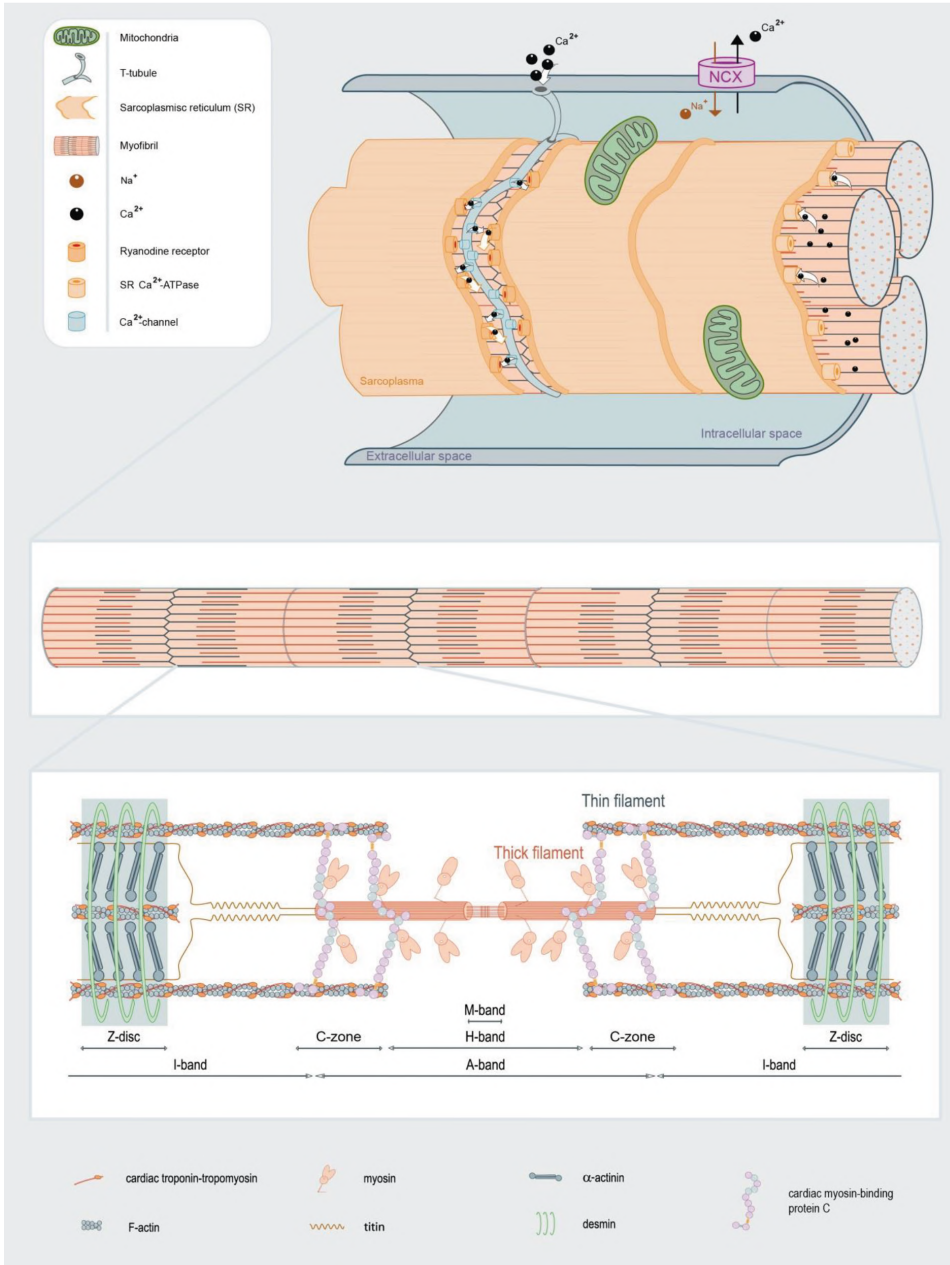

Figure 1.1: Activation of a cardiomyocyte triggers calcium entry and release of calcium from the sarcomplasmic reticulum (*SR*), which results in contraction of the cardiac myofibrils. To relax the cardiomyocyte, calcium is pumped back into the SR, and out of the cell via the sodium-calcium exchanger (*NCX*). Myofibrils consist of sarcomeres composed of the thin actin and thick myosin filament, and the third filament titin. Sarcomeres consist of sub-regions (depicted by the different bands), which underlie the striated pattern of cardiac muscle. Gene variants that cause cardiomyopathies are frequently found in myosin heavy chain, troponin T, cardiac myosin-binding protein C (located in the Z zone) and titin. (Figure is adapted from Sequeira et al.[6]).

Since cardiomyopathies continue to constitute one of the most common causes of sudden cardiac death in the young and still represent major causes for cardiac transplantation, adequate identification of additional disease triggers and understanding the pathomechanisms is of utmost importance. The clinical approach is furthermore complicated since inherited cardiomyopathies are clinically heterogeneous: age-dependent penetrance and disease-severity differ greatly between patients with the identical genetic variant. The mechanisms that underlie the variation in disease expression are still largely unknown. By combining cellular, genetic and clinical data from well-phenotyped national patient cohorts, DOSIS strived to define disease factors (i.e. secondary hits) that in addition to the pathogenic gene variant cause and aggravate cardiac disease in cardiomyopathy patients (Figure 1.2; Table 1.1). Several recent observations are highlighted below.

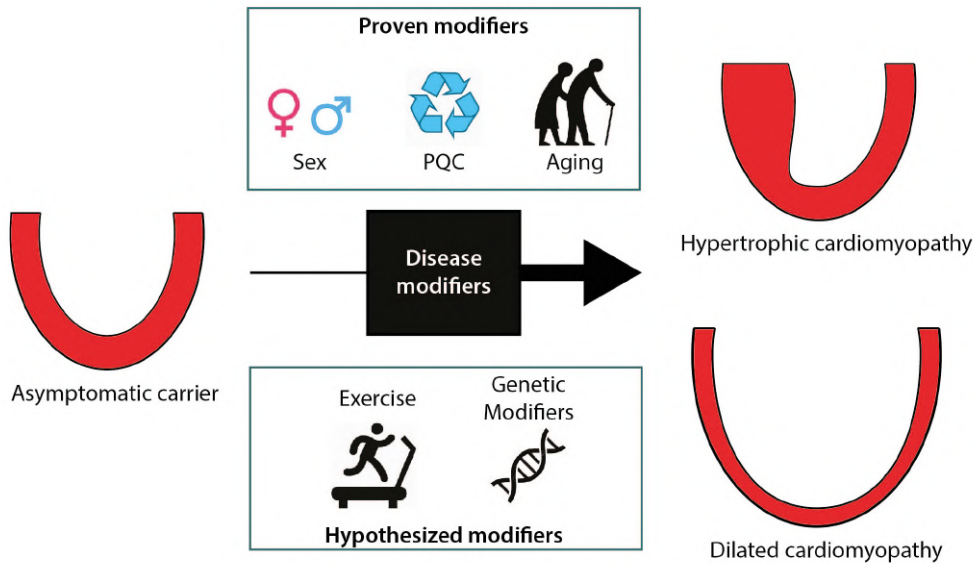

Figure 1.2: Disease modifiers in inherited cardiomyopathies (PQC, protein quality control).

Table 1.1: Cohorts of DOSIS

Cohort	Participating centres	Population	Biobank collection	Aim
Erasmus HCM observational cohort	Erasmus MC	HCM patients and gene variant carriers	DNA	Identify predictive clinical markers for major cardiac events
BIO FOr CARe observational cohort	UMC Utrecht, UMC Groningen, Amsterdam UMC, Erasmus MC	All sarcomere gene variants	DNA, RNA (from blood), plasma and serum	Identify predictive biomarkers for major cardiac events

Table 1.1: Continued

Cohort	Participating centres	Population	Biobank collection	Aim
Telephone interviews	UMC Utrecht, UMC Groningen, Amsterdam UMC	*MYBPC3* founder gene variant carriers	n.a.	Determine predictive value of environmental factors (especially exercise) for major cardiac events
ENERGY randomised placebo-controlled trial	Amsterdam UMC, Erasmus MC	Preclinical *MYH7* gene variant carriers	Serum	Determine effects of trimetazidine on improving myocardial energy efficiency in the pre-clinical disease stage
Myectomy cohort	Erasmus MC, UMC Utrecht	HCM patients undergoing septal myectomy	DNA, cardiac tissue	Collect myocardial tissue for use in aetiological studies

INDEXATION FOR BODY SIZE TO SET THE DIAGNOSTIC THRESHOLD FOR LEFT VENTRICULAR THICKENING

Using a large collection of myectomy samples from patients with obstructive HCM, we have shown that there is a sex-specific difference in diastolic function at the time of myectomy in HCM patients carrying pathogenic variants in *MYH7* and *MYBPC3*.[10] Women showed more diastolic dysfunction evident from significantly higher E/e' ratios, impaired left ventricular filling patterns, and higher tricuspid regurgitation velocities. Of the female patients, 50% showed grade III diastolic dysfunction, while the majority of male patients (56%) had only mild (grade I) diastolic dysfunction. Correction of maximal septal thickness and left atrial diameter for body surface area (BSA) resulted in significantly higher values in female compared with male patients. Histological and protein analyses revealed more advanced remodelling of the heart in female compared with male HCM patients evident from higher levels of fibrosis and activation of the cardiac foetal gene program, which is characteristic of heart failure. In **chapter 8** we performed a proteomics analysis in age-matched female and male HCM patients to define sex-specific changes in cardiac tissue at the time of myectomy. In addition to genetic screening, the current diagnostic criterion of hypertrophy is a maximal left ventricular wall thickness of $\geq$15 mm, or $\geq$13 mm in first-degree relatives of HCM patients. As the hearts of women, and in general relatively small persons, are smaller than the hearts of men, this threshold for the diagnosis of HCM should probably be corrected for body size.[11] The current diagnostic threshold, which does not take into account body size, may likely explain the male predominance in HCM patient cohorts, simply because males in general have larger hearts. A recent study in a Dutch cohort of 199 genotype-positive subjects, family members of HCM patients who were referred for cardiac screening between 1995 and 2018, indexation of wall thickness by BSA decreased the number of HCM diagnoses.[12] Moreover, predictive accuracy for HCM-related events

(mortality, cardiac transplantation, implantable cardioverter-defibrillator implantation and septal reduction therapy) improved significantly after indexation by BSA. These studies indicate that correcting left ventricular thickness for body size should be considered for the diagnosis of HCM and longitudinal follow-up studies in larger cohorts of preclinical genotype-positive individuals are needed to confirm this.

ALTERED PROTEIN QUALITY CONTROL AS DISEASE MODIFIER IN CARDIOMYOPATHY

An age-related decline in protein quality control (PQC) has been proposed as a contributor to disease progression in cardiomyopathy. As sarcomere proteins are the most abundant proteins in the heart, maintenance of sarcomere structure and function depends on PQC mechanisms. Pathogenic gene variants result in poison polypeptides or reduced protein levels (haploinsufficiency) and may trigger PQC and/or stress cellular protein homeostasis. DCM patients with truncating *TTN* variants show a relatively mild disease course, though with significant excess mortality in elderly patients. The latter may be explained by an age-related deterioration of the PQC mechanisms. As life expectancy increases, *TTN*-associated morbidity and mortality will likely become more prevalent.[13] Also in PLN-associated cardiomyopathy, protein aggregation and activation of PQC pathways has been observed in end-stage disease.[14]

Terminally misfolded and aggregation-prone proteins are cleared by the two degradation systems, the ubiquitin-proteasome system and autophagy.[15] Furthermore, pathways of PQC are strongly linked to cell architecture, such as the microtubules network. The role of the PQC in inherited cardiomyopathies is reviewed in **chapter 3**. Mutations in heat shock proteins, which are components of the PQC system, cause DCM (**chapter 4**), and oral geranylgeranylacetone (GGA), a HSP protein inducer, may activate specific HSPs to prevent cardiac dysfunction (**chapter 5**). As such, HSPs represent a key cellular component which may underlie development of cardiac disease, but also a target for drug therapy. Subsequent, DOSIS studies in a large set of cardiac tissues from a well-characterised HCM patient group showed altered PQC with several specific changes in gene-variant positive patients (genotype-positive) compared with genotype-negative patients and non-failing controls (**chapters 6**, **7** and **8**).

ALTERED METABOLISM AS KEY DRIVER OF DISEASE IN CARDIOMYOPATHIES

Several studies suggest an important role for secondary disease modifiers such as additional epigenetic and genetic variations and environmental disease triggers. Compelling data have accumulated that obesity is an overarching risk factor, also for age-of-onset and severity of cardiomyopathies. Proof that obesity contributes to disease onset and severity comes from cohort studies. The international HCM SHaRe registry showed that patients with a high body mass index have a significantly increased risk of heart failure, more advanced left ventricular outflow tract obstruction and more arrhythmias (i.e. HCM-related outcomes).[16] Moreover, a prospective study in adolescent men demonstrated that even mildly elevated body weight in late adolescence significantly increased the risk to develop dilated cardiomyopathy in adulthood.[17] At the heart level, a recent proteomics study

in human HCM tissue samples showed reduced levels of energy metabolism proteins.[18] We performed the largest proteomic study in HCM patient material and also observed this reduction in proteins involved in a wide array of metabolic processes (**chapter 6**). These observations are in line with studies in human HCM showing energy deficiency of the heart.[19,20] Energy deficiency has been proposed as the primary variant-induced pathomechanism of HCM,[21] which is supported by studies showing reduced cardiac efficiency in preclinical asymptomatic carriers of sarcomere gene variants in the absence of cardiac hypertrophy.[20,22] Accordingly, DCM caused by *TTN* gene variants has been linked with mitochondrial dysfunction and metabolic perturbations as cause of disease progression.[23] Overall, these studies indicate that timely disease stage-specific treatment of metabolic perturbations may slow down disease progression in cardiomyopathy patients.[24] An observational cohort to determine the predictive value of metabolic biomarkers (BIO FOr CARe: identification of biomarkers for development and progression of HCM in carriers of the Dutch *MYBPC3* founder carriers) and a clinical trial using metabolic drug therapy aimed to improve energetics of the heart at preclinical stage in HCM gene variant carriers are currently being performed by several DOSIS principal investigators (ENERGY trial).[25]

CELL-TO-CELL mRNA/PROTEIN VARIABILITY AS PATHOMECHANISM IN CARDIOMYOPATHY

As familial cardiomyopathies represent an autosomal dominant genetic disorder, most patients are heterozygous for the mutation and carry one variant and one normal wild-type allele. In cardiomyopathy patients, the heart of a genotype-positive individual produces the variant protein in addition to the normal protein. As indicated above, the homeostasis of cellular proteins is tightly regulated by the PQC system, but it is also regulated at the mRNA level by non-sense mediated mRNA decay. Both systems are needed to suppress the accumulation of variant protein while keeping the normal protein at sufficient levels in cardiac muscle cells. It was recently shown that transcription of both alleles occurs independently and in a stochastic manner, where one cell favours one allele and the next cell favours the other allele.[26] This burst-like, stochastic on/off switching of allele transcription does not affect mRNA and protein levels in case of homozygous wild-type alleles. However, heterozygosity of alleles as present in genotype-positive individuals may introduce cell-to-cell variation with one cardiomyocyte expressing high levels of variant protein, while variant levels may be low in another cardiomyocyte.[27] Indeed, it has been shown that *MYH7* gene variants cause a variable variant to wild-type ratio of mRNA expression in cardiomyocytes from the same heart.[26,28]

The DOSIS consortium showed intercellular variation of cMyBP-C myofilament protein expression due to truncating *MYBPC3* variants in the myocardium of HCM patients.[29] The functional consequences of the variable protein expression, which results in a mosaic pattern of cardiomyocytes with low and high variant/wild-type expression, remain to be determined. Loss of cMyBP-C causes severe dysfunction in mouse studies and engineered heart tissue.[30,31] We propose that the intercellular variation of cMyBP-C protein levels causes inhomogeneous contraction and relaxation and underlies the formation of myofibrillar disarray, a currently unexplained disease characteristic of HCM. As ageing reduces the quality of PQC, an age-dependent progression of the degree of allelic imbalance and cell-to-cell variation may contribute to cardiomyopathy development.

In conclusion, monogenetic cardiomyopathies have been intensely studied in the last three decades, and this has resulted in major progress in understanding what genes are involved. On the other hand, the striking heterogeneity, the highly variable age of onset, and the presence of gene variant carriers that never develop disease is as of yet largely unexplained. Given the profound repercussion for carriers, patients and family members we must improve our understanding of the individual's response to the presence of a pathogenic gene variant. DOSIS aims to study unexplored mechanisms that will probably modify the pathogenic gene variant (Figure 1.3).

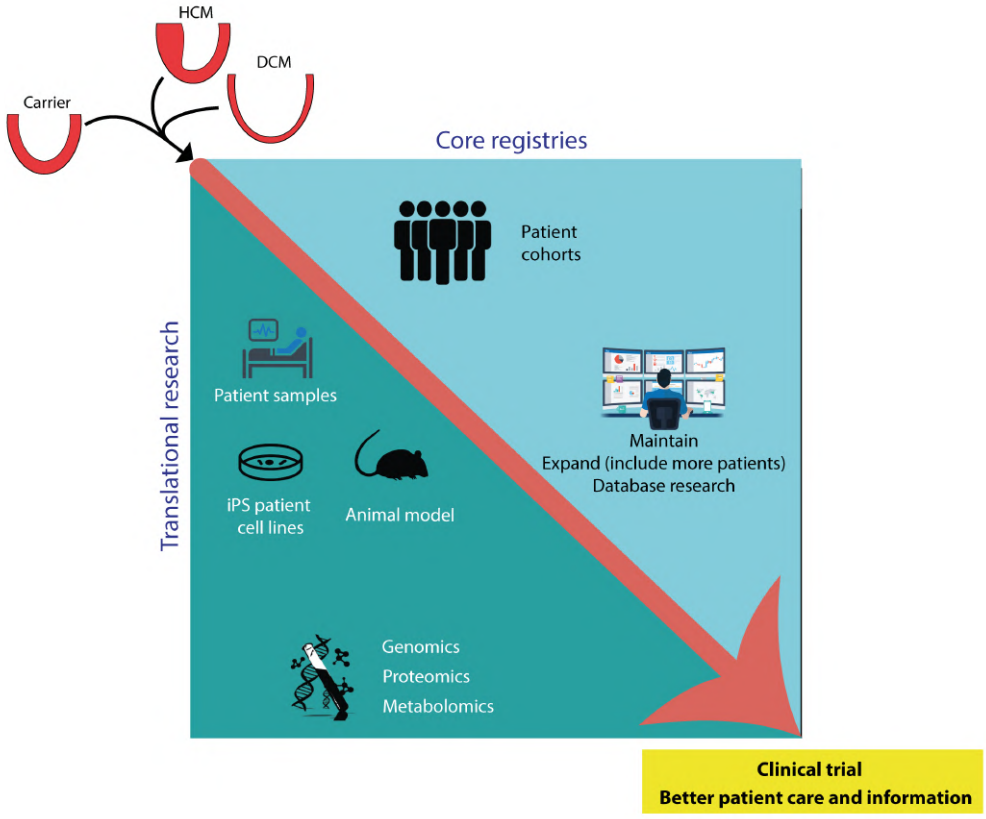

Figure 1.3: By combining cellular, genetic and clinical data from well-phenotyped national patient cohorts, DOSIS strives to define disease factors that in addition to the pathogenic gene variant cause and aggravate cardiac disease in cardiomyopathy patients.

We have set up important initiatives and collaborations and have generated preliminary results showing that environmental and genetic modifiers are indeed important in our understanding. In the future we will step up our initiatives and projects and have identified an agenda, which contains - what we feel - important additional factors that when fully understood will guide clinicians in proper diagnosis, risk prediction, prognostication and, ultimately, cause-specific novel treatments.

AIM AND OUTLINE OF THIS THESIS

I. DIVERSE CLINICAL PHENOTYPES

Variants in the exact same gene may cause diverse forms of cardiomyopathy. In **Chapter 2** we investigated three different *TPM1* variants observed in DCM and RCM. In addition to a comprehensive clinical evaluation showing the heterogeneous cardiomyopathy phenotype, we describe, for the first time, the compound heterozygote $TPM1_{E62Q/M281T}$ gene variants in a child with RCM. Since in thin filament cardiomyopathies, altered intracellular calcium homeostasis may contribute to contractile dysfunction and ultimately perturb cardiac structure,[32,33] we overexpressed the identified *TPM1* variants in HL-1 cardiomyocytes to measure the effect on the resulting calcium transients.

II. PROTEIN QUALITY CONTROL AND MICROTUBLE SIGNATURE IN CARDIOMYOPATHIES

The PQC is crucial for cardiac health and requires the collaboration of all its components to be functional. In **chapter 3**, we present recent mechanistic findings on the role of proteostasis derailment in inherited cardiomyopathies with a special focus on the presence of sarcomeric gene mutations. We were interested in whether key modulators of the PQC, such as heat shock proteins (HSPs), Ubiquitin-proteasome system and autophagy, are disease- and mutation-specifically altered and derailed in cardiomyopathies. Inter-individual differences in the capacity of the PQC and/or the specific effect of the sarcomeric gene mutation on the PQC may explain part of the disease heterogeneity. Since all three PQC components are pharmacologically targetable, we provide therapeutic strategy suggestions to improve the clinical outcome of cardiomyopathy patients.

In **chapter 4** the focus is shifted towards two gene variants in the small heat shock protein *HSPB5* (alpha-B crystallin) that cause dominantly inherited DCM.[34,35] HSPB5 function relies on oligomerization of HSPB5 proteins and oligomeric dynamics are important for HSPB5 to bind to destabilized client proteins.[36] In a first step, we overexpressed the two HSPB5 variants in various cell systems to measure loss of function of HSPB complexes, formation of aggregates, insolubilization and the effect on calcium transients. In a second step, we studied whether introduction of two different secondary gene variants alleviates protein aggregation and leads to regain of chaperone and contractile function.

The development of atrial fibrillation (AF) is an often complication of inherited cardiomyopathies either as a direct consequence of disease-specific defects, secondary to the primary illness, or a combination thereof.[37] In **chapter 5**, left and right atrial appendages of patients undergoing coronary artery bypass grafting were collected. Prior to surgery, oral geranylgeranylacetone (GGA), a HSP protein inducer, or placebo was administered for three days to determine HSPB1, HSPA1, HSPA5, HSPD1, heat shock factor-1 (HSF1) and phosphorylation HSF1 levels in the appendages and the occurrence of postoperative atrial fibrillation. The myofilament fraction was investigated for HSPB1 and HSPA1 to check whether GGA administration induces the expression levels of these two HSPs.

In more than half of HCM patients a causative mutation is identified in genes encoding sarcomere proteins. With more than 1500 identified HCM-causing mutations, the heterogeneity in genetic background of HCM is enormous.[38] We performed an unbiased proteomics approach in cardiac tissue from a clinically well-phenotyped HCM patient group to define if genotype-specific changes at the protein level may explain the heterogeneity in disease development (**chapter 6**). Furthermore, a novel *MYBPC3*$_{2373insG}$ mouse model was used to confirm functional relevance of our proteomic findings.

Sarcomere proteins are highly abundant proteins in cardiomyocytes and mutant forms of these likely stress the PQC system. As mentioned before, the PQC system relies on a functional microtubule network to maintain proteostasis. Therefore, in the same clinically well-phenotyped HCM patient group, we quantified microtubule network markers (for example acetylation of α-tubulin) and key PQC players, such as stabilizing and refolding HSPs and degradation markers (ubiquitinated proteins, p62, LC3BII) (**chapter 7**). We aimed to understand if the presence of a sarcomere mutation differentially affects PQC and assessed mutation-specific PQC changes by comparing HCM with missense mutations and haploinsufficiency-causing *MYBPC3* (cardiac myosin-binding protein-C) mutations.

Besides the different genotypes, sex-differences in clinical presentation contribute to the phenotypic heterogeneity of HCM patients. The observations so far point to a higher disease prevalence in men and a higher age of women at the time of diagnosis as well as at the time of myectomy.[10,39] Since the disease severity in female patients with HCM may be underestimated due to the smaller cardiac anatomy than men and setting the diagnostic criterion of $\geq$15 mm wall thickness without taking correction by body surface area into account,[11] it is important to study cellular differences which are caused by sex differences. In **chapter 8**, we analysed sex-differences at the protein level in proteomics data of HCM patient tissue to define sex-specific protein expression which may explain the differences in clinical presentation such as diastolic dysfunction.

Triggered by our findings of increased levels of α-tubulin and posttranslational modifications (acetylation and detyrosination) in genotype-positive HCM patients at the time of septal myectomy (**chapter 6** and **7**), we were interested whether we observe the same changes of the microtubule network in various model systems for hypertrophy and/or heart failure in mouse and swine (**chapter 9**). Furthermore, we investigated whether the observed changes are HCM-specific remodelling of the microtubule network or also apply to other inherited or acquired cardiac diseases, such as DCM and ischemic heart disease.

III. *DROSOPHILA MELANOGASTER* – A MODEL SYSTEM TO STUDY INHERITED CARDIOMYOPATHIES

In the third part of this thesis, we aimed to generate clustered regularly interspaced, short palindromic repeats (CRISPR)/CRISPR-associated (Cas)9-edited *Drosophila melanogaster* strains as a model system to study inherited cardiomyopathies and test drug interventions. In **chapter 10**, we intended to study two distinct *TNNI3* variants (*wupA* in *Drosophila melanogaster*), whereby one variant is causing DCM and the other one HCM in humans. In **chapter 11**, we introduced two distinct *Mhc* variants to investigate the effects of

HCM-causing variants in humans located in either the head or the tail region of the protein. All four variants represent orthologues of clinically relevant variants in humans.

Our attempt using scarless CRISPR/Cas9-mediated genome editing to make the *wupA*-mutant strains in **chapter 10** was not successful and therefore we provide various explanations for the observed dominant lethal phenotype of both CRISPR edited strains.

In **chapter 11**, we thoroughly describe the phenotype of the two *Mhc*-mutant *Drosophila melanogaster* strains.

In **chapter 12**, we summarize and discuss the data obtained in our experimental chapters and provide future perspectives related to PQC derailment and microtubule remodelling in inherited cardiomyopathies.

Sources of funding: CVON-DOSIS consortium 2014-40 Netherlands Heart Foundation

ACKNOWLEDGEMENT

We thank Salva R. Yurista and Vasco Sequeira with the design of the figures.

REFERENCES

1. Walsh R, Thomson KL, Ware JS, Funke BH, Woodley J, McGuire KJ, et al. Reassessment of Mendelian gene pathogenicity using 7,855 cardiomyopathy cases and 60,706 reference samples. *Genet Med*. 2017;19(2):192-203.
2. Herman DS, Lam L, Taylor MR, Wang L, Teekakirikul P, Christodoulou D, et al. Truncations of titin causing dilated cardiomyopathy. *N Engl J Med*. 2012;366(7):619-28.
3. van der Zwaag PA, van Rijsingen IA, Asimaki A, Jongbloed JD, van Veldhuisen DJ, Wiesfeld AC, et al. Phospholamban R14del mutation in patients diagnosed with dilated cardiomyopathy or arrhythmogenic right ventricular cardiomyopathy: evidence supporting the concept of arrhythmogenic cardiomyopathy. *Eur J Heart Fail*. 2012;14(11):1199-207.
4. van Spaendonck-Zwarts KY, van Rijsingen IA, van den Berg MP, Lekanne Deprez RH, Post JG, van Mil AM, et al. Genetic analysis in 418 index patients with idiopathic dilated cardiomyopathy: overview of 10 years' experience. *Eur J Heart Fail*. 2013;15(6):628-36.
5. van der Velden J, Stienen GJM. Cardiac Disorders and Pathophysiology of Sarcomeric Proteins. *Physiol Rev*. 2019;99(1):381-426.
6. Sequeira V, Nijenkamp LL, Regan JA, van der Velden J. The physiological role of cardiac cytoskeleton and its alterations in heart failure. *Biochim Biophys Acta*. 2014;1838(2):700-22.
7. Thomson KL, Ormondroyd E, Harper AR, Dent T, McGuire K, Baksi J, et al. Analysis of 51 proposed hypertrophic cardiomyopathy genes from genome sequencing data in sarcomere negative cases has negligible diagnostic yield. *Genet Med*. 2019;21(7):1576-84.
8. van Lint FHM, Mook ORF, Alders M, Bikker H, Lekanne Dit Deprez RH, Christiaans I. Large next-generation sequencing gene panels in genetic heart disease: yield of pathogenic variants and variants of unknown significance. *Neth Heart J*. 2019;27(6):304-9.
9. Akinrinade O, Helio T, Lekanne Deprez RH, Jongbloed JDH, Boven LG, van den Berg MP, et al. Relevance of Titin Missense and Non-Frameshifting Insertions/Deletions Variants in Dilated Cardiomyopathy. *Sci Rep*. 2019;9(1):4093.
10. Nijenkamp L, Bollen IAE, van Velzen HG, Regan JA, van Slegtenhorst M, Niessen HWM, et al. Sex Differences at the Time of Myectomy in Hypertrophic Cardiomyopathy. *Circ Heart Fail*. 2018;11(6):e004133.
11. van Driel B, Nijenkamp L, Huurman R, Michels M, van der Velden J. Sex differences in hypertrophic cardiomyopathy: new insights. *Curr Opin Cardiol*. 2019;34(3):254-9.
12. Huurman R, Schinkel AFL, van der Velde N, Bowen DJ, Menting ME, van den Bosch AE, et al. Effect of body surface area and gender on wall thickness thresholds in hypertrophic cardiomyopathy. *Neth Heart J*. 2020;28(1):37-43.
13. Jansen M, Baas AF, van Spaendonck-Zwarts KY, Ummels AS, van den Wijngaard A, Jongbloed JDH, et al. Mortality Risk Associated With Truncating Founder Mutations in Titin. *Circ Genom Precis Med*. 2019;12(5):e002436.
14. Te Rijdt WP, van der Klooster ZJ, Hoorntje ET, Jongbloed JDH, van der Zwaag PA, Asselbergs FW, et al. Phospholamban immunostaining is a highly sensitive and specific method for diagnosing phospholamban p.Arg14del cardiomyopathy. *Cardiovasc Pathol*. 2017;30:23-6.
15. Dorsch LM, Schuldt M, Knezevic D, Wiersma M, Kuster DWD, van der Velden J, et al. Untying the knot: protein quality control in inherited cardiomyopathies. *Pflugers Arch*. 2018.
16. Fumagalli C, Maurizi N, Day SM, Ashley EA, Michels M, Colan SD, et al. Association of Obesity With Adverse Long-term Outcomes in Hypertrophic Cardiomyopathy. *JAMA Cardiol*. 2020;5(1):65-72.
17. Robertson J, Schaufelberger M, Lindgren M, Adiels M, Schioler L, Toren K, et al. Higher Body Mass Index in Adolescence Predicts Cardiomyopathy Risk in Midlife. *Circulation*. 2019;140(2):117-25.
18. Coats CJ, Heywood WE, Virasami A, Ashrafi N, Syrris P, Dos Remedios C, et al. Proteomic Analysis of the Myocardium in Hypertrophic Obstructive Cardiomyopathy. *Circ Genom Precis Med*. 2018;11(12):e001974.
19. Guclu A, Knaapen P, Harms HJ, Parbhudayal RY, Michels M, Lammertsma AA, et al. Disease Stage-Dependent Changes in Cardiac Contractile Performance and Oxygen Utilization Underlie Reduced Myocardial Efficiency in Human Inherited Hypertrophic Cardiomyopathy. *Circ Cardiovasc Imaging*. 2017;10(5).
20. Crilley JG, Boehm EA, Blair E, Rajagopalan B, Blamire AM, Styles P, et al. Hypertrophic cardiomyopathy due to sarcomeric gene mutations is characterized by impaired energy metabolism irrespective of the degree of hypertrophy. *J Am Coll Cardiol*. 2003;41(10):1776-82.
21. Ashrafian H, Redwood C, Blair E, Watkins H. Hypertrophic cardiomyopathy:a paradigm for myocardial energy depletion. *Trends Genet*. 2003;19(5):263-8.
22. Witjas-Paalberends ER, Guclu A, Germans T, Knaapen P, Harms HJ, Vermeer AM, et al. Gene-specific increase in the energetic cost of contraction in hypertrophic cardiomyopathy caused by thick filament mutations. *Cardiovasc Res*. 2014;103(2):248-57.
23. Verdonschot JAJ, Hazebroek MR, Derks KWJ, Barandiaran Aizpurua A, Merken JJ, Wang P, et al. Titin cardiomyopathy leads to altered mitochondrial energetics, increased fibrosis and long-term life-threatening arrhythmias. *Eur Heart J*. 2018;39(10):864-73.
24. van der Velden J, Tocchetti CG, Varricchi G, Bianco A, Sequeira V, Hilfiker-Kleiner D, et al. Metabolic changes in hypertrophic cardiomyopathies: scientific update from the Working Group of Myocardial Function of the European Society of Cardiology. *Cardiovasc Res*. 2018;114(10):1273-80.
25. van Driel BO, van Rossum AC, Michels M, Huurman R, van der Velden J. Extra energy for hearts with a genetic defect: ENERGY trial. *Neth Heart J*. 2019;27(4):200-5.

26. Montag J, Kowalski K, Makul M, Ernstberger P, Radocaj A, Beck J, et al. Burst-Like Transcription of Mutant and Wildtype MYH7-Alleles as Possible Origin of Cell-to-Cell Contractile Imbalance in Hypertrophic Cardiomyopathy. *Front Physiol*. 2018;9:359.
27. Kraft T, Montag J, Radocaj A, Brenner B. Hypertrophic Cardiomyopathy: Cell-to-Cell Imbalance in Gene Expression and Contraction Force as Trigger for Disease Phenotype Development. *Circ Res*. 2016;119(9):992-5.
28. Brenner B, Seebohm B, Tripathi S, Montag J, Kraft T. Familial hypertrophic cardiomyopathy: functional variance among individual cardiomyocytes as a trigger of FHC-phenotype development. *Front Physiol*. 2014;5:392.
29. Parbhudayal RY, Garra AR, Gotte MJW, Michels M, Pei J, Harakalova M, et al. Variable cardiac myosin binding protein-C expression in the myofilaments due to MYBPC3 mutations in hypertrophic cardiomyopathy. *J Mol Cell Cardiol*. 2018;123:59-63.
30. McConnell BK, Jones KA, Fatkin D, Arroyo LH, Lee RT, Aristizabal O, et al. Dilated cardiomyopathy in homozygous myosin-binding protein-C mutant mice. *J Clin Invest*. 1999;104(9):1235-44.
31. Wijnker PJ, Friedrich FW, Dutsch A, Reischmann S, Eder A, Mannhardt I, et al. Comparison of the effects of a truncating and a missense MYBPC3 mutation on contractile parameters of engineered heart tissue. *J Mol Cell Cardiol*. 2016;97:82-92.
32. Tardiff JC. Thin filament mutations: developing an integrative approach to a complex disorder. *Circ Res*. 2011;108(6):765-82.
33. Fatkin D, McConnell BK, Mudd JO, Semsarian C, Moskowitz IG, Schoen FJ, et al. An abnormal Ca(2+) response in mutant sarcomere protein-mediated familial hypertrophic cardiomyopathy. *J Clin Invest*. 2000;106(11):1351-9.
34. Vicart P, Caron A, Guicheney P, Li Z, Prevost MC, Faure A, et al. A missense mutation in the alphaB-crystallin chaperone gene causes a desmin-related myopathy. *Nat Genet*. 1998;20(1):92-5.
35. Sacconi S, Feasson L, Antoine JC, Pecheux C, Bernard R, Cobo AM, et al. A novel CRYAB mutation resulting in multisystemic disease. *Neuromuscul Disord*. 2012;22(1):66-72.
36. Delbecq SP, Klevit RE. HSPB5 engages multiple states of a destabilized client to enhance chaperone activity in a stress-dependent manner. *J Biol Chem*. 2019;294(9):3261-70.
37. Yeung C, Enriquez A, Suarez-Fuster L, Baranchuk A. Atrial fibrillation in patients with inherited cardiomyopathies. *Europace*. 2019;21(1):22-32.
38. Ingles J, Burns C, Barratt A, Semsarian C. Application of Genetic Testing in Hypertrophic Cardiomyopathy for Preclinical Disease Detection. *Circ Cardiovasc Genet*. 2015;8(6):852-9.
39. Olivotto I, Maron MS, Adabag AS, Casey SA, Vargiu D, Link MS, et al. Gender-related differences in the clinical presentation and outcome of hypertrophic cardiomyopathy. *J Am Coll Cardiol*. 2005;46(3):480-7.

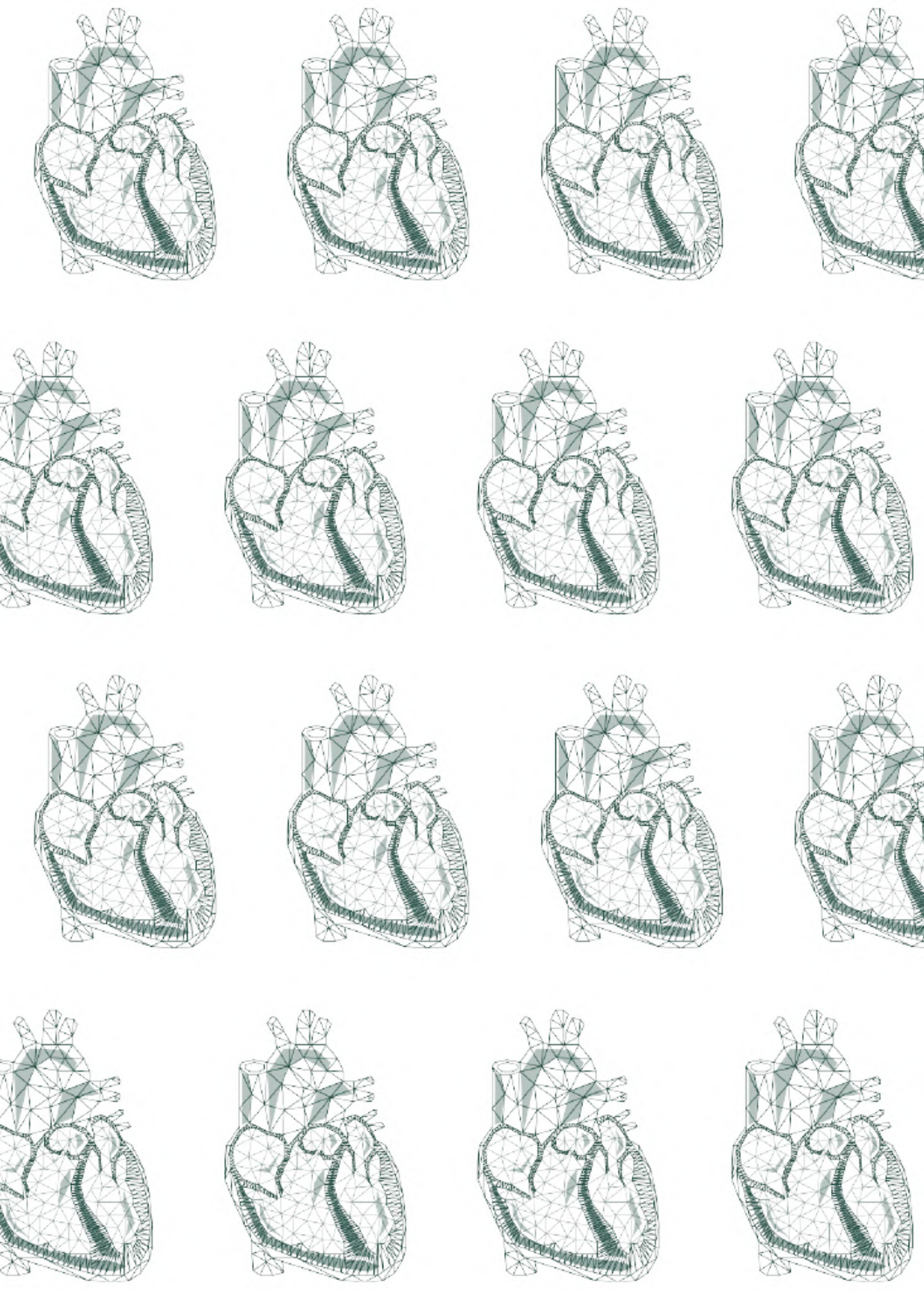

PART

DIVERSE CLINICAL PHENOTYPES

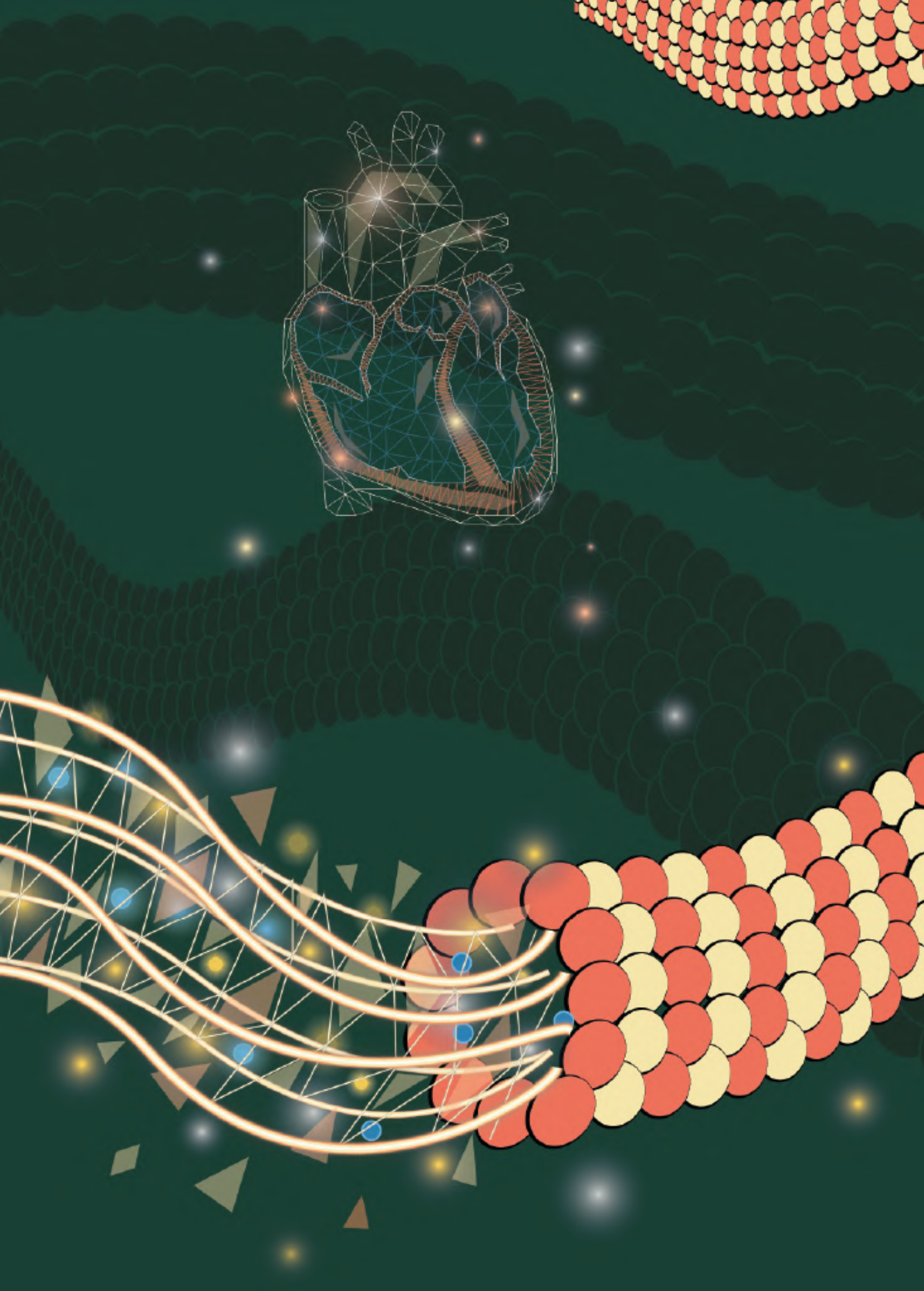

Chapter 2

The effect of tropomyosin variants on cardiomyocyte function and structure that underlie different clinical cardiomyopathy phenotypes

Larissa M. Dorsch, Diederik WD. Kuster, Jan DH. Jongbloed, Ludolf G. Boven, Karin Y. van Spaendonck-Zwarts, Albert JH. Suurmeijer, Aryan Vink, Gideon J. du Marchie Sarvaas, Maarten P. van den Berg, Jolanda van der Velden, Bianca JJM. Brundel, Paul A. van der Zwaag

Int J Cardiol. 323, 251-258 (2021).

ABSTRACT

BACKGROUND

Variants within the alpha-tropomyosin gene (*TPM1*) cause dominantly inherited cardiomyopathies, including dilated (DCM), hypertrophic (HCM) and restrictive (RCM) cardiomyopathy. Here we investigated whether *TPM1* variants observed in DCM and HCM patients affect cardiomyocyte physiology differently.

METHODS

We identified a large family with DCM carrying a recently identified *TPM1* gene variant (T201M) and a child with RCM with compound heterozygote *TPM1* variants (E62Q and M281T) whose family members carrying single variants show diastolic dysfunction and HCM. The effects of *TPM1* variants (T201M, E62Q or M281T) and of a plasmid containing both the E62Q and M281T variants on single-cell Ca^{2+} transients (CaT) in HL-1 cardiomyocytes were studied. To define toxic threshold levels, we performed dose-dependent transfection of *TPM1* variants. In addition, cardiomyocyte structure was studied in human cardiac biopsies with *TPM1* variants.

RESULTS

Overexpression of TPM1 variants led to time-dependent progressive deterioration of CaT, with the smallest effect seen for E62Q and larger and similar effects seen for the T201M and M281T variants. Overexpression of E62Q/M281T did not exacerbate the effects seen with overexpression of a single *TPM1* variant. T201M (DCM) replaced endogenous tropomyosin dose-dependently, while M281T (HCM) did not. Human cardiac biopsies with *TPM1* variants revealed loss of sarcomeric structures.

CONCLUSION

All *TPM1* variants result in reduced cardiomyocyte CaT amplitudes and loss of sarcomeric structures. These effects may underlie pathophysiology of different cardiomyopathy phenotypes.

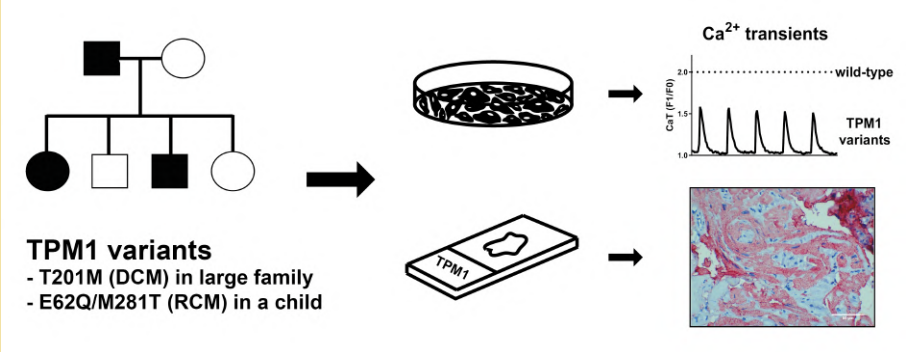

INTRODUCTION

Cardiomyopathies are a heterogeneous group of diseases of the myocardium that are associated with mechanical and/or electrical dysfunction and frequently caused by a genetic defect.[1] The working group on Myocardial and Pericardial Diseases of the European Society of Cardiology proposed a clinically oriented classification system in which heart muscle disorders are grouped into the following subtypes according to ventricular morphology and function: hypertrophic cardiomyopathy (HCM), dilated cardiomyopathy (DCM), restrictive cardiomyopathy (RCM), arrhythmogenic right ventricular cardiomyopathy (ARVC) and unclassified cardiomyopathies.[1,2]

Pathogenic variants in sarcomere genes are a frequent cause of cardiomyopathies and may lead to different cardiomyopathy subtypes.[3] One of these sarcomere genes is *TPM1* , which encodes alpha-tropomyosin and causes HCM (10 *TPM1* gene variants), DCM (11 *TPM1* variants), cardiomyopathy (2 *TPM1* variants) and left-ventricular non-compaction (3 *TPM1* variants) according to ClinVar database (January 2020).[4] All reported *TPM1* variants are missense variants that result in a single amino acid substitution, and they account for 1.5% of all likely pathogenic and pathogenic gene variants in HCM and 1.9% in DCM.[5]

Since distinct variants in the same sarcomere gene have been observed to cause either HCM or DCM, it has been proposed that these gene variants have to trigger two different series of events to culminate in the distinct cardiomyopathy subtypes.[6] Several studies have been published on the functional consequences of *TPM1* variants, adding to our understanding of the different pathophysiological processes that lead to distinct forms of cardiomyopathy.[7-9]

Here we describe a large family with DCM carrying a *TPM1* variant that was previously reported in a large Dutch cohort study.[10] We also identified compound heterozygote *TPM1* variants in a child with RCM, with family members carrying one of the two variants and showing HCM(-like) phenotypes. As changes in calcium-handling have been suggested to be central in determining the type of remodelling that occurs in genetic cardiomyopathies,[11] we expressed the three *TPM1* variants in HL-1 cardiomyocytes and measured the resulting Ca^{2+} transients (CaT).

METHODS

The comprehensive method section is available in the Data Supplement.

RESULTS

CLINICAL CHARACTERISTICS OF DCM FAMILY MEMBERS

Two probands (III:20 and IV:5) were investigated separately at the outpatient clinic and diagnosed with DCM. Clinical data of members of this DCM family (Figure 2.1A) are listed in Table 2.1. Individual III:20 complained of progressive dyspnoea, had a dilated LV and a LV ejection fraction (LVEF) of 15%, leading to a diagnosis of DCM at age 31. She received an implantable cardioverter defibrillator (ICD) at age 40. Ten years later, her LVEF was 18%. Genetic testing revealed that she carried the c.602C>T (p.(Thr201Met)) variant in exon 6 of *TPM1* (referred to as T201M), which had been previously identified in a large Dutch cohort study of DCM patients.[10] We classified T201M as likely pathogenic because it fulfills one strong and two moderate criteria (Table SI). This variant has not been further investigated so far.

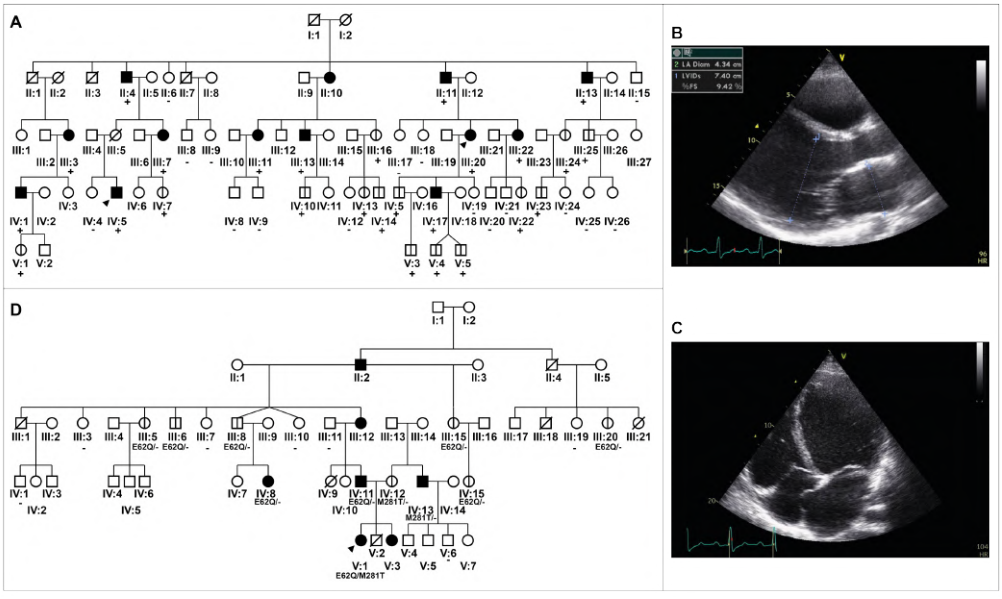

Figure 2.1: Pedigree of *TPM1* variant carrier and echocardiographic images of a DCM patient. (**A**) Pedigree of the DCM family. Presence (+) or absence (-) of the *TPM1* variant c.602C>T p.(Thr201Met) is indicated for the analysed subjects. (**B**) Parasternal long axis view and (**C**) apical 4-chamber view of patient IV:5 (DCM family) at presentation. The left ventricle is dilated (normal value <58 mm) and fractional shortening (FS) is reduced (normal value >25%). The left atrium is also enlarged (normal value <40 mm). (**D**) Pedigree of the family with the RCM patient. Presence (E62Q and/or M281T/-) or absence (-) of the *TPM1* variants c.184G>C p.(Glu62Gln) and c.842T>C p.(Met281Thr) is indicated for the analysed subjects. Squares represent males and circles represent females. Filled symbols indicate those with a diagnosis of (**A**) DCM and (**D**) RCM or HCM. Vertical lines indicate those who are asymptomatic or with mild signs or features of cardiomyopathies. Slashed symbols indicate deceased subjects. Arrowhead mark the index cases.

Table 2.1: Clinical data of members of DCM family.

Pedigree	*TPM1* genotype	1st presentation Age (years)	Reason	Echocardiogram LVEDd (mm)	LVESd (mm)	FS (%)	LVEF (%)	Phenotypes
II:1	**p.(Thr201Met)***	NA						D/83yr
II:4	**p.(Thr201Met)**	84	Screening	62	44	29	NA	DCM, atrial fibrillation
II:10	**p.(Thr201Met)***	NA						D/63yr, "enlarged heart"
II:11	**p.(Thr201Met)**	62	Dyspnoea	59	40	32	35	DCM, ICD at 66yr, replaced at 84yr, nsVTs
II:13	**p.(Thr201Met)**	70	Screening	61	50	18	35	DCM, atrial fibrillation at 75yr, no ICD
III:3	**p.(Thr201Met)**	53	CVA	60	45	25	NA	DCM, no follow-up available
III:5	**p.(Thr201Met)***	NA						D/44yr, traffic accident
III:7	**p.(Thr201Met)**	53	Screening	56	40	29	44	DCM, no follow-up available
III:11	**p.(Thr201Met)**	43	Dyspnoea	62	54	13	36	At 46yr discharged from follow-up after normalization echo
III:13	**p.(Thr201Met)**	53	Screening	52	37	29	50	No follow-up available
III:16	**p.(Thr201Met)**	48	Screening	42	29	31	55	At 57yr mild diastolic dysfunction, no DCM
III:20	**p.(Thr201Met)**	31	Dyspnoea	67	60	10	15	ICD at 40yr, LVEF 18% at 50yr
III:22	**p.(Thr201Met)**	38	Screening	58	47	19	28	DCM, no follow-up available
III:24	**p.(Thr201Met)**	47	Screening	48	30	38	60	Asymptomatic, no signs of DCM at 56yr
III:25	**p.(Thr201Met)**	45	Screening	51	34	33	55	Asymptomatic, no signs of DCM at 53yr
IV:1	**p.(Thr201Met)**	33	Screening	59	45	24	NA	No follow-up available
IV:5	**p.(Thr201Met)**	21	Dyspnoea	82	74	10	12	ICD at 21yr, at 34yr no ICD shocks, LVEF 40%
IV:7	**p.(Thr201Met)**	24	Screening					No signs of DCM, no follow-up available
IV:10	**p.(Thr201Met)**	18	Screening	52	37	29	60	Asymptomatic, LVEF 54% at 25yr
IV:13	**p.(Thr201Met)**	14	Screening	51	32	37	68	Asymptomatic, no signs of DCM at 22yr
IV:14	**p.(Thr201Met)**	12	Screening	51	33	35	62	Asymptomatic, no signs of DCM at 19yr
IV:15	**p.(Thr201Met)**	21	Screening				41	Mild DCM, no follow-up available
IV:17	**p.(Thr201Met)**	13	Screening	48	32	33	62	Died of heart failure at 24yr
IV:22	**p.(Thr201Met)**	7	Screening	41	29	29	55	Asymptomatic, LVEF 50% at 19yr
IV:23	**p.(Thr201Met)**	19	Screening	58	37	36	60	Asymptomatic, no signs of DCM at 27yr
V:1	**p.(Thr201Met)**	6	Screening	41	28	32	62	Asymptomatic, LVEF 41% at 17yr
V:3	**p.(Thr201Met)**	6	Screening	39	26	33	NA	No signs of DCM at 6yr

Table 2.1: Continued

Pedigree	*TPM1* genotype	1st presentation Age (years)	Reason	Echocardiogram LVEDd (mm)	LVESd (mm)	FS (%)	LVEF (%)	Phenotypes
V:4	**p.(Thr201Met)**	3	Screening	36	23	36	NA	No signs of DCM at 3yr
V:5	**p.(Thr201Met)**	3	Screening	37	22	41	NA	No signs of DCM at 3yr

* obligate carrier; CVA, cerebrovascular accident; D/, death; DCM, dilated cardiomyopathy; echo, echocardiogram; FS, fractional shortening; ICD, implantable cardioverter-defibrillator; LVEDd, left ventricular end-diastolic diameter; LVEF, left ventricular ejection fraction; LVESd, left ventricular end-systolic diameter; NA, not available; nsVT, non-sustained ventricular tachycardia; yr, years.

This proband's son (IV:17) died at age 24 from heart failure that had worsened after a high energy trauma (car accident) two months before his death. Her sister (III:22) was diagnosed with DCM at age 38 following family screening, but no follow-up is available. Two other siblings tested negative for the familial *TPM1* variant. The father of the proband (II:11) was diagnosed with DCM at age 62. At age 66, he received an ICD, which was replaced at age 84. No ICD shocks were recorded.
The other proband in this family (IV:5) was diagnosed with DCM (Figures 2.1B-C) and received an ICD at age 21. After 13 years of follow-up, he had not experienced any ICD shocks and his LVEF was 40%. His mother (III:5) died at age 44 in a traffic accident. His maternal aunt (III:7) was diagnosed with DCM at age 53 following family screening. His maternal grandfather (II:4), who had not undergone prior cardiac evaluations, was diagnosed with DCM and atrial fibrillation at age 84 following family screening.
Both probands were linked to the same ancestral couple (I:1 and I:2). After cascade family screening, 29 family members were identified as carriers of the familial *TPM1* variant. The phenotypic variability and age-related penetrance is further illustrated by III:24 and III:25, who were asymptomatic and without signs of DCM at ages 56 and 53, respectively. The penetrance, as indicated by age at DCM diagnosis, is shown in Figure SI. The youngest age at diagnosis was 17 (V:1), though this individual was asymptomatic at that time. At age 60, a diagnosis of DCM was made in 55% of the family members who carried the T201M variant.

CLINICAL CHARACTERISTICS OF RCM FAMILY MEMBERS

We describe, for the first time, compound heterozygote *TPM1* variants in a child with RCM, with family members carrying one of the two variants and showing HCM(-like) phenotypes (Figure 2.1D).
An asymptomatic 6-year-old girl (V:1) was referred to the paediatrician after the sudden death of her brother (V:2) at 22 months of age. No autopsy was performed, and no DNA was available for genetic testing. At age six, the proband's cardiac evaluation was normal. At age nine, she was referred to a paediatric cardiologist because she reported chest pain during exercise. Cardiac evaluation showed bi-atrial dilatation with near-normal LV volume and raised ventricular end-diastolic pressures at cardiac catheterization. There was no evidence of LV hypertrophy or constrictive pericarditis. Based on these findings, a diagnosis of RCM was made in this patient. At age 12, she received an orthotopic cardiac transplantation, and she reached adult age in good clinical condition. Genetic

screening identified two missense variants in *TPM1* : c.184G>C (p.(Glu62Gln)) (referred to as E62Q) and c.842T>C (p.(Met281Thr)) (referred to as M281T). Both variants had previously been identified in HCM patients.[12,13] We classified both variants as likely pathogenic, with E62Q fulfilling one strong and two moderate criteria and M281T fulfilling two moderate and $\geq$2 supporting criteria (Table SI).

The proband's sister (V:3) had a normal cardiac evaluation at age seven and has so far not undergone genetic testing. The proband's father (IV:11), a carrier of the E62Q variant, had minor abnormalities suggestive for RCM, with mild LV diastolic dysfunction on echo. Her mother (IV:12), a carrier of the M281T variant, was asymptomatic but had a mildly enlarged left atrium at age 40. The maternal uncle (IV:13), also a carrier of the M281T variant, was asymptomatic, but echocardiography at age 40 showed mild LV hypertrophy (13 mm). The paternal grandmother (III:12) and other carriers in her generation (III) who were positive for the E62Q variant showed stable diastolic dysfunction and atrial dilatation in an age range of 51-69 years. Notably, a cousin of the father (IV:8), a carrier of the E62Q variant, was diagnosed with HCM at age 17 with an LV wall thickness of 18 mm.

TIME-DEPENDENT REDUCTION OF CALCIUM TRANSIENT AMPLITUDE BY *TPM1* VARIANTS

Variants in *TPM1* may lead to disturbed intracellular calcium handling that contributes to contractile dysfunction,[14] and different changes in calcium handling have been linked to the development of either DCM or HCM.[11] We therefore overexpressed the three identified *TPM1* variants (untagged, 0.75 µg/µL) in HL-1 cardiomyocytes and determined the effect on CaT. All three *TPM1* variants significantly reduced CaT amplitude 48 h post-transfection when compared to HL-1 cardiomyocytes overexpressing untagged wild-type *TPM1* (Figures 2.2A,G and SII).

The reduction in CaT amplitude was significantly larger for $TPM1_{T201M}$ and $TPM1_{M281T}$ compared to $TPM1_{WT}$, with means $\pm$ SEM of 34.90% $\pm$ 0.05 and 35.78% $\pm$ 0.04, respectively, while the reduction for the $TPM1_{E62Q}$ variant was smaller (19.33% $\pm$ 0.07). As the RCM patient carried both the E62Q and M281T variants ($TPM1_{E62Q/M281T}$), we studied if expression of both variants exacerbated the phenotype and found that $TPM1_{E62Q/M281T}$ expression did not significantly decrease CaT (24.64% $\pm$ 0.06) in comparison to the reductions we saw for the individual variants. Longer overexpression (72 h) of all *TPM1* variants further reduced the CaT amplitude, but did not change the variant-specific effects that we had observed 48 h post-transfection (Figures 2.2B,E). With the exception of $TPM1_{E62Q/M281T}$ 48 h post-transfection, no significant differences in calcium re-uptake kinetics were observed between the wild-type and variant *TPM1* forms 48 h and 72 h post-transfection (Figure 2.2C-D,F-G).

DOSE-DEPENDENT EFFECT OF *TPM1* VARIANTS EXPRESSION

Since overexpression of $TPM1_{T201M}$ and $TPM1_{M281T}$ 48 h post-transfection resulted in a strong reduction in CaT amplitudes, we wanted to see if this effect is dose-dependent. Using

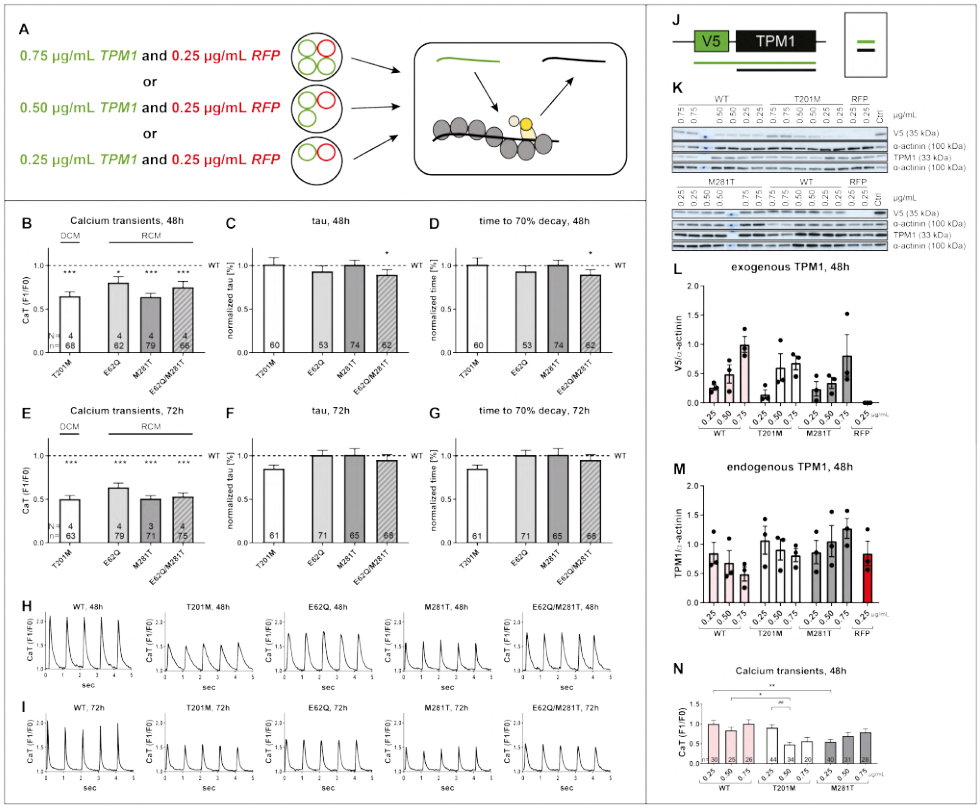

Figure 2.2: Time- (B-I) and dose-dependent (J-N) transfection of *TPM1* variants.
(**A**) Schematic representation of the ratio of double transfected DNA. 0.25 µg/mL DNA encoding RFP (red circle) was co-transfected with 0.75 (used in **B-I**), 0.50 or 0.25 µg/mL DNA encoding TPM1 (green circle). Green circles: *TPM1* plasmids. Red circle: *RFP* plasmid. Thick green line: exogenous TPM1 encoded by *TPM1* plasmid. Thick black line: endogenous TPM1. Grey circles: actin. Complex of yellow circles: troponin complex. (**B**) Quantified CaT amplitude data of single HL-1 cardiomyocytes 48 h post-transfection. N = number of transfections; n = number of measured HL-1 cardiomyocytes that were *RFP*-positive transfected. Exponential curve fitting was applied to obtain (**C**) the mean time constant of CaT decay (tau) and (**D**) the time to 70% decay. (**E**) Quantified CaT amplitude data of single HL-1 cardiomyocytes 72 h post-transfection, (**F**) tau and (**G**) time to 70% decay. Representative CaT traces detected (**H**) 48 h and (**I**) 72 h post-transfection. (**J**) Due to the amino-terminal V5-tag, exogenous TPM1 (green line) was larger and therefore displayed migration on Western blot that was distinguishable from endogenous TPM1 (black line). (**K**) Representative blot images for endogenous (TPM1-antibody) and exogenous (V5-antibody) TPM1 expression level after dose-dependent double transfection of *TPM1* and *RFP*. Ctrl: Control cell lysate to compare different membranes. (**L**) Dose-dependent expression of exogenous V5-tagged $TPM1_{WT}$, $TPM1_{T201M}$ and $TPM1_{M281T}$. Each dot represents one transfection and each value was normalized to the mean of $TPM1_{WT\_0.75µg/mL}$. (**M**) Endogenous TPM1 levels after dose-dependent transfection. (**N**) Quantified CaT amplitude data of single HL-1 cardiomyocytes 48 h after dose-dependent double transfection (N = 2) of untagged wild-type/variant *TPM1* and *RFP*. Per transfection, each CaT value was normalized to the mean value of overexpressed (**B-I**) $TPM1_{WT}$ and (**N**) $TPM1_{WT\_0.25µg/mL}$. *p<0.05, **p<0.01, ***p<0.001 versus $TPM1_{WT}$ and $^{\#\#}p$<0.01 versus $TPM1_{T201M\_0.25µg/µL}$.

different ratios of *RFP* (0.25 µg/mL) and V5-tagged *TPM1* (0.25, 0.50 and 0.75 µg/mL (used in previous experiment)), we were able to express TPM1 in a dose-dependent manner (Figures 2.2J-L and SIII). Transfection of $TPM1_{WT}$ and $TPM1_{T201M}$ resulted in partial replacement of endogenous TPM1 (Figure 2.2M). Notably, endogenous TPM1 levels increased with higher doses of transfected $TPM1_{M281T}$. Dose-dependent transfection of untagged *TPM1* variants and CaT assessment 48 h post-transfection showed that calcium handling dysfunction was influenced by the dose of $TPM1_{T201M}$ (Figure 2.2N), showing significant effects at 0.5 µg/mL and a trend toward significance at 0.75 µg/mL $TPM1_{T201M}$ levels. Transfection of 0.25 µg/mL $TPM1_{T201M}$, however, had no detrimental effect on CaT amplitude, while transfection of 0.25 µg/mL $TPM1_{M281T}$ already significantly decreased CaT amplitude. A lower transfection dose of $TPM1_{M281T}$ reduced CaT amplitude more than a higher one.

TPM1 VARIANTS HAVE NO EFFECT ON AUTOPHAGY AND F-ACTIN

Based on the increase in endogenous TPM1 after high-dose transfection of $TPM1_{M281T}$, we defined the effect of *TPM1* variants on components of cellular protein quality control. Immunofluorescent staining of V5-tagged TPM1 revealed no difference in localization of TPM1 variants 48 h post-transfection, nor the formation of aggregates (Figure SIVA). We also observed unaltered levels of markers for cardiac-specific proteins (α-actinin and myosing heavy chain 7 (MYH7)), autophagy (LC3B and p62), endoplasmic reticulum stress (phosphorylation of translation-initiation factor eIF2α) and stress fibers (F-actin) in HL-1 cardiomyocytes transfected with TPM1 variants as compared to wild-type TPM1-transfected cardiomyocytes (Figures SIV-V).

LOSS OF SARCOMERIC STRUCTURES IN HUMAN TISSUE BIOPSIES WITH *TPM1* VARIANTS

As HL-1 cardiomyocytes do not show the highly organized myofilament structure of adult cardiomyocytes,[15,16] we determined the localization of TPM1 in the myocardium of patients carrying either the $TPM1_{T201M}$ variant or the $TPM1_{E62Q/M281T}$ variants. We stained patient samples (small endomyocardial biopsies) with antibodies against TPM1 and α-actinin. Both biopsies showed a loss of cardiomyocyte-typical architecture indicated by a loss of sarcomere striations and a loss of intact cardiac muscle fibers (Figure 2.3). TPM1 epitopes appeared disrupted and were not organized in the characteristic contractile filaments, and this was accompanied by an almost complete loss of α-actinin. Biopsies from end-stage ischemic heart failure and non-failing subjects were used as controls, and these show the expected sarcomere striation and distribution of TPM1 and α-actinin.

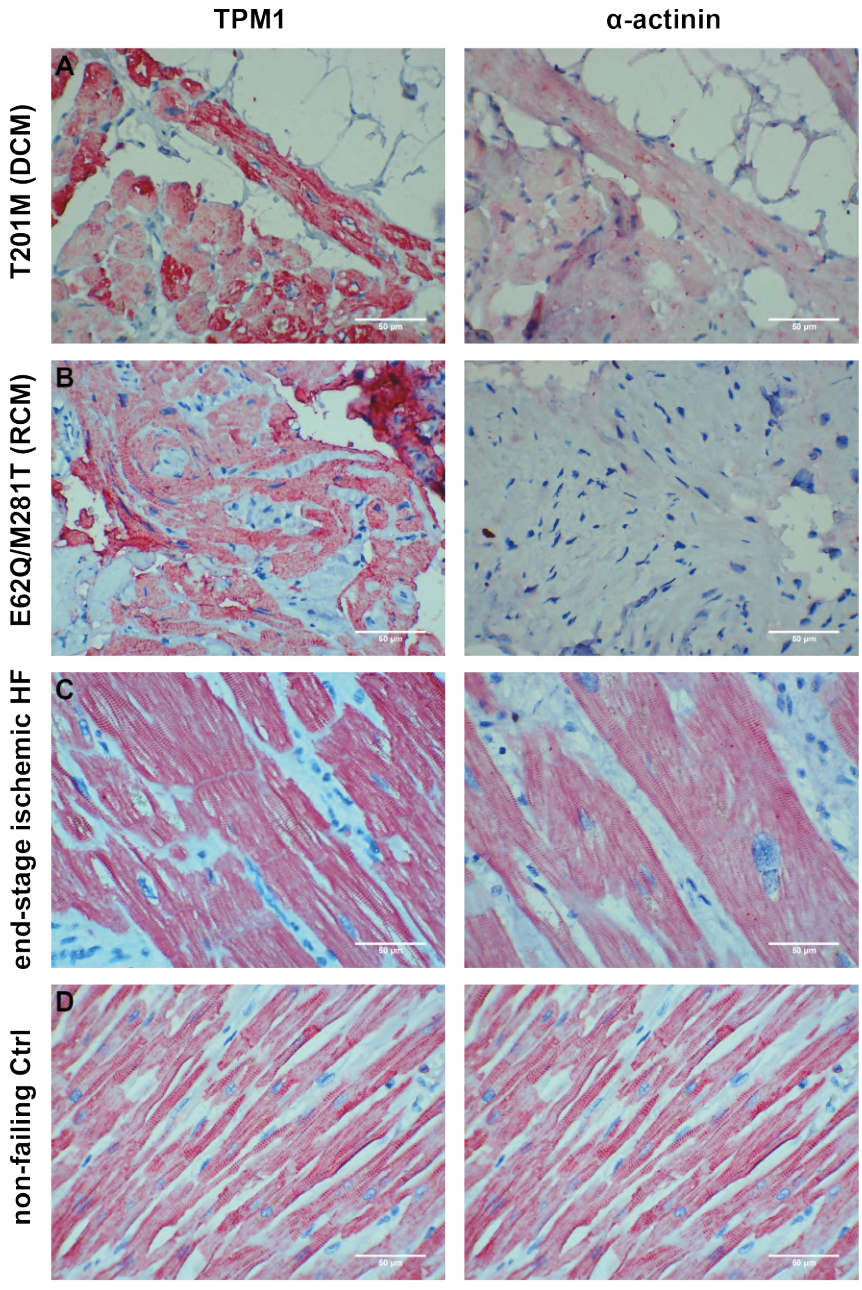

Figure 2.3: Representative images of immunohistochemical staining for TPM1 (left column) and α-actinin (right column) of endomyocardial biopsies. (**A**) Subject (III:11) with *TPM1* T201M variants, (**B**) proband (V:1) with *TPM1* E62Q/M281T variants, (**C**) remote area biopsies from the left ventricle of one of three patients with end-stage ischemic heart failure (HF) and (**D**) septal tissue from one of four subjects that died due to a non-cardiac cause of death (non-failing Ctrl). Scale bar represents 50 µm.

DISCUSSION

Gene variants in thin filament components, including alpha-tropomyosin, are known to cause a complex heterogeneous pattern of progressive ventricular remodelling and clinical phenotypes.[17] Our study confirms this clinical heterogeneity in two families with *TPM1* variants and different cardiomyopathy subtypes, namely $TPM1_{T201M}$ (DCM) and $TPM1_{E62Q}$ and $TPM1_{M281T}$ (HCM; and in combination RCM). We also describe, for the first time, compound heterozygote $TPM1_{E62Q/M281T}$ variants in a child with RCM. Overall, the genotypes and diverse clinical characteristics of the family members of the DCM and RCM probands suggest that additional causal factors are necessary for the development of cardiac abnormalities in carriers of a heterozygous *TPM1* variant, whereas compound heterozygosity for *TPM1* variants causes severe cardiomyopathy in childhood.

IMPAIRED CARDIAC PERFORMANCE DUE TO REDUCED CALCIUM TRANSIENT AMPLITUDES

In thin filament cardiomyopathies, altered myocellular Ca^{2+} homeostasis may trigger events that remodel the cardiomyocyte and ultimately perturb cardiac structure.[17,18] Data from experiments in which adenovirus was used to express human HCM-causing variants in isolated guinea pig left ventricular cardiomyocytes showed that altered CaT were one of the primary effects of HCM-causing variants expression.[14] We therefore measured CaT amplitudes in HL-1 cardiomyocytes. Cardiac muscle cell properties have been measured in this model system before.[19,20] In our experimental model system, production of all *TPM1* variants resulted in reduced CaT amplitudes that were independent of the clinical cardiomyopathy phenotype. Previous studies on HCM- and DCM-related thin filament gene variants have shown opposing changes in myofilament Ca^{2+}-sensitivity, specifically an increase for HCM variants and a decrease for DCM variants (reviewed in [21]). Tardiff and colleagues suggested that the observed primary alterations in Ca^{2+}-sensitivity at the myofilament level indicate a disruption of the Ca^{2+}-dependent sarcomeric activation by thin filament gene variants.[17] These Ca^{2+}-sensitivity changes were associated with similar opposite effects in the Ca^{2+} affinity of myofilaments, i.e. an increase for HCM variants and a decrease for DCM variants.[14] These opposing changes may alter cytosolic Ca^{2+} buffering in different ways, and thereby alter cellular CaT. Davis and colleagues provided evidence for diverse changes in developed tension and CaT when comparing HCM- and DCM-related cardiac troponin C variants, a finding they related to diverse activation of signaling pathways leading to either concentric or eccentric remodelling.[11] While previous studies on *TPM1* variants have also reported a similar opposite effect on the Ca^{2+}-sensitivity of myofilaments for HCM- and DCM-associated variants,[8] two DCM-related *TPM1* variants have shown opposite effects: the Glu40Lys variant decreased Ca^{2+} affinity, while the Glu54Lys variant increased Ca^{2+} affinity (but at 100% variant level).[14] Importantly, no effect on Ca^{2+} affinity was observed when a mixture of 50% variant:50% wild-type TPM1 was studied.[14]

In contrast, we observed a decrease in CaT for both HCM- and DCM-related *TPM1* variants. The previous study and our current data indicate that *TPM1* variant-related changes in Ca^{2+} affinity and CaT are independent of the type of cardiac remodelling, which

suggests that the diverse clinical cardiac phenotypes seen in affected subjects may rather involve modifier genes and/or environmental factors.[17]

Reduced CaT amplitudes may affect tension development of cardiomyocytes. Comparing the CaT amplitudes at 48 h and 72 h post-transfection revealed that longer overexpression of all *TPM1* variants further reduced CaT amplitude, suggesting a progressive pathogenic process. This is in line with a series of longitudinal studies of patients with thin filament variants in whom the ventricle, in particular, was progressively remodeled.[22,23] Reduced CaT amplitudes have been associated with impaired cell-shortening of HL-1 myocytes, indicating contractile dysfunction.[19] Taken together, reduced CaT amplitudes may contribute to the poor cardiac contraction seen in affected individuals.

DOSE-DEPENDENT TRANSFECTION: MAINTENANCE TPM1 STOICHIOMETRY

Previous studies in several transgenic mouse models revealed that increasing the expression of *Tpm1* variants causes a concomitant decrease in wild-type TPM1 levels, histopathological changes and severe impairment of both contractility and relaxation.[24,25] Given the large decrease in CaT amplitude 48 h post-transfection induced by production of $TPM1_{T201M}$ (DCM) and $TPM1_{M281}$ (HCM) (Figure 2.2B), and the previously reported dose-effects of *TPM1* variants, we studied the effect of dose-dependent transfection of these particular variants. A dose-dependent decrease in endogenous TPM1 was observed upon transfection with $TPM1_{T201M}$, and this coincided with a reduction in CaT. These data illustrate that a heterozygous gene variant, which results in a mixture of the variant and wild-type TPM1, is sufficient to suppress CaT. We therefore propose for $TPM1_{T201M}$ that total TPM1 levels seem to be kept constant to preserve stoichiometry of sarcomere proteins. Furthermore, "threshold" levels of $TPM1_{T201M}$ seem to have been reached when $TPM1_{T201M}$ was transfected between 0.25 and 0.50 µg/mL since functional compensation by wild-type TPM1 became insufficient. This is in line with *Tpm1* transgenic mouse experiments indicating that there may be "threshold" levels of TPM1 expression that lead to defined phenotypes rather than a gradient of physiological or pathological conditions.[24,25] While the total amount of TPM1 protein remained unchanged in these *Tpm1* transgenic mice, wild-type TPM1 levels were reduced by 35 to 65%.[24,25]

In contrast to the $TPM1_{T201M}$-induced reduction of endogenous wild-type TPM1, higher transfection doses of the $TPM1_{M281T}$ variant did not lower endogenous TPM1, instead resulting in higher levels of wild-type TPM1. This indicates that synthesis of TPM1 is increased and/or its degradation decreased in the presence of an increasing dose of the $TPM1_{M281T}$ variant. The largest drop in CaT was observed at the lowest dose of $TPM1_{M281T}$ transfection, which coincided with the lowest level of wild-type TPM1.

Overall, we observed that the dose-dependent effect on CaT may be determined by the mixture of variant and wild-type TPM1. DCM- and HCM-associated *TPM1* variants led to opposite effects, and this difference may be related to the ability to replace/reduce endogenous sarcomeric tropomyosin.

DESTRUCTION OF HUMAN CARDIOMYOCYTES IN TISSUE BIOPSIES WITH LONG-TERM EXPRESSION OF *TPM1* VARIANTS

In contrast to our observations in short-term *TPM1* overexpression experiments and previous findings suggesting that *Tpm1* variants expressed in isolated rat cardiomyocytes or 12-month-old transgenic mice were normally incorporated into the sarcomeres without altering sarcomeric structures,[26,27] cardiomyocytes in the respective human tissue biopsies displayed obvious structural changes. To our knowledge this is the first time that cardiac biopsies with these *TPM1* variants have been immunohistochemically analysed for intracellular localization of TPM1 and α-actinin. We used α-actinin as a Z-disc marker to assess normal myofilament structure. The combination of chronic expression of *TPM1* variants and cardiomyopathy-associated pathological remodelling may have been responsible for the loss of cardiomyocyte-typical architecture. Cardiac histopathologic findings of myocyte disarray and interstitial fibrosis have also been reported in an affected subject with the $TPM1_{D175N}$ variant,[28] and myofibril loss has been observed in subjects with HCM, DCM and RCM.[29-31] Reduced myofibril density may subsequently impair contractility and enhance the respective cardiomyopathy-associated pathomechanisms.

Since the TPM1 epitopes appeared disrupted and not organized in the characteristic contractile filaments and α-actinin was almost completely lost, we hypothesize that these *TPM1* variants affect the sarcomeric organization, especially assembly of α-actinin. *TPM1*-deficient cardiomyocytes have been shown to assemble aberrant F-actin fibrils with α-actinin puncta dispersed irregularly along their lengths.[32] Moreover, disrupting the tropomodulin–TPM1 interaction in chicken cardiac myocytes led to thin filament depolymerization and disassembly that was accompanied by perturbation of Z-lines, thick filaments and titin filaments.[33] Likewise, the *TPM1* variants we studied may disrupt interactions of TPM1, leading to its depolymerization and, as a consequence, to disassembly of α-actinin.

LIMITATIONS OF HL-1 CARDIOMYOCYTES

As sarcomeric structures are immature,[15,16] HL-1 cardiomyocytes present with limited contractility.[16] We therefore focused on the effect on Ca^{2+} transients since disturbed Ca^{2+} handling will impair contractility. CaT data in HL-1 cardiomyocytes has been shown to be similar to that of isolated rat and dog atrial cardiomyocytes, indicating that HL-1 cardiomyocytes represent a cardiac cell model to trace changes in Ca^{2+} transients in relation to cardiac diseases.[19,34]

HL-1 cardiomyocytes are immortalized cells of mouse atrial origin and therefore do not precisely recapitulate a cellular milieu that reflects the ventricular cardiac myocytes in human or of acutely isolated ventricular cardiomyocytes.[35] In future, it is important to test these *TPM1* variants in a human cell-based model such as human iPSC-derived cardiomyocytes.

CONCLUSION

In conclusion, various *TPM1* variants lead to heterogeneous clinical manifestations of different cardiomyopathy subtypes. Overexpression of *TPM1* variants led to time-dependent progressive deterioration of cardiomyocyte CaT amplitudes. The dose-dependent effect on CaT was opposite for DCM- and HCM-associated *TPM1* variants. Overall, our data indicate that reduced cardiomyocyte CaT amplitudes and loss of sarcomeric structures are independent of the *TPM1* variant and of the clinical cardiomyopathy phenotype.

Source of funding: This work was supported by the Netherlands Cardiovascular Research Initiative: An initiative with support of the Dutch Heart Foundation [grant numbers CVON2014-40 DOSIS, CVON-STW2016-14728 AFFIP] and Netherlands Organization for Sciences (NWO)-ZonMW [grant number VICI 91818602].

ACKNOWLEDGEMENTS

We acknowledge the Microscopy and Cytometry Core Facility at the Amsterdam UMC – Location VUmc for providing assistance in microscopy, Petra van der Kraak and Pedro Espinosa González for technical assistance with the immunostains and Kate Mc Intyre for reviewing the manuscript.

SUPPLEMENTARY FILES - ONLINE

https://www.internationaljournalofcardiology.com/article/S0167-5273(20)33728-1/fulltext#supplementaryMaterial

REFERENCES

1. Maron BJ, Towbin JA, Thiene G, Antzelevitch C, Corrado D, Arnett D, et al. Contemporary definitions and classification of the cardiomyopathies: an American Heart Association Scientific Statement from the Council on Clinical Cardiology, Heart Failure and Transplantation Committee; Quality of Care and Outcomes Research and Functional Genomics and Translational Biology Interdisciplinary Working Groups; and Council on Epidemiology and Prevention. *Circulation*. 2006;113(14):1807-16.
2. Elliott P, Andersson B, Arbustini E, Bilinska Z, Cecchi F, Charron P, et al. Classification of the cardiomyopathies: a position statement from the European Society Of Cardiology Working Group on Myocardial and Pericardial Diseases. *Eur Heart J*. 2008;29(2):270-6.
3. Walsh R, Mazzarotto F, Whiffin N, Buchan R, Midwinter W, Wilk A, et al. Quantitative approaches to variant classification increase the yield and precision of genetic testing in Mendelian diseases: the case of hypertrophic cardiomyopathy. *Genome Med*. 2019;11(1):5.
4. Redwood C, Robinson P. Alpha-tropomyosin mutations in inherited cardiomyopathies. *J Muscle Res Cell Motil*. 2013;34(3-4):285-94.
5. Walsh R, Thomson KL, Ware JS, Funke BH, Woodley J, McGuire KJ, et al. Reassessment of Mendelian gene pathogenicity using 7,855 cardiomyopathy cases and 60,706 reference samples. *Genet Med*. 2017;19(2):192-203.
6. Kamisago M, Sharma SD, DePalma SR, Solomon S, Sharma P, McDonough B, et al. Mutations in sarcomere protein genes as a cause of dilated cardiomyopathy. *N Engl J Med*. 2000;343(23):1688-96.
7. Mirza M, Marston S, Willott R, Ashley C, Mogensen J, McKenna W, et al. Dilated cardiomyopathy mutations in three thin filament regulatory proteins result in a common functional phenotype. *J Biol Chem*. 2005;280(31):28498-506.
8. Chang AN, Harada K, Ackerman MJ, Potter JD. Functional consequences of hypertrophic and dilated cardiomyopathy-causing mutations in alpha-tropomyosin. *J Biol Chem*. 2005;280(40):34343-9.
9. Rajan S, Ahmed RP, Jagatheesan G, Petrashevskaya N, Boivin GP, Urboniene D, et al. Dilated cardiomyopathy mutant tropomyosin mice develop cardiac dysfunction with significantly decreased fractional shortening and myofilament calcium sensitivity. *Circ Res*. 2007;101(2):205-14.
10. van Spaendonck-Zwarts KY, van Rijsingen IA, van den Berg MP, Lekanne Deprez RH, Post JG, van Mil AM, et al. Genetic analysis in 418 index patients with idiopathic dilated cardiomyopathy: overview of 10 years' experience. *Eur J Heart Fail*. 2013;15(6):628-36.
11. Davis J, Davis LC, Correll RN, Makarewich CA, Schwanekamp JA, Moussavi-Harami F, et al. A Tension-Based Model Distinguishes Hypertrophic versus Dilated Cardiomyopathy. *Cell*. 2016;165(5):1147-59.
12. Jongbloed RJ, Marcelis CL, Doevendans PA, Schmeitz-Mulkens JM, Van Dockum WG, Geraedts JP, et al. Variable clinical manifestation of a novel missense mutation in the alpha-tropomyosin (TPM1) gene in familial hypertrophic cardiomyopathy. *J Am Coll Cardiol*. 2003;41(6):981-6.
13. Van Driest SL, Ellsworth EG, Ommen SR, Tajik AJ, Gersh BJ, Ackerman MJ. Prevalence and spectrum of thin filament mutations in an outpatient referral population with hypertrophic cardiomyopathy. *Circulation*. 2003;108(4):445-51.
14. Robinson P, Liu X, Sparrow A, Patel S, Zhang YH, Casadei B, et al. Hypertrophic cardiomyopathy mutations increase myofilament Ca(2+) buffering, alter intracellular Ca(2+) handling, and stimulate Ca(2+)-dependent signaling. *J Biol Chem*. 2018;293(27):10487-99.
15. Claycomb WC, Lanson NA, Jr., Stallworth BS, Egeland DB, Delcarpio JB, Bahinski A, et al. HL-1 cells: a cardiac muscle cell line that contracts and retains phenotypic characteristics of the adult cardiomyocyte. *Proc Natl Acad Sci U S A*. 1998;95(6):2979-84.
16. Dias P, Desplantez T, El-Harasis MA, Chowdhury RA, Ullrich ND, Cabestrero de Diego A, et al. Characterisation of connexin expression and electrophysiological properties in stable clones of the HL-1 myocyte cell line. *PLoS One*. 2014;9(2):e90266.
17. Tardiff JC. Thin filament mutations: developing an integrative approach to a complex disorder. *Circ Res*. 2011;108(6):765-82.
18. Fatkin D, McConnell BK, Mudd JO, Semsarian C, Moskowitz IG, Schoen FJ, et al. An abnormal Ca(2+) response in mutant sarcomere protein-mediated familial hypertrophic cardiomyopathy. *J Clin Invest*. 2000;106(11):1351-9.
19. Brundel BJ, Shiroshita-Takeshita A, Qi X, Yeh YH, Chartier D, van Gelder IC, et al. Induction of heat shock response protects the heart against atrial fibrillation. *Circ Res*. 2006;99(12):1394-402.
20. Huang JH, Chen YC, Lee TI, Kao YH, Chazo TF, Chen SA, et al. Glucagon-like peptide-1 regulates calcium homeostasis and electrophysiological activities of HL-1 cardiomyocytes. *Peptides*. 2016;78:91-8.
21. van der Velden J, Stienen GJM. Cardiac Disorders and Pathophysiology of Sarcomeric Proteins. *Physiol Rev*. 2019;99(1):381-426.
22. Mogensen J, Kubo T, Duque M, Uribe W, Shaw A, Murphy R, et al. Idiopathic restrictive cardiomyopathy is part of the clinical expression of cardiac troponin I mutations. *J Clin Invest*. 2003;111(2):209-16.
23. Revera M, Van der Merwe L, Heradien M, Goosen A, Corfield VA, Brink PA, et al. Long-term follow-up of R403WMYH7 and R92WTNNT2 HCM families: mutations determine left ventricular dimensions but not wall thickness during disease progression. *Cardiovasc J Afr*. 2007;18(3):146-53.
24. Muthuchamy M, Pieples K, Rethinasamy P, Hoit B, Grupp IL, Boivin GP, et al. Mouse model of a familial hypertrophic cardiomyopathy mutation in alpha-tropomyosin manifests cardiac dysfunction. *Circ Res*. 1999;85(1):47-56.

25. Prabhakar R, Boivin GP, Grupp IL, Hoit B, Arteaga G, Solaro RJ, et al. A familial hypertrophic cardiomyopathy alpha-tropomyosin mutation causes severe cardiac hypertrophy and death in mice. *J Mol Cell Cardiol*. 2001;33(10):1815-28.
26. Michele DE, Albayya FP, Metzger JM. Direct, convergent hypersensitivity of calcium-activated force generation produced by hypertrophic cardiomyopathy mutant α-tropomyosins in adult cardiac myocytes. *Nature Medicine*. 1999;5(12):1413-7.
27. Michele DE, Gomez CA, Hong KE, Westfall MV, Metzger JM. Cardiac dysfunction in hypertrophic cardiomyopathy mutant tropomyosin mice is transgene-dependent, hypertrophy-independent, and improved by beta-blockade. *Circ Res*. 2002;91(3):255-62.
28. Coviello DA, Maron BJ, Spirito P, Watkins H, Vosberg HP, Thierfelder L, et al. Clinical features of hypertrophic cardiomyopathy caused by mutation of a "hot spot" in the alpha-tropomyosin gene. *J Am Coll Cardiol*. 1997;29(3):635-40.
29. Nijenkamp L, Bollen IAE, van Velzen HG, Regan JA, van Slegtenhorst M, Niessen HWM, et al. Sex Differences at the Time of Myectomy in Hypertrophic Cardiomyopathy. *Circ Heart Fail*. 2018;11(6):e004133.
30. Bollen IAE, Schuldt M, Harakalova M, Vink A, Asselbergs FW, Pinto JR, et al. Genotype-specific pathogenic effects in human dilated cardiomyopathy. *J Physiol*. 2017;595(14):4677-93.
31. Jaffer F, Murphy SM, Scoto M, Healy E, Rossor AM, Brandner S, et al. BAG3 mutations: another cause of giant axonal neuropathy. *J Peripher Nerv Syst*. 2012;17(2):210-6.
32. McKeown CR, Nowak RB, Gokhin DS, Fowler VM. Tropomyosin is required for cardiac morphogenesis, myofibril assembly, and formation of adherens junctions in the developing mouse embryo. *Dev Dyn*. 2014;243(6):800-17.
33. Mudry RE, Perry CN, Richards M, Fowler VM, Gregorio CC. The interaction of tropomodulin with tropomyosin stabilizes thin filaments in cardiac myocytes. *J Cell Biol*. 2003;162(6):1057-68.
34. Zhang D, Hu X, Li J, Liu J, Baks-Te Bulte L, Wiersma M, et al. DNA damage-induced PARP1 activation confers cardiomyocyte dysfunction through NAD(+) depletion in experimental atrial fibrillation. *Nat Commun*. 2019;10(1):1307.
35. Peter AK, Bjerke MA, Leinwand LA. Biology of the cardiac myocyte in heart disease. *Mol Biol Cell*. 2016;27(14):2149-60.

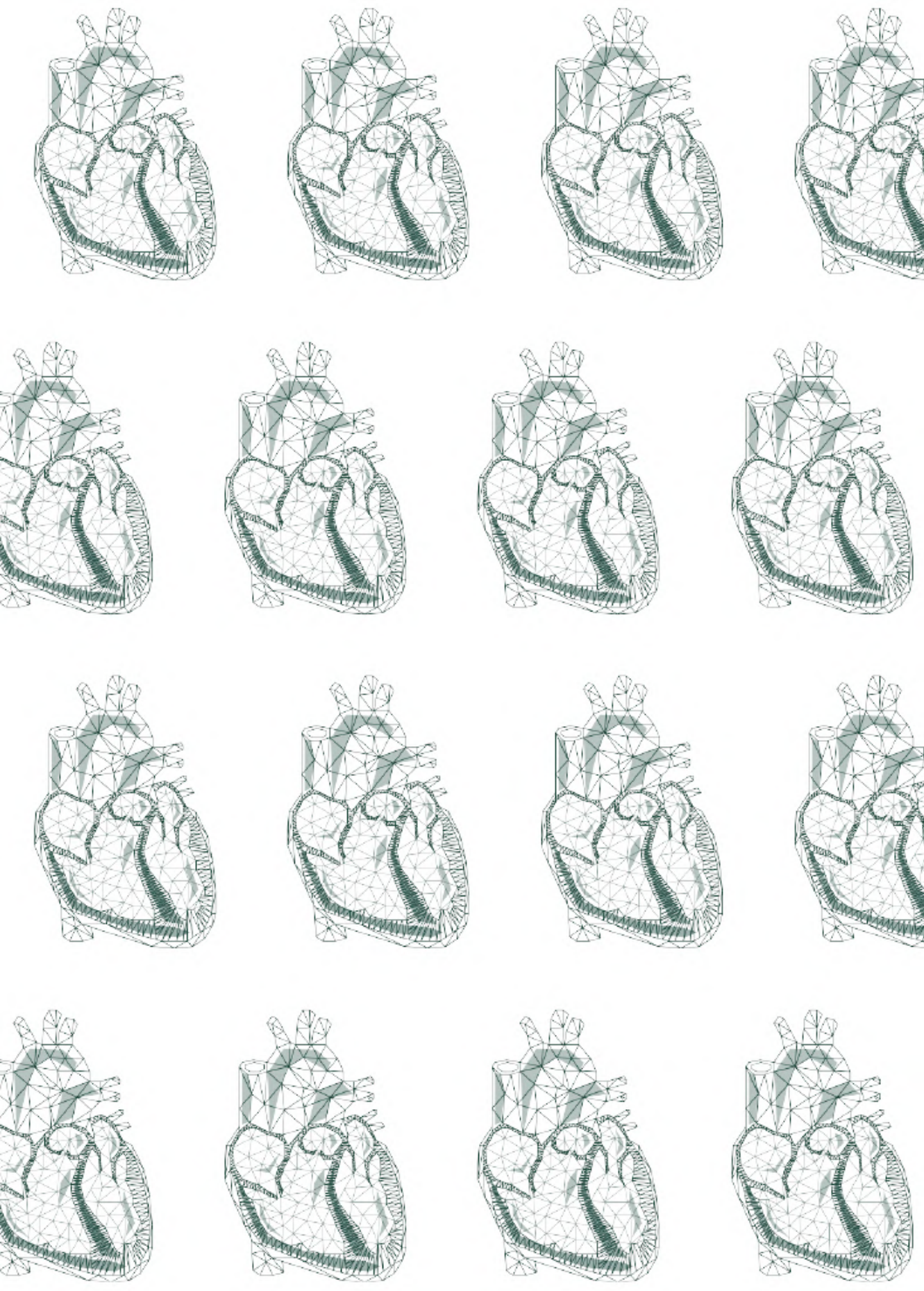

PART

PROTEIN QUALITY CONTROL AND MICROTUBLE SIGNATURE IN CARDIOMYOPATHIES

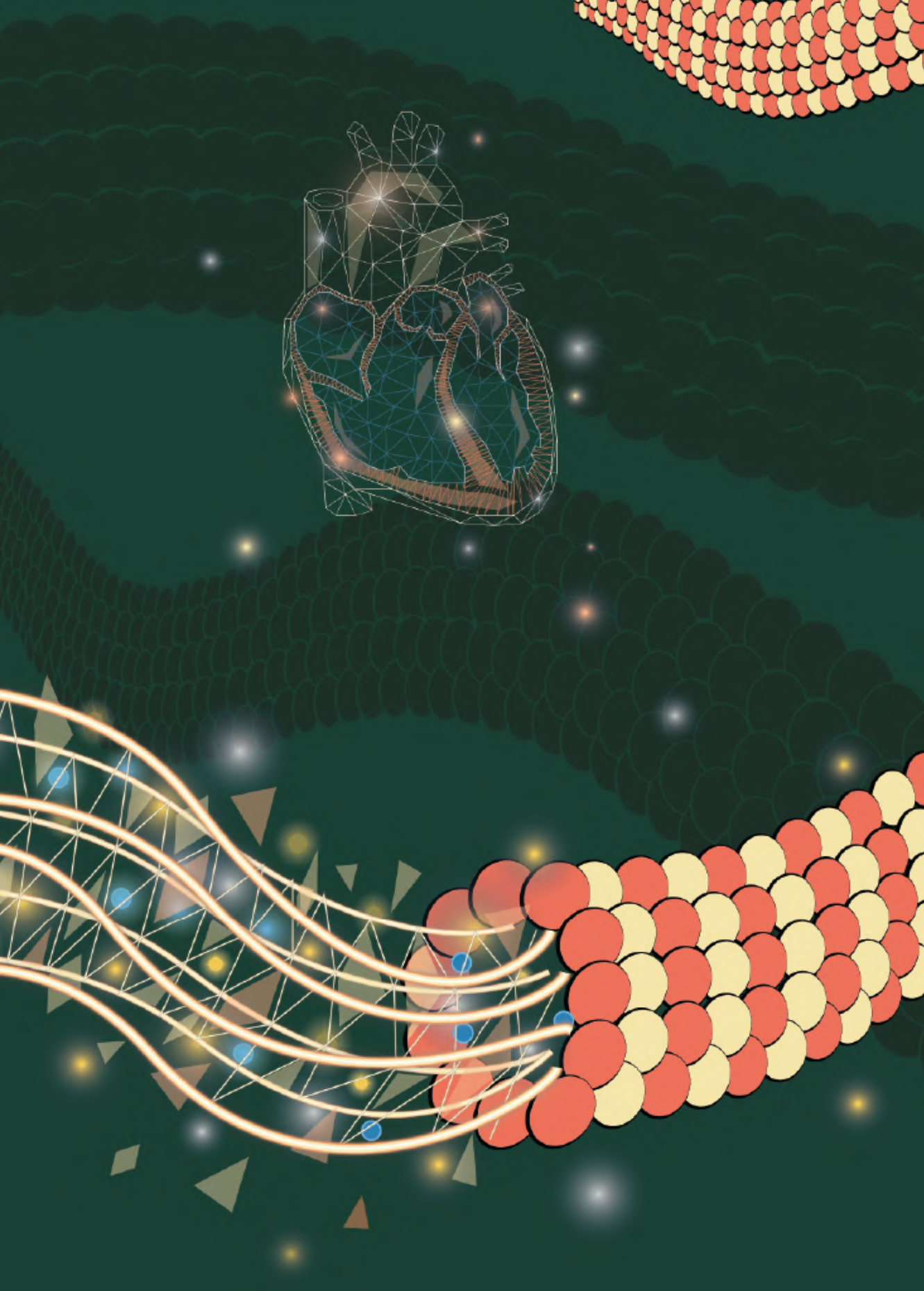

Chapter 3

Untying the knot: protein quality control in inherited cardiomyopathies

Larissa M. Dorsch[*], Maike Schuldt[*], Dora Knežević, Marit Wiersma, Diederik WD. Kuster, Jolanda van der Velden, Bianca JJM. Brundel

[*] *contributed equally*

Pflugers Arch - Eur J Physiol 471, 795–806 (2019).

ABSTRACT

Mutations in genes encoding sarcomeric proteins are the most important cause of inherited cardiomyopathies, which are a major cause of mortality and morbidity worldwide. Although genetic screening procedures for early disease detection have been improved significantly, treatment to prevent or delay mutation-induced cardiac disease onset is lacking. Recent findings indicate that loss of protein quality control (PQC) is a central factor in the disease pathology leading to derailment of cellular protein homeostasis. Loss of PQC includes impairment of heat shock proteins, the ubiquitin-proteasome system and autophagy. This may result in accumulation of misfolded and aggregation-prone mutant proteins, loss of sarcomeric and cytoskeletal proteins, and, ultimately, loss of cardiac function. PQC derailment can be a direct effect of the mutation-induced activation, a compensatory mechanism due to mutation-induced cellular dysfunction or a consequence of the simultaneous occurrence of the mutation and a secondary hit. In this review, we discuss recent mechanistic findings on the role of proteostasis derailment in inherited cardiomyopathies, with special focus on sarcomeric gene mutations and possible therapeutic applications.

CLASSIFICATION OF CARDIOMYOPATHIES

Cardiomyopathies (CM) constitute one of the most common causes of sudden cardiac death in young adults and represent major causes for cardiac transplantation.[1] Disease onset generally ranges between 20-50 years of age. CMs are defined by abnormal myocardial structure and function in the absence of any other diseases sufficient to cause these abnormalities.[2] These can be sub-classified based on their functional phenotype and their specific morphological changes. The most common types are hypertrophic CM (HCM), characterized by increased left ventricular (LV) wall thickness often occurring asymmetrically, and dilated CM (DCM), in which the presence of LV dilatation is accompanied by contractile dysfunction.[2] Besides HCM and DCM, there are less frequent forms such as restrictive CM (RCM) and desmin-related cardiomyopathy.[2] All these cardiomyopathies can be familial and are typically inherited in an autosomal dominant manner. Mutations in genes encoding sarcomeric proteins are the most common cause of these types of CMs.[3] However, the genotype-phenotype relationship is far from clear. The variations in age of CM onset and disease phenotype suggest that additional factors play a role in CM pathogenesis.

Accumulating evidence indicates the presence of derailed proteostasis in CMs as well as its contribution to CM onset and progression. This derailment could either be caused directly by the mutation or indirectly due to a compensatory mechanism. In the former case, the mutant protein might be instable or improperly folded leading to direct activation of the protein quality control (PQC). In the latter case, the mutation does not interfere with protein folding or stability but causes functional impairment which in turn leads to cellular stress and indirect activation of the PQC. Furthermore, the "secondary-hit" model may apply in CMs, in which a primary sarcomere mutation enhances vulnerability to secondary stressors which increases cellular burden resulting in PQC derailment. This review summarizes the current knowledge about perturbations in the different components of the PQC in CMs that are caused by mutations in sarcomeric proteins.

PROTEOSTASIS NETWORK ENSURES CARDIAC HEALTH

The heart has a very limited regenerative capacity and therefore requires surveillance by a system that maintains protein homeostasis to ensure cardiac health.[4] The PQC system sustains proteostasis by refolding misfolded proteins or removing them if refolding is impossible. It is composed of heat shock proteins (HSPs), the ubiquitin-proteasome system (UPS) and autophagy. PQC is only then functional when all three components are operative and interact with each other. This means that derailment of one of the parts might impair the function of the others in a direct or indirect manner. In a physiological state, protein folding and refolding is ensured by HSPs and their regulators. Terminally misfolded and aggregation-prone proteins are cleared by the two degradation systems, i.e. the UPS and autophagy, that work in collaboration with the HSPs (Figure 3.1). First, the different parts of the PQC in normal physiology are described, before addressing their role in CMs.

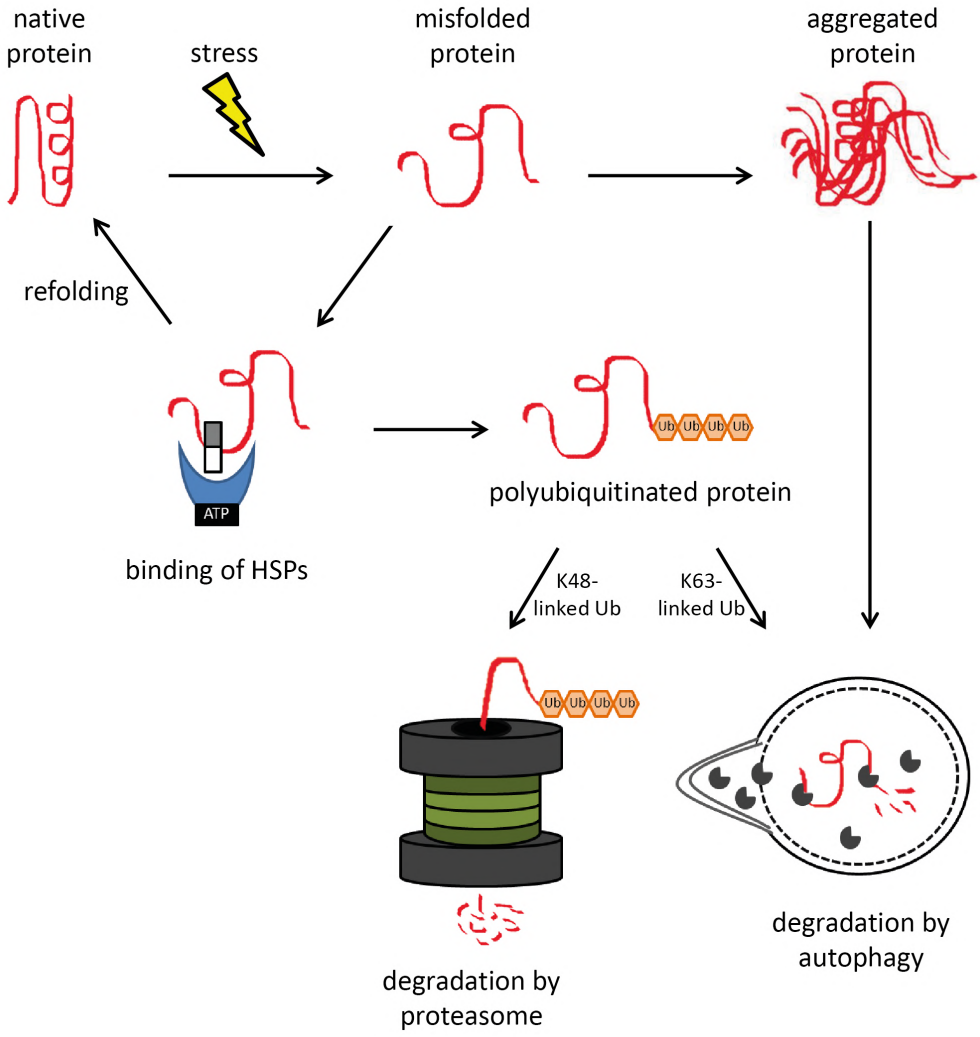

Figure 3.1: Collaboration of the protein quality control components.
Stress leads to misfolding of proteins which may result in abnormal interaction and subsequent aggregation. Small HSPs (white/grey rectangle) and HSPs with ATPase activity (blue moon shape with black rectangle) prevent aggregation formation by binding to the hydrophobic surfaces of misfolded protein. They either refold the misfolded protein to its native structure or initiate its polyubiquitination (Ub, orange hexagon). Misfolded proteins with polyubiquitin chains linked to lysine 48 (K48) are mainly degraded by the proteasome. Misfolded proteins carrying K63-linked polyubiquitin chains and aggregated proteins enter the autophagic pathway.

HEAT SHOCK PROTEINS

HSPs, originally identified as heat responsive proteins, are constitutively expressed in the cell to serve as molecular chaperones to ensure correct folding and assembly of proteins. HSPs are classified in two categories: the small HSPs with a low molecular weight (15-30 kDa) and the chaperones with a high molecular weight (>30 kDa).
One functional group of HSPs are chaperonin complexes, which are ATP-dependent chaperones with a barrel-like structure, that provide correct folding of nascent proteins after translation. Besides their folding function during protein translation, HSPs are also induced in response to cellular and environmental stressors to maintain a healthy cellular proteostasis by clearance of misfolded proteins.[5,6]
As reviewed by Garrido et al, small HSPs show an ATP-independent holdase activity. This means that they bind to misfolded proteins, keep them in a state competent for either refolding or degradation, and thereby prevent or attenuate their aggregation. Due to the association of small HSPs with the HSPs that have an ATP-dependent folding activity, the misfolded proteins can be refolded into their native and functional conformation.[7]
The binding affinity of HSPs to the misfolded protein is dependent on the chaperone cofactors bound to the HSPs. Furthermore, this binding of chaperone cofactors determines the processing of the misfolded protein for either refolding or degradation. Chaperone cofactors involved in degradation pathways can switch off the refolding activity of HSPs by inhibiting their ATPase activity and assist the HSPs and the UPS or autophagy in the breakdown of misfolded proteins (Figure 3.2).[8,9] The degradation of the thick filament protein myosin-binding protein-C (MyBP-C), for instance, is mediated via the chaperone cofactor HSC70 playing a major role in regulating MyBP-C protein turnover.[10] These degradation pathways are addressed in the following sections.

To maintain the structure and function of the highly dynamic cardiac sarcomeres, HSPs play an important role. The molecular chaperones GimC (Prefoldin), chaperonin TCP-1 Ring Complex (TRiC), αB-crystallin and HSP27 ensure correct folding and assembly of proteins, maturation of actin and prevent aggregate formation.[11-14] HSP27 is mostly found as high–molecular weight oligomers in the cytosol of unstressed cells.[15] Upon stress, HSP27 deoligomerizes and translocates to F-actin and thereby stabilizes the F-actin network.[16]
To assemble the myosin thick filament, the chaperones UNC-45, HSP90 and HSP70 are required, whereas the actin filament is self-assembled.[17-19] Several members of the small HSPs family are expressed in the heart and associate with cytoskeletal proteins.[20,21] These HSPBs stabilize cytoskeletal structures and improve coping with stress situations.[21-23]

UBIQUITIN-PROTEASOME SYSTEM

In case of terminally misfolded proteins, that failed be refolded, HSPs and their chaperone cofactors recruit enzymes to mediate polyubiquitination of the target substrate and thereby mark them for the appropriate degradation pathway. Short-lived proteins are typically degraded by the UPS, whereas autophagy is mainly used for degrading long-lived proteins and entire organelles.[24,25]
The polyubiquitination of the target substrate requires the sequential action of three enzymes. The ubiquitin-activating enzyme (E1) activates ubiquitin which is then

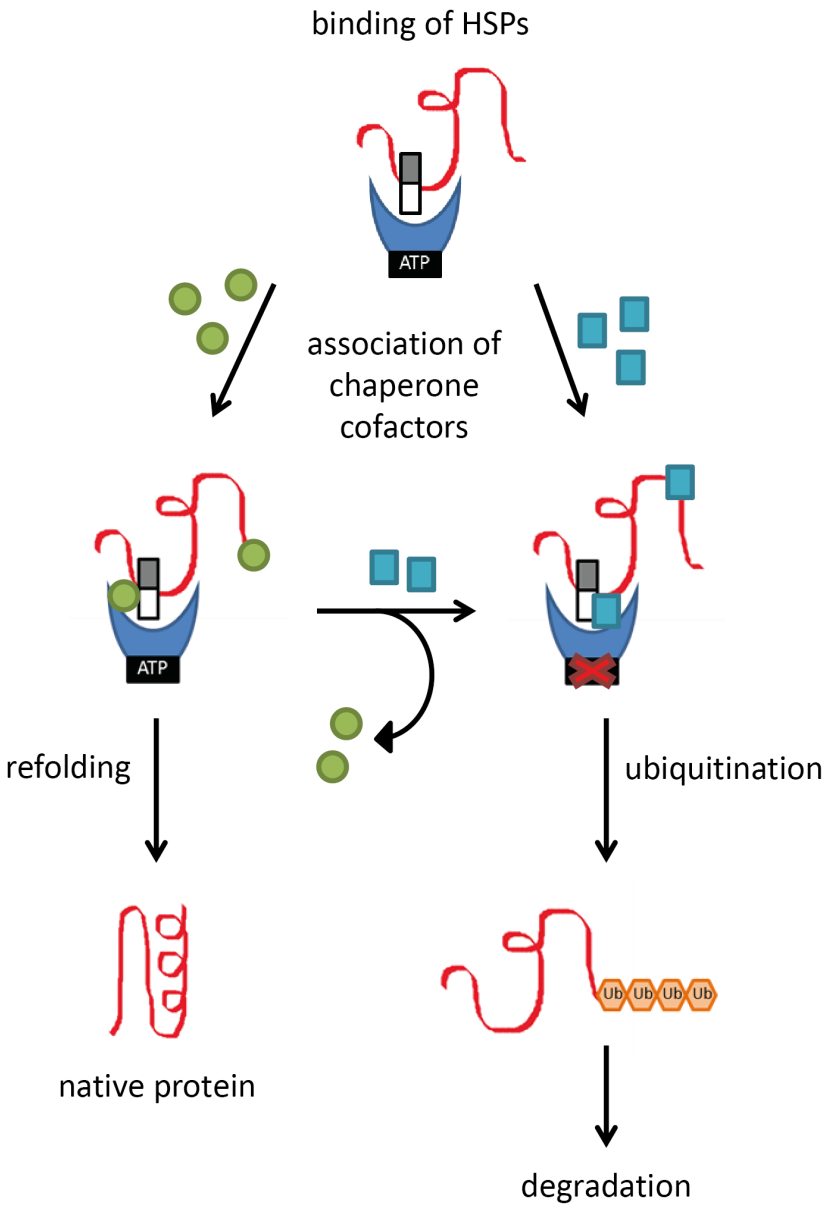

Figure 3.2: Chaperone cofactor binding determines the heat shock protein (HSP) function. Small HSPs (white/grey rectangle) and HSPs with ATPase activity (blue moon shape with black rectangle) bind to the misfolded protein to stabilize it. Dependent on the chaperone cofactors (green circles or turquoise squares), the misfolded protein gets either refolded or ubiquitinated for subsequent degradation. If refolding is impossible, the chaperone cofactors can be exchanged to promote degradation. In case of ubiquitination, the chaperone cofactors can switch off the HSP refolding activity by blocking the ATPase activity and, together with HSPs, assist in clearance of the misfolded protein via the degradation pathways.

transferred to a ubiquitin-conjugating enzyme (E2). In the last step, a ubiquitin ligase (E3) links ubiquitin from the E2 enzyme to a lysine residue of the target protein. There are only two E1 enzymes, several E2 enzymes and many E3 ligases, each of which recognizes one or several specific protein motifs. Therefore, the substrate specificity is achieved by the selectivity of the different E3 ligases.[26,27] Dependent on the combination of E2 enzyme and E3 ligase, polyubiquitin chains are linked to the preceding ubiquitin molecule either via lysine 48 (K48) or via lysine 63 (K63) which marks the protein for degradation. Therefore, the polyubiquitination process determines the degradation pathways: Proteins carrying K48-linked polyubiquitin chains are predominantly targeted to proteasomal degradation, and proteins carrying K63-linked polyubiquitin chains enter the autophagic pathways as discussed in the following paragraph.[28]

K48-linked polyubiquitinated proteins are transferred to the proteasome, which is almost exclusively the 26S proteasome in eukaryotic cells. This protein complex consist of one 20S core- and two 19S regulatory subunits forming a barrel-like structure. The regulatory subunits have ubiquitin-binding sites to recognize polyubiquitinated proteins and unfold them using their ATPase activity. The unfolded proteins are transferred to the catalytic core and proteolytically cleaved.[29] Sarcomeric proteins have an average turnover rate of 5-10 days.[30,31] Therefore, they rely on a proper functioning UPS to regulate their clearance. Once dissociated from the myofibrils, ubiquitin-conjugating enzymes mark the proteins for proteasomal degradation by adding K48-linked polyubiquitin chains.[31,32] In cardiomyocytes, this step is mediated by the MuRF family of E3 ligases.[33,34]

AUTOPHAGY

Autophagy cleans up aggregates or proteins via lysosomal breakdown that cannot be refolded by chaperones or processed by the UPS.[35] During macroautophagy, herein referred to as autophagy, membrane enclosed vesicles are formed containing the targeted cellular components. First, an isolation membrane is formed engulfing the cytoplasmic material. The membrane expands until the edges fuse to form the autophagosome.[36] Fusion of the autophagosome with a lysosome leads to an autolysosome which breaks down the cargo.[37] During selective autophagy, proteins carrying a K63-linked polyubiquitin chain are degraded. In the case the proteasome is overwhelmed with proteins carrying a K48-linked ubiquitin chain, such as aggregated proteins, they can also be cleared via autophagy. Their polyubiquitin chain docks to the adaptor protein p62/SQSTM1 which enables the translocation into the autophagosome.[38] Acidic lysosomal hydrolases degrade the captured material together with the inner membrane and the resulting macromolecules are recycled into ATP, amino acids and fatty acids.

Autophagy is found to be upregulated in response to starvation, growth factor withdrawal or high bioenergetic demands.[39-42] The ability to sequester and break down entire organelles, such as mitochondria, peroxisomes, endoplasmic reticulum and intact intracellular microorganisms, makes autophagy a unique and essential process in the cell. Especially in post-mitotic cells like cardiomyocytes, basal activation of autophagy is important to maintain a balanced proteostasis by degradation of long-lived proteins, lipid droplets and dysfunctional organelles.[24] Cardiomyocytes have a low basal autophagic activity under

normal conditions. Upon stress, the formation of protein aggregates is facilitated and triggers activation of autophagy.[43] Furthermore, cardiac autophagy is initiated in response to energy stress during periods of nutrient deprivation or high metabolic demand.[44]

PROTEOSTASIS DERAILMENT IN INHERITED CARDIOMYOPATHIES

The PQC is of great importance in many cardiac diseases caused by 'wear and tear', including cardiac amyloidosis, myocardial infarction and atrial fibrillation.[45-48] The activation of PQC in a variety of cardiac stress conditions can be considered as a positive compensatory response to maintain proteostasis. This might be especially true in the case of inherited CMs, where mutant protein expression is the disease-causing mechanism. Recent studies provide evidence for a causative role of the PQC in CM. On one hand, mutations in components of the PQC itself can cause CM. This has been described for the R120G mutation in *CRYAB* encoding for the chaperone αB-crystallin, causing desmin-related CM, and the P209L mutation in the chaperone cofactor BAG3, leading to juvenile DCM.[49,50] Mutations in PQC components as causes of inherited CM are rare, but PQC impairment can also occur as a result of CM-causing sarcomeric mutations. In this case, mutant sarcomeric proteins may impair the function of the PQC through overload of its components including HSPs, UPS and autophagy. This could lead to increased levels of mutant protein, exacerbating CM disease progression.
So far, the role of PQC has been investigated only in a limited number of studies on CM caused by sarcomeric gene mutations. *In vitro* information is available for HCM- and DCM-causing mutations in *ACTC1*. Furthermore, it has been studied *in vivo* with HCM-causing mutations in *MYBPC3*, *MYH7* and *MYOZ2*, DCM-causing *NEBL* mutations and RCM-causing *TNNI3* mutations (Table 3.1). In the following sections, the interaction between CM and derailments of the different parts of the PQC are described in detail.

Table 3.1: Overview of structural changes and adaptations in the protein quality control system related to cardiomyopathies.

Gene	Phenotype	Morphological abnormalities	Chaperones	UPS	Autophagy
ACTC1	HCM	not reported	+ (*in vitro*)[51]	not reported	not reported
	DCM	not reported	+ (*in vitro*)[51]	not reported	not reported
	RCM	not reported	not reported	not reported	not reported
ACTN2	HCM	cytoplasmic vacuolization, perinuclear halo, dysmorphic nuclei (human)[52]	not reported	not reported	not reported
	DCM	not reported	not reported	not reported	not reported
MYBPC3	HCM	large irregular vacuoles (infant)[53]	αB-crystallin ↑ (mice)[54]	↓ (mice)[55]	↑ (human)[56] ↓ (mice)[55]
	DCM	not reported	not reported	not reported	not reported
MYH6	HCM	not reported	not reported	not reported	not reported

Table 3.1: Continued

Gene	Phenotype	Morphological abnormalities	Chaperones	UPS	Autophagy
	DCM	not reported	not reported	not reported	not reported
MYH7	HCM	not reported	not reported	not reported	↑ (human)[56]
	DCM	not reported	not reported	not reported	not reported
	RCM	not reported	not reported	not reported	not reported
MYL2	HCM	not reported	not reported	not reported	not reported
MYL3	HCM	not reported	not reported	not reported	not reported
	RCM	ultrastructural defects (mice)[57]	not reported	not reported	not reported
MYOZ2	HCM	not reported	not reported	↑ (mice)[58]	not reported
NEBL	HCM	myocyte vacuolization (human)[59]	not reported	not reported	not reported
	DCM	enlarged and deformed mitochondria, lipid accumulation (mice)[60]	not reported	not reported	abnormal lysosomes (mice)[60]
TNNC1	HCM	not reported	not reported	not reported	not reported
	DCM	no evidence of vacuolization (human)[61]	not reported	not reported	not reported
	RCM	degeneration of myocardial fibres (human)[62]	not reported	not reported	not reported
TNNI3	HCM	not reported	not reported	not reported	not reported
	DCM	not reported	not reported	not reported	not reported
	RCM	irregularly shaped megamitochondria (human)[63]	not reported	↓proteasomal activity (mice)[64]	not reported
TNNT2	HCM	myocyte atrophy (mice)[65]	not reported	↓(mice)[66]	not reported
	DCM	not reported	not reported	not reported	not reported
	RCM	abnormal mitochondria (human)*[67]	not reported	not reported	not reported
TPM1	HCM	nuclear gigantism[68]	not reported	not reported	not reported
	DCM	accumulation of TPM1 (mice)[69]	not reported	not reported	not reported
	RCM	not reported	not reported	not reported	not reported

Mixed genotypes are indicated with *. A "+" indicates a positive finding, whereas a "-" indicates that it has been studied with a negative outcome.

DIVERSE ABNORMALITIES IN HEAT SHOCK PROTEIN FUNCTION

HSP impairment or activation contribute to disease pathology in CMs. Desmin-related CM displays HSP impairment and is either caused by mutant desmin itself or mutant chaperone αB-crystallin. In a normal state, αB-crystallin binds to desmin and thereby prevents its aggregation.[13] Mutant desmin, however, impairs the interaction with αB-crystallin leading to desmin accumulation and cardiomyocyte dysfunction.[70] This suggests aberrant protein aggregation can cause CM. Correspondingly, the R120G mutation in *CRYAB* results in desmin-related-CM as well and also presents with aggregates containing desmin and mutant αB-crystallin.[49] Sanbe et al. showed that upregulation of HSPB8 due to geranylgeranylacetone treatment reduces the amount of mutant αB-crystallin-containing aggregates.[71] This implies that other HSPs can compensate for the loss of function to remove aggregates. Furthermore, *in vitro* experiments have shown that HCM- or DCM-causing mutations in *ACTC1*, encoding cardiac actin, can interfere with its folding by the TRiC chaperonin complex resulting in inefficient incorporation of actin into the myofilament and its subsequent aggregation.[51] Mutations in one specific subdomain of actin affect protein stability or polymerization, making actin more prone for degradation. Whereas mutations in other subdomains of actin cause alterations in protein-protein interactions.[72] A gene co-expression analysis of human controls and HCM samples identified the TRiC chaperonin complex as the most differential pathway thereby further highlighting its importance in HCM.[73]

By contrast, various studies on the role of PQC in CMs report on increased levels of HSPs due to PQC activation. However, it still remains unresolved whether the increased levels of HSPs are a direct effect of the mutant protein or a compensatory secondary effect due to increased cellular stress. Therefore, the direct interaction of mutant protein and HSPs needs to be studied. In mice with a truncating *MYBPC3* mutation and an HCM phenotype, increased levels of αB-crystallin have been found.[54] In other CM mouse models, independent of a sarcomeric mutation, increased levels of HSP70 have been observed.[74] A study in patients with chronic heart failure due to DCM revealed a correlation of serum HSP60 levels with disease severity.[75] Since increased levels of HSP27 and HSP70 are associated with a protective effect in models for atrial fibrillation, by maintaining cardiomyocyte function, one can speculate that increased expression of these HSPs might be part of a compensatory protective mechanism in CM.[74,76]
In general, research findings indicate that HSP impairment is detrimental for cardiomyocyte function due to a higher risk of impaired protein folding and aggregate formation. By contrast, HSP activation in CM is considered as a beneficial effect and is most likely a compensatory mechanism of the cell.

DERAILMENT OF THE UBIQUITIN-PROTEASOME SYSTEM

Derailed UPS function in CM affects the degradation of terminally misfolded proteins. *MYBPC3* mutations often lead to expression of truncated protein, which is not incorporated into the sarcomere because the most C-terminal domain needed for incorporation is missing.[77] Truncated MyBP-C has not been detected in cardiac samples of HCM patients.[78] In addition, very low levels ($<4\%$) of truncated MyBP-C, which were not

incorporated into the sarcomeres, were found in engineered heart tissue made of *MYBPC3* knock-out mouse cardiomyocytes transfected with a truncating *MYBPC3* mutation.[79] Therefore, it is likely that either the mutant mRNA is degraded via nonsense-mediated mRNA decay and/or the truncated MyBP-C forms a substrate for immediate degradation by the UPS or autophagy. Since MyBP-C is highly expressed in cardiomyocytes, high levels of truncated protein may lead to an increased UPS burden and competitive inhibition of the proteasome.[55,80] In this case, the UPS is overwhelmed by the amount of truncated protein that needs to be degraded. In line with this hypothesis are analyses of myectomy samples from HCM patients with sarcomeric mutations which show a decrease in proteolytic activity (Table 3.1).[55,81] Decreased processing through the UPS system is also indicated by the increase in overall levels of protein ubiquitination in HCM patients and animal models which is already detectable at an early postnatal phase prior to any other symptom development.[55,66,81,82] Consistent with the studies in *MYBPC3*-mutant samples, UPS perturbations have also been found in mouse heart tissue with *TNNT2* mutations.[66] Patient samples with a sarcomeric mutation showed higher levels of polyubiquitination and decreased proteolytic activity compared to healthy controls.[81]

In addition to overload of the UPS by mutant protein, increased oxidative stress can also impair the function of the proteasome. In this case, the proteasomal dysfunction would not be a direct effect of the mutant protein but a consequence of secondary cellular changes. In CM samples, an increase in oxidation of cytosolic protein content as well as the 19S proteasome, thereby decreasing the overall proteolytic function of the 26S proteasome subunit, has been identified.[66,81,83] In addition to the proteasome itself, the expression of ubiquitin ligases can be altered. In an HCM mouse model with mutant *Mybpc3*, the muscle specific E3 ligase Asb2β showed decreased mRNA levels compared to wild-type mice.[84] Since one of its targets is desmin, accumulation of desmin could contribute to the HCM phenotype, as observed for desmin-related CMs. A large HCM patient cohort and matched healthy controls were screened for genetic variants in all three members of the MuRF family, since mutations in the gene encoding MuRF1 were reported to cause HCM.[85] In this study, a higher prevalence of rare variants of the cardiac-specific E3 ligases MuRF1 and MuRF2 was found in HCM patients.[86] These were associated with earlier disease onset and higher penetrance implying that disturbances of the UPS might act as a disease modifier contributing to HCM.

In contrast to HCM, in DCM the reported UPS derailments could not yet be linked to sarcomeric mutations. A likely reason for this is that the DCM patient samples did not carry a sarcomeric mutation and/or the underlying disease cause was not known. Tissue analysis from explanted DCM hearts revealed increased expression of both E1 and/or E2 enzymes.[87,88] Further evidence of increased ubiquitin-conjugating enzyme activity was detected in end-stage DCM. Here, increased levels of MuRF1 and MAFbx were associated with increased UPS degradation activity, which might be the cause of ventricle wall thinning as observed in end-stage DCM patients.[89] In line with the increased ubiquitin-conjugating enzyme levels, increased levels of polyubiquitinated proteins have been detected in DCM samples.[87,88,90,91] This finding is further supported by a 2.3-fold reduced expression of the deubiquitinating enzyme isopeptidase-T in DCM patients.[88] Furthermore, increased

proteolytic activity of the 26S proteasome as well as the 20S subunit peptidase activity have been found.[89-91] In contrast to HSPs, the answer to the question whether UPS activation or inhibition would be beneficial in HCM and DCM, is not as straight forward. In an HCM phenotype, proteasome activation might improve the hypertrophic phenotype due to increased mutant protein degradation. However, in DCM, increased proteasome function might augment wall thinning and therefore DCM might benefit from proteasome inhibition.

UNRESOLVED ROLE OF THE AUTOPHAGIC RESPONSE IN CARDIOMYOPATHIES

Autophagy is a crucial mechanism in CMs that only fulfills its cytoprotective mechanisms when it is in balance.[42] Moderate activation of autophagy has beneficial effects in CM patients by removing aggregates and supplying the cell with energy.
However, protein degradation due to excessive autophagy has been associated with different types of CM, including HCM, DCM, ischemic CM and chemotherapy-induced CM.[92-97] This could lead to loss of myofibrils, as observed in end-stage HCM and DCM patients.[98,99] In a recent study, the expression of vacuolar protein sorting 34 (Vps34), an important autophagy regulator, was shown to be decreased in the myocardium of HCM patients and deletion of Vsp34 resulted in an HCM-like phenotype in mice. Furthermore, decreased expression of Vsp34 impaired the HSP-autophagy axis, as indicated by αB-crystallin-positive aggregates.[97] HCM patients with mutations in *MYBPC3* or *MYH7* revealed an upregulation of autophagic vacuoles and markers, indicating increased autophagic activity.[56] In a homozygous *Mybpc3*-mutant HCM mouse model, levels of autophagy markers were increased on protein level implying autophagic activation. However, mRNA levels of these markers were not increased. This rather suggests an accumulation of autophagic proteins due to defective autophagic-lysosomal degradation instead of activation on transcriptional level.[55] In explanted hearts from DCM patients, the imbalance of high uibiquitination rate and insufficient degradation may contribute to autophagic cell death.[88] Vacuolization in CMs has been reported with mutations in *ACTN2*, *MYBPC3* and *NEBL*.[52,53,59] This observation suggests that the accumulation of autophagic vacuoles implies cardiomyocyte stress. However, the interpretation of vacuole accumulation remains unclear since it could reflect an increase in autophagic activity or an impairment of autophagosome-lysome fusion. For a correct interpretation of the role of autophagy in CM, autophagic flux in combination with gene and protein expression data have to be studied in the future.

ENVIRONMENTAL STRESSORS INFLUENCING THE PROTEOSTASIS NETWORK

Besides the upper mentioned effects of the sarcomeric gene mutations on the PQC, other environmental stressors, including physiological stress, genetic and epigenetic pathways and inflammation, can also impair its function.[100,101] In CM patients with a sarcomeric mutation, these stressors can act as second hit and thereby determine disease severity. Since most of CM patients become symptomatic only in a later stage of their life, the influence of drugs directed at the PQC system as treatment modality for co-morbidities and the age-related decline of the PQC are discussed below.

Several anti-cancer agents block the PQC to cause a lethal proteotoxicity in cancer cells. Anthracyclines, for example, directly impair its function by enhancing proteasomal degradation due to increased expression of E3 ligases and increased proteasome activity as well as inhibition of autophagy in cardiomyocytes.[102-105] Furthermore, they disturb Ca^{2+} homeostasis, leading to endoplasmic reticulum stress, which derails protein folding.[102] In CM patients, dealing already with a sarcomeric mutation, treatment of another non-cardiac disease can trigger the onset of CM or worsen the clinical outcome. Cardiotoxic side effects of anthracyclines can lead to anthracycline-associated cardiomyopathy (AACM) which presents as LV dysfunction and DCM in adults and RCM in children.[106,107] Even a low dose treatment caused anti-cancer agents-induced CM in cancer patients without a history of cardiac disease. Genetic screening of these patients revealed truncating titin variants which are known as a genetic cause of DCM. These variants may increase the susceptibility for anti-cancer agents-induced CM.[108] In general, patients having a genetic predisposition for DCM are more prone to develop AACM after anthracycline treatment.[109,110] It can be speculated that the impairment of the PQC due to the anti-cancer treatment is an additional burden to the cardiomyocyte. The clinical cardiac phenotype is caused by insufficient clearance of the mutant protein via UPS and/or autophagy. Therefore, these findings suggest that PQC impairment by anthracyclines can act as catalysts in the development of CM in patients with underlying sarcomeric gene mutation.

Ageing represents another cellular stressor leading to toxic mutation effects because of the late disease onset and development of symptoms in inherited CMs. Clinical characteristics, such as wall thickness and diastolic function, worsen with increasing age.[111] This could be related to an age-associated decline in proteostatic function, which is supported by the presence of damaged macromolecules and mitochondria in aged cardiomyocytes.[112] Dysfunctional mitochondria generate high levels of reactive oxygen species, which promote proteotoxic stress and accelerate detrimental effects on the cardiomyocyte.[113] Also, the activity of the 26S proteasome is decreased during ageing which is possibly caused by oxidation of its components.[66,83,114,115] The age-dependent decline in proteasome function increases the burden for the autophagic pathway. However, not only the proteasome, but also the autophagy-lysosomal system declines during ageing.[116] As an example, mTOR, a negative regulator of autophagy, was upregulated during ageing in a mouse study which indicates decreased autophagic activity.[117] As a result, the activity of the autophagic response might not be sufficient. However, similar to findings related to the UPS, autophagy was enhanced during ageing in some animal models, suggesting an increased need for autophagy in aged cells.[118] Further research is warranted to investigate whether the age-related decline of the PQC is causative for CM onset and/or progression.

FUTURE THERAPEUTIC IMPLICATIONS

To improve the clinical outcome of CM patients, modulation of PQC components might serve as a novel therapeutic strategy. Figure 3.3 summarizes the three different ways and illustrates how a sarcomeric gene mutation can lead to PQC derailment. In case of a direct mutation effect on the PQC as well as in combination with secondary hits, targeting of the PQC would be most beneficial and the most direct way to prevent cardiomyocyte

dysfunction. In case where the PQC derailment is a consequence of mutation-induced cellular disturbances, it is important to also target the cellular dysfunction to prevent further worsening of the PQC.

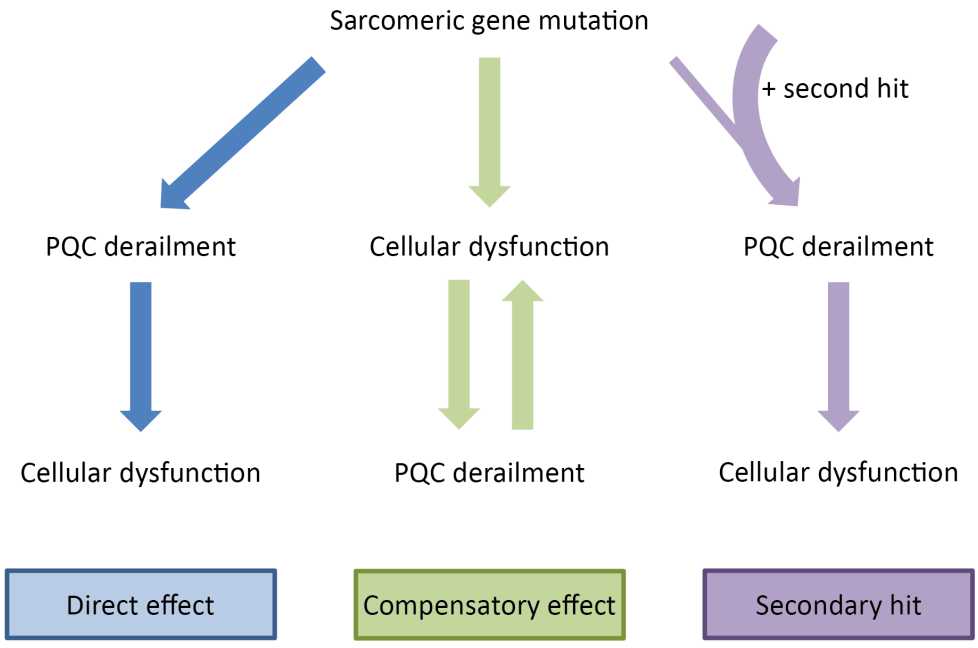

Figure 3.3: Effects of sarcomeric gene mutations on the protein quality control (PQC) system. Sarcomeric gene mutations can directly derail PQC function leading to cardiomyocyte dysfunction. PQC derailments in cardiomyopathies (CMs) can also be a compensatory mechanism to counteract cardiomyocyte dysfunction caused by the sarcomeric gene mutation. The secondary hit hypothesis suggests that the PQC of cardiomyocytes carrying a sarcomeric gene mutation is more prone to derail in response to additional cellular stressors, thereby resulting in cardiomyocyte dysfunction.

As extensively discussed in this review, PQC alterations in CMs are disease- and mutation-specific leading to either increased or reduced function in one or several of its components. Therefore, personalized treatment strategies are required to restore a balanced proteostasis. Potentially, all three PQC components can be therapeutically targeted with the appropriate compounds.

HSP expression can be induced by the drug geranylgeranylacetone. In animal models of desmin-related CM, the induction of HSP expression by geranylgeranylacetone resulted in a beneficial effect on heart function because desmin-aggregate formation was reduced.[71] This example suggests that activation of HSPs might also be beneficial in other types of inherited CMs since HSPs play a crucial role in coping with the mutant protein.

The derailment of the UPS is context dependent: proteasomal function is decreased in HCM, RCM and desmin-related CM and increased in DCM.[89] Decreased proteasomal function suggest that the misfolded proteins hamper the UPS by overwhelming it due to permanent degradation of misfolded proteins. As a consequence, the activity of the UPS is throttled. Therefore, UPS activation might be a beneficial therapeutic strategy in HCM and desmin-related CM.[89] In line with this, in HCM patients with a *TNNT2* mutation increased proteasomal activity was correlated with a better clinical outcome.[66] In contrast, over-activation of the UPS indicates a direct response of the UPS to the misfolded proteins to ensure optimal clearance. However, excessive activation of the UPS transforms the initially beneficial effects into a detrimental maladaptation that possibly contribute to loss of myofibrils.[89] Nevertheless, complete proteasome inhibition itself triggered cardiac dysfunction and a CM-like phenotype in healthy pigs.[119] Therefore, it is important to achieve a moderate UPS response in DCM to prevent the detrimental effects of complete proteasome inhibition.

The altered autophagic flux in CMs can be caused on the one hand directly by the misfolded protein itself or on the other hand indirectly by compensating for the impaired functionality of the UPS. To optimize the degradation response, the autophagic activity needs to be pharmacologically titrated into its proteostasis promoting range.[120]

CONCLUSION

The PQC is crucial for cardiac health and requires the collaboration of all its components to be functional. Key modulators of the PQC are disease- and mutation-specifically altered and derailed in CM. Pharmacological targeting of PQC components represents a novel therapeutic strategy to treat CMs. Since most of the described findings are retrieved from single CM patients or experimental animal models, systematic studies in larger CM patient populations are warranted to untie the knot of disease- and mutation-specific derailments of the PQC.

Conflict of Interest: The authors declare that they have no conflict of interest.

Source of Funding: We acknowledge support from the Netherlands Cardiovascular Research Initiative - an initiative with support of the Dutch Heart Foundation, CVON: The Netherlands CardioVascular Research Committee, CVON2014-40 DOSIS. Furthermore, this research has been supported by LSH-TKI (40-43100-98-008), the Dutch Heart Foundation (2013T096, 2013T144) and the Netherlands Organisation for Scientific Research (NWO), as part of their joint strategic research programme: 'Earlier recognition of cardiovascular diseases' (AFFIP: 14728). Van der Velden is supported by a VICI grant from the Netherlands Organization for Scientific Research (NWO-ZonMW; 91818602).

REFERENCES

1. Semsarian C, Ingles J, Wilde AA. Sudden cardiac death in the young: the molecular autopsy and a practical approach to surviving relatives. *Eur Heart J*. 2015;36(21):1290-6.
2. Elliott P, Andersson B, Arbustini E, Bilinska Z, Cecchi F, Charron P, et al. Classification of the cardiomyopathies: a position statement from the European Society Of Cardiology Working Group on Myocardial and Pericardial Diseases. *Eur Heart J*. 2008;29(2):270-6.
3. Arbustini E, Narula N, Dec GW, Reddy KS, Greenberg B, Kushwaha S, et al. The MOGE(S) classification for a phenotype-genotype nomenclature of cardiomyopathy: endorsed by the World Heart Federation. *J Am Coll Cardiol*. 2013;62(22):2046-72.
4. Wang X, Su H, Ranek MJ. Protein quality control and degradation in cardiomyocytes. *J Mol Cell Cardiol*. 2008;45(1):11-27.
5. Morimoto RI. Proteotoxic stress and inducible chaperone networks in neurodegenerative disease and aging. *Genes Dev*. 2008;22(11):1427-38.
6. Willis MS, Patterson C. Hold me tight: Role of the heat shock protein family of chaperones in cardiac disease. *Circulation*. 2010;122(17):1740-51.
7. Garrido C, Paul C, Seigneuric R, Kampinga HH. The small heat shock proteins family: the long forgotten chaperones. *Int J Biochem Cell Biol*. 2012;44(10):1588-92.
8. Esser C, Alberti S, Hohfeld J. Cooperation of molecular chaperones with the ubiquitin/proteasome system. *Biochim Biophys Acta*. 2004;1695(1-3):171-88.
9. Bozaykut P, Ozer NK, Karademir B. Regulation of protein turnover by heat shock proteins. *Free Radic Biol Med*. 2014;77:195-209.
10. Glazier AA, Hafeez N, Mellacheruvu D, Basrur V, Nesvizhskii AI, Lee LM, et al. HSC70 is a chaperone for wild-type and mutant cardiac myosin binding protein C. *JCI Insight*. 2018;3(11).
11. Hansen WJ, Cowan NJ, Welch WJ. Prefoldin-nascent chain complexes in the folding of cytoskeletal proteins. *J Cell Biol*. 1999;145(2):265-77.
12. Grantham J, Ruddock LW, Roobol A, Carden MJ. Eukaryotic chaperonin containing T-complex polypeptide 1 interacts with filamentous actin and reduces the initial rate of actin polymerization in vitro. *Cell Stress Chaperones*. 2002;7(3):235-42.
13. Bennardini F, Wrzosek A, Chiesi M. Alpha B-crystallin in cardiac tissue. Association with actin and desmin filaments. *Circ Res*. 1992;71(2):288-94.
14. Brown DD, Christine KS, Showell C, Conlon FL. Small heat shock protein Hsp27 is required for proper heart tube formation. *Genesis*. 2007;45(11):667-78.
15. Ehrnsperger M, Lilie H, Gaestel M, Buchner J. The dynamics of Hsp25 quaternary structure. Structure and function of different oligomeric species. *J Biol Chem*. 1999;274(21):14867-74.
16. Bryantsev AL, Loktionova SA, Ilyinskaya OP, Tararak EM, Kampinga HH, Kabakov AE. Distribution, phosphorylation, and activities of Hsp25 in heat-stressed H9c2 myoblasts: a functional link to cytoprotection. *Cell Stress Chaperones*. 2002;7(2):146-55.
17. Barral JM, Hutagalung AH, Brinker A, Hartl FU, Epstein HF. Role of the myosin assembly protein UNC-45 as a molecular chaperone for myosin. *Science*. 2002;295(5555):669-71.
18. Srikakulam R, Winkelmann DA. Chaperone-mediated folding and assembly of myosin in striated muscle. *J Cell Sci*. 2004;117(Pt 4):641-52.
19. Barral JM, Epstein HF. Protein machines and self assembly in muscle organization. *Bioessays*. 1999;21(10):813-23.
20. Vos MJ, Kanon B, Kampinga HH. HSPB7 is a SC35 speckle resident small heat shock protein. *Biochim Biophys Acta*. 2009;1793(8):1343-53.
21. Golenhofen N, Perng MD, Quinlan RA, Drenckhahn D. Comparison of the small heat shock proteins alphaB-crystallin, MKBP, HSP25, HSP20, and cvHSP in heart and skeletal muscle. *Histochem Cell Biol*. 2004;122(5):415-25.
22. Landry J, Huot J. Modulation of actin dynamics during stress and physiological stimulation by a signaling pathway involving p38 MAP kinase and heat-shock protein 27. *Biochem Cell Biol*. 1995;73(9-10):703-7.
23. Lavoie JN, Lambert H, Hickey E, Weber LA, Landry J. Modulation of cellular thermoresistance and actin filament stability accompanies phosphorylation-induced changes in the oligomeric structure of heat shock protein 27. *Mol Cell Biol*. 1995;15(1):505-16.
24. Cecconi F, Levine B. The role of autophagy in mammalian development: cell makeover rather than cell death. *Dev Cell*. 2008;15(3):344-57.
25. Hershko A, Ciechanover A. The ubiquitin system. *Annu Rev Biochem*. 1998;67:425-79.
26. Finley D. Recognition and processing of ubiquitin-protein conjugates by the proteasome. *Annu Rev Biochem*. 2009;78:477-513.
27. Ravid T, Hochstrasser M. Diversity of degradation signals in the ubiquitin-proteasome system. *Nat Rev Mol Cell Biol*. 2008;9(9):679-90.
28. Amm I, Sommer T, Wolf DH. Protein quality control and elimination of protein waste: the role of the ubiquitin-proteasome system. *Biochim Biophys Acta*. 2014;1843(1):182-96.
29. Wang J, Maldonado MA. The ubiquitin-proteasome system and its role in inflammatory and autoimmune diseases. *Cell Mol Immunol*. 2006;3(4):255-61.

30. Boateng SY, Goldspink PH. Assembly and maintenance of the sarcomere night and day. *Cardiovasc Res*. 2008;77(4):667-75.
31. Willis MS, Schisler JC, Portbury AL, Patterson C. Build it up-Tear it down: protein quality control in the cardiac sarcomere. *Cardiovasc Res*. 2009;81(3):439-48.
32. Solomon V, Goldberg AL. Importance of the ATP-ubiquitin-proteasome pathway in the degradation of soluble and myofibrillar proteins in rabbit muscle extracts. *J Biol Chem*. 1996;271(43):26690-7.
33. McElhinny AS, Perry CN, Witt CC, Labeit S, Gregorio CC. Muscle-specific RING finger-2 (MURF-2) is important for microtubule, intermediate filament and sarcomeric M-line maintenance in striated muscle development. *J Cell Sci*. 2004;117(Pt 15):3175-88.
34. Spencer JA, Eliazer S, Ilaria RL, Jr., Richardson JA, Olson EN. Regulation of microtubule dynamics and myogenic differentiation by MURF, a striated muscle RING-finger protein. *J Cell Biol*. 2000;150(4):771-84.
35. Klionsky DJ. Autophagy: from phenomenology to molecular understanding in less than a decade. *Nat Rev Mol Cell Biol*. 2007;8(11):931-7.
36. Yorimitsu T, Klionsky DJ. Autophagy: molecular machinery for self-eating. *Cell Death Differ*. 2005;12 Suppl 2:1542-52.
37. Baba M, Takeshige K, Baba N, Ohsumi Y. Ultrastructural analysis of the autophagic process in yeast: detection of autophagosomes and their characterization. *J Cell Biol*. 1994;124(6):903-13.
38. Kirkin V, McEwan DG, Novak I, Dikic I. A role for ubiquitin in selective autophagy. *Mol Cell*. 2009;34(3):259-69.
39. Scott RC, Schuldiner O, Neufeld TP. Role and regulation of starvation-induced autophagy in the Drosophila fat body. *Dev Cell*. 2004;7(2):167-78.
40. Lum JJ, Bauer DE, Kong M, Harris MH, Li C, Lindsten T, et al. Growth factor regulation of autophagy and cell survival in the absence of apoptosis. *Cell*. 2005;120(2):237-48.
41. Mizushima N, Yamamoto A, Matsui M, Yoshimori T, Ohsumi Y. In vivo analysis of autophagy in response to nutrient starvation using transgenic mice expressing a fluorescent autophagosome marker. *Mol Biol Cell*. 2004;15(3):1101-11.
42. Levine B, Kroemer G. Autophagy in the pathogenesis of disease. *Cell*. 2008;132(1):27-42.
43. Tannous P, Zhu H, Nemchenko A, Berry JM, Johnstone JL, Shelton JM, et al. Intracellular protein aggregation is a proximal trigger of cardiomyocyte autophagy. *Circulation*. 2008;117(24):3070-8.
44. Gustafsson AB, Gottlieb RA. Recycle or die: the role of autophagy in cardioprotection. *J Mol Cell Cardiol*. 2008;44(4):654-61.
45. Patterson C, Ike C, Willis PWt, Stouffer GA, Willis MS. The bitter end: the ubiquitin-proteasome system and cardiac dysfunction. *Circulation*. 2007;115(11):1456-63.
46. Meijering RA, Zhang D, Hoogstra-Berends F, Henning RH, Brundel BJ. Loss of proteostatic control as a substrate for atrial fibrillation: a novel target for upstream therapy by heat shock proteins. *Front Physiol*. 2012;3:36.
47. Yan L, Vatner DE, Kim SJ, Ge H, Masurekar M, Massover WH, et al. Autophagy in chronically ischemic myocardium. *Proc Natl Acad Sci U S A*. 2005;102(39):13807-12.
48. Henning RH, Brundel B. Proteostasis in cardiac health and disease. *Nat Rev Cardiol*. 2017;14(11):637-53.
49. Wang X, Osinska H, Klevitsky R, Gerdes AM, Nieman M, Lorenz J, et al. Expression of R120G-alphaB-crystallin causes aberrant desmin and alphaB-crystallin aggregation and cardiomyopathy in mice. *Circ Res*. 2001;89(1):84-91.
50. Selcen D, Muntoni F, Burton BK, Pegoraro E, Sewry C, Bite AV, et al. Mutation in BAG3 causes severe dominant childhood muscular dystrophy. *Ann Neurol*. 2009;65(1):83-9.
51. Vang S, Corydon TJ, Borglum AD, Scott MD, Frydman J, Mogensen J, et al. Actin mutations in hypertrophic and dilated cardiomyopathy cause inefficient protein folding and perturbed filament formation. *FEBS J*. 2005;272(8):2037-49.
52. Girolami F, Iascone M, Tomberli B, Bardi S, Benelli M, Marseglia G, et al. Novel alpha-actinin 2 variant associated with familial hypertrophic cardiomyopathy and juvenile atrial arrhythmias: a massively parallel sequencing study. *Circ Cardiovasc Genet*. 2014;7(6):741-50.
53. Wessels MW, Herkert JC, Frohn-Mulder IM, Dalinghaus M, van den Wijngaard A, de Krijger RR, et al. Compound heterozygous or homozygous truncating MYBPC3 mutations cause lethal cardiomyopathy with features of noncompaction and septal defects. *Eur J Hum Genet*. 2015;23(7):922-8.
54. Yang Q, Osinska H, Klevitsky R, Robbins J. Phenotypic deficits in mice expressing a myosin binding protein C lacking the titin and myosin binding domains. *J Mol Cell Cardiol*. 2001;33(9):1649-58.
55. Schlossarek S, Englmann DR, Sultan KR, Sauer M, Eschenhagen T, Carrier L. Defective proteolytic systems in Mybpc3-targeted mice with cardiac hypertrophy. *Basic Res Cardiol*. 2012;107(1):235.
56. Song L, Su M, Wang S, Zou Y, Wang X, Wang Y, et al. MiR-451 is decreased in hypertrophic cardiomyopathy and regulates autophagy by targeting TSC1. *J Cell Mol Med*. 2014;18(11):2266-74.
57. Yuan CC, Kazmierczak K, Liang J, Kanashiro-Takeuchi R, Irving TC, Gomes AV, et al. Hypercontractile mutant of ventricular myosin essential light chain leads to disruption of sarcomeric structure and function and results in restrictive cardiomyopathy in mice. *Cardiovasc Res*. 2017;113(10):1124-36.
58. Ivandic BT, Mastitsky SE, Schonsiegel F, Bekeredjian R, Eils R, Frey N, et al. Whole-genome analysis of gene expression associates the ubiquitin-proteasome system with the cardiomyopathy phenotype in disease-sensitized congenic mouse strains. *Cardiovasc Res*. 2012;94(1):87-95.
59. Perrot A, Tomasov P, Villard E, Faludi R, Melacini P, Lossie J, et al. Mutations in NEBL encoding the cardiac Z-disk protein nebulette are associated with various cardiomyopathies. *Arch Med Sci*. 2016;12(2):263-78.

60. Purevjav E, Varela J, Morgado M, Kearney DL, Li H, Taylor MD, et al. Nebulette mutations are associated with dilated cardiomyopathy and endocardial fibroelastosis. *J Am Coll Cardiol*. 2010;56(18):1493-502.
61. Kaski JP, Burch M, Elliott PM. Mutations in the cardiac Troponin C gene are a cause of idiopathic dilated cardiomyopathy in childhood. *Cardiol Young*. 2007;17(6):675-7.
62. Ploski R, Rydzanicz M, Ksiazczyk TM, Franaszczyk M, Pollak A, Kosinska J, et al. Evidence for troponin C (TNNC1) as a gene for autosomal recessive restrictive cardiomyopathy with fatal outcome in infancy. *Am J Med Genet A*. 2016;170(12):3241-8.
63. Yang SW, Hitz MP, Andelfinger G. Ventricular septal defect and restrictive cardiomyopathy in a paediatric TNNI3 mutation carrier. *Cardiol Young*. 2010;20(5):574-6.
64. Cui Z, Venkatraman G, Hwang SM, Gomes AV. Effect of the Troponin I Restrictive Cardiomyopathy Mutation R145W on Protein Expression in Murine Hearts. *Biophys J*. 2013b;104:312a.
65. Tardiff JC, Factor SM, Tompkins BD, Hewett TE, Palmer BM, Moore RL, et al. A truncated cardiac troponin T molecule in transgenic mice suggests multiple cellular mechanisms for familial hypertrophic cardiomyopathy. *J Clin Invest*. 1998;101(12):2800-11.
66. Gilda JE, Lai X, Witzmann FA, Gomes AV. Delineation of Molecular Pathways Involved in Cardiomyopathies Caused by Troponin T Mutations. *Mol Cell Proteomics*. 2016;15(6):1962-81.
67. Peddy SB, Vricella LA, Crosson JE, Oswald GL, Cohn RD, Cameron DE, et al. Infantile restrictive cardiomyopathy resulting from a mutation in the cardiac troponin T gene. *Pediatrics*. 2006;117(5):1830-3.
68. Muthuchamy M, Pieples K, Rethinasamy P, Hoit B, Grupp IL, Boivin GP, et al. Mouse model of a familial hypertrophic cardiomyopathy mutation in alpha-tropomyosin manifests cardiac dysfunction. *Circ Res*. 1999;85(1):47-56.
69. Rajan S, Ahmed RP, Jagatheesan G, Petrashevskaya N, Boivin GP, Urboniene D, et al. Dilated cardiomyopathy mutant tropomyosin mice develop cardiac dysfunction with significantly decreased fractional shortening and myofilament calcium sensitivity. *Circ Res*. 2007;101(2):205-14.
70. Liu J, Tang M, Mestril R, Wang X. Aberrant protein aggregation is essential for a mutant desmin to impair the proteolytic function of the ubiquitin-proteasome system in cardiomyocytes. *J Mol Cell Cardiol*. 2006;40(4):451-4.
71. Sanbe A, Daicho T, Mizutani R, Endo T, Miyauchi N, Yamauchi J, et al. Protective effect of geranylgeranylacetone via enhancement of HSPB8 induction in desmin-related cardiomyopathy. *PLoS One*. 2009;4(4):e5351.
72. Mundia MM, Demers RW, Chow ML, Perieteanu AA, Dawson JF. Subdomain location of mutations in cardiac actin correlate with type of functional change. *PLoS One*. 2012;7(5):e36821.
73. Chen XM, Feng MJ, Shen CJ, He B, Du XF, Yu YB, et al. A novel approach to select differential pathways associated with hypertrophic cardiomyopathy based on gene coexpression analysis. *Mol Med Rep*. 2017;16(1):773-7.
74. Min TJ, Jo WM, Shin SY, Lim HE. The protective effect of heat shock protein 70 (Hsp70) in atrial fibrillation in various cardiomyopathy conditions. *Heart Vessels*. 2015;30(3):379-85.
75. Niizeki T, Takeishi Y, Watanabe T, Nitobe J, Miyashita T, Miyamoto T, et al. Relation of serum heat shock protein 60 level to severity and prognosis in chronic heart failure secondary to ischemic or idiopathic dilated cardiomyopathy. *Am J Cardiol*. 2008;102(5):606-10.
76. Brundel BJ, Shiroshita-Takeshita A, Qi X, Yeh YH, Chartier D, van Gelder IC, et al. Induction of heat shock response protects the heart against atrial fibrillation. *Circ Res*. 2006;99(12):1394-402.
77. Miyamoto CA, Fischman DA, Reinach FC. The interface between MyBP-C and myosin: site-directed mutagenesis of the CX myosin-binding domain of MyBP-C. *J Muscle Res Cell Motil*. 1999;20(7):703-15.
78. van Dijk SJ, Dooijes D, dos Remedios C, Michels M, Lamers JM, Winegrad S, et al. Cardiac myosin-binding protein C mutations and hypertrophic cardiomyopathy: haploinsufficiency, deranged phosphorylation, and cardiomyocyte dysfunction. *Circulation*. 2009;119(11):1473-83.
79. Wijnker PJ, Friedrich FW, Dutsch A, Reischmann S, Eder A, Mannhardt I, et al. Comparison of the effects of a truncating and a missense MYBPC3 mutation on contractile parameters of engineered heart tissue. *J Mol Cell Cardiol*. 2016;97:82-92.
80. Sarikas A, Carrier L, Schenke C, Doll D, Flavigny J, Lindenberg KS, et al. Impairment of the ubiquitin-proteasome system by truncated cardiac myosin binding protein C mutants. *Cardiovasc Res*. 2005;66(1):33-44.
81. Predmore JM, Wang P, Davis F, Bartolone S, Westfall MV, Dyke DB, et al. Ubiquitin proteasome dysfunction in human hypertrophic and dilated cardiomyopathies. *Circulation*. 2010;121(8):997-1004.
82. Bahrudin U, Morisaki H, Morisaki T, Ninomiya H, Higaki K, Nanba E, et al. Ubiquitin-proteasome system impairment caused by a missense cardiac myosin-binding protein C mutation and associated with cardiac dysfunction in hypertrophic cardiomyopathy. *J Mol Biol*. 2008;384(4):896-907.
83. Day SM, Divald A, Wang P, Davis F, Bartolone S, Jones R, et al. Impaired assembly and post-translational regulation of 26S proteasome in human end-stage heart failure. *Circ Heart Fail*. 2013;6(3):544-9.
84. Thottakara T, Friedrich FW, Reischmann S, Braumann S, Schlossarek S, Kramer E, et al. The E3 ubiquitin ligase Asb2beta is downregulated in a mouse model of hypertrophic cardiomyopathy and targets desmin for proteasomal degradation. *J Mol Cell Cardiol*. 2015;87:214-24.
85. Chen SN, Czernuszewicz G, Tan Y, Lombardi R, Jin J, Willerson JT, et al. Human molecular genetic and functional studies identify TRIM63, encoding Muscle RING Finger Protein 1, as a novel gene for human hypertrophic cardiomyopathy. *Circ Res*. 2012;111(7):907-19.
86. Su M, Wang J, Kang L, Wang Y, Zou Y, Feng X, et al. Rare variants in genes encoding MuRF1 and MuRF2 are modifiers of hypertrophic cardiomyopathy. *Int J Mol Sci*. 2014;15(6):9302-13.

87. Weekes J, Morrison K, Mullen A, Wait R, Barton P, Dunn MJ. Hyperubiquitination of proteins in dilated cardiomyopathy. *Proteomics*. 2003;3(2):208-16.
88. Kostin S, Pool L, Elsasser A, Hein S, Drexler HC, Arnon E, et al. Myocytes die by multiple mechanisms in failing human hearts. *Circ Res*. 2003;92(7):715-24.
89. Baumgarten A, Bang C, Tschirner A, Engelmann A, Adams V, von Haehling S, et al. TWIST1 regulates the activity of ubiquitin proteasome system via the miR-199/214 cluster in human end-stage dilated cardiomyopathy. *Int J Cardiol*. 2013;168(2):1447-52.
90. Birks EJ, Latif N, Enesa K, Folkvang T, Luong le A, Sarathchandra P, et al. Elevated p53 expression is associated with dysregulation of the ubiquitin-proteasome system in dilated cardiomyopathy. *Cardiovasc Res*. 2008;79(3):472-80.
91. Otsuka K, Terasaki F, Shimomura H, Tsukada B, Horii T, Isomura T, et al. Enhanced expression of the ubiquitin-proteasome system in the myocardium from patients with dilated cardiomyopathy referred for left ventriculoplasty: an immunohistochemical study with special reference to oxidative stress. *Heart Vessels*. 2010;25(6):474-84.
92. Matsui Y, Takagi H, Qu X, Abdellatif M, Sakoda H, Asano T, et al. Distinct roles of autophagy in the heart during ischemia and reperfusion: roles of AMP-activated protein kinase and Beclin 1 in mediating autophagy. *Circ Res*. 2007;100(6):914-22.
93. Decker RS, Wildenthal K. Lysosomal alterations in hypoxic and reoxygenated hearts. I. Ultrastructural and cytochemical changes. *Am J Pathol*. 1980;98(2):425-44.
94. Shimomura H, Terasaki F, Hayashi T, Kitaura Y, Isomura T, Suma H. Autophagic degeneration as a possible mechanism of myocardial cell death in dilated cardiomyopathy. *Jpn Circ J*. 2001;65(11):965-8.
95. Nowis D, Maczewski M, Mackiewicz U, Kujawa M, Ratajska A, Wieckowski MR, et al. Cardiotoxicity of the anticancer therapeutic agent bortezomib. *Am J Pathol*. 2010;176(6):2658-68.
96. Lu L, Wu W, Yan J, Li X, Yu H, Yu X. Adriamycin-induced autophagic cardiomyocyte death plays a pathogenic role in a rat model of heart failure. *Int J Cardiol*. 2009;134(1):82-90.
97. Kimura H, Eguchi S, Sasaki J, Kuba K, Nakanishi H, Takasuga S, et al. Vps34 regulates myofibril proteostasis to prevent hypertrophic cardiomyopathy. *JCI Insight*. 2017;2(1):e89462.
98. Hoorntje ET, Bollen IA, Barge-Schaapveld DQ, van Tienen FH, Te Meerman GJ, Jansweijer JA, et al. Lamin A/C-Related Cardiac Disease: Late Onset With a Variable and Mild Phenotype in a Large Cohort of Patients With the Lamin A/C p.(Arg331Gln) Founder Mutation. *Circ Cardiovasc Genet*. 2017;10(4).
99. Nijenkamp L, Bollen IAE, van Velzen HG, Regan JA, van Slegtenhorst M, Niessen HWM, et al. Sex Differences at the Time of Myectomy in Hypertrophic Cardiomyopathy. *Circ Heart Fail*. 2018;11(6):e004133.
100. Sadoul K, Boyault C, Pabion M, Khochbin S. Regulation of protein turnover by acetyltransferases and deacetylases. *Biochimie*. 2008;90(2):306-12.
101. Zhang K, Kaufman RJ. From endoplasmic-reticulum stress to the inflammatory response. *Nature*. 2008;454(7203):455-62.
102. Fu HY, Sanada S, Matsuzaki T, Liao Y, Okuda K, Yamato M, et al. Chemical Endoplasmic Reticulum Chaperone Alleviates Doxorubicin-Induced Cardiac Dysfunction. *Circ Res*. 2016;118(5):798-809.
103. Arai M, Yoguchi A, Takizawa T, Yokoyama T, Kanda T, Kurabayashi M, et al. Mechanism of doxorubicin-induced inhibition of sarcoplasmic reticulum Ca(2+)-ATPase gene transcription. *Circ Res*. 2000;86(1):8-14.
104. Ling YH, Priebe W, Perez-Soler R. Apoptosis induced by anthracycline antibiotics in P388 parent and multidrug-resistant cells. *Cancer Res*. 1993;53(8):1845-52.
105. Minotti G, Licata S, Saponiero A, Menna P, Calafiore AM, Di Giammarco G, et al. Anthracycline metabolism and toxicity in human myocardium: comparisons between doxorubicin, epirubicin, and a novel disaccharide analogue with a reduced level of formation and [4Fe-4S] reactivity of its secondary alcohol metabolite. *Chem Res Toxicol*. 2000;13(12):1336-41.
106. Lipshultz SE, Lipsitz SR, Sallan SE, Dalton VM, Mone SM, Gelber RD, et al. Chronic progressive cardiac dysfunction years after doxorubicin therapy for childhood acute lymphoblastic leukemia. *J Clin Oncol*. 2005;23(12):2629-36.
107. Meinardi MT, van der Graaf WT, van Veldhuisen DJ, Gietema JA, de Vries EG, Sleijfer DT. Detection of anthracycline-induced cardiotoxicity. *Cancer Treat Rev*. 1999;25(4):237-47.
108. Linschoten M, Teske AJ, Baas AF, Vink A, Dooijes D, Baars HF, et al. Truncating Titin (TTN) Variants in Chemotherapy-Induced Cardiomyopathy. *J Card Fail*. 2017;23(6):476-9.
109. Wasielewski M, van Spaendonck-Zwarts KY, Westerink ND, Jongbloed JD, Postma A, Gietema JA, et al. Potential genetic predisposition for anthracycline-associated cardiomyopathy in families with dilated cardiomyopathy. *Open Heart*. 2014;1(1):e000116.
110. van den Berg MP, van Spaendonck-Zwarts KY, van Veldhuisen DJ, Gietema JA, Postma A, van Tintelen JP. Familial dilated cardiomyopathy: another risk factor for anthracycline-induced cardiotoxicity? *Eur J Heart Fail*. 2010;12(12):1297-9.
111. Luo HC, Pozios I, Vakrou S, Sorensen L, Abraham RM, Abraham T. Age-related changes in familial hypertrophic cardiomyopathy phenotype in transgenic mice and humans. *J Huazhong Univ Sci Technolog Med Sci*. 2014;34(5):634-9.
112. Terman A, Dalen H, Eaton JW, Neuzil J, Brunk UT. Mitochondrial recycling and aging of cardiac myocytes: the role of autophagocytosis. *Exp Gerontol*. 2003;38(8):863-76.
113. Simonsen A, Cumming RC, Brech A, Isakson P, Schubert DR, Finley KD. Promoting basal levels of autophagy in the nervous system enhances longevity and oxidant resistance in adult Drosophila. *Autophagy*. 2008;4(2):176-84.

114. Gilda JE, Gomes AV. Proteasome dysfunction in cardiomyopathies. *J Physiol*. 2017;595(12):4051-71.

115. Jana NR. Protein homeostasis and aging: role of ubiquitin protein ligases. *Neurochem Int*. 2012;60(5):443-7.

116. Rubinsztein DC, Marino G, Kroemer G. Autophagy and aging. *Cell*. 2011;146(5):682-95.

117. Baar EL, Carbajal KA, Ong IM, Lamming DW. Sex- and tissue-specific changes in mTOR signaling with age in C57BL/6J mice. *Aging Cell*. 2016;15(1):155-66.

118. Wohlgemuth SE, Julian D, Akin DE, Fried J, Toscano K, Leeuwenburgh C, et al. Autophagy in the heart and liver during normal aging and calorie restriction. *Rejuvenation Res*. 2007;10(3):281-92.

119. Herrmann J, Wohlert C, Saguner AM, Flores A, Nesbitt LL, Chade A, et al. Primary proteasome inhibition results in cardiac dysfunction. *Eur J Heart Fail*. 2013;15(6):614-23.

120. Xie M, Morales CR, Lavandero S, Hill JA. Tuning flux: autophagy as a target of heart disease therapy. *Curr Opin Cardiol*. 2011;26(3):216-22.

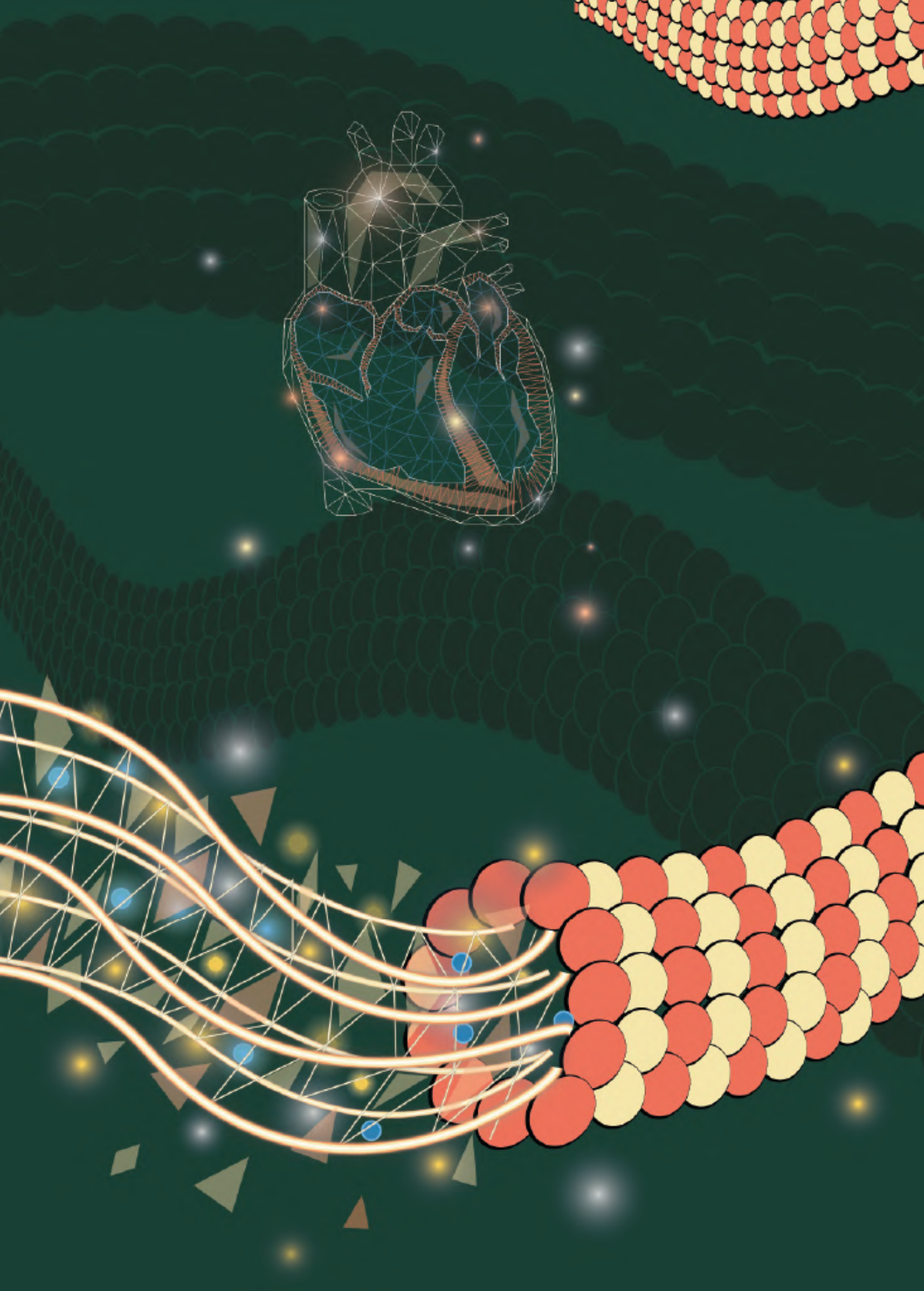

Chapter 4

Functional rescue of disease-causing HSPB5 mutants by interfering with interactions of the C-terminal tail and the hydrophobic β4-β8 groove in the α-crystallin domain

Jan J. Vonk[*], **Larissa M. Dorsch**[*], Christopher N. Woods[*], Rebecca Freilich[*], Jolanda van der Velden, Bianca JJM. Brundel, Jason E. Gestwicki[‡], Rachel E. Klevit[‡], Harm H. Kampinga[‡]

[*] *contributed equally*
[‡] *shared last author*

Manuscript in preparation.

ABSTRACT

BACKGROUND/OBJECTIVES

Dilated cardiomyopathy (DCM) is defined by the presence of left ventricular dilation and contractile dysfunction. R120G and D109H mutations in the small heat shock protein HSPB5 (αB-crystallin) are associated with formation of HSPB5 aggregates and dominantly inherited DCM. HSP5 has the ability to form dynamic oligomeric complexes for which a key role in substrate recognition and chaperoning functions is suggested. Interaction between HSPB5 C-terminal isoleucine-proline-isoleucine (IPI) domain and a hydrophobic groove including the amino acid serine 135 of the α-crystallin domain enables this oligomerization. Our aim is to study the underlying mechanism of aggregate formation by HSPB5 mutations and its effect on chaperone activity and cardiomyocyte function in experimental model systems.

METHODS

Purified proteins and overexpression of wild-type and mutant forms of HSPB5 in HL-1 cardiomyocytes, HEK293 and S2 cells were used to study the formation of aggregates including insolubilization, oligomer size, exchange rate, chaperone activity and the effect on calcium transients (CaT).

RESULTS

$HSPB5^{R120G}$ and $HSPB5^{D109H}$ overexpression resulted in the formation of aggregates with increased oligomer size and reduced exchange rate, insolubilization, loss of chaperone activity and CaT amplitudes. Substitution of HSPB5 IPI domain to AAA and the S135Q mutation in the $HSPB5^{R120G}$ and $HSPB5^{D109H}$ background decreased oligomer size, regained solubility, partially prevented aggregate formation and partially restored chaperone activity. Elevated expression of $HSPB5^{D109H;\ S135Q}$ completely protected against CaT loss. Pharmaceutical targeting of the IPI domain with a small peptide resolubilized $HSPB5^{R120G}$ and $HSPB5^{D109H}$.

CONCLUSION

This study shows that substitution of IPI domain to AAA or the S135Q mutation in the $HSPB5^{R120G}$ and $HSPB5^{D109H}$ background, partially prevent aggregate formation and restores chaperone activity suggesting a role for altered oligomerization dynamics in cardiomyocytes remodelling and disease progression. Targeting the altered oligomerization dynamics may represent a novel strategy to treat DCM patients carrying $HSPB5^{R120G}$ and $HSPB5^{D109H}$ mutations.

INTRODUCTION

Dilated cardiomyopathy (DCM) is a condition with left ventricular enlargement and reduced systolic output.[1] Features often observed in DCM patients include an irregular heartbeat (arrhythmia), shortness of breath (dyspnoea), extreme tiredness (fatigue), fainting episodes (syncope), and swelling of the legs and feet. Familial (inherited) DCM accounts for about 35 percent of affected individuals.[1] DCM-causing mutations affect genes encoding proteins regulating structure and function of the cardiomyocytes.[2] Interestingly, a restricted set of DCM-causing mutations are found to reside in genes encoding for chaperones, the caretakers of the cellular proteome.[1] Mutations in chaperone genes include gene variants in *BAG3*[3,4], *DNAJB6*[5], and *HSPB5* (αB-crystallin)[6,7]. This indicates that in a significant number of DCM cases, a collapse of protein homeostasis may be key to the disease pathology either caused by increased substrate fragility or by impaired protein quality control.[8]

In this paper, we focus on DCM-causing mutations in the small heat shock protein HSPB5 (also referred to as αB-crystallin). The frequency of HSPB5 mutations has not been systematically studied, but occurs less frequent than gene variants in desmin.[9] The small heat shock proteins are characterized by a conserved α-crystallin domain and variable N- and C-termini. There are 10 different human HSPBs (HSPB1-10) of which HSPB1 and HSPB5 are amongst the most highly and widely expressed members.[10,11] Together with HSPB8, these HSPBs increase their cellular expression levels upon a variety of intrinsic and extrinsic forms of stress.[12] HSPB5 binds unfolded proteins and prevents these from aggregating irreversibly.[13,14] Unlike the ATP-driven chaperones (HSPA, HSPC, chaperonins) all HSPBs, including HSPB5, lack ATPase activity, therefore bound substrates are generally not released spontaneously. Rather, substrates are released by the ATP-fuelled HSPA machines to either help them refold or target them towards degradation.[15-17]

HSPB5 forms homo-oligomeric and hetero-oligomeric complexes with HSPB1, HSPB4, HSPB6 and HSPB8.[18-20] Although the precise role of HSPB5 oligomerization for its function is not known, oligomeric dynamics seem to determine the state at which HSPB5 binds to the destabilized client protein and are considered to be crucial for HSPB5 function.[21-24] Several interactions contribute to HSPB5 oligomerization. The best characterized interaction is between the IPI sequence in the C-terminus and a hydrophobic β4-β8 groove in the α-crystallin domain (ACD). Mutation of the IPI sequence to three alanines results in a weakening of the interactions within the oligomers and a faster exchange of the subunits.[18,19] Such an increase in oligomer dynamics has been suggested to increase the chaperone function of HSPB5.[25] Inversely, compared to wild-type HSPB5, mutations in HSPB5 which are associated with diseases, including myofibrillar myopathy, cataract and DCM, have been shown to result in an increase in oligomeric size,[26] which could possibly underlie decreased oligomeric dynamics and substrate handling/chaperone function. This in particular has been suggested for the $HSPB5^{R120G}$ and $HSPB5^{D109H}$ mutations that cause dominantly inherited DCM and cataract and result in early fatality.[6,7,27] The R120 and D109 are located at opposite positions in the ACD at the dimer interface and interact through hydrogen bonds.[28,29] The R120G mutation causes a change in conformation of

the α-crystallin domain and results in a decreased chaperone function.[27,28] In patients, the HSPB5^{R120G} mutation is associated with insolubilization of the protein itself in muscle tissue.[6] HSPB5^{R120G} insolubilization is accompanied by aggregation of desmin, an intermediate filament protein, resulting in desmin-related cardiomyopathy.[6] In cell models, ectopic expression of HSPB5^{R120G} and HSPB5^{D109H} also leads the insolubilization of the mutant proteins whereas ectopic expression of HSPB5^{WT} remains detergent soluble.[30-32] The underlying mechanism for this aggregation phenotype and how this phenotype contributes to cellular dysfunction and disease onset is unknown.

In the current study, we demonstrate that expression of HSPB5^{R120G} and HSPB5^{D109H} in HL-1 cardiomyocytes results in loss of function of HSPB complexes and is associated with insolubilization of HSPB5 and contractile dysfunction. Introducing a secondary mutation in the IPI sequence or the hydrophobic groove where the IPI sequence interacts, partially alleviates protein aggregation and also leads to a partial regain of chaperone function and coincident improvement of contractile function. Also, addition of IPV peptides, which bind to the β4-β8 groove in the α-crystallin domain, to lysates of HSPB5^{R120G} and HSPB5^{D109H} expressing cells results in partial resolubilization of the mutant HSPB5 proteins. These results demonstrate that interfering with the binding of the IPI domain into the hydrophobic groove of the ACD results in improved chaperone and contractile function. Therapies directed at the IPI domain and/or hydrophobic groove may represent a viable strategy for the treatment of DCM associated with HSPB5 mutations.

METHODS

PLASMIDS

pCMV-Myc-HSPB5, pCMV-Myc-HSPB5^{R120G} and pCMV-Myc-HSPB5^{D109H} were provided kindly by Katie Mitzelfelt and Ivor Benjamin. The GFP-Luciferase construct was used from.[33] The V5-HSPA1A and V5-DNAJB1, V5-HSPB1 and V5-HSPB7 constructs were created in our lab.[34,35] Mutations were created by using the Quickchange kit (Qiagen) using the primers provided in Table S1. For cloning HSPB constructs into a Drosophila pUAST vector, restriction with Bgl2 and Xho1 was used.

CELL CULTURE AND TRANSFECTION

HL-1 cardiomyocytes were cultured in Claycomb medium containing 100 µM Norepinephrine, 0.3 mM L-ascorbic acid, 4 mM L-glutamine, 10% (v/v) FBS and 100 units/mL penicillin and 100 mg/mL streptomycin (Invitrogen) in gelatin (0.02%) coated flasks. $2*10^5$ cells were plated in gelatin (0.02%) coated wells and transfected after three days with Lipofectamine 2000 (Invitrogen) using a standard protocol. The experiments were performed two days after transfection.

HEK293 cells were cultured in Dulbecco's modified eagles medium (DMEM, Gibco) supplemented with 10% (v/v) fetal calf serum (Greiner Bio-one, Long wood, FL, USA) plus 100 units/mL penicillin and 100 mg/mL streptomycin (Invitrogen). One day before

transfection 3,5*10^5 cells were plated in Poly-L lysin (0.001%, Sigma) coated wells. Transfection of HEK cells was performed using polyethylenimine (PEI) according to the manufacturer's protocol.

S2 cells were cultured in Schneiders medium (Gibco) containing 10% (v/v) FBS and 100 units/mL penicillin and 100 mg/mL streptomycin (Invitrogen). The cells were transfected using Effectene (Qiagen) according to standard protocol. The cells were harvested for Western blot two days after transfection.

NP40 FRACTIONATION AND WESTERN BLOTTING

Cells were washed with PBS, lysed in 200 µL NP40 lysis buffer (60 mM KCl, 2 mM MgCl, 10% (v/v) glycerol, 0.4% (v/v) NP40, 50 mM HEPES, pH 7.5) containing fresh protease inhibitors (EDTA free Complete, Sigma), sonicated and a 40 µL whole cell extract was taken. Subsequently the samples were spun at 20.000g at 4°C for 20 min and a 40 µL supernatant fraction (NP40 soluble) was taken. The pellet was washed with lysis buffer and resuspended in 40 µL 1x Laemmli sample buffer (2% (w/v) SDS, 10% (v/v) glycerol, 0.004% (w/v) bromophenol blue, 0.125 M Tris HCl pH 6,8) and sonicated. 2x Laemmli sample buffer was added to the whole cell extract and the supernatant fractions. 5% (v/v) β-Mercapthoethanol was added to all samples and they were boiled for 5 min.

Samples were run on 12% (w/v) polyacrylamide gels and transferred onto nitrocellulose using a semi-dry transfer system (BioRad). The membranes were blocked for at least 1 h in 5% (w/v) milk and incubated in 3% BSA in PBST (PBS 0.1% (v/v) Tween-20) containing the primary antibody at 4°C overnight. Subsequently the membranes were washed with PBST and incubated with the secondary antibody (1:4000 in PBST) for 1.5 h. After washing with PBST the membranes were detected using ECL (ThermoFischer) in the dark room or on a BioRad Chemidoc Touch.

The antibodies used for Western blot: Myc-tag (1:1000, PL14, Enzo Life Sciences), β-Actin (1:1000, 8H10D10, Cell Signaling), HSPB5 (1:1000, 1A7.D5, StresMarq) and GFP (1:1000, JL8, Clontech), HSPB1 (1:1000, ADI-SPA-800, Enzo Life Sciences) and HSPA6 (1:1000, ADI-SPA-754).

SUCROSE GRADIENT FRACTIONATION

HL-1 cardiomyocytes were transfected and samples in NP40 lysis buffer were made as previously described. Sucrose gradients of 20% to 60% (w/v) sucrose in 10 mM Tris–HCl, pH 8, 5 mM EDTA, 50 mM NaCl were made using a Biocomp gradient master 108. The samples were loaded on top and the gradient was spun overnight at 100.000g for 20 h at 4°C in a Sorvall discovery 90SE with an SW41 rotor. Samples of 700 µL were taken from the top and the protein was precipitated by adding an equal volume of 25% TCA. After an incubation of 30 min on ice the samples were spun for 15 min at 14.000 rpm 4°C. The supernatant was removed and the pellet was washed with 500 µL 80% aceton. The samples were spun for 15 min at 14.000 rpm 4°C, supernatant was removed and the pellets were air

dried. The pellets were solubilized in 40 µL 1% SDS, 0.1 M NaOH. 40 µL 2x Laemmli buffer and 5% β-Mercapthoethanol were added and the samples were boiled for 5 min.

LUCIFERASE REFOLDING ASSAY

The luciferase assay was performed in HEK293 cells 1 day after transfection using a protocol described previously.[36]

IMMUNOFLUORESCENCE STAINING AND MICROSCOPY

HL-1 cells were plated on gelatine (0.02% gelatine, Sigma) coated cover slips three days before transfection. Transfection was done as described previously. Two days after transfection the cells were washed twice with PBS and fixed in 3,7% formaldehyde in PBS for 20 min. The cover slips were washed twice with 0.1% triton x-100 in PBS (PBT 0.1%) and permeabilized for 20 min in 0.2% PBT . Blocking was done for 1 h using 5% BSA in 0.1% PBT . Staining with primary antibody was done overnight at 4°C. After a wash with 0.1% PBT the cover slips were incubated with secondary antibody in 0.1% PBT for 2 h (including DAPI or Rhodamine Phalloidin) and mounted using citifluor (Agar Scientific). The slides were imaged with a Leica CLSM microscope. The quantifications were done by a person blinded to the experimental conditions. Antibodies used for immunofluorescence: Myc-tag (1:250, PL14, Enzo Life Sciences) and ubiquitylated proteins (1:250, FK2, Enzo Life Sciences).

RECOMBINANT PROTEIN PURIFICATION

Constructs for full length and ACD HSPB5, R120G HSPB5 and HSPB1 were a gift from the Klevit laboratory (University of Washington), and proteins were expressed and purified as described.[37,38] Briefly, all constructs were transformed in E. coli BL21 (DE3) cells, grown to an OD600 of 0.6 in Terrific Broth (TB), and induced with 0.5 mM IPTG overnight at 18°C. For full length constructs, cells were pelleted and re-suspended in 50 mM Tris-HCl pH 8.0, 10 mM imidazole, 500 mM NaCl and lysed by sonication. The cleared lysate was loaded onto the Ni-NTA spin column (Qiagen) and eluted with buffer containing 300 mM imidazole. Proteins were concentrated and further purified by size exclusion on a Superdex 200 16/600 column (GE Healthcare) equilibrated with SEC Buffer (50 mM sodium phosphate pH 7.5, 100 mM NaCl). For ACD constructs, ammonium sulphate was added to a final concentration of 16.9% (w/v), centrifuged, pellet discarded, and then an additional 16.9% (w/v) ammonium sulfate was added to the supernatant to precipitate the protein from solution. Precipitated protein was brought up and dialyzed into MonoQ Buffer A (20 mM Tris, pH 8.0) overnight, followed by a MonoQ column (0–1 M NaCl gradient), and finally an SEC on a Superdex S75 (GE Healthcare) equilibrated in SEC Buffer.

ISOTHERMAL TITRATION CALORIMETRY

Small HSPs were dialyzed overnight against SEC Buffer, and peptides were dissolved in dialysis buffer. Concentration of proteins was determined using BCA assays (Thermo Scientific), and ITC experiments were performed with a MicroCal ITC200 (GE Healthcare)

at 25°C. For experiments, 1 mM peptide solution was titrated into a cell containing specified small HSP at 100 µM. Calorimetric parameters were calculated using Origin® 7.0 software and fit with a one-site binding model.

LIGHT SCATTERING ASSAYS

Solutions of R120G HSPB5 (30 µM) in SEC Buffer with listed binding partners or buffer controls were placed in triplicate wells of a clear bottom 384-well plate. The aggregation reaction was carried out at 37°C with continuous shaking and the OD350 was measured in a Spectramax M5 microplate reader (Molecular Devices). Readings were taken every 2 min for 3 h. Baseline curves of non-induced controls (3 replicates) were subtracted from induced samples (3 replicates).

CALCIUM TRANSIENT MEASUREMENTS

For calcium transient (CaT) measurements, HL-1 cardiomyocytes were co-transfected with 0.75 µg/mL HSPB5 plasmid (wild-type or mutant) and 0.25 µg/mL RFP plasmid. 48 h post-transfection, HL-1 cardiomyocytes were loaded and incubated at room temperature for 30 min with 1 µM of calcium indicator Fluo-4 AM (Invitrogen, Carlsbad) in Hanks Balanced Salt Solution (HBSS) buffer (Lonza, Basel) supplemented with 1.7 µM $CaCl_2 \cdot H_2O$ and 0.8 mM $MgSO_4 \cdot 7H_2O$ 48 h after lipofectamine transfection. HL-1 cardiomyocytes were washed 3 times with supplemented HBSS buffer before adding Claycomb medium without supplements. The Fluo-4 loaded HL-1 cardiomyocytes, stimulated at 1 Hz and 40 V by a C-Pace system (IonOptix, Westwood), were excited at 488 nm and the light emitted at 500-550 nm was live recorded with a 40 x 1.3 NA oil-objective of a high-speed Nikon A1R confocal microscope (Nikon, Minato). Temperature (37°C) and CO_2 (5%) were kept constant in the microscope incubator. Absolute fluorescent signals were recorded and single cell CaTs of *RFP*-positive transfected cells were analysed with ImageJ software (National Institute of Health, Bethesda). To compare fluorescent signals between experiments, the fluorescent signal at any given time (F) was divided by the fluorescent signal at rest (F0) (Fcal = F/F0)[39] CaTs were at least measured three times. Per experimental day, each CaT value was normalized to the mean value of overexpressed wild-type HSPB5. Exponential curve fitting was applied to obtain tau and time to 70% baseline.

QUANTIFICATION AND STATISTICAL ANALYSIS

The Western blots were quantified using ImageJ (NIH). Statistical analysis was done and graphs were made using Graphpad Prism 5. Plotted values show the average of at least 3 independent experiments and error bars show the standard error of the mean. The Student's t-test was used to calculate significance. Statistical significance in CaT measurements was estimated with Kruskal-Wallis test and Dunn's multiple comparisons post-hoc test. *P*-values below 0.05 were considered significant. In the figures $p<0.05$ is indicated by a *, $p<0.01$ by **, and $p<0.001$ by ***.

RESULTS

HSPB5^{R120G} AND HSPB5^{D109H} FORM AGGREGATES WHEN EXPRESSED IN HL-1 CARDIOMYOCYTES

The DCM-associated, dominant HSPB5^{R120G} or HSPB5^{D109H} mutants (Figure 4.1A) can accumulate protein aggregates in cardiac tissue.[6] To model this effect *in vitro*, we expressed wild-type HSPB5, HSPB5^{R120G} or HSPB5^{D109H} in HL-1 cardiomyocytes.[40] While wild-type HSPB5 was homogeneously distributed in the cytosol of HL-1 cardiomyocytes, both the HSPB5^{R120G} and HSPB5^{D109H} formed puncta throughout the cardiomyoyctes (Figure 4.1B), suggesting formation of aggregates. To confirm aggregation, we fractionated cardiomyocytes expressing HSPB5 wild-type or mutants using a mild detergent and found that both mutants, but not wild-type HSPB5 were mainly present in the NP40 insoluble fraction (Figures 4.1C-D). Immunofluorescence staining showed that ubiquitin partially co-localized with the HSPB5^{R120G} and HSPB5^{D109H} puncta in the cardiomyoycytes (Figure 4.1E).

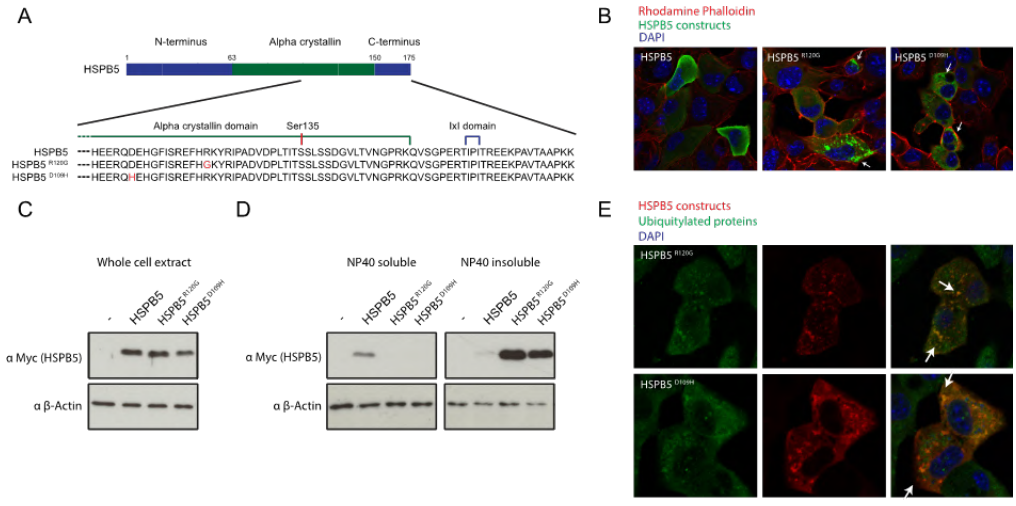

Figure 4.1: HSPB5^{R120G} and HSPB5^{D109H} form aggregates when expressed in HL-1 cardiomyocytes. (**A**) Schematic representation of the HSPB5 protein. The amino acid sequences of Myc-HSPB5, Myc-HSPB5^{R120G} and Myc-HSPB5^{D109H} are indicated. (**B**) Immunofluorescence staining of HL-1 cardiomyocytes expressing Myc-HSPB5, Myc-HSPB5^{R120G} and Myc-HSPB5^{D109H} stained for the Myc-tag (green), polymerized Actin (Rhodamine Phalloidin, red) and DNA (DAPI, blue). (**C**) Myc-HSPB5, Myc-HSPB5^{R120G} and Myc-HSPB5^{D109H} were transiently expressed in HL-1. The samples were separated in a NP40 soluble and NP40 insoluble fraction and analysed by Western blot (**D**). (**E**) Immunofluorescence staining of HL-1 cardiomyocytes expressing Myc-HSPB5^{R120G} and Myc-HSPB5^{D109H} stained for the Myc-tag (red), ubiquitylated proteins (green) and DNA (DAPI, blue).

We previously demonstrated that the insolubilization of HSPB5^{R120G} is preventable by co-expression of proteins of the HSPB family due to formation of hetero-oligomeric complexes with HSPB5.[30] To confirm this result in HL-1 cardiomyocytes and to test whether the same is true for the HSPB5^{D109H} mutant, we co-expressed either HSPB1 or HSPB7 with the HSPB5^{R120G} and HSPB5^{D109H} mutants. While overexpression of HSPB1, which forms hetero-oligomers with HSPB5, increased the soluble fraction of both HSPB5^{R120G} and HSPB5^{D109H}, HSPB7, which does not form hetero-oligomers with HSPB5, did not (Figure S1). Similarly, co-expression of HSPA1A or DNAJB1 did not prevent or rescue insolubilization of the two HSPB5 mutants (Figure S1). This suggests that intrinsic misfolding can be excluded because HSPA1A and/or DNAJB1 should have rescued the intrinsic misfolding. Moreover, the insolubilization is likely related to the formation of oligomeric complexes as HSPB1 can compete it away.

MUTATION OF THE IPI DOMAIN REDUCES HSPB5^{R120G} AND HSPB5^{D109H} INSOLUBILIZATION

To follow up the suggestion that the oligomerization of mutant HSPB5 is crucial for its presence in protein aggregates, we interfered with the stability of HSPB5 oligomers. The IPI domain in the C-terminus of HSPB5 is key to oligomer stability. When the IPI sequence is mutated, it no longer binds to the hydrophobic groove on the ACD. This weakens interactions within the oligomers and results in formation of smaller oligomers *in vitro*.[18,19,21-23,29] Consistently, sucrose gradient centrifugation revealed that mutating the IPI motif into triple alanines (HSPB5$^{IPI > AAA}$) resulted in smaller complexes than HSPB5^{WT} (Figure 4.2A).

Just as observed *in vitro* for HSPB5^{R120G},[27] the HSPB5^{R120G} and HSPB5^{D109H} mutants formed complexes of increased size (Figure 4.2A). Introduction of the IPI>AAA mutation in HSPB5^{R120G} and HSPB5^{D109H} to HSPB5$^{R120G; IPI > AAA}$ and HSPB5$^{D109H; IPI > AAA}$, respectively also reduced the formation of the very large complexes present in fraction 17 (Figures 4.2A and S2A). In line with these results and consistent with our prediction, HSPB5$^{R120G; IP > AAA}$ and HSPB5$^{D109H; IPI > AAA}$ had regained solubility (Figures 4.2B and S2B) and puncta formation was drastically reduced (Figures 4.2C-D).

MUTATION OF THE HYDROPHOBIC GROOVE DECREASES HSPB5^{R120G} AND HSPB5^{D109H} INSOLUBILIZATION

The IPI domain binds in a hydrophobic groove formed by the β4 and β8 strands of HSPB5. Serine 135 is part of the β8 strand and is located in between two pockets in which the isoleucines of the IPI domain bind. Mutating this serine to a glutamine has been shown to significantly reduce the affinity of the IPI domain for the hydrophobic groove.[21-23] As found for the IPI>AAA mutants, the insolubilization of the double mutants HSPB5$^{R120G; S135Q}$ and HSPB5$^{D109H; S135Q}$ was significantly reduced when compared to HSPB5^{R120G} and HSPB5^{D109H} (Figure 4.3A).

However, the S135Q mutation also resulted in lower expression levels of HSPB5 protein (Figure 4.3B). By increasing plasmid concentrations during transfection, we

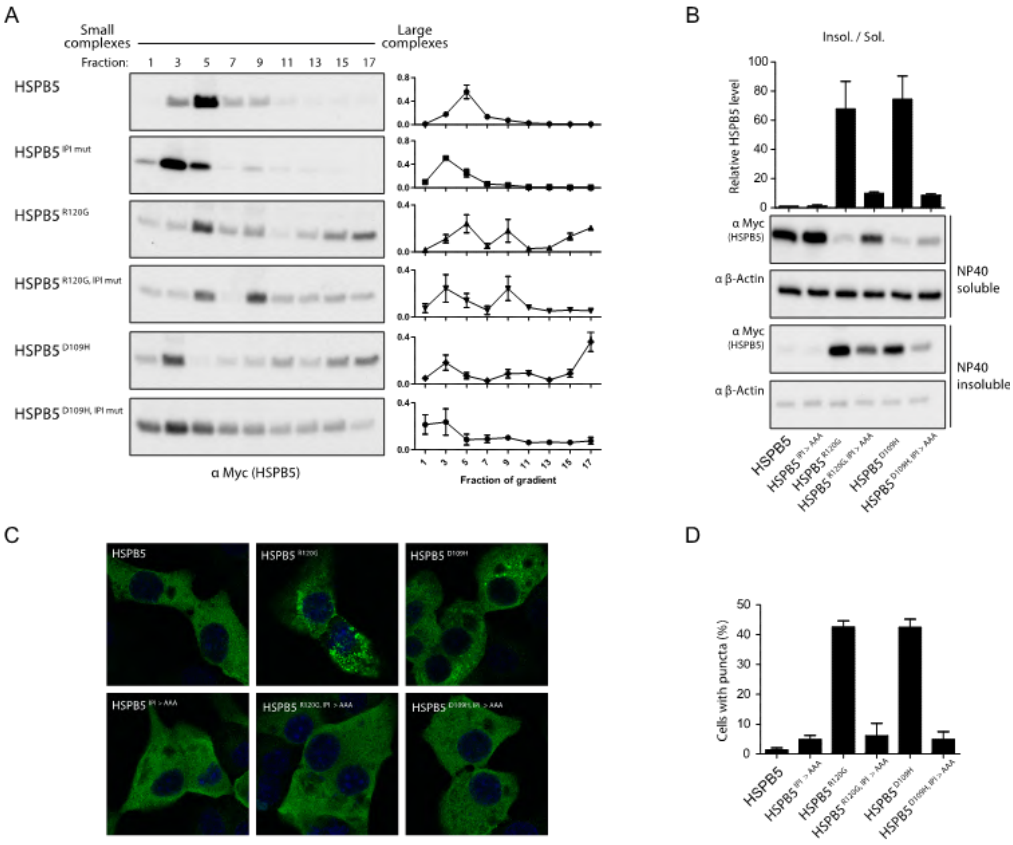

Figure 4.2: Mutation of the IPI domain decreases Myc-HSPB5^{R120G} and Myc-HSPB5^{D109H} aggregation. (**A**) Samples from HL-1 cardiomyocytes transiently expressing the indicated Myc-HSPB5 proteins were run on a 20% to 60% sucrose gradient and the fractions were analysed by Western blot. The quantifications indicate the distribution of the Myc-HSPB5 protein over the sucrose gradient. (**B**) The indicated Myc-HSPB5 constructs were transiently expressed in HL-1 cardiomyocytes and separated in a NP40 soluble and insoluble fraction. The quantification shows the relative amount of the Myc-HSPB5 protein. (**C**) Immunofluorescence staining of HL-1 cardiomyocytes expressing the indicated Myc-tagged HSPB5 variants (green) and DNA (DAPI, blue). The quantification shows the percentage of cells with puncta (**D**).

expressed different S135Q mutants to levels comparable to those without this mutation and still found that this reduced the insolubilization compared to HSPB5^{R120G} and HSPB5^{D109H} proteins (Figures S3A-B).

In order to investigate whether the Myc-tag influences the solubility of the HSPB5 mutants, we expressed untagged HSPB5^{R120G} in Drosophila S2 cells (Figure S3C). These experiments showed that also the IPI>AAA and S135Q mutations restored the solubility of untagged HSPB5^{R120G} (Figure S3D). We next generated triple mutants (IPI>AAA and S135Q in the HSPB5^{R120G} and HSPB5^{D109H}). These also increased the NP40 solubility compared to the single mutants (HSPB5^{R120G} and HSPB5^{D109H}), but these were not

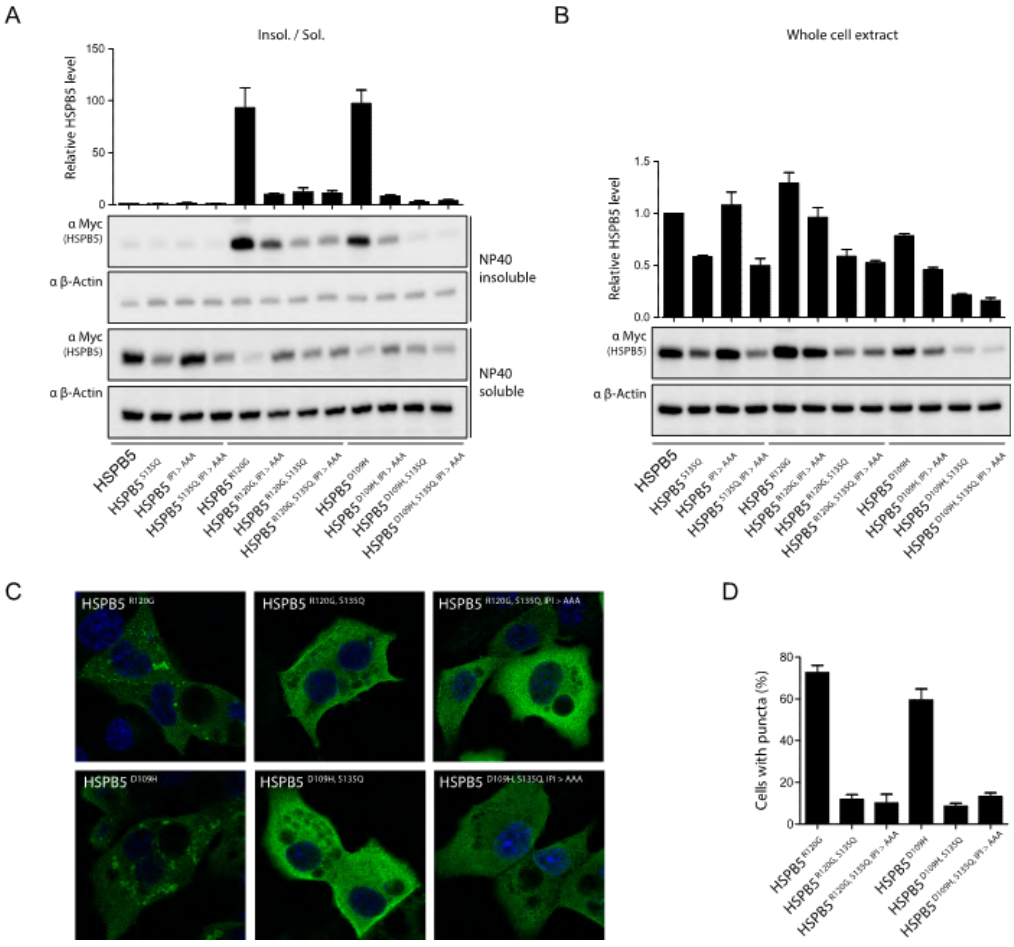

Figure 4.3: The S135Q mutation decreases Myc-HSPB5^{R120G} and Myc-HSPB5^{D109H} aggregation. (**A**) The indicated Myc-HSPB5 constructs were transiently expressed in HL-1 cardiomyocytes. The quantification shows the relative amount of the Myc-HSPB5 proteins. The samples were separated in a NP40 soluble and insoluble fraction (**B**). (**C**) Immunofluorescence staining of HL-1 cardiomyocytes expressing the indicated Myc-tagged HSPB5 variants (green) and DNA (DAPI, blue). The quantification shows the percentage of cells with puncta (**D**).

more soluble than the HSPB5$^{R120G;\ S135Q}$ and HSPB5$^{D109H;\ S135Q}$ or HSPB5$^{R120G;\ IPI\ >\ AAA}$ and HSPB5$^{D109H;\ IPI\ >\ AAA}$ (Figures 4.3A-B). This is consistent with the notion of direct contact between the IPI motif and S135 and that abrogation of either one of them suffices to lower oligomeric stability. The data on solubility were also fully recapitulated when the formation of puncta in cells was analysed (Figures 4.3C-D). Together, these data show that insolubilization of HSPB5^{R120G} and HSPB5^{D109H} is mediated via a dominant negative effect, i.e. the abnormal stabilization of HSPB5 complexes.

MUTATION OF THE IPI DOMAIN AND S135Q IMPROVE HSPB5^{R120G} AND HSPB5^{D109H} FUNCTION

In vitro, it has been shown that HSPB5 is a chaperone maintaining heat-unfolded or chemically unfolded proteins in a state competent for refolding by the ATP-dependent HSPA-chaperone machinery.[17] In contrast, HSPB5^{R120G} lost almost completely such chaperone activity.[27] Besides the diminished formation of HSPB5 aggregates when the contact between the IPI motif and ACD of HSPB5^{R120G} and HSPB5^{D109H} is disrupted, we wondered whether this also affects chaperone function. In human HEK293 cells, elevated expression of HSPB5^{WT} enhances the cellular ability to refold the ectopically expressed model protein firefly luciferase after heat shock (Figures 4.4A-B).[36] Consistent with the *in vitro* data,[27] HSPB5^{R120G} and HSPB5^{D109H} have almost completely lost this chaperone activity (Figure 4.4B). Like in HL-1 cardiomyocytes, both the IPI to AAA substitution and the S135Q mutation reduced the insolubilization of the HSPB5^{R120G} and HSPB5^{D109H} in HEK293 cells (Figures 4.4A and S4A).

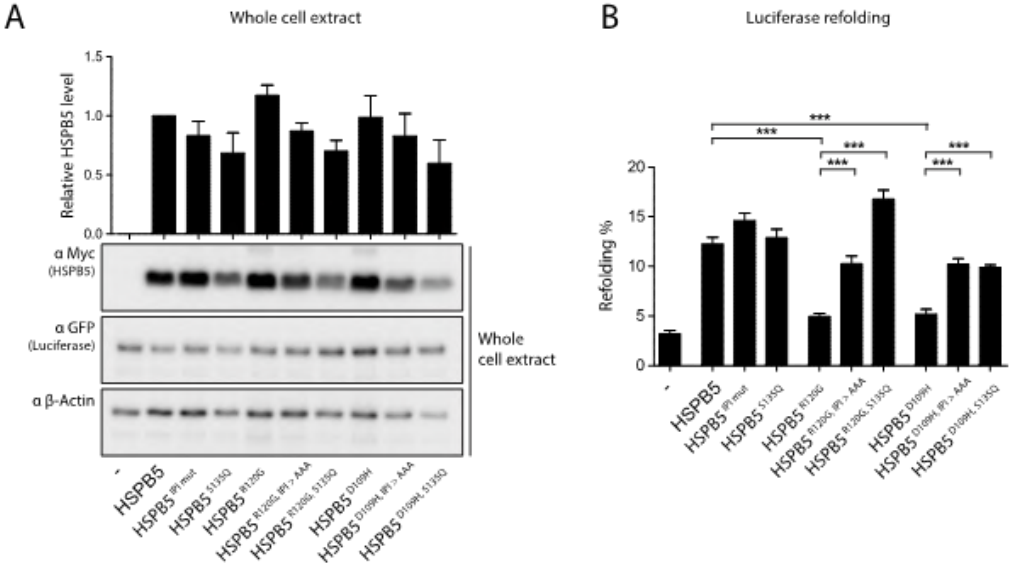

Figure 4.4: The IPI to AAA and the S135Q mutation improve chaperone activity of the HSPB5^{R120G} and HSPB5^{D109H} mutants. (**A**) HEK293 cells were transiently transfected with the indicated Myc-HSPB5 constructs and the expression was analysed by Western blot. (**B**) The indicated Myc-HSPB5 variants were co-expressed with GFP-Luciferase. The cells were heat shocked for 30 min at 43°C and re-incubated for 2 h after 37°C. The graph indicates the Luciferase activity 2 h after heat shock, relative to the Luciferase activity before the heat shock.

Excitingly, the HSPB5$^{R120G;\ IPI\ >\ AAA}$ and HSPB5$^{D109H;\ IPI\ >\ AAA}$ double mutants as well as the HSPB5$^{R120G;\ S135Q}$ and HSPB5$^{D109H;\ S135Q}$ double mutants had regained significant chaperone function (Figure 4.4B). This effect was not due to a promiscuous activation of HSF-1 as evidenced by the lack of induction of the expression of typical HSF-1 regulated chaperones like HSPB1 and HSPA6 (Figure S4B).

MUTATION OF THE HYDROPHOBIC GROOVE RESTORES CALCIUM TRANSIENT LOSS IN HL-1 CARDIOMYOCYTE OVEREXPRESSING HSPB5^{D109H}

Since mutation-related alterations in CaT may contribute to contractile dysfunction,[41-43] the effect of the different HSPB5 mutants on intracellular calcium handling were assessed in HL-1 transfected cardiomyocytes. Elevated expression of HSPB5^{R120G} and HSPB5^{D109H} resulted in a reduction of peak CaT by approximately 30% compared to CaT in cardiomyocytes overexpressing wild-type HSPB5 (Figures 4.5A-B and S5). Modifying the IPI domain (HSPB5e$^{IPI\ mut}$) or the hydrophobic groove (HSPB5^{S135Q}) had no effect on CaT. Introduction of the IPI>AAA mutation and S135Q in HSPB5^{R120G} to HSPB5$^{R120G;\ IPI\ mut}$ and HSPB5$^{R120G;\ S135Q}$, respectively, did not restore CaT loss.

These findings show that the presence of both R120G and D109H mutation results in CaT loss independent of the second mutation. Interestingly, elevated expression of HSPB5$^{D109H;\ S135Q}$ completely protected against CaT loss in contrast to HSPB5^{D109H} and HSPB5$^{D109H;\ IPI\ mut}$. In addition, the effect of wild-type HSPB5, HSPB5^{D109H} and HSPB5$^{D109H;\ S135Q}$ on CaT morphology, including time to 70% decay and mean time constant of CaT decay (tau) were calculated, to determine an effect on relaxation of HL-1 cardiomyocytes. Compared to wild-type HSPB5, HSPB5^{D109H} overexpression resulted in slightly accelerated, but not significant different, Ca^{2+} decay indicated by reduction in time to 70% decay and mean time constant of CaT decay (tau) (Figures 4.5C-D). Elevated levels of HSPB5$^{D109H;\ S135Q}$ increased the rate of relaxation and thereby attenuated defective Ca^{2+} handling.

Thus, the findings indicate that aggregated HSPB5^{R120G} and HSPB5^{D109H} cause CaT loss and that the S135Q mutation in the hydrophobic groove protects against CaT loss in case of HSPB5^{D109H} mutation.

OLIGOMERIC DYNAMICS AND SIZE OF THE HSPB5 VARIANTS DO NOT CORRELATE WITH FUNCTIONALITY *IN VITRO*

Based on the cellular data, we decided to purify a subset of the HSPB5 variants to assess their biochemical behaviour and functionality *in vitro*. As expected, the oligomeric size of the two disease-associated mutants HSPB5^{R120G} and HSPB5^{D109H} was higher than that of wild-type HSPB5 (Figure 4.6A).

Figure 4.5: Effect of HSPB5 variants on calcium transient amplitudes in HL-1 cardiomyocytes. (**A**) Representative CaT traces and (**B**) quantified CaT amplitude data of single HL-1 cardiomyocytes overexpressing wild-type and mutant HSPB5 48 h post-transfection, indicating HSPB5$^{D109H;\ S135Q}$ double mutant to rescue CaT function . Exponential curve fitting was applied to obtain (**C**) the time to 70% decay and (**D**) the mean time constant of CaT decay (tau). N = number of transfections; n = number of measured HL-1 cardiomyocytes that were *RFP*-positive transfected; *$p<0.05$, **$p<0.01$ and ***$p<0.001$ versus HSPB5 and $^{\#\#\#}p<0.001$ versus HSPB5^{D109H}.

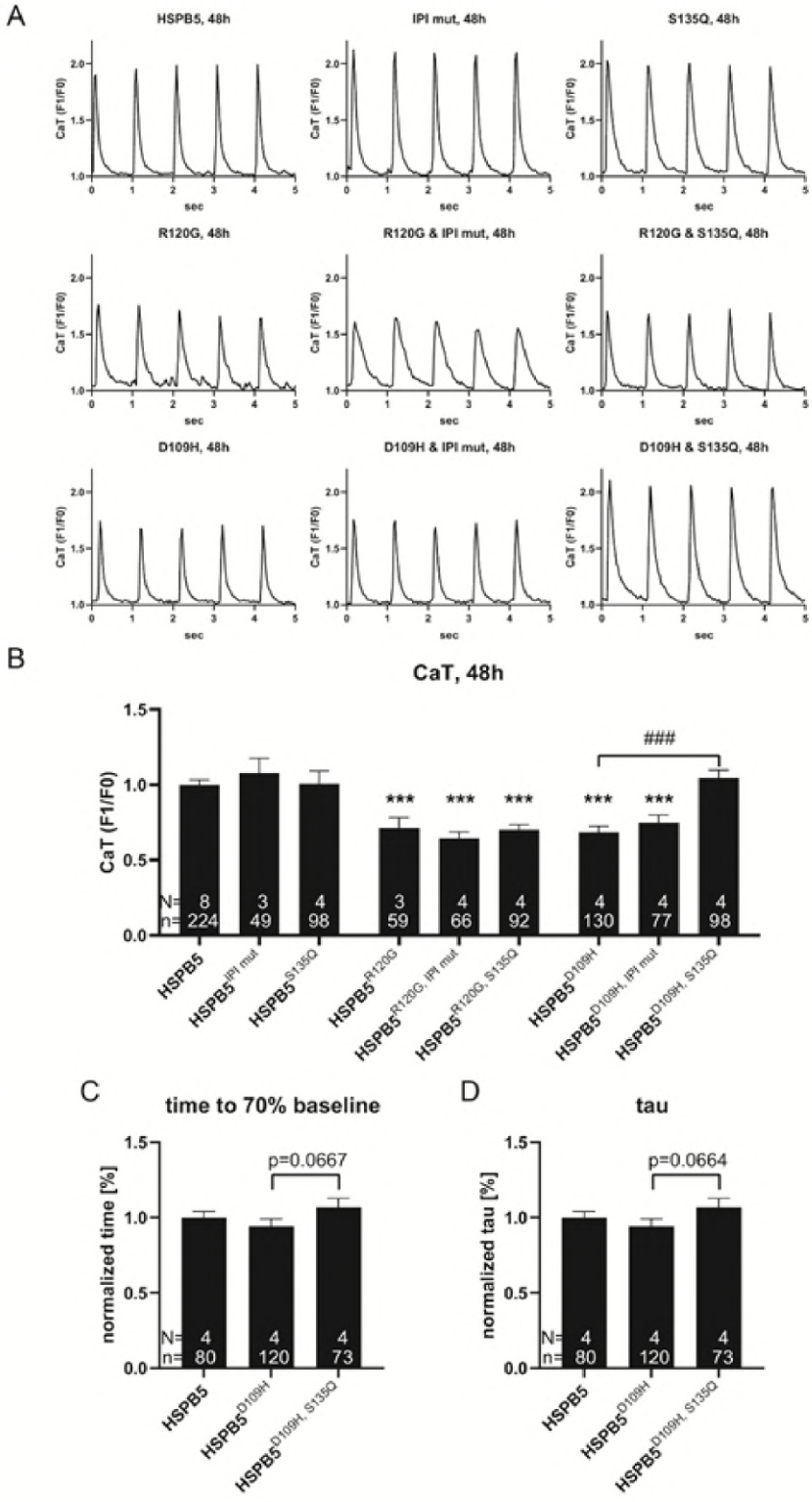
A
HSPB5, 48h
IPI mut, 48h
S135Q, 48h
R120G, 48h
R120G & IPI mut, 48h
R120G & S135Q, 48h
D109H, 48h
D109H & IPI mut, 48h
D109H & S135Q, 48h
CaT (F1/F0)
sec
B
CaT, 48h
CaT (F1/F0)
###
***
N= 8 3 4 3 4 4 4 4 4
n= 224 49 98 59 66 92 130 77 98
HSPB5
HSPB5IPI mut
HSPB5S135Q
HSPB5R120G
HSPB5R120G, IPI mut
HSPB5R120G, S135Q
HSPB5D109H
HSPB5D109H, IPI mut
HSPB5D109H, S135Q
C
time to 70% baseline
normalized time [%]
p=0.0667
N= 4 4 4
n= 80 120 73
HSPB5
HSPB5D109H
HSPB5D109H, S135Q
D
tau
normalized tau [%]
p=0.0664
N= 4 4 4
n= 80 120 73
HSPB5
HSPB5D109H
HSPB5D109H, S135Q

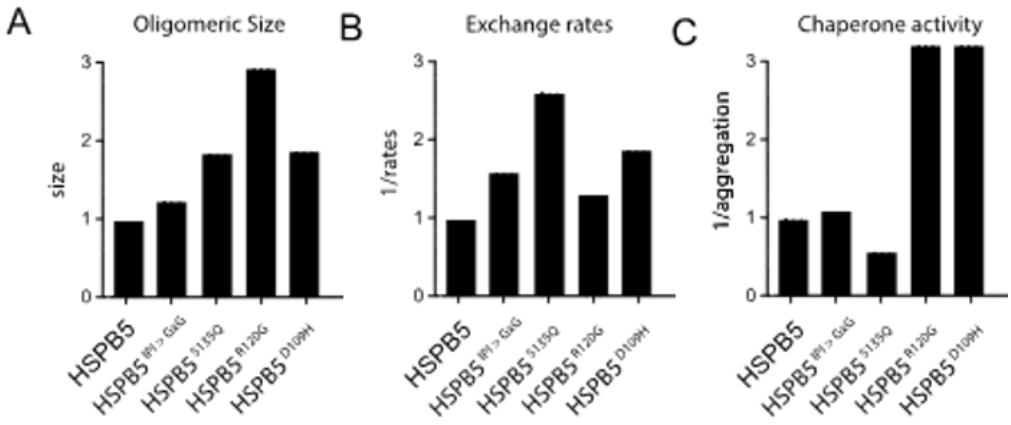

Figure 4.6: *In vitro* characteristics of HSPB5 variants.
(**A**) Oligomeric size of the complexes of the indicated HSPB5 variants relative to HSPB5 wild-type (= 1.0) (**B**) Inverse of the exchange rates of complexes of the indicated variants relative to HSPB5 wild-type (= 1.0) (**C**) Inverse of the anti-aggregation effects of the indicated variants relative to HSPB5 wild-type (= 1.0); substrate = α-lactalbumin.

Intriguingly, however, the HSPB5^{S135Q} as well as the IPI mutant HSPB5$^{IPI > GxG}$ that decrease the IPI-ACD interaction between HSPB5 monomers formed larger oligomers than the wild-type HSPB5 (Figure 4.6A).[21-23]
In addition, we were unable to purify the IPI and S135Q variants in the background of the disease-associated mutants (data not shown), suggesting they are only stable in the context of mammalian cells expressing HSPB5 or/and other HSPB family members. We next used fluorescent exchange experiments to test whether oligomeric exchange rates were different between the HSPB5 variants in a manner that would explain their cellular functionality. The exchange rates *in vitro* were higher for wild-type HSPB5 than for both HSPB5^{R120G} and HSPB5^{D109H}. Furthermore, the exchange rates for HSPB5^{R120G} were higher than for HSPB5^{S135Q} as well as the IPI mutant HSPB5$^{IPI > GxG}$ (Figure 4.6B). In general, among the HSPB5 variants tested, there was no correlation between oligomeric size (Figure 4.6A) and exchange rates (Figure 4.6B). Moreover, when assaying HSPB5 chaperone activity *in vitro*, using α-lactalbumin as substrate, both disease-variants were largely inactive (Figure 4.6C), as expected.[21] There was no correlation with oligomeric size (Figure 4.6A), nor with subunit exchange rates (Figure 4.6B), nor with the cellular data. Together these data imply that the functionality and aggregation phenotypes of the HSPB5 variants in cells cannot be attributed to intrinsic properties of the homo-oligomeric proteins only, but must be a combined effect of these intrinsic properties and interactions with other (wild-type) HSPB partners and chaperone substrates.

IPV PEPTIDES RESOLUBILIZE HSPB5^{R120G} AND HSPB5^{D109H}

Despite the absence of a correlation between intrinsic oligomeric behaviour of the HSPB5 variants and their chaperone function or the cellular findings, the data using the various

genetic single and double mutant HSPB5 variants in cells suggested that targeting the IPI-ACD interaction rescues the adverse phenotypes of the disease-associated variants and may thus have therapeutic potential. We therefore investigated whether the functionality of the mutants is restorable in a pharmaceutical manner using a small peptide EIT**IPV**THE (IPV peptide). *In vitro*, the IPV peptide, but not a control EIT**APV**THE peptide (APV) binds to the β4-β8 groove of the crystallin dimer of both wild-type HSPB5 and HSPB5^{R120G} with equal affinity (Figures 4.7A-B).

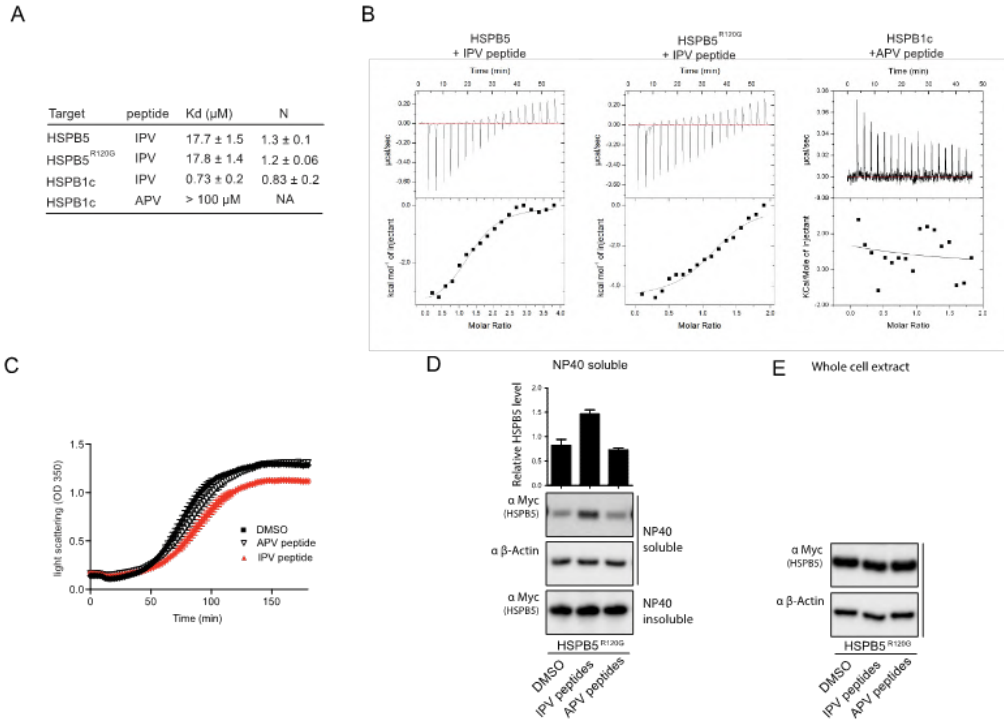

Figure 4.7: IPV peptides resolubilize Myc-HSPB5^{R120G} aggregates. (**A, B**) IPV peptide binds to HSPB5, HSPB5^{R120G} and HSPB1c. Representative ITC results for binding of IPV and control peptide, APV, are shown. The average of two independent replicates is shown in the table. Error is standard error of the mean (SEM). (**C**) Light scattering of purified, human HSPB5 (30 μM) treated with IPV peptide (30 μM), APV peptide control (30 μM) or DMSO. Results are the average of triplicate wells. The error bars represent standard deviation (SD), but are often too small to be seen. Additionally, the results are representative of three independent experiments. (**D, E**) Myc-HSPB5^{R120G} was expressed in HEK293 cells and lysed in NP40 lysis buffer. The cell lysates were incubated overnight at 4°C with DMSO, IPV peptides or APV peptides and separated in a NP40 soluble and insoluble fraction.

Using light scattering analyses, the IPV, but not APV peptide reduced the size of the HSPB5^{R120G} oligomers significantly (Figure 4.7C). Unfortunately, the hydrophobic IPV peptides are not effectively taken up by cells. Yet, as a proof of concept to test whether the peptides are also effective within the context of the cell, we generated lysates of HEK293 cells expressing HSPB5^{R120G}, added the peptides and subsequently compared the fraction

of HSPB5^{R120G} in the NP40 insoluble with and without addition of the IPV peptides. Like for the purified proteins, also in cell lysates addition of the IPV peptides, but not the APV peptides resulted in partial resolubilization of the HSPB5^{R120G} mutant (Figures 4.7D-E). Together, our data imply that targeting the IPI-ACD interaction has therapeutic potential in HSPB5-related cardiomyopathies.

DISCUSSION

The HSPB5^{R120G} and HSPB5^{D109H} mutations lead to dilated cardiomyopathy, myopathy and cataract. Misfolding and aggregation of HSPB5 has been proposed as part of the pathomechanisms. Here, we show that aggregation of both HSPB5^{R120G} and HSPB5^{D109H} can be reduced by interference with the IPI-ACD interactions between HSPB5 molecules. This decrease in aggregation is accompanied by a partial restoration of its chaperone and contractile function.

HSPB5 forms oligomers of heterogeneous size. The dynamics of this oligomerization, i.e. the constant and rapid disassembly and reassembly of mono- and/or dimers of HSPB5 from and to the oligomers, has been proposed to be important for its chaperone function.[21-24] One of the best characterized interactions in the HSPB5 oligomers is between the IPI motif in the N-terminus of one HSPB5 monomer with the ACD of an adjacent HSPB molecule. Our cellular data, using both genetic and pharmacological approaches, reveal that targeting this IPI-ACD interaction not only decreases the steady state oligomeric sizes of the mutant HSPB5 complexes, but also counteracts their aggregation-proneness and partially restores their chaperone and contractile function. This would suggest that the HSPB5^{R120G} and HSPB5^{D109H} mutants may not be intrinsically dysfunctional chaperones, but that they have lost their dynamics within the cellular context with either wild-type HSPB5 or other HSPB members. Therefore, these complexes become trapped with their substrates and no longer serve as entities from which the ATP-dependent chaperones can extract the client proteins.

Unexpectedly, whereas our *in vitro* data confirmed the larger steady state oligomeric sizes and defective chaperone activities of the HSPB5^{R120G} and HSPB5^{D109H} mutants (Figure 4.6),[27,28] they did not reveal a correlation between oligomeric size and function (*in vitro* nor in cells). These experiments also did not reveal a correlation of oligomeric size with the *in vitro* subunit exchange rates of the HSPB5 variants when assayed in isolation. This implies that the functionality of HSPB proteins may not only be related to intrinsic properties of the monomers and their oligomeric behaviours. Rather, they seem to also, and maybe even to a large extent, be determined by interactions that they have within the context of living cells. One such interaction is, obviously, the interaction with wild-type HSPB5 and other HSPB family members with whom they may from homo- or hetero-oligomers. In this context, it is intriguing to note that co-expression of those members of the small heat shock protein family that form hetero-oligomeric complexes with HSPB5 can block the insolubilization of HSPB5^{R120G} (Figure S1).[30] In fact, also *in vitro* mixing of wild-type HSPB5, that by itself shows no light scattering (not shown), completely blocks the light scattering of the large HSPB5^{R120G} oligomers (Figure S6). This

would imply that besides HSPB5-HSPB interactions, also interactions with the cellular client proteins play a role in the eventual complex stability and dynamics which do or do not allow efficient substrate recovery by ATP-dependent chaperones.

Irrespective of the lack of understanding of the main determinants of HSPB5 chaperone function, our data show that preformed aggregates of $HSPB5^{R120G}$ and $HSPB5^{D109H}$ with their client proteins are not unresolvable aggregated material, but can be reversed by a pharmaceutical intervention. Therefore, our data provide a proof-of-concept that interference with IPI-ACD interactions between HSPB5 molecules alters oligomerization dynamics. This has putative therapeutic value as shown before using chemical chaperones for $HSPB5^{R120G}$ related cataract treatment.[44] Since the peptide used in our experiments is very hydrophobic and has a very poor membrane permeability, its clinical applicability is limited and further research is warranted to investigate whether it can be developed into a therapeutic option.

Calcium handing in cardiac muscle cells is central in cell signalling, contractility and regulation of rhythm. Here we used HL-1 cardiomyocytes to also define the impact of HSPB5 mutants on intracellular calcium handling. HL-1 cardiomyocytes share characteristics with human adult cardiomyocytes and have therefore been successfully utilized to study pathomechanisms of human atrial fibrillation[41-43] and for drug screening studies.[45] Previous studies showed that changes in the expression level of HSPs coincide with alterations in intracellular calcium handling and cardiac disease progression. Depletion of HSPB1 decreased CaT amplitudes and changed expression of calsequestrin, a calcium-binding protein which interacts directly with the ryanodine receptor.[46] Comparative proteomics of HSPB1-null mice revealed that absence of HSPB1 mainly impacted proteins involved in Ca^{2+} homeostasis, contraction, energy metabolism and HSPA9.[47] HSP20 directly interacts with protein phosphatase 1 and overexpression of HSP20 resulted in phosphorylation of phospholamban at both Ser16 and Thr17 and thereby enhanced sarcoplasmic reticulum Ca^{2+} cycling.[48] HSPB5 and HSPB2 deficiency in myocardial ischemia in aging mice caused a reduction of Ca^{2+} -dependent metabolism and respiration.[49] Currently, knowledge about the effects of mutant HSP caused by point mutations on calcium handling is limited. Our study shows that the presence of R120G or D109H mutation have an effect on CaT amplitudes (Figure 4.5). Loss of CaT coincides with loss of chaperone activity as demonstrated by overexpression of $HSPB5^{R120G}$ and $HSPB5^{D109H}$ (Figure 4.6). In contrast, overexpression of $HSPB5^{WT}$ and $HSPB5^{S135Q}$ does not affect CaT amplitude and chaperone activity.

Our finding of R120G mutation disturbing/altering calcium handling is in line with literature.[50] *HspB5* R120G transgenic mice showed endoplasmic reticulum (ER) stress and impaired Ca^{2+} regulation, including alterations in the expression of Ca^{2+} -handling proteins, leading to ageing-related cardiac dysfunction and arrhythmias. Especially for the R120G, it seems that the sole presence of the mutation will have an effect on Ca^{2+} handling. Introduction of a second mutation in the hydrophobic groove or IPI domain did not correct perturbed CaT.

So far, nothing is published on how the D109H mutation affects Ca^{2+} handling. Our findings suggest (1) that aggregated $HSPB5^{D109H}$ causes CaT loss and (2) that the location of the secondary mutation in $HSPB5^{D109H}$ determines the protection against CaT loss. While the second mutation in the hydrophobic groove restores the CaT loss, modifying the IPI domain has no rescuing effect on CaT loss. Moreover, 48 h overexpression of $HSPB5^{D109H}$ results in mild alterations of CaT decay which may affect relaxation of cardiomyocytes. Further experiments are required to explain the underlying mechanism for the difference in CaT amplitudes for $HSPB5^{D109H;\ IPI\ mut}$ and $HSPB5^{D109H;\ S135Q}$.

Except for $HSPB5^{D109H;\ S135Q}$, overexpression of mutant HSPB5 results in a reduction of peak CaT. These altered CaTs may impair cardiac function. For instance, reduction of peak CaT in HL-1 cardiomyocytes were accompanied by reduced cell shortening[41] and this diminished cardiac contractility is a characteristic feature of DCM.[51] Mutant HSPB5 may alter cardiomyocyte function via perturbations in Ca^{2+} kinetics, and thereby contribute to depressed contractility and to the development of DCM.[52]

CONCLUSION

This study shows that aggregation of both $HSPB5^{R120G}$ and $HSPB5^{D109H}$ can be reduced by interference with the IPI-ACD interactions between HSPB5 molecules. This decrease in aggregation is accompanied by increased solubilisation, a partial restoration of its chaperone function and in the case $HSPB5^{D109H;\ S135Q}$ a complete protection against CaT loss. Targeting the altered oligomerization dynamics may represent a novel strategy to treat cellular dysfunction in DCM patients carrying $HSPB5^{R120G}$ and $HSPB5^{D109H}$ mutations.

Sources of funding: We acknowledge the support from the Netherlands Cardiovascular Research Initiative: An initiative with support of the Dutch Heart Foundation, CVON2014-40 DOSIS and CVON-STW2016-14728 AFFIP, and Hartedroom funding.

SUPPLEMENTARY FILES - ONLINE

https://drive.google.com/drive/folders/142Qu-xSO28VI2zAZVxI77v0M6fnDZogr

REFERENCES

1. Hershberger RE, Hedges DJ, Morales A. Dilated cardiomyopathy: the complexity of a diverse genetic architecture. *Nat Rev Cardiol*. 2013;10(9):531-47.
2. Walsh R, Thomson KL, Ware JS, Funke BH, Woodley J, McGuire KJ, et al. Reassessment of Mendelian gene pathogenicity using 7,855 cardiomyopathy cases and 60,706 reference samples. *Genet Med*. 2017;19(2):192-203.
3. Selcen D, Muntoni F, Burton BK, Pegoraro E, Sewry C, Bite AV, et al. Mutation in BAG3 causes severe dominant childhood muscular dystrophy. *Ann Neurol*. 2009;65(1):83-9.
4. Norton N, Li D, Rieder MJ, Siegfried JD, Rampersaud E, Zuchner S, et al. Genome-wide studies of copy number variation and exome sequencing identify rare variants in BAG3 as a cause of dilated cardiomyopathy. *Am J Hum Genet*. 2011;88(3):273-82.
5. Ding Y, Long PA, Bos JM, Shih YH, Ma X, Sundsbak RS, et al. A modifier screen identifies DNAJB6 as a cardiomyopathy susceptibility gene. *JCI Insight*. 2017;2(8).
6. Vicart P, Caron A, Guicheney P, Li Z, Prevost MC, Faure A, et al. A missense mutation in the alphaB-crystallin chaperone gene causes a desmin-related myopathy. *Nat Genet*. 1998;20(1):92-5.
7. Sacconi S, Feasson L, Antoine JC, Pecheux C, Bernard R, Cobo AM, et al. A novel CRYAB mutation resulting in multisystemic disease. *Neuromuscul Disord*. 2012;22(1):66-72.
8. Dorsch LM, Schuldt M, Knezevic D, Wiersma M, Kuster DWD, van der Velden J, et al. Untying the knot: protein quality control in inherited cardiomyopathies. *Pflugers Arch*. 2018.
9. van Spaendonck-Zwarts KY, van Hessem L, Jongbloed JD, de Walle HE, Capetanaki Y, van der Kooi AJ, et al. Desmin-related myopathy. *Clin Genet*. 2011;80(4):354-66.
10. Kampinga HH, Garrido C. HSPBs: small proteins with big implications in human disease. *Int J Biochem Cell Biol*. 2012;44(10):1706-10.
11. Golenhofen N, Perng MD, Quinlan RA, Drenckhahn D. Comparison of the small heat shock proteins alphaB-crystallin, MKBP, HSP25, HSP20, and cvHSP in heart and skeletal muscle. *Histochem Cell Biol*. 2004;122(5):415-25.
12. Garrido C, Paul C, Seigneuric R, Kampinga HH. The small heat shock proteins family: the long forgotten chaperones. *Int J Biochem Cell Biol*. 2012;44(10):1588-92.
13. Haslbeck M, Weinkauf S, Buchner J. Small heat shock proteins: Simplicity meets complexity. *J Biol Chem*. 2019;294(6):2121-32.
14. Janowska MK, Baughman HER, Woods CN, Klevit RE. Mechanisms of Small Heat Shock Proteins. *Cold Spring Harb Perspect Biol*. 2019;11(10).
15. Jakob U, Gaestel M, Engel K, Buchner J. Small heat shock proteins are molecular chaperones. *J Biol Chem*. 1993;268(3):1517-20.
16. Ehrnsperger M, Graber S, Gaestel M, Buchner J. Binding of non-native protein to Hsp25 during heat shock creates a reservoir of folding intermediates for reactivation. *EMBO J*. 1997;16(2):221-9.
17. Strauch A, Haslbeck M. The function of small heat-shock proteins and their implication in proteostasis. *Essays Biochem*. 2016;60(2):163-72.
18. Hilton GR, Hochberg GK, Laganowsky A, McGinnigle SI, Baldwin AJ, Benesch JL. C-terminal interactions mediate the quaternary dynamics of alphaB-crystallin. *Philos Trans R Soc Lond B Biol Sci*. 2013;368(1617):20110405.
19. Hochberg GKA, Shepherd DA, Marklund EG, Santhanagoplan I, Degiacomi MT, Laganowsky A, et al. Structural principles that enable oligomeric small heat-shock protein paralogs to evolve distinct functions. *Science*. 2018;359(6378):930-5.
20. Arrigo AP, Gibert B. Protein interactomes of three stress inducible small heat shock proteins: HspB1, HspB5 and HspB8. *Int J Hyperthermia*. 2013;29(5):409-22.
21. Delbecq SP, Klevit RE. HSPB5 engages multiple states of a destabilized client to enhance chaperone activity in a stress-dependent manner. *J Biol Chem*. 2019;294(9):3261-70.
22. Delbecq SP, Klevit RE. One size does not fit all: the oligomeric states of alphaB crystallin. *FEBS Lett*. 2013;587(8):1073-80.
23. Delbecq SP, Jehle S, Klevit R. Binding determinants of the small heat shock protein, alphaB-crystallin: recognition of the 'IxI' motif. *EMBO J*. 2012;31(24):4587-94.
24. Preis W, Bestehorn A, Buchner J, Haslbeck M. An alternative splice variant of human alphaA-crystallin modulates the oligomer ensemble and the chaperone activity of alpha-crystallins. *Cell Stress Chaperones*. 2017;22(4):541-52.
25. Pasta SY, Raman B, Ramakrishna T, Rao Ch M. The IXI/V motif in the C-terminal extension of alpha-crystallins: alternative interactions and oligomeric assemblies. *Mol Vis*. 2004;10:655-62.
26. Kumar LV, Ramakrishna T, Rao CM. Structural and functional consequences of the mutation of a conserved arginine residue in alphaA and alphaB crystallins. *J Biol Chem*. 1999;274(34):24137-41.
27. Bova MP, Yaron O, Huang Q, Ding L, Haley DA, Stewart PL, et al. Mutation R120G in alphaB-crystallin, which is linked to a desmin-related myopathy, results in an irregular structure and defective chaperone-like function. *Proc Natl Acad Sci U S A*. 1999;96(11):6137-42.
28. Clark AR, Naylor CE, Bagneris C, Keep NH, Slingsby C. Crystal structure of R120G disease mutant of human alphaB-crystallin domain dimer shows closure of a groove. *J Mol Biol*. 2011;408(1):118-34.

29. Jehle S, Vollmar BS, Bardiaux B, Dove KK, Rajagopal P, Gonen T, et al. N-terminal domain of alphaB-crystallin provides a conformational switch for multimerization and structural heterogeneity. *Proc Natl Acad Sci U S A*. 2011;108(16):6409-14.
30. Hussein RM, Benjamin IJ, Kampinga HH. Rescue of alphaB Crystallin (HSPB5) Mutants Associated Protein Aggregation by Co-Expression of HSPB5 Partners. *PLoS One*. 2015;10(5):e0126761.
31. Raju I, Abraham EC. Mutants of human alphaB-crystallin cause enhanced protein aggregation and apoptosis in mammalian cells: influence of co-expression of HspB1. *Biochem Biophys Res Commun*. 2013;430(1):107-12.
32. Chavez Zobel AT, Loranger A, Marceau N, Theriault JR, Lambert H, Landry J. Distinct chaperone mechanisms can delay the formation of aggresomes by the myopathy-causing R120G alphaB-crystallin mutant. *Hum Mol Genet*. 2003;12(13):1609-20.
33. Gupta R, Kasturi P, Bracher A, Loew C, Zheng M, Villella A, et al. Firefly luciferase mutants as sensors of proteome stress. *Nat Methods*. 2011;8(10):879-84.
34. Hageman J, Rujano MA, van Waarde MA, Kakkar V, Dirks RP, Govorukhina N, et al. A DNAJB chaperone subfamily with HDAC-dependent activities suppresses toxic protein aggregation. *Mol Cell*. 2010;37(3):355-69.
35. Vos MJ, Zijlstra MP, Kanon B, van Waarde-Verhagen MA, Brunt ER, Oosterveld-Hut HM, et al. HSPB7 is the most potent polyQ aggregation suppressor within the HSPB family of molecular chaperones. *Hum Mol Genet*. 2010;19(23):4677-93.
36. Vos MJ, Kanon B, Kampinga HH. HSPB7 is a SC35 speckle resident small heat shock protein. *Biochim Biophys Acta*. 2009;1793(8):1343-53.
37. Jehle S, van Rossum B, Stout JR, Noguchi SM, Falber K, Rehbein K, et al. alphaB-crystallin: a hybrid solid-state/solution-state NMR investigation reveals structural aspects of the heterogeneous oligomer. *J Mol Biol*. 2009;385(5):1481-97.
38. Clouser AF, Klevit RE. pH-dependent structural modulation is conserved in the human small heat shock protein HSBP1. *Cell Stress Chaperones*. 2017;22(4):569-75.
39. Paredes RM, Etzler JC, Watts LT, Zheng W, Lechleiter JD. Chemical calcium indicators. *Methods*. 2008;46(3):143-51.
40. Claycomb WC, Lanson NA, Jr., Stallworth BS, Egeland DB, Delcarpio JB, Bahinski A, et al. HL-1 cells: a cardiac muscle cell line that contracts and retains phenotypic characteristics of the adult cardiomyocyte. *Proc Natl Acad Sci U S A*. 1998;95(6):2979-84.
41. Brundel BJ, Shiroshita-Takeshita A, Qi X, Yeh YH, Chartier D, van Gelder IC, et al. Induction of heat shock response protects the heart against atrial fibrillation. *Circ Res*. 2006;99(12):1394-402.
42. Zhang D, Hu X, Li J, Liu J, Baks-Te Bulte L, Wiersma M, et al. DNA damage-induced PARP1 activation confers cardiomyocyte dysfunction through NAD(+) depletion in experimental atrial fibrillation. *Nat Commun*. 2019;10(1):1307.
43. Qi XY, Diness JG, Brundel BJ, Zhou XB, Naud P, Wu CT, et al. Role of small-conductance calcium-activated potassium channels in atrial electrophysiology and fibrillation in the dog. *Circulation*. 2014;129(4):430-40.
44. Makley LN, McMenimen KA, DeVree BT, Goldman JW, McGlasson BN, Rajagopal P, et al. Pharmacological chaperone for alpha-crystallin partially restores transparency in cataract models. *Science*. 2015;350(6261):674-7.
45. van Marion DM, Hu X, Zhang D, Hoogstra-Berends F, Seerden JG, Loen L, et al. Screening of novel HSP-inducing compounds to conserve cardiomyocyte function in experimental atrial fibrillation. *Drug Des Devel Ther*. 2019;13:345-64.
46. Das T, Yoo YS, Rhim H, Song EJ. Potential role of Hsp25 in calcium-modulated cardiomyocytes. *Proteomics*. 2012;12(3):411-20.
47. Picard B, Kammoun M, Gagaoua M, Barboiron C, Meunier B, Chambon C, et al. Calcium Homeostasis and Muscle Energy Metabolism Are Modified in HspB1-Null Mice. *Proteomes*. 2016;4(2).
48. Qian J, Vafiadaki E, Florea SM, Singh VP, Song W, Lam CK, et al. Small heat shock protein 20 interacts with protein phosphatase-1 and enhances sarcoplasmic reticulum calcium cycling. *Circ Res*. 2011;108(12):1429-38.
49. Benjamin IJ, Guo Y, Srinivasan S, Boudina S, Taylor RP, Rajasekaran NS, et al. CRYAB and HSPB2 deficiency alters cardiac metabolism and paradoxically confers protection against myocardial ischemia in aging mice. *Am J Physiol Heart Circ Physiol*. 2007;293(5):H3201-9.
50. Jiao Q, Sanbe A, Zhang X, Liu JP, Minamisawa S. alphaB-Crystallin R120G variant causes cardiac arrhythmias and alterations in the expression of Ca(2+) -handling proteins and endoplasmic reticulum stress in mice. *Clin Exp Pharmacol Physiol*. 2014;41(8):589-99.
51. Maron BJ, Towbin JA, Thiene G, Antzelevitch C, Corrado D, Arnett D, et al. Contemporary definitions and classification of the cardiomyopathies: an American Heart Association Scientific Statement from the Council on Clinical Cardiology, Heart Failure and Transplantation Committee; Quality of Care and Outcomes Research and Functional Genomics and Translational Biology Interdisciplinary Working Groups; and Council on Epidemiology and Prevention. *Circulation*. 2006;113(14):1807-16.
52. Burke MA, Cook SA, Seidman JG, Seidman CE. Clinical and Mechanistic Insights Into the Genetics of Cardiomyopathy. *J Am Coll Cardiol*. 2016;68(25):2871-86.

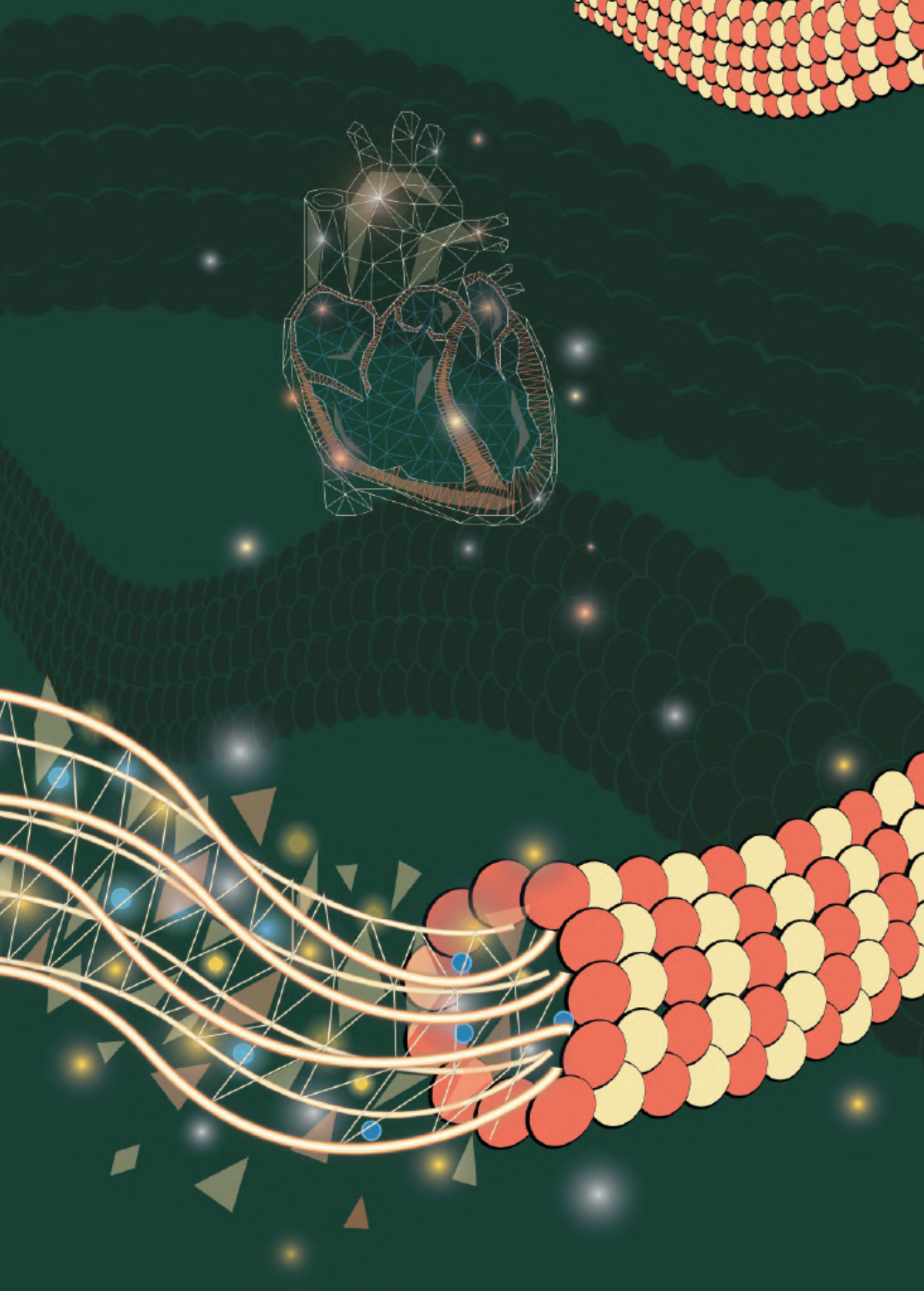

Chapter 5

Oral geranylgeranylacetone treatment increases heat shock protein expression in human atrial tissue

Denise MS. van Marion, **Larissa M. Dorsch**, Femke Hoogstra-Berends, Tea Kakuchaya, Leo Bockeria, Natasja MS. de Groot, Bianca JJM. Brundel

Heart Rhythm 17(1):115-122 (2020).

ABSTRACT

BACKGROUND

Heat shock proteins (HSPs) are important chaperones which regulate the maintenance of a healthy protein quality control in the cell. Impairment of HSPs is associated with ageing-related neurodegenerative and cardiac diseases. A well-known compound to increase HSPs, through the activation of heat shock factor-1 (HSF1), is geranylgeranylacetone (GGA). GGA increases HSPs in various tissues, but so far, it is unknown whether GGA can increase HSP expression in human heart tissue.

OBJECTIVE

Test whether oral GGA treatment increases HSP expression in atrial appendages of patients undergoing cardiac surgery.

METHODS

HSPB1, HSPA1, HSPD1, HSPA5, HSF1 and phosphorylated HSF1 levels were measured by Western blot analysis in right and left atrial appendages (RAAs and LAAs, respectively) collected from patients undergoing coronary artery bypass grafting (CABG) who were treated with placebo (n=13) or GGA 400 mg/day (n=13) 3 days before surgery. Myofilament fractions were isolated from LAAs to determine the level of HSPB1 and HSPA1 present in these fractions.

RESULTS

GGA treatment significantly increased HSPB1 and HSPA1 expression levels in RAA and LAA compared to the placebo group, while HSF1, phosphorylated HSF1, HSPD1 and HSPA5 were unchanged. In addition, GGA treatment significantly enhanced HSPB1 levels at the myofilaments compared to placebo.

CONCLUSION

Three days of GGA treatment is associated with higher HSPB1 and HSPA1 expression levels in RAA and LAA of patients undergoing CABG surgery and higher HSPB1 levels at the myofilaments. These findings pave the way to study the role of GGA as a protective compound against other cardiac diseases, including postoperative AF.

INTRODUCTION

Proteostasis, the balance in protein synthesis, folding, assembly, trafficking and clearance by protein degradation systems, is controlled by the protein quality control (PQC) system.[1] The PQC is an exquisitely regulated network in which the most important chaperones, heat shock proteins (HSPs), play a crucial role. In response to changes in the intra- and extracellular environment cells upregulate HSPs to maintain proteostasis. HSPs guide protein folding of nascent proteins, stabilize misfolded proteins, prevent protein aggregation, guide protein refolding and facilitate degradation of unwanted and damaged proteins.[1]
HSPs consist of five HSP families: HSPA (HSP70), HSPB (small HSPs), HSPC (HSP90), HSPD (HSP60), and DnaJB (HSP40), each with several family members and (specific) co-factors in various cellular localizations, with distinct and overlapping functions.[1] Previous studies reveal that especially HSPBs are abundant in cardiomyocytes and that they safeguard a balanced proteostasis in cardiomyocytes.[2] HSPBs interact with contractile and microtubule proteins, thereby stabilizing the cardiomyocyte structure, and conserving the contractile and electrophysiological function of the cardiomyocytes.[3-5] Upon cellular stress, such as heat shock, hypoxia, oxidative stress, inflammation and ischemia, the heat shock response (HSR) is stimulated by activation of heat shock transcription factors (HSF). HSF1 is the major regulator of HSP transcription in eukaryotes.[6] Upon phosphorylation, the activated HSF1 translocates to the nucleus, and binds to the heat shock elements in *hsp* genes, thereby resulting in the transcription and expression of HSPs[7] to maintain proteostasis. However, HSP levels decline with age and long term stress leading to a derailment in proteostasis by altered stability of proteins and accumulation of protein damage, unfolding and breakdown.[1,8] Therefore, impairment of tissue HSP levels is associated with ageing-related misfolded protein diseases such as Parkinson's, Huntington's, and Alzheimer's disease, as well as cardiac diseases, including AF and myocardial infarction.[1] It is because of the central role of HSPs in PQC that pharmacological modulation of HSP levels represents an interesting target to treat ageing-related diseases.

A well-known compound to induce HSPs levels, via activation of the heat shock transcription factor-1 (HSF1), is geranylgeranylacetone (GGA).[9] This nontoxic acyclic isoprenoid compound is since 1984 clinically applied as an anti-ulcer drug in Asian countries.[10,11] Since then, GGA has been examined in numerous disease models in animals, where it was found to induce HSPs in various tissues, including gastric mucosa, intestine, liver, peritoneum, kidney, retina, central nervous system, skeletal muscle and the myocardium.[9,12-14] Moreover, pharmacologically induction of HSPs with GGA revealed pleiotropic protective effects by attenuating electrical as well as structural changes in experimental models for heart failure, myocardial infarction, desmin-related cardiomyopathy and AF.[4,8,15-19] Therefore, GGA may also represent a protective agent in human heart diseases, but so far it is unknown whether GGA can increase HSP expression in human heart tissue. In the current study, we tested whether oral GGA treatment can increase HSF1-mediated HSP expression in atrial appendages of patients undergoing cardiac surgery.

METHODS

STUDY POPULATION

Patients scheduled for coronary artery bypass grafting (CABG) surgery received GGA (Selbex®, Teprenone Eisai Japan) (GGA) (n=13) or placebo (n=13) for 3 days before and 3 days after on-pump CABG in a dosage of 400 mg per day. Patients selected for this study did not have a history of AF, confirmed by Holter monitoring and high-resolution ECG to measure signal-averaged P-wave duration (cut off point of >150 ms for AF indication). Both patients and physicians were blinded for the treatment. Patients were recruited at the A.N. Bakulev National Medical Research Center of Cardiovascular Surgery in Moscow, Russia. The study was approved by the Institutional Committee on Human Research (MEC Bakulev 12-029/12323). Prior to study enrolment, each patient is provided an oral and written explanation of the study procedure and written informed consent is obtained from all patients. The study was carried out according to the principals of the Declaration of Helsinki. Clinical data from the patients were obtained from electronic patient files.

SAMPLING

Tissue samples of RAA and LAA were collected just before aortic cross-clamping, snap frozen in liquid nitrogen and stored at -80°C.

WHOLE PROTEIN ISOLATION

Part of the frozen tissue was homogenized on ice with SDS sample buffer (10% (w/v) SDS, 50% (v/v) glycerol, 0.33 M Tris–HCl pH 6.8, 10% (v/v) β-mercaptoethanol, 0.05% (w/v) bromophenol blue and protease and phosphatase inhibitors) using an Ultra-Turrax. The lysates were centrifuged, supernatant was collected, passed through an insulin syringe and boiled for 6 min.

MYOFILAMENT FRACTIONATION

Part of the frozen tissue was dissected in F60 buffer (0.447% (w/v) KCl, 0.204% (w/v) Imidazole and 0.041% (w/v) $MgCl_2 \cdot 6H_2O$) containing protease and phosphatase inhibitors. Supernatant containing cell debris was discarded. A precooled metal homogenizer bead was placed in the sample tubes and 2 cycles of (a) adding cold F60 buffer including 1% triton, (b) homogenization in the Qiagen Tissuelyser II for 3 min at maximum speed, (c) centrifugation at 14,000×g (10 min at 4°C) and (d) removal of the supernatant (soluble fraction) were performed. Subsequently the pellet was homogenized in RIPA buffer (R0278, Merck, USA). Supernatant was collected obtaining the myofilament fraction, which was mixed with 4x NuPage Buffer (6.68% (w/v) Tris-HCl, 6.84% (w/v) Tris base, 8% (w/v) lithium dodecyl sulphate, 40% (v/v) glycerol, 0.060% (w/v) EDTA, 0.075% (w/v) Serva Blue G250, 0.025% (w/v) phenol red) and 10% (w/v) Dithiothreitol.

WESTERN BLOT ANALYSIS

Equal amounts of protein were analysed by Western blot analysis as described in detail in the Supplementary Information and Supplementary Information Table S1.

STATISTICAL ANALYSIS

A detailed description of the statistical analysis can be found in the Supplementary Information.

RESULTS

STUDY POPULATION

The study population consisted of 26 CABG patients, of whom 13 were treated with placebo and 13 with GGA. All of them received beta-blockers before surgery. All patients had normal resting heart rate between 65-70 beats per min, normal cardiac output, with normal left ventricular ejection fraction between 59-60%. Baseline characteristics of the study population are summarized in Table 5.1.

Table 5.1: Clinical characteristics.

Treatment	Patient number	Age (years)	Gender	Multifocal atherosclerosis	LVEF (%)	Anterior-posterior LA size (cm)	NYHA or CCS class	Number of CABG conduits	poAF
Placebo	1	58	Male	Yes	60	4,3	II	3	No
	2	46	Male	No	58	4,3	II	3	No
	3	54	Male	Yes	59	5,5	II	2	Yes(*)
	4	62	Male	Yes	65	3,9	II	1	No
	5	53	Female	Yes	60	4,1	II	2	No
	6	46	Male	No	58	4,0	II	3	No
	7	48	Male	No	59	3,7	II	2	No
	8	59	Male	Yes	56	4,2	II	2	No
	9	57	Male	No	60	4,9	II	3	No
	10	48	Male	Yes	60	4,4	II	3	No
	11	41	Female	No	63	4,7	II	2	No
	12	59	Male	Yes	60	4,7	II	1	No
	13	50	Male	No	58	4,5	II	2	No
GGA	1	61	Male	Yes	56	4,5	II	3	No
	2	60	Male	Yes	60	5,3	III	2	Yes(*)
	3	50	Male	No	59	4,2	II	3	No
	4	45	Male	Yes	56	4,0	III	2	No
	5	50	Male	Yes	60	4,2	II	3	No
	6	56	Male	No	60	4,0	II	3	No
	7	53	Male	Yes	62	4,0	II	2	No
	8	42	Male	Yes	56	4,4	III	2	No
	9	55	Male	Yes	57	4,3	III	3	No
	10	51	Male	No	58	4,4	III	3	No
	11	63	Male	Yes	60	4,9	II	3	No
	12	50	Male	Yes	60	4,2	II	3	No

Table 5.1: Continued

Treatment	Patient number	Age (years)	Gender	Multifocal atherosclerosis	LVEF (%)	Anterior-posterior LA size (cm)	NYHA or CCS class	Number of CABG conduits	poAF
	13	50	Male	Yes	55	4,5	III	2	No

NYHA - New York Heart Association; CCS - The Canadian Cardiovascular Society grading scale for angina; LVEF - left ventricular ejection fraction. (*) Tachy-form of AF developed at second day after surgery with heart rate 180-190 per min, which lasted for 8-12 h and was eliminated after amiodarone infusion.

There was no difference in age (placebo 53 [47 – 59] vs GGA 51 [50 – 58] years, p=0.797), gender (placebo 11 (84.6%) male vs GGA 13 (100%) male, p=0.480), multifocal atherosclerosis (placebo 7 (53.8%) vs GGA 10 (76.9%), p=0.411), left ventricular ejection fraction (LVEF) (placebo 59.7 $\pm$ 2.29 vs GGA 58.4 $\pm$ 2.18, p=0.149) and left atrial size (placebo: 4.40 $\pm$ 0.474, GGA: 4.38 $\pm$ 0.375, p=0.892), yet left atrial enlargement is correlated with increased risk of poAF (cut-off value >5.0 cm) (p<0.001). All patients in the placebo group have a NYHA class II, while for the GGA group there are 7 (53.8%) patients with NYHA class II and 6 (46.2%) with class III (p=0.015). In total, two patients, one in the placebo and one in the GGA group developed poAF. Both patients revealed enlarged LA (cut-off value >5.0 cm), which significantly correlates with poAF (p<0.001).

GGA INDUCES HSPB1 AND HSPA1 EXPRESSION IN ATRIAL TISSUE

To study whether GGA increases the expression of HSF1 related HSPs, HSPA1, HSPB1, HSPD1, HSF1 and phosphorylated HSF1 levels were measured in the atrial appendages. Expression of HSPA5, which is not HSF1 related, was determined as a negative control. GGA significantly induced HSPB1 and HSPA1 levels compared to the placebo (p=0.019 and p=0.021, respectively) (Figures 5.1A-B). Similar levels for HSPD1, a mitochondrial HSP, and HSPA5, were observed in both the placebo and GGA treated group (Figures 5.1C-D). HSF1 and phosphorylated HSF1 levels were measured to test whether the HSP-inducing effect is via HSF1 activation. GGA did not increase protein expression levels of HSF1 and pHSF1 (Figures 5.1E-F). Lower HSPD1 levels correlated with larger LA size (p<0.01), higher HSF1 levels correlated with larger LA size (p<0.05) and higher HSPA1 levels correlated with lower LVEF (p<0.05) (Supplementary Information Table S2).

GGA ENHANCES HSPB1 LEVELS AT THE MYOFILAMENTS

While HSPA1 reveals its protective actions mainly in the cytosol,[8] HSPB1 (co)-localizes with myofilament proteins, including α-actinin, actin and myosin, to stabilize the myofilaments and/or shielding the contractile proteins from cleavage by cysteine proteases, such as calpain.[8,19-20] Both HSPB1 and HSPA1 levels were higher in RAA and LAA of patients treated with GGA in the RAA and LAA with the effect more clearly observed in LAA for HSPB1 (p<0.05) (Figure 5.2).

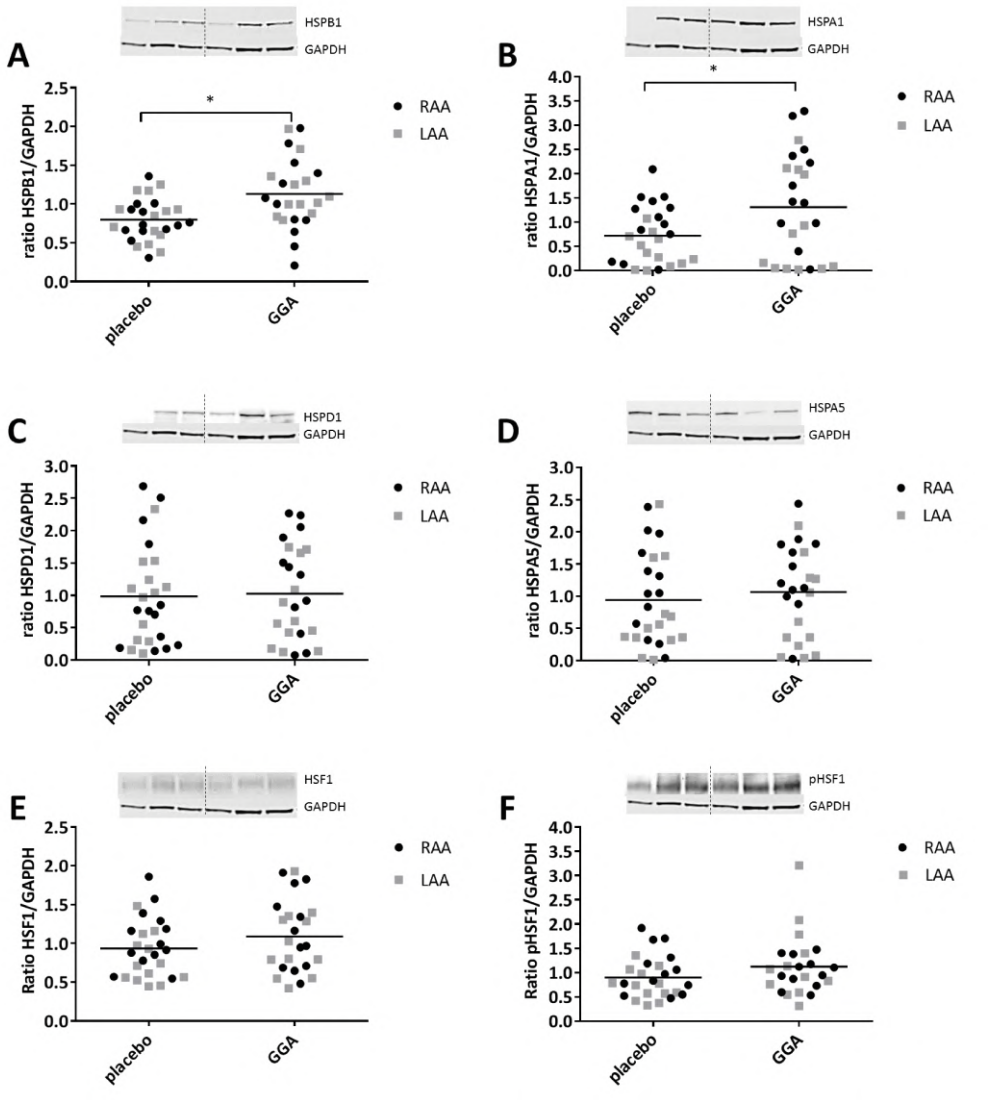

Figure 5.1: GGA increases HSF1-mediated HSP expression in atrial appendages of patients undergoing CABG surgery. Representative Western blots (left 3 lanes placebo, right 3 lanes GGA treated) and quantified Western blot results for HSPB1 (**A**), HSPA1 (**B**), HSPD1 (**C**), HSPA5 (**D**), HSF1 (**E**) and phosphorylated HSF1 (**F**) relative to GAPDH in LAA and RAA of patients treated with placebo or GGA. * is $p<0.05$ compared to placebo.

To investigate whether the GGA-induced increase in HSPB1 and HSPA1 results in enhanced co-localization at the myofilaments in human heart tissue, myofilament fractions were isolated from LAAs and utilized for Western blot analysis. Interestingly, GGA significantly enhanced HSPB1 levels (p=0.042), but not HSPA1 levels (p=0.851), at the myofilaments compared to placebo (Figure 5.3).

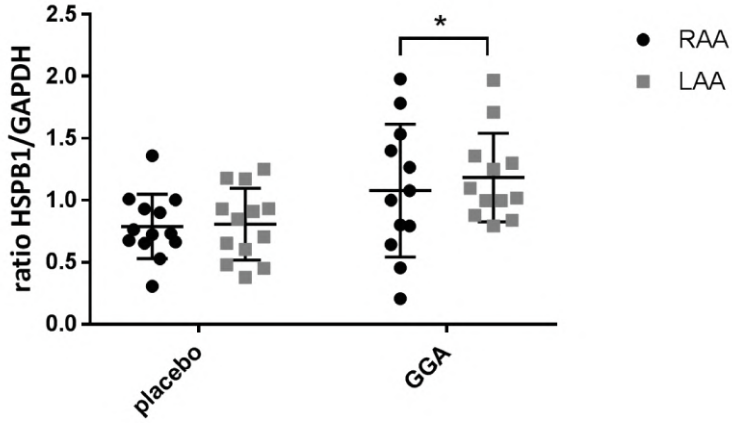

Figure 5.2: GGA enhances HSPB1 more in LAA than RAA.
Quantified Western blot results for HSPB1 in RAA and LAA of patients treated with placebo and GGA. * is $p<0.05$ compared to placebo.

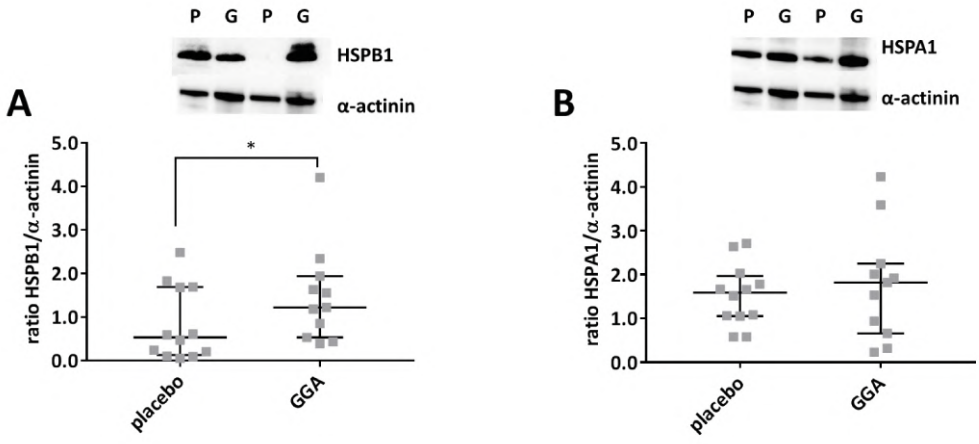

Figure 5.3: GGA enhances HSPB1 and not HSPA1 levels at the myofilaments compared to placebo. Quantified Western blot results for (**A**) HSPB1 and (**B**) HSPA1 relative to α-actinin in LAA of patients treated with placebo (P) and GGA (G). * is $p<0.05$ compared to placebo.

DISCUSSION

Preclinical studies showed HSF1-mediated HSP induction by GGA treatment and subsequent protection against various cardiac diseases.[4,8,15-19] With this study we aimed to obtain proof of concept for oral GGA treatment to increase HSP levels in human heart tissue. HSPB1, HSPA1, HSPD1, HSPA5, HSF1 and phosphorylated HSF1 levels were measured by Western blot analysis in RAAs and LAAs collected from patients undergoing CABG surgery who were treated with placebo or GGA (400 mg/day for 3 days). GGA treatment associated

with higher HSPB1 and HSPA1 levels, which are both HSF1 regulated, while it did not have an effect on mitochondrial HSPD1 and endoplasmic reticulum HSPA5, latest is not HSF1 regulated. HSF1 and, the activated form of HSF1, phosphorylated HSF1, were both unchanged. Previous studies showed HSPB1 to protect against cardiac diseases by (co)-localization to the myofilaments, thereby safeguarding cardiomyocytes from protein damage and derailment of proteostasis by stabilizing the contractile apparatus.[8,19-20] By utilizing isolated myofilaments, we were able to show that HSPB1, but not HSPA1 levels, were enhanced at the myofilaments by GGA treatment, in contrast to the placebo treated atrial tissue samples. Taken together, these data indicate for the first time, that three days of GGA treatment (400 mg/day) associated with higher HSPB1 and HSPA1 expression levels in atrial tissue samples of patients undergoing CABG surgery and increased localization of HSPB1 levels specifically at the myofilaments. These findings pave the way to study the role of GGA as a protective compound in cardiac diseases, including (po)AF.

INCREASED HSPA1 AND HSPB1 LEVELS IN HEART TISSUE BY GGA

The observed increase in HSPB1 and HSPA1 expression levels in human atrial tissue is in line with the effect of GGA in preclinical studies. In rabbits, oral GGA treatment increased HSPA1 expression in the heart (LA), which was associated with protection against HF-induced electrical and structural remodelling.[15] Rats showed enhanced recovery after ischemia reperfusion injury when treated with GGA (oral 200 mg/kg). In the GGA treated rats, HSPA1 expression was increased and thereby preserved the structure of the cardiomyocytes, compared to controls.[16] In a myocardial infarction model in rats, oral GGA treatment increased HSPB1 and HSPB8 levels, resulting in preserved mitochondrial and cardiac pump function.[17] Also, oral GGA treatment in HSPB5 R120G transgenic mice, a model for desmin-related cardiomyopathy, improved cardiac function and increased survival via HSPB1 and HSPB8 upregulation.[18] Furthermore, GGA's protective effects have been extensively studied in various experimental models for AF, including tachypaced HL-1 cardiomyocytes, *Drosophila melanogaster* and dogs, where GGA treatment increased HSPB1 levels and protected against structural and electrical remodelling and conserved contractile function upon tachypacing.[4,8,19,21] The observed increase in HSPB1 and HSPA1 expression levels in human atrial tissue, revealed a more pronounced effect in LAA versus RAA. This is in line with previous studies showing enhanced structural remodelling in LAA compared to RAA and suggests an increased stress response in LAA.[22]

Although no dose response and pharmacokinetic studies were conducted in the dog model for AF, an oral dosage of 4 gr/day was used to reveal a protective effect against AF progression.[4,21] The registered clinical dose for treating gastic ulcers in Japan is 150 mg GGA per day, revealing a maximal concentration of 2.1 µg/mL GGA in serum at 5 h after administration. In the current study, three days of oral treatment with 400 mg GGA was sufficient to increase HSPB1 and HSPA1 levels in human atria. So far, it is unknown whether this clinical dose will suffice protection of the heart from developing poAF. In both the placebo and GGA treated groups, one patient developed poAF, and these patients revealed LA size of $>$5 cm and average HSPA1 and HSPB1 levels, suggesting the atrial dilation was the cause of poAF onset. Future studies in larger patient groups should elucidate whether three days treatment with 400 mg GGA suffices protection against development of poAF.

ENHANCED HSPB1 LEVELS AT THE MYOFILAMENTS UPON GGA TREATMENT

Previously, preclinical studies showed that the protective action of GGA against contractile dysfunction is critically dependent on the induction of HSPB1, as knockdown of HSPB1 abrogated the protective effect.[4,9] The current study revealed that GGA treatment associated with higher HSPB1 levels at the myofilaments in human atrial tissue. This suggests that HSPB1, (re-)localizes to the myofilaments, thereby shielding the contractile machinery during stress.[8,19-20] This is in line with experimental studies in rats where HSPB1 binds to cytoskeletal, structural and contractile proteins to conserve proteostasis and thereby contractile function.[23-25] We recently observed that GGA-induced HSPB1 expression also restores contractile function an experimental model for AF recovery,[9] indicating that, next to prevention of damage, HSPB1 also aids in the recovery from contractile protein damage. With this proof of concept for GGA to increase HSPs in human atrial tissue, the next logical step is to investigate in larger study populations, whether GGA protects against cardiac diseases, including AF, heart failure, myocardial infarction and cardiomyopathy. Monitoring HSP levels before and, periodically, after GGA treatment in serum/plasma could facilitate in predicting treatment outcome and possible (progression of) the disease.

POSSIBLE MECHANISMS OF GGA TO INCREASE HSP EXPRESSION

The exact mode of action of HSP induction by GGA in unknown. GGA is thought to act via HSF1-activation. Although we did not observe an increase in (p)HSF1 by GGA treatment in the current study, this can be attributed to (p)HSF1's early and temporary activation upon stress.[9] Recently, we observed that a GGA-derivative enhances hyperphosphorylation of HSF1, resulting in prolonged binding of HSF1 to the heat shock element (HSE) in the promotor regions of *hsp* genes, thereby prolonging *hsp* gene transcription and HSP protein expression.[9] GGA is expected to work on a similar mechanism.

Next to enhanced phosphorylation of HSF1 by GGA, GGA is described to bind the C-terminus of HSPA1 *in vitro*, thereby dissociating HSPA1 from HSF1, which are bound in non-stressed situations in the cytosol. Free HSF1 can become phosphorylated, resulting in translocalization to the nucleus and binding to the HSE within the promotor regions of *hsp* genes.[26] As an alternative mechanism, we previously observed that active RhoA abrogates HSF1 transcriptional activity by suppressing HSF1 binding to the HSE of *hsp* genes.[27] Activation of RhoA is regulated by natural occurring prenylation. Prenylation, the addition of C15 (farnesyl) or C20 (geranylgeranyl) isoprenoids to proteins, acts as posttranslational modifiers of proteins and thereby regulate protein function.[28] GGA may compete with endogenous geranyl groups, thereby resulting in the inhibition of RhoA activation, and consequently enhancing binding of HSF1 to the HSE region.[29] As such, GGA may enhance HSF1-mediated HSP induction via inhibition of RhoA activation. However, this mode of action of GGA should be further explored by genetic ablation, competition and enhanced binding experiments to elucidate the mechanism of action.

POTENTIAL PROTECTIVE ROLE FOR HSP INDUCTION IN AF

Various studies in human atrial tissue revealed that induction of HSPA1 and HSPB1 expression may have cardioprotective effects against AF. Higher HSPA1 expression levels in atrial tissue related to a lower incidence of poAF.[30-31] In the current study we showed that GGA treatment associated with higher expression levels of HSPA1 and HSPB1 in human atria and therefore it is of interest to further explore the effect of GGA in the prevention of poAF.

A possible protective role for HSPB1 in patients was previously indicated by two independent studies that report on elevated HSPB1 expression levels in atrial tissue from patients with short duration of AF and low level of atrial structural changes, including degradation of sarcomeres.[8,32] In addition, elevated HSPB1 levels were found in patients with paroxysmal AF, while patients with persistent AF revealed lower levels of HSPB1, suggesting that the HSP response gets activated upon short duration of AF, while it becomes exhausted with longer duration of AF. Possibly, lower levels of HSPB1 may indicate derailment of proteostasis, in turn leading to progression of structural changes and persistence of AF. Thus, securing HSP(B) levels at an adequate level with GGA treatment may thus limit the induction and progression of AF.

GGA IN CLINICAL PERSPECTIVE

Several experimental studies already indicate a potential beneficial role for HSP induction via GGA in the prevention cardiac diseases, including AF, heart failure, ischemia reperfusion injury, myocardial infarction and desmin-related cardiomyopathy.[4,8,15-19] As GGA is marketed in various Asian countries for decades, well tolerated and with a solid safety profile,[33] GGA is a viable approach to treat various cardiac diseases. Future studies including larger study populations may reveal possible associations between HSP(B1) levels and demographic and clinical parameters, including NYHA class, atrial pressure, cardiac output and atrial interstitial fibrosis levels. In the current study, lower HSPD1 levels correlated with larger LA size, higher HSF1 levels correlated with larger LA size and higher HSPA1 levels correlated with lower LVEF, which can be explained by a larger stress response and thus increased HSF1 and HSPA1 levels in these patients. Since the size of the current patient groups was small, further studies are warranted to study the relation between HSPs and LA size and LVEF.

Particularly, it would be of interest to study the effect of GGA in reducing the incidence of poAF, since poAF affects 20-40% of the patients undergoing CABG surgery,[34] with an even higher prevalence for patients undergoing valve surgery, either alone or in combination with CABG.[35] Also, GGA may enhance successful recovery of heart function after elective electrical cardioversion of patients with paroxysmal and/or persistent AF. If successful, this approach may ultimately result in reduced hospital time, increased quality of life for the patient and lower costs for the society.

Since most patients with cardiac disease reveal cardiomyocyte remodelling at the moment of diagnosis, compounds that reverse cardiomyocyte remodelling are clinically

highly relevant. In a recent study, GGA and GGA-derivatives were shown both to prevent and also reverse contractile dysfunction in experimental models for AF.[9] As such, this study substantiates previous findings that GGA treatment has high potential as a novel approach to prevent and reverse cardiac diseases, including AF.

CONCLUSION

Three days of GGA treatment associated with higher HSPB1 and HSPA1 expression levels in RAA and LAA of patients undergoing CABG surgery and enhances HSPB1 levels at the myofilaments. These findings pave the way to further study GGA for its protective effects against cardiac diseases in larger study populations.

Source of funding: The current study has been supported by the LSH-Impulse grant (40-43100-98-008), the Dutch Heart Foundation (2013T144 and 2013T096) and CVON-STW2016-14728 AFFIP.

ACKNOWLEDGEMENTS

We are grateful to all participating patients. Many thanks to the staff and personnel of the A.N. Bakulev National Medical Research Center of Cardiovascular Surgery in Moscow for their participation in this study. Thanks to Mieke van Schaik for performing one of the Western blot experiments.

SUPPLEMENTARY FILES - ONLINE

https://www.sciencedirect.com/science/article/pii/S1547527119306423?via%3Dihub#appsec1

REFERENCES

1. Henning RH, Brundel B. Proteostasis in cardiac health and disease. *Nat Rev Cardiol*. 2017;14(11):637-53.
2. Golenhofen N, Perng MD, Quinlan RA, Drenckhahn D. Comparison of the small heat shock proteins alphaB-crystallin, MKBP, HSP25, HSP20, and cvHSP in heart and skeletal muscle. *Histochem Cell Biol*. 2004;122(5):415-25.
3. Kotter S, Unger A, Hamdani N, Lang P, Vorgerd M, Nagel-Steger L, et al. Human myocytes are protected from titin aggregation-induced stiffening by small heat shock proteins. *J Cell Biol*. 2014;204(2):187-202.
4. Brundel BJ, Shiroshita-Takeshita A, Qi X, Yeh YH, Chartier D, van Gelder IC, et al. Induction of heat shock response protects the heart against atrial fibrillation. *Circ Res*. 2006;99(12):1394-402.
5. Ghosh JG, Houck SA, Clark JI. Interactive domains in the molecular chaperone human alphaB crystallin modulate microtubule assembly and disassembly. *PLoS One*. 2007;2(6):e498.
6. Baler R, Dahl G, Voellmy R. Activation of human heat shock genes is accompanied by oligomerization, modification, and rapid translocation of heat shock transcription factor HSF1. *Mol Cell Biol*. 1993;13(4):2486-96.
7. Benjamin IJ, McMillan DR. Stress (heat shock) proteins: molecular chaperones in cardiovascular biology and disease. *Circ Res*. 1998;83(2):117-32.
8. Brundel BJ, Henning RH, Ke L, van Gelder IC, Crijns HJ, Kampinga HH. Heat shock protein upregulation protects against pacing-induced myolysis in HL-1 atrial myocytes and in human atrial fibrillation. *J Mol Cell Cardiol*. 2006;41(3):555-62.
9. van Marion DM, Hu X, Zhang D, Hoogstra-Berends F, Seerden JG, Loen L, et al. Screening of novel HSP-inducing compounds to conserve cardiomyocyte function in experimental atrial fibrillation. *Drug Des Devel Ther*. 2019;13:345-64.
10. Murakami M, Oketani K, Fujisaki H, Wakabayashi T, Ohgo T. Antiulcer effect of geranylgeranylacetone, a new acyclic polyisoprenoid on experimentally induced gastric and duodenal ulcers in rats. *Arzneimittelforschung*. 1981;31(5):799-804.
11. Nakazawa S, Tsuboi Y, Tsukamoto Y, Yoshino J, Okada M. Serum and stomach tissue levels of geranylgeranylacetone in patients. *Int J Clin Pharmacol Ther Toxicol*. 1983;21(6):267-70.
12. Latchman DS. Heat shock proteins and cardiac protection. *Cardiovasc Res*. 2001;51(4):637-46.
13. Mao H, Li Z, Zhou Y, Li Z, Zhuang S, An X, et al. HSP72 attenuates renal tubular cell apoptosis and interstitial fibrosis in obstructive nephropathy. *Am J Physiol Renal Physiol*. 2008;295(1):F202-14.
14. Goto K, Kojima A, Morioka S, Naito T, Akema T, Matsuba Y, et al. Geranylgeranylaceton induces heat shock protein 72 in skeletal muscle cells. *Biochem Biophys Res Commun*. 2007;358(1):331-5.
15. Chang SL, Chen YC, Hsu CP, Kao YH, Lin YK, Lai YJ, et al. Heat shock protein inducer modifies arrhythmogenic substrate and inhibits atrial fibrillation in the failing heart. *Int J Cardiol*. 2013;168(4):4019-26.
16. Ooie T, Takahashi N, Saikawa T, Nawata T, Arikawa M, Yamanaka K, et al. Single oral dose of geranylgeranylacetone induces heat-shock protein 72 and renders protection against ischemia/reperfusion injury in rat heart. *Circulation*. 2001;104(15):1837-43.
17. Marunouchi T, Inomata S, Sanbe A, Takagi N, Tanonaka K. Protective effect of geranylgeranylacetone via enhanced induction of HSPB1 and HSPB8 in mitochondria of the failing heart following myocardial infarction in rats. *Eur J Pharmacol*. 2014;730:140-7.
18. Sanbe A, Daicho T, Mizutani R, Endo T, Miyauchi N, Yamauchi J, et al. Protective effect of geranylgeranylacetone via enhancement of HSPB8 induction in desmin-related cardiomyopathy. *PLoS One*. 2009;4(4):e5351.
19. Zhang D, Ke L, Mackovicova K, Van Der Want JJ, Sibon OC, Tanguay RM, et al. Effects of different small HSPB members on contractile dysfunction and structural changes in a Drosophila melanogaster model for Atrial Fibrillation. *J Mol Cell Cardiol*. 2011;51(3):381-9.
20. Lavoie JN, Lambert H, Hickey E, Weber LA, Landry J. Modulation of cellular thermoresistance and actin filament stability accompanies phosphorylation-induced changes in the oligomeric structure of heat shock protein 27. *Mol Cell Biol*. 1995;15(1):505-16.
21. Sakabe M, Shiroshita-Takeshita A, Maguy A, Brundel BJ, Fujiki A, Inoue H, et al. Effects of a heat shock protein inducer on the atrial fibrillation substrate caused by acute atrial ischaemia. *Cardiovasc Res*. 2008;78(1):63-70.
22. Zhang D, Wu CT, Qi X, Meijering RA, Hoogstra-Berends F, Tadevosyan A, et al. Activation of histone deacetylase-6 induces contractile dysfunction through derailment of alpha-tubulin proteostasis in experimental and human atrial fibrillation. *Circulation*. 2014;129(3):346-58.
23. Sakamoto K, Urushidani T, Nagao T. Translocation of HSP27 to sarcomere induced by ischemic preconditioning in isolated rat hearts. *Biochem Biophys Res Commun*. 2000;269(1):137-42.
24. Stacchiotti A, Bonomini F, Lavazza A, Rodella LF, Rezzani R. Adverse effects of cyclosporine A on HSP25, alpha B-crystallin and myofibrillar cytoskeleton in rat heart. *Toxicology*. 2009;262(3):192-8.
25. Lu XY, Chen L, Cai XL, Yang HT. Overexpression of heat shock protein 27 protects against ischaemia/reperfusion-induced cardiac dysfunction via stabilization of troponin I and T. *Cardiovasc Res*. 2008;79(3):500-8.
26. Otaka M, Yamamoto S, Ogasawara K, Takaoka Y, Noguchi S, Miyazaki T, et al. The induction mechanism of the molecular chaperone HSP70 in the gastric mucosa by Geranylgeranylacetone (HSP-inducer). *Biochem Biophys Res Commun*. 2007;353(2):399-404.

27. Meijering RA, Wiersma M, van Marion DM, Zhang D, Hoogstra-Berends F, Dijkhuis AJ, et al. RhoA Activation Sensitizes Cells to Proteotoxic Stimuli by Abrogating the HSF1-Dependent Heat Shock Response. *PLoS One*. 2015;10(7):e0133553.
28. Shack S, Gorospe M, Fawcett TW, Hudgins WR, Holbrook NJ. Activation of the cholesterol pathway and Ras maturation in response to stress. *Oncogene*. 1999;18(44):6021-8.
29. Sysa-Shah P, Xu Y, Guo X, Pin S, Bedja D, Bartock R, et al. Geranylgeranylacetone blocks doxorubicin-induced cardiac toxicity and reduces cancer cell growth and invasion through RHO pathway inhibition. *Mol Cancer Ther*. 2014;13(7):1717-28.
30. St Rammos K, Koullias GJ, Hassan MO, Argyrakis NP, Voucharas CG, Scarupa SJ, et al. Low preoperative HSP70 atrial myocardial levels correlate significantly with high incidence of postoperative atrial fibrillation after cardiac surgery. *Cardiovasc Surg*. 2002;10(3):228-32.
31. Mandal K, Torsney E, Poloniecki J, Camm AJ, Xu Q, Jahangiri M. Association of high intracellular, but not serum, heat shock protein 70 with postoperative atrial fibrillation. *Ann Thorac Surg*. 2005;79(3):865-71; discussion 71.
32. Yang M, Tan H, Cheng L, He M, Wei Q, Tanguay RM, et al. Expression of heat shock proteins in myocardium of patients with atrial fibrillation. *Cell Stress Chaperones*. 2007;12(2):142-50.
33. Yanaka A, Zhang S, Sato D, Tauchi M, Suzuki H, Shibahara T, et al. Geranylgeranylacetone protects the human gastric mucosa from diclofenac-induced injury via induction of heat shock protein 70. *Digestion*. 2007;75(2-3):148-55.
34. Aranki SF, Shaw DP, Adams DH, Rizzo RJ, Couper GS, VanderVliet M, et al. Predictors of atrial fibrillation after coronary artery surgery. Current trends and impact on hospital resources. *Circulation*. 1996;94(3):390-7.
35. Yaksh A, Kik C, Knops P, van Ettinger MJ, Bogers AJ, de Groot NM. Early, de novo atrial fibrillation after coronary artery bypass grafting: Facts and features. *Am Heart J*. 2017;184:62-70.

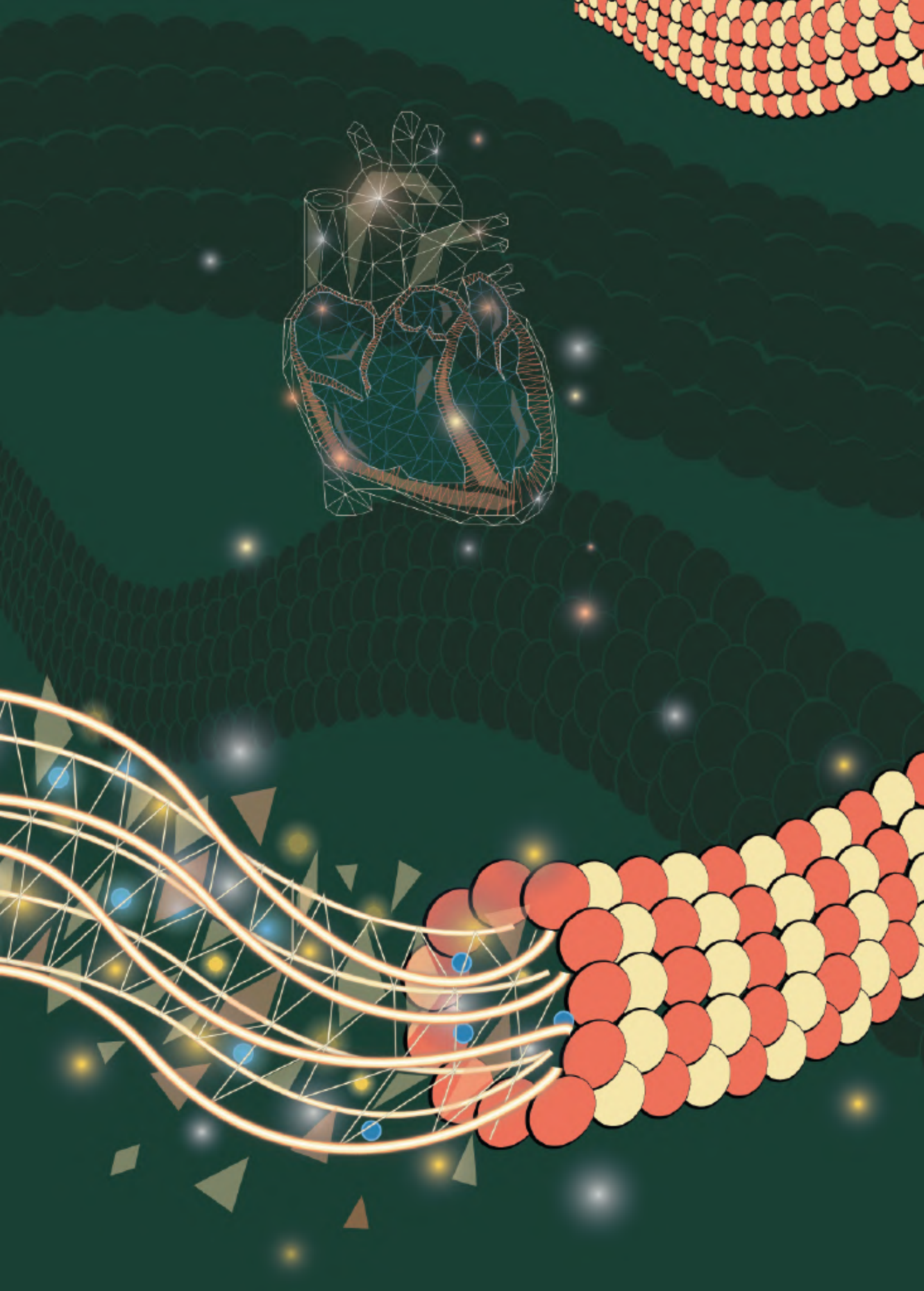

Chapter 6

Proteomic and functional studies reveal detyrosinated tubulin as treatment target in sarcomere mutation-induced hypertrophic cardiomyopathy

Maike Schuldt, Jiayi Pei, Magdalena Harakalova, **Larissa M. Dorsch**, Saskia Schlossarek, Michal Mokry, Jaco C. Knol, Thang V. Pham, Tim Schelfhorst, Sander R. Piersma, Cris dos Remedios, Michiel Dalinghaus, Michelle Michels, Folkert W. Asselbergs, Marie-Jo Moutin, Lucie Carrier, Connie R. Jimenez, Jolanda van der Velden[‡], Diederik W.D. Kuster[‡]

[‡]*shared last author*

Circ Heart Fail. Epub p.CIRCHEARTFAILURE120007022 (2021).

ABSTRACT

BACKGROUND

Hypertrophic cardiomyopathy (HCM) is the most common genetic heart disease. While 50% of HCM patients carry a sarcomere gene mutation (HCM_{SMP}), the genetic background is unknown in the other half of the patients (sarcomere mutation-negative, HCM_{SMN}). Genotype-specific differences have been reported in cardiac function. Moreover, HCM_{SMN} patients have later disease onset and better prognosis than HCM_{SMP} patients. To define if genotype-specific derailments at the protein level may explain the heterogeneity in disease development, we performed a proteomic analysis in cardiac tissue from a clinically well-phenotyped HCM patient group.

METHODS

A proteomics screen was performed in cardiac tissue from 39 HCM_{SMP}, 11 HCM_{SMN} patients and 8 non-failing controls. HCM patients had obstructive cardiomyopathy with left ventricular outflow tract obstruction and diastolic dysfunction. A novel *MYBPC3*$_{2373insG}$ mouse model was used to confirm functional relevance of our proteomic findings.

RESULTS

In all HCM patient samples we found lower levels of metabolic pathway proteins and higher levels of extracellular matrix proteins. Levels of total and detyrosinated α-tubulin were markedly higher in HCM_{SMP} than in HCM_{SMN} and controls. Higher tubulin detyrosination was also found in two unrelated *MYBPC3* mouse models and its inhibition with parthenolide normalized contraction and relaxation time of isolated cardiomyocytes.

CONCLUSION

Our findings indicate that microtubules and especially its detyrosination contribute to the pathomechanism of HCM_{SMP} patients. This is of clinical importance since it represents a potential treatment target to improve cardiac function in HCM_{SMP} patients, whereas a beneficial effect may be limited in HCM_{SMN} patients.

CLINICAL PERSPECTIVE

WHAT IS NEW?

This study shows that the most prominent derailment at the protein level in cardiac tissue obtained during myectomy of HCM patients in an advanced disease stage is reduced levels of proteins involved in metabolic pathways. This is common for all genotypes.
The study further demonstrates that increased levels of detyrosinated tubulin are specific for sarcomere mutation-positive HCM patients.
The increase in tubulin detyrosination is resembled in a mouse model with the Dutch founder mutation *MYBPC3*$_{2373insG}$. Pharmacological inhibition of tubulin detyrosination normalizes contractile function in isolated cardiomyocytes.

WHAT ARE THE CLINICAL IMPLICATIONS?

Recent and ongoing clinical trials investigate the therapeutic effect of targeting the energy metabolism in HCM patients which is supported by our proteomic data showing metabolic derailment.
Lowering tubulin detyrosination presents a potential novel treatment strategy that may improve contractile function in sarcomere mutation-positive HCM patients. Since HCM is characterized by diastolic dysfunction, enhancing cardiomyocyte relaxation by lowering detyrosination of microtubules is considered to be beneficial for HCM patients.
This study provides evidence that there is a need for genotype-specific treatment in HCM. Due to differences in pathomechanism, not every therapeutic strategy may be beneficial in all patient groups.

INTRODUCTION

Hypertrophic cardiomyopathy (HCM) is characterized by diastolic dysfunction and asymmetric left ventricular (LV) hypertrophy, which lead to LV outflow tract obstruction (LVOTO) in the majority of cases.[1] Mutations in genes encoding sarcomere proteins cause HCM and are identified in more than half of the patients (sarcomere mutation-positive, HCM_{SMP}). The heterogeneity in genetic background of HCM is large with more than 1500 identified HCM-causing mutations.[2] Approximately 80% of mutations are located in *MYH7* and *MYBPC3*. Less frequent are mutations in *TNNT2* and *TNNI3*.[3,4]

Previous research in HCM mouse models and humans showed genotype-specific differences in cellular characteristics and cardiac remodelling and function. Gene-specific differences in cellular redox and mitochondrial function were reported in mice harbouring a *MYH7* or *TNNT2* mutation.[5] In accordance with studies in HCM mouse models, studies on patient myectomy samples reported gene-specific differences in the response to calcium, ADP, protein kinase A, and length-dependent activation of myofilaments compared to non-failing cardiomyocytes.[6,7] Also, a comparison of two different patient-specific induced pluripotent stem cell-derived cardiomyocyte cell lines, carrying either a mutation in *MYBPC3* or *TPM1*, showed differences in calcium handling and electrophysiological properties.[8] These *in vitro* studies are strengthened by clinical patient studies which revealed a more severe decline in myocardial efficiency in *MYH7* than in *MYBPC3* mutation carriers,[9] accompanied by a different response to therapy.[10] Notably, there is also a large patient population in which a disease-causing mutation cannot be identified, the so-called sarcomere mutation-negative patients (HCM_{SMN}). While the cause of the disease in these patients is unknown, they present with the same clinical phenotype as HCM_{SMP} patients albeit at older age.[3] Moreover, recent data from the SHaRe registry indicate that HCM_{SMP} have a 2-fold greater risk of adverse outcomes than HCM_{SMN}.[11] Whereas LVOTO can be invasively corrected by surgical myectomy, other symptoms can only be managed by pharmacological therapies, which do not halt or reverse cardiac disease.[1] Knowledge about the cellular changes that cause cardiac dysfunction and hypertrophy in HCM patients is needed to design new therapies.

The main goal of this study was to define HCM- and genotype-specific derailments at the protein level, which may explain the heterogeneity in cardiac characteristics and disease initiation and progression. Therefore, we used an unbiased proteomics approach in a large number of myectomy samples from a clinically well-characterized HCM patient group with (HCM_{SMP}) and without (HCM_{SMN}) sarcomere mutations. We show that lower levels of metabolic pathway proteins and higher levels of extracellular matrix (ECM) proteins are the most prominent genotype-independent HCM-specific disease characteristics at the time of myectomy. However, abundance and detyrosination of α-tubulin was significantly higher in HCM_{SMP} than in non-failing (NF) controls, with intermediate levels in HCM_{SMN}. Recent studies in human heart failure identified a central role for detyrosinated microtubules in regulating cardiomyocyte function and demonstrated the functional benefit upon reversal of this modification.[12,13] Our study in a European HCM patient cohort and genetic HCM mouse models strengthens the concept that targeting the microtubule network represents

a therapeutic strategy to correct impaired function, and extends it to HCM caused by sarcomere mutations.

METHODS

The proteomics data have been deposited to the ProteomeXchange Consortium via the PRIDE partner repository with the dataset identifier PXD012467 and are publicly available.

HUMAN CARDIAC SAMPLES

Tissue of the IVS of 50 HCM patients was obtained during myectomy surgery to relieve LVOTO or after heart transplantation (1 sample, HCM 164). Samples of IVS from 8 healthy NF donors (5 males, 3 females; mean age 45.9 $\pm$ 9.7 years) with no history of cardiac abnormalities was obtained from the Sydney Heart Bank (HREC Univ Sydney 2012/030) and served as controls. The parameters of all HCM and NF individuals are summarized in Table S1. In this table we organized HCM patients based on their genotype into 5 sub-groups: Patients with the Dutch *MYBPC3* founder mutation (2373insG), where the truncating mutation resulted in MYBPC3 haploinsufficiency;[14] Patients with *MYBPC3* mutations other than the 2373insG mutation of which 81.8% were truncating mutations as well; Patients with *MYH7* mutations; Patients with mutations in less frequently affected sarcomere genes (*TNNT2*, *TNNI3* and *MYL2*); and HCM_{SMN} patients. In line with studies in other cohorts,[15] almost all mutations in *MYBPC3* were truncating mutations, whereas mutations in other sarcomeric proteins were missense except the truncating mutation c.814C>T in *TNNT2*.

PROTEOMICS ANALYSIS

TISSUE HOMOGENIZATION

Pulverized frozen tissue was homogenized in 40 µL/mg tissue 1x reducing sample buffer (106 mM Tris-HCl, 141 mM Tris-base, 2% (w/v) lithium dodecyl sulphate (LDS), 10% (v/v) glycerol, 0.51 mM EDTA, 0.22 mM SERVA Blue G250, 0.18 mM Phenol Red, 100 mM DTT) using a glass tissue grinder. Proteins were denatured by heating to 99°C for 5 min, after which samples were sonicated and heated again. Debris was removed by centrifugation at maximum speed for 10 min in a microcentrifuge (Sigma, 1-15K).

PROTEIN FRACTIONATION

Proteins were separated using 1D SDS-PAGE. Samples from each group were loaded alternating on the gels to avoid bias. Equal volumes of sample (30 µL protein homogenate per sample, containing approximately 20-30 µg of protein) were loaded on a precast 4-12% NuPAGE Novex Bis-Tris 1.5 mm mini gel (Invitrogen). Electrophoresis was performed at 200 V in NuPAGE MES SDS running buffer until the dye front reached the bottom of the gel. Gels were fixed in a solution of 50% ethanol and 3% phosphoric acid, and stained with 0.1% Coomassie brilliant blue G-250 solution (containing 34% methanol, 3% phosphoric acid and 15% ammonium sulphate). Images of all gels are provided in Figure S1.

IN-GEL DIGESTION AND NANO-LC-MS/MS

Each gel lane was cut into 5 pieces and in-gel digestion was performed as described previously.[16] Samples were measured by LC-MS per gel band starting at the high molecular weight (MW) fraction for all samples, before continuing with the next gel band until the last (low MW fraction) band. Injections alternated between all different group samples to minimize experimental bias between groups. Analysis of the experiment was performed as described in Piersma et al.[17] Peptides were separated using an Ultimate 3000 Nano LC-MS/MS system (Dionex LC-Packings, Amsterdam, The Netherlands) equipped with a 40 cm x 75 µm ID fused silica column custom packed with 1.9 µm, 120 Å ReproSil Pur C18 aqua (Dr Maisch GMBH, Ammerbuch-Entringen, Germany). Eluting peptides were ionized at a potential of +2 kV into a Q Exactive mass spectrometer (Thermo Fisher, Bremen, Germany). MS/MS spectra were acquired at resolution 17,500 (at m/z 200) in the orbitrap using an AGC target value of $1x10^6$ charges, a maxIT of 60 ms and an underfill ratio of 0.1%. Dynamic exclusion was applied with a repeat count of 1 and an exclusion time of 30 s (additional details to in-gel-digestion and nano-LC-MS/MS are provided in the Supplemental Methods).

DATA ANALYSIS

MS/MS spectra were searched against a Uniprot human reference proteome FASTA file (Swissprot_2017_03_human_canonical_and_isoform.fasta, 42161 entries) using MaxQuant version 1.5.4.1 (details to search settings are provided in the Supplemental Methods). The mass spectrometry proteomics data are provided in Table S5 and the raw data have been deposited to the ProteomeXchange Consortium via the PRIDE[18] partner repository with the dataset identifier PXD012467. Beta-binominal statistics were used to assess differential protein expression between groups, after normalization on the sum of the counts for each sample.[19] Proteins with a *p*-value below 0.05 were considered significantly differentially expressed. Proteins which were present in less than 25% of the samples or had an average normalized count of less than 1.4 were excluded from further functional analysis. Principal component analysis was performed in R. Therefore quantile normalization and log2 transformation was performed on the normalized counts. The 95th Percentile was taken, the data median centered and the principal components calculated. Hierarchical clustering was performed after a statistical multi-group comparison. Proteins with a raw *p*-value <0.05 were selected for the pathway analysis. Protein networks were generated utilizing the STRING database (Search Tool for the Retrieval of Interacting Genes/Proteins) and visualized with Cytoscape software.[20] Protein interaction networks were generated with ClusterONE and gene ontology (GO) analysis was performed using the BiNGO application in cytoscape.[21,22] Heatmaps for a specific GOs were created with ToppGene Suite[23] and Graphpad Prism v7 software. Venn diagrams were created with InteractiVenn tool[24] and the layout modified if needed.

ANIMAL EXPERIMENTS

The *MYBPC3*$_{2373insG}$ mouse model was engineered using CRISPR/Cas9 (details are provided in the Supplemental Methods). Echocardiographic phenotyping (Vevo 2100, Visualsonics) was performed on 7 homozygous *MYBPC3*$_{2373insG}$ mice (3 females, 4 males) and 8 WT littermates (3 females, 5 males). The age of the mice ranged from 20-28

weeks. Group size of 7 was determined by a power calculation to achieve a power of 0.8 and an alpha of 0.05 and to detect an effect size of 20% in echocardiography. The *MYBPC3*$_{772G>A}$ mice were developed previously[25] and maintained on a blackswiss genetic background. Western blot analysis was performed of the cytosolic fraction of LV tissue in 6 homozygous *MYBPC3*$_{772G>A}$ mice (2 females, 4 males) and 6 WT littermates (2 females, 4 males). The age of these mice was 55-59 weeks.

INTACT CARDIOMYOCYTE ISOLATION AND MEASUREMENTS

Intact adult cardiomyocytes were isolated from 4 WT and 6 homozygous *MYBPC3*$_{2373insG}$ mice as described previously.[26] Cells were suspended in plating medium composed of Medium 199 (Lonza), 1% penicillin/streptomycin and 5% bovine serum and plated on a laminin coated dish (10 µg/ml, Sigma-Aldrich). The cells were incubated for 1 h at 37°C in humidified air with 5% CO_2 to let them attach to the coated dish. Afterwards, non-attached cells were removed by washing cells with pre-heated culture medium (Medium 199 (Lonza), 1% penicillin/streptomycin, 1x ITS supplement (Sigma-Aldrich) and 0.5 µM cytochalasin D (Life technologies)). Cells were incubated with DMSO (0.1% v/v) or 10 µM parthenolide (Sigma) for 2 h. Contractility measurements were performed in tyrode solution (HEPES 10 mM, NaCl 133.5 mM, KCl 5 mM, NaH_2PO_4 1.2 mM, $MgSO_4$ 1.2 mM, glucose 11.1 mM, sodium pyruvate 5 mM; pH 7.4 at 37°C) at 37°C using the MultiCell system (CytoCypher, the Netherlands). The dish was field-stimulated at 2 Hz, 25 V and a 4 ms pulse duration. Changes in sarcomere length were recorded with a high-speed camera and Ionoptix software (Ionoptix, Westwood MA, USA). The contractility profiles were analysed with the automated batch analysis software CytoSolver (CytoCypher, Amsterdam, NL). An R^2 for peak and recovery fit >0.95 was selected as inclusion criteria for contraction data.

For protein analysis, cells were incubated with DMSO (0.1% v/v) or 10 µM parthenolide (Sigma) for 2 h, washed with PBS and directly lysed in loading buffer.

STUDY APPROVAL

The study protocol for the human tissue samples was approved by the local medical ethics review committees and written informed consent was obtained from each patient prior to surgery. Animal experiments were performed in accordance with the Guide for the Animal Care and Use Committee of the VU University Medical Center (VUmc) and with approval of the Animal Care Committee of the VUmc (CCD-number AVD114002016700) and conform the guidelines from Directive 2010/63/EU of the European Parliament on the protection of animals used for scientific purposes.

Extended methods section in the supplementary materials.

RESULTS

NO MAJOR GENOTYPE-SPECIFIC PROTEIN CHANGES

We performed an unbiased proteomics approach to compare the protein expression profile of 50 interventricular septum (IVS) samples from HCM patients at the time of myectomy

with 8 NF_{IVS} samples (Table 6.1, Table S1; patient characteristics). Patient characteristics are shown in Table 6.1.

Table 6.1: Clinical characteristics of the HCM_{SMP} and HCM_{SMN} patient group.

	HCM_{SMP} (n=38)	**HCM_{SMN} (n=11)**	***p*-value**
Sex, male	65.8% (25)	63.6% (7)	>0.9999
Age at myectomy (years)	46.2 ± 17.4	53.6 ± 13.9	0.2084
Dimensions			
IVS (mm)	21.0 [18.8-23.3]	16.0 [15.0-18.0]	<0.0001
LAD (mm)	46.0 ± 6.5	48.1 ± 5.4	0.3861
EDD (mm)	42.5 ± 5.2	44.3 ± 6.4	0.4466
ESD (mm)	21.7 ± 5.0	26.0 ± 2.8	0.2595
Diastolic parameters			
E/A ratio	1.16 [0.81-1.54]	0.92 [0.67-1.15]	0.1795
E/e' ratio	16.2 [13.1-20.1]	21.7 [16.0-33.4]	0.0226
TR velocity (cm/s)	2.3 ± 0.5	*NA*	
Stadium of diastolic dysfunction			
1	46.9% (15)	40.0% (4)	>0.9999
2	31.3% (10)	40.0% (4)	0.7071
3	21.9% (7)	20.0% (2)	>0.9999
Systolic parameter			
FS (%)	47.4 ± 11.7	47.5 ± 0.7	0.9942
LVOTg (mmHg)	54.9 ± 31.9	91.7 ± 40.9	0.0034
Medication			
beta blocker	79.5% (31)	63.6% (7)	0.4240
calcium channel blocker	33.3% (13)	45.5% (5)	0.4945
Statins	12.8% (5)	18.2% (2)	0.6407

Displayed are the mean±SD or the median with interquartile range when appropriate. EDD indicates end-diastolic diameter; ESD, end-systolic diameter; FS, fractional shortening; HCM, hypertrophic cardiomyopathy; IVS, interventricular septum; LAD, left atrial diameter; LVOTg, left ventricular outflow tract gradient; SMN, sarcomere mutation-negative; SMP, sarcomere mutation-positive; and TR, tricuspid regurgitation.*$p<0.05$.

Echocardiographic parameters were assessed as described previously.[27] All HCM patients had obstructive HCM and showed impaired diastolic function evident from increased LV filling pressure indicated by an E/e' ratio >15 and atrial dilation indicated by increased left atrial diameter (LAD) compared to reference values.[28,29] IVS thickness was higher in HCM_{SMP} compared to HCM_{SMN}. We identified 3,811 proteins of which we included 2,127 into our analysis after applying our inclusion criteria of an average normalized count of >1.4 and the protein being detected in >25% of samples. This filtered out low-level proteins that could not be reliably quantified. Samples were grouped based on their genotype and protein expression changes were analysed in different group-wise comparisons. Table S2 lists all group-wise comparisons and the corresponding number of significantly deregulated proteins that contributed to the subsequent cluster and gene ontology (GO) analysis. An unbiased principal component analysis (PCA) of the protein expression data revealed

separate clustering of the NF_{IVS} and HCM samples, indicating different protein expression profiles between controls and patients (Figure 6.1A).

Supervised hierarchical clustering of a multi-group comparison revealed separate clusters for NF_{IVS} and HCM samples (Figure 6.1B). However, in both analysis the HCM samples did not cluster according to their genotypes, indicating that the protein profile at the time of myectomy surgery is relatively homogeneous with differences between genotypes that are not sufficiently large to distinguish them with cluster analysis. Sample HCM 83 did not cluster with any of the other HCM or NF_{IVS} samples and turned out to have a very high serum albumin content. This implicated contamination with blood and therefore we excluded this sample from all further analyses. Sample HCM 164 also showed a unique protein expression pattern. It may reflect the infant proteome due to the young age (2 months), or the very severe disease stage since this is the only sample obtained from a heart transplantation. Since the variation in this sample is due to a biological reason, we did not exclude it.

To validate our experimental approach, we checked the expression of proteins involved in pathways that are known to be altered in HCM (Figure S2, Table S3). Fibrosis, characterized by an increase in ECM components, is a well-established feature of HCM as shown by data from myectomy biopsies and cardiac magnetic resonance imaging of patients.[27,30] In line with the presence of fibrosis in patients, we found increased levels of fibronectin, thrombospondin 4 and periostin (Figures S2A-C). Since hypertrophy is a morphological hallmark of HCM, we checked FHL2 expression as a negative regulator of hypertrophy.[31] In line with pro-hypertrophic signalling, reduced FHL2 protein expression was observed (Figure S2D). The hypertrophic phenotype was also evident from reduced α-MHC encoded by *MYH6*, and increased CSRP3 expression in HCM samples (Figures S2E-F).[32,33] Finally, MYBPC3 haploinsufficiency was confirmed in samples with a mutation in *MYBPC3* irrespective of whether the mutation is a truncation or missense mutation (Figures S2G-H, Table S4).[14,34]

Additionally, we performed RNA sequencing in a subset of samples. Similar to the proteomics data, the PCA plot of the RNA data did not show clustering based on genotype (Figure S3A). The MA-plot depicts all genes with the differentially expressed genes in red (Figure S3B). Gene set enrichment analysis of the proteomics and transcriptomics data revealed a significant correlation of upregulated proteins with genes that showed higher expression levels in HCM compared to NF_{IVS} (FDR$<$0.001), while less expressed proteins are positively correlated with genes that showed lower expression levels in HCM (FDR=0.008). This observation suggested that protein expression changes were well correlated with the mRNA expression changes between HCM and NF_{IVS} (Figures S3C-D).

HCM-SPECIFIC PROTEIN CHANGES

To identify HCM disease-specific protein expression patterns at the time of myectomy we grouped all HCM samples (HCM_{all}) and compared them to NF_{IVS}. We identified clusters of interacting proteins for higher and lower expressed proteins separately.

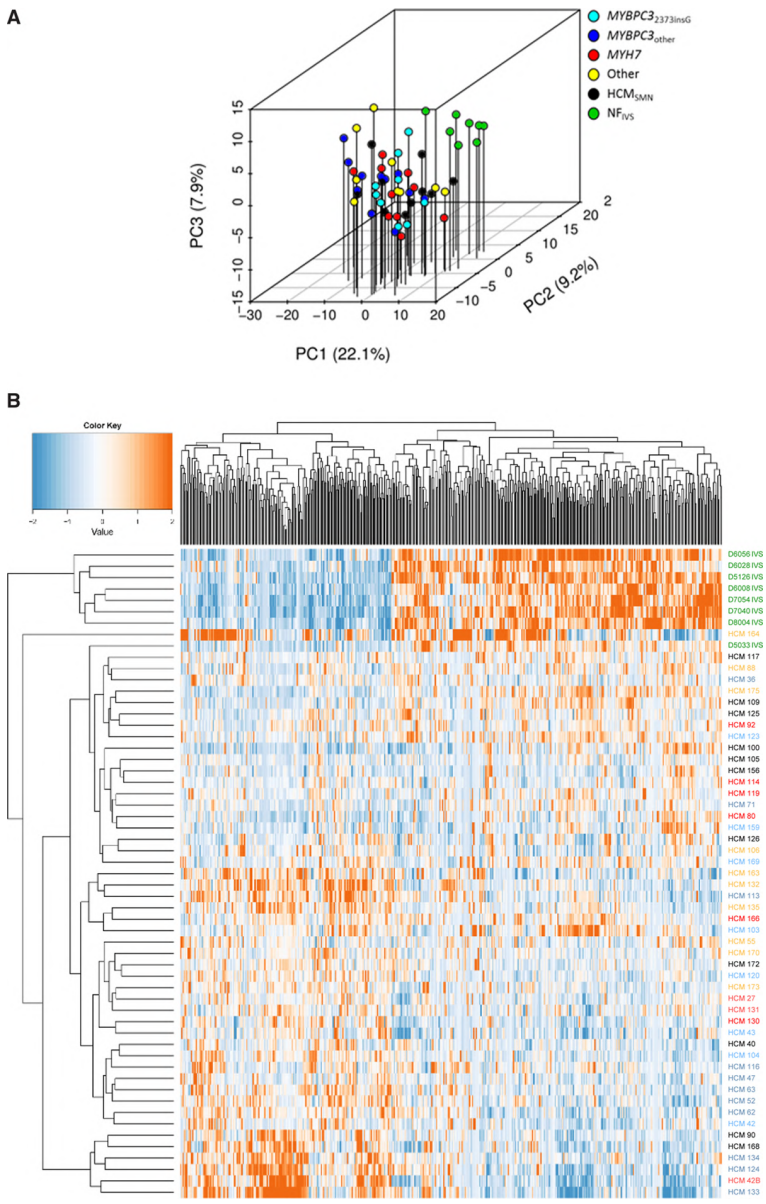

Figure 6.1: Clustering of proteome of controls and patient samples.
(**A**) Principal component (PC) analysis of the filtered protein expression data reveals separate clustering of the NF_{IVS} samples (n=8) and the HCM samples (n=50) showing that the overall protein expression profile between NF_{IVS} and HCM samples differs. HCM samples did not form separate clusters based on genotypes, indicating that genotype does not lead to major changes in protein expression profile. (**B**) Hierarchical clustering of a multi-group comparison of all proteins that are differently expressed at $p<0.05$ when comparing HCM_{all} with NF_{IVS}. Hierarchical clustering of all significantly different proteins between HCM_{all} and NF_{IVS} shows that the NF_{IVS} samples cluster together and are most different from the HCM samples. Also among this selection of proteins, the HCM samples do not cluster based on genotype.

Analysis of all significantly lower expressed proteins of HCM_{all} compared to NF_{IVS} uncovered the highest enrichment in oxidative phosphorylation, generation of precursor metabolites and energy, NAD metabolic process, translation, fatty acid catabolic process, regulated exocytosis and neutrophil degranulation (Figure 6.2A, more extensive list in Figure S4). This shows that the major changes in tissue of HCM patients are in metabolic pathways related to energy metabolism including both glucose and fatty acid metabolism. We selected all significantly lower expressed proteins annotated to the pathways and created a heatmap displaying the log2-fold change for a detailed visualization of protein changes in the pathway. We included RNA expression data of the corresponding genes to check if the protein changes coincide with changes at the RNA level. Strikingly, most of these proteins are not changed on RNA level (Figure S5).

The top clusters of the higher expressed proteins are associated with the GO terms ECM organization, actin filament-based process, myofibril assembly, muscle contraction, post-translational protein modification, protein folding and microtubule cytoskeleton organization (Figure 6.2B, more extensive list in Figure S6). The biggest cluster of more abundant proteins is ECM organization representing different collagens that are components of fibrotic tissue. Interestingly, many of these genes showed unaltered RNA levels compared to NF_{IVS}. The same was observed for the other top clusters of higher expressed proteins, namely actin filament-based process, myofibril assembly and muscle contraction, where RNA levels were unaltered or even lower than in NF_{IVS} (Figure S7).

Since HCM at the time of myectomy is characterized by pronounced hypertrophy of the myocardium, we expected a protein cluster related to hypertrophy among the significantly increased proteins. Surprisingly, we did not find this. This could be because the myocardium is not in a state of active hypertrophic growth at the time of sample collection, or because we did not detect low abundant hypertrophy promoting signalling proteins. It is also known that several signalling proteins are regulated by post-translational modifications rather than by abundance on which our proteomics screen was based. Western blot analysis of the expression and phosphorylation of AKT and ERK, two well-known inducers of hypertrophy,[35,36] showed higher AKT and ERK phosphorylation in HCM_{all} samples, indicating activation of hypertrophic signalling (Figure S8).

Subsequently, we repeated the cluster and GO analysis restricted to proteins that are higher and lower expressed if all 5 genotype HCM groups are compared individually to NF_{IVS} to extract the most consistent and robust changes. Venn diagrams (Figures S9 and S10) were made to identify overlapping protein changes (76 higher and 92 lower expressed), which were subsequently used as analysis input.

The results confirmed the findings from the initial analysis showing that the major HCM-specific protein changes include reduced metabolism, increased ECM remodelling, and pathways including muscle related processes.

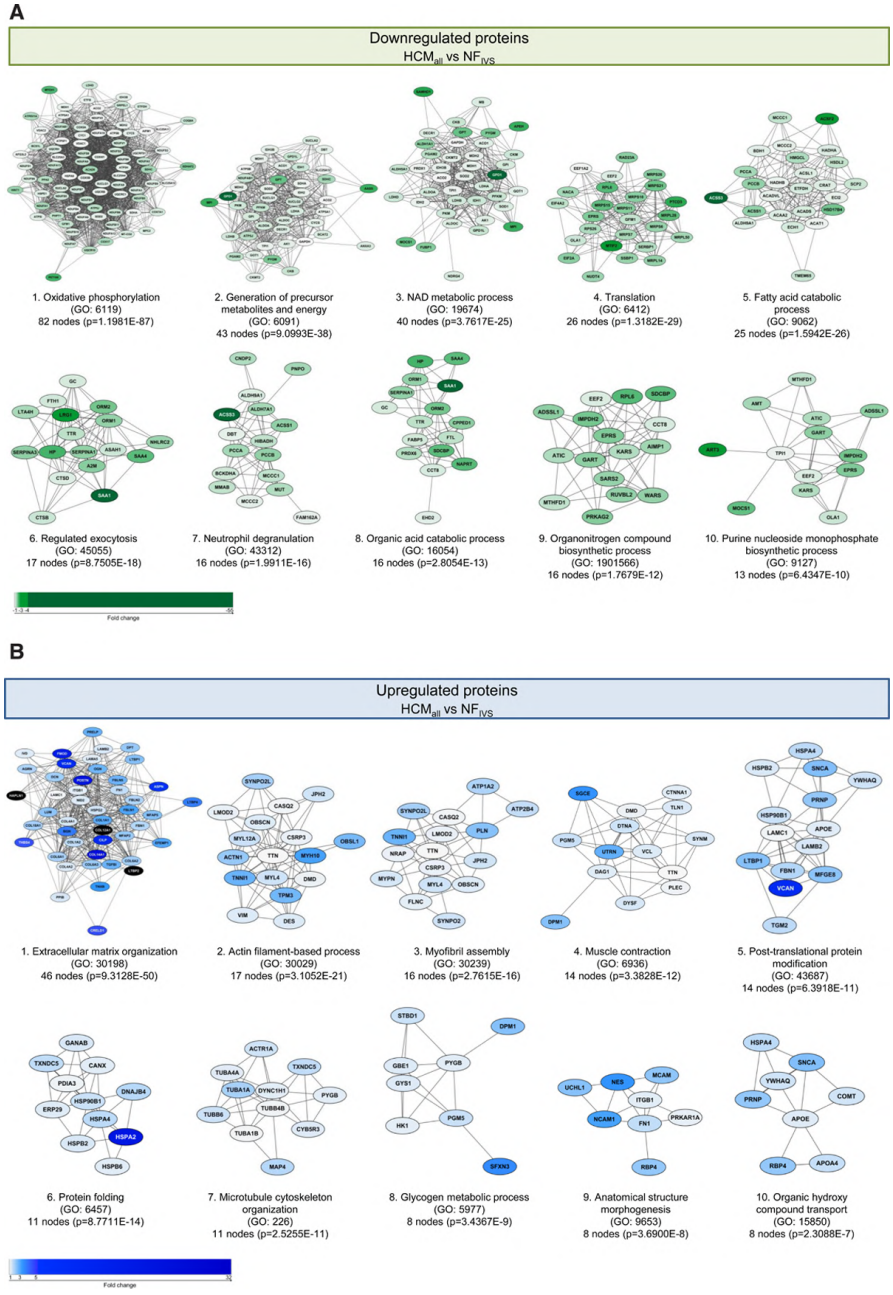

Figure 6.2: HCM-specific changes in biological processes.
Protein interaction cluster of significantly different proteins between HCM_{all} and NF_{IVS} were identified and are displayed with the most significant corresponding gene ontology (GO) term. (**A**) Top 10 downregulated protein interaction cluster based on cluster size with the most significant biological process related to this cluster. (**B**) Top 10 upregulated protein interaction cluster based on cluster size with the most significant biological process related to this cluster. The colour gradient from light to dark indicates an increase in fold change.

SPECIFIC CHANGES FOR HCM_{SMP} AND HCM_{SMN}

To study the pathways that are characteristic for HCM_{SMP} or HCM_{SMN} and might explain sarcomere mutation-specific changes in cardiac function, we created a Venn diagram of significantly different proteins in HCM_{SMP} and HCM_{SMN} compared to NF_{IVS}. The Venn diagrams (Figures 6.3 and S11) illustrate that the majority of significantly different proteins are similar in HCM_{SMP} and HCM_{SMN} (191 lower and 121 higher expressed proteins). However, a substantial number of proteins is only changed in either HCM_{SMP} or HCM_{SMN}, when compared to NF_{IVS}.

The 130 proteins that are specifically less abundant in HCM_{SMP} overlap to a large degree with the biological processes of the 194 proteins that are significantly less abundant in both HCM_{SMP} and HCM_{SMN} when compared to NF_{IVS} (Figure S12). Analysis of the 62 proteins that are specifically less expressed in HCM_{SMN} results in clusters related to stress granule assembly, translational initiation and protein folding (Figure S11).

The majority of the shared higher expressed proteins involve ECM organization (Figure S13). GO analysis of the 68 proteins that are specifically more abundant in HCM_{SMP} identified amongst others a protein clusters related to microtubule cytoskeleton organization (Figure 6.3).

This cluster representing tubulin subunits is solely more abundant in HCM_{SMP} when compared to NF_{IVS}, and is also among the functional protein cluster of proteins that are significantly upregulated in HCM_{SMP} when directly compared to HCM_{SMN} (Figure S14). Since the tubulin network is highly regulated by post-translational modifications, we determined the levels of total α-tubulin, tyrosinated and detyrosinated tubulin by Western blot (Figures 6.4 and S15A).

In line with the proteomics data we found an increase in total α-tubulin which is more prominent in HCM_{SMP} than in HCM_{SMN} (Figure 6.4A). We validated this with another primary antibody and obtained very comparable results (Figure S15A). A post-translational modification of tubulin that leads to increased stiffness of cardiomyocytes is detyrosination of α-tubulin.[12] We found markedly elevated detyrosinated tubulin only in HCM_{SMP} samples (Figure 6.4C), while levels of tyrosinated tubulin were slightly increased in both HCM_{SMP} and HCM_{SMN} (Figure 6.4B). Within the HCM_{SMP} group, levels of α-tubulin tend to be highest in the $MYBPC3_{other}$ group and lowest in the *MYH7* group, whereas desmin levels tend to be highest in *MYH7*.

Levels of tyrosinated and detyrosinated tubulin do not show any genotype-specific differences. Levels of tyrosinated and detyrosinated tubulin normalized to total α-tubulin are depicted in Figures S15B-C. Our data show that high levels of tubulin in HCM_{SMP} represent mostly the detyrosinated form. We also determined desmin protein levels by Western blot since this protein is associated with microtubules in cardiomyocytes. Accordingly, desmin levels were elevated in HCM with the largest increase in HCM_{SMP} (Figure 6.4D).

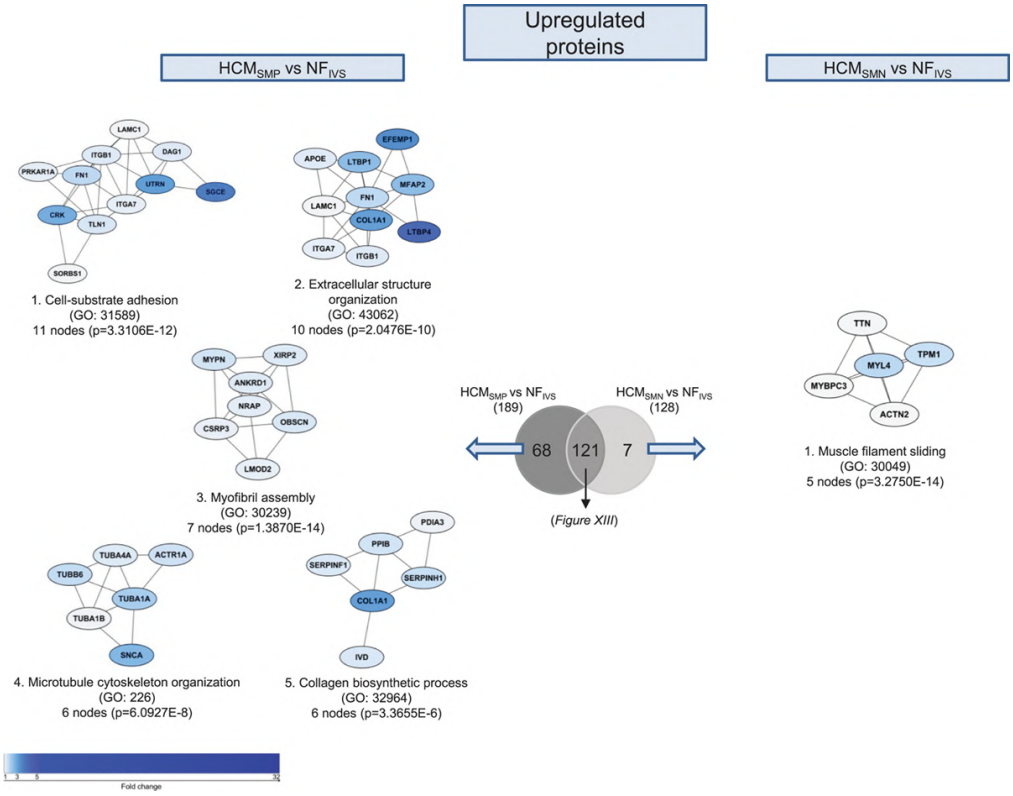

Figure 6.3: Differences in upregulated proteins between HCM_{SMP} and HCM_{SMN}.
Protein interaction cluster of proteins that are only significantly upregulated for the HCM_{SMP} vs NF_{IVS} or the HCM_{SMN} vs NF_{IVS} comparison were identified and are displayed with the most significant corresponding gene ontology (GO) term. The top 5 protein interaction clusters of upregulated proteins are displayed The colour gradient from light to dark indicates an increase in fold change.

INHIBITION OF TUBULIN DETYROSINATION CORRECTS CARDIOMYOCYTE DYSFUNCTION IN *MYBPC3*$_{2373insG}$ MICE

Based on previous studies in human heart failure,[13] our data in human myectomy samples indicate that microtubules may represent a treatment target to correct cardiac dysfunction in HCM. To provide proof for a role of tubulin in modulating cardiomyocyte function in HCM caused by a sarcomere gene mutation, we generated a HCM knock-in (KI) mouse model of the Dutch founder mutation c.2373insG in *MYBPC3* (Figures S16A-B). This mutation introduces a new splice donor site in exon 25 leading to a frameshift and premature stop codon resulting in an expected truncated protein of 95 kDa.[37] As no truncated protein is found in HCM patients carrying this mutation at the heterozygous state,[14] degradation of mutant mRNA and/or protein is likely. Accordingly, Western blot analysis did not reveal any truncated MYBPC3 protein in homozygous *MYBPC3*$_{2373insG}$ mice (Figure S16C).

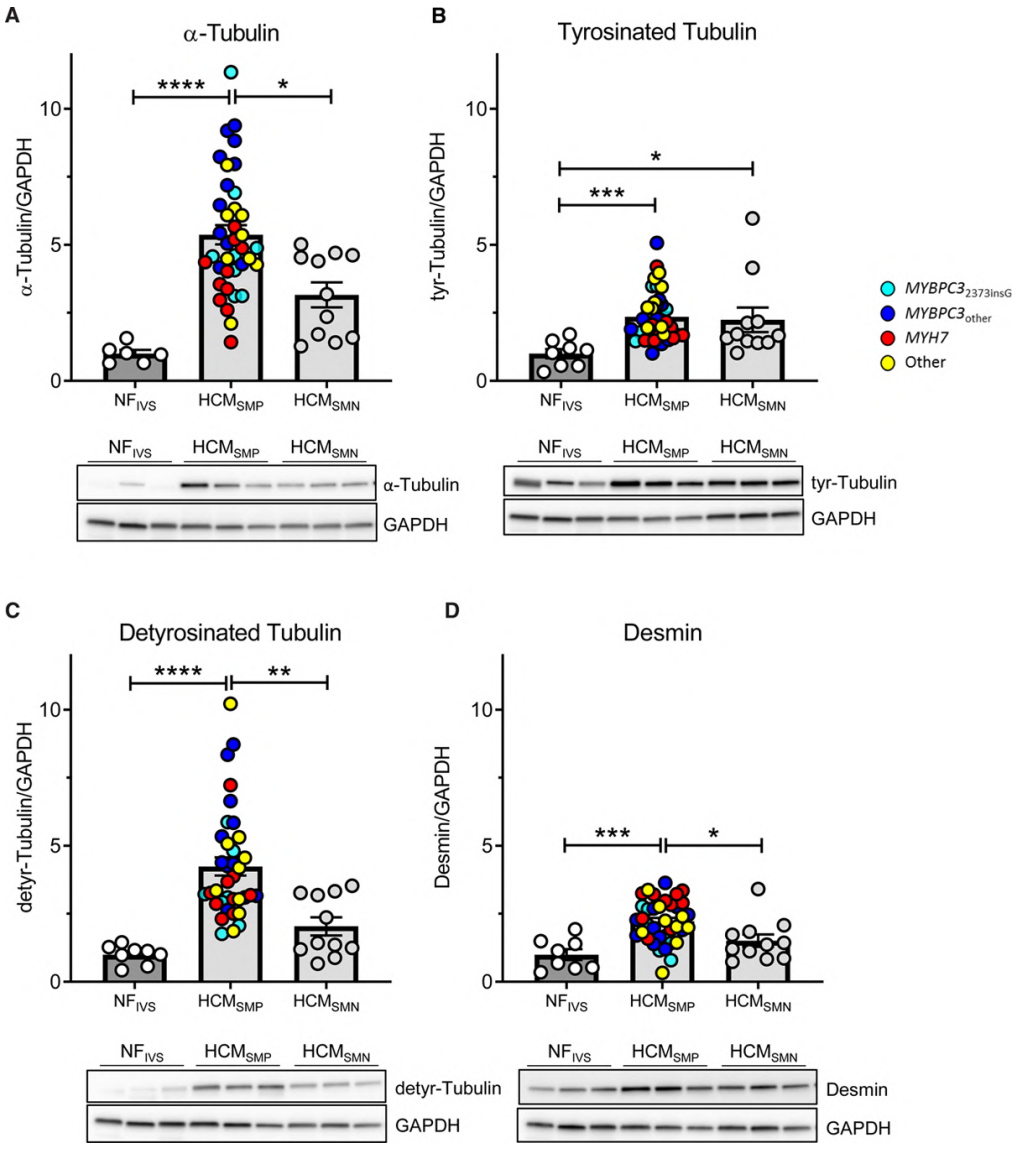

Figure 6.4: Tubulin expression and posttranslational modifications in HCM patients. Protein levels of α-tubulin (**A**), its tyrosinated (**B**) and detyrosinated forms (**C**) and desmin (**D**), all normalized to GAPDH, in tissue of HCM patients. Kruskal-Wallis test with Dunn's multiple comparisons test, ****$p<0.0001$, ***$p=0.0003$ in (**B**), ***$p=0.0009$ in (**D**), **$p=0.0074$, *$p=0.0437$ in (**A**), *$p=0.0499$ in (**B**) and *$p=0.0357$ in (**D**). Average of the control group is set to 1. $n(NF_{IVS}/HCM_{SMP}/HCM_{SMN})=6/38/11$ for (**A**), 8/36/11 for (**B-C**), 8/37/11 for (**D**).

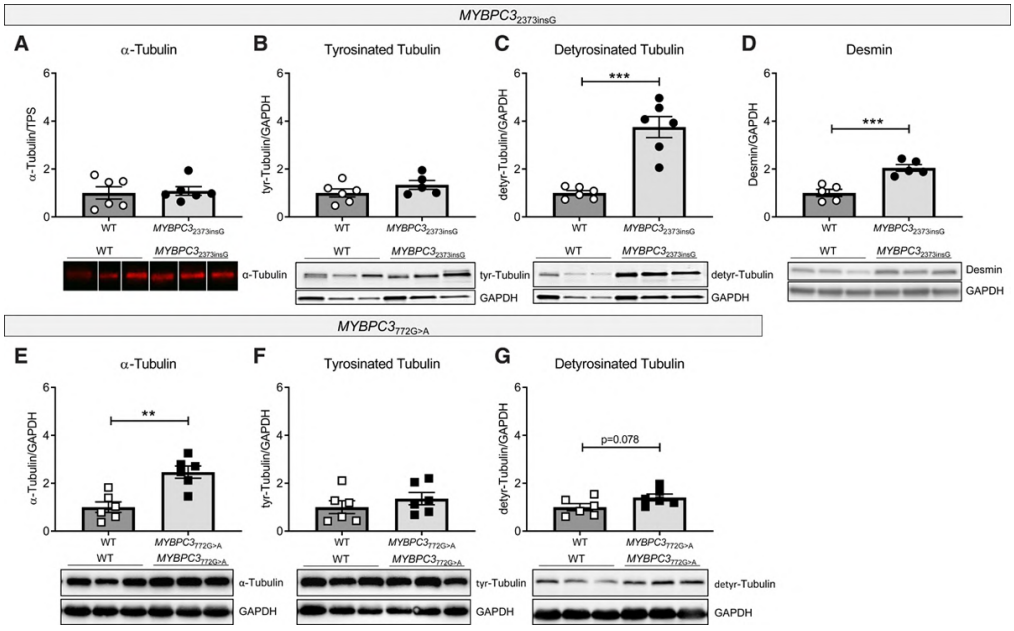

Figure 6.5: Tubulin composition in *MYBPC3*$_{2373insG}$ and *MYBPC3*$_{772G>A}$ mouse models. Quantification and representative Western blot images of (**A**) α-tubulin, (**B**) tyrosinated tubulin, (**C**) detyrosinated tubulin and (**D**) desmin in *MYBPC3*$_{2373insG}$ mice and (**E**) α-tubulin, (**F**) tyrosinated tubulin and (**G**) detyrosinated tubulin in *MYBPC3*$_{772G>A}$ mice, respectively. (**A**) is normalized to total protein stain (TPS, image provided in Figure S15D), (**B**-**G**) are normalized to GAPDH. Lanes in (**A**) were run on the same gel but were non-contiguous. n(WT/*MYBPC3*$_{2373insG/772G>A}$)=6/6 (4 females, 2 males/3 females, 3 males of 20-27 weeks for *MYBPC3*$_{2373insG}$ and the corresponding WT; 2 females, 4 males for of 55-59 weeks for *MYBPC3*$_{772G>A}$ and the corresponding WT) for (**A, C, E**-**G**), 6/5 (4 females, 2 males/3 females, 2 males; 20-27 weeks) for (**B**) and 5/5 (3 females, 2 males/2 females, 3 males; 20-27 weeks) for (**D**), unpaired two-tailed t-test, ***p=0.0001 in (**C**) and p=0.009 in (**D**), **p=0.0014.

Levels of total and tyrosinated α-tubulin did not differ between the groups, whereas the detyrosinated tubulin and desmin levels were markedly higher in *MYBPC3*$_{2373insG}$ than in wild-type (WT) mice (Figures 6.5A-D, loading control to panel A shown in Figure S15D).

To evaluate whether these findings were specific to this model, we assessed the levels of total and detyrosinated tubulin in a second HCM mouse model carrying a different *MYBPC3* mutation.[25] Homozygous *MYBPC3*$_{772G>A}$ mice showed a strong accumulation of α-tubulin and no difference in tyrosinated tubulin compared to their WT littermates. In addition, a trend to higher levels of detyrosinated tubulin was observed (Figures 6.5E-G). Overall, these mouse models consistently show tubulin changes in cardiomyopathy caused by *MYBPC3* gene mutations.

MYBPC3$_{2373insG}$ mice had a severe cardiac phenotype characterized by higher ventricular weight to body weight ratio, increased LV anterior wall diameter and interventricular

septum thickness, lower ejection fraction, increased left ventricular internal diameter and longer isovolumetric relaxation time than WT mice (Figures 6.6A-F). Single cardiomyocytes from $MYBPC3_{2373insG}$ hearts showed contractile deficits compared to WT as shown by an increase in time to peak of contraction and an impaired relaxation shown by an increase in time to baseline (Figures 6.6G-H). Inhibition of detyrosination by treatment with parthenolide (PTL) reduced levels of detyrosinated tubulin by 36% (Figure 6.6J) and normalized the contraction and relaxation times in $MYBPC3_{2373insG}$ mice to baseline WT levels (Figures 6.6G-H), whereas it had no effect on calcium release and reuptake time in $MYBPC3_{2373insG}$ mice (Figure S17A-B), indicating a direct effect on myofilament function.

Figure 6.6: Morphometric and phenotypic analysis of $MYBPC3_{2373insG}$ mice and contractile function of isolated $MYBPC3_{2373insG}$ cardiomyocytes upon inhibition of tubulin detyrosination. Quantification of the hypertrophy parameters (**A**) ventricle weight (VW)/body weight (BW) ratio and (**B**) anterior wall thickness in diastole (LWADd) and (**C**) interventricular septum thickness in diastole (IVSd) measured by echocardiography. (**D**) and (**E**) show parameters of systolic function measured by ejection fraction and left ventricular internal diameter (LVID) and (**F**) displays diastolic function assessed by isovolumetric relaxation time (IVRT). n(WT/$MYBPC3_{2373insG}$)=9/9 (4 females, 5 males; 20-27 weeks) for (**A**) and 8/7 (3 females, 5 resp. 4 males; 25-27 weeks) for (**B**-**F**), unpaired two-tailed t-test, ****$p<0.0001$, ***$p=0.0001$, *$p=0.0215$. (**G**) displays the effect of tubulin detyrosination inhibition by PTL on the contractile parameter time to peak 70% and (**H**) on the diastolic parameter time to baseline 70%. The dotted line visualizes the WT baseline level. (**I**) shows example force transients for each condition of the single cell measurements. For (**G**-**H**) N(WT mice)=4 (2 females and 2 males, 13-33 weeks) with total n(cells DMSO/PTL)=191/99 and N($MYBPC3_{2373insG}$ mice)=6 (2 females and 4 males, 13-35 weeks) with total n(cells DMSO/PTL)=169/123. (**G**) and (**H**) were analysed by 2way-ANOVA, **$p<0.01$, ****$p<0.0001$. (**J**) Levels of detyrosinated tubulin normalized to GAPDH in isolated $MYBPC3_{2373insG}$ cardiomyocytes upon inhibition of tubulin detyrosination by PTL. Every PTL treated sample was normalized to the DMSO control condition from the same animal. N($MYBPC3_{2373insG}$ mice)=6 (2 females, 4 males, 13-19 weeks); (**J**) was analysed with an unpaired two-tailed t-test, ***$p=0.0004$.

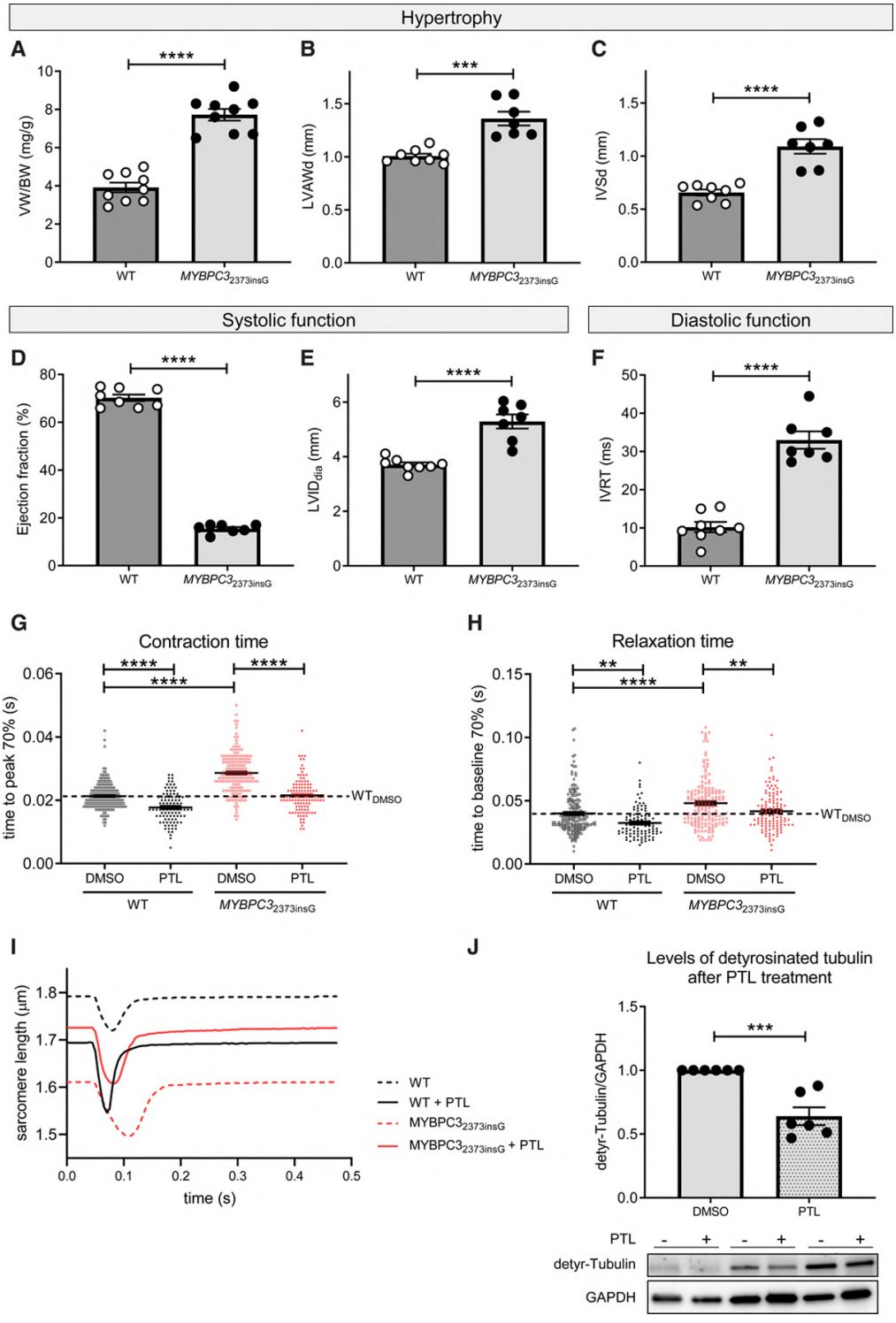
Hypertrophy
A
VW/BW (mg/g)
****
WT
MYBPC3 2373insG
B
LVAWd (mm)
***
C
IVSd (mm)
Systolic function
D
Ejection fraction (%)
E
LVIDdia (mm)
Diastolic function
F
IVRT (ms)
G
Contraction time
time to peak 70% (s)
WTDMSO
DMSO
PTL
H
Relaxation time
time to baseline 70% (s)
**
I
sarcomere length (µm)
time (s)
WT
WT + PTL
MYBPC3 2373insG
MYBPC3 2373insG + PTL
J
Levels of detyrosinated tubulin after PTL treatment
detyr-Tubulin/GAPDH
PTL
detyr-Tubulin
GAPDH

DISCUSSION

In this study we compared the protein profile of cardiac tissue from HCM patients with different disease-causing gene mutations to identify common HCM disease changes as well as genotype-specific protein changes at the time of myectomy. The majority of detected protein changes were common for all HCM samples and independent of the underlying gene mutation. Our approach revealed different protein profiles in the presence or absence of a sarcomere gene mutation. While hypertrophic remodelling in HCM_{SMP} is characterized by an increase in the levels of proteins involved in microtubule cytoskeleton organization, HCM_{SMN} samples show reduced levels of proteins involved in protein translation.

DEREGULATED ENERGY METABOLISM PROTEOME

Our analysis revealed that the majority of deregulated proteins are related to energy metabolism and show a consistent lower expression of proteins involved in oxidative phosphorylation, glycolysis and fatty acid oxidation. Especially subunits of mitochondrial respiratory chain complex I, that are part of cluster 1 in Figure 6.2A, are consistently lower expressed. This is in line with another recent proteomics study of HCM tissue samples in which reduced levels of energy metabolism proteins was one of the main findings.[38] It also matches observations of energy deficiency in animal models[39] and human studies.[40,41] Energy deficiency has been proposed as the primary mutation-induced pathomechanism leading to compensatory hypertrophy,[42] which is supported by the fact that even asymptomatic mutation carriers without hypertrophy display reduced cardiac energetic status.[9,41] The reduced cardiac efficiency was larger in *MYH7* mutation carriers compared to *MYBPC3* mutation carriers pointing towards genotype-specific functional differences.[9] Our proteomic analyses did not show gene-dependent differences in proteins involved in cardiac energy metabolism. This indicates that the deregulated energy metabolism proteome is a secondary consequence due to cellular stress that is similar in patients with advanced HCM.

PROTEIN HOMEOSTASIS DIFFERS BETWEEN HCM_{SMP} AND HCM_{SMN}

Interestingly, proteins involved in protein translation are less abundant, particularly in HCM_{SMN} patient tissue when compared to NF_{IVS}, implying that the protein translation system is either more impaired or differently regulated in HCM_{SMN}. Among the more abundant proteins, we observed a protein cluster related to protein folding. Protein folding proteins (chaperones) are needed for correct folding of de novo synthesized proteins as well as for refolding of misfolded mutant or damaged proteins. Since our data show downregulation of protein translation, it is unlikely that protein folding proteins are upregulated for folding of newly synthesized proteins. Instead, we speculate that their expression is upregulated to repair or remove misfolded (mutant) proteins.[43] This is in line with recent data describing an upregulation of protein folding proteins specifically in HCM_{SMP} samples.[44] Protein folding proteins represent potential treatment targets since boosting their expression has already shown beneficial effects in animal models of other cardiac diseases and in cardiomyopathies.[45-47]

IMPACT OF INCREASED TUBULIN NETWORK ON CARDIOMYOCYTE FUNCTION IN HCM

A striking observation was the specific upregulation of microtubule subunits and post-translational modification detyrosination in HCM_{SMP} compared to HCM_{SMN}, when comparing both to NF_{IVS}. Previous studies indicated important regulatory roles of microtubules in cardiomyocyte function.[48] Recent reports showed that the translation of the sarcomere proteins is localized to the myofilaments which points to a role of microtubules in the transportation of mRNA to the myofilament.[49,50] Increased expression of tubulin subunits strengthens the microtubule network and facilitates the transportation of mRNAs to the sarcomere and concomitant increasing cardiomyocyte stability. In addition to tubulins, desmin protein level was significantly higher in HCM_{SMP} than in HCM_{SMN}. In the healthy heart, desmin is localized at the Z-discs forming a striated pattern and playing a central role in cardiomyocyte mechanical stability.[51] Overall, these protein changes suggest a compensatory mechanism of the cell to ensure sarcomere stability in the presence of a sarcomere gene mutation.

Furthermore, microtubules and their post-translational modifications play an important role in cardiomyocyte mechanics, especially in regulating cardiomyocyte stiffness.[52,53] Detyrosinated tubulin stabilizes microtubules by inhibiting disassembly[54] and can anchor microtubules to the Z-discs of the sarcomere, most likely via desmin, and enhance stability and stiffness of the myofilaments and the microtubular network.[52] The *TUBA4A* transcript is directly synthesized in it is detyrosinated form and an upregulation could at least partly explain the increase in detyrosinated tubulin. In our RNA sequencing data, the *TUBA4A* transcript is however significantly downregulated when comparing HCM with NF_{IVS} and it is not differentially expressed in the direct comparison of HCM_{SMP} and HCM_{SMN}.

Tubulin detyrosination is enzymatically regulated by the tubulin tyrosine ligase (TTL) and tubulin carboxypeptidases (TCPs) that have detyrosinating activity and also the *TUBA4A* transcript can undergo these reactions.[55] Recently, vasohibins have been identified as the first tubulin detyrosinating enzymes,[56,57] and act in complex with small vasohibin-binding protein (SVBP). In accordance with findings by Robison et al. in explanted hearts of heart failure and cardiomyopathy patients,[12] we observed a specific upregulation of tubulins and enhanced detyrosination in our genetically well-characterized HCM myectomy samples. Notably, we found the increase in tubulin detyrosination specific for HCM_{SMP} samples. Although levels of detyrosinated tubulin are equal between HCM_{SMP} and HCM_{SMN} when normalized to total levels of α-tubulin, the absolute levels of α-tubulin and detyrosinated tubulin are much higher in HCM_{SMP} and thereby have a much greater impact on contractile function in these patients. Chen et al. have already demonstrated the reversibility of tubulin detyrosination in isolated cardiomyocytes from explanted HCM hearts associated with an improvement of contractile function.[13,58] Here we performed proof-of-concept studies in HCM mouse models to define the impact of tubulin detyrosination in the presence of a sarcomere mutation. Homozygous $MYBPC3_{2373insG}$ mice replicated the tubulin detyrosination without an increase in total α-tubulin levels, whereas homozygous $MYBPC3_{772G>A}$ mice display an increase in total α-tubulin with a trend to increased tubulin detyrosination. Considering the age difference of the mice with the $MYBPC3_{772G>A}$

mice being much older than the *MYBPC3*$_{2373insG}$ mice at the time of analysis, we speculate that the increase in tubulin detyrosination is an early disease change together with an increase in desmin protein levels, which is followed by an increase of total α-tubulin during disease progression and ageing. In *MYBPC3*$_{2373insG}$ mice we showed that the increase in tubulin detyrosination is accompanied by reduced contraction and relaxation kinetics in isolated intact cardiomyocytes. Inhibition of tubulin detyrosination by PTL restored contraction and relaxation kinetics to WT levels in *MYBPC3*$_{2373insG}$ cardiomyocytes. The used concentration of PTL has already been proven to be sufficient to reduce detyrosination of tubulin[12,59] and Chen et al. and Robison et al. have demonstrated that the PTL-induced effects on kinetics of contraction are the same as obtained by overexpression of TTL,[12,13] which specifically lowers tubulin detyrosination. The positive effect of PTL on cardiomyocyte function of *MYBPC3*$_{2373insG}$ cardiomyocytes is therefore explained by a decrease in cardiomyocyte stiffness due to lower levels of detyrosinated tubulin.

Overall, our findings in a European HCM patient cohort strengthens the evidence that increased detyrosination of microtubules contributes to cardiomyocyte stiffness and dysfunction in HCM. Importantly, we show that this is especially true in the presence of a sarcomere mutation.

STUDY LIMITATIONS AND CLINICAL IMPLICATIONS

We sex- and age-matched our experimental groups as good as the availability of human samples allowed us. As seen in Table 6.1, sex and age, as well as most clinical parameters, are not statistically different between groups. We cannot exclude that differences in disease progression, as displayed by the difference in IVS thickness, E/e' ratio and LVOTg between HCM_{SMP} and HCM_{SMN}, may influence the results. However, collection of patient heart tissue is only possible at the time of myectomy. Therefore, all our samples have the same clinical endpoint, i.e. time of myectomy. This is likely the cause for the low number of genotype-specific protein changes and we cannot exclude that genotype-specific differences might have occurred at earlier disease stages. Due to unavailability of myocardial biopsies from asymptomatic mutation carriers, animal models and human-derived cardiomyocyte muscle models should provide insight into gene-specific pathomechanisms at early disease stages.

Most of the patients in this study have been on drug therapy, therefore we cannot exclude that some of the proteomic changes are caused by medication. However, some of the main findings, e.g. energy deficiency, have also been observed in animal models,[39] and the number of patients on the most commonly used drugs does not differ between HCM_{SMP} and HCM_{SMN} (Table 6.1). Therefore it is more likely that the observed changes are driven by disease rather than medication.

Although we detected and quantified a large number of proteins in this study, we do not reach full coverage of the proteome as this method only reliably quantifies the more abundant proteins. Therefore, our list of differentially expressed proteins is not comprehensive. Also, we did not assess post-translational modifications in the proteomics

study which have important regulatory functions. The changes at the protein level reflect whole tissue alterations and cannot be solely assigned to the mutation-carrying cardiomyocytes but might also arise from other cell types. However, cardiomyocytes are responsible for most of the tissue volume and therefore drive most of the protein changes.

Homozygous *MYBPC3*$_{2373insG}$ mice do not fully resemble human HCM patients, since patients typically carry heterozygous mutations. Whilst both patients and the homozygous *MYBPC3*$_{2373insG}$ mouse model show hypertrophy and diastolic dysfunction, the prominent LV systolic dysfunction as observed in the homozygous *MYBPC3*$_{2373insG}$ mice is not seen in most HCM patients. But due to the lack of phenotype in heterozygous mice they provide a suitable genetic model of loss of MYBPC3 protein levels.

In our proteomic screen in a large set of human HCM samples we identified reduced levels of proteins involved in metabolic pathways as the most prominent derailment. This finding supports recent and ongoing clinical trials investigating the therapeutic effect of targeting the metabolism in HCM. Based on the proteomic data and functional studies in a novel HCM mouse model, we propose that an increase in detyrosinated tubulin contributes to the clinical and cellular differences that we see between HCM_{SMP} and HCM_{SMN} samples (Figure 6.7).

Detyrosinated microtubules may represent a target for therapeutic intervention in genetic heart disease because reducing detyrosination improves contractile function in isolated cardiomyocytes. Since the increase in detyrosinated tubulin is largest in HCM_{SMP}, this treatment strategy is proposed to be most beneficial in mutation-positive HCM patients. A specific inhibitor of detyrosination needs to be developed due to the known off-target effects of PTL. As sarcomere mutation carriers are identified before disease onset, targeting the microtubules may represent a preventive treatment option.

Figure 6.7: Schematic representation of genotype-independent changes in HCM and genotype-specific differences in the microtubular system. Our analysis shows that all HCM patients display downregulation of metabolic pathways (electron transport chain (ETC), tricarboxylic acid (TCA) cycle, β-oxidation (β-oxid)) and ribosomal proteins (Translation), as well as an upregulation of protein folding proteins (heat shock proteins, HSPs) and extracellular matrix (ECM) proteins. HCM_{SMP} patients have a large increase in microtubules and levels of its detyrosinated form, whereas HCM_{SMN} patients only have a slight increase compared to non-failing controls.

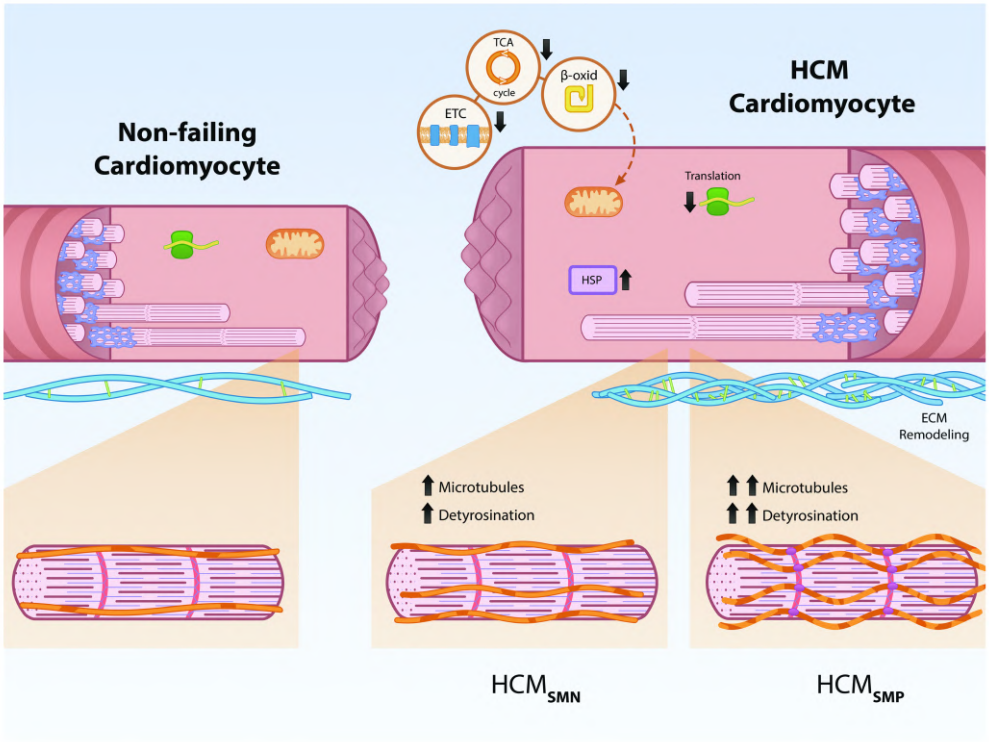

Sources of funding: We acknowledge the support from the Netherlands Cardiovascular Research Initiative: An initiative with support of the Dutch Heart Foundation, CVON2014-40 DOSIS and NWO (NWO-ZonMW; 91818602 VICI grant to Jolanda van der Velden). Folkert Asselbergs is supported by UCL Hospitals NIHR Biomedical Research Centre. Magdalena Harakalova is supported by NWO VENI grant (no. 016.176.136). Lucie Carrier and Saskia Schlossarek are supported by the German Centre for Cardiovascular Research (DZHK), the German Ministry of Research Education (BMBF), the Deutsche Herzstiftung and the Helmut und Charlotte Kassau Stiftung.

ACKNOWLEDGEMENTS

We would like to thank Ruud Zaremba, Valentijn Jansen and Max Goebel for technical assistance. We thank Feng Zhang for providing the Addgene plasmid #42230.

SUPPLEMENTARY FILES - ONLINE

https://www.ahajournals.org/doi/suppl/10.1161/CIRCHEARTFAILURE.120.007022

REFERENCES

1. Michels M, Olivotto I, Asselbergs FW, van der Velden J. Life-long tailoring of management for patients with hypertrophic cardiomyopathy : Awareness and decision-making in changing scenarios. *Neth Heart J*. 2017;25(3):186-99.
2. Ingles J, Burns C, Barratt A, Semsarian C. Application of Genetic Testing in Hypertrophic Cardiomyopathy for Preclinical Disease Detection. *Circ Cardiovasc Genet*. 2015;8(6):852-9.
3. Authors/Task Force, Elliott PM, Anastasakis A, Borger MA, Borggrefe M, Cecchi F, et al. 2014 ESC Guidelines on diagnosis and management of hypertrophic cardiomyopathy: the Task Force for the Diagnosis and Management of Hypertrophic Cardiomyopathy of the European Society of Cardiology (ESC). *Eur Heart J*. 2014;35(39):2733-79.
4. Richard P, Charron P, Carrier L, Ledeuil C, Cheav T, Pichereau C, et al. Hypertrophic cardiomyopathy: distribution of disease genes, spectrum of mutations, and implications for a molecular diagnosis strategy. *Circulation*. 2003;107(17):2227-32.
5. Vakrou S, Fukunaga R, Foster DB, Sorensen L, Liu Y, Guan Y, et al. Allele-specific differences in transcriptome, miRNome, and mitochondrial function in two hypertrophic cardiomyopathy mouse models. *JCI Insight*. 2018;3(6).
6. Sequeira V, Wijnker PJM, Nijenkamp LLaM, Kuster DWD, Najafi A, Witjas-Paalberends ER, et al. Perturbed length-dependent activation in human hypertrophic cardiomyopathy with missense sarcomeric gene mutations. *Circulation research*. 2013;112(11):1491-505.
7. Sequeira V, Najafi A, Wijnker PJ, Dos Remedios CG, Michels M, Kuster DW, et al. ADP-stimulated contraction: A predictor of thin-filament activation in cardiac disease. *Proc Natl Acad Sci U S A*. 2015;112(50):E7003-12.
8. Ojala M, Prajapati C, Polonen RP, Rajala K, Pekkanen-Mattila M, Rasku J, et al. Mutation-Specific Phenotypes in hiPSC-Derived Cardiomyocytes Carrying Either Myosin-Binding Protein C Or alpha-Tropomyosin Mutation for Hypertrophic Cardiomyopathy. *Stem Cells Int*. 2016;2016:1684792.
9. Witjas-Paalberends ER, Guclu A, Germans T, Knaapen P, Harms HJ, Vermeer AM, et al. Gene-specific increase in the energetic cost of contraction in hypertrophic cardiomyopathy caused by thick filament mutations. *Cardiovasc Res*. 2014;103(2):248-57.
10. Ho CY, Lakdawala NK, Cirino AL, Lipshultz SE, Sparks E, Abbasi SA, et al. Diltiazem treatment for pre-clinical hypertrophic cardiomyopathy sarcomere mutation carriers: a pilot randomized trial to modify disease expression. *JACC Heart Fail*. 2015;3(2):180-8.
11. Ho CY, Day SM, Ashley EA, Michels M, Pereira AC, Jacoby D, et al. Genotype and Lifetime Burden of Disease in Hypertrophic Cardiomyopathy: Insights from the Sarcomeric Human Cardiomyopathy Registry (SHaRe). *Circulation*. 2018;138(14):1387-98.
12. Robison P, Caporizzo MA, Ahmadzadeh H, Bogush AI, Chen CY, Margulies KB, et al. Detyrosinated microtubules buckle and bear load in contracting cardiomyocytes. *Science*. 2016;352(6284):aaf0659.
13. Chen CY, Caporizzo MA, Bedi K, Vite A, Bogush AI, Robison P, et al. Suppression of detyrosinated microtubules improves cardiomyocyte function in human heart failure. *Nat Med*. 2018;24(8):1225-33.
14. van Dijk SJ, Dooijes D, dos Remedios C, Michels M, Lamers JM, Winegrad S, et al. Cardiac myosin-binding protein C mutations and hypertrophic cardiomyopathy: haploinsufficiency, deranged phosphorylation, and cardiomyocyte dysfunction. *Circulation*. 2009;119(11):1473-83.
15. Alfares AA, Kelly MA, McDermott G, Funke BH, Lebo MS, Baxter SB, et al. Results of clinical genetic testing of 2,912 probands with hypertrophic cardiomyopathy: expanded panels offer limited additional sensitivity. *Genetics In Medicine*. 2015;17:880.
16. Warmoes M, Jaspers JE, Pham TV, Piersma SR, Oudgenoeg G, Massink MP, et al. Proteomics of mouse BRCA1-deficient mammary tumors identifies DNA repair proteins with potential diagnostic and prognostic value in human breast cancer. *Mol Cell Proteomics*. 2012;11(7):M111 013334.
17. Piersma SR, Broxterman HJ, Kapci M, de Haas RR, Hoekman K, Verheul HM, et al. Proteomics of the TRAP-induced platelet releasate. *J Proteomics*. 2009;72(1):91-109.
18. Perez-Riverol Y, Csordas A, Bai J, Bernal-Llinares M, Hewapathirana S, Kundu DJ, et al. The PRIDE database and related tools and resources in 2019: improving support for quantification data. *Nucleic Acids Res*. 2019;47(D1):D442-D50.
19. Pham TV, Piersma SR, Warmoes M, Jimenez CR. On the beta-binomial model for analysis of spectral count data in label-free tandem mass spectrometry-based proteomics. *Bioinformatics*. 2010;26(3):363-9.
20. Shannon P, Markiel A, Ozier O, Baliga NS, Wang JT, Ramage D, et al. Cytoscape: a software environment for integrated models of biomolecular interaction networks. *Genome Res*. 2003;13(11):2498-504.
21. Maere S, Heymans K, Kuiper M. BiNGO: a Cytoscape plugin to assess overrepresentation of gene ontology categories in biological networks. *Bioinformatics*. 2005;21(16):3448-9.
22. Nepusz T, Yu H, Paccanaro A. Detecting overlapping protein complexes in protein-protein interaction networks. *Nat Methods*. 2012;9(5):471-2.
23. Chen J, Bardes EE, Aronow BJ, Jegga AG. ToppGene Suite for gene list enrichment analysis and candidate gene prioritization. *Nucleic Acids Res*. 2009;37(Web Server issue):W305-11.
24. Heberle H, Meirelles GV, da Silva FR, Telles GP, Minghim R. InteractiVenn: a web-based tool for the analysis of sets through Venn diagrams. *BMC Bioinformatics*. 2015;16:169.

25. Vignier N, Schlossarek S, Fraysse B, Mearini G, Kramer E, Pointu H, et al. Nonsense-mediated mRNA decay and ubiquitin-proteasome system regulate cardiac myosin-binding protein C mutant levels in cardiomyopathic mice. *Circ Res*. 2009;105(3):239-48.
26. Najafi A, Schlossarek S, van Deel ED, van den Heuvel N, Guclu A, Goebel M, et al. Sexual dimorphic response to exercise in hypertrophic cardiomyopathy-associated MYBPC3-targeted knock-in mice. *Pflugers Arch*. 2015;467(6):1303-17.
27. Nijenkamp L, Bollen IAE, van Velzen HG, Regan JA, van Slegtenhorst M, Niessen HWM, et al. Sex Differences at the Time of Myectomy in Hypertrophic Cardiomyopathy. *Circ Heart Fail*. 2018;11(6):e004133.
28. Nagueh SF, Appleton CP, Gillebert TC, Marino PN, Oh JK, Smiseth OA, et al. Recommendations for the evaluation of left ventricular diastolic function by echocardiography. *J Am Soc Echocardiogr*. 2009;22(2):107-33.
29. Lang RM, Bierig M, Devereux RB, Flachskampf FA, Foster E, Pellikka PA, et al. Recommendations for chamber quantification: a report from the American Society of Echocardiography's Guidelines and Standards Committee and the Chamber Quantification Writing Group, developed in conjunction with the European Association of Echocardiography, a branch of the European Society of Cardiology. *J Am Soc Echocardiogr*. 2005;18(12):1440-63.
30. Maron MS, Appelbaum E, Harrigan CJ, Buros J, Gibson CM, Hanna C, et al. Clinical profile and significance of delayed enhancement in hypertrophic cardiomyopathy. *Circ Heart Fail*. 2008;1(3):184-91.
31. Purcell NH, Darwis D, Bueno OF, Muller JM, Schule R, Molkentin JD. Extracellular signal-regulated kinase 2 interacts with and is negatively regulated by the LIM-only protein FHL2 in cardiomyocytes. *Mol Cell Biol*. 2004;24(3):1081-95.
32. Lowes BD, Minobe W, Abraham WT, Rizeq MN, Bohlmeyer TJ, Quaife RA, et al. Changes in gene expression in the intact human heart. Downregulation of alpha-myosin heavy chain in hypertrophied, failing ventricular myocardium. *J Clin Invest*. 1997;100(9):2315-24.
33. Nakao K, Minobe W, Roden R, Bristow MR, Leinwand LA. Myosin heavy chain gene expression in human heart failure. *J Clin Invest*. 1997;100(9):2362-70.
34. Marston S, Copeland O, Gehmlich K, Schlossarek S, Carrier L. How do MYBPC3 mutations cause hypertrophic cardiomyopathy? *J Muscle Res Cell Motil*. 2012;33(1):75-80.
35. Heineke J, Molkentin JD. Regulation of cardiac hypertrophy by intracellular signalling pathways. *Nat Rev Mol Cell Biol*. 2006;7(8):589-600.
36. Matsui T, Nagoshi T, Rosenzweig A. Akt and PI 3-kinase signaling in cardiomyocyte hypertrophy and survival. *Cell Cycle*. 2003;2(3):220-3.
37. Moolman Ja, Reith S, Uhl K, Bailey S, Gautel M, Jeschke B, et al. A newly created splice donor site in exon 25 of the MyBP-C gene is responsible for inherited hypertrophic cardiomyopathy with incomplete disease penetrance. *Circulation*. 2000;101(12):1396-402.
38. Coats CJ, Heywood WE, Virasami A, Ashrafi N, Syrris P, Dos Remedios C, et al. Proteomic Analysis of the Myocardium in Hypertrophic Obstructive Cardiomyopathy. *Circ Genom Precis Med*. 2018;11(12):e001974.
39. Luedde M, Flogel U, Knorr M, Grundt C, Hippe HJ, Brors B, et al. Decreased contractility due to energy deprivation in a transgenic rat model of hypertrophic cardiomyopathy. *J Mol Med (Berl)*. 2009;87(4):411-22.
40. Guclu A, Knaapen P, Harms HJ, Parbhudayal RY, Michels M, Lammertsma AA, et al. Disease Stage-Dependent Changes in Cardiac Contractile Performance and Oxygen Utilization Underlie Reduced Myocardial Efficiency in Human Inherited Hypertrophic Cardiomyopathy. *Circ Cardiovasc Imaging*. 2017;10(5).
41. Crilley JG, Boehm EA, Blair E, Rajagopalan B, Blamire AM, Styles P, et al. Hypertrophic cardiomyopathy due to sarcomeric gene mutations is characterized by impaired energy metabolism irrespective of the degree of hypertrophy. *J Am Coll Cardiol*. 2003;41(10):1776-82.
42. Ashrafian H, Redwood C, Blair E, Watkins H. Hypertrophic cardiomyopathy:a paradigm for myocardial energy depletion. *Trends Genet*. 2003;19(5):263-8.
43. Tarone G, Brancaccio M. Keep your heart in shape: molecular chaperone networks for treating heart disease. *Cardiovasc Res*. 2014;102(3):346-61.
44. Dorsch LM, Schuldt M, dos Remedios CG, Schinkel AFL, de Jong PL, Michels M, et al. Protein Quality Control Activation and Microtubule Remodeling in Hypertrophic Cardiomyopathy. *Cells*. 2019;8(7).
45. Dorsch LM, Schuldt M, Knezevic D, Wiersma M, Kuster DWD, van der Velden J, et al. Untying the knot: protein quality control in inherited cardiomyopathies. *Pflugers Arch*. 2018.
46. Sanbe A, Daicho T, Mizutani R, Endo T, Miyauchi N, Yamauchi J, et al. Protective effect of geranylgeranylacetone via enhancement of HSPB8 induction in desmin-related cardiomyopathy. *PLoS One*. 2009;4(4):e5351.
47. Bhuiyan MS, Pattison JS, Osinska H, James J, Gulick J, McLendon PM, et al. Enhanced autophagy ameliorates cardiac proteinopathy. *J Clin Invest*. 2013;123(12):5284-97.
48. Grimes KM, Prasad V, McNamara JW. Supporting the heart: Functions of the cardiomyocyte's non-sarcomeric cytoskeleton. *J Mol Cell Cardiol*. 2019;131:187-96.
49. Lewis YE, Moskovitz A, Mutlak M, Heineke J, Caspi LH, Kehat I. Localization of transcripts, translation, and degradation for spatiotemporal sarcomere maintenance. *J Mol Cell Cardiol*. 2018;116:16-28.
50. Scholz D, Baicu CF, Tuxworth WJ, Xu L, Kasiganesan H, Menick DR, et al. Microtubule-dependent distribution of mRNA in adult cardiocytes. *Am J Physiol Heart Circ Physiol*. 2008;294(3):H1135-44.
51. Thottakara T, Friedrich FW, Reischmann S, Braumann S, Schlossarek S, Kramer E, et al. The E3 ubiquitin ligase Asb2beta is downregulated in a mouse model of hypertrophic cardiomyopathy and targets desmin for proteasomal degradation. *J Mol Cell Cardiol*. 2015;87:214-24.
52. Robison P, Prosser BL. Microtubule mechanics in the working myocyte. *J Physiol*. 2017;595(12):3931-7.

53. Zile MR, Koide M, Sato H, Ishiguro Y, Conrad CH, Buckley JM, et al. Role of microtubules in the contractile dysfunction of hypertrophied myocardium. *J Am Coll Cardiol*. 1999;33(1):250-60.
54. Infante AS, Stein MS, Zhai Y, Borisy GG, Gundersen GG. Detyrosinated (Glu) microtubules are stabilized by an ATP-sensitive plus-end cap. *J Cell Sci*. 2000;113 (Pt 22):3907-19.
55. Nieuwenhuis J, Brummelkamp TR. The Tubulin Detyrosination Cycle: Function and Enzymes. *Trends Cell Biol*. 2019;29(1):80-92.
56. Aillaud C, Bosc C, Peris L, Bosson A, Heemeryck P, Van Dijk J, et al. Vasohibins/SVBP are tubulin carboxypeptidases (TCPs) that regulate neuron differentiation. *Science*. 2017;358(6369):1448-53.
57. Nieuwenhuis J, Adamopoulos A, Bleijerveld OB, Mazouzi A, Stickel E, Celie P, et al. Vasohibins encode tubulin detyrosinating activity. *Science*. 2017;358(6369):1453-6.
58. Kerr JP, Robison P, Shi G, Bogush AI, Kempema AM, Hexum JK, et al. Detyrosinated microtubules modulate mechanotransduction in heart and skeletal muscle. *Nat Commun*. 2015;6:8526.
59. Swiatlowska P, Sanchez-Alonso JL, Wright PT, Novak P, Gorelik J. Microtubules regulate cardiomyocyte transversal Young's modulus. *Proc Natl Acad Sci U S A*. 2020;117(6):2764-6.

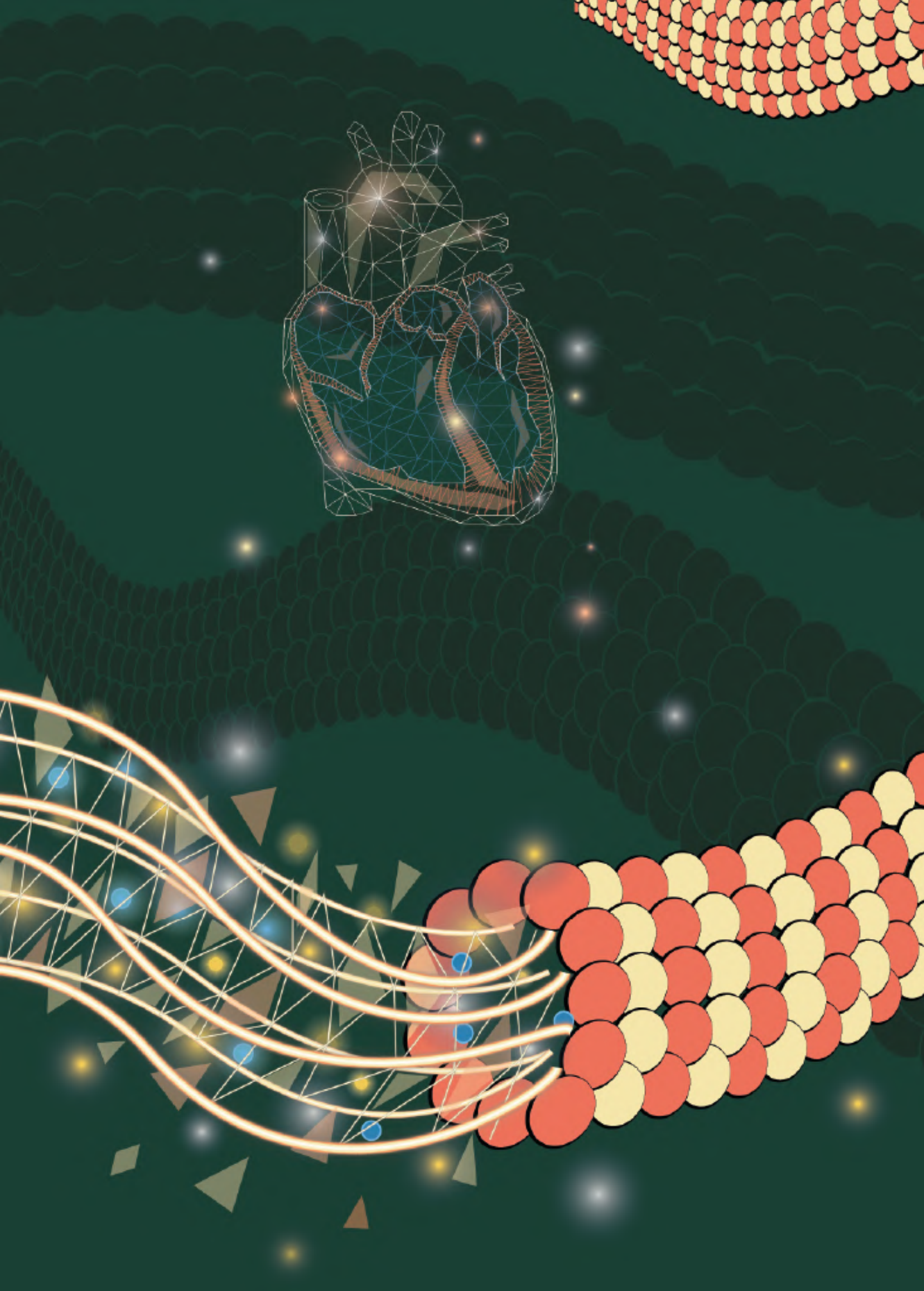

Chapter 7

Protein quality control activation and microtubule remodeling in hypertrophic cardiomyopathy

Larissa M. Dorsch, Maike Schuldt, Cristobal G. dos Remedios, Arend FL. Schinkel, Peter L. de Jong, Michelle Michels, Diederik WD. Kuster, Bianca JJM. Brundel, Jolanda van der Velden

Cells.; 8(7):741 (2019).

ABSTRACT

BACKGROUND

Hypertrophic cardiomyopathy (HCM) is the most common inherited cardiac disorder. It is mainly caused by mutations in genes encoding sarcomere proteins. Mutant forms of these highly abundant proteins likely stress the protein quality control (PQC) system of cardiomyocytes. The PQC system together with a functional microtubule network maintains proteostasis.

METHODS

We compared left ventricular (LV) tissue of 9 donors (controls) with 38 sarcomere mutation-positive (HCM_{SMP}) and 14 sarcomere mutation-negative (HCM_{SMN}) patients to define HCM and mutation-specific changes in PQC. Mutations in HCM_{SMP} result in poison polypeptides or reduced protein levels (haploinsufficiency, HI).

RESULTS

The main findings are: 1) Several key PQC players were more abundant in HCM compared to controls; 2) After correction for sex and age, stabilizing heat shock protein (HSP)B1, and refolding HSPD1 and HSPA2 were increased in HCM_{SMP} compared to controls; 3) α-tubulin and acetylated α-tubulin levels were higher in HCM compared to controls, especially in HCM_{HI}; 4) Myosin-binding protein-C (cMyBP-C) levels were inversely correlated with α-tubulin; 5) α-tubulin levels correlated with acetylated α-tubulin and HSPs.

CONCLUSION

Overall, carrying a mutation affects PQC and α-tubulin acetylation. Haploinsufficiency of cMyBP-C may trigger HSPs and α-tubulin acetylation. Our study indicates that proliferation of the microtubular network may represent a novel pathomechanism in cMyBP-C haploinsufficiency-mediated HCM.

INTRODUCTION

Hypertrophic cardiomyopathy (HCM) is a common familial cardiac disease with an estimated prevalence of 1:200.[1] It is characterized by an asymmetrically hypertrophied, non-dilated left ventricle and impaired diastolic function.[2] More than 1500 pathogenic mutations have been identified which most frequently encode proteins in the sarcomere. Previous studies have shown that sarcomere mutations alter myofilament function (reviewed recently in [3]) However, while the same sarcomere mutation is present in members of one family, age of onset and disease severity vary greatly between patients spanning from asymptomatic mutation carriers to symptomatic patients with severe cardiac remodelling.[4] This large clinical heterogeneity implies that HCM pathophysiology is more complex than the functional defects triggered by the gene mutation. Furthermore, pathogenic mutations were only found in ~50% of all HCM patients.[4] Moreover, a recent large international clinical HCM study showed that patients with a mutation in a sarcomere gene have a 2-fold higher risk of adverse outcomes (e.g. heart failure and atrial fibrillation) compared to patients with no known mutations.[5] The exact mechanisms underlying the difference in disease severity between sarcomere mutation-positive (HCM_{SMP}) and mutation-negative (HCM_{SMN}) patients are currently unknown.

A mechanism implicated in HCM progression is perturbed protein quality control (PQC).[6,7] Cardiomyocytes contain a multi-layered PQC system for maintaining proper protein conformation, and for reorganizing and removing misfolded or aggregated (mutant) proteins.[8] The PQC system comprises heat shock proteins (HSPs), the ubiquitin-proteasome system (UPS), and autophagy.[9] HSPs are involved at all stages of sustaining protein homeostasis: during protein biosynthesis and maturation, in chaperoning the folding, in protection from environmental stress, in rearrangements of cellular macromolecules during functional cycles of assembly and disassembly, and finally in targeting proteins for degradation.[10] Terminally misfolded and aggregation-prone proteins are cleared by the two degradation systems, UPS and autophagy.[11] Furthermore, pathways of PQC are strongly linked to cell architecture, such as the microtubules network.[12] As sarcomere proteins are the most abundant proteins in the heart, maintenance of sarcomere structure and functions depends on functioning PQC mechanisms. Perturbations in PQC mechanisms may be aggravated by the presence of sarcomere gene mutations that may explain the difference in disease severity between HCM_{SMP} and HCM_{SMN} patient groups. Moreover, the proteotoxic burden on PQC may depend on the type of mutation: in HCM, gene mutations either result in a 'poison polypeptide' (an expressed protein containing a mutated sequence) or haploinsufficiency where up-regulation of the wild-type protein levels failed to compensate for reduced total protein.[13,14]

Here, we identified and quantified key PQC players, such as HSPs and degradation markers (ubiquitinated proteins, p62, LC3BII) and microtubule network markers (for example acetylation of α-tubulin) in a large set of myectomy samples from HCM_{SMP} and HCM_{SMN} patients to define if the presence of a sarcomere mutation differentially affects PQC. In addition, mutation-specific PQC changes were assessed by comparing HCM with missense mutations and *MYBPC3* (cardiac myosin-binding protein-C) mutations, which cause haploinsufficiency.

METHODS

SEPTAL MYECTOMY

Cardiac tissue from the interventricular septum was obtained during myectomy surgery to relieve left ventricular (LV) outflow tract obstruction. Patients are selected for surgery at our HCM centre on the basis of the following indications: (1) peak left ventricular outflow tract (LVOT) gradient $\geq$50 mmHg at rest or on provocation and (2) presence of unacceptable symptoms despite maximally tolerated medications consisting of β-blocking agents and/or calcium channel blockers. The decision to perform surgery was made after consensus of a heart team consisting of a cardiothoracic surgeon, an interventional cardiologist, and a cardiologist specialized in HCM care.[15] Hypertrophic obstructive cardiomyopathy was evident from the increased septal thickness with a mean ($\pm$ SD) of 21 ($\pm$ 6) mm and high LV outflow tract pressure gradient with a mean ($\pm$ SD) of 66 ($\pm$ 37) mmHg. Next-generation-sequencing was used to check 48 different HCM-associated genes for variants.[16]

This study included 52 septal myectomy patients and they are summarized in Table 7.1. 38 HCM patients were tested positive for carrying a gene variant in one of the genes encoding for sarcomeric protein. Ages of all 38 HCM_{SMP} patients ranged between 15 and 72 with a mean ($\pm$ SD) of 49 ($\pm$ 16) years and 68% of these were males. Dependent on the reported pathomechanism, this group was subdivided into haploinsufficiency (HI) and poison polypeptide (PP) subgroups.

Seven patients of the HCM_{HI} group were identified as carrying the Dutch founder mutation (c.2373dupG) in *MYBPC3*, the gene encoding the A band protein, cardiac myosin-binding protein-C (cMyBP-C) and twelve patients carried other mutations in *MYBPC3* of which three were missense and the remainder were truncations. Patient ages ranged between 21 and 71 years with a mean ($\pm$ SD) of 43 ($\pm$ 15) years. 79% of these were males. We collected 19 myectomy samples from HCM_{PP} patients carrying a missense mutation. Nine patients presented with mutations in the gene for cardiac myosin heavy chain (*MYH7*), the second most commonly mutated gene in HCM patients. Four patients carried mutations in the gene for troponin I (*TNNI3*), three patients carried troponin T (*TNNT2*) mutations and two patients carried myosin light chain 2 (*MYL2*) mutations. HCM_{PP} patients were aged between 15 and 72 years with a mean ($\pm$ SD) of 55 ($\pm$ 15) years. 58% of these were males.

Our study included 14 patients with no known sarcomere gene mutation. HCM_{SMN} patient ages ranged between 22 to 74 with a mean ($\pm$ SD) of age 57 ($\pm$ 14). 64% of these were males. Not all myectomy samples were sufficiently large to perform all analyses.

Finally, the 52 HCM samples were compared with nine samples of healthy donor hearts that were not used for heart transplantation, often because of poor tissue matching against patients in the heart failure clinic of St Vincent's Hospital. While these controls had no history of cardiac disease, their validity as "controls" is based on their extensive use as such in publications from a wide range of other laboratories. We therefore assume

these donors are representative of diverse human population. Consistent with the HCM patients, these donor were 67% male, with a mean age (± SD) of 43 (± 14) years, ranging from 19 to 65. All donor hearts were perfused with ice-cold cardioplegia, transported on ice to the Sydney Heart Bank where ~1 g samples were snap frozen and stored in liquid nitrogen. The average values of control cardiac samples (n=9) are indicated by the dotted lines in Figures 7.1 to 7.4 and Figure 7.6. The distribution of the controls are shown in the Supplementary Materials (Figure S1) as well as uncropped full-width images of the membranes (Figure S2). The patients study protocol was approved by the local ethics committees and donor hearts were approved by the University of Sydney (HREC #7326). All collections were made with written informed consent obtained from each patient prior to surgery and from the donors' next of kin.

Table 7.1: Characteristics of controls and manifest HCM patients.

Number	Code	Reported pathomechanism	Affected gene	Gene/ protein variant	Type of mutation	Sex (F/ M)	Age	ST (mm)	LVOT (mmHg)
1	HCM 42[17-20]	HI	MYBPC3	c.2373dupG	truncation	M	32	23	64
2	HCM 43[18-22]	HI	MYBPC3	c.2373dupG	truncation	M	60	23	77
3	HCM 103[20]	HI	MYBPC3	c.2373dupG	truncation	M	26	20	13
4	HCM 104[20]	HI	MYBPC3	c.2373dupG	truncation	M	33	24	31
5	HCM 120[20]	HI	MYBPC3	c.2373dupG	truncation	M	27	24	61
6	HCM 123[20]	HI	MYBPC3	c.2373dupG	truncation	F	59	12	64
7	HCM 169[20]	HI	MYBPC3	c.2373dupG	truncation	M	52	-	-
8	HCM 34[18,20,23]	HI	MYBPC3	c.1790G>A; p.Arg597Gln	missense	F	47	20	38
9	HCM 36 [17,18,20-25]	HI	MYBPC3	c.927-2A>G	truncation	M	22	30	71
10	HCM 47 [19,20,23,25]	HI	MYBPC3	c.3407_ 3409delACT	truncation	M	55	25	96
11	HCM 52[18-20]	HI	MYBPC3	c.2827C>T	truncation	F	24	24	34
12	HCM 62 [17,18,20,23]	HI	MYBPC3	c.772G>A; p.Glu258Lys	missense	M	35	27	3
13	HCM 63[20,23]	HI	MYBPC3	c.2827C>T	truncation	M	33	21	25
14	HCM 71[20]	HI	MYBPC3	c.2827C>T	truncation	M	49	16	9
15	HCM 82[20]	HI	MYBPC3	c.2783C>T; p.Ser928Leu	missense	M	71	20	64
16	HCM 113[17,20]	HI	MYBPC3	c.2827C>T	truncation	M	21	45	27
17	HCM 116[20]	HI	MYBPC3	c.2827C>T	truncation	F	53	-	-
18	HCM 124[20]	HI	MYBPC3	c.2827C>T	truncation	M	53	21	41
19	HCM 133[20]	HI	MYBPC3	c.442G>A	truncation	M	58	-	-
1	HCM 27[18-20,25]	PP	MYH7	c.4130C>T; p.Thr1377Met	missense	F	58	20	100
2	HCM 42B [18-20,23,25]	PP	MYH7	c.1816G>A; p.Val606Met	missense	F	46	20	77
3	HCM 80[20]	PP	MYH7	c.1291G>C & c.4327G>A; p.Val431Leu & p.Asp1443Asn	missense	M	34	17	85
4	HCM 92[20]	PP	MYH7	c.2685A>C; p.Glen895His	missense	M	66	-	-

Table 7.1: Continued

Number	Code	Reported pathomechanism	Affected gene	Gene/ protein variant	Type of mutation	Sex (F/ M)	Age	ST (mm)	LVOT (mmHg)
5	HCM 106[20]	PP	MYH7	c.2783A>T; p.Asp928Val	missense	M	35	16	16
6	HCM 114[20]	PP	MYH7	c.976G>C; p.Ala326Pro	missense	M	69	19	71
7	HCM 119[20]	PP	MYH7	c.3367G>A; p.Glu1123Gln	missense	M	41	20	81
8	HCM 130[20]	PP	MYH7	c.976G>C; p.Ala326Pro	missense	M	72	18	27
9	HCM 131	PP	MYH7	c.1987C>T; p.Arg663Cys	missense	F	52	21	41
10	HCM 166[20]	PP	MYH7	c.2080C>T; p.Arg694Cys	missense	F	66	-	-
11	HCM 55[18,23,25]	PP	TNNI3	c.433C>T; p.Arg145Trp	missense	M	46	23	100
12	HCM 59[18,25]	PP	TNNI3	c.433C>T; p.Arg145Trp	missense	M	66	16	67
13	HCM 163	PP	TNNI3	c.433C>T; p.Arg145Trp	missense	F	64	-	-
14	HCM 170	PP	TNNI3	c.433C>T; p.Arg145Trp	missense	F	69	-	-
15	HCM 132	PP	TNNT2	c.814C>T; p.Arg272Cys	missense	F	15	-	-
16	HCM 173	PP	TNNT2	c.832C>T; p.Arg278Cys	missense	M	58	-	-
17	HCM 175	PP	TNNT2	c.832C>T; p.Arg278Cys	missense	M	61	-	-
18	HCM 135	PP	MYL2	c.64G>A; p.Glu22Lys	missense	M	68	-	-
19	HCM 88	PP	MYL2	c.401A>C; p.Glu134Ala	missense	F	57	-	-
1	3145[27-39]	Ctrl			-	M	39	-	-
2	4021[33-45]	Ctrl			-	F	53	-	-
3	4049[33-42,46-51]	Ctrl			-	M	65	-	-
4	5126[46-49,52]	Ctrl			-	F	55	-	-
5	6008[42,53-55]	Ctrl			-	M	40	-	-
6	7012[27-32,56,57]	Ctrl			-	M	19	-	-
7	7040[33-36,55,58]	Ctrl			-	M	37	-	-
8	7054[55,59]	Ctrl			-	M	33	-	-
9	8004[55]	Ctrl			-	F	50	-	-

HI: haploinsufficiency; PP: poison polypeptide; SMN: sarcomere mutation-negative; Ctrl: healthy donor hearts; F: female; M: male; Age at time of surgery; ST: septal thickness; LVOT: left outflow tract pressure gradient at rest. Patients without significant obstruction (LVOT gradient <20 mmHg), but with severe heart failure symptoms, received an extended myectomy in order to increase LV filling.

WHOLE PROTEIN ISOLATION

Frozen tissue was dissected on dry ice and homogenized with RIPA buffer (0.05 M $C_4H_{11}NO_3 \cdot HCl$ pH 8.0, 0.15 M NaCl, 1% (v/v) IGEPAL CA-630, 0.5% (w/v) sodium

deoxycholate, 1% (w/v) sodium dodecyl sulphate) using a Tissuelyser II (Qiagen). The lysates were centrifuged, supernatant was collected and passed through an insulin syringe (Becton Dickinson Microlance needle, 25 gauge). Whole protein lysate was mixed with 4x Laemmli sample buffer (8% (w/v) sodium dodecyl sulphate, 40% (v/v) glycerol, 0.04% (w/v) bromophenol blue, 0.240 M $C_4H_{11}NO_3 \cdot HCl$ pH 6.8, 10 mM β-mercaptoethanol, 0.01 M NaF, 0.001 M Na_3VO_4, cOmplete mini protease inhibitor cocktail (Roche)), boiled for 5 min and stored at -80°C.

ELECTROPHORESIS AND WESTERN BLOTS

Equal amounts of protein (10 µg) were separated on pre-cast SDS-PAGE 4-12% criterion gels (Bio-Rad) and transferred onto nitrocellulose membranes (Bio-Rad). Membranes were blocked in 5% (w/v) skim milk/1x TBST for 1 h at room temperature and incubated overnight at 4°C with the following primary antibodies in 3% (w/v) BSA/1x TBST: mouse anti-acetylated α-tubulin (T7451, Sigma-Aldrich), mouse anti-α-actinin (A7811, Merck KGaA), mouse anti-HSPA1 (ADI-SPA-810, Enzo Life Sciences), mouse anti-HSPA2 (66291-1, Proteintech Group), mouse anti-HSPB1 (ADI-SPA-800, Enzo Life Sciences), rabbit anti-HSPB5 (ADI-SPA-223, Enzo Life Sciences), rabbit anti-HSPB7 (ab150390, Abcam), rabbit anti-HSPD1 (ADI-SPA-805, Enzo Life Sciences), mouse anti-GAPDH (10R-G109a, Fitzgerald Industries International), mouse anti-LC3B (#2775, Cell Signaling Technology), rabbit anti-p62 (#5114, Cell Signaling Technology), mouse anti-α-tubulin (T9026, Sigma-Aldrich), rabbit anti-ubiquitin (#3933, Cell Signaling Technology). Membranes were incubated for 1 h at room temperature with horseradish peroxidase-conjugated secondary antibody (DakoCytomation), raised in goat, in 3% (w/v) BSA/1x TBST. Signals were detected by Amersham Imager 600 (GE Healthcare) and quantified by densitometry (ImageQuant TL, GE Healthcare). To correct for loading differences, protein amounts were expressed relative to GAPDH.

STATISTICAL ANALYSES

Data were analysed with SPSS Statistics version 22.0 for Windows (IBM Corporation, US) and GraphPad Prism version 7.0 (GraphPad Software Inc., US). Data in figures are presented as means ± standard errors of the mean (SEM) per group and in text, data are presented as means ± standard deviations (SD). Distribution of each data set was determined by Q-Q plots and then double checked by Kolmogorov-Smirnov and Shapiro Wilk tests after data collection was completed. Normally distributed data was analysed with unpaired t-test (comparing 2 groups) and ordinary one-way ANOVA (comparing $>$ 2 groups) with Tukey's multiple comparisons post-hoc test (comparing $\leq$ 3 groups) and Dunnett's multiple comparisons post-hoc test (comparing $>$ 3 groups). To analyse non-parametric data, Mann-Whitney U test (comparing 2 groups) and Kruskal-Wallis test with Dunn's multiple comparisons post-hoc test (comparing $>$ 2 groups) were used. A two-sided $p<0.05$ was considered to indicate statistical significance. Multivariate generalized linear model testing (detailed description in the Supplementary Materials) was performed to study the main effects of different mutation groupings, sex, and age at operation on PQC proteins which were used as dependent variables.

RESULTS

CHANGES OF PROTEIN QUALITY CONTROL IN HCM_{SMP} AND HCM_{SMN}

We investigated the expression levels of key PQC proteins to determine if they are altered in patients with HCM at the time of myectomy compared with the levels in LV samples from healthy controls. As the mutant sarcomere proteins may directly affect PQC, we used Western blots to compare myectomy samples from 38 HCM_{SMP} and 14 HCM_{SMN} patients with LV tissue from nine healthy controls that were age- and sex-matched to the HCM samples (Table 7.1).

HSPs THAT STABILIZE TARGET PROTEINS

Dependent on their function, HSPs are classified in two categories: stabilizing HSPs and HSPs with refolding capacity. Stabilizing HSPs (HSPB1 (also known as HSP27), HSPB5 (αB-crystallin), HSPB7 (cardiovascular HSP)) have relatively low molecular weights (15-30 kDa). They stabilize misfolded proteins using an ATP-independent holdase activity, thereby preventing their aggregation (Figure 7.1A). Compared to controls, the HCM_{SMP} samples expressed significantly higher levels of HSPB1 and HSPB7, while HSPB5 appeared to be unaltered (Figure 7.1C; Table 7.2).

Table 7.2: Overview of results on statistical testing for differences between controls, HCM_{SMP} and HCM_{SMN}.

Proteins	Statistical test	*p*-value	Adjusted *p*-value post-hoc testing		
			Controls vs. HCM_{SMP}	Controls vs. HCM_{SMN}	HCM_{SMP} vs. HCM_{SMN}
Stabilizing HSPs					
HSPB1	Kruskal-Wallis	0.0019	0.0018	0.2113	0.3302
HSPB5	Ordinary one-way ANOVA	0.1297	0.1090	0.3807	0.8174
HSPB7	Kruskal-Wallis	0.0060	0.0048	0.0341	>0.9999
Refolding HSPs					
HSPD1	Ordinary one-way ANOVA	0.0004	0.0003	0.0530	0.2123
HSPA1	Kruskal-Wallis	0.3636	0.6382	>0.9999	>0.9999
HSPA2	Ordinary one-way ANOVA	0.0101	0.0071	0.1008	0.7334
Protein degradation					
Ubiquitin	Kruskal-Wallis	0.2159	0.3094	>0.9999	0.9890
p62	Ordinary one-way ANOVA	0.1087	0.5822	0.7531	0.1046
LC3BII	Kruskal-Wallis	0.0451	0.0384	0.2455	>0.9999
Tubulin network					
α-tubulin	Ordinary one-way ANOVA	<0.0001	<0.0001	0.0119	0.0019
Acetylated α-tubulin	Kruskal-Wallis	<0.0001	<0.0001	0.0451	0.0516

$p<0.05$ is considered to be significant.

We then quantified the protein levels of these stabilizing HSPs (HSPB1, HSPB5 and HSPB7) in HCM_{SMN} samples. Only HSPB7 was significantly higher in HCM_{SMN} compared to controls (Figure 7.1C; Table 7.2). Despite this, there were no significant differences in stabilizing HSPs levels between HCM_{SMP} and HCM_{SMN}.

HSPs THAT REFOLD TARGET PROTEINS

Next we investigated the expression levels of HSPD1 (HSP60), HSPA1 (HSP70 and HSP72) and HSPA2 (HSP70-2) that have an ATP-dependent folding activity. These HSPs have molecular weights >30 kDa and either refold misfolded proteins or assist in their degradation. HSPD1 is mainly located in mitochondria while HSPA1 and HSPA2 are cytosolic, but when they are exposed to heat stress, both translocate to the nucleus.[60,61] Compared to controls, significantly higher levels of HSPD1 and HSPA2 were observed in HCM_{SMP} samples, while HSPA1 levels were not significantly changed. Levels of HSPs with refolding capacity were not significantly different in HCM_{SMN} compared to controls, although HSPD1 and HSPA2 showed a trend to higher levels. There were no significant differences in HSPs with refolding capacity between the two HCM groups (Figure 7.2; Table 7.2).

DEGRADATION OF PROTEINS

PQC is also involved in the degradation of proteins and therefore levels of ubiquitination, p62 and LC3BII were assessed. The antibody used for ubiquitin recognizes polyubiquitinated proteins without distinguishing between K48-linked polyubiquitin chains (predominantly targeted by proteasomal degradation) and K63-linked polyubiquitin chains (targeted by autophagic degradation).[62] Levels of ubiquitin and the ubiquitin-binding autophagic adaptor protein p62 were unaltered in both HCM groups compared to controls. Levels of the autophagosome marker LC3BII were significantly higher in HCM_{SMP} compared to controls, while only some samples of the HCM_{SMN} group had higher levels of LC3BII (Figure 7.3; Table 7.2).

To ensure that the significant differences detected by ANOVA testing were not related to differences in age and/or sex of the myectomy patients, we performed multivariate testing (Wilks' Lambda test). This test uses age, sex and the HCM grouping (controls, HCM_{SMP} and HCM_{SMN}) as the effects and the HSPs, ubiquitination, p62, and LC3BII as dependent variables. We found an overall significant difference in levels of key PQC players based on the different mutation groups (Table 7.3), while sex and age at operation had no significant effect on levels of key PQC players.

Table 7.3: Multivariate Tests[a]: HCM grouping (controls, HCM_{SMP}, and HCM_{SMN}), sex and age at operation.

Effect	Value	F	Hypothesis df	Error df	Significance	Partial eta squared
Intercept	0.260	14.561[b]	9.000	46.000	<0.001	0.740
HCM grouping	0.479	2.278[b]	18.000	92.000	0.006	0.308
Sex	0.754	1.664[b]	9.000	46.000	0.126	0.246

Table 7.3: Continued

Effect	Value	F	Hypothesis df	Error df	Significance	Partial eta squared
Age at operation	0.717	2.016[b]	9.000	46.000	0.059	0.283

[a] Design: Intercept and HCM grouping and sex and age at operation; [b] exact statistic; F: F statistic for the given effect and test statistic; Hypothesis df: Number of degrees of freedom in the model; Error df: Number of degrees of freedom associated with the model errors; Partial eta squared: estimate of effect size; $p<0.05$ is considered to be significant.

To determine which of the individual key PQC players differ among groups when taking into account sex and age, we performed tests for between-subjects effects. This test revealed statistically significant differences among groups for HSPB1 and HSPD1 (Table 7.4).

Table 7.4: Tests for between-subjects: HCM grouping (controls, HCM_{SMP}, HCM_{SMN}) as an effect and correction for differences in sex and age at operation.

	Type III Sum of Squares	df	Mean Square	F	Significance	Partial eta squared	R squared
Stabilizing HSPs							
HSPB1	23.286	2	11.643	6.031	0.004	0.182	0.261
HSPB5	1.777	2	0.889	2.495	0.092	0.085	0.088
HSPB7	9.725	2	4.863	3.319	0.044	0.109	0.162
Refolding HSPs							
HSPD1	11.104	2	5.552	10.543	<0.001	0.281	0.323
HSPA1	0.258	2	0.129	0.981	0.381	0.035	0.055
HSPA2	1.724	2	0.862	5.114	0.009	0.159	0.171
Protein degradation							
Ubiquitin	1.433	2	0.716	2.101	0.132	0.072	0.097
p62	0.733	2	0.367	2.498	0.092	0.085	0.122
LC3BII	12.839	2	6.420	2.276	0.112	0.078	0.111

df: Number of degrees of freedom in the model; F: F statistic for the given effect and test statistic; Partial eta squared: estimate of effect size; R squared: proportion of the variance in the dependent variable that is predictable from the independent variable; Bonferroni correction: statistical significance at $p<0.0056$ ($\alpha/9 = 0.05/9 = 0.0056$).

Since we found between-subjects main effects, we performed contrast analysis to determine significant pairwise differences between controls and the two HCM patient groups corrected for age and sex. A simple main effects analysis revealed significantly higher levels of HSPB1, HSPD1 and HSPA2 in HCM_{SMP} compared to controls (Table 7.5), while a trend to higher levels of HSPD1 was observed in HCM_{SMN}. Overall, our analyses showed increased levels of several HSPs in HCM_{SMP} and HCM_{SMN} compared to controls, while no significant differences between HCM_{SMP} and HCM_{SMN} were observed.

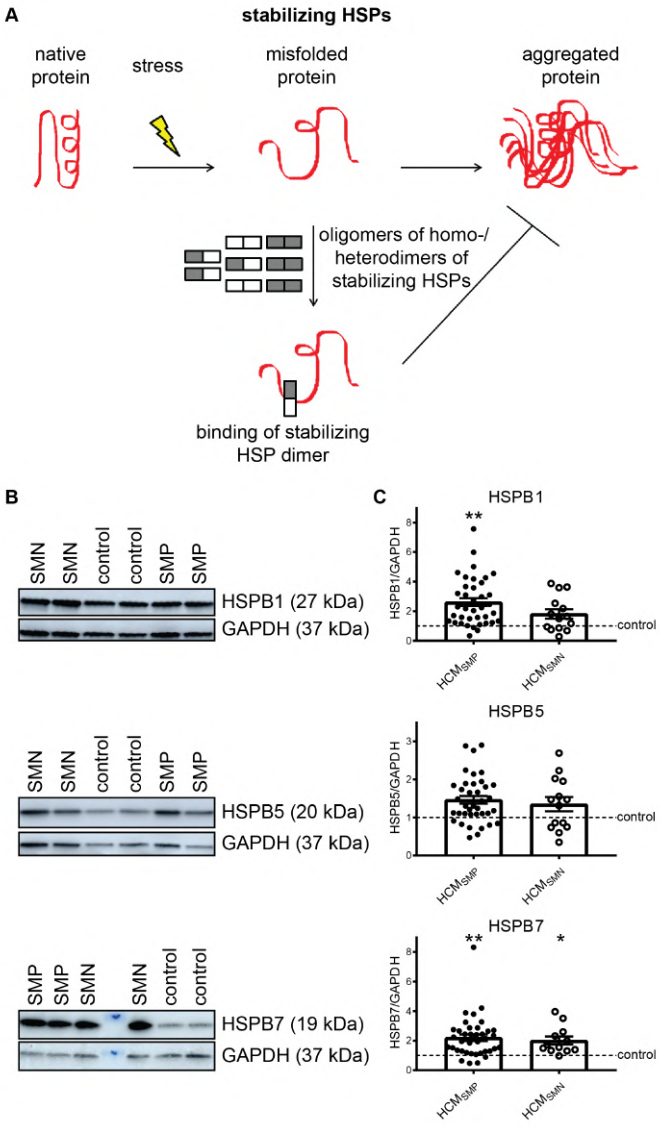

Figure 7.1: Stabilizing HSPs.
(**A**) Under stress conditions when native proteins are destabilized and begin to unfold, stabilizing HSPs dissociate from homo- and/or heterogeneous oligomeric complexes into dimers to bind these partially misfolded proteins. Thereby, stabilizing HSPs prevent the aggregation of misfolded proteins. Figure reproduced and adapted with permission from Dorsch, L.M. et al., Pflügers Archiv – European Journal of Physiology; published by Springer Berlin Heidelberg, 2018. (**B**) Representative blot images for HSPB1, HSPB5, and HSPB7 expression. (**C**) Higher levels of HSPB1 and HSPB7 in HCM_{SMP} (n=38) compared to controls. Higher HSPB7 levels in HCM_{SMN} (n=12) compared to controls (n=9; average is shown as dotted line). HSPB1 and HSPB5 protein levels were not different in HCM_{SMP} (n=14) compared to controls. There were no significant differences between HCM_{SMP} and HCM_{SMN}. Each dot in the scatter plots represents an individual sample. *$p<0.05$ and **$p<0.01$ versus controls.

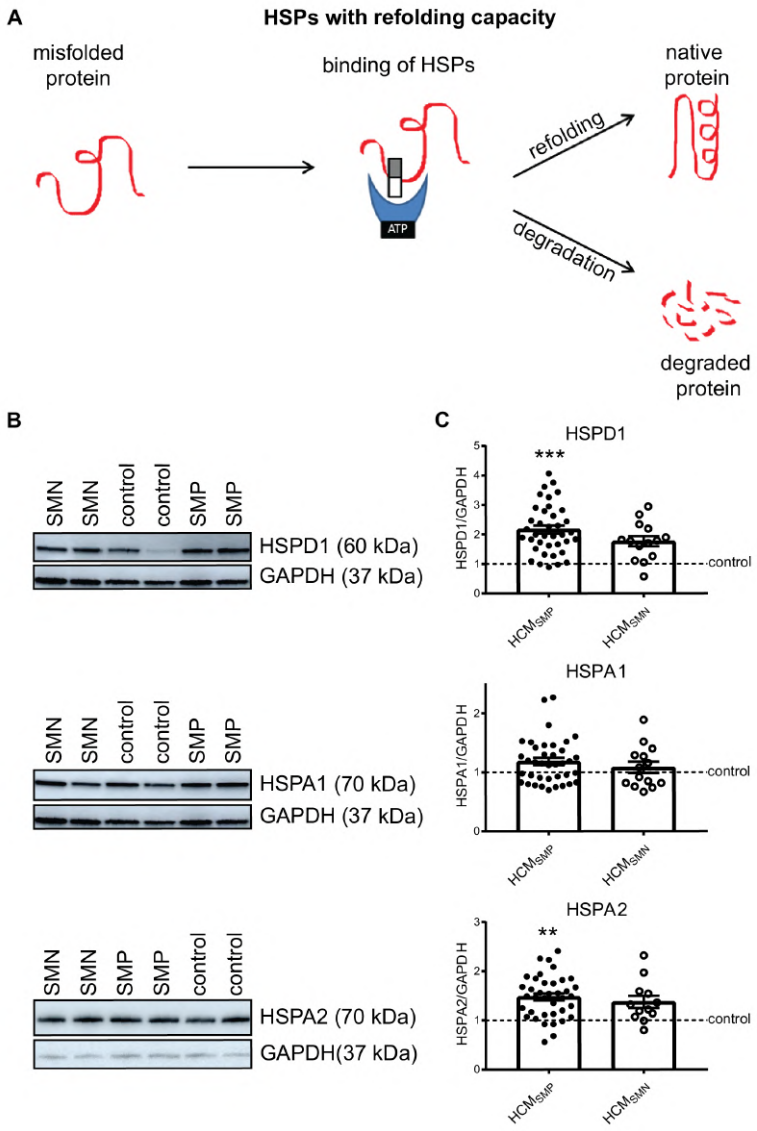

Figure 7.2: HSPs with refolding capacity.
(**A**) HSPs with ATPase activity and stabilizing HSPs bind to the misfolded protein to stabilize and further process it. HSPs with refolding capacity either refold the misfolded protein to its native structure or, if refolding is impossible, the HSPs assist in the degradation pathways to degrade the misfolded protein. Figure reproduced and adapted with permission from Dorsch, L.M. et al., Pflügers Archiv – European Journal of Physiology; published by Springer Berlin Heidelberg, 2018. (**B**) Representative blot images for HSPD1, HSPA1, and HSPA2 expression. (**C**) Higher levels of HSPD1 and HSPA2 in HCM_{SMP} (n=38) compared to controls. HSPs with refolding capacity were unaltered in HCM_{SMN} (HSPD1, HSPA1: n=14; HSPA2: n=12) compared to controls. There were no significant differences between HCM_{SMP} and HCM_{SMN}. Each dot in the scatter plots represents an individual sample. $^{**}p<0.01$ and $^{***}p<0.001$ versus controls.

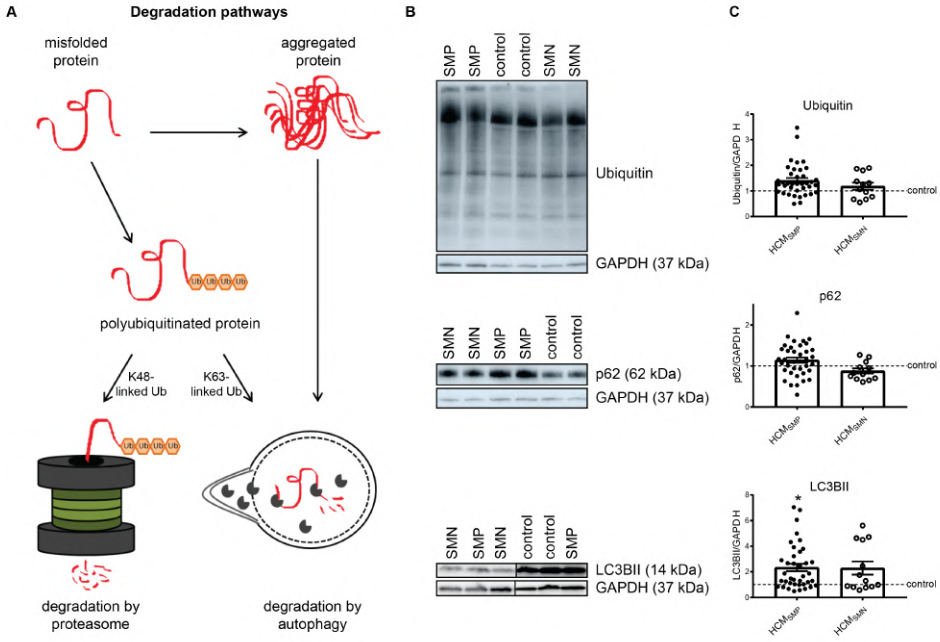

Figure 7.3: Degradation pathways.
(**A**) Misfolded proteins with polyubiquitin chains linked via lysine 48 (K48) are mainly degraded by the proteasome. Misfolded proteins carrying K63-linked polyubiquitin chains and aggregated proteins enter the autophagic pathway. Figure reproduced and adapted with permission from Dorsch, L.M. et al., Pflügers Archiv – European Journal of Physiology; published by Springer Berlin Heidelberg, 2018. (**B**) Representative blot images for ubiquitin, p62, and LC3BII expression. (**C**) Protein levels of ubiquitin and p62 did not differ between HCM and controls samples. Higher levels of LC3BII in HCM_{SMP} (n=38) compared to controls. There were no significant differences between HCM_{SMP} and HCM_{SMN} (ubiquitin, p62: n=12; LC3BII: n=13). Each dot in the scatter plots represents an individual sample. *p<0.05 versus controls.

Table 7.5: Simple Contrast Results (K Matrix) for HCM grouping (controls, HCM_{SMP}, HCM_{SMN}) as an effect and correction for differences in age at operation and sex.

		Dependent Variable								
		Stabilizing HSPs			Refolding HSPs			Protein degradation		
		HSPB1	HSPB5	HSPB7	HSPD1	HSPA1	HSPA2	Ubiquitin	p62	LC3BII
HCM_{SMP} vs. controls	Contrast Estimate	1.804	0.447	1.164	1.242	0.177	0.491	0.441	0.128	1.319
	Standard error	0.520	0.223	0.453	0.271	0.136	0.154	0.218	0.143	0.628
	Significance	0.001	0.050	0.013	<0.001	0.198	0.002	0.049	0.375	0.040
	95% CI Lower Bound	0.761	-<0.001	0.257	0.698	-0.095	0.183	0.003	-0.159	0.060
	95% CI Upper Bound	2.848	0.895	2.072	1.786	0.449	0.799	0.878	0.415	2.578
HCM_{SMN} vs. controls	Contrast Estimate	1.522	0.178	0.929	0.961	0.086	0.452	0.301	-0.160	1.335
	Standard error	0.650	0.279	0.565	0.339	0.169	0.192	0.273	0.179	0.784
	Significance	0.023	0.524	0.106	0.006	0.613	0.031	0.274	0.374	0.094
	95% CI Lower Bound	0.220	-0.380	-0.204	0.282	-0.253	0.041	-0.245	-0.519	-0.236
	95% CI Upper Bound	2.825	0.737	2.062	1.641	0.426	0.810	0.848	0.198	2.907

CI: Confidence Interval; Bonferroni correction: statistical significance at p<0.0028 ($\alpha/18 = 0.05/18 = 0.0028$).

CHANGES OF PROTEIN QUALITY CONTROL: HCM DISEASE MECHANISM

All studied HCM_{SMP} patients are heterozygous for the mutation implying the potential to produce either/or both the mutant and wild-type protein.[14] Either the expression of mutant protein, which above a threshold (the 'poison polypeptide' mechanism) level might become toxic or an inability to upregulate the haplotype protein levels to meet the needs of the heart (the 'haploinsufficiency' mechanism) might underlie HCM.[14] Truncation and missense *MYBPC3* mutations usually involve haploinsufficiency as the disease mechanism since total cMyBP-C protein level is lower and the mutant protein has not been detected in human myectomy samples.[13,63]

We determined whether key PQC players are differently changed in samples with haploinsufficiency (HI) and poison polypeptide (PP) by comparing 19 *MYBPC3* mutation samples (HCM_{HI}) with 19 HCM_{SMP} samples carrying a missense mutation (HCM_{PP}). Proteomics analysis using mass spectrometry revealed significantly lower cMyBP-C protein levels in the HCM_{HI} samples compared to the HCM_{PP} patients, consistent with a protein haploinsufficiency mechanism (Figure 7.4).[64]

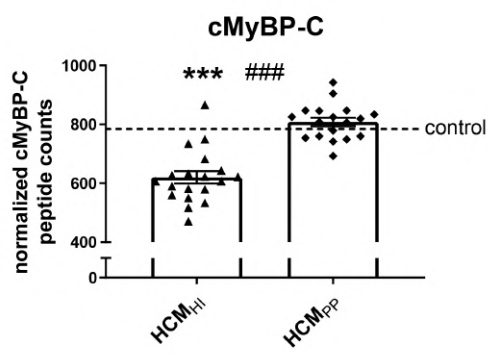

Figure 7.4: cMyBP-C haploinsufficiency.
Mass spectrometry-based proteomics analysis revealed lower levels of cMyBP-C in HCM_{HI} (n=19) compared to controls (n=5) and HCM_{PP} (n=18). Each dot in the scatter plot represents an individual sample. $^{***}p<0.001$ versus controls and $^{\#\#\#}p<0.001$ versus HCM_{PP}.

No significant differences in PQC components were observed between HCM_{HI} and HCM_{PP} (Figure 7.5; Table 7.6).

Table 7.6: Overview of results on statistical testing for differences between HCM_{HI} and HCM_{PP}.

	Statistical test	*p*-value
Stabilizing HSPs		
HSPB1	Unpaired t-test	0.4040
HSPB5	Unpaired t-test	0.6236
HSPB7	Mann-Whitney U test	0.4181
Refolding HSPs		
HSPD1	Unpaired t-test	0.1712

Table 7.6: Continued

	Statistical test	*p*-value
HSPA1	Unpaired t-test	0.8044
HSPA2	Unpaired t-test	0.2096
Protein degradation		
Ubiquitin	Unpaired t-test	0.6099
p62	Unpaired t-test	0.5868
LC3BII	Unpaired t-test	0.4297
Tubulin network		
α-tubulin	Unpaired t-test	0.0074
Acetylated α-tubulin	Unpaired t-test	0.0079
Acetylated α-tubulin/α-tubulin	Mann-Whitney U test	0.1629

$p<0.05$ is considered to be significant.

MICROTUBLE NETWORK

Microtubule-based transport of proteins is required for autophagy and is thus an essential part of PQC. Acetylation of α-tubulin is associated with stable microtubules and is used as a marker of their stability.[65,66] Mouse models of familial HCM showed higher levels of acetylated α-tubulin.[67] Compared to controls, α-tubulin expression levels were significantly higher in both HCM_{SMP} and HCM_{SMN} (Figures 7.6A-B; Table 7.2).

In addition, acetylation of α-tubulin was significantly higher in both HCM patient groups compared to controls (Figures 7.6A-B). The increases in levels of α-tubulin and acetylated α-tubulin were significantly higher in HCM_{SMP} compared to HCM_{SMN}.

When comparing mutation type, significantly higher levels of α-tubulin and acetylated α-tubulin were observed in HCM_{HI} compared to HCM_{PP} (Figure 7.6C, Table 7.6). The levels of acetylated α-tubulin significantly correlated with α-tubulin (Figure 7.6D), which is in line with the observation that acetylation of α-tubulin compartmentalizes on the stable microtubules. Moreover, a significant inverse linear correlation was present between cMyBP-C protein level and α-tubulin in HCM with a sarcomere gene mutation (Figure 7.6E). Overall, these data show that the presence of a sarcomere mutation coincides with a more extensive and stabilized microtubule network in HCM.

STRONG CORRELATION OF HSPs WITH α-TUBULIN

Since the PQC is strongly linked to the microtubules network, we performed multivariate testing (Wilks' Lambda test) using levels of α-tubulin, sex and age at operation as effects and the HSPs, ubiquitination, p62, and LC3BII as dependent variables. There was an overall statistically significant difference in levels of key PQC players based on α-tubulin levels (Table 7.7).

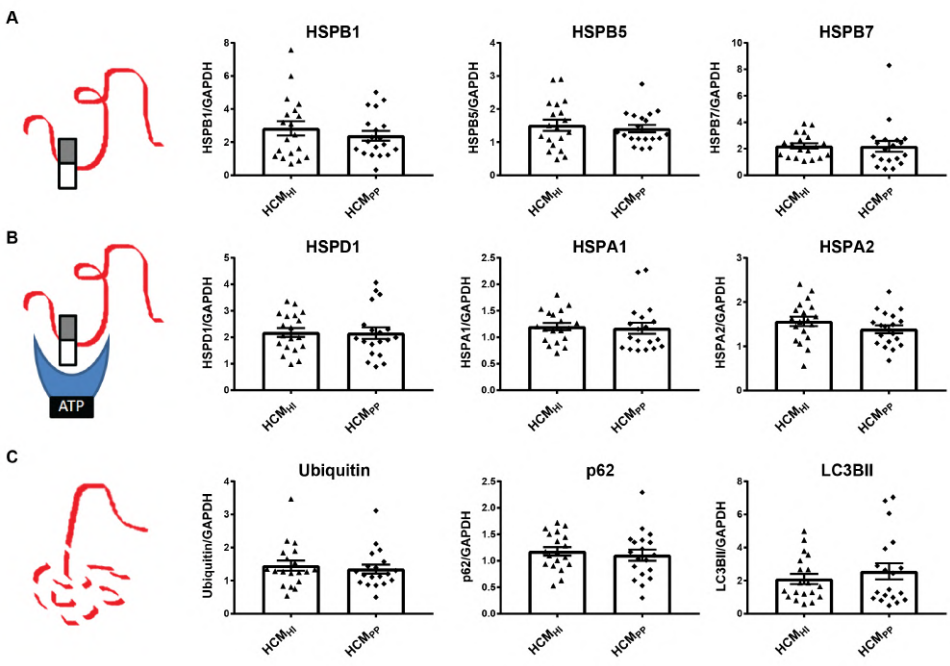

Figure 7.5: Pathomechanism of HCM and key PQC players.
(**A**) Stabilizing HSPs (HSPB1, HSPB5, HSPB7), (**B**) HSPs with refolding capacity (HSPD1, HSPA1 HSPA2) and (**C**) degradation markers (ubiquitin, p62, LC3BII) were not significantly different between HCM_{HI} (n=19) and HCM_{PP} (n=19). Each dot in the scatter plots represents an individual sample. Figure reproduced and adapted with permission from Dorsch, L.M. et al., Pflügers Archiv – European Journal of Physiology; published by Springer Berlin Heidelberg, 2018.

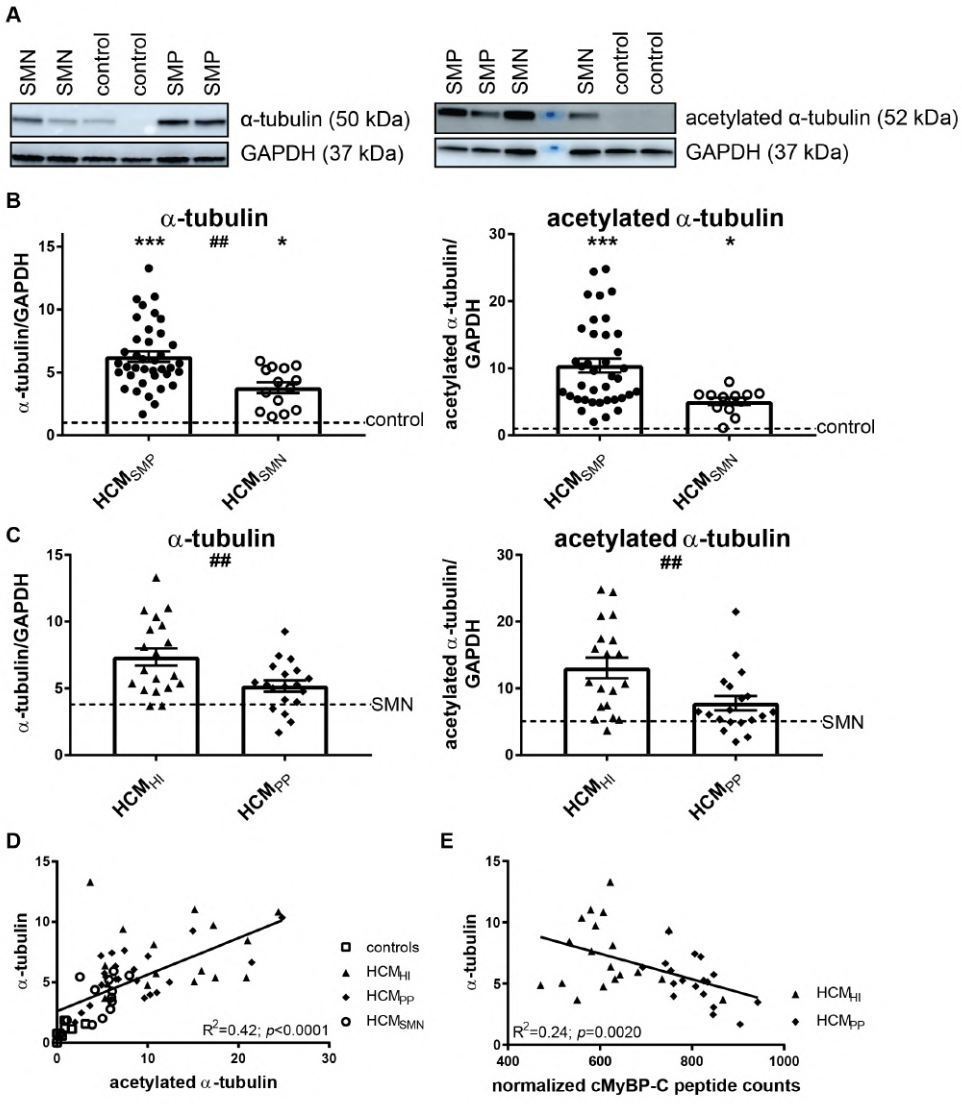

Figure 7.6: Pathomechanism of HCM and acetylation of α-tubulin.
(**A**) Representative blot images for α-tubulin and acetylated α-tubulin. (**B**) Higher levels of α-tubulin and acetylated α-tubulin in HCM_{SMP} (n=38) and HCM_{SMN} (α-tubulin: n=14; acetylated α-tubulin: n=12) compared to controls. Significant difference of α-tubulin levels between HCM_{SMP} and HCM_{SMN} ($^{\#\#}p<0.01$). (**C**) Higher levels of α-tubulin and acetylated α-tubulin in HCM_{HI} (n=19) than HCM_{PP} (n=19). (**D**) The levels of α-tubulin correlated well with acetylated α-tubulin (**E**) Significant inverse linear correlation of α-tubulin with cMyBP-C. Controls = open squares, HCM_{SMP} = filled circles, HCM_{SMN} = open circles, HCM_{HI} = filled triangles, HCM_{PP} = filled rhomboids. Each dot in the scatter plots and the correlation analyses represents an individual sample. $^{*}p<0.05$ and $^{***}p<0.001$ versus controls and $^{\#\#}p<0.01$ and $^{\#\#\#}p<0.001$ versus HCM_{PP}.

,

Table 7.7: Multivariate Tests[a]: α-tubulin (all samples), sex, and age at operation.

Effect	Value	F	Hypothesis df	Error df	Significance	Partial eta squared
Intercept	0.389	8.186[b]	9.000	47.000	<0.001	0.611
α-tubulin	0.427	7.009[b]	9.000	47.000	<0.001	0.573
Sex	0.774	1.523[b]	9.000	47.000	0.168	0.226
Age at operation	0.791	1.384[b]	9.000	47.000	0.223	0.209

[a] Design: Intercept and α-tubulin and sex and age at operation; [b] exact statistic; F: F statistic for the given effect and test statistic; Hypothesis df: Number of degrees of freedom in the model; Error df: Number of degrees of freedom associated with the model errors; Partial eta squared: estimate of effect size; $p<0.05$ is considered to be significant.

To determine which of the key PQC players differ when α-tubulin levels are changing, we performed tests for between-subjects effects. This testing revealed that α-tubulin had a significant effect on all measured HSPs, but not on the degradation markers (Table 7.8). The correlation of HSPs and α-tubulin levels is visualized in Figure S3.
,

Table 7.8: Tests for between-subjects: α-tubulin as an effect and correction for differences in sex and age at operation.

	Type III Sum of Squares	df	Mean Square	F	Significance	Partial eta squared	R squared
Stabilizing HSPs							
HSPB1	38.460	1	38.460	23.663	>0.001	0.301	0.368
HSPB5	3.630	1	3.630	11.485	0.001	0.173	0.176
HSPB7	14.246	1	14.246	10.504	0.002	0.160	0.209
Refolding HSPs							
HSPD1	10.273	1	10.273	19.305	>0.001	0.260	0.303
HSPA1	1.370	1	1.370	12.580	0.001	0.186	0.203
HSPA2	1.723	1	1.723	10.410	0.002	0.159	0.171
Protein degradation							
Ubiquitin	0.419	1	0.419	1.187	0.281	0.021	0.047
p62	0.418	1	0.418	2.793	0.100	0.048	0.087
LC3BII	3.849	1	3.849	1.312	0.257	0.023	0.058

df: Number of degrees of freedom in the model; F: F statistic for the given effect and test statistic; Partial eta squared: estimate of effect size; R squared: proportion of the variance in the dependent variable that is predictable from the independent variable; Bonferroni correction: statistical significance at $p<0.0056$ ($\alpha/9 = 0.05/9 = 0.0056$).

DISCUSSION

The incomplete penetrance, age-related onset and the large clinical variability in disease severity imply a complex HCM pathophysiology mechanism. Especially, patients with a sarcomere mutation have a higher risk for adverse outcomes. The underlying causes for difference in disease between HCM_{SMP} and HCM_{SMN} remain unclear.

Here we determined protein levels of key PQC players, including HSPs and degradation markers, and acetylation of α-tubulin by Western blot analysis in a large set of cardiac samples from HCM_{SMP} and HCM_{SMN} patients to define PQC changes in HCM at the time of myectomy, and identified if the presence of a sarcomere mutation mediates changes in PQC mechanisms and tubulin network. One of the limitations of the current study is that patients had a severe phenotype with LVOT obstruction. Therefore, this group may not be representative for all patients with HCM.

Main findings of our PQC assessment are that: 1) Several HSPs and autophagy markers are higher in HCM compared to controls, but there are no major differences between HCM_{SMP} and HCM_{SMN} or mutation type (haploinsufficiency versus poison polypeptide) at the time of myectomy; 2) After correction for sex and age at operation, the major increases in HCM_{SMP} compared to controls were observed in the stabilizing HSPB1 and the refolding HSPD1 and HSPA2; 3) The most significant increase compared to control samples was observed in the levels of α-tubulin and acetylated α-tubulin with significant differences between mutation group: $HCM_{HI} > HCM_{PP} > HCM_{SMN}$; and 4) Levels of α-tubulin significantly correlated with levels of acetylated α-tubulin and all HSPs (Figure 7.7).

Overall, our analyses indicate that carrying a HCM-causing mutation affects PQC and α-tubulin acetylation. We propose that reduced levels of cMyBP-C caused by *MYBPC3* mutations trigger HSPs and α-tubulin acetylation, and may present a pathomechanism in cMyBP-C haloinsufficiency-mediated HCM. The possible impact of the observed PQC changes is discussed below.

ELEVATED LEVELS OF HSPs IN HUMAN HCM

We identified higher levels of HSPB1, HSPD1, and HSPA2 in HCM_{SMP} compared to controls which could not be explained by differences in sex and age at operation (Table 7.5). Our findings are in line with studies in human end-stage heart failure studies samples, which showed increases in HSPD1 and HSPB1 compared to controls.[68]

HSPB1 is implicated in different cardio-protective processes involving interception of misfolded proteins, cytoskeletal organization, anti-apoptotic and anti-oxidant properties.[69] Therefore, its expression may improve the resistance of tissue exposed to stress and injuries.[70] While moderate cardiac expression of HSPB1 protects against doxorubicin-induced cardiac dysfunction through anti-oxidative stress, reports on effects of HSPB1 overexpression are inconsistent.[71] Overexpression of HSPB1 conferred protection against myocardial ischemia-reperfusion injury[72] whereas overexpression of HSPB1 caused reductive stress

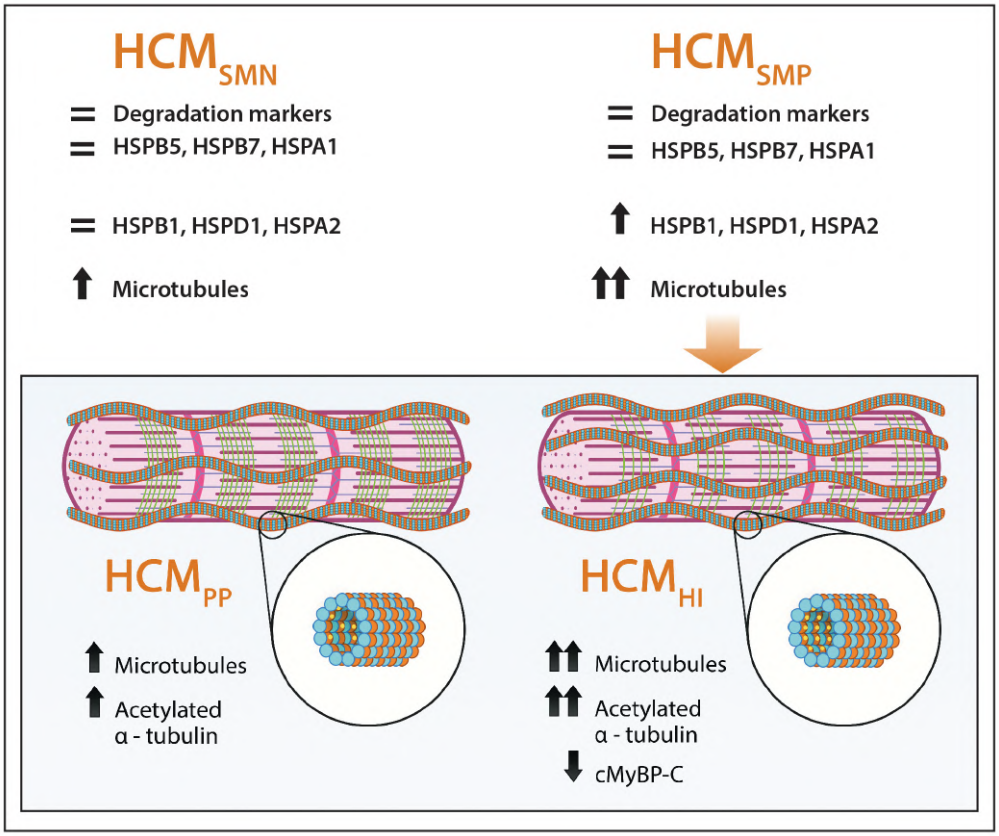

Figure 7.7: Schematic representation of PQC and microtubular system assessment in HCM. Our analyses show that HSPB1, HSPD1 HSPA2, α-tubulin and acetylated α-tubulin are increased in HCM, especially when a sarcomere mutation is present, while HSPB5, HSPB7, HSPA1 and degradation markers are not changed in HCM compared to controls. Levels of α-tubulin (orange balls) and acetylated α-tubulin (small yellow balls attached to α-tubulin in the lumen of polymerized microtubules (blue and orange balls)) are more increased when haploinsufficiency (HI), characterized by lower levels of cardiac myosin-binding protein-C (green lines), is the underlying pathomechanism instead of poison polypeptides (PP). =: similar to controls; ↑: significantly increased compared to controls; ↓: significantly decreased compared to controls.

and cardiomyopathy in another study.[73] Further experiments are needed to clarify if the observed increase in HSPB1 is actually beneficial and may be a response to stress exposure.

HSPD1 fulfils multiple tasks in a cell by refolding key proteins after their import into the mitochondria, transporting of proteins between the mitochondrial matrix and the cytoplasm of the cell, and binding to cytosolic pro-apoptotic proteins to sequester them.[74] Upregulation of HSPD1 due to mitochondrial impairment is suggested to be an indicator of mitochondrial stress.[75] 15-20% of HSPD1 is located at extra-mitochondrial sites suggesting important physiological roles at other locations.[61] In human end-stage

heart failure, HSPD1 localizes to the plasma membrane thereby losing anti-apoptotic and protective effects and becoming detrimental to the cell.[76] Impairment of HSPD1-mediated anti-stress response has been reported in dilated cardiomyopathy (DCM) which progressed to end stage heart failure.[77] Here, we identified higher levels of HSPD1 which may indicate mitochondrial stress, which has been reported in HCM.[78]

Western blot analysis, showed higher levels of HSPA2 in HCM_{SMP} compared to controls. In our mass-spectrometry based proteomics study, HSPA2 was highly upregulated in cardiac disease (Figure 7.8A).[64]

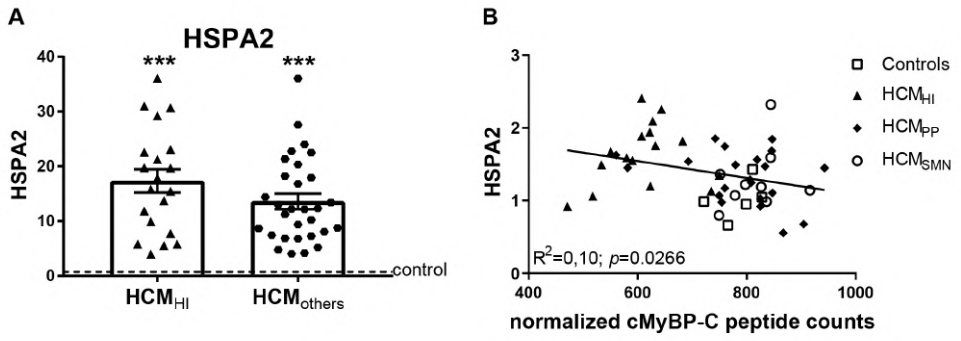

Figure 7.8: Upregulated HSPA2 in HCM in proteomics screen.
(**A**) In a mass-spectrometry based proteomics study, HSPA2 levels were higher in HCM_{HI} (n=20) and HCM_{others} (n=30) samples, including HCM_{PP} and HCM_{SMN}, compared to controls (n=8). (**B**) Significant inverse correlation of HSPA2 levels determined by Western blot analysis with cMyBP-C. Controls = open squares, HCM_{HI} = filled triangles, HCM_{PP} = filled rhomboids, HCM_{SMN} = open circles, HCM_{others} = hexagons. Each dot in the scatter plots and correlation analysis represents an individual sample. ***$p<0.001$ versus controls.

HSPA2 has been reported in heart tissue and low expression was identified in fibroblasts.[60,79] Recently, HSPA-family chaperones have been suggested to interact with cMyBP-C to regulate its turnover.[80] Moreover, a significant inverse linear correlation was present between cMyBP-C protein levels and HSPA2 (Figure 7.8B). Therefore, HSPA2 may be an additional regulator of cMyBP-C. Further experiments are warranted to explain the role of HSPA2 in haploinsufficiency for cMyBP-C.

In contrast, levels of HSPB5 and HSPA1 in HCM samples were not different compared to controls after adjusting for sex and age differences. Several studies have shown that HSPB5 and HSPA1 are both increased early in response to acute hypertrophic signalling, but with opposite functions. While HSPB5 is involved in counteracting acute cardiac remodelling by suppressing hypertrophic signalling pathways, HSPA1 supports pro-hypertrophic signalling pathways[81,82] The increase of HSPA1 was transient and attenuated 14 days after isoproterenol-infusion in a mouse model for cardiac hypertrophy.[82] Consistent with our findings in myectomy samples from patient with advanced disease, HSPA1 levels were not changed in septal myectomy samples of HCM patients and end-stage heart failure patients

compared to controls.[68,80] Increased HSPA1 in the heart protects against acute cardiac stress, but not against chronic cardiac stress.[83]

Based on these studies, we propose that HSPB5 and HSPA1 levels are not changed in HCM myectomy samples because of persistent chronic hypertrophic stimuli leading to their blunted response. Further research is warranted to investigate if the failure to increase HSPB5 implies a loss of responsiveness at advanced disease stage because HSPB5 seems to play a beneficial role in hypertrophic signalling.

PROTEIN DEGRADATION IN HCM

Defects in the turnover of key sarcomere proteins may account for both hypertrophic and functional defects.[9] UPS dysfunction is characterized by accumulation of ubiquitinated proteins, altered proteasome activity, and changes in expression of UPS proteins or E2 and E3 enzymes.[84] Upon correction for sex and age, no significant changes were observed in levels of degradation-associated markers in HCM, such as HSPB7, ubiquitin, p62 and LC3BII. Compared to the protein folding-supportive HSPB1 and HSPB5, HSPB7 plays a critical role in preventing protein aggregation.[85] Genetic variants in *HSPB7* have been associated with advanced heart failure and systolic dysfunction.[86] In a zebrafish model, HSPB7 is involved in early post-damage processing of large cytoskeletal proteins and the loss of HSPB7 function is accompanied by increased damaged protein load, protein aggregation and risk for cardiomyopathy.[87]

Due to the use of an antibody recognizing both K48- and K63-linked polyubiquitinated chains, we do not know if the ratio between K48- and K63-linked polyubiquitinated proteins is altered in HCM. Therefore, we cannot draw any conclusion about the functionality of the proteasome which would be indicated by an increase in K48-linked polyubiquitinated proteins. LC3BII and p62 are both markers for autophagosomes because in selective autophagy, the cargo adapter protein p62 links polyubiquitinated proteins to the autophagic machinery via LC3.[88] We did not find a change in autophagosome markers, but this finding does not exclude the prospect that the autophagic flux might be impaired. Autophagy has been implicated in the pathogenesis of a wide range of cardiac pathologies.[62,88] Pre-clinical models of pressure overload-induced cardiac hypertrophy show that the increase of autophagic flux correlates with the degree of hypertrophy and therapeutic inhibition of autophagy is accompanied by reduced amount of fibrosis.[89]

Our analysis of protein degradation markers, indicate that there is no enhancement of protein degradation pathways at the time of myectomy. This may indicate that boosting protein degradation may actually represent a treatment option to prevent cardiac dysfunction and remodelling.

INCREASED MUTATION-DEPENDENT PROLIFERATION AND ACETYLATION OF α-TUBULIN

Our protein analyses revealed significantly increased levels of α-tubulin in both HCM groups (Figure 7.6A), which correlated with an increase in α-tubulin acetylation and levels of all HSPs. Changes of microtubules distribution occur at the onset of hypertrophy.[90] In chronically hypertrophied hearts, the increase of microtubules has been shown to be a major cause of contractile defects.[91] Two different hypotheses may explain microtubule densification: (1) Microtubules may be involved in myofibrillogenesis and an increase in microtubules would be required when new myofibrils are formed in hypertrophied cardiomyocytes, and (2) Microtubules may be intracellular compression-bearing elements needed to cope with increased contractile stress on cardiomyocytes.[92,93] In failing human hearts, accumulation of microtubules impedes sarcomere motion and contributes to decreased ventricular compliance.[94] Our results are in line with literature, showing an increase in α-tubulin in the HCM myocardial tissue.[95]

The underlying pathomechanism seems to have an effect on extent of increase in α-tubulin and acetylated α-tubulin, since we observed the largest increase in samples with haploinsufficiency for cMyBP-C. An intact microtubule-based cytoskeleton contributes to the stabilization of myofibril structure in the cardiomyocytes and HSPs may preserve this relationship.[96] Post-chaperonin tubulin-folding cofactors, such as HSPs and other tubulin-associated proteins, regulate the synthesis, transport, and storage of α- and β-tubulin.[97] For instance, HSPA1 binds to native tubulin dimers and microtubules to assist in proper tubulin folding.[98] In addition, HSPB5 prevents aggregation of tubulin and the chaperone activity is accompanied by the formation of large complexes between HSPB5 and tubulin.[99] We identified that α-tubulin level significantly correlates with all investigated HSPs.

In addition to HSPs, acetylation of α-tubulin was higher in both HCM groups (Figure 7.6B). Acetylation of α-tubulin directly tunes the compliance and resilience from mechanical breakage to ensure the persistence of long-lived microtubules.[100] Moreover, acetylation of α-tubulin most often compartmentalizes on the stable microtubules and is suggested to increase assembly of autophagic cargo along microtubules, thereby initiating augmented autophagic degradation in the heart.[101,102] Interestingly, there is a strong linear relation between acetylated and total α-tubulin levels (Figure 7.6D). This may suggest hyperacetylation of α-tubulin which is a common response to several cellular stresses. For example, acetyltransferase induction is triggered by the release of mitochondrial reactive oxygen species (ROS) and by AMP kinase.[103,104] Noteworthy, the underlying pathomechanism (HI versus PP) seems to have an effect on extent of increase in α-tubulin and acetylation of α-tubulin, since we observed the largest increase in samples with haploinsufficiency for cMyBP-C. As such, our analyses suggest that proliferation of the microtubular network represents a pathomechanism in HI-mediated HCM. Based on previous studies,[100-104] we propose that the increased tubulin network may function to maintain cellular stability and enhance autophagic flux of damaged proteins, while it may impair contractile function.[95,105] Future studies are warranted to establish the link (cause-consequence) between reduced cMyBP-C protein levels, increased α-tubulin

acetylation and cardiomyocyte contractile function and hypertrophy that may underlie initiation and progression of cardiac disease in *MYBPC3* mutation carriers.

INTER-INDIVIDUAL DIFFERENCES

We observed large inter-individual differences in various key PQC players and tubulin network, especially in the presence of a sarcomere mutation. This variability may be explained by the large variability among HCM-causing mutations, which may all have a distinct effect on cellular PQC. Most of the mutation sites of proteins affect stability and aggregation but rarely its function.[106] This concept is supported by the fact that HCM_{HI} mutations cause a rather heterogeneous cMyBP-C haploinsufficiency, with some samples having relatively low cMyBP-C, and others having still relatively high protein level. Loss of cMyBP-C levels correlates very well with α-tubulin, thereby supporting the diverse response to a change in sarcomere protein composition in the case of HCM_{HI}. The microtubule response correlates significantly with the expression level of cMyBP-C, and may represent a direct compensation for the loss of cMyBP-C as cMyBP-C is known to have a central regulatory role in myofibril development and stability.[107] In line with this, reduced myofibril density was detected in septal myectomy samples from HCM_{SMP} patients compared to HCM_{SMN} patients.[18] While the excessive microtubular response to cMyBP-C haploinsufficiency may be an attempt to maintain myofibril stability, it may aggravate cardiac dysfunction by altering cytoskeletal mechanical properties.[95,105]

CONCLUSION

In summary, our data show that the hypertrophied muscle of HCM patients is characterized by an increased and stabilized tubular network which may be an adaptive response to cardiomyocyte growth. While this compensatory response may aid to stabilize cardiomyocyte architecture, this structural adaption may contribute to reduced function of the HCM myocardium.

Conflict of Interest: The authors declare no conflict of interest.

Sources of funding: We acknowledge the support from the Netherlands Cardiovascular Research Initiative: An initiative with support of the Dutch Heart Foundation, CVON2014-40 DOSIS and CVON-STW2016-14728 AFFIP.

ACKNOWLEDGEMENTS

We would like to thank Ruud Zaremba for technical assistance with the LC3BII Western blots and Peter van de Ven for statistical analyses.

SUPPLEMENTARY FILES - ONLINE

https://www.mdpi.com/2073-4409/8/7/741/s1

REFERENCES

1. Semsarian C, Ingles J, Maron MS, Maron BJ. New perspectives on the prevalence of hypertrophic cardiomyopathy. *J Am Coll Cardiol*. 2015;65(12):1249-54.
2. Michels M, Olivotto I, Asselbergs FW, van der Velden J. Life-long tailoring of management for patients with hypertrophic cardiomyopathy : Awareness and decision-making in changing scenarios. *Neth Heart J*. 2017;25(3):186-99.
3. van der Velden J, Stienen GJM. Cardiac Disorders and Pathophysiology of Sarcomeric Proteins. *Physiol Rev*. 2019;99(1):381-426.
4. Maron BJ, Olivotto I, Spirito P, Casey SA, Bellone P, Gohman TE, et al. Epidemiology of hypertrophic cardiomyopathy-related death: revisited in a large non-referral-based patient population. *Circulation*. 2000;102(8):858-64.
5. Ho CY, Day SM, Ashley EA, Michels M, Pereira AC, Jacoby D, et al. Genotype and Lifetime Burden of Disease in Hypertrophic Cardiomyopathy: Insights from the Sarcomeric Human Cardiomyopathy Registry (SHaRe). *Circulation*. 2018;138(14):1387-98.
6. Willis MS, Patterson C. Proteotoxicity and cardiac dysfunction–Alzheimer's disease of the heart? *N Engl J Med*. 2013;368(5):455-64.
7. Henning RH, Brundel B. Proteostasis in cardiac health and disease. *Nat Rev Cardiol*. 2017;14(11):637-53.
8. Wang X, Robbins J. Heart failure and protein quality control. *Circ Res*. 2006;99(12):1315-28.
9. Wang X, Su H, Ranek MJ. Protein quality control and degradation in cardiomyocytes. *J Mol Cell Cardiol*. 2008;45(1):11-27.
10. Latchman DS. Heat shock proteins and cardiac protection. *Cardiovasc Res*. 2001;51(4):637-46.
11. Tannous P, Zhu H, Nemchenko A, Berry JM, Johnstone JL, Shelton JM, et al. Intracellular protein aggregation is a proximal trigger of cardiomyocyte autophagy. *Circulation*. 2008;117(24):3070-8.
12. Sontag EM, Vonk WIM, Frydman J. Sorting out the trash: the spatial nature of eukaryotic protein quality control. *Curr Opin Cell Biol*. 2014;26:139-46.
13. Marston S, Copeland O, Jacques A, Livesey K, Tsang V, McKenna WJ, et al. Evidence from human myectomy samples that MYBPC3 mutations cause hypertrophic cardiomyopathy through haploinsufficiency. *Circ Res*. 2009;105(3):219-22.
14. Seidman JG, Seidman C. The genetic basis for cardiomyopathy: from mutation identification to mechanistic paradigms. *Cell*. 2001;104(4):557-67.
15. Vriesendorp PA, Schinkel AF, Soliman OI, Kofflard MJ, de Jong PL, van Herwerden LA, et al. Long-term benefit of myectomy and anterior mitral leaflet extension in obstructive hypertrophic cardiomyopathy. *Am J Cardiol*. 2015;115(5):670-5.
16. van Velzen HG, Vriesendorp PA, Oldenburg RA, van Slegtenhorst MA, van der Velden J, Schinkel AFL, et al. Value of Genetic Testing for the Prediction of Long-Term Outcome in Patients With Hypertrophic Cardiomyopathy. *Am J Cardiol*. 2016;118(6):881-7.
17. Parbhudayal RY, Garra AR, Gotte MJW, Michels M, Pei J, Harakalova M, et al. Variable cardiac myosin binding protein-C expression in the myofilaments due to MYBPC3 mutations in hypertrophic cardiomyopathy. *J Mol Cell Cardiol*. 2018;123:59-63.
18. Witjas-Paalberends ER, Piroddi N, Stam K, van Dijk SJ, Oliviera VS, Ferrara C, et al. Mutations in MYH7 reduce the force generating capacity of sarcomeres in human familial hypertrophic cardiomyopathy. *Cardiovasc Res*. 2013;99(3):432-41.
19. Witjas-Paalberends ER, Guclu A, Germans T, Knaapen P, Harms HJ, Vermeer AM, et al. Gene-specific increase in the energetic cost of contraction in hypertrophic cardiomyopathy caused by thick filament mutations. *Cardiovasc Res*. 2014;103(2):248-57.
20. Nijenkamp L, Bollen IAE, van Velzen HG, Regan JA, van Slegtenhorst M, Niessen HWM, et al. Sex Differences at the Time of Myectomy in Hypertrophic Cardiomyopathy. *Circ Heart Fail*. 2018;11(6):e004133.
21. van Dijk SJ, Paalberends ER, Najafi A, Michels M, Sadayappan S, Carrier L, et al. Contractile dysfunction irrespective of the mutant protein in human hypertrophic cardiomyopathy with normal systolic function. *Circ Heart Fail*. 2012;5(1):36-46.
22. Kuster DW, Mulders J, Ten Cate FJ, Michels M, Dos Remedios CG, da Costa Martins PA, et al. MicroRNA transcriptome profiling in cardiac tissue of hypertrophic cardiomyopathy patients with MYBPC3 mutations. *J Mol Cell Cardiol*. 2013;65:59-66.
23. Sequeira V, Najafi A, Wijnker PJ, Dos Remedios CG, Michels M, Kuster DW, et al. ADP-stimulated contraction: A predictor of thin-filament activation in cardiac disease. *Proc Natl Acad Sci U S A*. 2015;112(50):E7003-12.
24. van Dijk SJ, Boontje NM, Heymans MW, Ten Cate FJ, Michels M, Dos Remedios C, et al. Preserved cross-bridge kinetics in human hypertrophic cardiomyopathy patients with MYBPC3 mutations. *Pflugers Arch*. 2014;466(8):1619-33.
25. Sequeira V, Wijnker PJ, Nijenkamp LL, Kuster DW, Najafi A, Witjas-Paalberends ER, et al. Perturbed length-dependent activation in human hypertrophic cardiomyopathy with missense sarcomeric gene mutations. *Circ Res*. 2013;112(11):1491-505.

26. Witjas-Paalberends ER, Ferrara C, Scellini B, Piroddi N, Montag J, Tesi C, et al. Faster cross-bridge detachment and increased tension cost in human hypertrophic cardiomyopathy with the R403Q MYH7 mutation. *J Physiol*. 2014;592(15):3257-72.
27. Robinson AA, Dunn MJ, McCormack A, dos Remedios C, Rose ML. Protective effect of phosphorylated Hsp27 in coronary arteries through actin stabilization. *J Mol Cell Cardiol*. 2010;49(3):370-9.
28. Polden J, McManus CA, Dos Remedios C, Dunn MJ. A 2-D gel reference map of the basic human heart proteome. *Proteomics*. 2011;11(17):3582-6.
29. Narolska NA, Piroddi N, Belus A, Boontje NM, Scellini B, Deppermann S, et al. Impaired diastolic function after exchange of endogenous troponin I with C-terminal truncated troponin I in human cardiac muscle. *Circ Res*. 2006;99(9):1012-20.
30. Zhang P, Kirk JA, Ji W, dos Remedios CG, Kass DA, Van Eyk JE, et al. Multiple reaction monitoring to identify site-specific troponin I phosphorylated residues in the failing human heart. *Circulation*. 2012;126(15):1828-37.
31. Kooij V, Zhang P, Piersma SR, Sequeira V, Boontje NM, Wijnker PJ, et al. PKCalpha-specific phosphorylation of the troponin complex in human myocardium: a functional and proteomics analysis. *PLoS One*. 2013;8(10):e74847.
32. Wijnker PJ, Li Y, Zhang P, Foster DB, dos Remedios C, Van Eyk JE, et al. A novel phosphorylation site, Serine 199, in the C-terminus of cardiac troponin I regulates calcium sensitivity and susceptibility to calpain-induced proteolysis. *J Mol Cell Cardiol*. 2015;82:93-103.
33. Krysiak J, Unger A, Beckendorf L, Hamdani N, von Frieling-Salewsky M, Redfield MM, et al. Protein phosphatase 5 regulates titin phosphorylation and function at a sarcomere-associated mechanosensor complex in cardiomyocytes. *Nat Commun*. 2018;9(1):262.
34. Gotzmann M, Grabbe S, Schone D, von Frieling-Salewsky M, Dos Remedios CG, Strauch J, et al. Alterations in Titin Properties and Myocardial Fibrosis Correlate With Clinical Phenotypes in Hemodynamic Subgroups of Severe Aortic Stenosis. *JACC Basic Transl Sci*. 2018;3(3):335-46.
35. Kruger M, Kotter S, Grutzner A, Lang P, Andresen C, Redfield MM, et al. Protein kinase G modulates human myocardial passive stiffness by phosphorylation of the titin springs. *Circ Res*. 2009;104(1):87-94.
36. Kotter S, Gout L, Von Frieling-Salewsky M, Muller AE, Helling S, Marcus K, et al. Differential changes in titin domain phosphorylation increase myofilament stiffness in failing human hearts. *Cardiovasc Res*. 2013;99(4):648-56.
37. Huang ZP, Ding Y, Chen J, Wu G, Kataoka M, Hu Y, et al. Long non-coding RNAs link extracellular matrix gene expression to ischemic cardiomyopathy. *Cardiovasc Res*. 2016;112(2):543-54.
38. Lin Z, Guo H, Cao Y, Zohrabian S, Zhou P, Ma Q, et al. Acetylation of VGLL4 Regulates Hippo-YAP Signaling and Postnatal Cardiac Growth. *Dev Cell*. 2016;39(4):466-79.
39. Kong SW, Hu YW, Ho JW, Ikeda S, Polster S, John R, et al. Heart failure-associated changes in RNA splicing of sarcomere genes. *Circ Cardiovasc Genet*. 2010;3(2):138-46.
40. Lu Z, Xu X, Hu X, Lee S, Traverse JH, Zhu G, et al. Oxidative stress regulates left ventricular PDE5 expression in the failing heart. *Circulation*. 2010;121(13):1474-83.
41. Fermin DR, Barac A, Lee S, Polster SP, Hannenhalli S, Bergemann TL, et al. Sex and age dimorphism of myocardial gene expression in nonischemic human heart failure. *Circ Cardiovasc Genet*. 2008;1(2):117-25.
42. McNamara JW, Li A, Lal S, Bos JM, Harris SP, van der Velden J, et al. MYBPC3 mutations are associated with a reduced super-relaxed state in patients with hypertrophic cardiomyopathy. *PLoS One*. 2017;12(6):e0180064.
43. Montag J, Syring M, Rose J, Weber AL, Ernstberger P, Mayer AK, et al. Intrinsic MYH7 expression regulation contributes to tissue level allelic imbalance in hypertrophic cardiomyopathy. *J Muscle Res Cell Motil*. 2017;38(3-4):291-302.
44. Montag J, Kowalski K, Makul M, Ernstberger P, Radocaj A, Beck J, et al. Burst-Like Transcription of Mutant and Wildtype MYH7-Alleles as Possible Origin of Cell-to-Cell Contractile Imbalance in Hypertrophic Cardiomyopathy. *Front Physiol*. 2018;9:359.
45. Iorga B, Schwanke K, Weber N, Wendland M, Greten S, Piep B, et al. Differences in Contractile Function of Myofibrils within Human Embryonic Stem Cell-Derived Cardiomyocytes vs. Adult Ventricular Myofibrils Are Related to Distinct Sarcomeric Protein Isoforms. *Front Physiol*. 2017;8:1111.
46. Messer AE, Gallon CE, McKenna WJ, Dos Remedios CG, Marston SB. The use of phosphate-affinity SDS-PAGE to measure the cardiac troponin I phosphorylation site distribution in human heart muscle. *Proteomics Clin Appl*. 2009;3(12):1371-82.
47. Hoskins AC, Jacques A, Bardswell SC, McKenna WJ, Tsang V, dos Remedios CG, et al. Normal passive viscoelasticity but abnormal myofibrillar force generation in human hypertrophic cardiomyopathy. *J Mol Cell Cardiol*. 2010;49(5):737-45.
48. Bayliss CR, Jacques AM, Leung MC, Ward DG, Redwood CS, Gallon CE, et al. Myofibrillar Ca(2+) sensitivity is uncoupled from troponin I phosphorylation in hypertrophic obstructive cardiomyopathy due to abnormal troponin T. *Cardiovasc Res*. 2013;97(3):500-8.
49. Messer AE, Bayliss CR, El-Mezgueldi M, Redwood CS, Ward DG, Leung MC, et al. Mutations in troponin T associated with Hypertrophic Cardiomyopathy increase Ca(2+)-sensitivity and suppress the modulation of Ca(2+)-sensitivity by troponin I phosphorylation. *Arch Biochem Biophys*. 2016;601:113-20.
50. Mamidi R, Gresham KS, Li A, dos Remedios CG, Stelzer JE. Molecular effects of the myosin activator omecamtiv mecarbil on contractile properties of skinned myocardium lacking cardiac myosin binding protein-C. *J Mol Cell Cardiol*. 2015;85:262-72.

51. Mamidi R, Li J, Gresham KS, Verma S, Doh CY, Li A, et al. Dose-Dependent Effects of the Myosin Activator Omecamtiv Mecarbil on Cross-Bridge Behavior and Force Generation in Failing Human Myocardium. *Circ Heart Fail*. 2017;10(10).
52. Coats CJ, Heywood WE, Virasami A, Ashrafi N, Syrris P, Dos Remedios C, et al. Proteomic Analysis of the Myocardium in Hypertrophic Obstructive Cardiomyopathy. *Circ Genom Precis Med*. 2018;11(12):e001974.
53. Mollova M, Bersell K, Walsh S, Savla J, Das LT, Park SY, et al. Cardiomyocyte proliferation contributes to heart growth in young humans. *Proc Natl Acad Sci U S A*. 2013;110(4):1446-51.
54. Polizzotti BD, Ganapathy B, Walsh S, Choudhury S, Ammanamanchi N, Bennett DG, et al. Neuregulin stimulation of cardiomyocyte regeneration in mice and human myocardium reveals a therapeutic window. *Sci Transl Med*. 2015;7(281):281ra45.
55. Bollen IAE, Ehler E, Fleischanderl K, Bouwman F, Kempers L, Ricke-Hoch M, et al. Myofilament Remodeling and Function Is More Impaired in Peripartum Cardiomyopathy Compared with Dilated Cardiomyopathy and Ischemic Heart Disease. *Am J Pathol*. 2017;187(12):2645-58.
56. Bergmann O, Zdunek S, Felker A, Salehpour M, Alkass K, Bernard S, et al. Dynamics of Cell Generation and Turnover in the Human Heart. *Cell*. 2015;161(7):1566-75.
57. Gomez-Arroyo J, Mizuno S, Szczepanek K, Van Tassell B, Natarajan R, dos Remedios CG, et al. Metabolic gene remodeling and mitochondrial dysfunction in failing right ventricular hypertrophy secondary to pulmonary arterial hypertension. *Circ Heart Fail*. 2013;6(1):136-44.
58. Martin-Garrido A, Biesiadecki BJ, Salhi HE, Shaifta Y, Dos Remedios CG, Ayaz-Guner S, et al. Monophosphorylation of cardiac troponin-I at Ser-23/24 is sufficient to regulate cardiac myofibrillar Ca(2+) sensitivity and calpain-induced proteolysis. *J Biol Chem*. 2018;293(22):8588-99.
59. Piroddi N, Witjas-Paalberends ER, Ferrara C, Ferrantini C, Vitale G, Scellini B, et al. The homozygous K280N troponin T mutation alters cross-bridge kinetics and energetics in human HCM. *J Gen Physiol*. 2019;151(1):18-29.
60. Brocchieri L, Conway de Macario E, Macario AJ. hsp70 genes in the human genome: Conservation and differentiation patterns predict a wide array of overlapping and specialized functions. *BMC Evol Biol*. 2008;8:19.
61. Soltys BJ, Gupta RS. Immunoelectron microscopic localization of the 60-kDa heat shock chaperonin protein (Hsp60) in mammalian cells. *Exp Cell Res*. 1996;222(1):16-27.
62. Dorsch LM, Schuldt M, Knezevic D, Wiersma M, Kuster DWD, van der Velden J, et al. Untying the knot: protein quality control in inherited cardiomyopathies. *Pflugers Arch*. 2018.
63. van Dijk SJ, Dooijes D, dos Remedios C, Michels M, Lamers JM, Winegrad S, et al. Cardiac myosin-binding protein C mutations and hypertrophic cardiomyopathy: haploinsufficiency, deranged phosphorylation, and cardiomyocyte dysfunction. *Circulation*. 2009;119(11):1473-83.
64. Schuldt M, Pei J, Harakalova M, Dorsch LM, Mokry M, Knol JC, et al. Detyrosinated tubulin as treatment target in genetic heart disease: proteomic and functional studies in hypertrophic cardiomyopathy. status: manuscript in preparation.
65. Matsuyama A, Shimazu T, Sumida Y, Saito A, Yoshimatsu Y, Seigneurin-Berny D, et al. In vivo destabilization of dynamic microtubules by HDAC6-mediated deacetylation. *EMBO J*. 2002;21(24):6820-31.
66. Hubbert C, Guardiola A, Shao R, Kawaguchi Y, Ito A, Nixon A, et al. HDAC6 is a microtubule-associated deacetylase. *Nature*. 2002;417(6887):455-8.
67. Ng DC, Ng IH, Yeap YY, Badrian B, Tsoutsman T, McMullen JR, et al. Opposing actions of extracellular signal-regulated kinase (ERK) and signal transducer and activator of transcription 3 (STAT3) in regulating microtubule stabilization during cardiac hypertrophy. *J Biol Chem*. 2011;286(2):1576-87.
68. Knowlton AA, Kapadia S, Torre-Amione G, Durand JB, Bies R, Young J, et al. Differential expression of heat shock proteins in normal and failing human hearts. *J Mol Cell Cardiol*. 1998;30(4):811-8.
69. Benjamin IJ, McMillan DR. Stress (heat shock) proteins: molecular chaperones in cardiovascular biology and disease. *Circ Res*. 1998;83(2):117-32.
70. Arrigo AP. Mammalian HspB1 (Hsp27) is a molecular sensor linked to the physiology and environment of the cell. *Cell Stress Chaperones*. 2017;22(4):517-29.
71. Liu L, Zhang X, Qian B, Min X, Gao X, Li C, et al. Over-expression of heat shock protein 27 attenuates doxorubicin-induced cardiac dysfunction in mice. *Eur J Heart Fail*. 2007;9(8):762-9.
72. Efthymiou CA, Mocanu MM, de Belleroche J, Wells DJ, Latchmann DS, Yellon DM. Heat shock protein 27 protects the heart against myocardial infarction. *Basic Res Cardiol*. 2004;99(6):392-4.
73. Zhang X, Min X, Li C, Benjamin IJ, Qian B, Zhang X, et al. Involvement of reductive stress in the cardiomyopathy in transgenic mice with cardiac-specific overexpression of heat shock protein 27. *Hypertension*. 2010;55(6):1412-7.
74. Knowlton AA, Srivatsa U. Heat-shock protein 60 and cardiovascular disease: a paradoxical role. *Future Cardiol*. 2008;4(2):151-61.
75. Pellegrino MW, Nargund AM, Haynes CM. Signaling the mitochondrial unfolded protein response. *Biochim Biophys Acta*. 2013;1833(2):410-6.
76. Lin L, Kim SC, Wang Y, Gupta S, Davis B, Simon SI, et al. HSP60 in heart failure: abnormal distribution and role in cardiac myocyte apoptosis. *Am J Physiol Heart Circ Physiol*. 2007;293(4):H2238-47.
77. Sidorik L, Kyyamova R, Bobyk V, Kapustian L, Rozhko O, Vigontina O, et al. Molecular chaperone, HSP60, and cytochrome P450 2E1 co-expression in dilated cardiomyopathy. *Cell Biol Int*. 2005;29(1):51-5.
78. Unno K, Isobe S, Izawa H, Cheng XW, Kobayashi M, Hirashiki A, et al. Relation of functional and morphological changes in mitochondria to myocardial contractile and relaxation reserves in asymptomatic to mildly symptomatic

patients with hypertrophic cardiomyopathy. *Eur Heart J*. 2009;30(15):1853-62.

79. Roux AF, Nguyen VT, Squire JA, Cox DW. A heat shock gene at 14q22: mapping and expression. *Hum Mol Genet*. 1994;3(10):1819-22.
80. Glazier AA, Hafeez N, Mellacheruvu D, Basrur V, Nesvizhskii AI, Lee LM, et al. HSC70 is a chaperone for wild-type and mutant cardiac myosin binding protein C. *JCI Insight*. 2018;3(11).
81. Kumarapeli AR, Su H, Huang W, Tang M, Zheng H, Horak KM, et al. Alpha B-crystallin suppresses pressure overload cardiac hypertrophy. *Circ Res*. 2008;103(12):1473-82.
82. Kee HJ, Eom GH, Joung H, Shin S, Kim JR, Cho YK, et al. Activation of histone deacetylase 2 by inducible heat shock protein 70 in cardiac hypertrophy. *Circ Res*. 2008;103(11):1259-69.
83. Bernardo BC, Weeks KL, Patterson NL, McMullen JR. HSP70: therapeutic potential in acute and chronic cardiac disease settings. *Future Med Chem*. 2016;8(18):2177-83.
84. Day SM. The ubiquitin proteasome system in human cardiomyopathies and heart failure. *Am J Physiol Heart Circ Physiol*. 2013;304(10):H1283-93.
85. Vos MJ, Zijlstra MP, Kanon B, van Waarde-Verhagen MA, Brunt ER, Oosterveld-Hut HM, et al. HSPB7 is the most potent polyQ aggregation suppressor within the HSPB family of molecular chaperones. *Hum Mol Genet*. 2010;19(23):4677-93.
86. Villard E, Perret C, Gary F, Proust C, Dilanian G, Hengstenberg C, et al. A genome-wide association study identifies two loci associated with heart failure due to dilated cardiomyopathy. *Eur Heart J*. 2011;32(9):1065-76.
87. Mercer EJ, Lin YF, Cohen-Gould L, Evans T. Hspb7 is a cardioprotective chaperone facilitating sarcomeric proteostasis. *Dev Biol*. 2018;435(1):41-55.
88. Lavandero S, Troncoso R, Rothermel BA, Martinet W, Sadoshima J, Hill JA. Cardiovascular autophagy: concepts, controversies, and perspectives. *Autophagy*. 2013;9(10):1455-66.
89. Weng LQ, Zhang WB, Ye Y, Yin PP, Yuan J, Wang XX, et al. Aliskiren ameliorates pressure overload-induced heart hypertrophy and fibrosis in mice. *Acta Pharmacol Sin*. 2014;35(8):1005-14.
90. Samuel JL, Bertier B, Bugaisky L, Marotte F, Swynghedauw B, Schwartz K, et al. Different distributions of microtubules, desmin filaments and isomyosins during the onset of cardiac hypertrophy in the rat. *Eur J Cell Biol*. 1984;34(2):300-6.
91. Tagawa H, Rozich JD, Tsutsui H, Narishige T, Kuppuswamy D, Sato H, et al. Basis for increased microtubules in pressure-hypertrophied cardiocytes. *Circulation*. 1996;93(6):1230-43.
92. Stamenovic D, Mijailovich SM, Tolic-Norrelykke IM, Chen J, Wang N. Cell prestress. II. Contribution of microtubules. *Am J Physiol Cell Physiol*. 2002;282(3):C617-24.
93. Watkins SC, Samuel JL, Marotte F, Bertier-Savalle B, Rappaport L. Microtubules and desmin filaments during onset of heart hypertrophy in rat: a double immunoelectron microscope study. *Circ Res*. 1987;60(3):327-36.
94. Heling A, Zimmermann R, Kostin S, Maeno Y, Hein S, Devaux B, et al. Increased expression of cytoskeletal, linkage, and extracellular proteins in failing human myocardium. *Circ Res*. 2000;86(8):846-53.
95. Robison P, Caporizzo MA, Ahmadzadeh H, Bogush AI, Chen CY, Margulies KB, et al. Detyrosinated microtubules buckle and bear load in contracting cardiomyocytes. *Science*. 2016;352(6284):aaf0659.
96. Decker RS, Decker ML, Nakamura S, Zhao YS, Hedjbeli S, Harris KR, et al. HSC73-tubulin complex formation during low-flow ischemia in the canine myocardium. *Am J Physiol Heart Circ Physiol*. 2002;283(4):H1322-33.
97. Lopez-Fanarraga M, Avila J, Guasch A, Coll M, Zabala JC. Review: postchaperonin tubulin folding cofactors and their role in microtubule dynamics. *J Struct Biol*. 2001;135(2):219-29.
98. Sanchez C, Padilla R, Paciucci R, Zabala JC, Avila J. Binding of heat-shock protein 70 (hsp70) to tubulin. *Arch Biochem Biophys*. 1994;310(2):428-32.
99. Ohto-Fujita E, Fujita Y, Atomi Y. Analysis of the alphaB-crystallin domain responsible for inhibiting tubulin aggregation. *Cell Stress Chaperones*. 2007;12(2):163-71.
100. Xu Z, Schaedel L, Portran D, Aguilar A, Gaillard J, Marinkovich MP, et al. Microtubules acquire resistance from mechanical breakage through intralumenal acetylation. *Science*. 2017;356(6335):328-32.
101. Geeraert C, Ratier A, Pfisterer SG, Perdiz D, Cantaloube I, Rouault A, et al. Starvation-induced hyperacetylation of tubulin is required for the stimulation of autophagy by nutrient deprivation. *J Biol Chem*. 2010;285(31):24184-94.
102. McLendon PM, Ferguson BS, Osinska H, Bhuiyan MS, James J, McKinsey TA, et al. Tubulin hyperacetylation is adaptive in cardiac proteotoxicity by promoting autophagy. *Proc Natl Acad Sci U S A*. 2014;111(48):E5178-86.
103. Mackeh R, Lorin S, Ratier A, Mejdoubi-Charef N, Baillet A, Bruneel A, et al. Reactive oxygen species, AMP-activated protein kinase, and the transcription cofactor p300 regulate alpha-tubulin acetyltransferase-1 (alphaTAT-1/MEC-17)-dependent microtubule hyperacetylation during cell stress. *J Biol Chem*. 2014;289(17):11816-28.
104. Li L, Yang XJ. Tubulin acetylation: responsible enzymes, biological functions and human diseases. *Cell Mol Life Sci*. 2015;72(22):4237-55.
105. Caporizzo MA, Chen CY, Salomon AK, Margulies KB, Prosser BL. Microtubules Provide a Viscoelastic Resistance to Myocyte Motion. *Biophys J*. 2018;115(9):1796-807.
106. DePristo MA, Weinreich DM, Hartl DL. Missense meanderings in sequence space: a biophysical view of protein evolution. *Nat Rev Genet*. 2005;6(9):678-87.
107. Ehler E, Gautel M. The sarcomere and sarcomerogenesis. *Adv Exp Med Biol*. 2008;642:1-14.

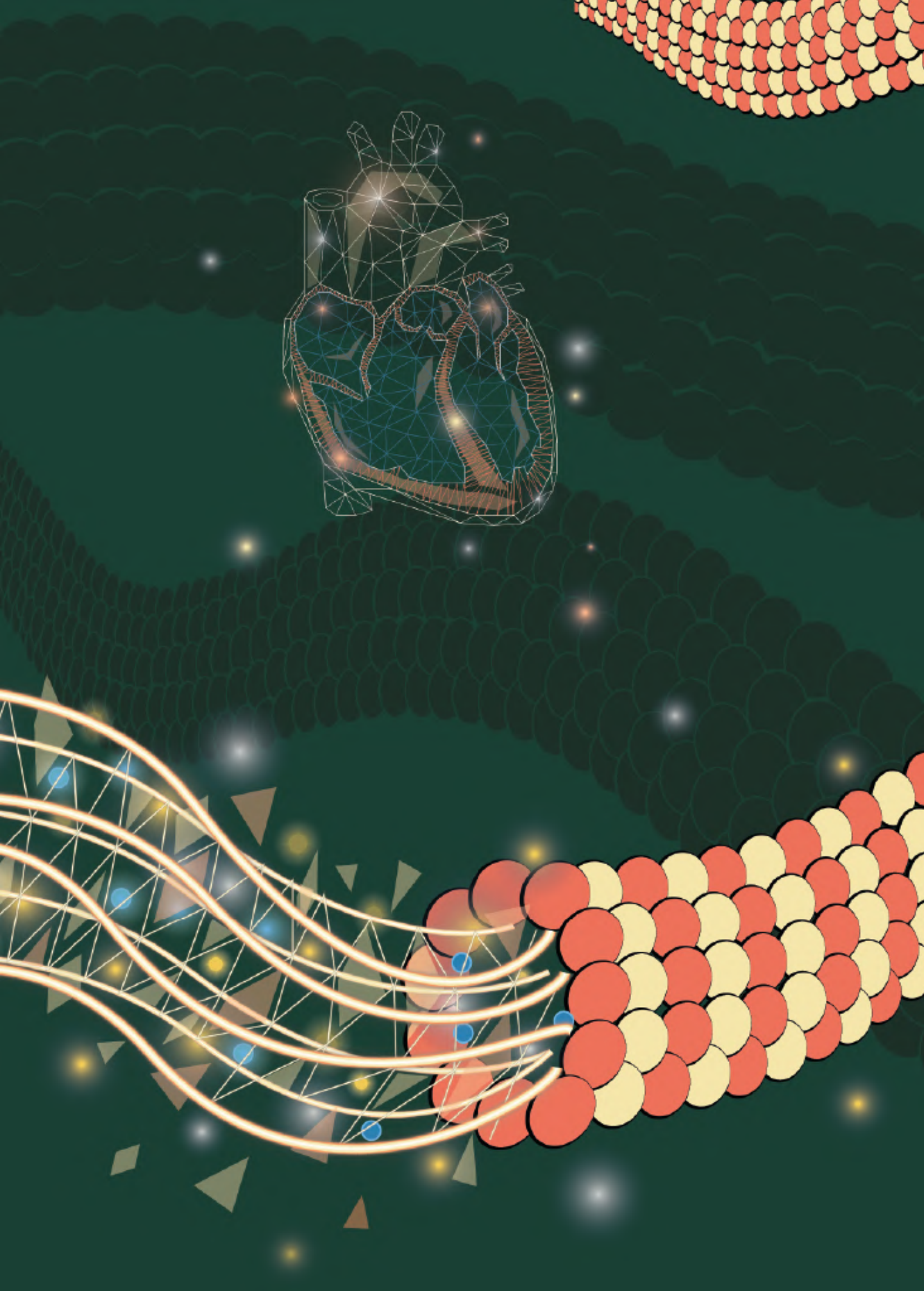

Chapter 8

Sex-related differences in protein expression in sarcomere mutation-positive hypertrophic cardiomyopathy

Maike Schuldt, **Larissa M. Dorsch**, Jaco C. Knol, Thang V. Pham, Tim Schelfhorst, Sander R. Piersma, Cris dos Remedios, Michelle Michels, Connie R. Jimenez, Diederik WD. Kuster, Jolanda van der Velden

Front Cardiovasc Med 8, 129 (2021)

ABSTRACT

BACKGROUND

Sex-differences in clinical presentation contribute to the phenotypic heterogeneity of hypertrophic cardiomyopathy (HCM) patients. While disease prevalence is higher in men, women present with more severe diastolic dysfunction and worse survival. Until today, little is known about the cellular differences underlying sex-differences in clinical presentation.

METHODS

To define sex-differences at the protein level, we performed a proteomic analysis in cardiac tissue obtained during myectomy surgery to relieve left ventricular outflow tract obstruction of age-matched female and male HCM patients harbouring a sarcomere mutation (n=13 in both groups). Furthermore, these samples were compared to 8 non-failing controls. Women presented with more severe diastolic dysfunction.

RESULTS

Out of 2099 quantified proteins, direct comparison of male and female HCM samples revealed only 46 significantly differentially expressed proteins. Increased levels of tubulin and heat shock proteins were observed in female compared to male HCM patients. Western blot analyses confirmed higher levels of tubulin in female HCM samples. In addition, proteins involved in carbohydrate metabolism were significantly lower in female compared to male samples. Furthermore, we found lower levels of translational proteins specifically in male HCM samples. The disease-specificity of these changes were confirmed by a second analysis in which we compared female and male samples separately to non-failing control samples. Transcription factor analysis showed that sex hormone-dependent transcription factors may contribute to differential protein expression, but do not explain the majority of protein changes observed between male and female HCM samples.

CONCLUSION

In conclusion, based on our proteomics analyses we propose that increased levels of tubulin partly underlie more severe diastolic dysfunction in women compared to men. Since heat shock proteins have cardioprotective effects, elevated levels of heat shock proteins in females may contribute to later disease onset in woman, while reduced protein turnover in men may lead to the accumulation of damaged proteins which in turn affects proper cellular function.

INTRODUCTION

Hypertrophic cardiomyopathy (HCM) is the most prevalent inherited cardiac disease with a prevalence of 1:200-500.[1,2] Clinically, it is characterized by unexplained asymmetric left ventricular hypertrophy and diastolic dysfunction.[3,4] A pathogenic mutation is identified in about 50-60% of all patients.[5] Both genetic and clinical heterogeneity is large, with more than 1500 identified gene mutations, and mutation carriers who are asymptomatic, die of acute cardiac arrest or show end-stage heart failure.[6]

Sex-differences in clinical presentation contribute to the phenotypic heterogeneity of HCM. Several large cohort studies observed a higher disease prevalence in men representing 55-65% of the total HCM population.[7-11] At HCM diagnosis, women are on average 9 years older than men,[7,12] and at the time of myectomy surgery women are on average 7 years older than men.[13] While women display less ventricular remodelling,[14,15] several studies have demonstrated more severe diastolic dysfunction[13,16-18] and worse survival compared to men.[19] Based on recent studies, our group put forward the hypothesis that disease severity in female patients with HCM is underestimated because females have smaller hearts than men, and the diagnostic criterion of $\geq$15 mm wall thickness does not take into account a correction by body surface area (BSA).[20] Consequently, women may be diagnosed at a later disease stage, since it takes more time for them to reach the diagnostic threshold of 15 mm wall thickness. This is supported by the observation that differences in wall thickness between genotype-positive men and women, that presented for cardiac screening, are mitigated after correction for BSA.[21]

Recently, efforts have been made to understand the sex-specific phenotypical differences on a cellular level. Single cardiomyocyte studies did not observe sex-specific changes in passive stiffness compared to non-failing controls, and the HCM-related increase in myofilament Ca^{2+}-sensitivity was similar in male and female HCM patients, implying that the sex-difference in diastolic dysfunction is not explained by sarcomere function itself.[13] However, women had more fibrosis compared to men, expressed more compliant titin and showed reduced levels of calcium-handling proteins.[13] These findings are first indications of differences between males and females on a cellular level. To further investigate cellular alterations that may underlie the sex-differences in HCM, we analysed protein expression data of males and females in a proteomics data set of septal myocardial tissue that was collected during myectomy surgery.

By direct comparison of male and female samples we found higher levels of tubulin subunits and heat shock proteins in females. The levels of α-tubulin, determined by Western blot analysis, correlate with diastolic function displayed as E/e' and may therefore at least partly underlie the sex-difference in diastolic dysfunction. The increased levels of heat shock proteins in females are proposed to be cardioprotective[22,23] and may contribute to later disease onset in women.

METHODS

PROTEOMICS ANALYSIS

The proteomics data in this study is a new analysis of a subset of the samples that were included of the study from Schuldt et al. 2021, where we identified HCM-specific protein changes compared to non-failing controls. We here focus on sex-specific protein changes in HCM by comparing cardiac samples from age-matched female and male genotype-positive HCM patients. In addition, a comparison was made between the proteomics data from the female and the male group, and the proteomic data from the non-failing control group. HCM patient tissue from the interventricular septum (IVS) of HCM patients was obtained during myectomy surgery to relieve left ventricular outflow tract obstruction (LVOTO). The study protocol for the human tissue samples was approved by the local medical ethics review committees and written informed consent was obtained from each patient prior to surgery.

For the analysis of sex-differences age-matched sarcomere mutation-positive (SMP) female (n=13) and male (n=13) samples were compared in a group-wise comparison using the beta binomial test as described previously.[24,25] Furthermore, the male and female SMP samples were compared to 8 non-failing healthy controls (NF_{IVS}; 5 females and 3 males) obtained from the Sydney Heart Bank (HREC Univ Sydney 2012/030). The non-failing controls have no history of cardiac disease and do not take any medication. The clinical characteristics of the groups are summarized in Table 8.1, individual patient characteristics are displayed in Table S1.

Table 8.1: Clinical characteristics.

	HCM_{female} (n=13)	HCM_{male} (n=13)	p
Age at myectomy (years)	48.5 ± 17.7	49.8 ± 15.5	0.85
LVOTg (mmHg)	60.4 ± 31.8	55.6 ± 32.2	0.72
LV parameters			
LAD (mm)	45.5 ± 4.3	48.4 ± 7.3	0.25
IVS (mm)	21.0 [20.0-23.0]	21.0 [18.3-23.0]	0.80
IVS_i	12.5 [10.0-13.8]	10.0 [8.3-10.8]	0.07
EDD (mm)	41.5 [39.3-42.8]	43.5 [40.0-46.5]	0.39
ESD (mm)	16.7 ± 1.2	24.9 ± 4.7	*0.02
Systolic parameter			
FS (%)	56.7 ± 2.5	44.4 ± 12.3	0.13
Diastolic parameters			
E/A ratio	1.20 [0.79-2.17]	0.87 [0.74-1.40]	0.34
E/e' ratio	20.3 [17.9-32.7]	13.9 [12.6-16.0]	***0.0003
TR velocity (cm/s)	2.6 [2.1-2.9]	2.3 [2.2-2.4]	0.20
Grade of diastolic dysfunction			
1	11.1% (1)	75.0% (9)	**0.008
2	55.6% (5)	8.3% (1)	*0.046
3	33.3% (3)	16.7% (2)	0.61
Medication			
beta blocker	84.6% (11)	84.6% (11)	>0.9999
calcium channel blocker	46.2% (6)	23.1% (3)	0.41

Table 8.1: Continued

	HCM_{female} (n=13)	HCM_{male} (n=13)	p
statins	15.4% (2)	23.1% (3)	>0.9999

Table displays clinical characteristics of female and male HCM patient group with testing for statistical differences. Abbreviations: LVOTg, left ventricular outflow tract gradient; LAD, left atrial diameter; IVS, interventricular septum; IVS_i, indexed interventricular septum thickness corrected for body surface area (BSA); EDD, end-diastolic diameter; ESD, end-systolic diameter; FS, fractional shortening.

TISSUE HOMOGENIZATION

Pulverized frozen tissue was homogenized in 40 µL/mg tissue 1x reducing sample buffer (106 mM Tris-HCl, 141 mM Tris-base, 2% (w/v) lithium dodecyl sulphate (LDS), 10% (v/v) glycerol, 0.51 mM EDTA, 0.22 mM SERVA Blue G250, 0.18 mM Phenol Red, 100 mM DTT) using a glass tissue grinder. Proteins were denatured by heating to 99°C for 5 min, after which samples were sonicated and heated again. Debris was removed by centrifugation at maximum speed for 10 min in a microcentrifuge (Sigma, 1-15K).

PROTEIN FRACTIONATION

Proteins were separated using 1D SDS-PAGE. Samples from each group were loaded alternating on the gels to avoid bias. Equal volumes of sample (30 µL protein homogenate per sample, containing approximately 20-30 µg of protein) were loaded on a precast 4-12% NuPAGE Novex Bis-Tris 1.5 mm mini gel (Invitrogen). Electrophoresis was performed at 200V in NuPAGE MES SDS running buffer until the dye front reached the bottom of the gel. Gels were fixed in a solution of 50% ethanol and 3% phosphoric acid, and stained with 0.1% (w/v) Coomassie brilliant blue G-250 solution (containing 34% (v/v) methanol, 3% (v/v) phosphoric acid and 15% (w/v) ammonium sulphate).

IN-GEL-DIGESTION

In-gel digestion was performed as described previously.[26] The proteins were in-gel reduced with 10 mM DTT and alkylated with 54 mM iodoacetamide. Each gel lane was cut into 5 pieces which were subsequently sliced into 1 mm^3 cubes. Proteins were digested in-gel with 6.3 ng/ml trypsin. Peptides were extracted from gel slices with 1% formic acid and 5% formic acid/50% acetonitrile and concentrated in a vacuum centrifuge prior to nano-LC-MS/MS measurement. Samples were measured by LC-MS per gel band starting at the high molecular weight (MW) fraction for all samples, before continuing with the next gel band until the last (low MW fraction) band was measured. Injections alternated between all different group samples to minimize experimental bias between groups.

NANO-LC-MS/MS

Analysis of the experiment was performed as described in Piersma et al.[27] Peptides were separated using an Ultimate 3000 Nano LC-MS/MS system (Dionex LC-Packings, Amsterdam, The Netherlands) equipped with a 40 cm x 75 µm ID fused silica

column custom packed with 1.9 µm,120 Å ReproSil Pur C18 aqua (Dr Maisch GMBH, Ammerbuch-Entringen, Germany). After injection, peptides were trapped at 6 µL/min on a 10 mm × 100 µm ID trap column packed with 5 µm, 120 Å ReproSil Pur C18aqua at 2% buffer B (buffer A: 0.5% acetic acid (Fischer Scientific), buffer B: 80% acetonitrile, 0.5% acetic acid) and separated at 300 nl/min in a 10–40% buffer B gradient in 60 min (90 min inject-to-inject). Eluting peptides were ionized at a potential of + 2 kV into a Q Exactive mass spectrometer (Thermo Fisher, Bremen, Germany). Intact masses were measured at resolution 70,000 (at m/z 200) in the orbitrap using an automatic gain control (AGC) target value of $3x10^6$ charges. The top 10 peptide signals (charge-states 2+ and higher) were submitted to MS/MS in the HCD (higher-energy collision) cell using 1.6 amu isolation width and 25% normalized collision energy. MS/MS spectra were acquired at resolution 17,500 (at m/z 200) in the orbitrap using an AGC target value of $1x10^6$ charges, a maxIT of 60 ms and an underfill ratio of 0.1%. Dynamic exclusion was applied with a repeat count of 1 and an exclusion time of 30 s.

DATA ANALYSIS

MS/MS spectra were searched against a Uniprot human reference proteome FASTA file (Swissprot_2017_03_human_canonical_and_isoform.fasta, 42161 entries) using MaxQuant version 1.5.4.1. Enzyme specificity was set to trypsin and up to two missed cleavages were allowed. Cysteine carboxamidomethylation was treated as fixed modification, and methionine oxidation and N-terminal acetylation as variable modifications. Peptide precursor ions were searched with a maximum mass deviation of 4.5 parts per million (ppm) and fragment ions with a maximum mass deviation of 20 ppm. Peptide and protein identifications were filtered at a false discovery rate (FDR) of 1% using the decoy database strategy. The minimal peptide length was 7 amino acids, the minimum Andromeda score for modified peptides was 40, and the minimum delta score was 6. Proteins that could not be differentiated based on MS/MS spectra alone were grouped to protein groups (default MaxQuant settings). Searches were performed with the label-free quantification option selected. The mass spectrometry proteomics data have been deposited to the ProteomeXchange Consortium via the PRIDE[28] partner repository with the dataset identifier PXD012467. Beta-binominal statistics were used to assess differential protein expression between groups, after normalization on the sum of the counts for each sample.[24] Proteins with a *p*-value below 0.05 were considered significantly differentially expressed. Proteins which were present in less than 25% of the samples or had an average normalized count of less than 1.4 were excluded from further functional analysis. Principal component analysis was performed in R. Therefore quantile normalization and log2 transformation was performed on the normalized counts. The 95th Percentile was taken, the data median centred and the principal components calculated. Hierarchical clustering was performed after a statistical multi-group comparison. Protein networks were generated utilizing the STRING database (Search Tool for the Retrieval of Interacting Genes/Proteins) and visualized with Cytoscape software.[29] Protein interaction networks were generated with ClusterONE and gene ontology (GO) analysis was performed using the BiNGO application in cytoscape.[30,31] Venn diagrams were created with InteractiVenn tool[32] and the layout modified if needed.

TRANSCRIPTION FACTOR ANALYSIS

The ToppFun tool from the ToppGene Suite was used to identify transcription factors of significantly different proteins between HCM_{female} and HCM_{male} .[33] All significantly different proteins between HCM_{female} and HCM_{male} were used as input.

WESTERN BLOT

For analysis of protein levels by Western blot, whole tissue lysates were used from either the proteomic analysis or were prepared as described previously.[34] Proteins were separated on precast SDS-PAGE 4-12% criterion gels (Bio-Rad) and transferred to polyvinylidene difluoride or nitrocellulose membranes. Site-specific antibodies directed to acetylated α-tubulin (Sigma, T7451), HSPA1 (Enzo Life Sciences, ADI-SPA-810), HSPA2 (Proteintech group, 66291-1), HSPB1 (Enzo Life Sciences, ADI-SPA-800), HSPB5 (Enzo Life Sciences, ADI-SPA-223), HSPB7 (abcam, ab150390), HSPD1 (Enzo Life Sciences, ADI-SPA-805), HSPA4 (Cell Signaling, 3303S), HSP90 (Cell Signaling, 4874S), α-tubulin (Sigma, T9026), tyrosinated tubulin (Sigma, T9028), detyrosinated tubulin (abcam, ab48389), and GAPDH (Cell Signaling, 2118S; Fitzgerald, 10R-G109a) were used to detect the proteins which were visualized with an enhanced chemiluminescence detection kit (Amersham) and scanned with Amersham Imager 600. Protein levels were determined by densitometric analysis and normalized to GAPDH.

STATISTICS

Graphpad Prism v8 software was used for statistical analysis. Normally distributed data (except proteomics data) were statistically analysed with the Student's *t*-test when comparing 2 groups and with one-way ANOVA when comparing more than 2 groups. Non-normally distributed data were analysed with Mann-Whitney test. Linear regression was statistically tested with Pearson correlation. Data are presented as means ± standard errors of the mean, clinical characteristics are presented as mean ± standard deviation or median with interquartile range when appropriate. Categorical data was statistically analysed using Fisher's exact test and presented as frequencies. A p-value ≤ 0.05 was considered as significantly different.

RESULTS

To define sex-specific protein changes in HCM, we compared the protein expression profile of male and female HCM samples. We performed a new analysis on a subset of patients from our proteomics data set.[25] We compared age-matched samples from 13 male and 13 female sarcomere mutation-positive (SMP) HCM patients. The genotype distribution of both groups is depicted in Figure 8.1 and shows that the majority of mutations in both groups are located in the thick filament genes *MYBPC3* and *MYH7*.

Clinical characteristics of the groups are summarized in Table 8.1. Both male and female patients had obstructive HCM. While male patients presented with a larger LV end-systolic diameter (ESD), females displayed more severe diastolic dysfunction, indicated by a higher E/e' ratio compared to male patients, and more females with diastolic dysfunction

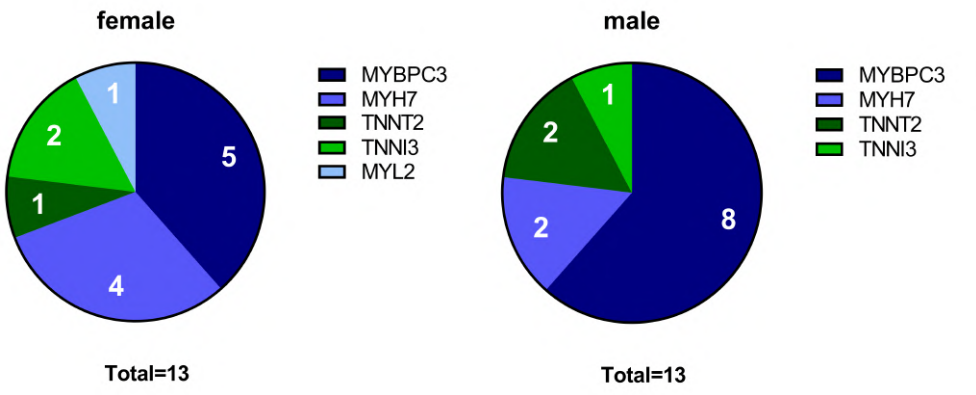

Figure 8.1: Genotypes in female and male HCM patient groups.
The pie charts indicate the number of patients with a mutation in *MYBPC3*, *MYH7*, *TNNT2*, *TNNI3* and *MYL2* for the female and male group, respectively.

stage 2.[35,36] Although there is no difference between women and men in absolute IVS thickness, the women included in this study showed a higher IVS thickness when corrected for BSA compared to males (25% increase, p=0.07; Table 8.1). This is in line with a previous study showing significant differences in IVS thickness between women and men when corrected for BSA.[13]

FEMALES EXPRESS MORE TUBULIN AND HEAT SHOCK PROTEINS

Out of 2099 quantified proteins, only 46 proteins were significantly differentially expressed in the direct comparison of the female and male group. Two functional protein interaction clusters were identified for both the 14 downregulated and the 32 upregulated proteins in females compared to males. The functional protein clusters that were less expressed in females compared to males were related to muscle filament sliding and carbohydrate catabolic process (Figure 8.2A).
The functional protein clusters of proteins that are more expressed in females compared to males are chaperone-mediated protein complex assembly and action potential (Figure 8.2B). Chaperone-mediated complex assembly is, based on the number of proteins in this cluster (18, 39% of the differentially expressed proteins), the dominating protein cluster in the comparison of female and male SMP HCM samples. Interestingly, this cluster contains mainly heat shock proteins (HSPs) and tubulin subunits. HSPs and tubulin have already been investigated before by our group in the context of SMP and sarcomere mutation-negative HCM samples.[25,34] Therefore, we now further determined if there are any sex-differences at the protein levels of tubulin and a selection of HSPs that were assessed by Western blot. While we did not observe significant sex-differences in the levels of HSPA1, HSPA2, HSPB5, HSPB7, HSPA4 and HSP90, we found a trend to higher levels of HSPD1 (p=0.0957) and HSPB1 (p=0.0850) in female compared to male samples (Figure 8.3, re-analysed from the dataset from Dorsch et al.[34]).

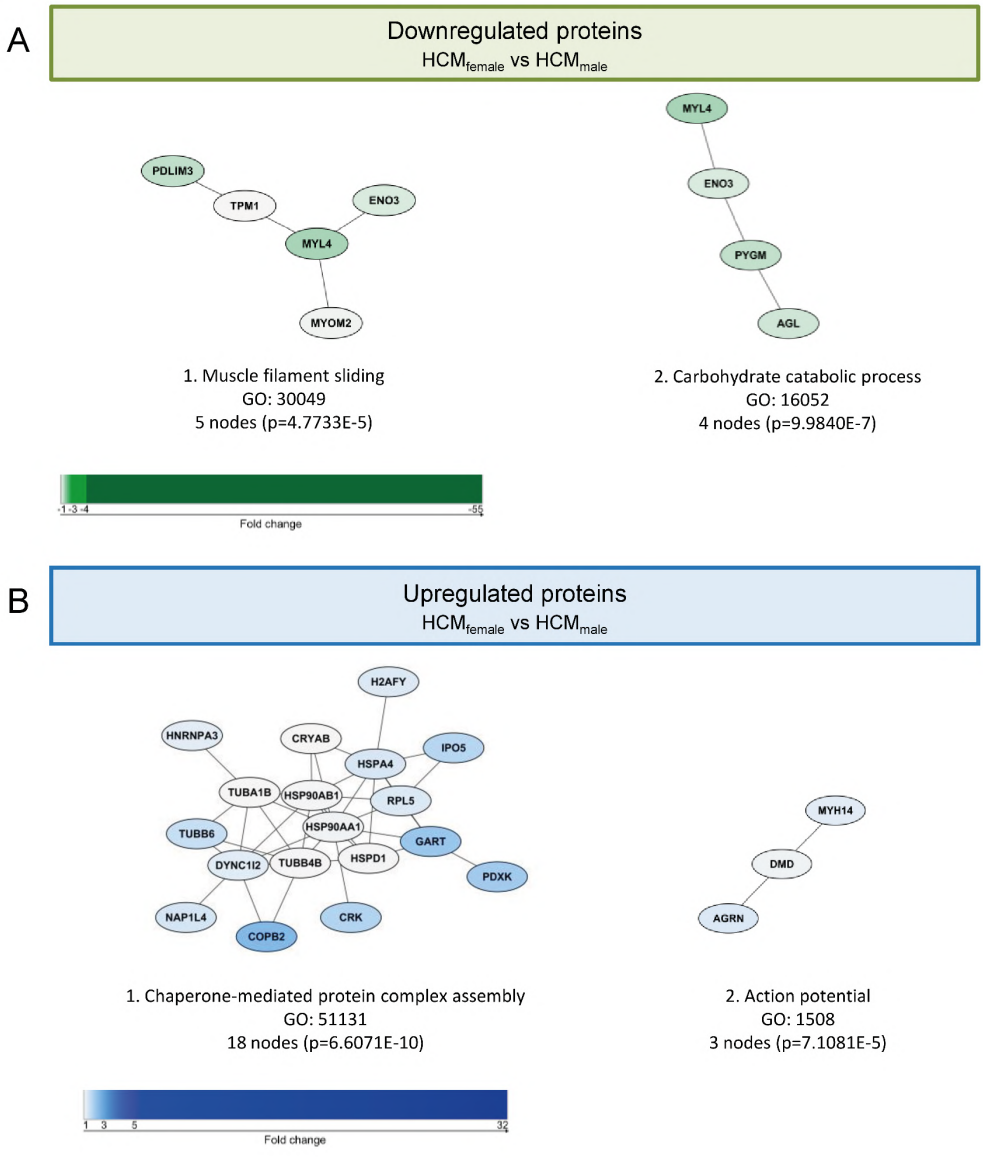

Figure 8.2: Functional protein cluster of the direct comparison of HCM_{female} and HCM_{male}. (**A**) illustrates the functional protein cluster of the proteins that are significantly lower expressed in females compared to males. (**B**) shows the functional protein cluster of the proteins that are significantly higher expressed in females compared to males. For each protein cluster the most significant biological process is given. Proteins with a p-value <0.05 were used for the analysis.

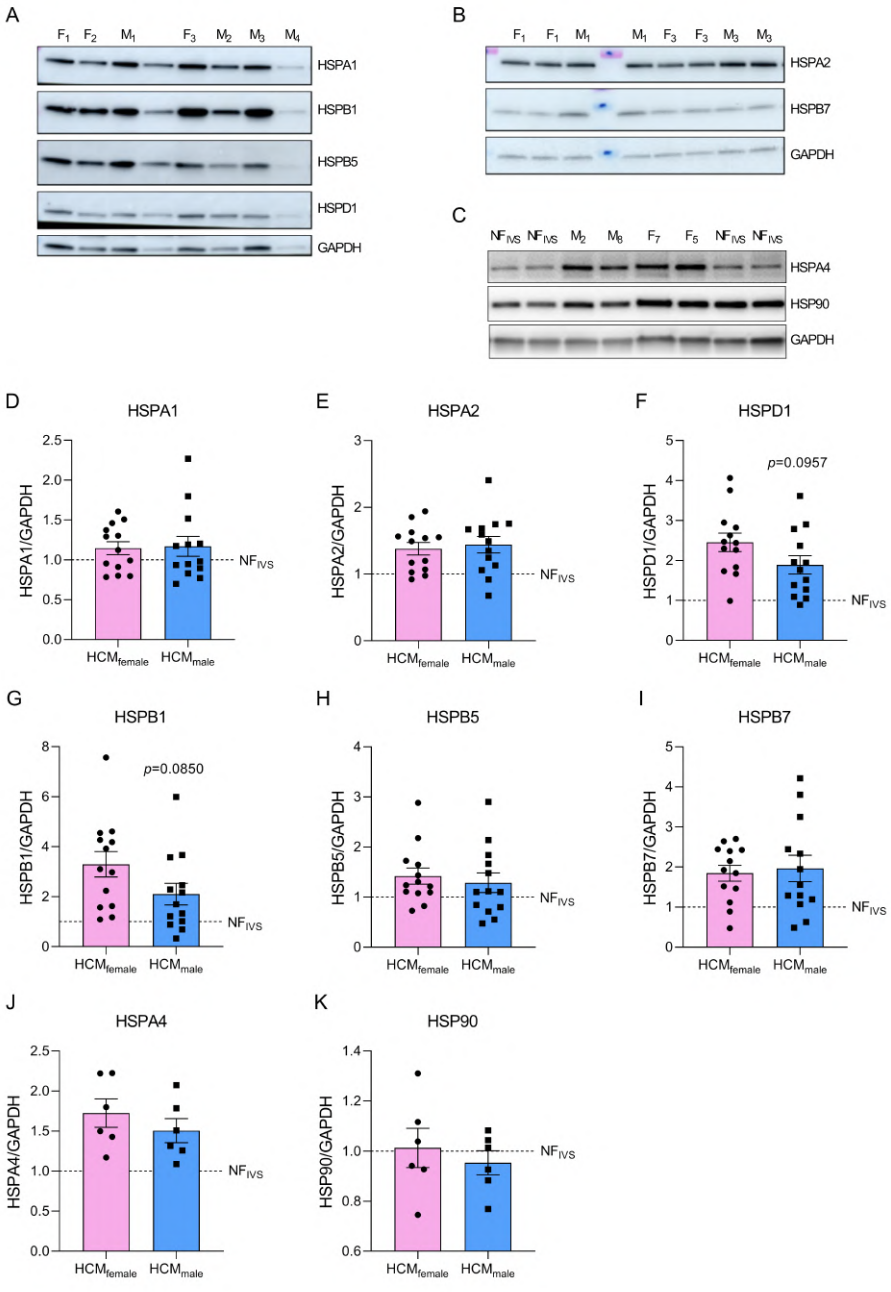

Figure 8.3: Protein levels of heat shock proteins determined by Western blot.
Panel (**A**), (**B**) and (**C**) show representative Western blot images. Panel (**D**-**K**) display quantified protein levels for HSPA1, HSPA2, HSPD1, HSPB1, HSPB5, HSPB7, HSPA4 and HSP90, respectively. Data were statistically analysed by unpaired two-tailed t-test. Dashed line indicates protein levels in the NF_{IVS}. Western blot dataset is partly derived from Dorsch et al. and re-analysed for the age-matched samples included in the current study.[34]

Although the HSPs assessed by Western blot do not show significant differences between females and males, the data are in line with the small fold changes found in the proteomics data and point towards higher levels of HSPs in female compared to male HCM tissue. Likewise, we analysed the sex-differences in our tubulin data set (Figure 8.4, re-analysed from the datasets from Dorsch et al. 2019 and Schuldt et al. 2021.[25,34]

In line with the proteomics data, levels of α-tubulin were significantly higher in females compared to males, whereas we did not find any sex-differences in the posttranslational modifications acetylation, tyrosination and detyrosination. To determine if elevated levels of tubulin may correlate with diastolic dysfunction, we plotted levels of α-tubulin with the clinical parameter E/e' for male and female patients separately (Figure 8.4E). Female patients have higher levels of α-tubulin in combination with more severe diastolic dysfunction, as indicated by increased E/e', compared to male patients who show lower levels of α-tubulin with less severe diastolic dysfunction.

PROTEINS INVOLVED IN TRANSLATION ARE SPECIFICALLY DOWNREGULATED IN MALE HCM PATIENTS COMPARED TO NON-FAILING CONTROL MYOCARDIUM

As an additional approach, we compared the protein expression of both the male and the female group to NF_{IVS} to look at specific sex-related protein changes compared to non-failing myocardium, thereby identifying proteins that are not only sex- but also disease-specific. We have identified 236 proteins that are less expressed and 214 proteins that are more expressed in the female HCM patients versus NF_{IVS}. In the male HCM patients we identified 251 lower expressed proteins and 156 more abundant proteins compared to NF_{IVS}. The top 10 functional protein interaction clusters of the females compared to NF_{IVS} are listed in Table 8.2 and the top 10 protein clusters of the male samples compared to NF_{IVS} are displayed in Table 8.3.

Table 8.2: Top 10 differentially regulated pathways in HCM_{female} vs NF_{IVS}.

Downregulated proteins			Upregulated proteins		
Pathway (GO ID)	**nodes**	***p***	**Pathway (GO ID)**	**nodes**	***p***
Cellular respiration (45333)	70	6.7945E-73	Extracellular structure organization (43062)	45	8.1156E-43
NAD metabolic process (19674)	28	1.7205E-22	Muscle contraction (6936)	19	1.9361E-16
Monocarboxylic acid metabolic process (32787)	22	2.3313E-25	Post-translational protein modification (43687)	17	1.4103E-11
Organic acid catabolic process (16054)	20	1.0701E-24	Organelle localization (51640)	13	1.6284E-8
Neutrophil degranulation	15	2.5257E-15	Response to unfolded protein (6986)	12	2.2706E-12
Cellular nitrogen compound biosynthetic process (44271)	12	3.4079E-11	Striated muscle cell development (55002)	12	6.9444E-9
Muscle contraction (6936)	12	5.6834E-9	Myofibril assembly (30239)	10	4.2003E-14
Acute-phase response (6953)	11	5.0201E-14	Regulation of cell migration (30334)	9	1.3513E-8

Table 8.2: Continued

Downregulated proteins			Upregulated proteins		
Pathway (GO ID)	**nodes**	***p***	**Pathway (GO ID)**	**nodes**	***p***
Cellular detoxification (1990748)	9	6.5002E-10	Cellular carbohydrate metabolic process (44262)	8	2.0038E-9
Cardiac muscle tissue development (48738)	8	9.5592E-12	Membrane organization (61024)	8	4.7889E-6

Table lists the top 10 functional protein cluster (based on size) of the down- and upregulated proteins for the comparison of HCM_{female} with NF_{IVS}. Displayed are the most significant biological process (gene ontology), the number of nodes in the cluster and the *p*-value.

,

Table 8.3: Top 10 differentially regulated pathways in HCM_{male} vs NF_{IVS}.

Downregulated proteins			Upregulated proteins		
Pathway (GO ID)	**nodes**	***p***	**Pathway (GO ID)**	**nodes**	***p***
Cellular respiration (45333)	62	9.9733E-62	Extracellular matrix organization (30198)	47	9.0957E-40
Small molecule metabolic process (44281)	29	3.0796E-22	Actin filament-based process (30029)	13	3.2873E-10
Amide biosynthetic process (43604)	27	2.6386E-19	Striated muscle cell development (55002)	12	4.8955E-11
Carboxylic acid catabolic process (46395)	26	3.3911E-26	Platelet aggregation (70527)	11	1.0179E-8
Regulated exocytosis (45055)	15	3.5280E-13	Muscle contraction (6936)	10	1.1585E-7
Translational initiation (6413)	15	6.4097E-8	Calcium-independent cell-matrix adhesion (7161)	8	5.7263E-7
Protein folding (6457)	15	1.9000E-7	Response to muscle inactivity involved in regulation of muscle adaptation (14877)	8	8.5753E-6
Organic acid catabolic process (16054)	13	1.0083E-14	Neutrophil degranulation (43312)	7	3.3963E-7
Acute-phase response (6953)	12	1.0023E-13	Carbohydrate metabolic process (5975)	6	6.4278E-8
Creatine metabolic process (6600)	12	3.2195E-12	Regulation of podosome assembly (71801)	6	9.2900E-6

Table lists the top 10 functional protein cluster (based on size) of the down- and upregulated proteins for the comparison of HCM_{male} with NF_{IVS}. Displayed are the most significant biological process (gene ontology), the number of nodes in the cluster and the *p*-value.

The complete set of protein interaction clusters resulting from this analysis is shown in Figures S1-S4. To identify differences between female and male HCM using this analysis approach, we created Venn diagrams of the significantly different proteins from the female vs NF_{IVS} and the male vs NF_{IVS} comparison to look at overlapping proteins that are shared by both comparisons, and proteins that are unique for either males or females compared to NF_{IVS} (Figures 8.5 and 8.6, Venn diagrams).

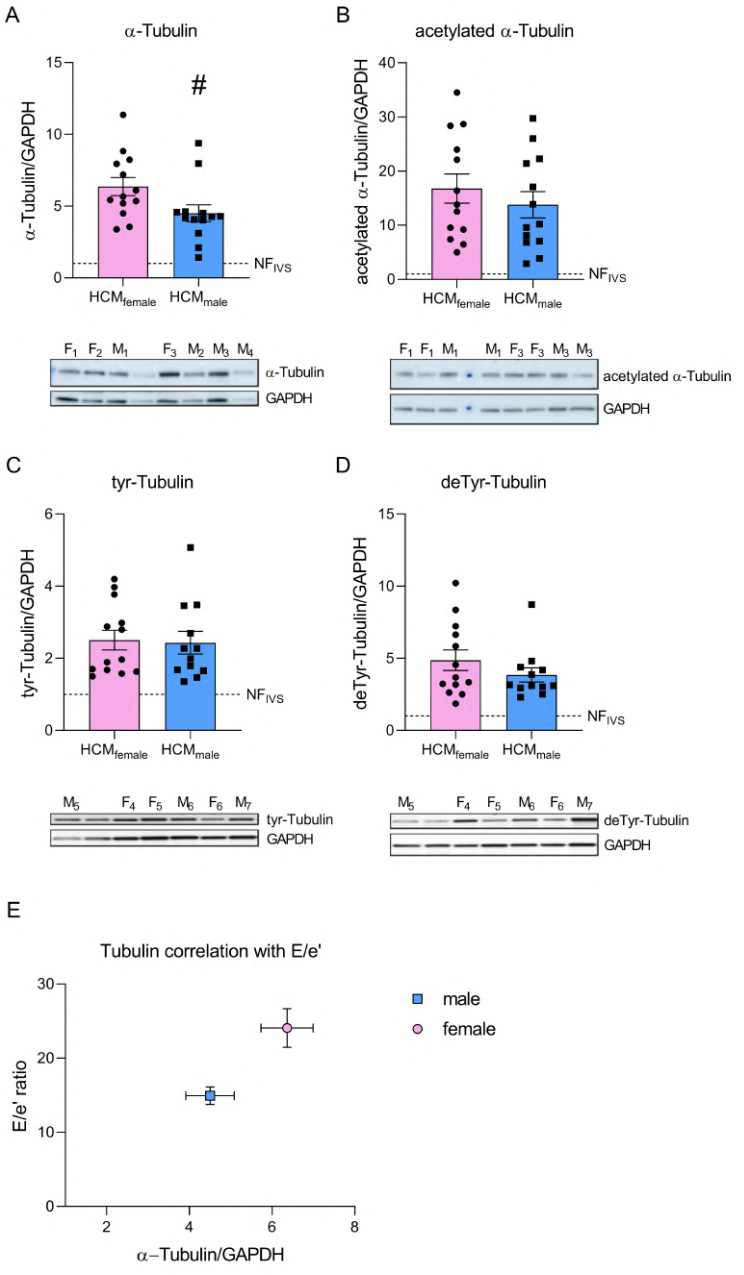

Figure 8.4: Protein levels of α-tubulin and its posttranslational modifications determined by Western blot. Panels (**A**-**D**) show protein levels of α-tubulin (**A**), acetylated tubulin (**B**), tyrosinated tubulin (**C**) and detyrosinated tubulin (**D**) with representative images. Data were statistically analysed by unpaired two-tailed t-test, $^{\#}p$=0.0407. Dashed line indicates protein levels in the NF_{IVS}. Western blot dataset is new analysis of a subset of samples from Dorsch et al. and Schuldt et al.[25,34] (**E**) shows correlation of α-tubulin levels with E/e' ratio.

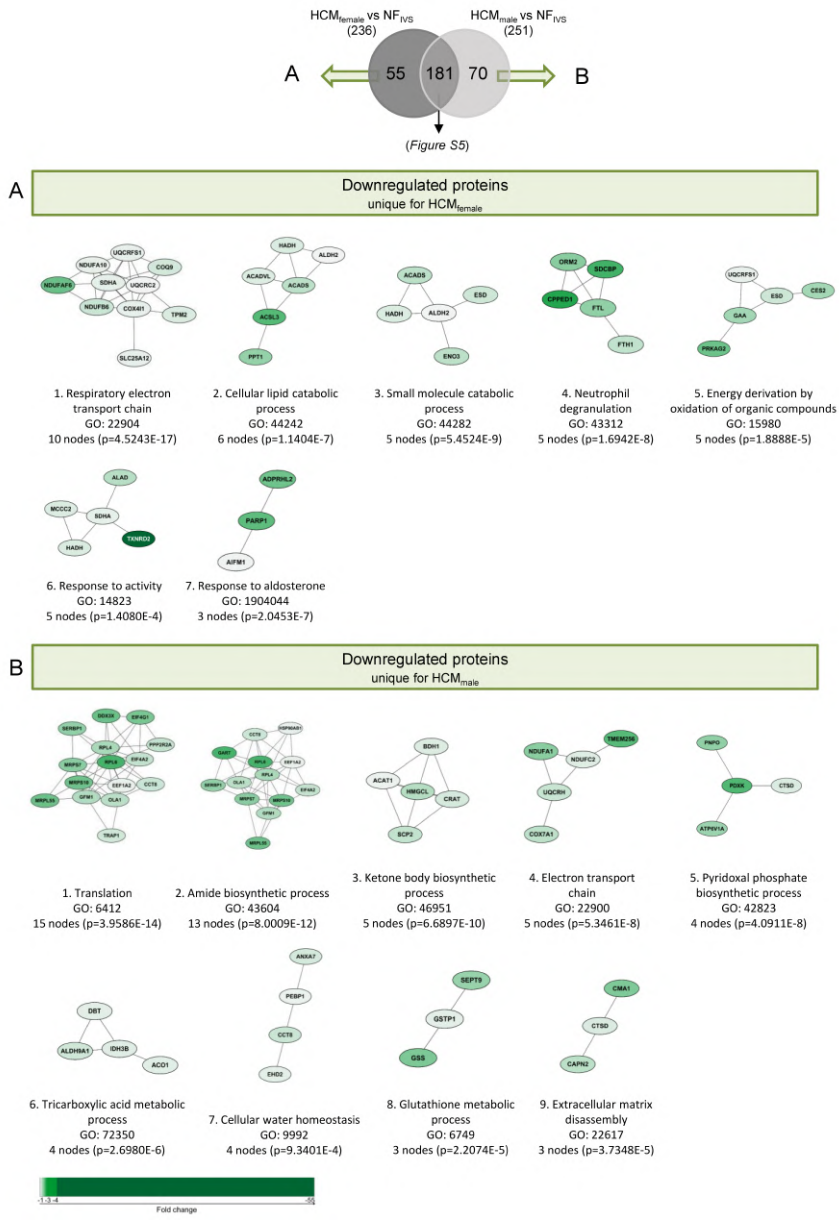

Figure 8.5: Functional protein cluster of the downregulated proteins that are unique for either HCM_{female} and HCM_{male} when compared separately to NF_{IVS}. A Venn diagram was created with the significantly lower expressed proteins between HCM_{female} and NF_{IVS} and HCM_{male} and NF_{IVS}, to identify the downregulated proteins that are unique for either males or females, or shared by both groups. Panel (**A**) illustrates the functional protein cluster of the proteins that are only significantly lower expressed in females when compared to NF_{IVS}, whereas (**B**) shows the functional protein cluster of the proteins that are significantly lower expressed in males when compared to NF_{IVS}. For each protein cluster the most significant biological process is given. Proteins with a p-value <0.05 were used for the analysis.

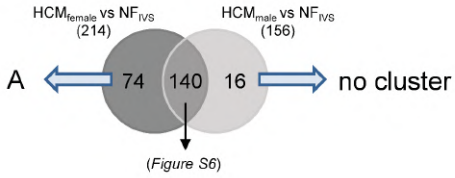

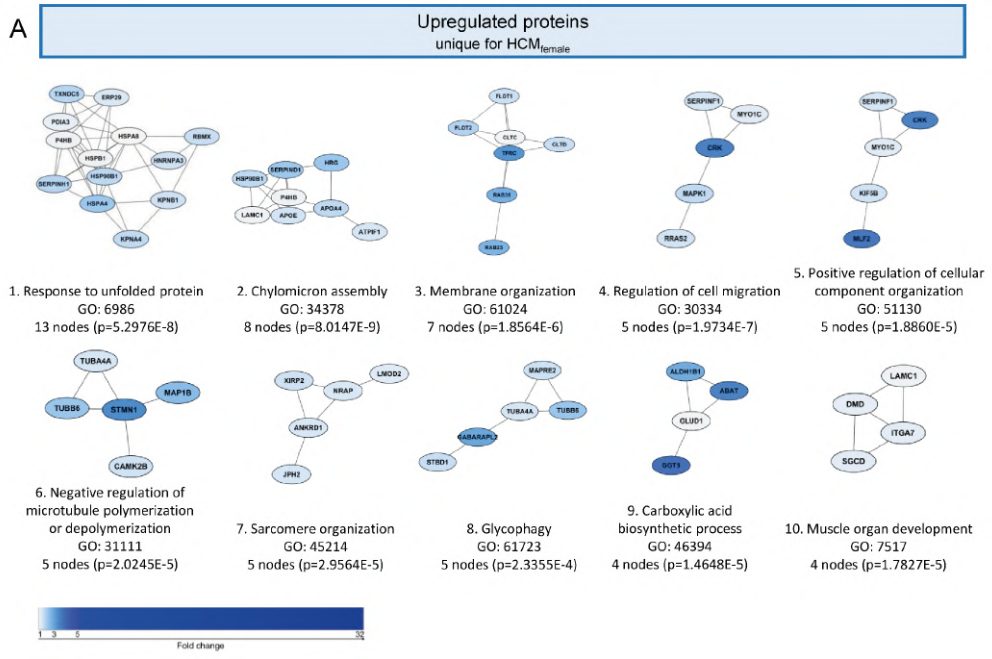

Figure 8.6: Functional protein cluster of the upregulated proteins that are unique for either HCM_{female} and HCM_{male} when compared separately to NF_{IVS}. A Venn diagram was created with the significantly higher expressed proteins between HCM_{female} and NF_{IVS} and HCM_{male} and NF_{IVS}, to identify the upregulated proteins that are unique for either males or females or shared by both groups. Panel (**A**) illustrates the functional protein cluster of the proteins that are only significantly higher expressed in females when compared to NF_{IVS}. The proteins only significant for HCM_{male} did not give any functional protein cluster. For each protein cluster the most significant biological process is given. Proteins with a p-value <0.05 were used for the analysis.

Of the proteins that are downregulated compared to NF_{IVS} we identified 181 proteins that are overlapping between males and females. These proteins belong mainly to metabolic pathways (Figure S5), and can be considered as general HCM-specific protein changes. 55 of the downregulated proteins are only significantly different for the females. The functional protein clusters of these proteins are related to respiratory electron transport chain, cellular lipid catabolic process, response to activity, small molecule catabolic process, neutrophil degranulation, energy deprivation by oxidation of organic compounds and response to aldosterone (Figure 8.5A). 70 downregulated proteins are only significantly different in the male group and cluster analysis revealed that the biggest protein cluster is related to the

biological process translation. It contains many ribosomal proteins that have a consistently high fold-change compared no NF_{IVS}. Other clusters are related to amide biosynthetic process and several processes related to energy metabolism like ketone body biosynthetic process, electron transport chain and tricarboxylic acid metabolic process. Furthermore, we obtained protein clusters related to pyridoxal phosphate biosynthetic process, cellular water homeostasis, glutathione metabolic process and extracellular matrix disassembly (Figure 8.5B).

MICROTUBULAR AND HEAT SHOCK PROTEINS ARE SPECIFICALLY UPREGULATED IN FEMALE HCM PATIENTS WHEN COMPARED TO CONTROLS

For the upregulated proteins, 140 proteins are significantly more expressed in both females vs NF_{IVS} and males vs NF_{IVS}. The functional protein interaction clusters are illustrated in Figure S6. The 74 proteins that are significantly higher in females compared to controls result in clusters related to response to unfolded protein, chylomicron assembly, membrane organization, regulation of cell migration, negative regulation of microtubule polymerization or depolymerization, positive regulation of cellular component organization, sarcomere organization, glycophagy, muscle organ development and carboxylic acid biosynthetic process (Figure 8.6A). With the cluster response to unfolded protein and negative regulation of microtubule polymerization or depolymerization the results of this approach are in line with the direct comparison of female and male HCM samples in which these proteins were represented by the cluster chaperone-mediated protein complex assembly. 8 of the 74 proteins that are significantly higher expressed only in females (CRK, HSPA4, TUBB6, ALDH1B1, DMD, LMOD2, HNRNPA3 and TFRC) overlap with the 46 proteins significantly different in the direct male and female comparison and may represent important candidates to define the female group (Figure 8.7).

The 16 proteins that are only significantly higher in HCM males compared to NF_{IVS} did not form any functional protein cluster. Of these proteins, only the protein SLC27A6 (solute carrier family 27 member 6/long chain fatty acid transport protein 6) overlaps with the 46 proteins that are significantly different in the direct comparison of females and males. As being significantly higher expressed compared to both NF_{IVS} and females, SLC27A6, involved in long chain fatty acid uptake, may be an important candidate defining the male HCM patients.

TRANSCRIPTIONAL REGULATION OF SIGNIFICANTLY DIFFERENT PROTEINS BETWEEN HCM_{female} AND HCM_{male} IS NOT DOMINATED BY SEX HORMONES

Since sex hormones also act as transcription factors, we analysed if sex-hormone-related transcription factors can be responsible for the 46 significantly differentially expressed proteins of the direct comparison between female and male HCM samples (Figure 8.2). Possible transcription factor bindings sites were analysed with the ToppFun database. 372 transcription factors were identified that have binding-sites in the 46 proteins that are significantly different between female and male HCM patient samples. The 10 most

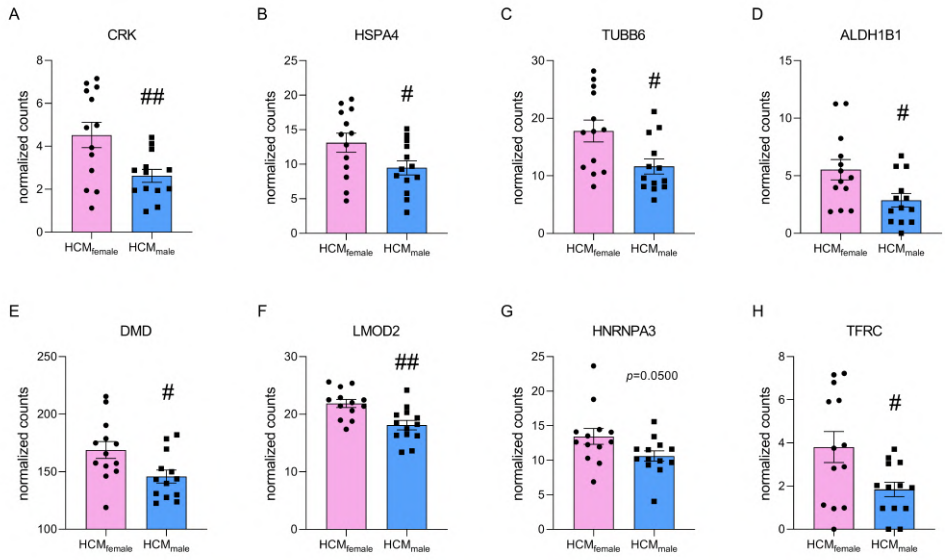

Figure 8.7: Normalized counts of proteins that are significantly upregulated in HCM_{female} compared to HCM_{male} and are uniquely upregulated in females when compared to NF_{IVS}. (**A**) CRK, (**B**) HSPA4), (**C**) TUBB6, (**D**) ALDH1B1, (**E**) DMD, (**F**) LMOD2, (**G**) HNRNPA3 and (**H**) TFRC. $^{\#}p<0.05$, $^{\#\#}p<0.01$, unpaired two-tailed t-test.

significant transcription factors are shown in Table S2. Of these we found 7 to be sex-hormone related (Table S3). These 7 transcription factors are involved in the regulation of 5 significantly different proteins between male and female HCM myocardium: HSPD1, PYGM, DMD, ENO3 and TFRC. Of these, DMD, ENO3 and TFRC are also significantly different when comparing females with NF_{IVS} (Figures 8.5 and 8.6). With PYGM and ENO3 involved in carbohydrate metabolism, DMD involved in muscle organization and HSPD1 as a member of the PQC, we thereby identified candidate proteins that may be regulated by sex hormone-related transcription factors. However, the bioinformatical analysis revealed that the 5 proteins also have binding sites for another 258 of the 372 identified transcription factors. Based on this we can conclude that the differences found between female and male samples may be partly due to transcriptional regulation by sex hormones but that this is not the dominant mechanism driving sex-dependent differential protein expression.

DISCUSSION

In this study we analysed sex-differences at the protein level in proteomics data of HCM patient tissue to define sex-specific protein expression which may explain the difference in clinical presentation. The direct comparison of the male and female patient groups resulted in only a small number of significantly different proteins. Compared to males, female HCM patients display lower levels of myofilament proteins related to the biological process muscle filament sliding and have elevated levels of tubulin and HSPs. Consistently, by subtracting

the baseline differences using an additional non-failing control group, we observed a more profound elevation of HSPs and the microtubule processes in female HCM patients.

SET OF 8 PROTEINS CONSISTENTLY DEFINES THE FEMALE HCM PATIENTS

A study investigating sex-differences in gene expression at the mRNA level in idiopathic cardiomyopathy patients found 1837 differently expressed genes between male and female patients, of which the large majority of 1377 genes had a fold change <1.2.[37] Considering these low fold changes on a gene expression level, little changes at the protein level are to be expected. We found expression levels of 8 proteins significantly higher in females when directly compared to males, and also uniquely significant for females when compared to NF_{IVS} (Figure 8.7). Thereby, these proteins are disease-specific and may play an important role in defining the female patient group. One of these proteins is CRK, which is an adaptor protein with SH2 and SH3 domains but no catalytic region. It functions in signal transduction processes and has been shown to be involved in cardiac development.[38] HSPA4 is a heat shock protein that acts as nucleotide exchange factor for HSP70 chaperones. Its expression is upregulated in response to pressure overload and in human heart failure, which is thought to be a beneficial response as it helps degrading misfolded proteins.[39] TUBB6 is a β-tubulin subtype that forms microtubules together with α-tubulin. Elevated levels of tubulin have been observed in heart failure.[40] ALDH1B1 is an aldehyde dehydrogenase that is involved in alcohol metabolism and has been shown to function in glucose metabolism.[41] DMD encodes for dystrophin and connects the actin cytoskeleton with the extracellular matrix. As actin cross-linker, it plays an important role for the mechanical properties of the cardiomyocyte. Elevated levels in females may be explained by its gene location on the X-chromosome. Mutations in DMD have been associated with muscular dystrophies and X-linked dilated cardiomyopathy.[42] LMOD2 is the cardiac isoform of leiomodin, an actin-binding protein involved in thin filament assembly. Studies in adult mice have shown that LMOD2 has an essential role in maintaining proper cardiac thin filament length and coinciding force generation.[43] HNRNPA3 is a heterogeneous nuclear ribonucleoprotein that binds to single-stranded telomeric repeats to stabilize them,[44] and TFRC encodes for the transferrin receptor that promotes iron uptake.[45]

ELEVATED LEVELS OF HSPs AND TUBULIN ARE IN LINE WITH A MORE SEVERE PHENOTYPE

The most prominent difference in our study were higher levels of tubulin and HSPs in female compared to male HCM patient samples taken at the time of myectomy. Interestingly, sex-differences in the expression of HSPs have been observed before. Higher levels of HSPA1A have been measured in healthy female rat hearts compared to male, and these increased levels were oestrogen dependent.[46] We also found by bioinformatical analysis that HSPD1, which is elevated in female compared to male HCM myocardium, can be regulated by the oestrogen-related receptor α. It may be speculated that the oestrogen-dependent HSP induction, that is known to be cardioprotective,[47] has also beneficial effects in HCM, leading to lower disease penetrance and later disease onset in women. Indeed, HSP activation has been shown to have beneficial effects on heart function in a mouse model of desmin-related cardiomyopathy in which HSP expression was induced

by geranylgeranylacetone.[48] In our study we observed increased protein expression of HSPs in tissue samples from symptomatic stage II HCM patients, which raises the question if the optimal therapeutic window for HSP induction might already be at an earlier preclinical stage of the disease. This warrants further studies in iPSC-derived human heart models and other cardiomyopathy animal models.

Cytoskeletal proteins like tubulin and desmin are known to be elevated in heart failure.[40] Our group has previously shown that tubulin protein levels are increased in HCM myectomy tissue compared to NF_{IVS}.[25,34] Interestingly, tubulin and desmin protein content has been shown to correlate well with left ventricular end-diastolic pressure (LVEDP) in heart failure.[40] As increased LVEDP indicates diastolic dysfunction, cytoskeletal protein levels correlate directly with diastolic dysfunction. Furthermore, tubulin has in combination with its posttranslational modifications a direct effect on contractile function, as detyrosinated tubulin binds to desmin and causes a stiffening of the myofilament.[49-51] As increased levels of tubulin in females compared to males correlate with more severe diastolic dysfunction,[13] proof-of-concept studies in model systems have to show whether this is a causal relationship during HCM development.

MALE SAMPLES DISPLAY LOWER LEVELS OF TRANSLATIONAL PROTEINS

Ribosomal and protein synthesis-related proteins, which form the cluster "translation", were significantly downregulated in male HCM patients compared to NF_{IVS}. Interestingly, it was recently shown that cMyBP-C protein synthesis and degradation rates were slowed down in induced pluripotent stem cell-derived cardiomyocytes harbouring a heterozygous *MYBPC3* mutation.[52] The authors proposed that cells harbouring a *MYBPC3* truncating mutation may have the capacity to attain normal levels of cMyBP-C protein and thereby preserve cardiomyocyte function. On the other hand, protein turnover is needed to replace aged/damaged proteins. Thus, while reduced protein turnover may preserve protein stoichiometry and thereby cardiomyocyte function, it may lead to accumulation of damaged proteins in the sarcomere. Our data are in line with the study of Helms and colleagues, and imply reduced protein turnover in particular in male HCM hearts at the time of myectomy. Increasing protein translation rate to maintain proper protein turnover represents an attractive avenue to further explore.

SEX-SPECIFIC DIFFERENCE IN CARBOHYDRATE METABOLISM

Downregulation of metabolic pathways is a general HCM disease hall mark[25,53] and accordingly we did not find major differences in these pathways between males and females. However, females showed lower levels of proteins related to carbohydrate catabolic process (Figure 8.2A), including muscle associated glycogen phosphorylase (PYGM) and β-enolase (ENO3). Mutations in both of these genes have been associated with glycogen metabolism disorders.[54] Consequently, reduced levels of PYGM and ENO3 impair glycogen metabolism in women. Our transcription factor analysis showed that both PYGM and ENO3 can be regulated by sex hormone transcription factors. The findings indicate that women may be less metabolically flexible to adapt to altered metabolic demand, at least during disease development. Imaging studies have shown that reduced cardiac efficiency occurs already

at the early disease stage in asymptomatic male and female mutation carriers[55,56] and may indicate that metabolic changes may be present in the very early stages before the onset of cardiac remodelling.

MORE FIBROSIS IN FEMALE PATIENTS IS NOT REFLECTED AT PROTEIN LEVEL

It has been observed that female HCM patient samples show more fibrosis compared to male samples.[13] Interestingly, this difference is not reflected at protein level. Neither in the direct comparison of female and male HCM samples, nor in the analysis compared to NF_{IVS}, we observed a specific increase in extracellular matrix proteins for females. In the current proteomics analysis, increased expression of extracellular matrix proteins was a general disease hallmark, and common for both female and male group. The methodological difference between quantifying proteins involved in extracellular matrix organization in this proteomics analysis and measuring the actual fibrotic area in tissue sections as performed by Nijenkamp et al. may underlie the divergent findings.

STUDY LIMITATIONS

The findings in this study are observational and provide a starting point for further validation in an independent cohort and proof-of-concept studies in disease models. Due to the limited availability of non-failing heart tissues, the male control samples used in this study are not age-matched with the male HCM samples, which may contribute to observed differences in protein expression. Furthermore, the group size of only female or male non-failing samples is too small to perform comparisons of HCM and controls of the same sex. Therefore, follow-up studies would benefit from age-matched and increased numbers of non-failing controls to differentiate between sex- and disease-specific differences in protein expression. As our findings point towards a possible role of sex hormone regulation, information about the hormonal state of the female subjects should be collected for future studies.

CONCLUSION

This proteomic analysis of female and male SMP HCM tissue highlights that elevated protein levels of tubulin correlate with more severe diastolic dysfunction in females. Another aspect which warrants further research is reduced protein turnover, in particular in male HCM, which may represent an adaptive mechanism to maintain protein stoichiometry, though may also have a negative impact and result in 'aged' sarcomeres. Further research in experimental model systems is needed to determine if targeting tubulin and protein quality control at an early disease stage prevent the progression of cardiac dysfunction.

Conflict of Interest: The authors declare that the research was conducted in the absence of any commercial or financial relationships that could be construed as a potential conflict of interest.

Sources of funding: We acknowledge the support from the Netherlands Cardiovascular

Research Initiative: An initiative with support of the Dutch Heart Foundation, CVON2014-40 DOSIS and NWO (NWO-ZonMW; 91818602 VICI grant to Jolanda van der Velden).

SUPPLEMENTARY FILES - ONLINE

https://www.frontiersin.org/articles/10.3389/fcvm.2021.612215/full#supplementary-material

REFERENCES

1. Maron BJ, Gardin JM, Flack JM, Gidding SS, Kurosaki TT, Bild DE. Prevalence of hypertrophic cardiomyopathy in a general population of young adults. Echocardiographic analysis of 4111 subjects in the CARDIA Study. Coronary Artery Risk Development in (Young) Adults. *Circulation*. 1995;92(4):785-9.
2. Semsarian C, Ingles J, Maron MS, Maron BJ. New Perspectives on the Prevalence of Hypertrophic Cardiomyopathy. *Journal of the American College of Cardiology*. 2015;65(12):1249-54.
3. Authors/Task Force, Elliott PM, Anastasakis A, Borger MA, Borggrefe M, Cecchi F, et al. 2014 ESC Guidelines on diagnosis and management of hypertrophic cardiomyopathy: the Task Force for the Diagnosis and Management of Hypertrophic Cardiomyopathy of the European Society of Cardiology (ESC). *Eur Heart J*. 2014;35(39):2733-79.
4. Michels M, Olivotto I, Asselbergs FW, van der Velden J. Life-long tailoring of management for patients with hypertrophic cardiomyopathy : Awareness and decision-making in changing scenarios. *Neth Heart J*. 2017;25(3):186-99.
5. Ho CY, Charron P, Richard P, Girolami F, Van Spaendonck-Zwarts KY, Pinto Y. Genetic advances in sarcomeric cardiomyopathies: state of the art. *Cardiovasc Res*. 2015;105(4):397-408.
6. Ingles J, Burns C, Barratt A, Semsarian C. Application of Genetic Testing in Hypertrophic Cardiomyopathy for Preclinical Disease Detection. *Circ Cardiovasc Genet*. 2015;8(6):852-9.
7. Olivotto I, Maron MS, Adabag AS, Casey SA, Vargiu D, Link MS, et al. Gender-related differences in the clinical presentation and outcome of hypertrophic cardiomyopathy. *J Am Coll Cardiol*. 2005;46(3):480-7.
8. Kubo T, Kitaoka H, Okawa M, Hirota T, Hayato K, Yamasaki N, et al. Gender-specific differences in the clinical features of hypertrophic cardiomyopathy in a community-based Japanese population: results from Kochi RYOMA study. *J Cardiol*. 2010;56(3):314-9.
9. Maron BJ, Casey SA, Poliac LC, Gohman TE, Almquist AK, Aeppli DM. Clinical course of hypertrophic cardiomyopathy in a regional United States cohort. *JAMA*. 1999;281(7):650-5.
10. Maron BJ, Olivotto I, Spirito P, Casey SA, Bellone P, Gohman TE, et al. Epidemiology of hypertrophic cardiomyopathy-related death: revisited in a large non-referral-based patient population. *Circulation*. 2000;102(8):858-64.
11. Marstrand P, Han L, Day SM, Olivotto I, Ashley EA, Michels M, et al. Hypertrophic Cardiomyopathy With Left Ventricular Systolic Dysfunction: Insights From the SHaRe Registry. *Circulation*. 2020;141(17):1371-83.
12. Bos JM, Theis JL, Tajik AJ, Gersh BJ, Ommen SR, Ackerman MJ. Relationship between sex, shape, and substrate in hypertrophic cardiomyopathy. *Am Heart J*. 2008;155(6):1128-34.
13. Nijenkamp L, Bollen IAE, van Velzen HG, Regan JA, van Slegtenhorst M, Niessen HWM, et al. Sex Differences at the Time of Myectomy in Hypertrophic Cardiomyopathy. *Circ Heart Fail*. 2018;11(6):e004133.
14. Schulz-Menger J, Abdel-Aty H, Rudolph A, Elgeti T, Messroghli D, Utz W, et al. Gender-specific differences in left ventricular remodelling and fibrosis in hypertrophic cardiomyopathy: insights from cardiovascular magnetic resonance. *Eur J Heart Fail*. 2008;10(9):850-4.
15. Leinwand LA. Sex is a potent modifier of the cardiovascular system. *J Clin Invest*. 2003;112(3):302-7.
16. Chen YZ, Qiao SB, Hu FH, Yuan JS, Yang WX, Cui JG, et al. Left ventricular remodeling and fibrosis: Sex differences and relationship with diastolic function in hypertrophic cardiomyopathy. *Eur J Radiol*. 2015;84(8):1487-92.
17. Borlaug BA, Redfield MM, Melenovsky V, Kane GC, Karon BL, Jacobsen SJ, et al. Longitudinal changes in left ventricular stiffness: a community-based study. *Circ Heart Fail*. 2013;6(5):944-52.
18. van Velzen HG, Schinkel AFL, Baart SJ, Huurman R, van Slegtenhorst MA, Kardys I, et al. Effect of Gender and Genetic Mutations on Outcomes in Patients With Hypertrophic Cardiomyopathy. *Am J Cardiol*. 2018;122(11):1947-54.
19. Geske JB, Ong KC, Siontis KC, Hebl VB, Ackerman MJ, Hodge DO, et al. Women with hypertrophic cardiomyopathy have worse survival. *Eur Heart J*. 2017.
20. van Driel B, Nijenkamp L, Huurman R, Michels M, van der Velden J. Sex differences in hypertrophic cardiomyopathy: new insights. *Curr Opin Cardiol*. 2019;34(3):254-9.
21. Huurman R, Schinkel AFL, van der Velde N, Bowen DJ, Menting ME, van den Bosch AE, et al. Effect of body surface area and gender on wall thickness thresholds in hypertrophic cardiomyopathy. *Neth Heart J*. 2020;28(1):37-43.
22. Latchman DS. Heat shock proteins and cardiac protection. *Cardiovasc Res*. 2001;51(4):637-46.
23. Golenhofen N, Perng MD, Quinlan RA, Drenckhahn D. Comparison of the small heat shock proteins alphaB-crystallin, MKBP, HSP25, HSP20, and cvHSP in heart and skeletal muscle. *Histochem Cell Biol*. 2004;122(5):415-25.
24. Pham TV, Piersma SR, Warmoes M, Jimenez CR. On the beta-binomial model for analysis of spectral count data in label-free tandem mass spectrometry-based proteomics. *Bioinformatics*. 2010;26(3):363-9.
25. Schuldt M, Pei J, Harakalova M, Dorsch LM, Schlossarek S, Mokry M, et al. Proteomic and Functional Studies Reveal Detyrosinated Tubulin as Treatment Target in Sarcomere Mutation-Induced Hypertrophic Cardiomyopathy. *Circ Heart Fail*. 2021:CIRCHEARTFAILURE120007022.
26. Warmoes M, Jaspers JE, Pham TV, Piersma SR, Oudgenoeg G, Massink MP, et al. Proteomics of mouse BRCA1-deficient mammary tumors identifies DNA repair proteins with potential diagnostic and prognostic value in human breast cancer. *Mol Cell Proteomics*. 2012;11(7):M111 013334.
27. Piersma SR, Broxterman HJ, Kapci M, de Haas RR, Hoekman K, Verheul HM, et al. Proteomics of the TRAP-induced platelet releasate. *J Proteomics*. 2009;72(1):91-109.

28. Perez-Riverol Y, Csordas A, Bai J, Bernal-Llinares M, Hewapathirana S, Kundu DJ, et al. The PRIDE database and related tools and resources in 2019: improving support for quantification data. *Nucleic Acids Res*. 2019;47(D1):D442-D50.
29. Shannon P, Markiel A, Ozier O, Baliga NS, Wang JT, Ramage D, et al. Cytoscape: a software environment for integrated models of biomolecular interaction networks. *Genome Res*. 2003;13(11):2498-504.
30. Maere S, Heymans K, Kuiper M. BiNGO: a Cytoscape plugin to assess overrepresentation of gene ontology categories in biological networks. *Bioinformatics*. 2005;21(16):3448-9.
31. Nepusz T, Yu H, Paccanaro A. Detecting overlapping protein complexes in protein-protein interaction networks. *Nat Methods*. 2012;9(5):471-2.
32. Heberle H, Meirelles GV, da Silva FR, Telles GP, Minghim R. InteractiVenn: a web-based tool for the analysis of sets through Venn diagrams. *BMC Bioinformatics*. 2015;16:169.
33. Chen J, Bardes EE, Aronow BJ, Jegga AG. ToppGene Suite for gene list enrichment analysis and candidate gene prioritization. *Nucleic Acids Res*. 2009;37(Web Server issue):W305-11.
34. Dorsch LM, Schuldt M, dos Remedios CG, Schinkel AFL, de Jong PL, Michels M, et al. Protein Quality Control Activation and Microtubule Remodeling in Hypertrophic Cardiomyopathy. *Cells*. 2019;8(7).
35. Lang RM, Bierig M, Devereux RB, Flachskampf FA, Foster E, Pellikka PA, et al. Recommendations for chamber quantification: a report from the American Society of Echocardiography's Guidelines and Standards Committee and the Chamber Quantification Writing Group, developed in conjunction with the European Association of Echocardiography, a branch of the European Society of Cardiology. *J Am Soc Echocardiogr*. 2005;18(12):1440-63.
36. Nagueh SF, Appleton CP, Gillebert TC, Marino PN, Oh JK, Smiseth OA, et al. Recommendations for the evaluation of left ventricular diastolic function by echocardiography. *J Am Soc Echocardiogr*. 2009;22(2):107-33.
37. Fermin DR, Barac A, Lee S, Polster SP, Hannenhalli S, Bergemann TL, et al. Sex and age dimorphism of myocardial gene expression in nonischemic human heart failure. *Circ Cardiovasc Genet*. 2008;1(2):117-25.
38. Park TJ, Boyd K, Curran T. Cardiovascular and craniofacial defects in Crk-null mice. *Mol Cell Biol*. 2006;26(16):6272-82.
39. Mohamed BA, Barakat AZ, Zimmermann WH, Bittner RE, Muhlfeld C, Hunlich M, et al. Targeted disruption of Hspa4 gene leads to cardiac hypertrophy and fibrosis. *J Mol Cell Cardiol*. 2012;53(4):459-68.
40. Heling A, Zimmermann R, Kostin S, Maeno Y, Hein S, Devaux B, et al. Increased expression of cytoskeletal, linkage, and extracellular proteins in failing human myocardium. *Circ Res*. 2000;86(8):846-53.
41. Singh S, Chen Y, Matsumoto A, Orlicky DJ, Dong H, Thompson DC, et al. ALDH1B1 links alcohol consumption and diabetes. *Biochem Biophys Res Commun*. 2015;463(4):768-73.
42. Pecorari I, Mestroni L, Sbaizero O. Current Understanding of the Role of Cytoskeletal Cross-Linkers in the Onset and Development of Cardiomyopathies. *Int J Mol Sci*. 2020;21(16).
43. Pappas CT, Farman GP, Mayfield RM, Konhilas JP, Gregorio CC. Cardiac-specific knockout of Lmod2 results in a severe reduction in myofilament force production and rapid cardiac failure. *J Mol Cell Cardiol*. 2018;122:88-97.
44. Tanaka E, Fukuda H, Nakashima K, Tsuchiya N, Seimiya H, Nakagama H. HnRNP A3 binds to and protects mammalian telomeric repeats in vitro. *Biochem Biophys Res Commun*. 2007;358(2):608-14.
45. Hentze MW, Muckenthaler MU, Andrews NC. Balancing acts: molecular control of mammalian iron metabolism. *Cell*. 2004;117(3):285-97.
46. Voss MR, Stallone JN, Li M, Cornelussen RN, Knuefermann P, Knowlton AA. Gender differences in the expression of heat shock proteins: the effect of estrogen. *Am J Physiol Heart Circ Physiol*. 2003;285(2):H687-92.
47. Knowlton AA, Korzick DH. Estrogen and the female heart. *Mol Cell Endocrinol*. 2014;389(1-2):31-9.
48. Sanbe A, Daicho T, Mizutani R, Endo T, Miyauchi N, Yamauchi J, et al. Protective effect of geranylgeranylacetone via enhancement of HSPB8 induction in desmin-related cardiomyopathy. *PLoS One*. 2009;4(4):e5351.
49. Robison P, Caporizzo MA, Ahmadzadeh H, Bogush AI, Chen CY, Margulies KB, et al. Detyrosinated microtubules buckle and bear load in contracting cardiomyocytes. *Science*. 2016;352(6284):aaf0659.
50. Chen CY, Caporizzo MA, Bedi K, Vite A, Bogush AI, Robison P, et al. Suppression of detyrosinated microtubules improves cardiomyocyte function in human heart failure. *Nat Med*. 2018;24(8):1225-33.
51. Caporizzo MA, Chen CY, Bedi K, Margulies KB, Prosser BL. Microtubules Increase Diastolic Stiffness in Failing Human Cardiomyocytes and Myocardium. *Circulation*. 2020;141(11):902-15.
52. Helms AS, Tang VT, O'Leary TS, Friedline S, Wauchope M, Arora A, et al. Effects of MYBPC3 loss-of-function mutations preceding hypertrophic cardiomyopathy. *JCI Insight*. 2020;5(2).
53. Coats CJ, Heywood WE, Virasami A, Ashrafi N, Syrris P, Dos Remedios C, et al. Proteomic Analysis of the Myocardium in Hypertrophic Obstructive Cardiomyopathy. *Circ Genom Precis Med*. 2018;11(12):e001974.
54. Tarnopolsky MA. Myopathies Related to Glycogen Metabolism Disorders. *Neurotherapeutics*. 2018;15(4):915-27.
55. Guclu A, Knaapen P, Harms HJ, Parbhudayal RY, Michels M, Lammertsma AA, et al. Disease Stage-Dependent Changes in Cardiac Contractile Performance and Oxygen Utilization Underlie Reduced Myocardial Efficiency in Human Inherited Hypertrophic Cardiomyopathy. *Circ Cardiovasc Imaging*. 2017;10(5).
56. Timmer SA, Germans T, Brouwer WP, Lubberink M, van der Velden J, Wilde AA, et al. Carriers of the hypertrophic cardiomyopathy MYBPC3 mutation are characterized by reduced myocardial efficiency in the absence of hypertrophy and microvascular dysfunction. *Eur J Heart Fail*. 2011;13(12):1283-9.

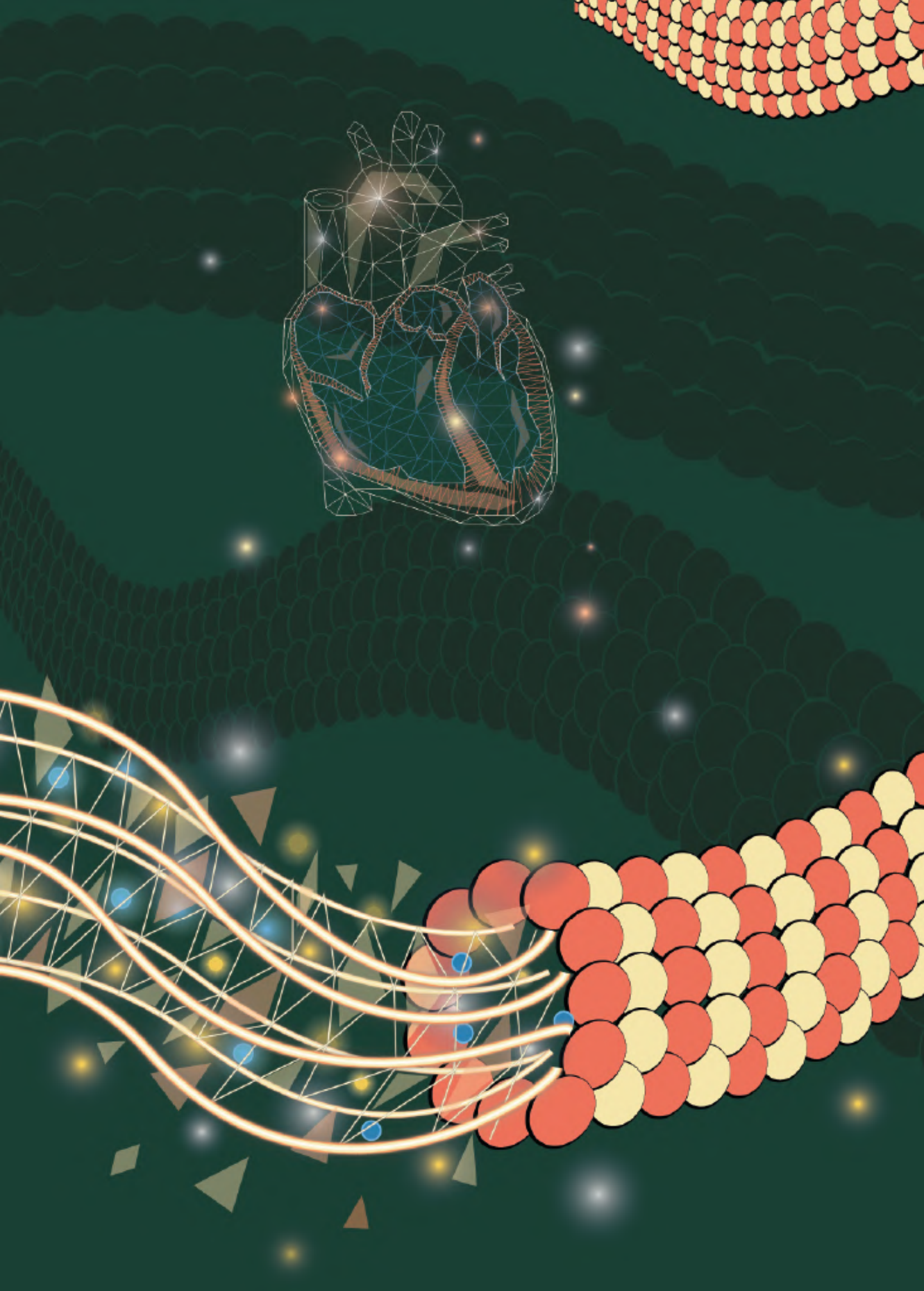

Chapter 9

Tubulin signature and desmin levels in pig and mouse models for cardiomyopathies and human heart failure samples

Larissa M. Dorsch, Oana Sorop, Aryan Vink, Michelle Michels, Cristobal G. dos Remedios, Michiel Dalinghaus, Lucie Carrier, Dirk JGM. Duncker, Diederik WD. Kuster, Jolanda van der Velden

Pilot study.

ABSTRACT

BACKGROUND

Hypertrophic (HCM) and dilated (DCM) cardiomyopathies are characterized by concentric and eccentric remodelling of the heart, respectively. HCM is associated with impaired diastolic function, while DCM patients show reduced systolic function, and both HCM and DCM can develop into end-stage heart failure (HF). The microtubular network and its post-translational modifications (tubulin signature) play a central role in cardiac structure and function. Animal models with concentric and eccentric cardiac remodelling may be used to study tubulin-mediated functional changes during disease progression. To study if animal models show changes in the tubulin signature that are observed in patients with HCM and DCM, we here defined the tubulin signature in myocardium of animal models with concentric and eccentric cardiac remodelling caused by pressure overload, myocardial infarction or a gene defect.

METHODS

We defined the levels of total, acetylated and detyrosinated α-tubulin and desmin in a pressure-overload concentric hypertrophic pig model, aged pigs with a heavy body weight and a disproportionately low stroke volume, mice carrying the HCM-associated $MYBPC3_{772G>A}$ mutation exposed to a voluntary wheel-running protocol and cardiac tissue from HCM and DCM patients, including paediatric DCM patients, ranging from NYHA class II-III to end-stage (NYHA class IV) heart failure with an idiopathic, ischemic and genetic origin.

RESULTS

The 18 months old pigs were characterized by an altered tubulin signature, including decreased levels of total, acetylated and detyrosinated α-tubulin. NYHA class II-III HCM patients had the strongest increase in tubulin signature. Within the HF cohorts, detyrosinated α-tubulin was increased in end-stage HCM and paediatric DCM patients and acetylated α-tubulin was increased in ischemic heart disease patients. Pressure overload or a genetic trigger initiating the development of hypertrophy resulted in increased desmin levels in biopsies from NYHA class II-III HCM patients, pressure-overload concentric hypertrophic pig model and homozygous $MYBPC3_{772G>A}$ mice.

CONCLUSION

Our data suggest increased desmin levels as an early event in compensated hypertrophy. Animal models only partially recapitulated the proliferated and modified tubulin signature and changes in desmin levels seen in patients. The most proliferated and modified microtubule network was observed in NYHA class II-III HCM patients indicating a target group for tubulin modifying therapies to re-write the tubulin signature.

INTRODUCTION

Cardiac disease has diverse etiologies ranging from valvular defects, hypertension, or an ischemic or genetic insult. Aortic stenosis and hypertension cause concentric remodelling of the heart which is characterized by increase of left ventricular (LV) wall thickness to a greater extent than the volume of the LV cavity, while an ischemic insult (myocardial infarction) causes eccentric remodelling in which the heart dilates and the wall becomes thin.[1] Gene defects may cause concentric or eccentric cardiac remodelling and are known as hypertrophic and dilated cardiomyopathy (HCM and DCM, respectively).

Cardiac function and structure is governed by the cytoskeleton which consists of sarcomeres and non-sarcomeric structures. The non-sarcomeric cytoskeleton is formed by microtubules and intermediate filaments. Little is known about the changes in non-sarcomeric structures during onset and progression of cardiac disease, while the microtubular network undergoes multiple post-translational modifications. Acetylation (ac) of α-tubulin at Lys40 decreases flexural rigidity of microtubules and thereby protects microtubules to mechanical bending-induced breakage and diassembly.[2,3] Previously in **chapter 7**, we reported increased levels of acetylated α-tubulin in septal myectomy samples of HCM patients, especially when a sarcomere gene mutation was present.[4] In samples with truncation or missense *MYBPC3* mutations causing haploinsufficieny of cMyBP-C we observed the biggest increase in α-tubulin and acetylation of α-tubulin.[4]

The Prosser's group reported proliferation of microtubules and intermediate filaments, and the posttranslational detyrosination of microtubules in hearts from transplant recipients.[5-7] Detyrosination (detyr) is the removal of tyrosine from the C-terminus of α-tubulin and significantly affects stability and density of the cardiomyocyte cytoskeleton and cell biomechanics.[8] The microtubule changes were causally linked to increased stiffness and viscoelasticity that reduce contractility and slow both contraction and relaxation.[5-7,9] Our group observed in **chapter 6** increased levels of detyrosinated α-tubulin at the time of septal myectomy of HCM patients.[10] In addition, increased levels of detyrosinated α-tubulin were found in a $MYBPC3_{2373insG}$ mouse model and its inhibition normalized contraction and relaxation kinetics of isolated cardiomyocytes.[10]

It has been shown before that intermediate filaments cross-link with microtubules in a detyrosination-dependent manner.[11,12] Recently, desmin, which forms structural bundles along the Z-disc,[13] was identified as a sarcomeric microtubule anchor.[7] Studies with desmin knock-out mice revealed that desmin cross-links with detyrosinated α-tubulin to structurally reinforce the microtubule network.[7] In addition, removal of desmin decreased cytoskeletal stiffness, disorganized the microtubule network and pharmacological inhibition of detyrosination did no longer modulate viscoelasticity.[7] In line with the increase in detyrosinated α-tubulin, increased desmin levels have been reported in heart failure (HF) patients and at the time of septal myectomy of HCM patients (**chapter 6**).[6,10]

We studied the microtubule network in cardiac tissue from HCM and DCM patients with different disease stages ranging from NYHA class II-III to end-stage HF (NYHA class

IV) with an idiopathic, ischemic and genetic origin. To define changes in microtubules and it post-translational modifications in cardiac remodelling at early disease development, we here studied the mircotubule network in different pig and mouse models. We compared sham-operated pigs to aortic banding (AoB)-treated pigs of the same age. AoB has been used to model pressure-overload concentric hypertrophy.[14-17] In addition, sham-operated, 4 months old pigs were compared to 18 months old pigs. These aged pigs had a heavy body weight (BW) and a disproportionately low stroke volume due to diastolic perturbations.[18] In a further data set, we used exercised wild-type (WT) mice and mice carrying *MYBPC3* point mutation on one or both alleles, which is associated with human HCM.

METHODS

HUMAN CARDIAC SAMPLES

Cardiac samples were collected from adult patients with obstructive HCM ($HCM_{St\ II}$; n=38; 26 males, 12 females; mean age 48±16 years), end-stage HCM ($HCM_{St\ IV}$; n=7; 3 males, 4 females; mean age 44±13 years), ischemic heart disease (ISHD; n=7; 6 males, 1 female; mean age 56±6 years), idiopathic DCM (IDCM; n=7; 4 males, 1 females; mean age 51±4 years), end-stage DCM with identified DCM-causing mutation (DCM_{end}; n=7; 5 males, 2 females; mean age 56±8 years) and 7 paediatric patients with DCM (DCM_{ped}; 2 males, 3 females; mean age 10±3 years). Samples from 8 healthy non-failing donors (5 males, 3 females; mean age 47±11 years) served as controls. Parameters of all HCM and DCM individuals and donors are summarized in Table 9.1. All samples were obtained after written informed consent from each patient prior to surgery and from the patients' or donors' next of kin.

Table 9.1: Characteristics of HCM, DCM and non-failing individuals.

Nr.	Group	Remark	Affected Genes	Sex (F/M)	Age	FS(%)	LVEF	LVEDD	LVESD
8	Ctrl	-	-	3 F, 5 M	47±11	-	-	-	-
38	$HCM_{St\ II}$	-	19 *MYBPC3*, 10 *MYH7*, 2 *MYL2*, 4 *TNNI3*, 3 *TNNT2*	12 F, 26 M	48±16	48±11 (n=15)	81±15 (n=2)	43±5 (n=31)	22±5 (n=15)
7	$HCM_{St\ IV}$	-	1 *MYBPC3*, 5 *MYH7*, 1 *TNNT2*	4 F, 3 M	44±13	-	-	57±9 (n=6)	-
7	ISHD	-	-	1 F, 6 M	56±6 (n=6)	-	24±6 (n=6)	72 (n=1)	66 (n=1)
7	IDCM	-	-	1 F, 4 M (n=5)	51±4 (n=5)	-	18±6 (n=3)	79±6 (n=2)	67±11 (n=2)

Table 9.1: Continued

Nr.	Group	Remark	Affected Genes	Sex (F/M)	Age	FS(%)	LVEF	LVEDD	LVESD
7	DCM_{end}	5 DCM, 2 DCM/ ACM	1 *DSP*, 1 *LMNA* & *TTN*, 2 *PLN*, 1 *TNNT2*, 2 *TTN*	2 F, 5 M	56±8	-	-	-	-
Nr.	**Group**	**Remark**	**Affected Genes**	**Sex (F/M)**	**Age**	**FS(%)**	**LVEF**	**LVEDD Z-score#**	**LVESD Z-score#**
7	DCM_{ped}	6 DCM, 1 RCM	1 *DES*, 1 *MYH7*, 1 *NKX2.5*, 1 *TPM1*	3 F, 2 M (n=5)	10±3 (n=5)	13±7 (n=6)	26±14 (n=6)	6±4 (n=6)	9±3 (n=6)

Nr.: Number; F: female; M: male; Age: age at septal myectomy/heart transplantation; FS: fractional shortening; LVEF: left ventricular ejection fraction; LVEDD: left ventricular end-diastolic dimension; LVESD: left ventricular end-systolic dimension; Ctrl: healthy donor hearts; $HCM_{St\ II}$: early HCM; $HCM_{St\ IV}$: end-stage HCM; ISHD: ischemic heart disease; IDCM: idiopathic DCM; DCM_{end}: adult end-stage DCM; DCM_{ped}: paediatric DCM; ACM: arrhythmogenic cardiomyopathy; #: LVEDD and LVESD expressed as Z-score for body surface are in paediatric samples.

Interventricular septum tissue of HCM patients was collected during myectomy surgery to relieve (LV) outflow tract obstruction. Cardiac tissue from end-stage HCM patients was obtained during heart transplantation surgery. HCM samples were approved by the local ethics board of the Erasmus Medical Center Rotterdam, the Netherlands (protocol number MEC-2010-40). LV tissue from ISHD and IDCM samples were acquired during transplantation from the University of Sydney, Australia, with the ethical approval of the Human Research Ethics Committee #2012/2814. Genetic DCM samples were acquired during transplantation from the Biobank of the University Medical Center Utrecht, the Netherlands and approved by the Biobank Research Ethics Committee, Utrecht, the Netherlands (protocol number WARB 12/387). Paediatric DCM samples were approved by the local ethics board of the Erasmus Medical Center Rotterdam, the Netherlands (protocol number MEC-2015-233). Five of these samples were obtained during transplantation and two samples were post-mortem.

Donor samples were obtained from the Sydney Heart Bank, Australia with the ethical approval of the Human Research Ethics Committee (HREC Univ Sydney 2012/030). Mostly because of poor tissue matching against patients in the heart failure clinic of St Vincent's Hospital, these hearts were not used for heart transplantation. Their validity as "controls" was based on their extensive use as such in publications from a wide range of other laboratories. We therefore assumed that these donors are representative of the diverse human population.

We acknowledge the uneven distribution between patient numbers and mutations and tissue locations (IVS and LV). However, our tissue characterization was dependent on available cardiac tissue and clinical parameters. Due to limited tissue availability, not all analyses could be performed in all patient/control samples.

PIGS: STUDY POPULATION

All studies were performed in accordance with the Council of Europe Convention (ETS123) and the Directive (2010/63/EU) for the protection of vertebrate animals used for experimental and other scientific purposes, and with approval of the Animal Care Committee of Erasmus University Medical Center Rotterdam, the Netherlands. Experiments were performed in Yorkshire x Landrace pigs and we included 3 study conditions (n=6): aortic banding (AoB)-treated and sham-operated pigs for 3 weeks of either sex and 4 months old when sacrificed weighing 18-29kg and 18 months old sows with a heavy BW (170–216kg). One week prior to surgery, pigs arrived for acclimatization at the central animal housing facility of Erasmus University Medical Center in Rotterdam, the Netherlands. Twice a day, pigs were fed compound feed in accordance with their BW and had free access to drinking water. Starting twelve hours before surgery, pigs were denied access to food.

SURGICAL INSTRUMENTATION AND MEASUREMENTS OF 18 MONTHS OLD PIGS

The surgical instrumentation and measurements have been described previously.[19,20] Briefly as outlined in,[18] pigs were sedated with a cocktail of Tiletamine/Zolazepam (5mg · kg-1), Xylazine (2.25mg · kg-1) and atropine (0.03mg · kg-1 i.m.), anaesthetized with sodium pentobarbital (6mg · kg-1 i.v.) and intubated for ventilation with O_2 and N_2 (1:3 v/v). A catheter was inserted into the right jugular vein and advanced into the superior vena cava for infusion of sodium pentobarbital (10-12mg/kg · h-1 i.v.) to maintain anaesthesia. A fluid-filled catheter was inserted into the right carotid artery for the measurement of mean arterial pressure.

A Swan-Ganz catheter (5 corodyn TD F7, Braun, Melsungen, Germany) was inserted into the left jugular vein, via a sheath introducer, and advanced into the pulmonary artery for the measurement of mean pulmonary artery pressure and pulmonary capillary wedge pressure, and for thermodilution-based measurement of CO (Abbott Laboratories, North Chicago, IL, USA). A 7F conductance catheter (CD Leycom, Hengelo, The Netherlands) was inserted into the left carotid artery, via a sheath introducer, and advanced into the left ventricle (LV) for measurement of LV volume. The conductance catheter was calibrated using the thermodilution CO measurements and hypertonic saline before LV volume measurements were obtained. Subsequently, the conductance catheter was replaced by a micro-manometer-tipped catheter (SPC-370s, Millar Instruments, Houston, TX, USA) for measurement of LV pressure (LVP) and its first derivative (LVdP/dt). LVdP/dt at a pressure of 40 mmHg (LVdP/dtP=40) was used as an afterload-independent index of systolic cardiac function. Heparin (10,000 I.U., i.v.) was administered before arterial blood gasses and haemodynamics were measured.

Subsequently, the chest was opened via sternotomy and the pericardial space was opened. After stabilization, ultrasound echocardiography recordings were made by placing the ultrasound probe directly onto the epicardium and obtaining short-axis recordings (Aloka SSD 4000; Aloka Company, Tokyo, Japan).

Just before sacrifice left ventricular biopsies were obtained, snap frozen and stored in liquid nitrogen until further analysis. Finally, animals were sacrificed, heart was excised and weighed. After removal of the large vessels, total heart weight (HW) was determined. Then, the atria and right ventricle were dissected and left ventricular weight (LVW) was determined.

AORTIC BANDING TREATMENT AND SHAM-OPERATION IN 4 MONTHS OLD PIGS
As previously described in Duncker's group, Swine were sedated with ketamine (20 mg/kg, i.m.) and midazolam (1 mg/kg, i.m.). Under isoflurane anaesthesia, a left thoracotomy was performed and the proximal ascending aorta was dissected free, and, in AoB-animals a band was placed, resulting in a systolic pressure gradient of 68±3 mmHg. Subsequently, the chest was closed and the animals were allowed to recover.

Three weeks later, swine were re-anaesthetised with sodium pentobarbital (15 mg/kg, i.v.), intubated, and placed on a positive-pressure ventilator (O_2:N_2=1:3 v/v). Catheters were inserted into the right external jugular vein for infusion of physiological saline and sodium pentobarbital (10-15 mg/kg/h) to maintain anaesthesia. Following sternotomy, fluid-filled catheters were surgically inserted into the aorta for measurement of aortic blood pressure. Subsequently, arterial and coronary venous blood samples were simultaneously obtained, Following arresting and excision of the heart, myocardial tissue samples from the left ventricular anterior wall were harvested.

MICE: EXERCISE PROTOCOL AND ECHOCARDIOGRAPHY

Experiments were performed in accordance with the Guide for the Animal Care and Use Committee of the VU University Medical Center (VUmc) and with approval of the Animal Care Committee of the VUmc (DEC-number FYS12-03) Amsterdam, the Netherlands. In total, 37 5-week-old mice were included in the study. Exercise wild-type (WT_{EX}; n=10) and heterozygous (HET_{EX}; n=9) and homozygous (HOM_{EX}; n=10) *MYBPC3*-targeted KI mice with a G>A transition on the last nucleotide of exon 6 (c.772G>A), in Black Swiss genetic background of either sex were exposed to an 8-week voluntary wheel-running protocol, and the running distances were monitored in individual animals.[21]

Wild-type sedentary mice (WTsed; n=7) and exercised mice (after the 8-week exercise protocol) of ~13 weeks of age were sedated with 4% isoflurane and ventilated with 0.25 l/min O_2 and 0.45 l/min air. To maintain the anaesthetized condition, mice were ventilated with ~2% isoflurane and identical O_2 and air flow rates. Subsequently, 2D-echocardiographic recording (Siemens Acuson Sequoia, Siemens Healthineers, Erlangen, GER) was performed on the LV short axis at mid-papillary level. LV end-diastolic as well as end-systolic lumen was determined from the M-mode images. Fractional shortening (FS) was calculated from the short axis M-mode images as 100% x (LV end-diastolic lumen-LV

end-systolic lumen)/LV end-diastolic lumen. After the echocardiogram, the LV (including the interventricular septum) and right ventricle (RV) were weighed and subsequently stored in liquid nitrogen (N_2). Due to limited tissue availability, not all analyses could be performed in all mice samples.

TISSUE HOMOGENIZATION

Pulverized frozen tissue was homogenized in 40 µL/mg tissue 1× reducing sample buffer (106 mM Tris-HCl, 141 mM Tris-base, 2% (w/v) lithium dodecyl sulfate, 10% (v/v) glycerol, 0.51 mM ethylenediaminetetraacetic acid, 0.22 mM SERVA Blue G250, 0.18 mM Phenol Red, and 100 mM dithiothreitol) using a glass tissue grinder. Proteins were denatured by heating to 99°C for 5 min, after which debris was removed by centrifugation at maximum speed for 10 min in a microcentrifuge (Sigma, 1-15K).

ELECTROPHORESIS AND WESTERN BLOTS

Equal amounts of protein (10 µg (pigs and human samples) and 5 µg (mice samples)) were separated on pre-cast SDS-PAGE 4–12% criterion gels (Bio-Rad, Hercules, CA, USA) and transferred onto PVDF membranes (GE Healthcare, Chicago, IL, USA). The membranes were blocked in 5% (w/v) skim milk/1× TBST (20 mM Tris, 150 mM NaCl, 0.1% (v/v) Tween-20) for 1 h at room temperature and incubated overnight at 4°C with the following primary antibodies in 3% (w/v) BSA/1× TBST: mouse anti-acetylated α-tubulin (T7451, Sigma-Aldrich, Saint Louis, MO, USA), rabbit anti-desmin (#5332, Cell Signaling Technology, Danvers, MA, USA), rabbit anti-detyrosinated α-tubulin (ab48389, Abcam, Cambridge, UK), mouse anti-GAPDH (10R-G109b, Fitzgerald Industries International, Acton, MA, USA), rabbit anti-GAPDH (#2118, Cell Signaling), mouse anti-MYBPC3 (sc-137180, Santa Cruz, Dallas, TX, USA), and mouse anti-α-tubulin (T9026, Sigma-Aldrich). Membranes were incubated for 1 h at room temperature with horseradish peroxidase-conjugated secondary antibody (DakoCytomation, Santa Clara, CA, USA), raised in goat, in 3% (w/v) BSA/1x TBST. Western blots were developed with Amersham ECL prime Western blotting detection reagent and images were acquired using Amersham Imager 600 and quantified by densitometry by ImageQuant TL software (all GE Healthcare). To correct for loading differences, protein amounts were expressed relative to GAPDH.

STATISTICAL ANALYSES

Data were analysed with SPSS Statistics version 26.0 for Windows (IBM Corporation, Armonk, NY, USA) and GraphPad Prism version 8.2.1 (GraphPad Software Inc., San Diego, CA, USA). Results are expressed as means ± standard errors of the mean (SEM) in graphs and as means ± standard deviation in text. After data collection, the distribution of each data set was determined by Q-Q plots and then double checked by Kolmogorov-Smirnov and Shapiro Wilk tests. Normally distributed data were analysed with unpaired t-test (comparing 2 groups) and ordinary one-way ANOVA (comparing $>$ 2 groups) with Tukey's multiple comparisons post-hoc test (comparing $\leq$ 3 groups). To analyse non-parametric data, the Mann-Whitney U test (comparing 2 groups) and the Kruskal-Wallis test with

Dunn's multiple comparisons post-hoc test (comparing > 2 groups) were used. A two-sided $p<0.05$ was considered statistically significant.

RESULTS

DEFINING THE TUBULIN SIGNATURE IN EARLY HCM AND END-STAGE HCM AND DCM

We defined the tubulin signature and desmin levels in cardiac tissue from HCM and DCM patients with different disease stages ranging from NYHA class II-III to end-stage HF (NYHA class IV) with an idiopathic, ischemic and genetic origin (Figure 9.1). We observed highly increased levels of α-tubulin, acetylated α-tubulin and desmin in $HCM_{St\ II}$ compared to Ctrl and $HCM_{St\ IV}$ (Figures 9.1B-C,E). Expression of detyrosinated α-tubulin was increased in both $HCM_{St\ II}$ and $HCM_{St\ IV}$ compared to Ctrl (Figure 9.1D). Normalization to α-tubulin revealed a trend to increased levels of acetylated α-tubulin in $HCM_{St\ II}$ compared to control and detyrosinated α-tubulin was increased in $HCM_{St\ IV}$ compared to Ctrl and $HCM_{St\ II}$ (Figures 9.1F-G).

When comparing different end-stage eccentric HF samples, we observed no changes in levels of α-tubulin, desmin and acetylated α-tubulin normalized to α-tubulin (Figures 9.1H,K-L). Compared to control, acetylated α-tubulin was increased in ISHD patients and detyrosinated α-tubulin (normalized to α-tubulin) in DCM_{ped} (Figures 9.1I,J,M).

Figure 9.1: Microtubule remodelling and increased desmin levels are most prominent in early HCM. (**A**) Representative blot images with uncropped membranes in Figure S1. In (**B**-**G**), early ($HCM_{St\ II}$) and end-stage ($HCM_{St\ IV}$) HCM samples were compared to controls (Ctrl) and in (**H**-**M**), end-stage DCM samples including ISHD, IDCM, adult (DCM_{end}) and paediatric (DCM_{ped}) were compared to Ctrl. Quantified levels of (**B, H**) α-tubulin, (**C, I**) acetylated α-tubulin, (**D, J**) detyrosinated α-tubulin, (**E, K**) desmin, (**F, L**) acetylated α-tubulin normalized α-tubulin and (**G, M**) detyrosinated α-tubulin . The average value of the Ctrl are indicated by the dotted line in the respective scatter plots. HCM samples = filled squares, $HCM_{St\ II}$ = brighter red bar, $HCM_{St\ IV}$ = darker red bar, DCM samples = filled triangles, ISHD = brown bar, IDCM = purple bar, DCM_{end} = darker blue bar, DCM_{ped} = brighter blue bar. Each dot in the scatter plots represents an individual sample. $^{*}p<0.05$ $^{**}p<0.01$ and $^{***}p<0.001$ versus Ctrl, $^{\#\#}p<0.01$ and $^{\#\#\#}p<0.001$ versus $HCM_{St\ IV}$. Measurements are mean ± SEM.

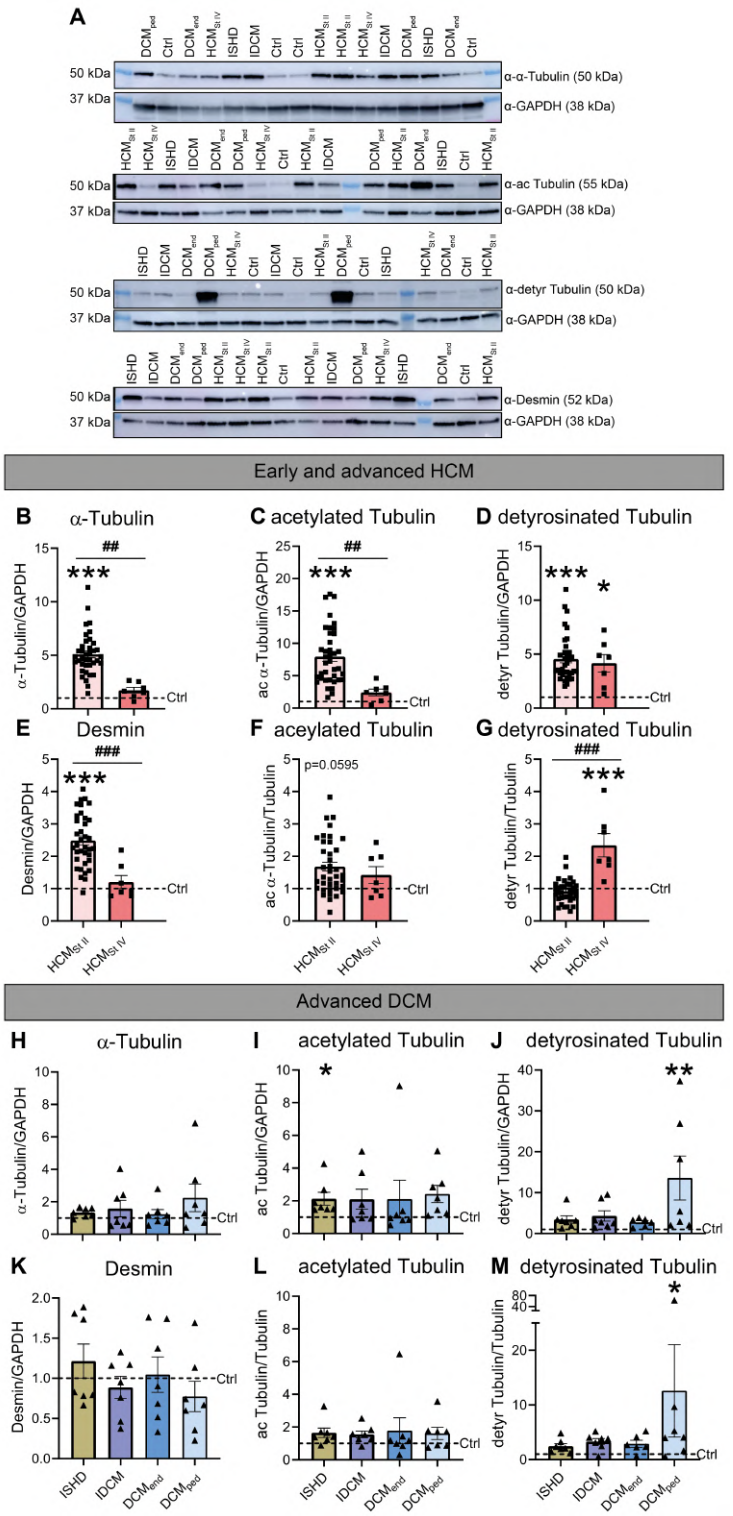
A
50 kDa
37 kDa
α-α-Tubulin (50 kDa)
α-GAPDH (38 kDa)
α-ac Tubulin (55 kDa)
α-detyr Tubulin (50 kDa)
α-Desmin (52 kDa)
Early and advanced HCM
B α-Tubulin
C acetylated Tubulin
D detyrosinated Tubulin
E Desmin
F aceylated Tubulin
G detyrosinated Tubulin
α-Tubulin/GAPDH
ac α-Tubulin/GAPDH
detyr Tubulin/GAPDH
Desmin/GAPDH
ac α-Tubulin/Tubulin
detyr Tubulin/Tubulin
p=0.0595
Ctrl
Advanced DCM
H α-Tubulin
I acetylated Tubulin
J detyrosinated Tubulin
K Desmin
L acetylated Tubulin
M detyrosinated Tubulin
ac Tubulin/GAPDH
ac Tubulin/Tubulin
ISHD
IDCM
DCMend
DCMped

DEFINING THE TUBULIN SIGNATURE IN AGED AND AORTIC BANDING TREATED PIGS

We compared sham-operated, 4 months old pigs to untreated, 18 months old pigs. Due to the age difference, the BW of both groups was different, therefore we used the formula LV weight = 0.6 x BW^0.78 to scale the LV weight to BW.[22,23] The 4 months old pigs showed a 22% reduced (p=0.0003) LV weight to BW ratio compared to expected value of 1.0. (Figure 9.2A).

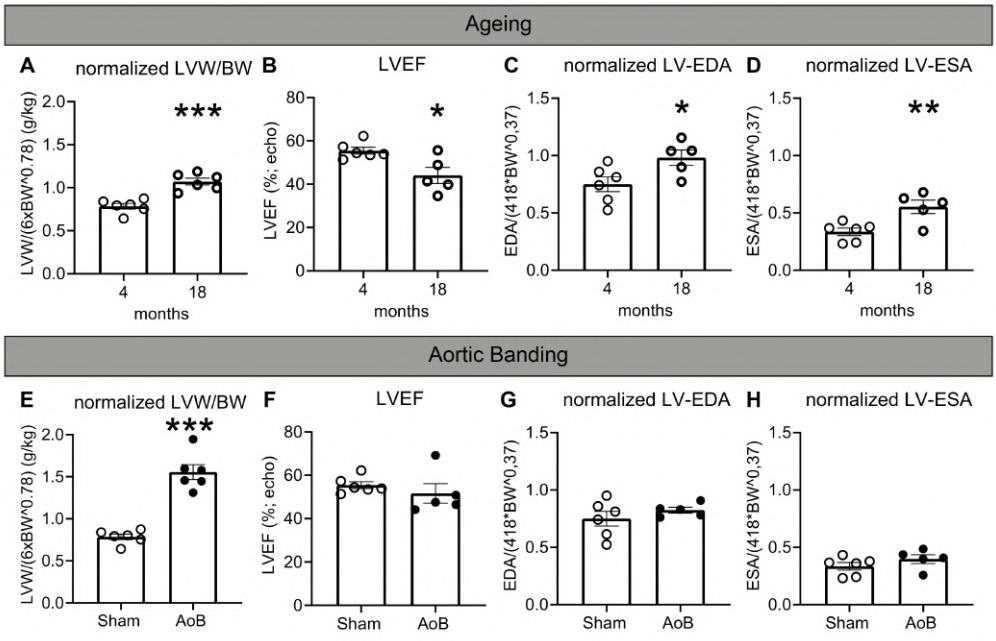

Figure 9.2: Cardiac characteristics in (A-D) 4 months (n=6) or 18 months old pigs (n=5 (A) or 6 (B-D)) and (E-H) sham-operated (same as 4 months old pigs in upper panel) or AoB-treated pigs (n=6). (**A, E**) Normalized left ventricular weight/body weight (LVW/BW) ratios. (**B, F**) Echo LV ejection fractions (LVEF). (**C, G**) Normalized LV end-diastolic lumen area (LV-EDA) and (**D, H**) normalized LV end-systolic lumen area (LV-ESA). Normalization was performed to take into account that cardiac geometry and function fail to scale proportionally with increasing BW.[18,22-23] 4 months, sham-operated = open circles, 18 months = bold open circles, AoB-treated = filled circles. Each dot in the scatter plots represents an individual sample. *p<0.05, **p<0.01 and ***p<0.001 versus 4 months, sham-operated pigs. Measurements are mean ± SEM.

This was accompanied by a 21% lower (p=0.01) LV ejection fraction (LVEF) in the aged pigs (Figure 9.2B). Since LV end-diastolic and end-systolic lumen area (LV-EDA and LV-ESA) fail to scale proportinally with increasing BW, we normalized EDA and ESA according to the formula EDV = 41 x BW^0.37 (Figures 9.2C-D).[18,24] Aged pigs were characterized by a 31% increase (p=0.03) in LV-EDA and a 65% increase (p=0.008) in LV-ESA.

We compared the same control cohort to AoB-treated animals. After three weeks of intervention, normalized LV weight to BW ratio was double ($p<0.001$) in AoB-treated pigs compared to sham-treated pigs (Figure 9.2E). In contrast to the difference in cardiac geometry, cardiac function, including LVEF, normalized LV-EDA and normalized LV-ESA, was comparable between AoB-treated and sham-operated pigs (Figures 9.2F-H).

As a next step, we studied the microtubule network and the respective post-translational modifications of LV biopsies in the ageing and aortic banding pig models (Figure 9.3). Compared to 4 months old pigs, we observed reduced levels of α-tubulin (46%; $p=0.04$), acetylated α-tubulin (51%, $p=0.005$) and detyrosinated α-tubulin (68%, $p=0.01$) in 18 months old pigs (Figures 9.3B-D). Levels of desmin and acetylated α-tubulin when normalized to α-tubulin were not different between both age groups (Figures 9.3E-F). In 18 months old pigs, levels of detyrosinated α-tubulin were 50% reduced ($p=0.02$) when normalized to α-tubulin (Figure 9.3G).

Levels of total, acetylated and detyrosinated α-tubulin were not different between AoB-treated and sham-operated pigs (Figures 9.3H-J). In AoB-treated pigs, levels of desmin were 83% increased ($p=0.04$) (Figure 9.3K).

NO DIFFERENT TUBULIN SIGNATURE IN EXERCISED MICE CARRYING A *MYBPC3* point mutation

In a further data set, we used exercised wild-type (WT_{EX}) mice and mice carrying $MYBPC3_{772G>A}$ point mutation on one (HET_{EX}) or both (HOM_{EX}) alleles. We observed no differences in cardiac characteristics, including LVW to tibia length ratio, fractional shortening, LV end-diastolic diameter (LV-EDD) and LV end-systolic diameter (LV-ESD) between sedentary (WT_{sed}) and WT_{EX} mice (Figure 9.4).

HOM_{EX} mice were characterized by an 88% increase ($p<0.0001$) in LVW to tibia length, a 49% decrease ($p=0.01$) in fractional shortening, a 22% increase ($p<0.0001$) in LV-EDD and a 26% increase ($p=0.007$) compared to WT_{sed} mice and the two other exercise mice groups.

When studying the effect on tubulin signature, we observed no changes in levels of total, acetylated and detyrosinated α-tubulin among sedentary WT_{sed}, WT_{EX} and mutant exercised mice (Figure 9.5). We observed a 168% increase ($p=0.005$) of desmin in HOM_{EX} mice compared to WT_{sed} mice (Figure 9.5E). Homozygous *MYBPC3* mice had 90% reduced levels ($p=0.002$) of cMyBP-C compared to WT_{sed} (Figure 9.5F). Also compared to the other exercise mice, the cMyBP-C were significantly reduced in HOM_{EX} mice.

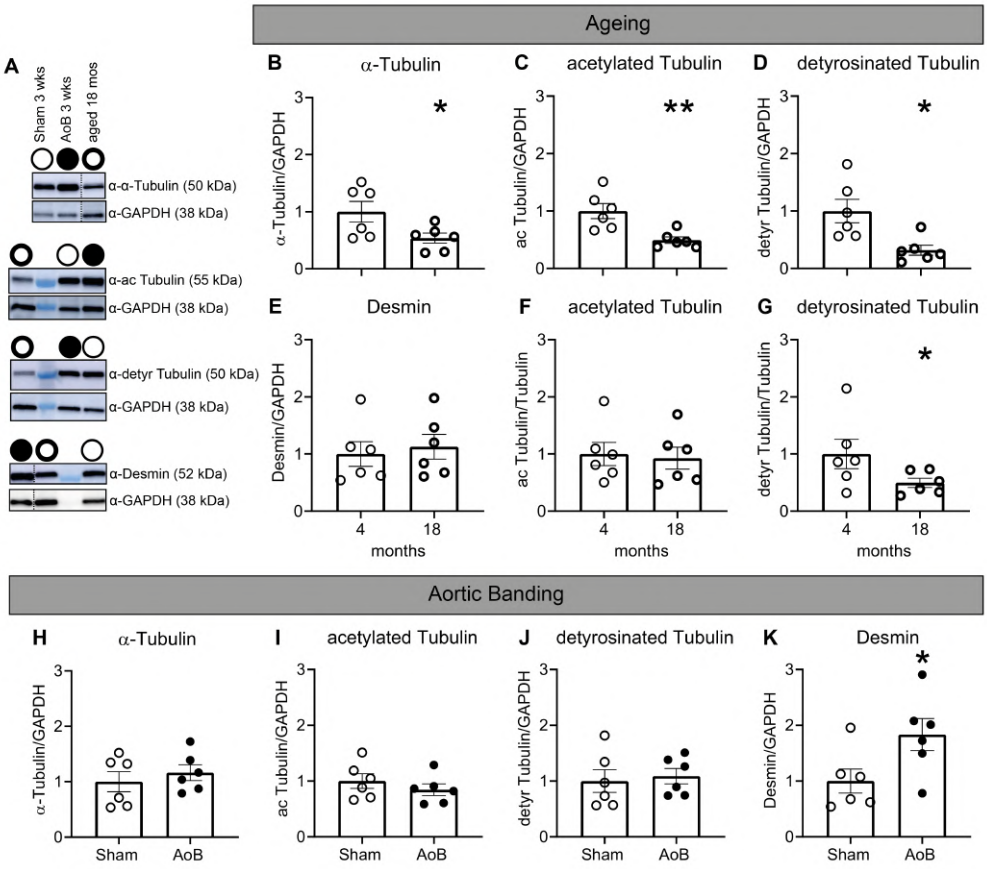

Figure 9.3: Reduced levels of microtubules and posttranslational modifications in aged pigs; increased desmin levels after AoB intervention. (**A**) Representative blot images; dashed lines indicate lanes which were run on the same membrane but were non-contiguous. Uncropped membranes are presented in Figure S2. In (**B-G**), 4 months old pigs were compared to 18 months old pigs and in (**H-K**), this 4 months, sham-operated pigs were compared to AoB-treated pigs (n=6 per group). Quantified levels of (**B, H**) α-tubulin, (**C, I**) acetylated α-tubulin, (**D, J**) detyrosinated α-tubulin, (**E, K**) desmin. Due to significant differences in α-tubulin levels, (**F**) acetylated α-tubulin and (**G**) detyrosinated α-tubulin were normalized to α-tubulin . 4 months, sham-operated = open circles, 18 months = bold open circles, AoB-treated = filled circles. Each dot in the scatter plots represents an individual sample. *$p<0.05$ and **$p<0.01$ versus 4 months, sham-operated pigs. Measurements are mean ± SEM.

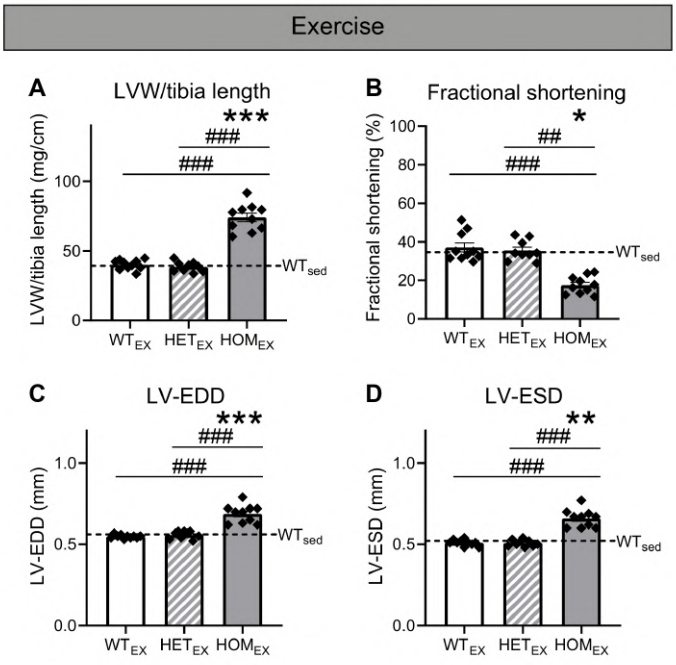

Figure 9.4: Cardiac characteristics in 13 weeks old *MYBPC3*$_{772G>A}$ mice.
(**A**) Normalized left ventricular weight (LVW)/tibia length ratios, (**B**) fractional Shortening, (**C**) LV end-diastolic diameter (LV-EDD) and (**D**) LV end-systolic diameter in sedentary wild-type (WT_{sed}, n=7), exercise wild-type (WT_{EX}, n=10), exercise heterozygous (HET_{EX}, n=9) and exercise homozygous (HOM_{EX}, n=10) mice. The average value of the WT_{sed} mice are indicated by the dotted line in the respective scatter plots. WT_{EX} = white bar, HET_{EX} = bar with diagonal lines, HOM_{EX} = grey bar, exercise mice = filled rhomboids. Each dot in the scatter plots represents an individual sample. *p<0.05, **p<0.01 and ***p<0.001 versus WT_{sed}, $^{\#\#}p$<0.01 and $^{\#\#\#}p$<0.001 versus HOM_{EX} mice. Measurements are mean ± SEM.

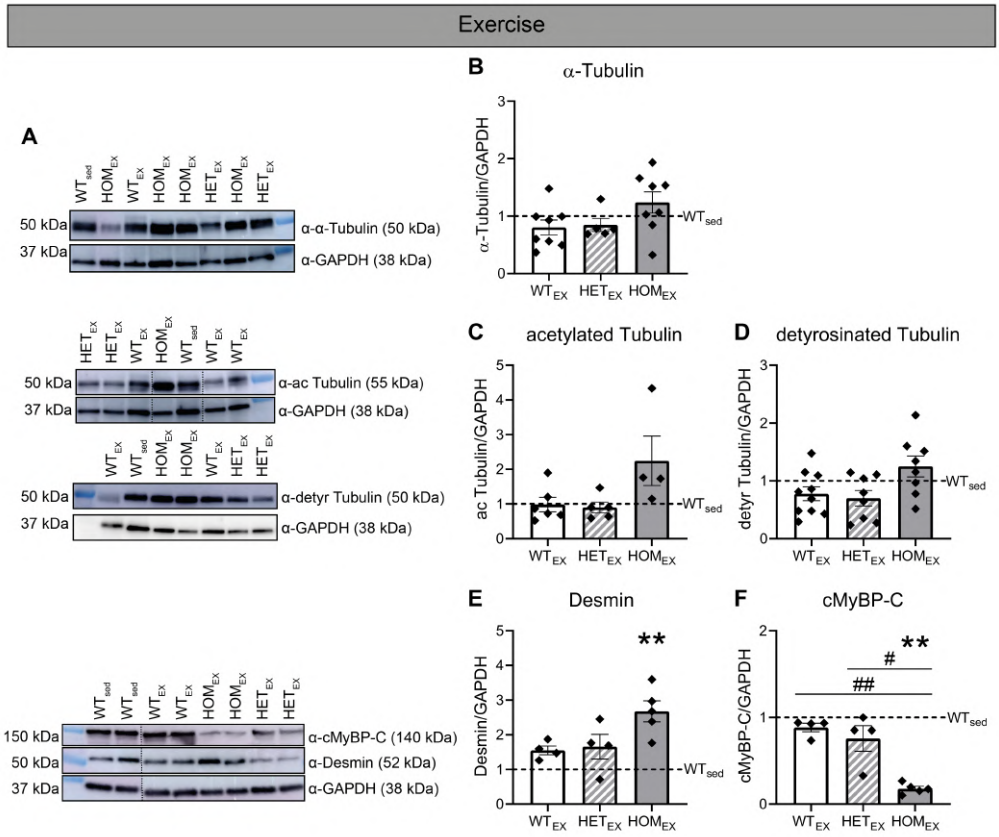

Figure 9.5: Increased levels of desmin and reduced levels of cardiac myosin binding protein C (cMyBP-C) in exercise mice which are homozygous for *MYBPC3* point mutation. (**A**) Representative blot images; dashed lines indicate lanes which were run on the same membrane but were noncontiguous. Uncropped membranes are presented in Figure S3. In (**B**-**F**), sedentary wild-type (WT_{sed}), exercise wild-type (WT_{EX}), exercise heterozygous (HET_{EX}) and exercise homozygous (HOM_{EX}) mice were used to determine levels of (**B**) α-tubulin, (**C**) acetylated α-tubulin, (**D**) detyrosinated α-tubulin, (**E**) desmin and (**F**) cMyBP-C. The average value of the WT_{sed} mice are indicated by the dotted line in the respective scatter plots. WT_{EX} = white bar, HET_{EX} = bar with diagonal lines, HOM_{EX} = grey bar, exercise mice = filled rhomboids. Each dot in the scatter plots represents an individual sample. $^{**}p<0.01$ versus WT_{sed}, $^{\#}p<0.05$ and $^{\#\#}p<0.01$ versus HOM_{EX} mice. Measurements are mean ± SEM.

DISCUSSION

In this study, we determined the tubulin signature and desmin expression in cardiac tissue from various pig and mouse models as well as HCM and DCM patients with different disease stages ranging from NYHA class II-III to end-stage HF (NYHA class IV) with an idiopathic, ischemic and genetic origin. Figure 9.6 visualizes and summarizes our findings of the different models and patient samples indicating the most proliferated and modified tubulin signature and desmin expression in early HCM patients compared to the respective controls.

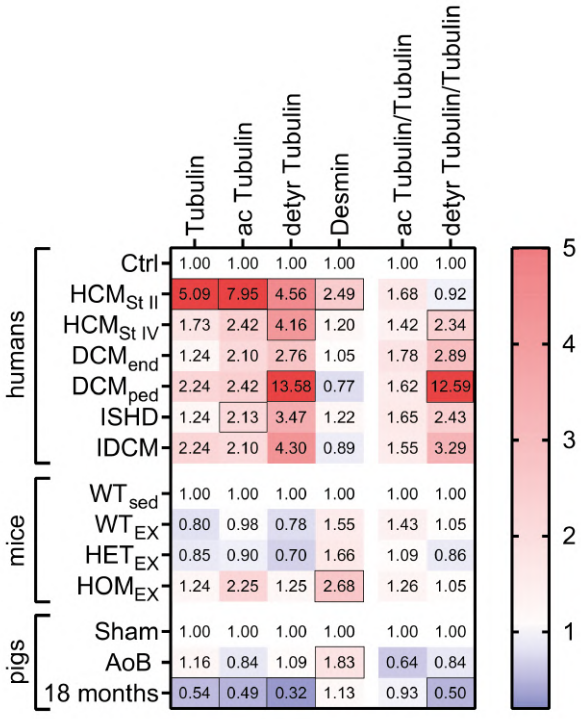

Figure 9.6: Heat map displaying the mean values of the Western blot analyses for the human (Figure 9.1), pig (Figure 9.3) and mouse samples (Figure 9.5). Blue colour indicates lower protein expression and red indicates higher protein expression compared to the respective control. Mean values above 5 are presented in dark red. Fields containing a statistically significant value are surrounded by boxes.

TUBULIN SIGNATURE IN EARLY HCM AND END-STAGE HCM AND DCM

We observed the strongest increase in tubulin signature in $HCM_{St\ II}$ patients. Interestingly, in end-stage HCM the levels of the tubulin signature were similar to control, except for detyrosinated α-tubulin which was strongly increased when normalized to α-tubulin. When comparing different end-stage eccentric HF samples, we mostly observed no changes

in tubulin signature. Compared to control, acetylated α-tubulin was increased in ISHD patients and detyrosinated α-tubulin in DCM_{ped}.

Whilst detyrosinated α-tubulin has been reported as a cardiomyocyte motion modifier,[5,7] the effect (compensation or consequence) of changes in acetylation of α-tubulin has not been studied. Available information suggests that acetylated α-tubulin compartmentalizes on stable microtubules and promotes autophagy due to increased assembly of autophagic cargo along microtubules.[25-26] Interestingly, stable, long-lived microtubules provide a substrate for luminal acetylation, but acetylation itself has been proposed to mechanically stabilize microtubules thereby prolonging the lifetime of microtubules and protecting them from mechanical ageing.[2] Moreover, an increase of tubulin acetylation has also been described in response to oxidative stress, for example inhibition of histone deacetylates has been suggested to protect the myocardium against oxidative stress induced injury.[27] Further research is needed to understand whether the observed increase in acetylated α-tubulin in $HCM_{St\ II}$ and ISHD samples is sufficient to promote autophagy and to buffer oxidative stress. In addition, it may also be interesting to investigate the functional effect of tubulin acetylation.

Partially in contrast to our findings, microtubule network was found to be highly proliferated and detyrosinated in failing myocytes of human LV explanted tissues collected from a myocardial rich, minimally fibrotic region of the mid LV wall.[6-7] Information whether the HCM and DCM patients had a genetic origin was not further investigated in both studies. The characteristics of the respective patient groups and tubulin modifications are listed in Table 9.2.

Table 9.2: Patient group characteristics and tubulin modifications.

	End-stage HCM	ISHD	End-stage DCM	Post-Vad DCM	Compensated hypertrophy
Study[6]					
Age ± SD [years]	49.9 ± 3.6	59.3 ± 1.5	55.5 ± 2.0	-	53.8 ± 1.5
LVEF ± SD [%]	42.9 ± 2.4	17.8 ± 2.2	14.1 ± 1.0	-	57.4 ± 1.8
Tubulin	↑↑	↑	↑↑↑	-	=
Detyrosination		↑↑↑		-	=
Study[7]					
Age ± SD [years]	50.9 ± 3.0	58.9 ± 1.6	57.8 ± 2.0	47 ± 4.9	50.8 ± 2.6
LVEF ± SD [%]	42.0 ± 4.3	13.3 ± 1.1	13.2 ± 0.8	31.1 ± 2.8	57.2 ± 2.7
Tubulin	↑↑↑	↑	↑↑↑	↑	=
Detyrosination	↑↑↑	↑	↑↑↑	↑	=

Post-Vad DCM: DCM following ventricular assist device support; SD: deviation; LVEF: left ventricular ejection fraction; ↑: increase, -: not measured; =: unchanged.

Natural co-founders such as differences in age ranges, sex, genotype and selection of cardiac regions from which the biopsies were taken may explain the partially different findings in

tubulin signature of HF patients in the various studies. For example, the HF patients with end-stage HCM included in our study were obviously younger than the ones in the studies of Prosser's group warranting the need to investigate how the tubulin signature changes with ageing. Moreover, in a proteomics analysis of septal myectomy samples from HCM patients (**chapter 8**), our group revealed an increased microtubule network in female compared to male HCM patients.[28] In another study, we observed the clear pattern that the levels of total and acetylated α-tubulin were changed dependent on the genotype in septal myectomies in the following order: HCM with haploinsufficiency > HCM with a poison polypeptide > genotype-negative HCM (**chapter 7**).[4] A description of the tubulin signature in the different regions of the heart is still lacking, but of utmost importance to understand how the selection of a specific region is introducing a bias when comparing different studies.

EFFECT OF AORTIC BANDING TO MODEL ACUTE PRESSURE-OVERLOAD CONCENTRIC HYPERTROPHY

We compared sham-operated to AoB-treated pigs of the same age. Since pressure-overload was initiated 3 weeks before sacrifice, we were able to study the consequences of acute concentric hypertrophy in the absence of any co-founding pathomechanisms such as a gene mutation. As expected, AoB-treated pigs were characterized by a double as high normalized LVW/BW ratio compared to sham-operated pigs. Interestingly, we did not observe any changes in tubulin signature which is in line with the fact that the cardiac function, including LVEF, LV-EDA and LV-ESA was comparable between AoB-treated and sham-operated pigs.

Previously, the effect on microtubule network of LV pressure overload has been studied in various animal models with contradictory results. In line with our findings, no microtubule proliferation was observed in guinea pigs[29-30] and cats[31] with pressure overload hypertrophy. In contrast to that, microtubule proliferation was shown in dogs[32] and mice[33] with LV pressure overload-induced cardiomyopathy. Potential reasons for these conflicting outcomes could be either underlying species differences in response to LV pressure overload or the differences in severity of the disease models. For example, compensated hypertrophy due to LV pressure overload in dogs did not affect tubulin expression, while microtubule proliferation was observed when hypertrophy transitioned from a compensated into a decompensated state.[32] Therefore, the normal cardiac function in our AoB-treated pigs may be reflected by an unchanged tubulin signature which may possibly be altered in decompensated hypertrophy. In the above mentioned animal models only total microtubule levels were studied and information about the fine-tuning of the tubulin code are lacking.

EFFECT OF AGEING AND BODY GROWTH IN PARALLEL

In our study, we used 18 months old pigs with a high BW. Previously, it has been reported that LV dimensions and function do not scale with BW in modern pigs according to allometric scaling laws.[18,22-23] In addition, high BW pigs were characterized by a high LV systolic pressure.[18] This chronic LV pressure overload was suggested to be responsible for the increase in interstitial collagen levels and the impaired LV relaxation contributing to diastolic perturbations as observed in our 18 months old pigs.[18,34] Since

we observed a weaker tubulin signature, including decreased levels of total, acetylated and detyrosinated α-tubulin in the 18 months old pigs, detyrosinated α-tubulin can be excluded as a potential contributor to the diastolic perturbations seen in this model. More research is needed to understand the causes and consequences for the weaker tubulin signature and whether modulation of the tubulin signature would have an effect on the disproportionately low stroke volume. Hereby, it is important to include healthy ageing pigs with a normal cardiac function as a control group to reduce the complexity of the model.

One limitation of our study is the comparison of the 18 months old pigs to sham-operated, 4 months old pigs. Part of the 18 months old pigs was obtained from another breeder. Moreover, the sham-operated pigs were studied several years before the 18 months old pigs, hence these animals likely have a slightly different genetic background. In addition, the 18 months old pigs were only females, while in the AoB study both males and females were used. Male pigs were selected for their rapid gain of skeletal muscle weight.[35] So this may have resulted in relatively lower normalized LVW/BW ratio's in sham-operated, 4 months old pigs as compared to the 18 months old female pigs. Furthermore, our proteomics study in **chapter 8** revealed sex differences in microtubule remodelling indicated by a proliferated microtubule network in female HCM patients.[28] In future, it would be interesting to determine the tubulin signature in female pigs of the lowest weight category of the van Essen study,[18] which is comparable to the weights of the sham-operated pigs.

TUBULIN SIGNATURE IN *MYBPC3* MICE

In a further data set, we used exercised WT mice and mice carrying the *MYBPC3* c.772G>A mutation on one or both alleles, which is associated with human HCM, to study the effect of this mutation under exercise. Exposure to an 8-week voluntary wheel-running protocol did not change the tubulin signature and levels of desmin as observed from our comparison of sedentary and exercised WT mice.

Interestingly, a similar tubulin signature as in WT mice was observed in hetero- and homozygous exercised mice and desmin levels were increased in HOM_{EX}. This unchanged tubulin signature differs from our previous study with older homozygous *MYBPC3* mice. We observed normal α-tubulin levels and increased levels of detyrosinated α-tubulin and desmin in homozygous, 20 to 28 weeks old $MYBPC3_{2373insG}$ mice and in homozygous, 55 to 59 weeks old $MYBPC3_{772G>A}$, we observed an increase in α-tubulin and a tendency to increased detyrosination of α-tubulin.[10] Desmin levels were not investigated in the latter group.

These findings suggest that the tubulin signature and desmin expression may be changed in a time-dependent sequence in response to a genetic trigger such as the strongly reduced cMyBP-C levels in HOM_{EX} mice which were accompanied by cardiac dysfunction and hypertrophy. Hereby, an intermediate stage may be represented by an increase in desmin levels, followed by more detyrosination of α-tubulin and lastly an increase in the microtubule network with a tendency to increased detyrosination of α-tubulin. Further research is needed to understand the age-dependent differences in tubulin signature and desmin expression and their functional ramifications in *MYBPC3* mice.

ASSESSMENT OF DESMIN EXPRESSION IN ANIMAL MODELS AND HEART FAILURE PATIENTS

Next to defining the tubulin signature, we assessed the desmin expression in our sample collection to better understand whether we could observe a pattern between the tubulin signature and desmin expression. This was especially relevant in the context that desmin has been identified as a sarcomeric microtubule anchor[7] and that intermediate filaments cross-link with microtubules in a detyrosination-dependent manner.[11-12] Compared to the respective control, we detected either normal or increased levels of desmin. The latter was the case in $HCM_{St\ II}$, HOM_{EX} mice and AoB-treated pigs. In line with our data, it has been suggested that increased desmin levels are observed during the development of hypertrophy in response to maintain organization of sarcomeres independent of the underlying pathology.[36-37] Moreover, one of the functions of desmin is to counteract external stresses.[38-39] In 4-week and 8-week thoracic aorta banded guinea-pigs to model compensated left ventricular pressure overload hypertrophy and decompensated congestive HF, an increase of desmin expression on the level of mRNA transcripts and proteins has been detected.[30] In contrast to our findings, investigating the cytoskeleton remodelling of explanted failing human myocardium revealed an increase of desmin filaments.[37] In comparison to non-failing and compensated hypertrophic hearts, upregulation of full-length desmin and some low molecular weight bands previously identified as post-translationally modified desmin products, that are prone to misfolding, aggregation and cleavage,[40] were detected in biopsies of HCM, DCM and ISHD patients with HF.[6] In our Western Blots analyses, we only detected full-length desmin due to usage of an anti-desmin antibody targeting a carboxy-terminal epitope. Besides the increase of desmin levels, disorganization of desmin filaments has been described coinciding with contractile dysfunction.[6,37] Higher levels of intact desmin are likely caused by either an increased desmin expression or a decreased capability of the cardiomyocytes to efficiently degrade desmin.[41] Since increased desmin levels in HF regardless of the underlying cause are often accompanied by posttranslational modification-driven formation of intracellular protein aggregates,[40-41] further research is warranted to improve our understandings about the extent of these changes and their functional ramifications.

Our data suggest that desmin levels are increased in early concentric hypertrophy, while our HF patient cohort was characterized by desmin levels comparable to controls. Furthermore, we observed that desmin expression was independent of the levels of detyrosinated α-tubulin. Along with reporting expression levels, it is also important to study the levels of low molecular weight post-translationally modified desmin products, the spatial organization patterns and formation of desmin aggregates in biopsies in future studies.

CONCLUSION

Cardiomyopathies underlie complex pathomechanisms and animal models only partially recapitulate the proliferated and modified tubulin signature and changes in desmin levels. Age, sex, genotype and selection of heart region are likely to introduce a bias in the tubulin signature. Our findings emphasize the necessity to establish better model systems to precisely elucidate the effect (compensation or consequence) on contractility, microtubule dynamics and stability of the observed tubulin signature in HCM and DCM patients and to test potential drugs re-writing the tubulin signature.

ACKNOWLEDGEMENTS

We would like to thank Michiel van Wijhe and Zubayda S. Sultan for technical assistance.

SUPPLEMENTARY FILES - ONLINE

https://drive.google.com/drive/folders/142Qu-xSO28VI2zAZVxI77v0M6fnDZogr

REFERENCES

1. Gaasch WH, Zile MR. Left ventricular structural remodeling in health and disease: with special emphasis on volume, mass, and geometry. *J Am Coll Cardiol*. 2011;58(17):1733-40.
2. Portran D, Schaedel L, Xu Z, Thery M, Nachury MV. Tubulin acetylation protects long-lived microtubules against mechanical ageing. *Nat Cell Biol*. 2017;19(4):391-8.
3. Xu Z, Schaedel L, Portran D, Aguilar A, Gaillard J, Marinkovich MP, et al. Microtubules acquire resistance from mechanical breakage through intralumenal acetylation. *Science*. 2017;356(6335):328-32.
4. Dorsch LM, Schuldt M, dos Remedios CG, Schinkel AFL, de Jong PL, Michels M, et al. Protein Quality Control Activation and Microtubule Remodeling in Hypertrophic Cardiomyopathy. *Cells*. 2019;8(7).
5. Caporizzo MA, Chen CY, Salomon AK, Margulies KB, Prosser BL. Microtubules Provide a Viscoelastic Resistance to Myocyte Motion. *Biophys J*. 2018;115(9):1796-807.
6. Chen CY, Caporizzo MA, Bedi K, Vite A, Bogush AI, Robison P, et al. Suppression of detyrosinated microtubules improves cardiomyocyte function in human heart failure. *Nat Med*. 2018;24(8):1225-33.
7. Robison P, Caporizzo MA, Ahmadzadeh H, Bogush AI, Chen CY, Margulies KB, et al. Detyrosinated microtubules buckle and bear load in contracting cardiomyocytes. *Science*. 2016;352(6284):aaf0659.
8. Kerr JP, Robison P, Shi G, Bogush AI, Kempema AM, Hexum JK, et al. Detyrosinated microtubules modulate mechanotransduction in heart and skeletal muscle. *Nat Commun*. 2015;6:8526.
9. Chen CY, Salomon AK, Caporizzo MA, Curry S, Kelly NA, Bedi K, et al. Depletion of Vasohibin 1 Speeds Contraction and Relaxation in Failing Human Cardiomyocytes. *Circ Res*. 2020;127(2):e14-e27.
10. Schuldt M, Pei J, Harakalova M, Dorsch LM, Schlossarek S, Mokry M, et al. Proteomic and Functional Studies Reveal Detyrosinated Tubulin as Treatment Target in Sarcomere Mutation-Induced Hypertrophic Cardiomyopathy. *Circ Heart Fail*. 2021:CIRCHEARTFAILURE120007022.
11. Liao G, Gundersen GG. Kinesin is a candidate for cross-bridging microtubules and intermediate filaments. Selective binding of kinesin to detyrosinated tubulin and vimentin. *J Biol Chem*. 1998;273(16):9797-803.
12. Gurland G, Gundersen GG. Stable, detyrosinated microtubules function to localize vimentin intermediate filaments in fibroblasts. *J Cell Biol*. 1995;131(5):1275-90.
13. Konieczny P, Fuchs P, Reipert S, Kunz WS, Zeold A, Fischer I, et al. Myofiber integrity depends on desmin network targeting to Z-disks and costameres via distinct plectin isoforms. *J Cell Biol*. 2008;181(4):667-81.
14. Kupper T, Pfitzer P, Schulte D, Arnold G. Pressure induced hypertrophy in the hearts of growing dwarf pigs. *Pathol Res Pract*. 1991;187(2-3):315-23.
15. Modesti PA, Vanni S, Bertolozzi I, Cecioni I, Polidori G, Paniccia R, et al. Early sequence of cardiac adaptations and growth factor formation in pressure- and volume-overload hypertrophy. *Am J Physiol Heart Circ Physiol*. 2000;279(3):H976-85.
16. Marshall KD, Muller BN, Krenz M, Hanft LM, McDonald KS, Dellsperger KC, et al. Heart failure with preserved ejection fraction: chronic low-intensity interval exercise training preserves myocardial O2 balance and diastolic function. *J Appl Physiol (1985)*. 2013;114(1):131-47.
17. Xiong Q, Zhang P, Guo J, Swingen C, Jang A, Zhang J. Myocardial ATP hydrolysis rates in vivo: a porcine model of pressure overload-induced hypertrophy. *Am J Physiol Heart Circ Physiol*. 2015;309(3):H450-8.
18. van Essen GJ, Te Lintel Hekkert M, Sorop O, Heinonen I, van der Velden J, Merkus D, et al. Cardiovascular Function of Modern Pigs Does not Comply with Allometric Scaling Laws. *Sci Rep*. 2018;8(1):792.
19. Sorop O, Merkus D, de Beer VJ, Houweling B, Pistea A, McFalls EO, et al. Functional and structural adaptations of coronary microvessels distal to a chronic coronary artery stenosis. *Circ Res*. 2008;102(7):795-803.
20. Duncker DJ, Boontje NM, Merkus D, Versteilen A, Krysiak J, Mearini G, et al. Prevention of myofilament dysfunction by beta-blocker therapy in postinfarct remodeling. *Circ Heart Fail*. 2009;2(3):233-42.
21. Najafi A, Schlossarek S, van Deel ED, van den Heuvel N, Guclu A, Goebel M, et al. Sexual dimorphic response to exercise in hypertrophic cardiomyopathy-associated MYBPC3-targeted knock-in mice. *Pflugers Arch*. 2015;467(6):1303-17.
22. West GB, Brown JH, Enquist BJ. A general model for the origin of allometric scaling laws in biology. *Science*. 1997;276(5309):122-6.
23. West GB, Brown JH. The origin of allometric scaling laws in biology from genomes to ecosystems: towards a quantitative unifying theory of biological structure and organization. *J Exp Biol*. 2005;208(Pt 9):1575-92.
24. Rovira S, Munoz A, Rodilla V. Allometric scaling of echocardiographic measurements in healthy Spanish foals with different body weight. *Res Vet Sci*. 2009;86(2):325-31.
25. Geeraert C, Ratier A, Pfisterer SG, Perdiz D, Cantaloube I, Rouault A, et al. Starvation-induced hyperacetylation of tubulin is required for the stimulation of autophagy by nutrient deprivation. *J Biol Chem*. 2010;285(31):24184-94.
26. McLendon PM, Ferguson BS, Osinska H, Bhuiyan MS, James J, McKinsey TA, et al. Tubulin hyperacetylation is adaptive in cardiac proteotoxicity by promoting autophagy. *Proc Natl Acad Sci U S A*. 2014;111(48):E5178-86.
27. Tang J, Zhuang S. Histone acetylation and DNA methylation in ischemia/reperfusion injury. *Clin Sci (Lond)*. 2019;133(4):597-609.
28. Schuldt M, Dorsch LM, Knol JC, Pham TV, Schelfhorst T, Piersma SR, et al. Sex-Related Differences in Protein Expression in Sarcomere Mutation-Positive Hypertrophic Cardiomyopathy. *Frontiers in Cardiovascular Medicine*. 2021;8(129).

29. Wang X, Li F, Campbell SE, Gerdes AM. Chronic pressure overload cardiac hypertrophy and failure in guinea pigs: II. Cytoskeletal remodeling. *J Mol Cell Cardiol*. 1999;31(2):319-31.
30. Collins JF, Pawloski-Dahm C, Davis MG, Ball N, Dorn GW, 2nd, Walsh RA. The role of the cytoskeleton in left ventricular pressure overload hypertrophy and failure. *J Mol Cell Cardiol*. 1996;28(7):1435-43.
31. Bailey BA, Dipla K, Li S, Houser SR. Cellular basis of contractile derangements of hypertrophied feline ventricular myocytes. *J Mol Cell Cardiol*. 1997;29(7):1823-35.
32. Tagawa H, Koide M, Sato H, Zile MR, Carabello BA, Cooper Gt. Cytoskeletal role in the transition from compensated to decompensated hypertrophy during adult canine left ventricular pressure overloading. *Circ Res*. 1998;82(7):751-61.
33. Zhang C, Chen B, Guo A, Zhu Y, Miller JD, Gao S, et al. Microtubule-mediated defects in junctophilin-2 trafficking contribute to myocyte transverse-tubule remodeling and Ca2+ handling dysfunction in heart failure. *Circulation*. 2014;129(17):1742-50.
34. Zile MR, Baicu CF, Gaasch WH. Diastolic heart failure–abnormalities in active relaxation and passive stiffness of the left ventricle. *N Engl J Med*. 2004;350(19):1953-9.
35. Gonzalez-Bulnes A, Ovilo C, Lopez-Bote CJ, Astiz S, Ayuso M, Perez-Solana ML, et al. Fetal and early-postnatal developmental patterns of obese-genotype piglets exposed to prenatal programming by maternal over- and undernutrition. *Endocr Metab Immune Disord Drug Targets*. 2013;13(3):240-9.
36. Rappaport L, Samuel JL. Microtubules in cardiac myocytes. *Int Rev Cytol*. 1988;113:101-43.
37. Hein S, Kostin S, Heling A, Maeno Y, Schaper J. The role of the cytoskeleton in heart failure. *Cardiovasc Res*. 2000;45(2):273-8.
38. Lazarides E, Granger BL, Gard DL, O'Connor CM, Breckler J, Price M, et al. Desmin- and vimentin-containing filaments and their role inthe assembly of the Z disk in muscle cells. *Cold Spring Harb Symp Quant Biol*. 1982;46 Pt 1:351-78.
39. Fuchs E, Cleveland DW. A structural scaffolding of intermediate filaments in health and disease. *Science*. 1998;279(5350):514-9.
40. Agnetti G, Halperin VL, Kirk JA, Chakir K, Guo Y, Lund L, et al. Desmin modifications associate with amyloid-like oligomers deposition in heart failure. *Cardiovasc Res*. 2014;102(1):24-34.
41. Singh SR, Kadioglu H, Patel K, Carrier L, Agnetti G. Is Desmin Propensity to Aggregate Part of its Protective Function? *Cells*. 2020;9(2).

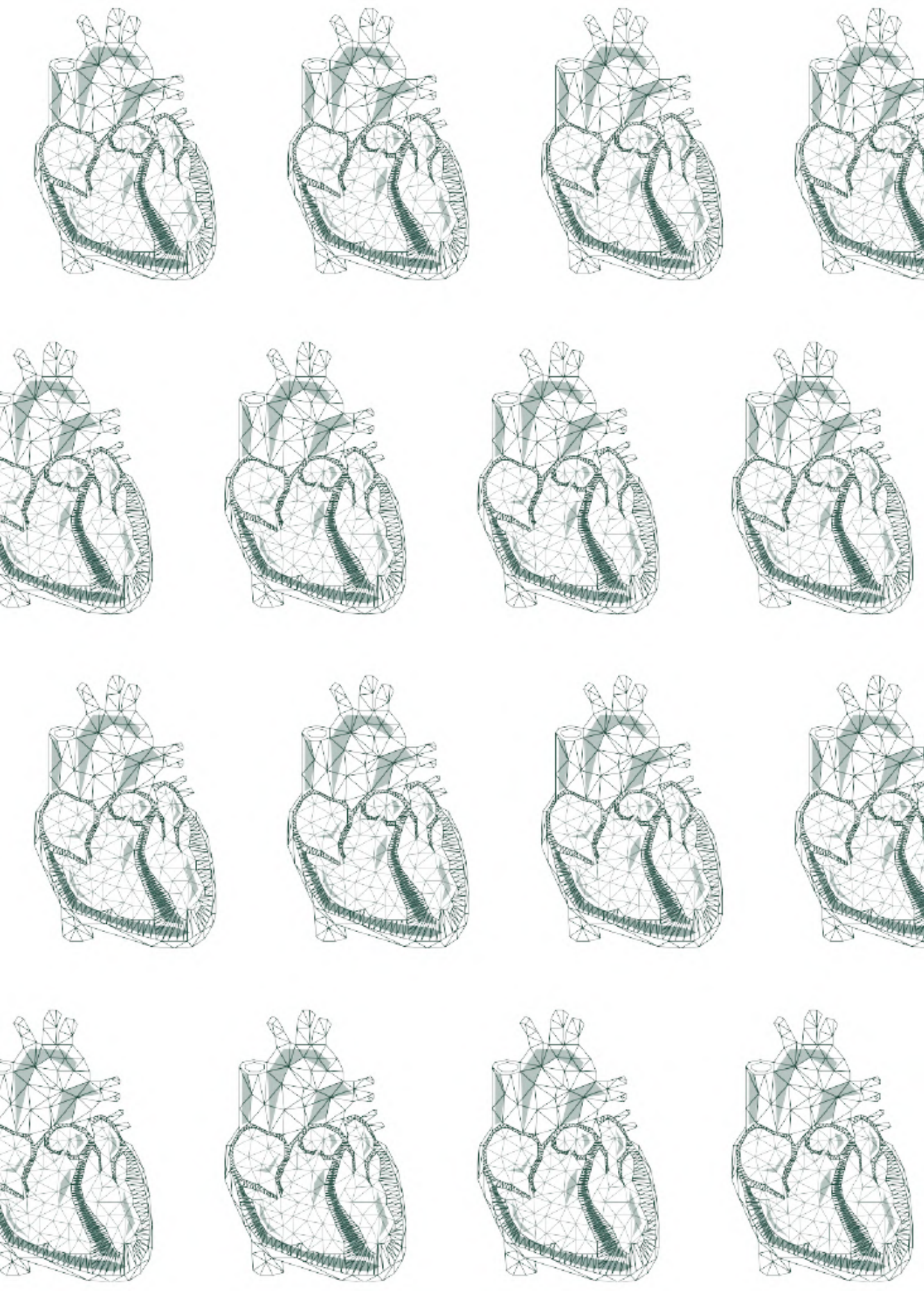

PART *DROSOPHILA MELANOGASTER* - A MODEL SYSTEM TO STUDY INHERITED CARDIOMYOPATHIES

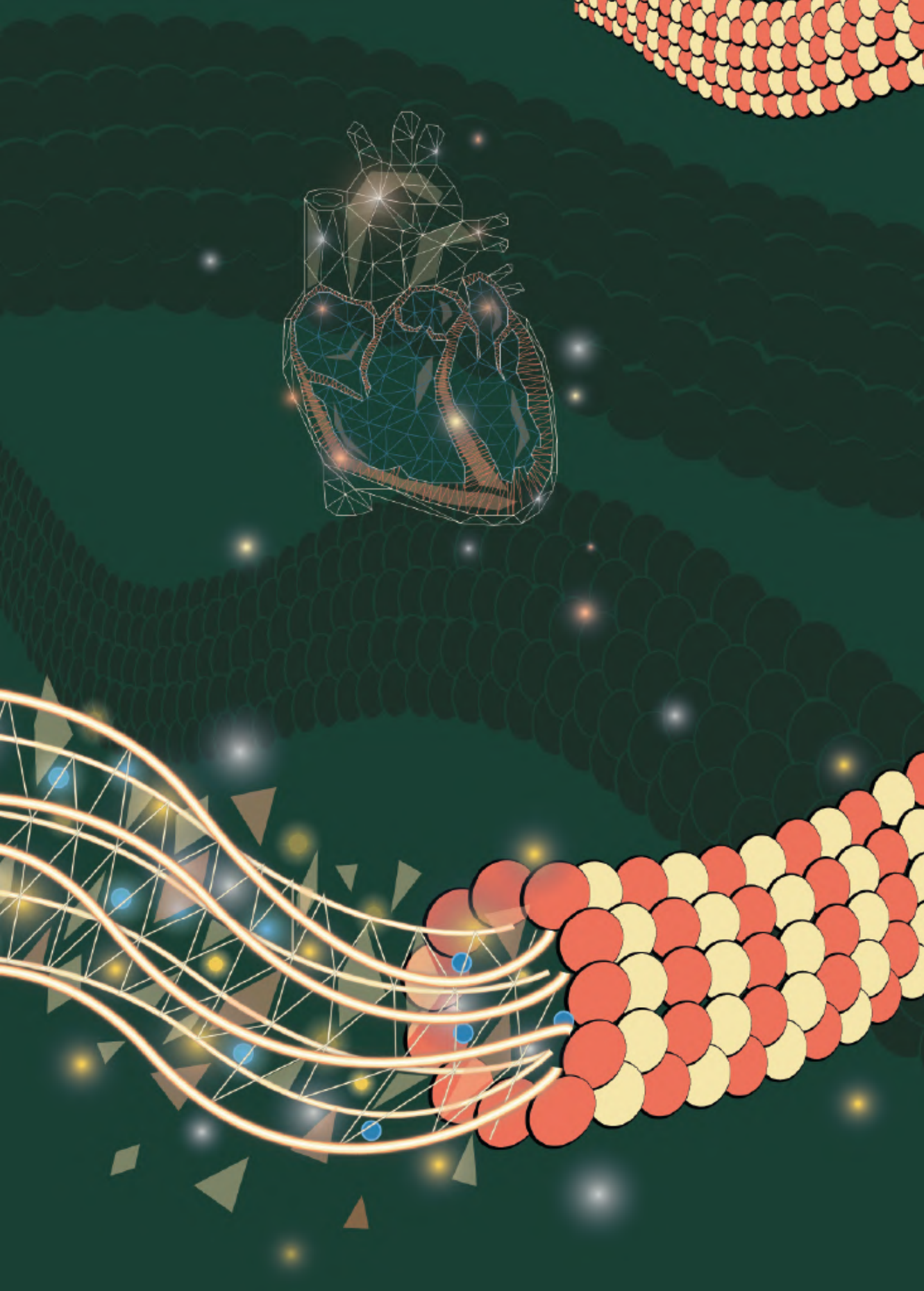

Chapter 10

Unsuccessful scarless CRISPR/Cas9 editing approach of haplolethal region 16F in *Drosophila melanogaster*

Larissa M. Dorsch, Bianca JJM. Brundel, Diederik WD. Kuster, Jolanda van der Velden

Manuscript in revision.

ABSTRACT

Variants in genes encoding contractile proteins can lead to diverse cardiomyopathy phenotypes and one of these genes is *TNNI3* which encodes cardiac Troponin I (TnI). We aimed to generate clustered, regularly interspaced, short palindromic repeats (CRISPR) / CRISPR-associated (Cas)9-edited *Drosophila melanogaster* as a model system to understand the pathomechanisms of two distinct gene variants E97X and K144W in *TNNI3* (*wupA* in *Drosophila melanogaster*). Both variants represent orthologues of the clinically relevant *TNNI3* variants R98X and R145W in humans. Our attempt using scarless CRISPR/Cas9-mediated genome editing to make these strains was not successful. This result was caused either by employing an experimental strategy which can lead to low or no activity of the Cas9/single-guide RNA (sgRNA) complexes or by targeting the haplolethal region 16F of *Drosophila melanogaster*. In the latter case, to introduce the nucleotide changes, the eye-specific 3xP3-DsRed selection marker was inserted during homology-directed repair which may affect one or several breakpoints in close proximity to the insertion site and thereby interrupt TnI protein expression. As a consequence, this may result in a lethal phenotype of both CRISPR edited strains. By sharing our unsuccessful attempt, we intend to create awareness about potential pitfalls of using our scarless CRISPR/Cas9 editing approach while targeting a haplolethal region.

INTRODUCTION

Cardiomyopathies are a heterogeneous group of diseases of the myocardium that are associated with mechanical and/or electrical dysfunction and are a major cause of morbidity and mortality.[1] Pathogenic variants in the sarcomere gene *TNNI3* which encodes cardiac Troponin I (TnI) can lead to diverse cardiomyopathy phenotypes.[2,3] Reported *TNNI3* variants account for 2.2% of all likely pathogenic and pathogenic gene variants in hypertrophic cardiomyopathy (HCM) and 0.6% in dilated cardiomyopathy (DCM).[4] Moreover, *TNNI3* gene variants are the most prevalent cause of restrictive cardiomyopathy (RCM).[5] In the literature, the gene encoding troponin I in *Drosophila melanogaster* has been referred to as *wings up A* (*wupA*), *held-up* (*hdp*), and *TnI*. Here, we use the FlyBase standard *wupA* (CG7178) name when referring to this gene. We aimed to introduce cardiomyopathy-specific *wupA* variants in *Drosophila melanogaster* to define underlying pathomechanisms.

Drosophila melanogaster is a relatively inexpensive model system, easy to keep and causes minimal ethical and safety issues. The relatively short life cycle of *Drosophila melanogaster* reduces enormously the time to wait until research material is available compared to vertebrate models. Material of adults can be studied 10 days after fertilization of the egg when maintained at 25°C.[6] The high reproduction rate makes it easy to generate and include large numbers of flies for experimental approaches.[6] Compared to transgenic mouse models, transgenic *Drosophila melanogaster* models are readily amenable to large scale genetic or pharmacologic screens.[7,8] *Drosophila melanogaster*, the simplest genetic model system with a heart, exhibits strong gene conservation with human genes, including 75% of disease-related genes.[9,10] Furthermore, it has been used as an efficient model for functional studies in cardiomyopathies.[9,10]

We performed sequence alignments of *Drosophila melanogaster* and cardiomyopathy-causing gene variants listed in our human tissue biobank. Here, we selected two *TNNI3* gene variants, the R98X and R145W. In addition, the R145W gene variant fulfilled our requirement for non-truncating mutations because the orthologous amino acid in *Drosophila melanogaster* belongs to the same physicochemical group. After evaluating the robustness of *Drosophila melanogaster* as a model system to study inherited cardiomyopathies, we intended to upscale the number of gene variants.

The R98X has been associated with different clinical phenotypes, i.e. DCM or HCM.[4,11] At a nucleotide level, R98X is caused by a 292 C→T mutation that is predicted to result in a premature stop codon at amino acid 98. The resulting truncated cardiac TnI protein lacks troponin C and actin binding domains.[5,11] Analysis of left ventricular cardiac tissue of patients with the truncating R98X gene variant showed reduced full length cTnI protein levels, i.e. while no truncated form of cTnI was observed indicating that the outcome of the R98X variant is haploinsufficiency instead of a dominant-negative effect and altered stoichiometry.[11]

The R145W mutation was initially detected in patients with idiopathic RCM.[12] Subsequent studies reported the R145W as an RCM- and HCM-causing variant in individuals with variable clinical characteristics leading to its classification as a pathogenic variant.[12-15] This variant is a Dutch founder mutation and represents 27% of all *TNNI3* gene variants.[15]

Previously, *wupA* mutant strains were set up by mutagenic chemicals, especially ethyl methane sulfonate mutagenesis.[16,17] Here, we applied, for the first time, scarless clustered, regularly interspaced, short palindromic repeats (CRISPR)/CRISPR-associated (Cas)9-mediated genome editing to specifically generate two *Drosophila melanogaster* strains with the *wupA* variants E97X and K144W, which are the orthologues changes for the two human *TNNI3* variants R98X and R145W, respectively. CRISPR/Cas9 system is a preferred tool to generate targeted mutations in *Drosophila melanogaster* because of the following benefits in comparison to other site-specific nuclease techniques such as zinc-finger nuclease (ZFN) and transcription activator-like effector nuclease (TALEN).[18] First, CRISPR/Cas9 is more feasible for upscaling gene editing project because only changing the 20-basepair guide RNA is sufficient for Cas9 to distinguish genes. Cas9 cutting sites are spread abundantly in the *Drosophila melanogaster* genome. To target another gene with ZFN or TALEN, the engineering of another protein is required.[18] Second, there are several established routes how Cas9 can be delivered into the model system which increased the likelihood of success and provides more flexibility.[19-21] Third, co-injection of a donor vector carrying a selection marker, such as 3xP3-DsRed, with Cas9 facilities and speeds up the screening process.[19]

Our scarless CRISPR/Cas9 approach is based on using Cas9 endonuclease complexes with a single-guide RNA (sgRNA), which is designed to match a ~20bp target sequence, and to cause double strand cleavage of the target sequence. The sgRNA is characterized by a protospacer-adjacent motif (PAM) (the trinucleotide 5'-NGG-3') immediately 3' of the 20bp target sequence.[22,23] Supplying a donor plasmid in excess was intended to be used as the desired homologous template and to introduce the defined changes in the target DNA.[24] Next to the defined changes to be introduced, our donor plasmid design also contains the promotor 3xP3 and the selection marker DsRed. This selection marker cassette is flanked by PBac transposon ends. The TTAA site, the PBac transposase recognition motif, is duplicated upon knock-in of the selection marker and restored to a single TTAA site upon excision of the selection marker by PBac transposase.[19,23] The workflow of the our seamless CRISPR/Cas9 approach is shown in Figure 10.1.

The *wupA* gene results in 13 transcripts and 13 protein isoforms. The transcripts RC and RF, the two most abundant transcripts in which both target sites are present, were used as reference transcripts to introduce the gene variants. Since hereditary cardiomyopathies are most commonly inherited by dominant transmission,[25] we aimed to generate strains that are heterozygous for the *wupA* variants.

It has been shown before that *wupA* variants can cause cardiomyopathies. For example, an alanine to valine change within all TnI isoforms (A116V in wupA-PG/PH; A31V in wupA-PK-PM; A55V in remaining isoforms) causes impaired systolic function

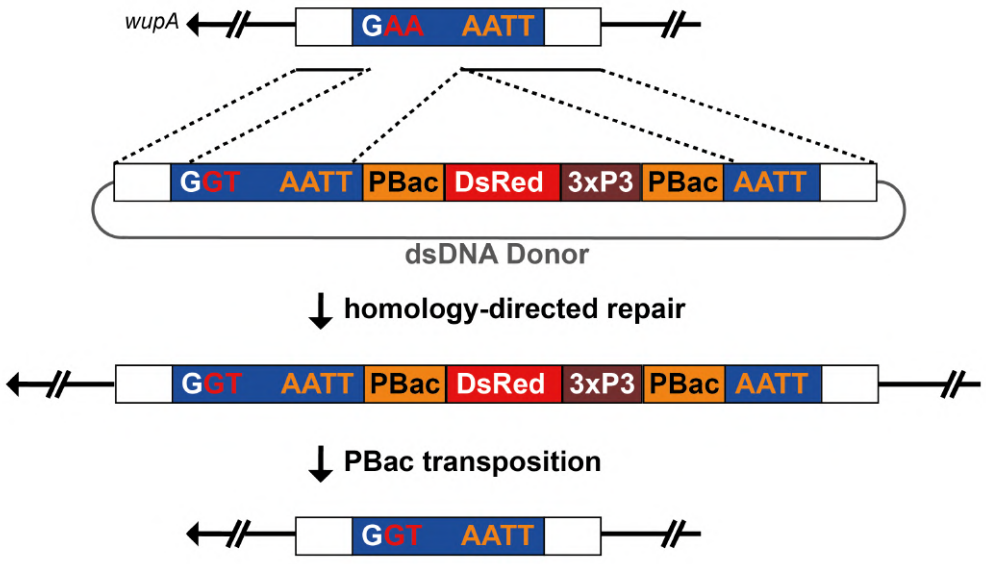

Figure 10.1: Workflow of seamless CRISPR/Cas9-based genome editing to introduce *wupA* variants. Double-stranded DNA donor plasmid contains the nucleotide changes (AAG to TGG) to introduce the K144W variant and the marker cassette PBacDsRed with the two PBac terminals, 3xP3-DsRed and two homology arms. Homology-directed repair of the CRISPR/Cas9-mediated double strand break in the genome results in insertion the of knock-in cassette PBacDsRed. This is an intermediate step for visible marker screening. Following DsRed-mediated identification of engineered strains, the marker cassette can be easily and scarlessly removed through a single cross to PBac transposase.

in heterozygote and homozygote $wupA^{hdp2}$ strains. Homozygote $wupA^{hdp2}$ *Drosophila melanogaster* also showed cardiac enlargement recapitulating the clinical phenotype of human DCM.[16] While *Drosophila melanogaster* thus represents an experimental tool to study cardiomyopathies, our usage of CRISPR/Cas9 editing to introduce *wupA* mutations in combination with knock-in of an eye-specific selection marker failed.

Instead of being able to provide any insight in these cardiomyopathy *wupA* variants and their impact, we share here our attempt and data on failure to generate these CRISPR-edited *Drosophila melanogaster* strains with the hope to prevent loss of time and research money by other groups who may want to use a similar method to target genes within haplolethal regions in *Drosophila melanogaster* and can inform future attempts to improve methodology.

METHODS

SEAMLESS CRISPR/CAS9-BASED GENOME EDITING WAS USED TO INTRODUCE THE E97X AND K144W VARIANTS

CRISPR/Cas9-mediated mutagenesis was performed by WellGenetics Inc. (Taipei City, Taiwan) using modified methods of Kondo and Ueda.[21] While Kondo and Ueda used transgenic CRISPR components, we used injected plasmids. In brief, genomic DNA was obtained from injection strain w^{1118}. PCR was performed using KOD FX DNA polymerase (TOYOBO, KFX-101) on BioRad S1000 Thermal Cycler. Sequencing results were BLAT against *Drosophila melanogaster* genome (August 2014 Assembly, BDGP Release 6) using UCSC Genome Bioinformatics and the genomic codons option was selected for codon colouring.[26,27] The respective guide RNA (Table 10.1) was cloned into U6:96Ab (U6-2) promoter plasmid.[21]

Table 10.1: Design of CRISPR target site, guide RNAs and homology arms.

	E97X		K144W	
	guide RNA1	**guide RNA2**	**guide RNA1**	**guide RNA2**
CRISPR target site [PAM]	GGGATCTGGA ATACGAAGTC [AGG]	TGAAGGCCAG AAATGGGATC [TGG]	CGTCAAGCCA GCCCTGAAGA [AGG]	CGTATTTGGA GACCTTCTTC [AGG]
CRISPR target strand	minus	minus	minus	plus
Cutting Site	+5135 nt from ATG of *wupA_RC/F*	+5121 nt from ATG of *wupA_RC/F*	+7821 nt from ATG of *wupA_RC/F*	+7821 nt from ATG of *wupA_RC/F*
Distance	+57 nt from breakpoint to cutting site of Cas9	+43 nt from breakpoint to cutting site of Cas9	+11 nt from breakpoint to cutting site of Cas9	+11 nt from breakpoint to cutting site of Cas9
Off target	0	on 3R:31180492.. 31180514; 3R:8415841.. 8415863; 3L:14787428.. 14787450; 2L:19469251.. 19469273	0	0
GC%	50%	50%	60%	45%
T number at 17th to 20th nucleotides	1	1	0	2
Guide RNA primers **Sense oligo**	5'– CTTCGGGATC TGGAATACGA AGTC	5'– CTTCGTGAAG GCCAGAAATG GGATC	5'– CTTCGCGTCA AGCCAGCCCT GAAGA	5'– CTTCGCGTAT TTGGAGACCT TCTTC

Table 10.1: Continued

		E97X		K144W	
		guide RNA1	**guide RNA2**	**guide RNA1**	**guide RNA2**
	Antisense oligo	5'–AAACGACTTCGTATTCCAGATCCC	5'–AAACGATCCCATTTCTGGCCTTCAC	5'–AAACTCTTCAGGGCTGGCTTGACGC	5'–AAACGAAGAAGGTCTCCAAATACGC
PAM mutation		GGGATCTGGAATACGAAGTC[AGA]	TGAAGGCCAGAAATGGGATC[TCG]	CGTCAAGCCAGCCCTGAAGA[AAG]	CGTATTTGGAGACCTTCTTC[ACG]
PAM mutation changes amino acid		no	no	no	no
Upstream homology arm	**Length**	1007bp	1007bp	1033bp	1033bp
	Location	+4068 nt to +5074 nt from ATG of *wupA_RC/F*	+4068 nt to +5074 nt from ATG of *wupA_RC/F*	6773 nt to +7805 nt from ATG of *wupA_RC/F*	6773 nt to +7805 nt from ATG of *wupA_RC/F*
	Forward oligo	5'–TTTGGAGGGCGATAAGTTTG	5'–TTTGGAGGGCGATAAGTTTG	5'–AGCCGAACAAACAAATCGAA	5'–AGCCGAACAAACAAATCGAA
	Reverse oligo	5'-CAAATCTCTTGCAATTCGCCT	5'-CAAATCTCTTGCAATTCGCCT	5'–CGCTAAAGTTATTCGAATGCAATC	5'–CGCTAAAGTTATTCGAATGCAATC
Down-stream homology arm	**Length**	1018bp	1018bp	1042bp	1042bp
	Location	+5079 nt to +6069 nt from ATG of *wupA_RC/F*	+5079 nt to +6069 nt from ATG of *wupA_RC/F*	+7810 nt to +8851 nt from ATG of *wupA_RC/F*	+7810 nt to +8851 nt from ATG of *wupA_RC/F*
	Forward oligo	5'–GAGTATTACGAGCGTATGTA	5'–GAGTATTACGAGCGTATGTA	5'–GCCAGCCCTGTGGAAGGTCTCC	5'–GCCAGCCCTGTGGAAGGTCTCC
	Reverse oligo	5'–GACAGCGGCACAAACAAAT	5'–GACAGCGGCACAAACAAAT	5'–CTGATCAAATCCATTGTGGACAC	5'–CTGATCAAATCCATTGTGGACAC

For both gene variants, guide RNA1 was used for the first round of injections and guide RNA2 was used for the second round of injections (Table 10.1). The donor plasmid containing a red fluorescent marker cassette with 3xP3 promoter driving DsRed expression in the eyes which was flanked by piggyBac (PBac) transposon ends and two homology arms with the gene variants was cloned into the pUC57-Kan vector (Figure 10.1; Supplementary Material: E97X and K144W Donor Designs).

WupA-targeting guide RNAs (100ng) and heat shock-inducible Cas9 (100ng) were supplied in DNA plasmids, together with donor plasmid (500ng) for microinjection into embryos of control strain w^{1118}. The first two rounds of microinjection of K144W were done on [LWG208] w^{1118}, which was newly obtained from Bloomington Stock Number

6326 (SNP mapping stock, isogenic 2nd and 3rd chromosomes).[28] Since this is the isogenic background for Exelixis P and PBac insertions, SNP variation for CRISPR editing would be reduced. However, it neither survived well nor gave any positive strains. All further microinjections of E97X and K144W were therefore done on [LWG012] w^{1118} strain, obtained from Bloomington Stock Center. Identification of engineered strains was performed via the 3xP3-DsRed marker by screening for DsRed expression in the eye.[19,29] F1 flies carrying the 3xP3-DsRed selection marker were further validated by genomic PCR and sequencing. CRISPR generated a break in *wupA* and was replaced by cassette PBacDsRed. The *TM6B* balancer was used for selection of heterozygous offspring at larval stage. Following DsRed-mediated identification of engineered strains, the marker cassette can be easily and scarlessly removed through a single cross to PBac transposase,[19,23] but was not applied in this study.

ANALYSIS OF CRISPR INTEGRATION OF THE SELECTION MARKER OF K144W VARIANT

Genomic DNA was obtained from a single fly of each stock following single-fly DNA preparation using Gloor's protocol.[30] Injection strain w^{1118} was used as a negative control and donor plasmid as a positive control for integration examination. PCR was performed using KOD FX DNA polymerase (TOYOBO, KFX-101) on BioRad S1000 Thermal Cycler (Table 10.2).

Table 10.2: Steps and conditions of thermo cycling for Integration and Validation PCR.

Steps	Temperature	Time	Cycles
Initial denaturation	94°C	2 min	1
Denaturation	98°C	10 sec	
Annealing	55°C	30 sec	30
Extension	68°C	2 min	
Final extension	68°C	5 min	1
End/Hold	15°C	Forever	

CRISPR/homology-directed repair may go through different repairing routes. Integration of donor plasmid in CRISPR editing alleles is a common phenomenon. "No integration" contains only one copy of selection marker. "Single integration of donor plasmid" contains the vector backbone, two copies of homology arms and selection marker.

Integration test is to exclude alleles with donor vector integration and only keep the strains with simple editing to avoid the genomic complications. For integration PCR 1, forward primer (5'–CAACTGTTGGGAAGGGCGAT) was designed outside the upstream homology arm in the backbone plasmid and reverse primer (5'–CGAGGGTTCGAAATCGATAA) was designed at 3xP3 promoter. For integration PCR 2, forward primer (5'-TTTGACTCACGCGGTCGTTA) was designed at 3' PBac terminal and reverse primer (5'–CATTAGGCACCCCAGGCTTT) was designed outside the downstream homology arm in the backbone plasmid. While single integration of donor

plasmid will have the amplicon, the corrected editing will not have the amplicon. 1kb Plus DNA RTU Ladder from Biomate (BR343-500) was used as reference on a 1.2% agarose gel and 0.5x TAE buffer.

CRISPR VALIDATION OF KNOCK-IN CASSETTE PBacDsRed FOR K144W VARIANT

Genomic DNA was obtained from a single fly of each stock following single-fly DNA preparation. Injection strain w^{1118} was used as a negative control. PCR was performed using KOD FX DNA polymerase (TOYOBO, KFX-101) on BioRad S1000 Thermal Cycler (Table 10.2). Using genomic PCR and sequencing methods to verify CRISPR alleles of *wupA* by testing if the knock-in cassette PBacDsRed was correctly used as template for homology-directed repair and was incorporated into guide RNA1 cutting site. For upstream PCR, forward primer (5'-TCTCTCTGTCACTTTTCTCTGTG) was designed at 5' outside the homology arm and reverse primer (5'-CGAGGGTTCGAAATCGATAA) was designed at 3xP3 promoter. For downstream PCR, forward primer (5'-TTTGACTCACGCGGTCGTTA) was designed at 3' PBac terminal repeat and reverse primer (5'-GGCATGGCAAGGTAGAAAGA) was designed at 3' outside the downstream homology arm. Only cassette PBacDsRed, which was inserted into the gene locus will have the amplicon. 1kb Plus DNA RTU Ladder from Biomate (BR343-500) was used as reference on a 1.2% agarose gel and 0.5x TAE buffer.

RESULTS

TARGET SEQUENCES OF GUIDE RNAs PRESENT IN INJECTION STRAIN

We designed the guide RNAs according to the following four criteria: distance from knock-in site to cutting site of Cas9, predicted off targets on other chromosomes, GC content of target sequence and thymine numbers at 17^{th} to 20^{th} nucleotide of the guide RNA target site. Quality of the guide RNA was considered as strong when the distance was shorter than 50 base pairs, without any off targets, 45%-70% GC content of the target sequence and 0 or 1 thymine. Quality of the guide RNA was classified as weak when the distance was between 50 to 100 base pairs, presence of potential off targets on untargeted chromosomes, 40% or 75% GC content of the target sequence and 2 thymines. All four designed guide RNAs showed at least three strong quality characteristics (Table 10.1).

Furthermore, we performed genomic sequencing of the injection strain to verify that all guide RNA loci for the E97X and K144W variants were as indicated. No SNPs were found on the guide RNAs in 3 independent reads in the injection strain. The target sequence of each guide RNA was present in the genome of the injection strain (Figures 10.2A-B and Supplementary Material). With this information, guide RNAs and donor plasmids were prepared. As illustrated in Figures 10.2C-D, for both gene variants the selection marker knock-in will be positioned within an exon.

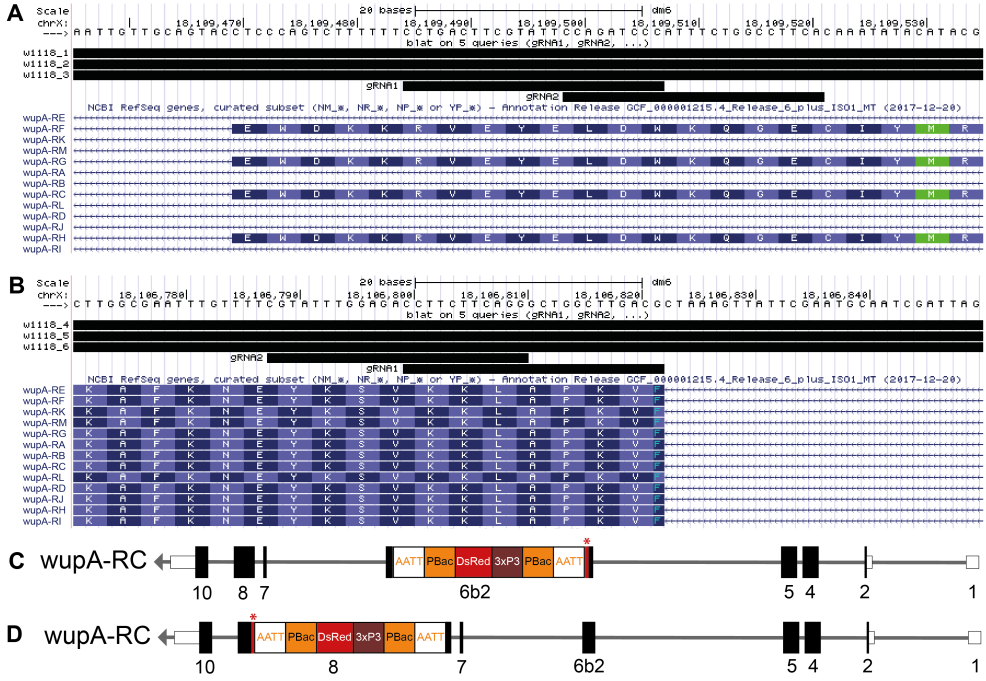

Figure 10.2: BLAT results to show alignment of the guide RNAs and independent reads of the injection strain with the *wupA* transcripts. The target sequence of both guide RNAs (gRNA1 and gRNA2; Table 10.1) for the (**A**) E97X variant and the (**B**) K144W variant were present in three independent reads (**A**) (w1118_1, w1118_2, w1118_3) and (**B**) (w1118_4, w1118_5, w1118_6) of the injection strain. The independent read sequences of the injection strain are available in the Supplementary Material. The 13 *wupA* transcripts were indicated below with codon boundaries depicted by alternating lighter and darker blue shades. Bright green codon indicates methionine and cyan text indicates spliced codon. Continuous black bars of the target sequence of guide RNAs and the independent reads of the injection strains indicate completely matched sequence overlap with the *wupA* transcripts. In (**A**) the targeted exon is present in 4 *wupA* transcripts and in (**B**) sequence is present in all 13 *wupA* transcripts. Schematic illustration of successful integration of selection marker cassette with (**C**) E97X and (**D**) K144W variant in the *wupA* locus. Red bar with asterisk on top indicates position of gene variant. Numbers below illustration indicate the exons.

NO POSITIVE STRAINS AFTER MICROINJECTION OF E97X DONOR PLASMID

We performed two rounds of microinjection in more than 400 embryos to introduce the E97X variant, but failed to get any 3xP3-DsRed-positive strain. In the first round after microinjection of guide RNA1, survival rate was low with 41 adults out of 207 injected embryos. In the second round after microinjection of guide RNA2, survival rate and fertile rate were all within normal range with 81 adults and 24 fertile crosses out of 222 injected embryos, but without any positive strain. Since we excluded failure to introduce the E97X

variant due to missing target sequence in the genome (Figure 10.2 and Supplementary Material), we also performed sequencing of the donor plasmid. Both upstream and downstream homology arms in the donor plasmid were sequenced to check if both are specific to *wupA* (Figure 10.3A and Supplementary Material). No mismatches were found in the coding sequence of *wupA*. Since the donor plasmid was correctly composed as designed, failure due to inaccurate design of donor plasmid was also excluded.

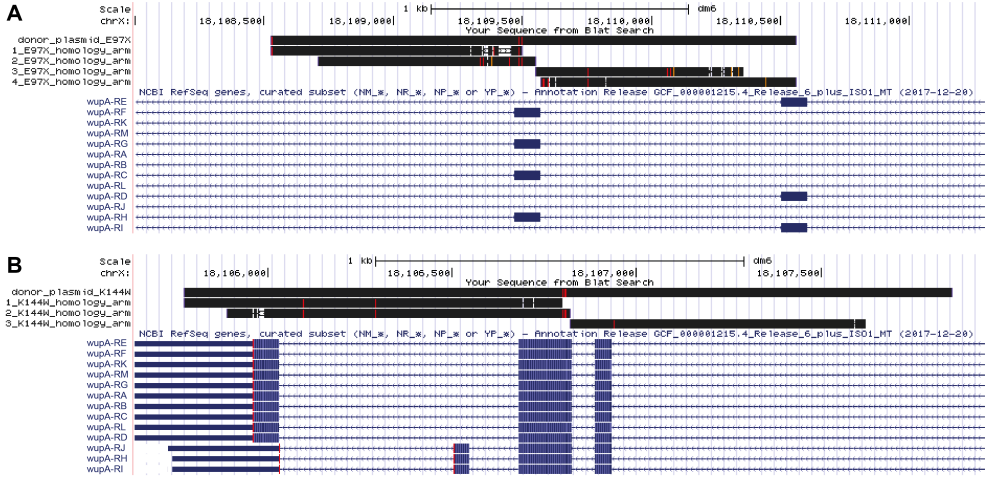

Figure 10.3: BLAT results of the homology arms.
Both upstream and downstream homology arms in the (**A**) E97X and (**B**) K144W donor plasmids were sequenced ((**A**) 1_E97X_homology_arm – 4_E97X_homology_arm; (**B**) 1_K144W_homology_arm – 3_K144W_homology_arm). The sequence reads were aligned to *wupA* transcripts and the donor plasmid designs. No mismatches were found in the coding sequence of *wupA*. The 13 *wupA* transcripts were indicated in blue below. Differences in nucleotides are highlighted as follows: red – genome and query sequence have different bases at this position; orange – the query sequence has an insertion (or genome has a deletion/alignment gap) at this point; purple – the query sequence extends beyond the end of the alignment. Double horizontal lines are drawn to indicate when the alignment has gaps in both the genome and query sequence.

ONE 3xP3-DsRed-POSITIVE STRAIN AFTER MICROINJECTION K144W DONOR PLASMID

We injected more than 400 embryos from two rounds of microinjection to introduce the K144W variant and got only one 3xP3-DsRed-positive strain, when guide RNA1 was used. This strain was further investigated. To exclude general mistakes in our genome editing approach leading to no K144W positive strains, we performed genomic sequencing of the injection strain (Figure 10.2 and Supplementary Material) and the donor plasmid. Sequencing of both upstream and downstream homology arms in the donor plasmid revealed that the donor plasmid sequence was as designed (Figure 10.3B and Supplementary Material). We, therefore, excluded inaccurate design of the donor plasmid as a possibility

for failure next to the presence of the target sequence in the genome (Figure 10.2 and Supplementary Material).

DONOR PLASMID INTEGRATION AND INCORRECT INCORPORATION OF KNOCK-IN CASSETTE PBacDsRed INTO GUIDE RNA CUTTING SITE

We checked the 3xP3-DsRed-positive strain to exclude strains with vector backbone integration, which is a common phenomenon in CRISPR edited alleles, and to only keep the strains with integration of selection marker at the correct guide RNA1 cutting site to avoid genomic complications and off-target strains. PCR bands at expected sizes for both integration PCR 1 (1508bp) and integration PCR 2 (1356bp) were observed from the donor plasmid which was used as positive control for the vector backbone (Figures 10.4A-B and S1). No bands at expected sizes were observed from negative control sample w^{1118}. Positive and negative control samples indicated that the primer pairs for integration test were highly specific. PCR bands at expected sizes for both integration PCR 1 and 2 were observed from the 3xP3-DsRed-positive strain suggesting that integration of the vector backbone has occurred.

In parallel, we tested if the knock-in cassette PBacDsRed was correctly used as template for homology-directed repair. No bands at expected sizes (upstream PCR: 1588bp; downstream PCR: 1480bp) were observed from negative control sample w^{1118}, indicating high specificity of the PCR reactions (Figures 10.4C-D and S1). In the lane loaded with the downstream PCR product of the 3xP3-DsRed-positive strain we observed a weak signal at approximately 1600bp. The intensity was weaker than normal and occurred at a wrong size. We observed no PCR product for upstream PCR. This suggests that the insertion of cassette PBacDsRed into *wupA* gene locus did not occur as designed.

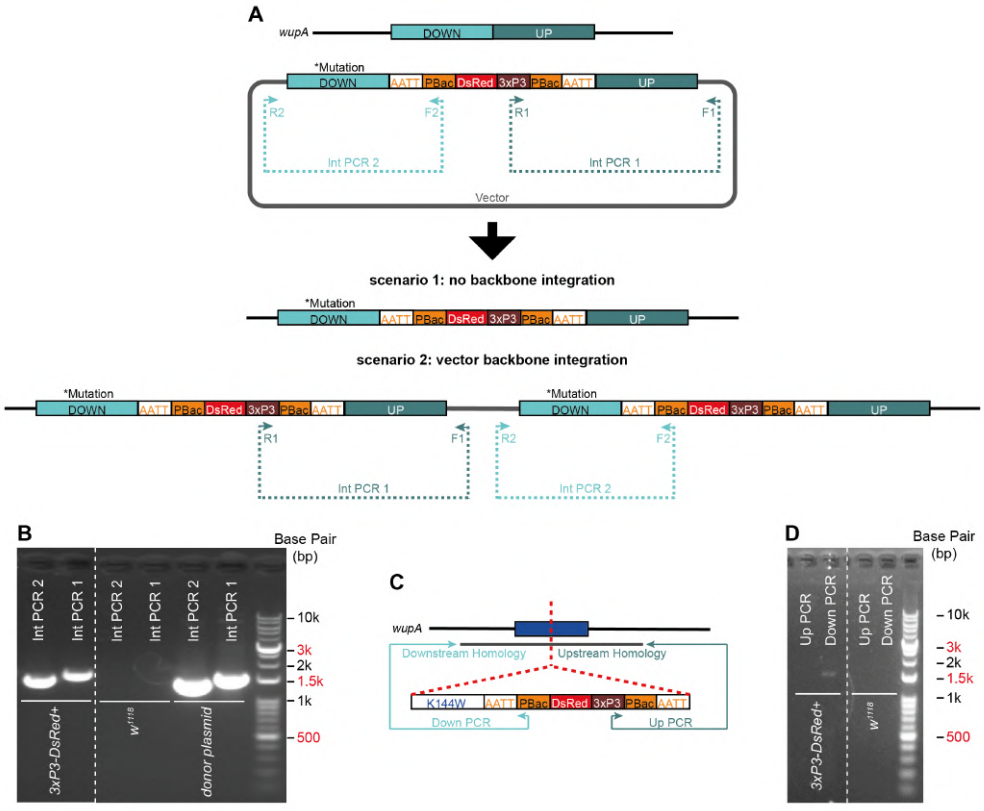

Figure 10.4: Donor plasmid integration and incorrect incorporation of knock-in cassette PBacDsRed into guide RNA cutting site. (**A**) Schematic of primer design (integration PCR 1 (Int PCR 1) and integration PCR 2 (Int PCR 2)) to check for integration of vector backbone in 3xP3-DsRed-positive strain. Correct editing will have no amplicon (scenario 1) and single integration of donor plasmid will have the amplicon (scenario 2). (**B**) Donor plasmid was used as a positive control and w^{1118} as a negative control. The 3xP3-DsRed-positive strain (*3xP3-DsRed+*) showed integration of vector backbone. (**C**) Schematic of the primer design to check for incorporation of knock-in cassette PBacDsRed into guide RNA cutting site to introduce K144W variant. (**D**) No bands were detected in upstream PCR (Up PCR) and downstream PCR (Down PCR) for negative control sample w^{1118}. The 3xP3-DsRed-positive strain (*3xP3-DsRed+*) showed a weak signal in the downstream PCR indicating that the knock-in cassette PBacDsRed was not located in the right locus due to missing amplicon in the upstream PCR. Primer sequences for both Int PCR and Up/Down PCR are provided in the Materials and Methods section. In both cases, (**B**) and (**D**), lanes were run on the same gel but were noncontiguous. Full-length gels are presented in Figure S1.

DISCUSSION

In the current study, we aimed to generate two *Drosophila melanogaster* strains heterozygous for the *wupA* variants E97X and K144W by the application of scarless CRISPR/Cas9-mediated genome editing to define cardiac pathomechanisms induced by *wupA* variants. We injected more than 800 embryos with in total 4 different guide RNAs to set up the two distinctive *wupA* mutant strains, but struggled to reach the step allowing screening for DsRed expression in the eyes for both variants (Figure 10.1). DsRed expression in the eyes suggests the introduction of the precise gene variant due to the simultaneous knock-in of the PBac-flanked 3xP3-DsRed selection marker. We observed that guide RNA1 to introduce E97X variant strongly affected survival rate.

Validation of our only 3xP3-DsRed-positive strain after CRISPR/Cas9-mediated genome editing to introduce the K144W variant in *wupA* revealed, that first, part of the backbone of the donor plasmid was inserted instead of only the selection marker. Second, the knock-in cassette PBacDsRed was not correctly incorporated into the guide RNA1 cutting site. We obtained a weak band at the wrong size in downstream PCR suggesting either a false-positive signal of an off-target strain or ends-in integration at the target locus. We did not further investigate the downstream PCR product by sequencing, even though it would have provided valuable information whether there was sufficient CRISPR/Cas9 activity to cause a double strand break. In addition, we know that vector backbone integration has occurred, therefore it would have been better to use a long PCR protocol. In line with that, complicated homology repair events may have occurred causing that the distance between the two primers became too long.

Due to genomic sequencing of the injection strain and the donor plasmids we were confident to exclude that a general mistake was made in the design of our genome editing approach which may be the explanation for having no positive stains with both distinctive *wupA* variants. Previously, this CRISPR/Cas9-mediated genome editing approach has been successfully used to generate variants in other *Drosophila melanogaster* genes such as *SH3PX1*, *tan* and *white*.[19,21,23] Therefore, we at least were confident that this genome editing approach is feasible for our model system. Nevertheless, CRISPR/Cas9 activity is highly dependent on guide RNA folding, thermodynamic stability of the sgRNA-DNA duplex as well as target accessibility within the context of chromatin.[31] These variabilities make it hard to predict activity at an untargeted locus such as the *wupA* gene. To maximise the chances of successful cleavage, it is advised to design multiple sgRNAs for each desired target[31] as we did (see Table 10.1). Since we injected more than 800 flies with 4 different guide RNAs, but only generated one 3xP3-DsRed-positive strain, this may suggest a low efficient design of the guide RNA plasmid. We selected the 20 nucleotide sequence of the guide RNA fulfilling many strong criteria (Table 10.1). Therefore the choice of U6:96Ab (U6-2) promotor may be causative for the low efficiency. Hence it would be interesting to test a more potent promoter, such as U6:3.[32]

In addition, generating one 3xP3-DsRed-positive strain out of 800 injected embryos also indicates a very low or no CRISPR/Cas9 activity. Furthermore our gel electrophoresis

was inconclusive whether the incorporation of the selection marker has happened at the target site or off-target. Our experimental strategy, injection of plasmids into wild-type seems to reveal low or no activity of CRISPR/Cas9-mediated double strand breaks at the target sites and therefore selecting a more optimized CRISPR tool such as a fully transgenic strategy may boost cleavage activity.[33] One disadvantage of this strategy is that first the fully transgenic flies need to be set up, so the overall time needed for the completion of the CRISPR/Cas9 approach will be longer.

The following explanations are based on the assumption that CRISPR/Cas9 activity was sufficient to cause double strand breaks. The inclusion of the large PBacDsRed cassette from the donor plasmid into the *wupA* gene may interrupt TnI expression and as a consequence affects viability of the CRISPR edited strains. Large indels such as the PBacDsRed cassette in the repair process of double strand breaks targeted to constitutively spliced coding exons may be sufficient to produce a non-functional protein.[34] We were then wondering if our intended changes affected constitutively spliced coding exons. According to Flybase, the *wupA* gene consists of 10 exons and differential splicing produces 13 transcripts leading to 13 protein isoforms (Figure 10.5A). There are four different variants of exon 6 (6a1/6a, 6a2/6b, 6b1/6c and 6b2/6d) and isoforms differing at this exon are mutually exclusive.[35] The E97X variant is located in exon 6b2 and since this exon is only spliced into the transcripts wupA-RC, wupA-RF, wupA-RG and wupA-RH, hence the E97X variant will affect four of the 13 transcripts. The K144W variant is located in exon 8 which is a mandatory exon of all transcripts. Therefore, by trying to introduce the E97X and K144W variants, a different number of transcripts was affected. In the case of K144W, this led to complete non-functional TnI proteins of one allele, while in the case of E97X only four TnI isoforms of one allele were affected.

Using the same technique to target constitutive exons of *Mhc*, another gene encoding the sarcomeric protein myosin heavy chain, resulted in the successful generation of mutant lines. In the Supplementary Material we provide the design and the validation of our *Mhc* mutant strain heterozygous for the R402Q gene variant (Figure S2 and Table S1).

Genome editing by CRISPR causing reduced numbers of TnI isoforms or complete depletion of TnI on one allele seems to be detrimental in *Drosophila melanogaster*. One reason may be that TnI plays an important role during early development in *Drosophila melanogaster*.[37] TnI-depleted cells lose apico-basal polarity and reduce proliferation.[38] Furthermore, TnI is expressed before muscle progenitors begin to fuse in *Drosophila melanogaster*, and sarcomere morphogenesis is affected by TnI depletion as Z discs fail to form.[39]

Another reason for having no positive strains may be the localization of the *wupA* itself. TnI is encoded in the haplolethal region 16F.[36] Haplolethality is caused by the one dose presence of a gene locus instead of the double dose.[40] Easy applicable genetic manipulation made *Drosophila melanogaster* to the preferred model system to study systematically this unusual phenomenon.[41,42] A comprehensive inventory of haploinsufficient genes revealed that six haplolethal genes are present *Drosophila melanogaster*.[43] The effect and consequence of

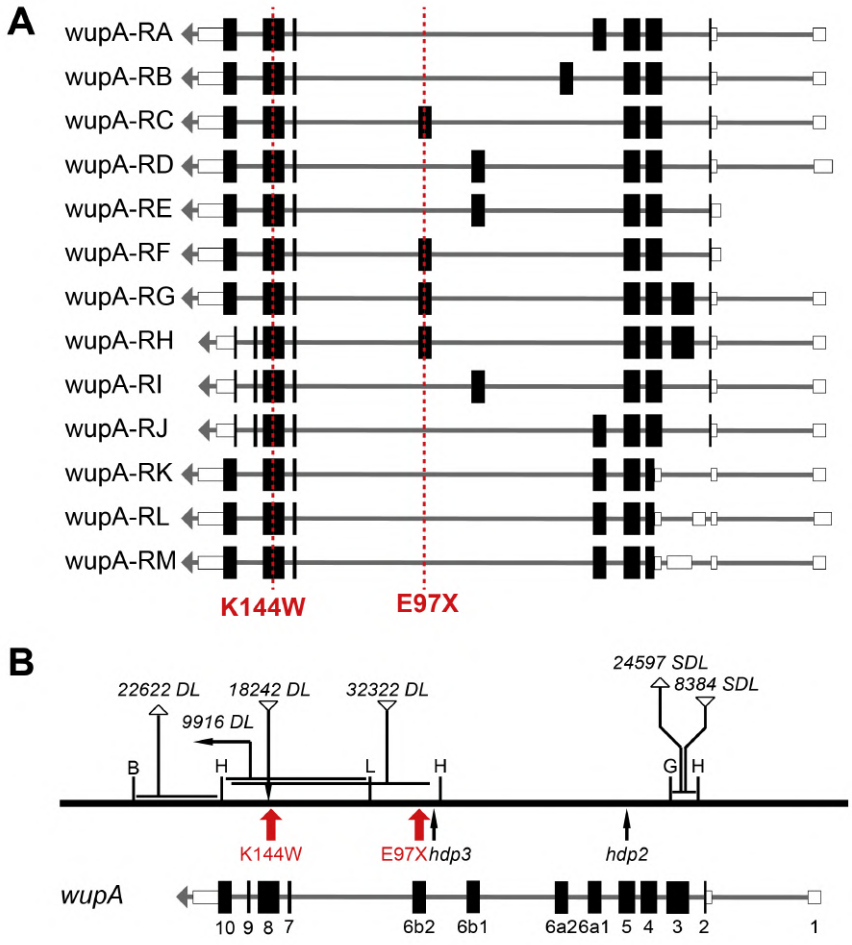

Figure 10.5: Transcripts of the *wupA* gene and molecular map of *wupA* gene variants. (**A**) Representation of the TnI-coding (black) and non-coding (white) exons of the 13 transcripts for *wupA*. Arrow head indicates the direction of transcription for this gene. Dashed red lines indicate the affected exons by introduction of the *wupA* gene variants E97X and K144W. (**B**) Different *wupA* gene variants lead to different phenotypes ranging from viable, semi-dominant lethal (SDL) to dominant lethal (DL). Rearrangements affecting at least one breakpoint in the *wupA* gene lead to a (semi)-dominant lethal phenotype. Single letter code indicates the restriction sites of the relevant restriction enzymes: B, BamHI; G, BglII; H, HindIII; P, PstI, R; EcoRI; L, SalI. Horizontal lines between restriction sites indicate the range of uncertainty in the location of each breakpoint. So far four dominant lethal and two semi-dominant lethal gene variants were mapped: 22622DL (deletion of the chromosomal segment 16F-18D), 9916DL (inversion), 18242DL (insertion of 540bp), 32322DL (insertion of ~3kb), 8384SDL (insertion of ~8kb) and 24597SDL (deletion of ~0.4kb). Changes in the point mutation category are viable: $wupA^{hdp2}$ *Drosophilae melanogaster* carry a point mutation on all transcript isoforms resulting in an alanine to valine change (A116V in wupA-RG/RH; A31V in wupA-PK-PM; A55V in remaining isoforms) and $wupA^{hdp3}$ *Drosophilae melanogaster* fail to produce all exon 6b1-containing isoforms due to one nucleotide displacement of the 3' AG splice site. Red arrows indicate the position of the insertion sites for the large PBacDsRed cassettes for two variants E97X and K144W. Molecular map was adapted from.[36]

CRISPR editing of haplolethal region is rarely studied and only single reports can be found in the context of reducing the transmission of vector-borne diseases.[44] In addition, targeting with CRISPR/Cas putative haplolethal X-linked genes led to significant lethality at the embryonic and subsequent stages.[45]

The 16F region extends along 100 kb and includes at least 14 genes and the normal haplolethal function depends on the integrity of a critical 4-kb window of mostly non-coding sequences within the *wupA* transcription located toward the 3' end.[36] Dominant lethal variants in the haplolethal region, which are even lethal in heterozygotes, result from chromosomal rearrangements including insertions, inversions and deletions with at least one breakpoint in the TnI-encoding gene within the critical 4-kb window (Figure 10.5B).[36]

Besides this dominant lethal domain, there are two additional domains in the *wupA* gene in which rearrangements lead to a semi-dominant lethal phenotype or a recessive lethal phenotype. The three domains are located in untranslated regions: dominant lethal and semi-dominant lethal within the *wupA* gene and recessive lethal immediately upstream of this gene.[36] As indicated in the molecular map (Figure 10.5B), both variants, E97X and K144W, are within the critical 4-kB window. This suggests that the introduction of the nucleotide changes in combination with knock-in of the PBacDsRed cassette may affect one or several breakpoints in close proximity to the insertion site and consequently resulted in a dominant lethal phenotype of both CRISPR edited strains. While dominant lethality caused by chromosomal rearrangement of exon 8 has been observed before, such as the 540 bp insertion variant *18242 DL*,[36] our report may suggest dominant lethality also caused by an insertion in exon 6b2. In addition, this would indicate that the four transcripts, wupA-RC, wupA-RF, wupA-RG and wupA-RH, as highly relevant for viability.

LIMITATION OF THIS STUDY

A limitation of our study is the lethality of the study material that made it impossible to provide direct evidence for the cause of failure to make the *wupA* mutant strains.

CONCLUSION

As far as we know, this was the first trial to make E97X and K144W *wupA* strains by the application of scarless CRISPR/Cas9-mediated genome editing, we did not succeed to get any positive strains. Our approach to introduce nucleotide changes in combination with knock-in of the 3xP3-DsRed selection marker in the critical 4-kb window of the haplolethal region 16F may have failed either due to our experimental strategy, such as injection of plasmids, usage of a low efficient guide RNA promoter and low CRISPR/Cas9 activity, or by targeting a haplolethal region. We recommend to pay attention to select a more successful CRISPR/Cas9 strategy to modify nucleotides of haplolethal genes, such as for example transgenic flies or plasmids with a more potent guide RNA promoter. In addition, selecting another CRISPR/Cas9 approach, such as for example a Co-CRISPR strategy,[46,47] may not result in lethality due to the prevention of large selection marker cassette, but

still allowing rapid screening for CRISPR/Cas9-induced events. In summary, we showed that it is difficult to target *wupA* with our experimental CRISPR/Cas9 strategy and more systematic research is required regarding genome editing of haplolethal genes.

Conflict of Interest: The authors declare no conflict of interest. The funders had no role in the design of the study; in the collection, analyses, or interpretation of data; in the writing of the manuscript, or in the decision to publish the results.

Sources of funding: We acknowledge the support from the Netherlands Cardiovascular Research Initiative: An initiative with support of the Dutch Heart Foundation, CVON2014-40 DOSIS, CVON-STW2016-14728 and the Medical Delta. The funders had no role in study design, data collection and analysis, decision to publish, or preparation of the manuscript.

SUPPLEMENTARY FILES - ONLINE

https://drive.google.com/drive/folders/142Qu-xSO28VI2zAZVxI77v0M6fnDZogr

REFERENCES

1. Maron BJ, Towbin JA, Thiene G, Antzelevitch C, Corrado D, Arnett D, et al. Contemporary definitions and classification of the cardiomyopathies: an American Heart Association Scientific Statement from the Council on Clinical Cardiology, Heart Failure and Transplantation Committee; Quality of Care and Outcomes Research and Functional Genomics and Translational Biology Interdisciplinary Working Groups; and Council on Epidemiology and Prevention. *Circulation*. 2006;113(14):1807-16.
2. Walsh R, Mazzarotto F, Whiffin N, Buchan R, Midwinter W, Wilk A, et al. Quantitative approaches to variant classification increase the yield and precision of genetic testing in Mendelian diseases: the case of hypertrophic cardiomyopathy. *Genome Med*. 2019;11(1):5.
3. Maron BJ, Towbin JA, Thiene G, Antzelevitch C, Corrado D, Arnett D, et al. Contemporary definitions and classification of the cardiomyopathies: an American Heart Association Scientific Statement from the Council on Clinical Cardiology, Heart Failure and Transplantation Committee; Quality of Care and Outcomes Research and Functional Genomics and Translational Biology Interdisciplinary Working Groups; and Council on Epidemiology and Prevention. *Circulation*. 2006;113(14):1807-16.
4. Walsh R, Thomson KL, Ware JS, Funke BH, Woodley J, McGuire KJ, et al. Reassessment of Mendelian gene pathogenicity using 7,855 cardiomyopathy cases and 60,706 reference samples. *Genet Med*. 2017;19(2):192-203.
5. Mogensen J, Hey T, Lambrecht S. A Systematic Review of Phenotypic Features Associated With Cardiac Troponin I Mutations in Hereditary Cardiomyopathies. *Can J Cardiol*. 2015;31(11):1377-85.
6. Stocker H, Gallant P. Getting started : an overview on raising and handling Drosophila. *Methods Mol Biol*. 2008;420:27-44.
7. Heineke J, Molkentin JD. Regulation of cardiac hypertrophy by intracellular signalling pathways. *Nat Rev Mol Cell Biol*. 2006;7(8):589-600.
8. Wolf MJ. Modeling dilated cardiomyopathies in Drosophila. *Trends Cardiovasc Med*. 2012;22(3):55-61.
9. Bier E, Bodmer R. Drosophila, an emerging model for cardiac disease. *Gene*. 2004;342(1):1-11.
10. Taghli-Lamallem O, Plantie E, Jagla K. Drosophila in the Heart of Understanding Cardiac Diseases: Modeling Channelopathies and Cardiomyopathies in the Fruitfly. *J Cardiovasc Dev Dis*. 2016;3(1).
11. Bollen IAE, Schuldt M, Harakalova M, Vink A, Asselbergs FW, Pinto JR, et al. Genotype-specific pathogenic effects in human dilated cardiomyopathy. *J Physiol*. 2017;595(14):4677-93.
12. Mogensen J, Kubo T, Duque M, Uribe W, Shaw A, Murphy R, et al. Idiopathic restrictive cardiomyopathy is part of the clinical expression of cardiac troponin I mutations. *J Clin Invest*. 2003;111(2):209-16.
13. Mogensen J, Murphy RT, Kubo T, Bahl A, Moon JC, Klausen IC, et al. Frequency and clinical expression of cardiac troponin I mutations in 748 consecutive families with hypertrophic cardiomyopathy. *J Am Coll Cardiol*. 2004;44(12):2315-25.
14. Andersen PS, Havndrup O, Hougs L, Sorensen KM, Jensen M, Larsen LA, et al. Diagnostic yield, interpretation, and clinical utility of mutation screening of sarcomere encoding genes in Danish hypertrophic cardiomyopathy patients and relatives. *Hum Mutat*. 2009;30(3):363-70.
15. van den Wijngaard A, Volders P, Van Tintelen JP, Jongbloed JD, van den Berg MP, Lekanne Deprez RH, et al. Recurrent and founder mutations in the Netherlands: cardiac Troponin I (TNNI3) gene mutations as a cause of severe forms of hypertrophic and restrictive cardiomyopathy. *Neth Heart J*. 2011;19(7-8):344-51.
16. Wolf MJ, Amrein H, Izatt JA, Choma MA, Reedy MC, Rockman HA. Drosophila as a model for the identification of genes causing adult human heart disease. *Proc Natl Acad Sci U S A*. 2006;103(5):1394-9.
17. Deak, II, Bellamy PR, Bienz M, Dubuis Y, Fenner E, Gollin M, et al. Mutations affecting the indirect flight muscles of Drosophila melanogaster. *J Embryol Exp Morphol*. 1982;69:61-81.
18. Lin SC, Chang YY, Chan CC. Strategies for gene disruption in Drosophila. *Cell Biosci*. 2014;4(1):63.
19. Gratz SJ, Ukken FP, Rubinstein CD, Thiede G, Donohue LK, Cummings AM, et al. Highly specific and efficient CRISPR/Cas9-catalyzed homology-directed repair in Drosophila. *Genetics*. 2014;196(4):961-71.
20. Gratz SJ, Cummings AM, Nguyen JN, Hamm DC, Donohue LK, Harrison MM, et al. Genome engineering of Drosophila with the CRISPR RNA-guided Cas9 nuclease. *Genetics*. 2013;194(4):1029-35.
21. Kondo S, Ueda R. Highly improved gene targeting by germline-specific Cas9 expression in Drosophila. *Genetics*. 2013;195(3):715-21.
22. Elliott P, Andersson B, Arbustini E, Bilinska Z, Cecchi F, Charron P, et al. Classification of the cardiomyopathies: a position statement from the European Society Of Cardiology Working Group on Myocardial and Pericardial Diseases. *Eur Heart J*. 2008;29(2):270-6.
23. Lamb AM, Walker EA, Wittkopp PJ. Tools and strategies for scarless allele replacement in Drosophila using CRISPR/Cas9. *Fly (Austin)*. 2017;11(1):53-64.
24. Shalem O, Sanjana NE, Zhang F. High-throughput functional genomics using CRISPR-Cas9. *Nat Rev Genet*. 2015;16(5):299-311.
25. Barbas JA, Galceran J, Torroja L, Prado A, Ferrus A. Abnormal muscle development in the heldup3 mutant of Drosophila melanogaster is caused by a splicing defect affecting selected troponin I isoforms. *Mol Cell Biol*. 1993;13(3):1433-9.
26. Prado A, Canal I, Ferrus A. The haplolethal region at the 16F gene cluster of Drosophila melanogaster: structure and function. *Genetics*. 1999;151(1):163-75.

27. Sahota VK, Grau BF, Mansilla A, Ferrus A. Troponin I and Tropomyosin regulate chromosomal stability and cell polarity. *J Cell Sci*. 2009;122(Pt 15):2623-31.
28. Casas-Tinto S, Ferrus A. Troponin-I mediates the localization of selected apico-basal cell polarity signaling proteins. *J Cell Sci*. 2019;132(8).
29. Marin MC, Rodriguez JR, Ferrus A. Transcription of Drosophila troponin I gene is regulated by two conserved, functionally identical, synergistic elements. *Mol Biol Cell*. 2004;15(3):1185-96.
30. Lindsley DL, Sandler L, Baker BS, Carpenter AT, Denell RE, Hall JC, et al. Segmental aneuploidy and the genetic gross structure of the Drosophila genome. *Genetics*. 1972;71(1):157-84.
31. Barbas JA, Galceran J, Krah-Jentgens I, de la Pompa JL, Canal I, Pongs O, et al. Troponin I is encoded in the haplolethal region of the Shaker gene complex of Drosophila. *Genes Dev*. 1991;5(1):132-40.
32. Keppy DO, Denell RE. A mutational analysis of the triplo-lethal region of Drosophila melanogaster. *Genetics*. 1979;91(3):421-41.
33. Cook RK, Christensen SJ, Deal JA, Coburn RA, Deal ME, Gresens JM, et al. The generation of chromosomal deletions to provide extensive coverage and subdivision of the Drosophila melanogaster genome. *Genome Biol*. 2012;13(3):R21.
34. Champer J, Wen Z, Luthra A, Reeves R, Chung J, Liu C, et al. CRISPR Gene Drive Efficiency and Resistance Rate Is Highly Heritable with No Common Genetic Loci of Large Effect. *Genetics*. 2019;212(1):333-41.
35. Fasulo B, Meccariello A, Morgan M, Borufka C, Papathanos PA, Windbichler N. A fly model establishes distinct mechanisms for synthetic CRISPR/Cas9 sex distorters. *PLoS Genet*. 2020;16(3):e1008647.
36. Beall CJ, Fyrberg E. Muscle abnormalities in Drosophila melanogaster heldup mutants are caused by missing or aberrant troponin-I isoforms. *J Cell Biol*. 1991;114(5):941-51.
37. Nongthomba U, Clark S, Cummins M, Ansari M, Stark M, Sparrow JC. Troponin I is required for myofibrillogenesis and sarcomere formation in Drosophila flight muscle. *J Cell Sci*. 2004;117(Pt 9):1795-805.
38. Nikonova E, Kao SY, Spletter ML. Contributions of alternative splicing to muscle type development and function. *Semin Cell Dev Biol*. 2020.
39. Kent WJ. BLAT–the BLAST-like alignment tool. *Genome Res*. 2002;12(4):656-64.
40. Kent WJ, Sugnet CW, Furey TS, Roskin KM, Pringle TH, Zahler AM, et al. The human genome browser at UCSC. *Genome Res*. 2002;12(6):996-1006.
41. Hoskins RA, Phan AC, Naeemuddin M, Mapa FA, Ruddy DA, Ryan JJ, et al. Single nucleotide polymorphism markers for genetic mapping in Drosophila melanogaster. *Genome Res*. 2001;11(6):1100-13.
42. Horn C, Jaunich B, Wimmer EA. Highly sensitive, fluorescent transformation marker for Drosophila transgenesis. *Dev Genes Evol*. 2000;210(12):623-9.
43. Gloor GB, Preston CR, Johnson-Schlitz DM, Nassif NA, Phillis RW, Benz WK, et al. Type I repressors of P element mobility. *Genetics*. 1993;135(1):81-95.

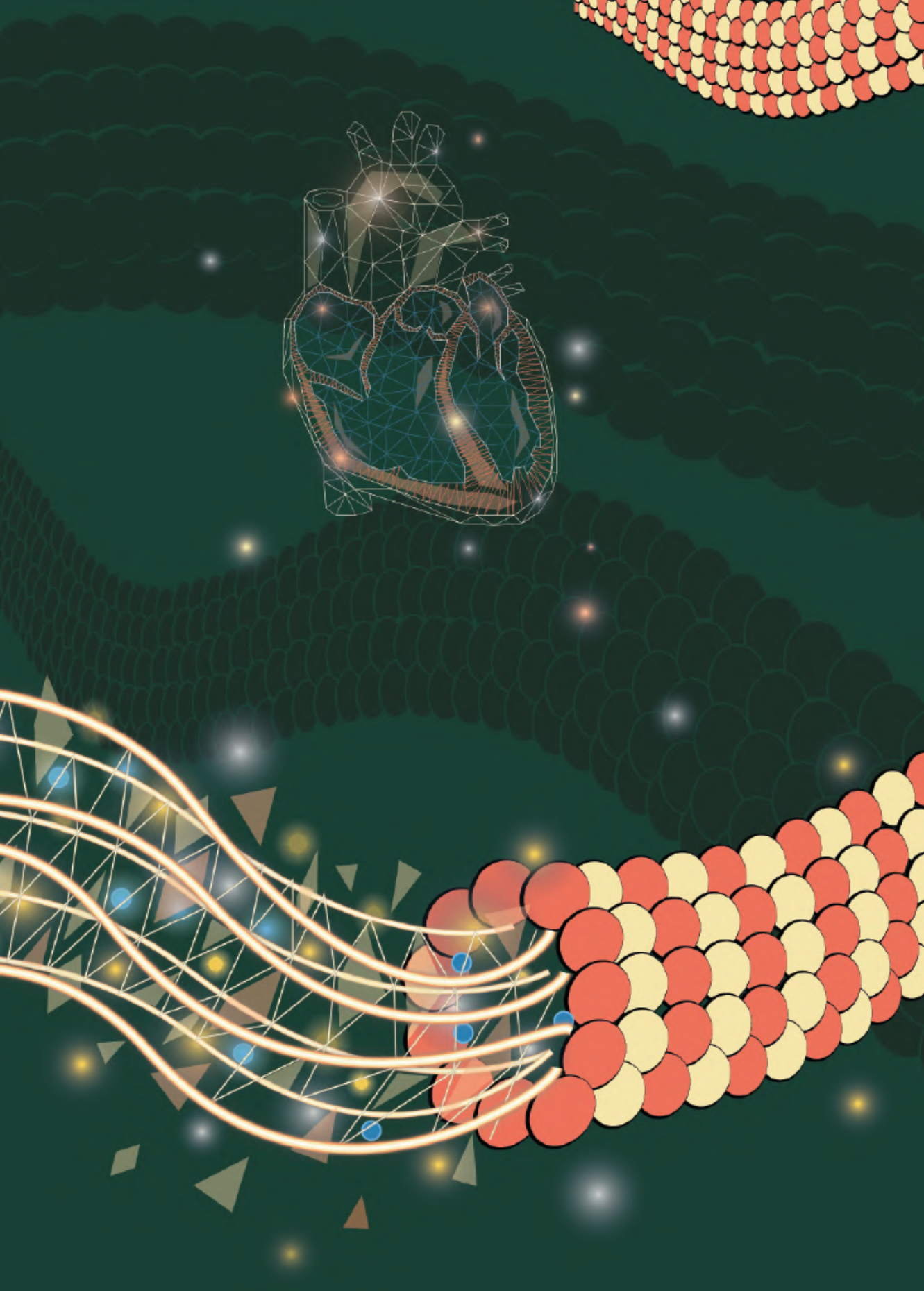

Chapter 11

Characterization of CRISPR/Cas9-edited *Drosophila melanogaster* strains with *Mhc* variants R402Q and S1376M

Larissa M. Dorsch, Pedro Espinosa González, Valentijn J. Jansen, Diederik WD. Kuster, Jolanda van der Velden

Manuscript in preparation.

ABSTRACT

BACKGROUND

Hypertrophic cardiomyopathy (HCM) is the most frequent inherited cardiac disease. In about one third of HCM patients the causative pathogenic gene variant is in *MYH7*, that encodes β-myosin heavy chain (β-MHC). Previously, *Drosophila melanogaster* has been demonstrated as a powerful tool to investigate Mhc function. Therefore, we aimed to assess the potential of *Drosophila melanogaster* as a model organism for HCM-causing *MYH7* variants.

METHODS

We generated clustered, regularly interspaced short palindromic repeats (CRISPR) / CRISPR-associated (cas)9-edited *Drosophila melanogaster* carrying either the *Mhc* gene variant R402Q or S1376M. Both variants represent orthologues of the clinically relevant human *MYH7* variants R403Q and T1377M. We determined contractile properties and the expression levels and phosphorylation of the sarcomeric proteins in semi-intact heart tube preparations. In addition, lumen and heart muscle areas of transversal cuts of the heart tube of female, homozygous transgenic flies were quantified and immunofluorescence of Mhc was performed.

RESULTS

We confirmed the successful set-up of scarless CRISPR/Cas9-edited hetero- and homozygous *Mhc* mutant flies. Our molecular analyses revealed no changes in expression of Mhc and other sarcomeric (phospho-)proteins. Morphological abnormalities were also absent in *Mhc* mutant strains illustrated by similar lumen and heart muscle areas, and Mhc localization and spacing as observed in control flies. However, both *Mhc* mutant strains revealed impaired contractility evident from reduced peak height, fractional shortening and time to peak compared to wild-type flies.

CONCLUSION

Taken together, we observed no molecular or morphological abnormalities in female flies homozygous for the *Mhc* variants R402Q and S1376M. Our data suggests that flies with *Mhc* R402Q and S1376M variants had a functional phenotype which was not caused by molecular biological and morphological abnormalities. Since our mutant *Drosophila melanogaster* strains show early mutation-mediated impaired contractile function, this model system may be used to study secondary disease mechanisms that underlie cardiac remodelling in HCM.

INTRODUCTION

Hypertrophic cardiomyopathy (HCM) is the most frequent inherited cardiac disease with a prevalence of 1:200 to 1:500.[1] HCM entails hypertrophy, that is often asymmetrical, of the left ventricle in the absence of other causes for hypertrophy, and histological features of myocyte hypertrophy, myofibrillar disarray and interstitial fibrosis.[2,3] Left ventricular diastolic dysfunction has been reported as a hallmark of HCM that occurs in the majority of patients.[4,5] Dominant pathogenic variants in genes that encode sarcomeric proteins cause inherited forms of HCM in 60% of all cases.[6] Two distinct genes (*MYH6* and *MYH7*) encode for two myosin heavy chain (MHC) isoforms, the α- and β-form, with β-MHC being the predominate in human ventricular myocardium.[7] Mutation hotspots are found at highly conserved residues of *MYH7* gene, encoding β-MHC, and in rare cases patients show a *MYH6/MYH7* hybrid gene.[7,8] About one third of the HCM cases are caused by heterozygous mutations in *MYH7*.[6] However, the genotype-phenotype relationship is not straightforward, as the age of onset and clinical presentation are highly variable even in people that carry the same mutation, spanning from asymptomatic gene variant carrier to development of severe hypertrophy at young age.[9,10] The first identified pathogenic variant to cause HCM was Arg403Gln (R403Q) in *MYH7*.[11] Until today, more than 400 different variants in *MYH7* have been identified to cause HCM.[12] In a large cohort of unrelated patients with HCM, *MYH7* variant carriers were diagnosed at a younger age and had more hypertrophy compared to HCM patients without *MYH7* variants, but sudden death among first-degree relatives had not a greater frequency.[9] In addition, the Sarcomeric Human Cardiomyopathy Registry (SHaRe) revealed that patients with mutations in *MYH7* had a higher risk of the overall composite outcome, atrial fibrillation and advanced heart failure compared to patients with *MYBPC3* mutations.[13]

Drosophila melanogaster is a well-studied genetic model organism for understanding molecular mechanisms of human disease and investigating disease gene functions. The *Drosophila melanogaster* proteome shows a 67% similarity and about 75% of human disease loci can be mapped to counterparts in *Drosophila melanogaster*.[14,15] In addition, it is a relatively inexpensive model system, easy to maintain with a short life cycle and causes minimal ethical and safety issues. Adult material becomes available 10 days post fertilization when kept at 25°C.[16] Previous studies revealed *Drosophila melanogaster* as an efficient model for functional studies in cardiomyopathies.[14,15] Likewise, *Drosophila melanogaster* serves as a powerful tool to investigate Mhc function because there is a single *Mhc* gene (CG17927), which encodes 20 unique Mhc isoforms via alternative RNA splicing.[17,18] The benefit of single gene rather than a multigene family is that there are no isoforms produced by other muscle myosin genes which could complicate the analysis or interfere with the results.

We aligned HCM-causing *MYH7* variants listed in our human tissue biobank with the *Mhc* sequence of *Drosophila melanogaster* to select two *MYH7* variants, the R403Q and Thr1377Met (T1377M). Our minimal requirement was that the orthologous amino acid to modify in *Drosophila melanogaster* should at least belong to the same physiochemical group. The MHC protein has two functional domains: the globular head region is mapped

from the amino-terminus until exon 22 and the elongated rod region starts at exon 23.[11] We studied the effect of the location of the gene variant by selecting one variant leading to an amino acid change in the head (R403Q) and one in the tail (T1377M) region of the protein. The selected R403Q variant has been associated with a shorter life expectancy.[7] Between different species including *Drosophila melanogaster*, this amino acid residue is highly conserved.[11] In a large cohort study, gene variants at the amino acid 1377 of β-MHC were identified as a mutational hot spot.[9] This variant is listed as "likely pathogenic" in ClinVar and *in silicon* prediction of pathogenicity suggests a deleterious effect on the mutant protein.[19]

In our study, we used scarless clustered, regularly interspaced, short palindromic repeats (CRISPR) / CRISPR-associated (Cas)9-mediated genome editing to specifically generate two *Drosophila melanogaster* strains with the *Mhc* variants R402Q and S1376M, which are the orthologues changes for the two human *MYH7* variants R403Q and T1377M, respectively. We chose the CRISPR/Cas9 approach because of the feasibility to co-inject Cas9 with a donor vector carrying the eye-specific selection marker 3xP3-DsRed which speeds up the screening process for mutant flies.[20] As mentioned before, there is one *Mhc* gene encoding multiple protein isoforms. Both gene variants are located in the constitutive exons 8 and 16 (exception Mhc-RT: exons 7 and 15, respectively) and therefore, will be present in all Mhc isoforms. To reflect the dominant transmission of inherited cardiomyopathies,[21] we aimed to engineer strains being heterozygous for the *Mhc* variants. The aim of this study was to assess the potential of *Drosophila melanogaster* as a model organism for HCM-causing *Mhc* variants.

METHODS

SEAMLESS CRISPR/CAS9-BASED GENOME EDITING WAS USED TO INTRODUCE THE R402Q AND S1376M VARIANTS

Clustered, regularly interspaced, short palindromic repeats (CRISPR)/CRISPR-associated (Cas)9-mediated mutagenesis was performed by WellGenetics Inc. (Taipei City, Taiwan) using modified methods of Kondo and Ueda,[22] such as injected plasmids instead of using transgenic CRISPR components. In brief, genomic DNA was obtained from injection strain w^{1118}. PCR was performed using KOD FX DNA polymerase (TOYOBO) on BioRad S1000 Thermal Cycler. Sequencing results were BLAT against *Drosophila melanogaster* genome (August 2014 Assembly, BDGP Release 6) using UCSC Genome Bioinformatics and the genomic codons option was selected for codon colouring.[23,24] The respective guide RNA (Table 11.1) was cloned into U6 promoter plasmid.

Table 11.1: Design of CRISPR target site, guide RNAs and homology arms.

	R402Q	**S1376M**
CRISPR target site [PAM]	CTTGCTGAAGCCCCGCATCA [AGG]	GCTGAGCAAGGCCAACGCTG [AGG]
CRISPR target strand	plus	plus

Table 11.1: Continued

		R402Q	S1376M
Cutting Site		+5981 nt from ATG of *Mhc*	+16356 nt from ATG of *Mhc*
Distance		-1 nt from breakpoint to cutting site of Cas9	+12 nt from breakpoint to cutting site of Cas9
Off target		0	0
GC%		60%	65%
T number at 17th to 20th nucleotides		1	1
Guide RNA primers	**Sense oligo**	5'– CTTCGCTTGCTGAAGC CCCGCATCA	5'– CTTCGCTGAGCAAGGC CAACGCTG
	Antisense oligo	5'– AAACTGATGCGGGGCT TCAGCAAGC	5'– AAACCAGCGTTGGCCT TGCTCAGC
PAM mutation		not required	GCTGAGCAAGGCCAACGCTG [AAG]
PAM mutation changes amino acid		no	no
Upstream homology arm	**Length**	1031bp	1033bp
	Location	+4950 nt to +5980 nt from ATG of *Mhc*	+15307 nt to +16339 nt from ATG of *Mhc*
	Forward oligo	5'- CGTTACCCAAGTTCCGT TTC	5'- ACAGCATGTTCCAACCA ACA
	Reverse oligo	5'- TCTGGGGCTTCAGCAAG TT	5'- CTGGCGCTGCAGATCGG C
	Synthesis fragment	-	5'- GCAAGGCCAACGCTGAA GCGCAAGTGTGGCGCAGCA AGTACGAGATGGATGGCGTT GCCCGCTCTGAGGAGCTGGA GGA
Down-stream homology arm	**Length**	1003bp	1058bp
	Location	+5985 nt to +6987 nt from ATG of *Mhc*	+16423 nt to +17480 nt from ATG of *Mhc*
	Forward oligo	5'- GGTCGGCAACGAGTTCG TCA	5'- AGCCAAGAGGAAGCTGC AG
	Reverse oligo	5'- TTTTTAGGGGGAAATGG TG	5'- GGCGGACACTTCGTTCA G

The donor plasmid containing a red fluorescent marker cassette with 3xP3 promoter driving DsRed expression in the eyes which was flanked by piggyBac (PBac) transposon ends and two homology arms with the gene variants was cloned into the pUC57-Kan vector (Supplementary Material: R402Q and S1376M Donor Designs). *Mhc*-targeting guide RNAs (100ng) and heat shock-inducible Cas9 (100ng) were supplied in DNA plasmids, together with donor plasmid (500ng) for microinjection into embryos of control strain w^{1118}. The first round of microinjection was done on [LWG208] w^{1118}, which was newly obtained from Bloomington Stock Number 6326 (SNP mapping stock, isogenic 2nd and 3rd chromosomes).[25] Since this is the isogenic background for Exelixis P and PBac insertions,

SNP variation for CRISPR editing would be reduced. However, it neither survived well nor gave high number of fertile crosses and positive strains. All further microinjections of R402Q and S1376M were therefore done on [LWG012] w^{1118} strain, obtained from Bloomington Stock Center. Identification of engineered strains was performed via the 3xP3-DsRed marker by screening for DsRed expression in the eye.[20,26] F1 flies carrying the 3xP3-DsRed selection marker were further validated by genomic PCR and sequencing. CRISPR generated a break in *Mhc* and was replaced by cassette PBacDsRed. Either *Sp* or *CyO* balancer was used for selection of heterozygous offspring. After molecular validation, the *Mhc* variants were balanced by *CyO*.

ANALYSIS OF CRISPR INTEGRATION OF THE SELECTION MARKER FOR R402Q AND S1376M VARIANTS

Genomic DNA was obtained from a single fly of each stock following single-fly DNA preparation using Gloor's protocol.[27] Injection strain w^{1118} was used as a negative control and both donor plasmids as positive controls for integration examination. PCR was performed using KOD FX DNA polymerase (TOYOBO, KFX-101) on BioRad S1000 Thermal Cycler (Table 11.2).

Table 11.2: Steps and conditions of thermo cycling for Integration and Validation PCR.

Steps	Temperature	Time	Cycles
Initial denaturation	94°C	2 min	1
Denaturation	98°C	10 sec	30
Annealing	55°C	30 sec	
Extension	68°C	2 min	
Final extension	68°C	5 min	1
End/Hold	15°C	Forever	

CRISPR/homology-directed repair may go through different repairing routes. Integration of donor plasmid in CRISPR editing alleles is a common phenomenon. "No integration" contains only one copy of selection marker. "Single integration of donor plasmid" contains the vector backbone, two copies of homology arms and selection marker. Integration test is to exclude alleles with donor vector integration and only keep the strains with simple editing to avoid the genomic complications.

For integration PCR 1, forward primer (R402Q: 5'-CAACTGTTGGGAAGGGCGAT; S1376M: 5'-CAACTGTTGGGAAGGGCGAT) was designed outside the upstream homology arm in the backbone plasmid and reverse primer (R402Q: 5'-CGAGGGTTCGAAATCGATAA; S1376M: 5'-CGAGGGTTCGAAATCGATAA) was designed at 3xP3 promoter. For integration PCR 2, forward primer (R402Q: 5'-TTTGACTCACGCGGTCGTTA; S1376M: 5'-TTTGACTCACGCGGTCGTTA) was designed at 3' PBac terminal and reverse primer (R402Q: 5'-CATTAGGCACCCCAGGCTTT; S1376M: 5'-CATTAGGCACCCCAGGCTTT) was designed outside the downstream homology arm in the backbone plasmid. While single integration of donor plasmid will have the amplicon, the corrected editing will not have the amplicon. 1kb Plus DNA RTU Ladder from Biomate (BR343-500) was used as reference

on a 1.2% (w/v) agarose gel and 0.5x TAE buffer.

CRISPR VALIDATION OF KNOCK-IN CASSETTE PBacDsRed FOR R402Q AND S1376M VARIANTS

Genomic DNA was obtained from a single fly of each stock following single-fly DNA preparation. Injection strain w^{1118} was used as a negative control. PCR was performed using KOD FX DNA polymerase (TOYOBO, KFX-101) on BioRad S1000 Thermal Cycler (Table 11.2). Using genomic PCR and sequencing methods to verify CRISPR alleles of *Mhc* by testing if the knock-in cassette PBacDsRed was correctly used as template for homology-directed repair and was incorporated into guide RNA1 cutting site. For upstream PCR, forward primer (R402Q: 5'-ATGTAAGTGGTCGCCAAACC; S1376M: 5'-TCTTCTTTCGAAGAGCTTTGGT) was designed at 5' outside the homology arm and reverse primer (R402Q: 5'-CGAGGGTTCGAAATCGATAA; S1376M: 5'-CGAGGGTTCGAAATCGATAA) was designed at 3xP3 promoter. For downstream PCR, forward primer (R 402Q: 5'-TTTGACTCACGCGGTCGTTA; S1376M: 5'-TTTGACTCACGCGGTCGTTA) was designed at 3' PBac terminal repeat and reverse primer (R402Q: 5'-GAGCGATGGCGGATAATTT; S1376M: 5'-CCTTCTTGCCTCCCTTGAG) was designed at 3' outside the downstream homology arm. Only cassette PBacDsRed, which was inserted into the gene locus will have the amplicon. 1kb Plus DNA RTU Ladder from Biomate (BR343-500) was used as reference on a 1.2% (v/v) agarose gel and 0.5x TAE buffer.

EXCISION OF 3xP3-DsRed SELECTION MARKER

Following DsRed-mediated identification of engineered strains, the marker cassette can be easily and scarlessly removed through a single cross to PBac transposase.[20,28] Therefore, either *w[1118]; Mhc R402Q CRISPR{PBacDsRed}/ CyO* or *w[1118]; Mhc S1376M CRISPR{PBacDsRed}/ CyO* were mated with Bloomington Stock Number 8285 *w[1118]; CyO, P{Tub-PBac\T}2/wg[Sp-1]*. To verify successful excision of selection marker (3xP3-DsRed) in either *w[1118]; Mhc R402Q CRISPR/ CyO* or *w[1118]; Mhc S1376M CRISPR/ CyO*, genomic DNA was obtained from single fly of each stock following single-fly DNA prep. Injection strain w^{1118} was used as a negative control. Forward primer (R402Q: 5'-ATACCAACAGCAAGCCTTCG; S1376M: 5'-CAGGTGTCTCAGCTGTCCAA) was designed at upstream homology arm and reverse primer (R402Q: 5'-TAGCAGGTCGACTGGTGATG; S1376M: 5'-GAGCGGGCAACGCCATCCAT) was designed at downstream homology arm. PCR was performed using KOD FX DNA polymerase (TOYOBO, KFX-101) on BioRad S1000 Thermal Cycler. 1kb Plus DNA RTU Ladder from Biomate (BR343-500) was used as reference on a 1.2% (w/v) agarose gel and 0.5x TAE buffer. Using the *w[1118]; Mhc R402Q CRISPR/ CyO* strain, the PCR product with expected size band (R402Q: 575bp) were excised and submitted to Mission Biotech for gel extraction and sequencing. Using the *w[1118]; Mhc S1376M CRISPR/ CyO* strain, the PCR product of the genomic PCR with the forward primer (5'-CAGGTGTCTCAGCTGTCCAA) and reverse primer (5'-GGAACAGCTCGGTGGAGTAG) was sequenced.

FLY STRAINS AND CULTURE

We used the following transgenic strains: *w[1118]; Mhc R402Q CRISPR/ CyO*, *w[1118]; Mhc R402Q CRISPR/ Mhc R402Q CRISPR*, *w[1118]; Mhc S1376M CRISPR/ CyO* and *w[1118]; Mhc S1376M CRISPR/ Mhc S1376M CRISPR*. [LWG012] w^{1118} injection strain was used as a wild-type control. Flies were maintained on a 2.6% (w/v) yeast, 1.7% (w/v) agar, 5.4% (w/v) sugar and 0.13% (w/v) nipagin medium in a humidified, temperature-controlled incubator at 25°C without a defined light-dark cycle.

PRO-Q DIAMOND AND SYPRO RUBY STAINING

Adult flies were anesthetized 21 days after birth with Fly Nap (Carolina Biological). Semi-intact heart tube preparations were made following Ocorr's protocol.[29] In brief, after an initial cut to remove the head, ventral nerve cord and legs, the preparation was submerged in an oxygenated, artificial hemolymph solution (108 mM NaCl, 8 mM $MgCl_2$, 5 mM KCl, 2 mM $CaCl_2$ dehydrate, 1 mM NaH_2PO_4, 5 mM HEPES, 4 mM $NaHCO_3$, 10 mM sucrose, 5 mM trehalose, pH 7.1). The posterior tip of the abdomen was cut off and the ventral abdominal cuticle including the abdominal organs was removed. The semi-intact heart tube preparations were collected in a microcentrifuge tube and homogenized in 10 µL/mg tissue 1× reducing sample buffer (106 mM Tris-HCl, 141 mM Tris-base, 2% (w/v) lithium dodecyl sulphate, 10% (v/v) glycerol, 0.51 mM ethylenediaminetetraacetic acid, 0.22 mM SERVA Blue G250, 0.18 mM Phenol Red, and 100 mM dithiothreitol) using a plastic tissue grinder. Proteins were denatured by heating to 99°C for 5 min. Debris was removed by centrifugation at maximum speed for 10 min in a microcentrifuge (Sigma, 1-15k).

Following the protocol of Zaremba,[30] 10 µg of protein lysates were separated on pre-cast SDS-PAGE 4-12% criterion gels. Gels were fixed in fixation solution (50% (v/v) methanol, 10% (v/v) acetic acid) for 1 h and according to the manufacturer's protocols stained for Pro-Q Diamond and SYPRO Ruby (both Life technologies). A Peppermint Stick molecular weight marker (Life technologies) and a precision Plus Protein Dual Colour Standards (Bio-Rad) were used for molecular weight estimation.

MYOSIN HEAVY CHAIN COMPOSITION

A specialized sodium dodecyl sulphate polyacrylamide gel electrophoresis (SDS-PAGE) was used to determine the myosin heavy chain isoform composition of semi-intact heart tube preparations. Female flies, age two weeks, were anesthetized with Fly Nap (Carolina Biological). Anesthetized flies were prepared so that of the abdomen only the dorsal cuticle with the heart tube surrounded by fat bodies was left. While dissecting, the preparation was submerged in F60 buffer (60 mM KCl, 30 mM Imidazole and 2 mM $MgCl_2$, pH 7.4) containing protease and phosphatase inhibitors. 5 semi-intact heart tube preparations were collected in a microcentrifuge tube, 100 µL F60 buffer including 1% (v/v) triton X-100 was added and the tissue was homogenized using a plastic tissue grinder. Supernatant was discarded after centrifugation at maximum speed for 10 min in a microcentrifuge (Sigma, 1-15k). Pellet was resuspended in 100 µL SDS sample buffer, boiled for 5 min at 95°C

and centrifuged at maximum speed for 10 min to remove cell debris. The stacking gel contained a 4% (w/v) acrylamide concentration (pH 6.7), and the separating gel contained 7% (w/v) acrylamide (pH 8.7) with 30% (v/v) glycerol. The gels were run for 24 h at 15°C and a constant voltage of 275 V. Thereafter, the gels were silver-stained, scanned, and analysed with ImageQuant TL (GE Healthcare) software.

HISTOLOGICAL ANALYSIS OF HEART MUSCLE AND LUMEN AREAS

Adult female flies were collected 21 days after birth and fixed in Telly's fixative (60% (v/v) ethanol, 3.33% (v/v) formalin, 4% (v/v) glacial acetic acid) overnight at 4°C. According to the protocol of Xu,[31] the samples were embedded in paraffin after ethanol dehydration through sequential gradients and xylene washes. Paraffin blocks were sectioned serially at 4 µm thickness in transverse orientation. Sections were rehydrated, stained with hematoxylin and eosin, and imaged using Microscope Zeiss FLM imager M.1 63x oil objective. The heart wall thickness was measured by QuPath software.

WHOLE MOUNT IMMUNOSTAINING AND MICROSCOPY

Semi-intact heart tube preparations of female flies were prepared 14 days after birth as described in the section *Pro-Q Diamond and SYPRO Ruby staining* for whole mount staining and arrested using 10 mM EGTA in artificial hemolymph for 10 min. The relaxed, semi-intact heart tubes were fixed in 4% (w/v) paraformaldehyde and bleached 2x 15 min in 1x TBS (20 mM Tris, 150 mM NaCl) including 3% (v/v) H_2O_2. Samples were permeablized in 1x phosphate buffered saline (PBS, 154 mM NaCl, 2.4 mM KH_2PO_4, 7.7 mM Na_2HPO_4, pH 7.4) containing 0.1% (v/v) Triton X-100 for 30 min, blocked in 1x PBS containing 1% (w/v) BSA and 10% (v/v) donkey serum for 30 min and then incubated overnight at 4°C with primary antibodies: mouse anti-Mhc (1:250; DSHB Hybridoma Product 3E8-3D3 deposited to DSHB by Saide, J.D.) and rabbit anti-α-tubulin (1:100; abcam ab52866). Secondary antibody incubation was performed at room temperature for 1h: Alexa Fluor 555- and Alexa Fluor 647-conjugated secondary antibodies (1:250; Invitrogen), DAPI (1:1.000; Sigma-Aldrich) and Alexa Fluor 488 Phalloidin (1:100; Thermo Fisher Scientific). The samples were then placed in slides and mounted with mowiol 4-88. The images were taken with a 60x 1.4 NA oil-objective on the Nikon A1R confocal microscope (Nikon) and analysed with ImageJ software (National Institute of Health).

MEASUREMENT OF CARDIAC PARAMETERS

Semi-intact heart tube preparations of female flies were prepared at 14 days after birth as described in the section *Pro-Q Diamond and Sypro Ruby staining* and artificial hemolymph was refreshed. The dish, containing on average 9 fly preparations, was placed in a high-throughput inverted microscope (Olympus 20x 0.75 aperture objective lens, Olympus, Shinjuku, Japan) set-up (CytoCypher, Amsterdam, the Netherlands) and the heart tubes were visualized. We used the camera-based MultiCell microscope system (CytoCypher, Amsterdam, the Netherlands) and Ionoptix LLC software (Westwood, Massachusetts) to measure functional cardiac parameters at 25°C. Temporal data were determined by pixel correlation (Sampling Units: Frequency (Hz)) and spatial data by SoftEdge as an acquisition

task and the Box mode (Sampling Units: Period (s)). Videos were recorded for 10 sec. The software CytoSolver (CytoCypher) was used to analyse the transients.

STATISTICAL ANALYSIS

Data were analysed with GraphPad Prism version 8.0 and data in the figures are presented as means ± standard errors of the mean (SEM) per group. The distribution of each data set was determined by Q-Q plots and then double checked by Kolmogorov-Smirnov and Shapiro Wilk tests after data collection was completed. Normally distributed data were analysed with ordinary one-way ANOVA and non-parametric data with Kruskal-Wallis test. In both cases, Dunnett's multiple comparisons was used as a post-hoc test. A two-sided $p<0.05$ was considered to indicate statistical significance. Figures were assembled with Adobe Illustrator CS6.

RESULTS

DESIGN OF GUIDE RNAs AND VALIDATION OF HOMOLOGY ARMS OF DONOR PLASMIDS

For the design of the guide RNAs the following four criteria were taken into account: distance from knock-in site to cutting site of Cas9, predicted off targets on other chromosomes, GC content of target sequence and thymine numbers at 17^{th} to 20^{th} nucleotide of the guide RNA target site. We considered the quality of the designed guide RNAs as strong because the distance was shorter than 50 base pairs (bp), no prediction of off-targets on other chromosomes, 45%-70% GC content of the target sequence and 0 or 1 thymine (Table 11.1).

To verify that all guide RNA loci for the *Mhc* R402Q and S1376M variants were as indicated, we performed genomic sequencing of the injection strain. Guide RNAs and the 3 independent reads of the injection strain were free of any SNPs. Per variant, the target sequence of the guide RNA was present in the genome of the injection strain (Figure 11.1 and Supplementary Material). With this information, guide RNAs and donor plasmids were prepared.

Both upstream and downstream homology arms in both donor plasmids were sequenced to confirm the specificity to *Mhc/CG17927*. BLAT results of the homology arms revealed two mismatches for the R402Q variant and four mismatches for the S1376M variant in the coding sequence of *Mhc/CG17927* (Figure 11.2 and Supplementary Material).
Five of the six mismatches did not lead to amino acid changes and were considered synonymous SNPs. One mismatch caused an amino acid change which was also observed in the injection strain, suggesting this mismatch is a missense mutation.

VALIDATION OF POSITIVE STRAINS AFTER MICROINJECTION OF R402Q AND S1376M DONOR PLASMIDS

We performed two rounds of microinjection in more than 400 embryos per gene variant. Microinjection of the injection strain [LWG208] w^{1118} was not successful as indicated by

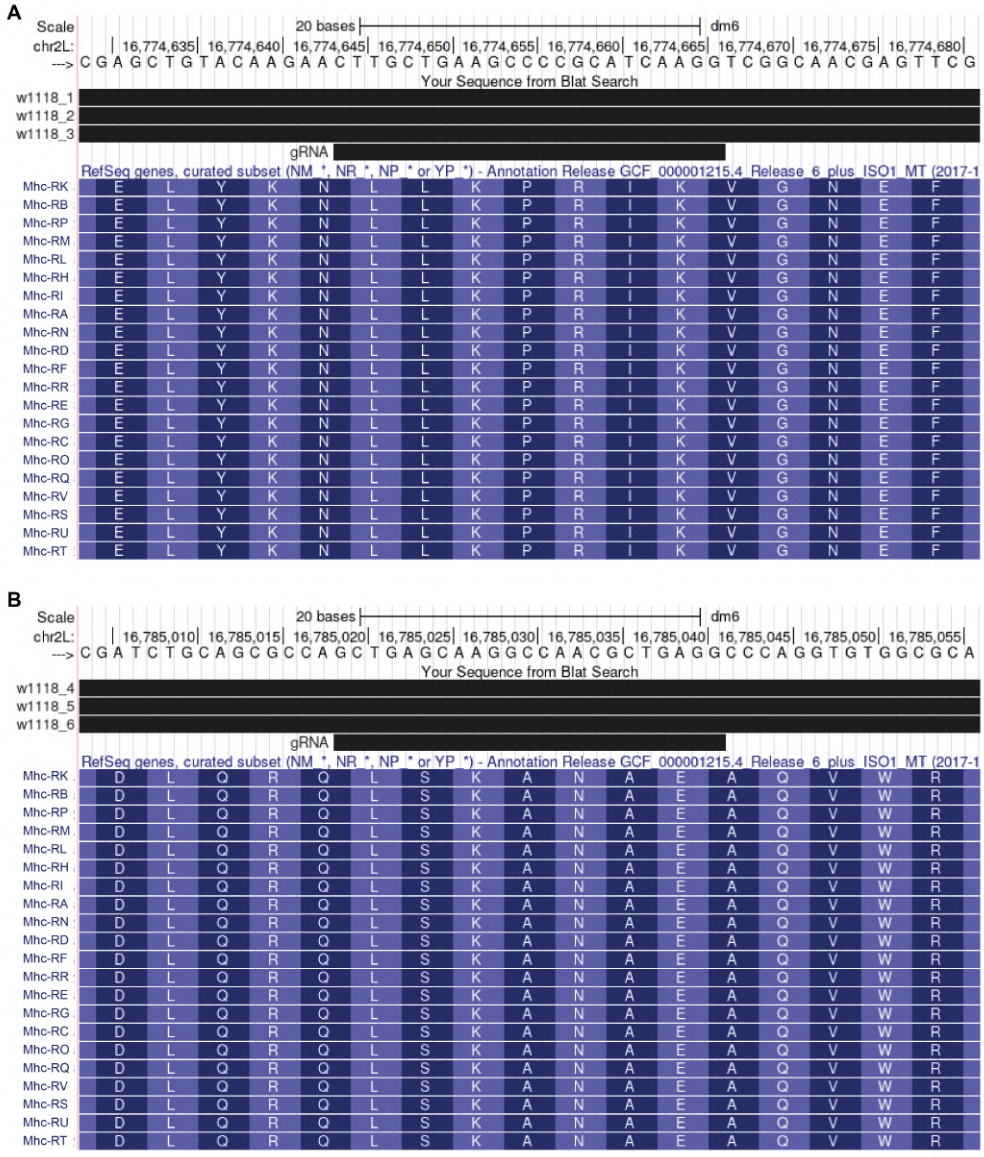

Figure 11.1: BLAT results show alignment of the guide RNAs and independent reads of the injection strain with the *Mhc* transcripts. The target sequence of both guide RNAs (Table 11.1) for the (**A**) R402Q and the (**B**) S1376M variant were present in three independent reads (**A**) (w1118_1, w1118_2, w1118_3) and (**B**) (w1118_4, w1118_5, w1118_6) of the injection strain. The independent read sequences of the injection strain are available in the Supplementary Material. The 21 *Mhc* transcripts were indicated below with codon boundaries depicted by alternating lighter and darker blue shades. Continuous black bars of the target sequence of guide RNAs and the independent reads of the injection strains indicate completely matched sequence overlap with the *Mhc* transcripts.

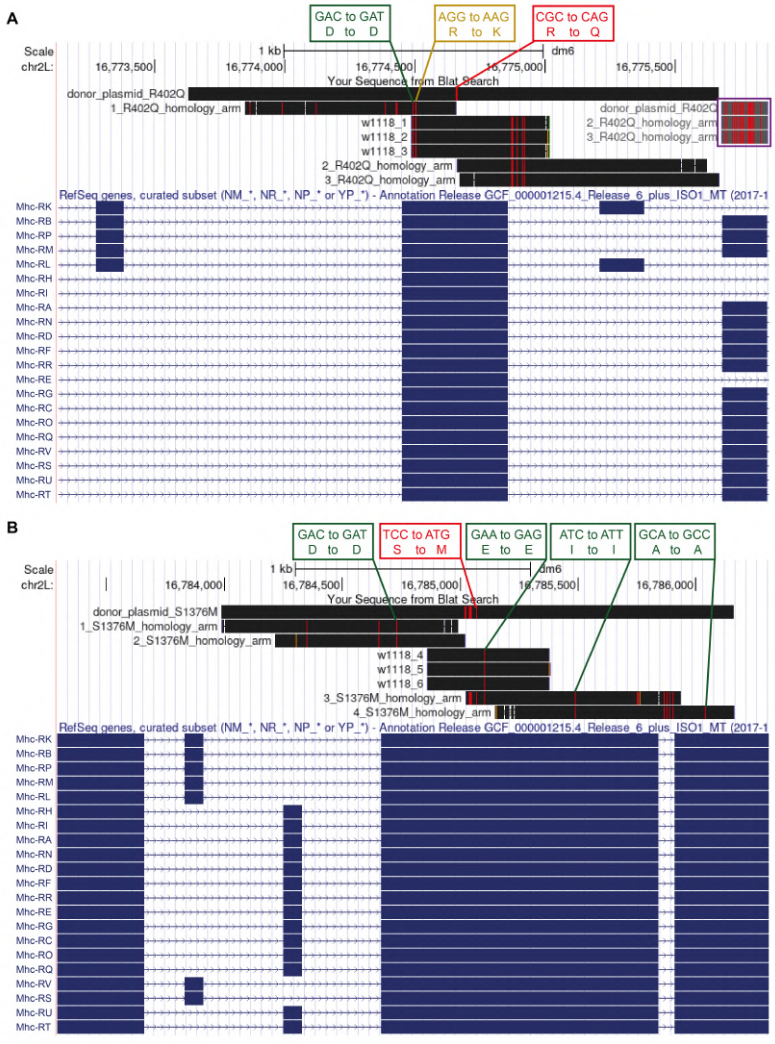

Figure 11.2: BLAT results of the homology arms.
Both upstream and downstream homology arms in the (**A**) R402Q and (**B**) S1376M donor plasmids were sequenced ((**A**) 1_R402Q_homology_arm – 3_R402Q_homology_arm; (**B**) 1_S1376M_homology_arm – 4_S1376M_homology_arm). The sequence reads were aligned to the 21 *Mhc* transcripts (indicated in blue below), the donor plasmid designs and the injection strain reads (w1118_1 to w1118_6). We found in (**A**) two mismatches and in (**B**) four mismatches in the coding sequence of *Mhc/CG17927*. Mismatches (boxed in green) that do not lead to amino acid changes were considered synonymous SNPs. The mismatch (boxed in orange) that leads to amino acid change was also found in the injection strain (w1118_1 to w1118_3). The disconnected grey/red mismatches regions (boxed in purple) are aligned to similar coding exons of *Mhc*. Red boxes indicate designed point mutations. Differences in nucleotides are highlighted in the black bars as follows: red – genome and query sequence have different bases at this position; orange – the query sequence has an insertion (or genome has a deletion/alignment gap) at this point; purple – the query sequence extends beyond the end of the alignment. Double horizontal lines are drawn to indicate when the alignment has gaps in both the genome and query sequence.

8 adults, 3 fertile crosses and no selection marker positive strains (*3xP3-DsRed+*) for the *Mhc* R402Q variant and by 3 adults, 1 fertile cross and 1 *3xP3-DsRed+* strain for the *Mhc* S1376M variant. We improved efficiency by performing microinjection in the [LWG012] w^{1118} strain. In total, 219 embryos were microinjected with the *Mhc* R402Q variant which resulted into 122 adults, 37 fertile crosses and 7 *3xP3-DsRed+* strains. Microinjection of 200 embryos with *Mhc* S1376M variant led to 68 adults, 40 fertile crosses and 4 *3xP3-DsRed+* strains.

The *3xP3-DsRed+* strains with either the *Mhc* R402Q or S1376M variant were further screened to exclude strains with vector backbone integration, which is a common phenomenon in CRISPR edited alleles. Moreover, we checked integration of selection marker at the correct guide RNA cutting sites to avoid genomic complications and off-target strains.

Both donor plasmids were used as a positive control for vector backbone integration and we observed the PCR bands at expected sizes for integration PCR 1 (R402Q: 1506bp; S1376M: 1508bp) and integration PCR 2 (R402Q: 1317bp: S1376M: 1451bp) (Figures 11.3 and S1). As expected, no bands were observed from negative control sample w^{1118}. Positive and negative control samples indicated that the primer pairs for integration tests were highly specific. In addition, we detected no PCR products from *3xP3-DsRed+* strains heterozygous for *Mhc* R402Q and S1376M variants, suggesting that no vector backbone integration has occurred at *Mhc/CG17927* gene locus.

Moreover, we investigated if the knock-in cassette PBacDsRed was correctly used as a template for homology-directed repair and as a consequence, has been incorporated into guide RNA cutting site. We observed no bands from negative control sample w^{1118}, indicating high specificity of the PCR reactions (Figures 11.4 and S2). PCR products at expected sizes for upstream PCR (R402Q: 1601bp; S1376M: 1583bp) and downstream PCR (R402Q: 1433bp; S1376M: 1606bp) were detected in samples from *3xP3-DsRed+* strains heterozygous for *Mhc* R402Q and S1376M variants, indicating PBacDsRed cassette insertion into *Mhc/CG17927* gene locus at correct orientation.

EXCISION OF SELECTION MARKER (3xP3-DsRed)

We used genomic PCR and sequencing to verify PiggyBac transposition alleles of *w[1118]; Mhc R402Q CRISPR [PBacDsRed]/ CyO* and *w[1118]; Mhc S1376M CRISPR [PBacDsRed]/ CyO* strains by testing if the selection marker (3xP3-DsRed) was precisely excised and left one TTAA sequence embedded in the coding region of *Mhc/CG17927*. We observed PCR bands at expected sizes for excised strains with *Mhc* R402Q (575bp) and S1376M (261bp) mutation suggesting the excision of the selection marker (Figures 11.5 and S3). In our control samples, including injection strain w^{1118} and unexcised strains with the selection marker, we detected the expected bands which indicated that the primer pairs for excision PCR were highly specific. Sequencing of the excision PCR products per strain confirmed the excision of the selection marker (3xP3-DsRed) and revealed the designed point mutation in both mutant strains as well as one exogenous TTAA motif embedded in the coding region of *Mhc*.

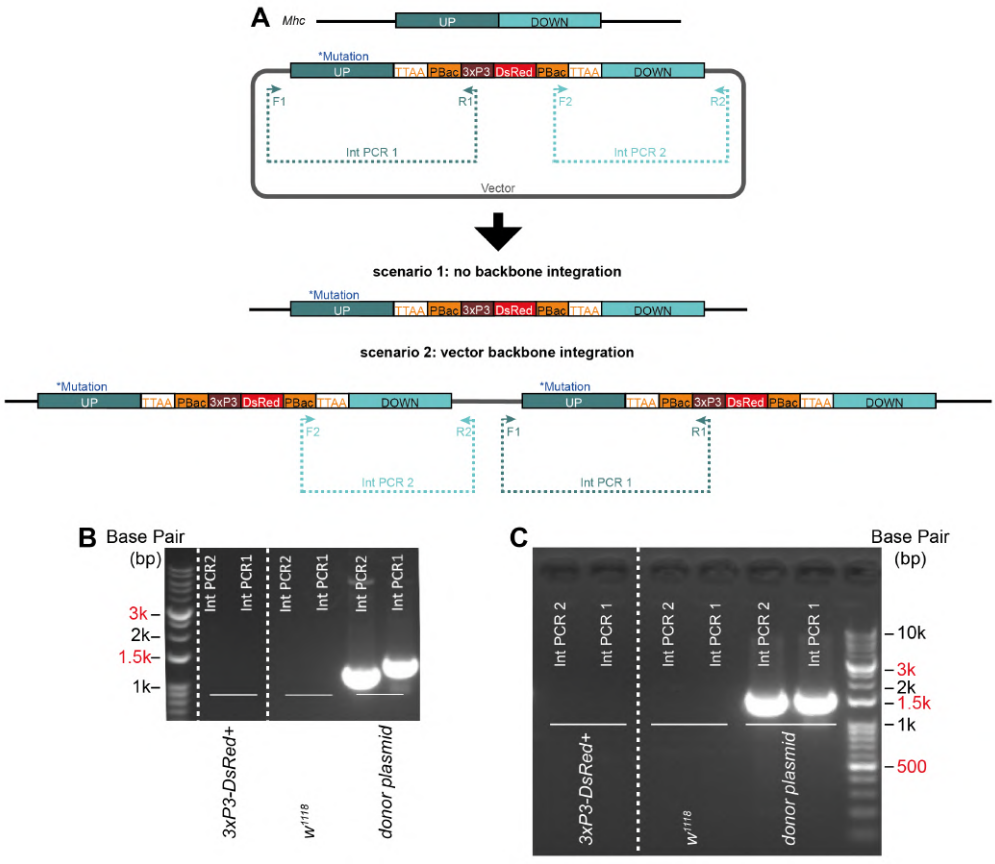

Figure 11.3: No donor plasmid integration in *3xP3-DsRed+* strains.
(**A**) Schematic of primer design (integration PCR 1 (Int PCR 1) and integration PCR 2 (Int PCR 2)) for *Mhc* R402 variant to check for integration of vector backbone in 3xP3-DsRed-positive strain. Correct editing will have no amplicon (scenario 1) and single integration of donor plasmid will have the amplicon (scenario 2). Donor plasmid of (**B**) *Mhc* R402Q and (**C**) S1376M variants were used as a positive control and w^{1118} as a negative control. The 3xP3-DsRed-positive strains (*3xP3-DsRed+*) showed single integration of vector backbone. Primer sequences for both Int PCR are provided in the Materials and Methods section. In both gels, (**B**) and (**C**), lanes were run on the same gel but were non-contiguous. Full-length gels are presented in Figure S1.

MOLECULAR BIOLOGICAL CHARACTERIZATION

We used semi-intact heart tube preparations to check the expression levels and phosphorylation levels of a variety of sarcomeric proteins. In our analysis, we included the following strains: w^{1118}, heterozygous and homozygous for *Mhc* R402Q ($R402Q^{+/-}$ and $R402Q^{+/+}$ respectively), heterozygous and homozygous for *Mhc* S1376M ($S1376M^{+/-}$ and $S1376M^{+/+}$ respectively).

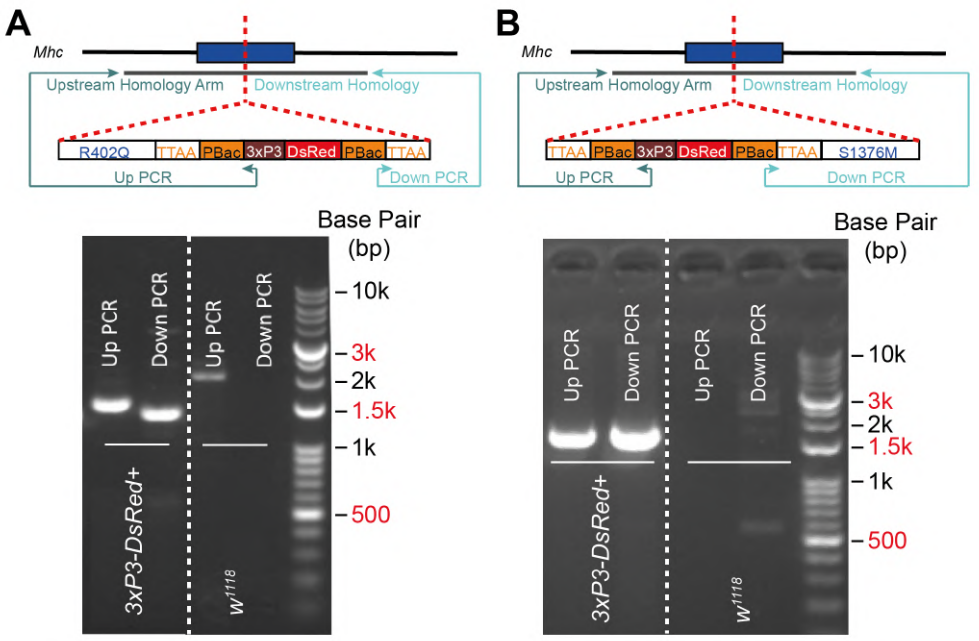

Figure 11.4: Correct incorporation of knock-in cassette 3xP3-DsRed into guide RNA cutting site. Schematic of the primer designs to check for incorporation of knock-in cassette 3xP3-DsRed into guide RNA cutting site to introduce (**A**) R402Q or (**B**) S1376M variant and the respective PCR products. No obvious bands were detected in upstream PCR (Up PCR) and downstream PCR (Down PCR) for negative control sample w^{1118}. The 3xP3-DsRed-positive strain (*3xP3-DsRed+*) showed an amplicon in Up/Down PCR. Primer sequences for Up/Down PCR are provided in the Materials and Methods section. In both cases, (**A**) and (**B**), lanes were run on the same gel but were non-contiguous. Full-length gels are presented in Figure S2.

Figure 11.5: Successful excision of selection marker (3xP3-DsRed) in *Mhc* R402Q (A-C) and S1376M (D-F) strains. PCR band at expected size of (**A**) 575bp or (**D**) 261bp was observed from heterozygous sample (excised) of (**A**) *w[1118]; Mhc R402Q CRISPR/ CyO* or (**D**) *w[1118]; Mhc S1376M CRISPR/ CyO* strains for excision PCR. (**A**) A 575bp product or (**D**) no PCR product was observed in negative control sample w^{1118}. (**A**) A 575bp and a 2271bp band or (**D**) a 1956bp band were detected in heterozygous un-excised line (*3xP3-DsRed+*). (**B, E**) Sequence read (Sbjct) was aligned with exercised donor sequence (Query) using Blast 2. (**C, F**) Sequencing chromatogram showing introduced gene variant and TTAA motif. One exogenous TTAA motif (boxed in purple) was left and embedded in the coding exon of *Mhc* after excision. Designed point mutation (**C**) R402Q or (**F**) S1376M of *Mhc* was boxed in orange. unrel. sample = sample unrelated to this study. In both cases, (**A**) and (**D**), lanes were run on the same gel, but were non-contiguous. Full-length gels are presented in Figure S3.

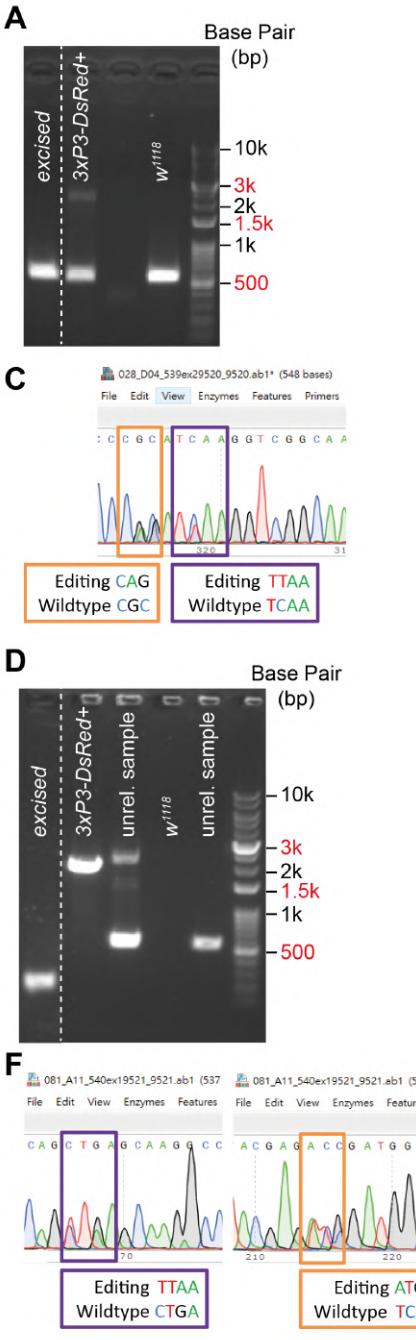
A
Base Pair
(bp)
excised
3xP3-DsRed+
w1118
10k
3k
2k
1.5k
1k
500
B
539ex29520_9520
Sequence ID: Query_62735 Length: 548 Number of Matches: 1
Range 1: 7 to 547 Graphics
Score
944 bits(511)
Expect
0.0
Identities
532/542(98%)
Gaps
2/542(0%)
Strand
Plus/Min
C
028_D04_539ex29520_9520.ab1* (548 bases)
File Edit View Enzymes Features Primers
Editing CAG
Wildtype CGC
Editing TTAA
Wildtype TCAA
D
Base Pair
(bp)
excised
3xP3-DsRed+
unrel. sample
w1118
unrel. sample
10k
3k
2k
1.5k
1k
500
E
540ex19521_9521
Sequence ID: Query_225815 Length: 537 Number of Matches: 1
Range 1: 6 to 521 Graphics
Score
917 bits(496)
Expect
0.0
Identities
511/518(99%)
Gaps
2/518(0%)
F
081_A11_540ex19521_9521.ab1
File Edit View Enzymes Features
Editing TTAA
Wildtype CTGA
Editing ATG
Wildtype TCC

We separated female from male flies. Compared to w^{1118}, we neither observed a difference in expression levels of Mhc, actin and Troponin I (TnI) nor in phosphorylation levels of Mhc, Troponin T (TnT) and TnI (Figure 11.6). In all *Mhc* mutant strains, we observed a signal around 80 kDa on the ProQ-stained gels, which suggests an additional phosphorylated protein in the mutant compared to control strains. Further investigation is warranted to align this signal to the respective protein.

To further investigate the Mhc expression in our *Mhc* mutant *Drosophila melanogaster* strains, we performed a SDS-PAGE analysis to separate Mhc isoforms of semi-intact heart tube preparations (Figure 11.7). We limited our selection to the extreme genotypes *Mhc* R402Q$^{+/+}$ and S1376M$^{+/+}$ and female flies due to the bigger body size. We limited our selection to the extreme genotypes *Mhc* R402Q$^{+/+}$ and S1376M$^{+/+}$ and female flies due to the bigger body size. All following experiments were therefore only performed in females. Using *Drosophila melanogaster* homogenates we detected a strong signal close to the band height of the skeletal slow MHC/cardiac β-MHC isoform. Quantification of this overall Mhc signal revealed no differences between the various genotypes. In some homogenates, the signal consisted of two bands, including a stronger upper band and a weaker lower band, which was closer to the skeletal slow MHC/cardiac β-MHC isoform. The composition of the *Drosophila melanogaster* Mhc signal is displayed in Figure 11.7C.

From the 9 pooled fly samples used in this analysis, 100% of the upper band was observed in 5 samples. In the pooled samples with both bands, the amount of the upper band was reduced up to 74%. We did not observe an obvious pattern between the genotype and the occurrence of two Mhc bands.

MORPHOLOGICAL CHARACTERIZATION

To examine the cardiac structure in more detail, hematoxylin and eosin staining was performed in transverse sections at three different selected regions of the heart tube on 3 week old female flies (Figure 11.8).
We observed that the *Drosophila melanogaster* heart is characterized by two single rows of contractile cells that form an inner lumen (myocardium), with opposite directionality (from lateral to medial, in the dorsal layer, and longitudinal in the ventral layer), and non-muscular pericardial cells aligned along the myocardium.[15] The first selected transverse cut was immediately posterior the conical chamber, the second one was located at half length of the heart tube when the first alary muscle bundle appeared and the last cut was close to the posterior end of the heart tube. Since hypertrophy of the heart wall would either increase the heart muscle area or decrease the lumen of heart tube,[32] we determined the lumen and heart muscle areas. We observed that both areas were similar in the mutant strains to w^{1118} at the different anatomical regions of the heart tube. We demonstrated that the heart tube sections closer to the conical chamber are characterized by a bigger heart muscle area independent of the analysed strains.

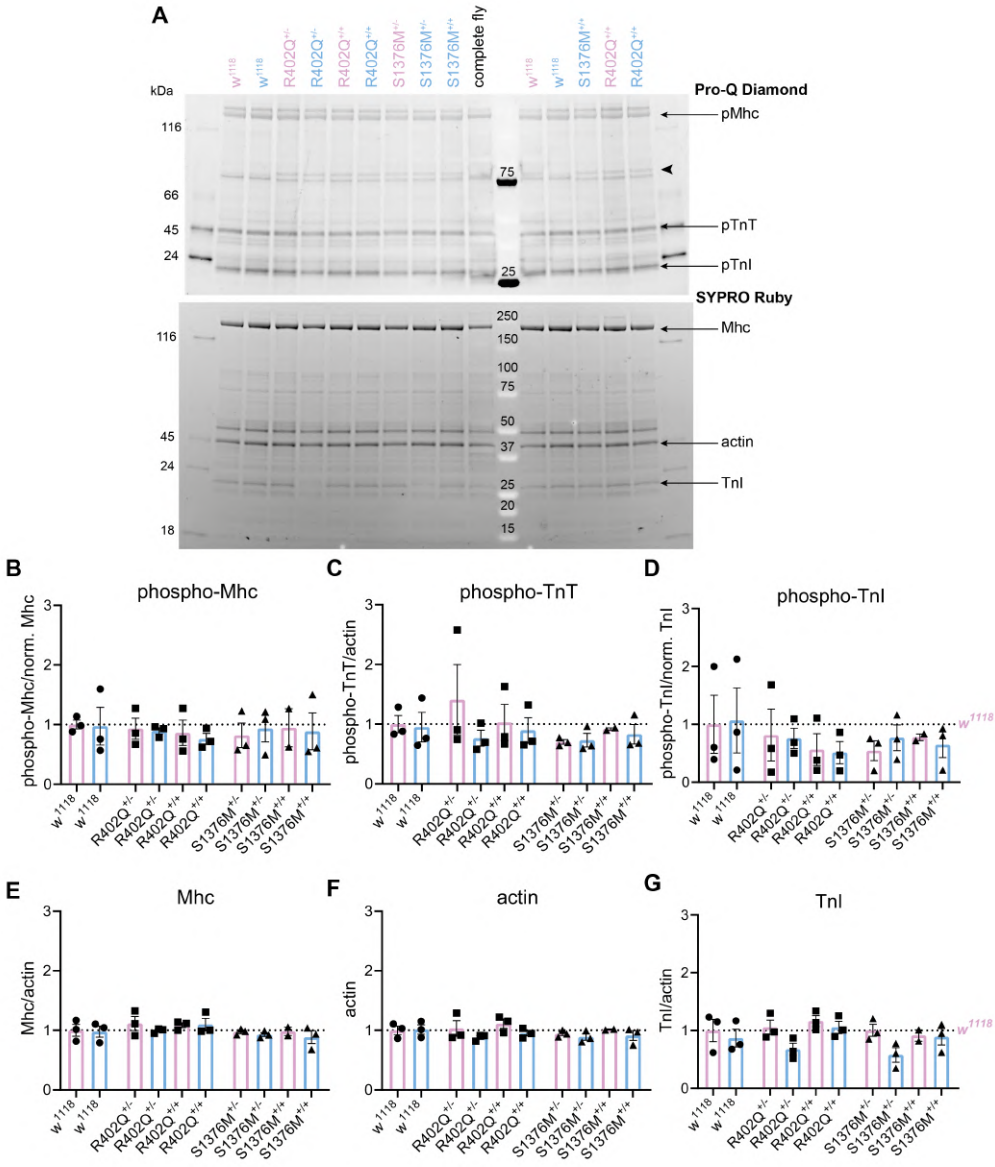

Figure 11.6: No changes in expression of (phospho-)proteins in semi-intact heart tube preparations. (**A**) Representative gel stained with Pro-Q Diamond and SYPRO Ruby. Arrows on the side indicate quantified sarcomere proteins. Arrow head at 80 kDa indicates additional phospho-band in mutants. Quantification of (**B**) phospho-Mhc, (**C**) phospho-TnT, (**D**) phospho-TnI, (**E**) Mhc, (**F**) actin (used as protein reference band) and (**G**) TnI. Purple color = female sample; blue colour = male sample. Each value per graph was normalized to the mean value of female w^{1118}.

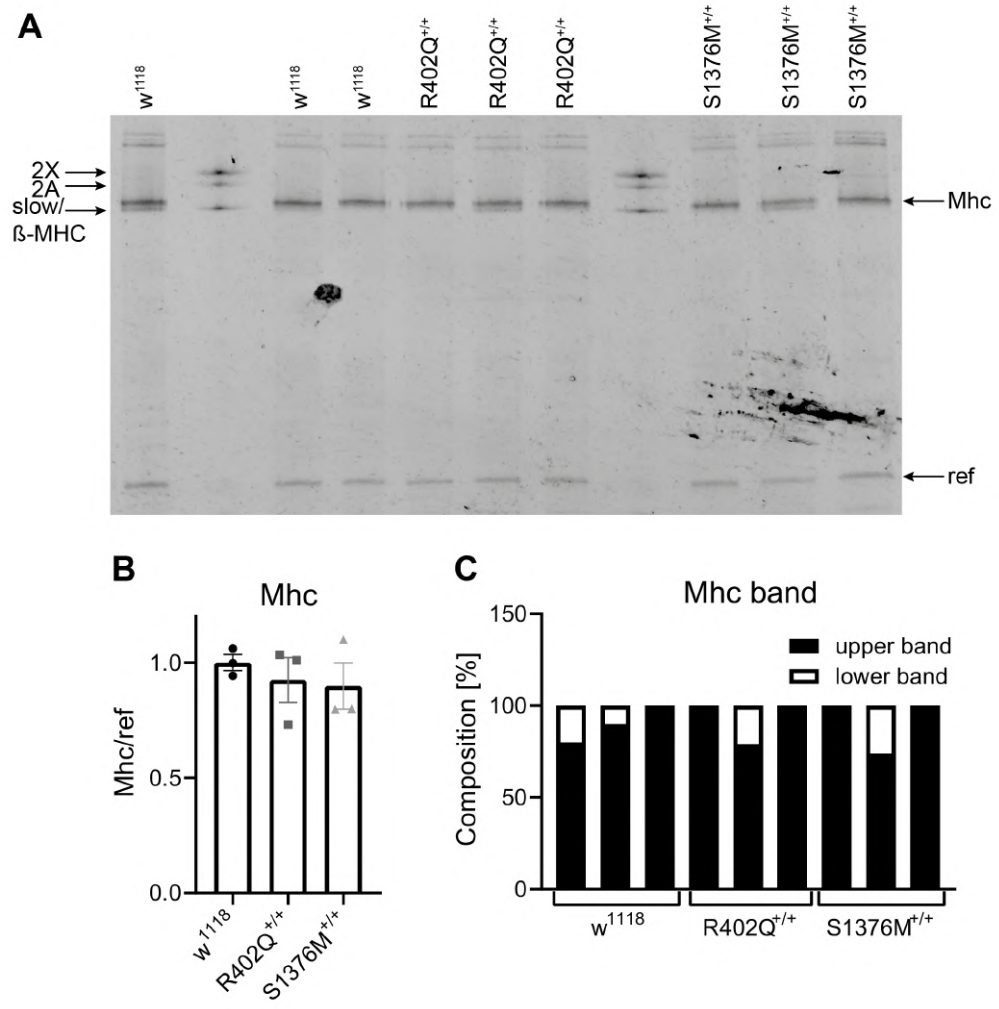

Figure 11.7: ***Drosophila melanogaster*** **Mhc signal close to the height of the skeletal slow/ cardiac β-MHC isoform.** (**A**) SDS-PAGE of semi-intact heart tube preparations in comparison to a human muscle homogenate expressing fast (2A and 2X) and slow/cardiac β-MHC isoforms. Ref: reference band used for normalization. (**B**) Quantification of the overall Mhc signal at the height of the slow/β-MHC isoform. (**C**) Quantification of the composition of the signal in (**B**) with a predominant upper band in all samples and a weaker lower band in some samples.

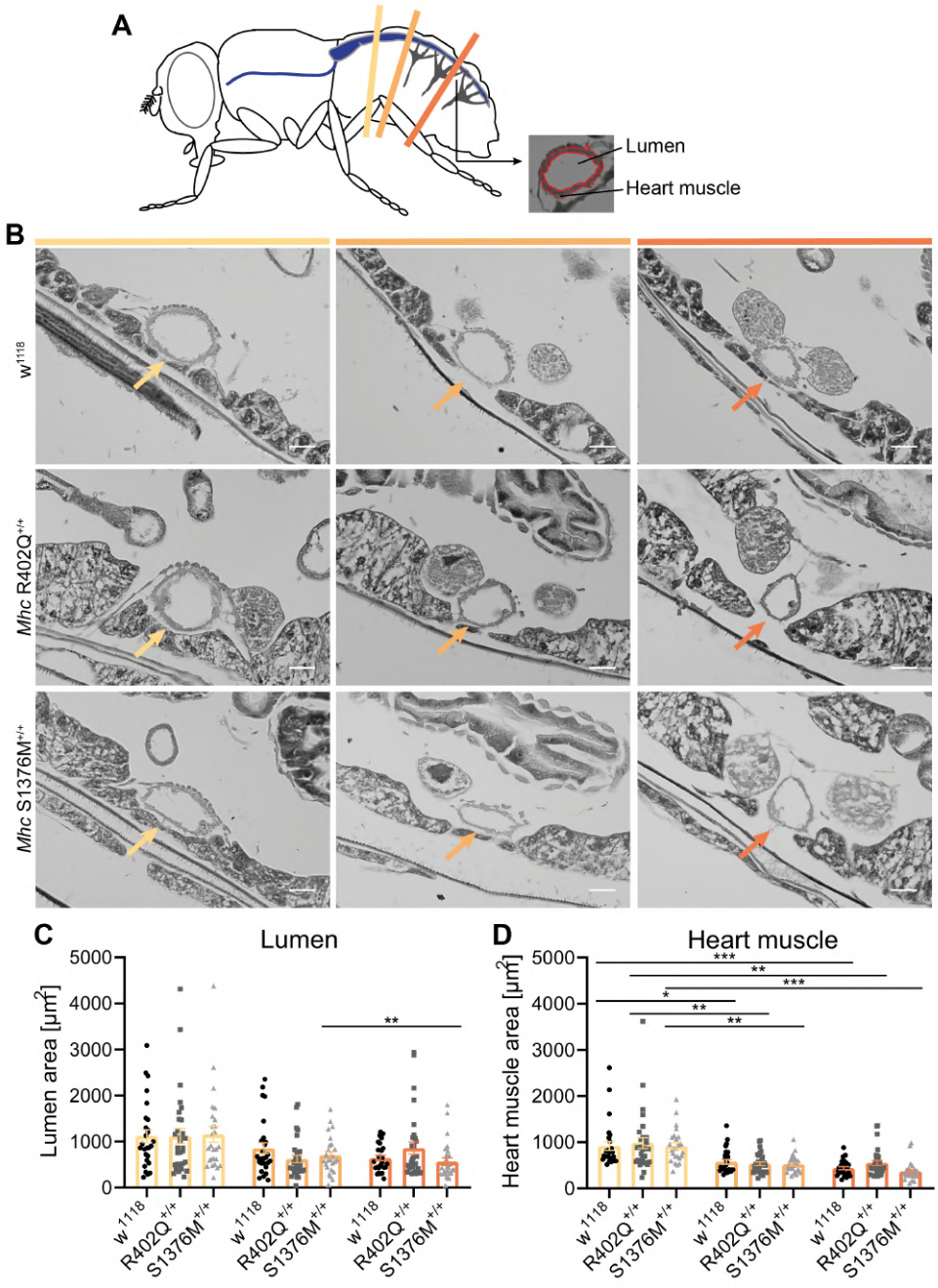

Figure 11.8: Lumen and heart muscle areas comparable to w^{1118}.
(**A**) Schematic illustration of the three selected transverse slides of the heart tube and the analysis mask. (**B**) Representative images with arrow pointing to the heart tubes (Scale bar = 20 µm). Quantified analysis of the (**C**) lumen and (**D**) heart muscle areas. Number of symbols per bar indicate the number of measured *Drosophilae melanogaster*. * denotes $p<0.05$, ** $p<0.01$ and *** $p<0.001$.

To investigate the effect of mutant Mhc on sarcomeric organization, we stained semi-intact heart tube preparations for Mhc, Phalloidin and α-tubulin. Again, we limited our selection to the extreme genotypes *Mhc* R402Q$^{+/+}$ and S1376M$^{+/+}$ and female flies due to the bigger body size. Although the sarcomeric structure and components of *Drosophila melanogaster* cardiomyocytes is similar to mammalian cardiac cells,[33] morphological differences can be observed. As mentioned before, two different cell layers can be observed. The heart tube is formed by contractile cells oriented from lateral to medial, and the ventral cell layer covering the heart tube is described as hybrid, non-myocardial muscle cells.[15] Our immunofluorescence staining revealed similar localization of mutant Mhc in the sarcomeres compared to controls, and regular arrangement of myofibrils along all z-stacks of the heart tube. We selected representative images for the ventral longitudinal muscle based on the straight appearance of myofibrils and determined the distance between consecutive Mhc bands (Figure 11.9).

Since a difference between the conical chamber, similar to the dorsal cells of the heart tube, and the remaining heart tube was clearly visible, we performed this analysis at two regions: at the half length of the heart tube and at the conical chamber near the aorta ring. In the latter region the cardiomyocytes can be representative from both areas (conical chamber and dorsal region). We observed in the ventral longitudinal muscle layer that consecutive Mhc bands were spaced closer to each other in the conical chamber than in the half length of the heart tube. The various genotypes did not show a difference in spacing of Mhc bands.

FUNCTIONAL CHARACTERIZATION

Female flies of 14 days of age with the extreme genotypes *Mhc* R402Q$^{+/+}$ and S1376M$^{+/+}$ were used for semi-intact heart tube preparations to determine heart function compared to age-matched controls (Figure 11.10). At baseline, there was no difference in distance of the two heart walls compared to w^{1118}. Both *Mhc* mutant strains showed functional impairments including reduced peak height (R402Q: 80%; S1376M: 91%) and fractional shortening (R402Q: 79%; S1376M: 90%) and shorter time to peak 50% (R402Q: 78%; S1376M: 76%), peak 90% (R402Q: 86%; S1376M: 86%) and return 50% (R402Q: 86%; S1376M: 87%). Time to return 90% was comparable to w^{1118}. While the contraction strength was more impaired in strains carrying the *Mhc* R402Q variant, time to peak parameters were similarly affected by both *Mhc* variants.

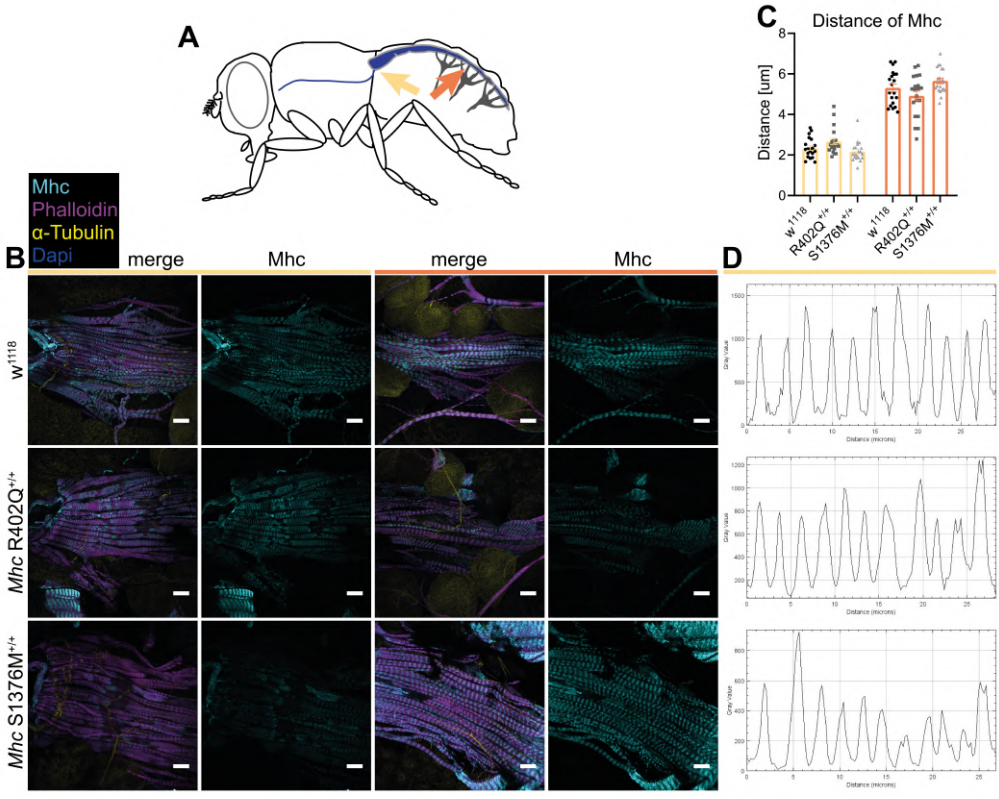

Figure 11.9: Normal Mhc localization and spacing in *Mhc* mutant strains.
(**A**) Schematic illustration of the two selected areas of the heart tube. (**B**) Representative images (merge and Mhc staining; Scale bar = 20 µm) for the ventral longitudinal muscle layer at the conical chamber near the aorta ring (left side) and at the half length of the heart tube (right side). (**C**) Quantification of the distance of consecutive Mhc bands in both regions. Number of symbols per bar indicate the number of measured distances. (**D**) Representative two-dimensional graphs of the pixel intensities (Gray Value) along a distance of 30 µm in a selected area of the conical chamber.

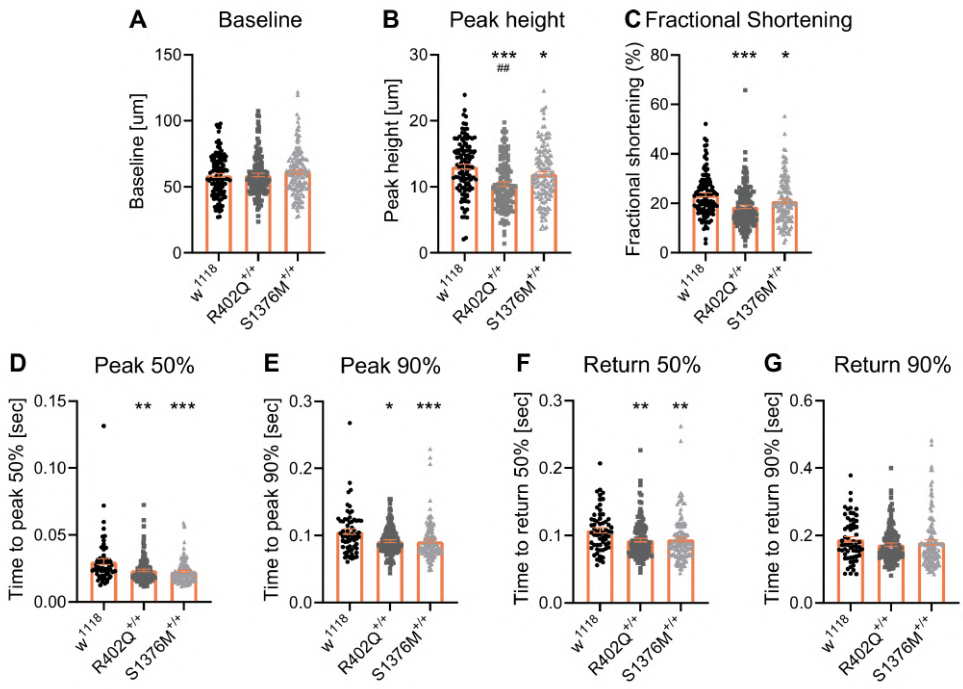

Figure 11.10: Functional impairment of *Mhc* mutant strains.
Quantified analysis of (**A**) the distance between the two heart walls during diastole, (**B**) peak height, (**C**) fractional shortening, (**D**) time to peak 50%, (**E**) time to peak 90%, (**F**) time to return 50% and (**G**) time to return 90%. Number of symbols per bar indicate the number of measured *Drosophilae melanogaster*. * denotes $p<0.05$, ** $p<0.01$ and *** $p<0.001$ compared to w^{1118} and $^{\#\#}$ denotes $p<0.01$ compared to S1376M mutation.

DISCUSSION

In the current study, we used scarless CRISPR/Cas9-mediated genome editing to specifically generate two *Drosophila melanogaster* strains with the orthologous HCM-causing *Mhc* variants R402Q and S1376M. Via PCR, we ensured that only strains without vector backbone integration and with correct orientation of the insertion were used for further analyses (Figure 11.4). We succeeded with our CRISPR/Cas9 approach to set up heterozygous strains for both variants and confirmed the excision of the selection marker 3xP3-DsRed by PCR and sequencing (Figure 11.5).

Maintaining the strains *w[1118]; Mhc R402Q CRISPR/ CyO* and *w[1118]; Mhc S1376M CRISPR/ CyO* revealed viable homozygous offspring (*w[1118]; Mhc R402Q CRISPR/ Mhc R402Q CRISPR* and *w[1118]; Mhc S1376M CRISPR/ Mhc S1376M CRISPR*, respectively). This provided us the opportunity to study the effect of 100% mutant protein in comparison to a mixture of wild-type and mutant protein in a single *Mhc* gene setting. In contrast to our *Drosophila melanogaster* model, which can live up to 50 days, *Myh6* R403Q$^{+/+}$ mice are viable for only 7 days after birth.[37] We performed molecular and histological analysis to investigate if these *Mhc* variants cause cardiac remodelling as observed in HCM, but did not observe any sign of structural abnormalities in the mutant lines compared to w^{1118}.

NO MOLECULAR ABNORMALITIES

We defined the levels of different sarcomeric proteins, especially the levels of Mhc, since myofilament protein stoichiometry can be altered in cardiac disease.[34] Moreover, reduced phosphorylation of cardiac TnI has been reported in HCM patients.[35] Therefore, we performed a Pro-Q Diamond and SYPRO Ruby staining to systematically assess the (phospho-)protein levels in semi-intact heart tube preparations including both sexes and all five different strains (Figure 11.6). Our Pro-Q Diamond staining revealed a strong signal for phospho-Mhc which was comparable between the different groups. This finding is in contrast to human and porcine cardiac samples which do not show any phosphorylation of MHC.[34,36] In comparison to w^{1118}, we observed similar expression of Mhc in the various *Mhc* mutant strains. This is in line with a *Myh6* R403Q$^{+/+}$ mouse model revealing no changes in expression levels of Mhc.[37] Therefore, our findings indicate that both variants do not affect overall Mhc expression, and in other assays phenotypical differences based on changes in protein expression can be excluded. Previously, it has been shown that TnT is readily phosphorylated,[38] and here we provided proof that TnT is endogenously phosphorylated in semi-intact heart of *Drosophila melanogaster* with similar levels in the different genotypes. In contrast to HCM patients,[35] we did not observe a reduction in phospho-TnI levels.

In addition, we analysed the Mhc expression in semi-intact heart tube preparations of female flies of the strains w^{1118}, *Mhc* R402Q$^{+/+}$ and S1376M$^{+/+}$ on a SDS-PAGE gel (Figure 11.7). This is a standard technique to investigate the various MHC isoforms in human cardiac and skeletal muscle.[39] We observed a Mhc signal slightly above the skeletal slow/cardiac β-MHC band. In line with the SYPRO Ruby staining, Mhc expression in the strains *Mhc* R402Q$^{+/+}$ and S1376M$^{+/+}$ was comparable to w^{1118}. In some lanes, the

Mhc signal consisted of two bands due to the occurrence of an additional lower band with a weaker signal which may suggest a mixture of various Mhc isoforms dependent on the preparations. Our semi-intact heart tube preparations contain various muscles, including the heart tube. Information about which Mhc isoforms are expressed in semi-intact heart tube preparations is lacking since there is no entry for the heart in the FlyAtlas2 database which provides data about transcripts expression in various tissues.[40] Spatially and temporally regulated expression of *Mhc* alternative exons has been studied during *Drosophila melanogaster* embryogenesis and revealed the expression of a single transcript containing the exon combination 3a-7a-9b-11d-15b in cardioblasts at late stage 15.[41] Similar to the human situation in which cardiac β-MHC isoform is expressed in both cardiac muscle and some skeletal muscles, this *Mhc* exon combination was also detected in dorsal acute and ventral oblique body wall muscles.[41] Unlike vertebrates, isoform changes within a particular muscle have not been documented during *Drosophila melanogaster* development.[18] Further research is warranted to investigate which Mhc isoforms are present in semi-intact heart tube preparations. This may help to understand why we observed different Mhc isoform compositions in some preparations.

NO MORPHOLOGICAL ABNORMALITIES

Transverse sections at three different regions of the heart tube were analysed and revealed no changes in the lumen and heart muscle areas in *Mhc* mutant strains compared to w^{1118} (Figure 11.8). This indicates that cardiac morphology is not affected by the presence of homozygous *Mhc* variants. One limitation of this study is that we only included 3-week old flies for this analysis meaning that we cannot exclude that hypertrophy might have occurred at an older age of *Mhc* mutant strains. In contrast to that, we know from a large unrelated cohort study that HCM patients harbouring *MYH7* variants are diagnosed at a younger age, have more hypertrophy and a higher risk for adverse cardiac outcomes than HCM patients without a *MYH7* variant.[9,13] Especially the *MYH7* variant R403Q is considered as pathogenic leading to a "malignant" course. Our data indicates that this pathogenicity and malignant disease course is not conserved in *Drosophila melanogaster*, even though the amino acid residue R402 and neighbouring residues are highly conserved.[11]

Staining semi-intact heart tube whole mounts of female flies of the strains w^{1118}, *Mhc* R402Q$^{+/+}$ and S1376M$^{+/+}$ showed a normal Mhc incorporation and localization, and myofibrils were arranged regularly (Figure 11.9). In line with previous findings, pericardial cells were Mhc-negative.[41] Moreover, we quantified the spacing of consecutive Mhc bands at two regions of the ventral longitudinal muscle layer and did not observe any difference in spacing of Mhc bands between the different genotypes. In contrast to our findings, morphological abnormalities, such as myofibril disarray and hypertrophy, have been reported for various model systems including in *MYH7* R403Q$^{+/-}$ 3D human iPSC-derived cardiac microtissue and *Myh6* R403Q$^{+/+}$ mice.[37,42] Myofibril disarray has also been reported in heterozygous transgenic flies expressing the *Drosophila melanogaster* equivalent of the human HCM-causing *MYH7* K146N variant which developed a phenotype including hypercontractility, increased tension generation periods and decreased diastolic/systolic.[43] The analysed flies were 1- and 3-week-old. There are no detailed reports about the morphological changes of HCM patients with *MYH7* R403Q and T1377M.

Overall, our data show no changes in myosin expression, sarcomere alignment or cardiomyocyte size in flies harbouring a homozygous R402Q and S1376M *Mhc* mutation at 14 and 21 days of age.

IMPARIED CONTRACTILITY

In line with our morphological analyses, our functional characterisation revealed that at baseline all strains showed a comparable distance between the two heart walls. The reduced peak height, fractional shortening and the shorter time to peak, observed in the *Mhc* mutant strains, indicates impaired contraction. Since we detected that time to return 50% was shorter in the mutant strains, but normalized when time to return 90% was reached, this may suggests different relaxation kinetics in mutant flies. Further research is necessary to understand the functional impairments and disease progression in *Mhc* mutant flies. Consistent with the pathogenicity of the R403Q variant in humans,[7] contraction strength, including peak height and fractional shortening, was more severely impaired in mutants carrying the R402Q variant.

CONCLUSION

In summary, our analyses revealed that heterozygous and homozygous strains with the R402Q and S1376M *Mhc* gene variants, do not alter expression level or incorporation of Mhc, and no morphological abnormality such as hypertrophy is induced. Homozygous R402Q and S1376M strains did show functional abnormalities, indicative for mutation-mediated effects independent of structural remodelling. In conclusion, our *Drosophila melanogaster* strains with R402Q and S1376M show early mutation-mediated impaired cardiac contractile function, and may be used as model system to study secondary disease mechanisms that underlie cardiac remodelling in HCM.

ACKNOWLEDGEMENTS

We would like to thank Ms. Z.S. Sultan for preparation of *Drosophila melanogaster* food and Mr. L. Begthel for performing the SDS-PAGE gels for Mhc isoform composition.

SUPPLEMENTARY FILES - ONLINE

https://drive.google.com/drive/folders/142Qu-xSO28VI2zAZVxI77v0M6fnDZogr

REFERENCES

1. Semsarian C, Ingles J, Maron MS, Maron BJ. New perspectives on the prevalence of hypertrophic cardiomyopathy. *J Am Coll Cardiol*. 2015;65(12):1249-54.
2. Maron BJ, Maron MS. Hypertrophic cardiomyopathy. *Lancet*. 2013;381(9862):242-55.
3. Varnava AM, Elliott PM, Sharma S, McKenna WJ, Davies MJ. Hypertrophic cardiomyopathy: the interrelation of disarray, fibrosis, and small vessel disease. *Heart*. 2000;84(5):476-82.
4. Kalra A, Harris KM, Maron BA, Maron MS, Garberich RF, Haas TS, et al. Relation of Doppler Tissue Imaging Parameters With Heart Failure Progression in Hypertrophic Cardiomyopathy. *Am J Cardiol*. 2016;117(11):1808-14.
5. Saccheri MC, Cianciulli TF, Lax JA, Guerra JE, Redruello HJ, Weich Glogier FL, et al. Impaired myocardial function in hypertrophic cardiomyopathy. *Echocardiography*. 2009;26(6):657-64.
6. Alfares AA, Kelly MA, McDermott G, Funke BH, Lebo MS, Baxter SB, et al. Results of clinical genetic testing of 2,912 probands with hypertrophic cardiomyopathy: expanded panels offer limited additional sensitivity. *Genet Med*. 2015;17(11):880-8.
7. Watkins H, Rosenzweig A, Hwang DS, Levi T, McKenna W, Seidman CE, et al. Characteristics and prognostic implications of myosin missense mutations in familial hypertrophic cardiomyopathy. *N Engl J Med*. 1992;326(17):1108-14.
8. Tanigawa G, Jarcho JA, Kass S, Solomon SD, Vosberg HP, Seidman JG, et al. A molecular basis for familial hypertrophic cardiomyopathy: an alpha/beta cardiac myosin heavy chain hybrid gene. *Cell*. 1990;62(5):991-8.
9. Van Driest SL, Jaeger MA, Ommen SR, Will ML, Gersh BJ, Tajik AJ, et al. Comprehensive analysis of the beta-myosin heavy chain gene in 389 unrelated patients with hypertrophic cardiomyopathy. *J Am Coll Cardiol*. 2004;44(3):602-10.
10. Perrot A, Schmidt-Traub H, Hoffmann B, Prager M, Bit-Avragim N, Rudenko RI, et al. Prevalence of cardiac beta-myosin heavy chain gene mutations in patients with hypertrophic cardiomyopathy. *J Mol Med (Berl)*. 2005;83(6):468-77.
11. Geisterfer-Lowrance AA, Kass S, Tanigawa G, Vosberg HP, McKenna W, Seidman CE, et al. A molecular basis for familial hypertrophic cardiomyopathy: a beta cardiac myosin heavy chain gene missense mutation. *Cell*. 1990;62(5):999-1006.
12. Colegrave M, Peckham M. Structural implications of beta-cardiac myosin heavy chain mutations in human disease. *Anat Rec (Hoboken)*. 2014;297(9):1670-80.
13. Ho CY, Day SM, Ashley EA, Michels M, Pereira AC, Jacoby D, et al. Genotype and Lifetime Burden of Disease in Hypertrophic Cardiomyopathy: Insights from the Sarcomeric Human Cardiomyopathy Registry (SHaRe). *Circulation*. 2018;138(14):1387-98.
14. Bier E, Bodmer R. Drosophila, an emerging model for cardiac disease. *Gene*. 2004;342(1):1-11.
15. Taghli-Lamallem O, Plantie E, Jagla K. Drosophila in the Heart of Understanding Cardiac Diseases: Modeling Channelopathies and Cardiomyopathies in the Fruitfly. *J Cardiovasc Dev Dis*. 2016;3(1).
16. Stocker H, Gallant P. Getting started : an overview on raising and handling Drosophila. *Methods Mol Biol*. 2008;420:27-44.
17. Bernstein SI, Mogami K, Donady JJ, Emerson CP, Jr. Drosophila muscle myosin heavy chain encoded by a single gene in a cluster of muscle mutations. *Nature*. 1983;302(5907):393-7.
18. Swank DM, Wells L, Kronert WA, Morrill GE, Bernstein SI. Determining structure/function relationships for sarcomeric myosin heavy chain by genetic and transgenic manipulation of Drosophila. *Microsc Res Tech*. 2000;50(6):430-42.
19. Montag J, Syring M, Rose J, Weber AL, Ernstberger P, Mayer AK, et al. Intrinsic MYH7 expression regulation contributes to tissue level allelic imbalance in hypertrophic cardiomyopathy. *J Muscle Res Cell Motil*. 2017;38(3-4):291-302.
20. Gratz SJ, Ukken FP, Rubinstein CD, Thiede G, Donohue LK, Cummings AM, et al. Highly specific and efficient CRISPR/Cas9-catalyzed homology-directed repair in Drosophila. *Genetics*. 2014;196(4):961-71.
21. Elliott P, Andersson B, Arbustini E, Bilinska Z, Cecchi F, Charron P, et al. Classification of the cardiomyopathies: a position statement from the European Society Of Cardiology Working Group on Myocardial and Pericardial Diseases. *Eur Heart J*. 2008;29(2):270-6.
22. Kondo S, Ueda R. Highly improved gene targeting by germline-specific Cas9 expression in Drosophila. *Genetics*. 2013;195(3):715-21.
23. Kent WJ. BLAT–the BLAST-like alignment tool. *Genome Res*. 2002;12(4):656-64.
24. Kent WJ, Sugnet CW, Furey TS, Roskin KM, Pringle TH, Zahler AM, et al. The human genome browser at UCSC. *Genome Res*. 2002;12(6):996-1006.
25. Hoskins RA, Phan AC, Naeemuddin M, Mapa FA, Ruddy DA, Ryan JJ, et al. Single nucleotide polymorphism markers for genetic mapping in Drosophila melanogaster. *Genome Res*. 2001;11(6):1100-13.
26. Horn C, Jaunich B, Wimmer EA. Highly sensitive, fluorescent transformation marker for Drosophila transgenesis. *Dev Genes Evol*. 2000;210(12):623-9.
27. Gloor GB, Preston CR, Johnson-Schlitz DM, Nassif NA, Phillis RW, Benz WK, et al. Type I repressors of P element mobility. *Genetics*. 1993;135(1):81-95.
28. Lamb AM, Walker EA, Wittkopp PJ. Tools and strategies for scarless allele replacement in Drosophila using CRISPR/Cas9. *Fly (Austin)*. 2017;11(1):53-64.
29. Vogler G, Ocorr K. Visualizing the beating heart in Drosophila. *J Vis Exp*. 2009(31).

30. Zaremba R, Merkus D, Hamdani N, Lamers JM, Paulus WJ, Dos Remedios C, et al. Quantitative analysis of myofilament protein phosphorylation in small cardiac biopsies. *Proteomics Clin Appl*. 2007;1(10):1285-90.
31. Xu P, Damschroder D, Zhang M, Ryall KA, Adler PN, Saucerman JJ, et al. Atg2, Atg9 and Atg18 in mitochondrial integrity, cardiac function and healthspan in Drosophila. *J Mol Cell Cardiol*. 2019;127:116-24.
32. Wolf MJ. Modeling dilated cardiomyopathies in Drosophila. *Trends Cardiovasc Med*. 2012;22(3):55-61.
33. Cammarato A, Ahrens CH, Alayari NN, Qeli E, Rucker J, Reedy MC, et al. A mighty small heart: the cardiac proteome of adult Drosophila melanogaster. *PLoS One*. 2011;6(4):e18497.
34. Stanley BA, Graham DR, James J, Mitsak M, Tarwater PM, Robbins J, et al. Altered myofilament stoichiometry in response to heart failure in a cardioprotective alpha-myosin heavy chain transgenic rabbit model. *Proteomics Clin Appl*. 2011;5(3-4):147-58.
35. van Dijk SJ, Dooijes D, dos Remedios C, Michels M, Lamers JM, Winegrad S, et al. Cardiac myosin-binding protein C mutations and hypertrophic cardiomyopathy: haploinsufficiency, deranged phosphorylation, and cardiomyocyte dysfunction. *Circulation*. 2009;119(11):1473-83.
36. Locher MR, Razumova MV, Stelzer JE, Norman HS, Moss RL. Effects of low-level & alpha;-myosin heavy chain expression on contractile kinetics in porcine myocardium. *Am J Physiol Heart Circ Physiol*. 2011;300(3):H869-78.
37. Tyska MJ, Hayes E, Giewat M, Seidman CE, Seidman JG, Warshaw DM. Single-molecule mechanics of R403Q cardiac myosin isolated from the mouse model of familial hypertrophic cardiomyopathy. *Circ Res*. 2000;86(7):737-44.
38. Domingo A, Gonzalez-Jurado J, Maroto M, Diaz C, Vinos J, Carrasco C, et al. Troponin-T is a calcium-binding protein in insect muscle: in vivo phosphorylation, muscle-specific isoforms and developmental profile in Drosophila melanogaster. *J Muscle Res Cell Motil*. 1998;19(4):393-403.
39. Reiser PJ, Kline WO. Electrophoretic separation and quantitation of cardiac myosin heavy chain isoforms in eight mammalian species. *Am J Physiol*. 1998;274(3):H1048-53.
40. Leader DP, Krause SA, Pandit A, Davies SA, Dow JAT. FlyAtlas 2: a new version of the Drosophila melanogaster expression atlas with RNA-Seq, miRNA-Seq and sex-specific data. *Nucleic Acids Res*. 2018;46(D1):D809-D15.
41. Zhang S, Bernstein SI. Spatially and temporally regulated expression of myosin heavy chain alternative exons during Drosophila embryogenesis. *Mech Dev*. 2001;101(1-2):35-45.
42. Cohn R, Thakar K, Lowe A, Ladha FA, Pettinato AM, Romano R, et al. A Contraction Stress Model of Hypertrophic Cardiomyopathy due to Sarcomere Mutations. *Stem Cell Reports*. 2019;12(1):71-83.
43. Kronert WA, Bell KM, Viswanathan MC, Melkani GC, Trujillo AS, Huang A, et al. Prolonged cross-bridge binding triggers muscle dysfunction in a Drosophila model of myosin-based hypertrophic cardiomyopathy. *Elife*. 2018;7.

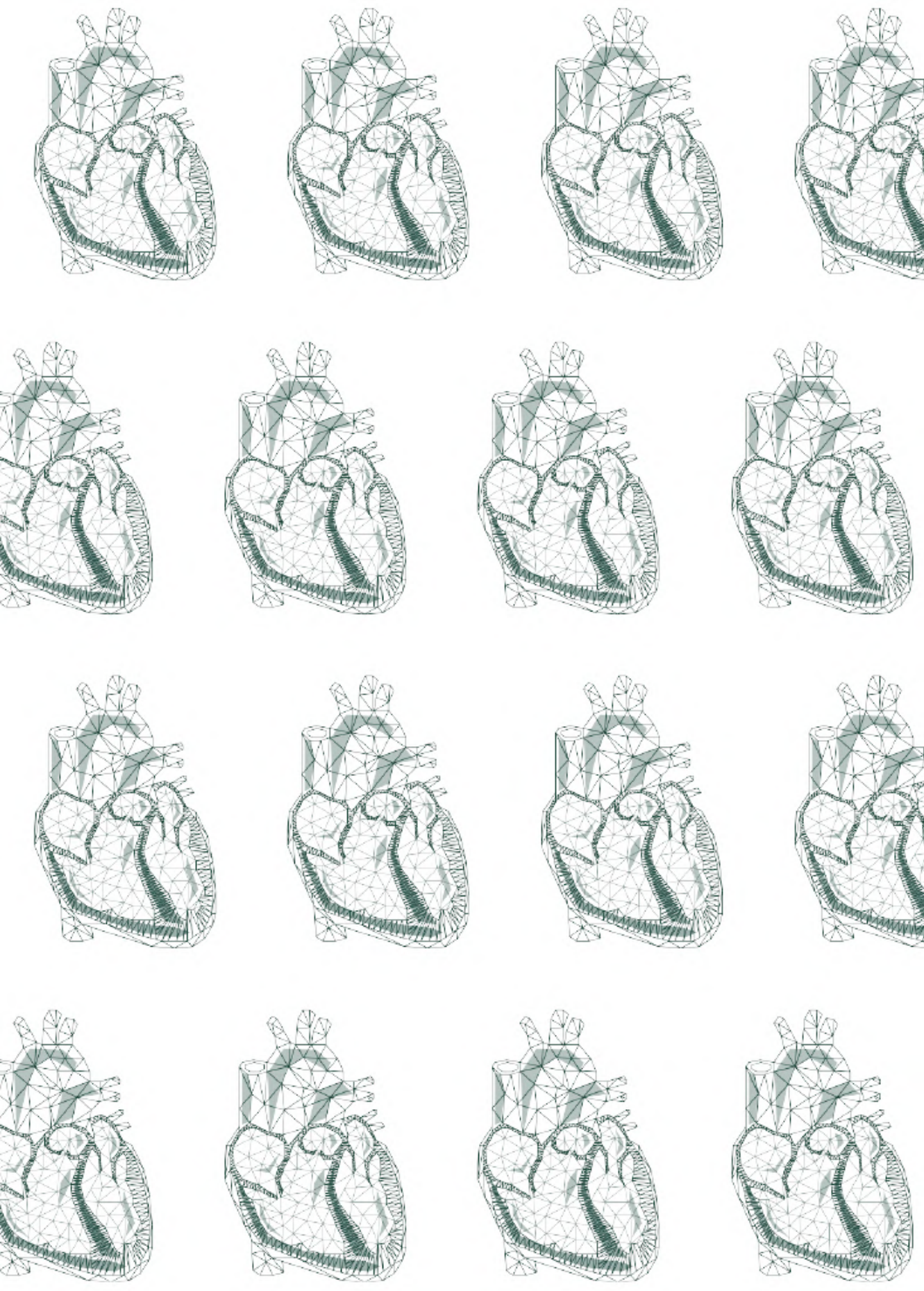

PART

DISCUSSION AND SUMMARY

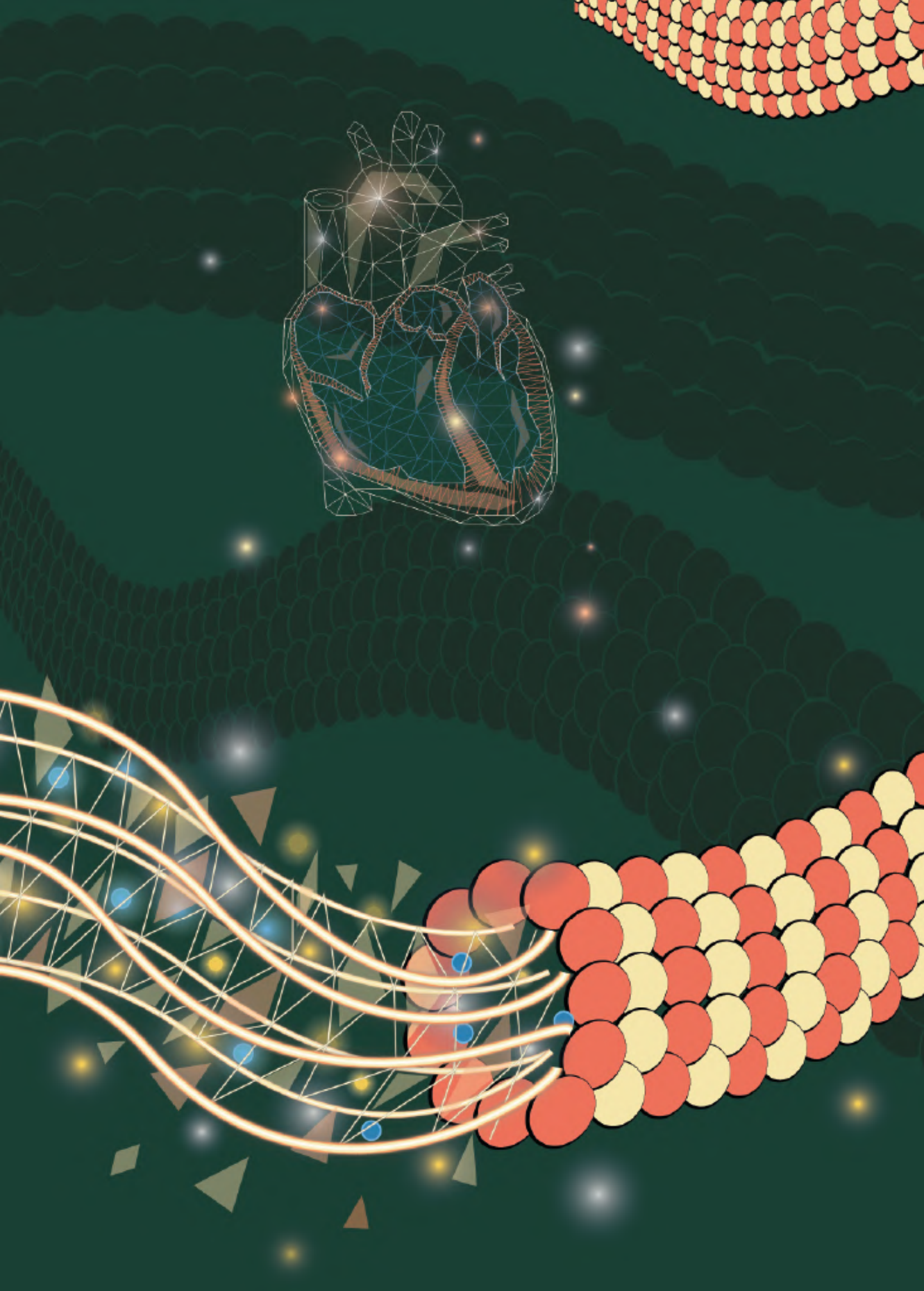

Chapter 12

Discussion and future perspective

According to the working group on Myocardial and Pericardial Diseases of the European Society of Cardiology, cardiomyopathies (CMs) are defined by abnormal myocardial structure and function in the absence of any other diseases sufficient to cause these abnormalities.[1] The two most common types are hypertrophic CM (HCM), characterized by increased left ventricular (LV) wall thickness often occurring asymmetrically and diastolic dysfunction, and dilated CM (DCM) with the hallmarks of LV dilation and systolic dysfunction.[1] Familial forms are characterized by an autosomal dominant inheritance pattern and many pathogenic gene variants (mutations) are localized in genes encoding sarcomeric proteins.[2] Both HCM and DCM can develop into advanced heart failure which poses a considerable mortality risk.[3]

Until today, there are no effective medical options to halt or reverse disease progression, and cardiac transplantation represents the best effective long-term treatment for all end-stage heart failure patients.[4] The heterogeneous clinical presentation of patients with inherited CMs further complicates clinical approaches and validation of new treatment strategies. In **chapter 2**, we provide a comprehensive clinical evaluation of two large families carrying gene variants in *TPM1*. Our data illustrate this clinical heterogeneity, which includes differences in age-dependent penetrance and disease severity between individuals with the identical genetic variant. Consequently, this striking heterogeneity and the highly variable age of onset imply that the pathophysiology of inherited CMs is more complex than the functional defects triggered by the gene variant. Therefore, it is of utmost importance to adequately identify additional disease triggers and understand the underlying pathomechanisms.

By combining cellular, genetic and clinical data from well-phenotyped patient cohorts and different disease models for CMs, we investigated potential disease triggers. In this thesis, we focused on assessing the status of the protein quality control (PQC) system and the microtubule network. Both systems are highly dynamic,[5,6] and proper functionality of the PQC system is dependent on the microtubule network and vice versa.[7] Especially, inter-individual differences in the capacity of the PQC[8] and the coincident derailed adaptations to stress triggers may contribute to the striking heterogeneity in clinical presentation.

Chapter 1 introduced the national research consortium CVON-DOSIS on cardiomyopathies that aimed to identify determinants of susceptibility in inherited cardiomyopathy and received funding by the Netherlands Heart Foundation. Clinically relevant observations of collaborations between clinical and preclinical researchers are: (1) Diastolic dysfunction in female is more severe at the time of septal myectomy than in male hypertrophic CM (HCM) patients; (2) Indexation for body size should be implemented to set the diagnostic threshold for LV thickening in HCM; (3) Cell-to-cell variability is present in the hearts of patients with a Dutch *MYBPC3* founder mutation; (4) Compelling evidence that altered metabolism and PQC are central disease modifiers in CMs. **Chapter 1** closed with an outline of this thesis.

CARDIOMYOPATHY IN A DISH: USING CELL CULTURE SYSTEMS TO MODEL INHERITED CARDIOMYOPATHIES

In **chapter 2**, we described a large family with a DCM-causing *TPM1* variant and identified compound heterozygote *TPM1* variants in a child with restrictive CM with family members carrying HCM(-like) phenotypes. Overexpression of *TPM1* variants in HL-1 cardiomyocytes led to time-dependent progressive deterioration of cardiomyocyte calcium transient (CaT) amplitudes. The dose-dependent effect on CaT was opposite for DCM- and HCM-associated *TPM1* variants and may be determined by the mixture of variant and wild-type TPM1. The reduced CaT amplitudes and structural changes occurred irrespective of *TPM1* variants and the clinical CM phenotype. Taken together, reduced CaT amplitudes may contribute to the poor cardiac contraction seen in affected individuals.

While HL-1 cardiomyocytes are a quick, cheap and easy *in vitro* model to check the effect of gene variant overexpression, it may be interesting to follow up our *TPM1* study with human induced pluripotent stem cells derived cardiomyocytes (hiPSC-CM). Patient derived hiPSC-CM provide a versatile new tool because they often recapitulate the respective hallmarks of inherited CMs, retain the genetic blueprint and thereby tremendously improve our understanding of underlying molecular mechanisms.[9] The advent of hiPSC-CM offers insights into the very early pathophysiology, such as contractile alterations that appear first in the course of the disease, unobscured by compensatory responses.[10] Moreover, using CRISPR/Cas9 technology to modify one allele better recapitulates the human disease situation than overexpression of mutant protein on top of the wild-type proteins which is important in a stoichiometry-controlled environment such as the myofilament proteins.

Whether our findings in HL-1 cardiomyocytes are recapitulated in hiPSC-CM, which have a higher potential to recapitulate the patient phenotype, is difficult to predict. Systematic functional characterization and comparison of HL-1 cardiomyocytes to stem cell-derived cardiomyocytes or hiPSC-CM is limited so far to electrophysiological properties.[11,12] In line with our data, Ca^{2+} handling abnormalities were observed in patient derived hiPSC-CM carrying the D175N variant in *TPM1*.[13] Especially the usage of a genetically encoded Ca^{2+} indicator may improve our understanding due to the direct visualization of changes in Ca^{2+} flux at the myofilaments.[14] Besides Ca^{2+} flux measurements in hiPSC-CM, there are diverse systems and methods for performing mechanical measurements of contractility, ranging from single cell techniques to multicellular tissue-like constructs.[15] Deciphering the mechanisms to enable the massive hiPSC-CM expansion made it possible to produce a sufficient number of cardiomyocytes needed for experiments such as large-scale drug screening and 3-dimensional tissue engineering applications.[16] hiPSC-CM represents a model with the potential to identify novel pathomechanisms and head into the direction of personalized medicine.

Besides the cell-culture systems (**chapter 2** and **4**), we used a variety of animal models for CMs spanning from *Drosophila melanogaster* (**chapter 10** and **11**) via *Mus musculus* (**chapter 6** and **9**) to *Sus scrofa domesticus* (**chapter 9**). We used all these models to recapitulate some hallmarks of CMs with the aim to improve our understanding of the underlying pathomechanisms and ultimately, to translate it back to the human phenotype. Each system has its weak points either by not mimicking a respective hallmark or by the inability to translate the findings to the human phenotype. Therefore, we want to highlight here the importance to evaluate firstly whether the used system is appropriate for the asked research question. In **chapter 9**, we assessed systematically the microtubule network in various pig and mouse models to define the recapitulating potential of each model system. In **chapter 11**, we phenotyped two point mutations in the myosin heavy chain gene of *Drosophila melanogaster*, which cause HCM in humans, to determine if these mutant *Drosophila melanogaster* strains represent a model for inherited CMs.

THE ROLE AND DERAILMENT ROUTE OF PQC IN INHERITED CARDIOMYOPATHIES

So far, studies investigating the role of PQC in CMs caused by sarcomeric gene mutations are limited. In **chapter 3**, we provided an overview of the reported structural changes and adaptations in PQC related to inherited CMs. Hereby, we observed that PQC derailment can be (1) a direct effect of the mutation-induced activation, (2) a compensatory mechanism due to mutation-induced cellular dysfunction or (3) a consequence of the simultaneous occurrence of the mutation and a secondary hit. Personalized treatment strategies should be addressed to the disease- and mutation-specific changes of key modulators in PQC.

Perturbations in PQC mechanisms may be aggravated by the presence of sarcomere gene mutations and may explain the difference in disease severity between genotype-positive and genotype-negative patients. Therefore, we defined HCM and mutation-specific changes in key PQC players and the microtubule network (**chapter 7**). We observed the following main findings: (1) Several key PQC players were more abundant in HCM compared to controls; (2) After correction for sex and age, stabilizing HSPB1 and refolding HSPD1 and HSPA2 were increased in sarcomere mutation-positive HCM compared to controls; (3) α-tubulin and acetylated α-tubulin levels were higher in HCM compared to controls, especially in HCM with cMyBP-C haploinsufficiency; (4) cMyBP-C levels were inversely correlated with α-tubulin; and (5) α-tubulin levels correlated with acetylated α-tubulin and HSPs.

In addition to measuring increased levels of a distinct set of HSPs in genotype-positive HCM patients (**chapter 6** and **7**), a histological characterization to determine the intracellular localization of these HSPs is similarly paramount due to the spatial organization of the PQC into compartments.[5,17] Localized translation and degradation processes are important to ensure robust and efficient spatial and stoichiometric control of sarcomere maintenance.[18] For example HSPD1 is a mitochondrial HSP[19] and its translocation to the plasma membrane is detrimental to the cell because of the loss of anti-apoptotic and protective effects.[20] Hence, the specific localization within the cells defines the functional properties of HSPs. Building a histopathological library to link the spatial expression of

the distinct HSPs with the mutant protein expression in patient and compare it to control samples will provide valuable information about how the PQC system may be derailed and which intervention should be considered at all.

To further assess whether our findings point towards proliferations of the microtubule network as a novel pathomechanisms in cMyBP-C haploinsufficiency-mediated HCM, a detailed histological characterization is mandatory. Previously, intercellular variation of cMyBP-C myofilament protein levels was described in cardiomyocytes of HCM patients with *MYBPC3* gene variants.[21,22] Hence, it would be similarly interesting to determine if there is an intercellular variability in the microtubule network. An enrichment of microtubules coinciding with cMyBP-C free patches may thereby suggest a direct compensation for the loss of cMyBP-C on a cellular level. In contrast, an overall increase in the microtubule network may indicate a secondary response regulated on the level of the myocardium due to the *MYBPC3*-caused impaired contractility. This cell-to-cell variability has also been described for *MYH7* mutations and substantial variability in contractility and mutant *MYH7*-mRNA levels were observed.[23,24]

HEAT SHOCK PROTEIN-BASED THERAPEUTIC OPTIONS FOR DCM PATIENTS WITH *HSPB5* GENE VARIANTS

DCM-causing mutations in *HSPB5* were studied in **chapter 4**. We observed that overexpression of mutant HSPB5 in various cell systems resulted in loss-of-function of HSPB complexes and coincided with insolubilisation of HSPB5 and loss of CaT amplitudes. Since oligomerization of HSPB5 proteins is enabled by interaction between C-terminal isoleucine-proline-isoleucine (IPI) domain and the hydrophobic groove in the α-crystallin domain, we studied the effect of loss-of-function mutations in both domains. Introducing a secondary mutation in one of these domains in addition to our *HSPB5* mutants, decreased formation of aggregates which was accompanied by increased solubilisation and a partial restoration of the chaperone function. In a next step, it is necessary to study the potential therapeutic effect in more complex models and include more functional measurements.

In addition, HSPs play a central role in PQC and for that reason pharmacologic modulation of HSP levels represents an interesting target in aging-related protein misfolding diseases. We tested whether oral geranylgeranylacetone (GGA) treatment increased HSP expression in atrial appendages of patients undergoing cardiac surgery (**chapter 5**). Three days of GGA treatment resulted in higher levels of HSPB1 and HSPA1 in the atrial appendages of patients undergoing surgery and higher HSPB1 levels at the myofilaments.

Here we provided direct proof that oral administration of GGA has an HSP boosting effect in human cardiac tissue. Previously, the *in vivo* HSP inducing effect of oral GGA treatment was studied in mutant HSPB5 mice containing the R120G mutation and controls.[25] Interestingly, GGA profoundly enhanced the induction of a discrete subset of small HSPs, including HSPB8 and HSPB1, in mutant mice compared to the induction of HSPA1 in controls.[25] Overall, this suggests that GGA induces the expression of distinct HSPs dependent on tissue-specific HSP expression profile and underlying stress trigger.

While we focused on determining various HSP expression levels after GGA treatment in **chapter 5**, the *in vivo* protective effects of HSP induction on disease development was investigated in studies with rodents. For example, overexpression of *HSPB8* or boosting by GGA treatment had a cardioprotective effect and led to a partial reduction of aggregates formation.[25,26] Therefore, combining the GGA treatment with peptides targeting the altered oligomerization dynamics, as discussed in **chapter 4**, may pave a new treatment strategy in DCM patients carrying *HSPB5* variants. In this case, the loss of function of HSPB complexes would be counteracted by the HSP boosting response of GGA and the peptide treatment would interfere with the oligomerization dynamics of mutant HSPB5 proteins and thereby prevent formation of aggregates.

DERAILED METABOLISM AS KEY DRIVER OF DISEASE IN HCM

Puzzled by the striking clinical heterogeneity and the aim to define genotype-specific changes at the protein levels, we performed an unbiased proteomics approach in cardiac tissue from a clinically well-phenotyped HCM patient group. Our proteomic analysis revealed derailment of metabolic pathways related to energy metabolism as the most prominent derailment in all HCM patients (**chapter 6**). We observed lower expression of proteins involved in oxidative phosphorylation, glycolysis, and fatty acid oxidation. Dysregulation of metabolic proteins was also a main finding of another proteomic study using HCM tissue samples.[27] Strikingly, studies with confirmed gene variant carriers and normal echocardiographic findings classified abnormality of cardiac energetics as an early feature in HCM pathogenesis.[28,29] Environmental and genetic factors have been suggested as dysregulators of the bioenergetic-metabolite interactome leading to a decreased capacity of the metabolic network to adapt and thereby causing progressive loss of cell and tissue function.[30] Therefore, metabolic modulators are currently under investigation to test whether they have a potential to alleviate HCM symptoms.[31,32]

Besides the direct contractile consequences, alterations in the energy metabolism may also affect other high energy dependent processes, such as protein synthesis and removal.[33] Recent insights have uncovered a complex interplay between PQC and metabolism, including bidirectional signalling, transcriptional control, and substrate provision.[34] Each component of the PQC, including HSPs, UPS and autophagy, is intimately linked to metabolism.[34,35] Further studies are mandatory to precisely dissect the impact of derailed energy metabolism on the functionality and adaptability of the PQC system in HCM patients.

SEX-DIFFERENCES IN CLINICAL MANIFESTATION AND CELLULAR PROPERTIES

As aforementioned, sex-differences are observed in the clinical presentation of HCM patients and contribute to the phenotypic heterogeneity.[36-38] In **chapter 8**, we analysed a proteomic data set of septal myocardial tissue of sarcomere mutation-positive HCM patients to investigate if molecular differences underlie sex-differences in clinical presentation. We found an increase in microtubule network and HSPs in female compared to male HCM patients. Due to the direct correlation of cytoskeletal proteins with diastolic dysfunction, we

suggested that elevated tubulin levels partly underlie the more severe diastolic dysfunction in women. In addition, the elevated HSPs levels in females may offer cardio-protective effects and could contribute to the later disease onset. In male HCM patients we observed lower levels of translational proteins which may result in 'aged' sarcomeres. In summary, our data revealed sex-specific differences in levels of tubulin and HSPs.

Our findings and the higher risk of mortality and developing severe heart failure symptoms of women point to the need to study the sex-effect on long-term myocardial performance in HCM.[38] While rodent models of HCM are an appropriate model to study sex-based differences in hypertrophy signalling pathways and cardiomyocyte calcium sensitivity,[39,40] murine studies failed to show a consistent effect of sex hormones on HCM development.[39] In line with our data showing increased levels of HSPs in women, also other components of the PQC system are affected in a sex-dependent manner. For example, diverse sex-related regulation of autophagy protein levels has been reported in a cardiac ischemia-reperfusion rat model.[41,42] Interestingly, organism-wide proteasome activity mapping revealed no sexual dimorphism in mice hearts, but a tremendous age-related decline in both sexes.[43] This highlights again the importance to use sex-specific longitudinal HCM model systems to study the microtubules dynamics and the age-related decline in PQC, as well as to allow the exposure to the different female hormone profiles. A longitudinal model system, including early and advanced disease stages, will help to determine if and when would be the optimal time frame to intervene with sex-specific treatment strategies targeting the microtubules and PQC.

TUBULIN SIGNATURE IN CARDIOMYOPATHIES

Pathways of PQC are strongly linked to the microtubule network and properties and function of this network are fine-tuned by the 'tubulin code' determined by alternative tubulin isotypes and a variety of post-translational modifications.[44] To study the changes in microtubules and its post-translational modifications in cardiac remodelling during disease development, we determined the tubulin signature at the time of septal myectomy (**chapter 6** and **7**). While increased levels of α-tubulin and acetylated α-tubulin were observed in all HCM samples, but more pronounced when a sarcomere mutation was present, increased levels of detyrosinated α-tubulin were specific for sarcomere mutation-positive patients with HCM. Moreover, our sex-based analysis (**chapter 8**) revealed elevated protein levels of tubulin correlate with more severe diastolic dysfunction in women.

Triggered by these findings, we investigated the microtubule signature and desmin levels, a sarcomeric microtubule anchor, in patients with advanced heart failure and various mouse and pig models for cardiac diseases (**chapter 9**). In contrast to HCM patients with NYHA class II-III, the levels of desmin, acetylated and total α-tubulin in a more advanced HCM stage were comparable to controls. Interestingly, detyrosinated α-tubulin was strongly uncoupled from the normal α-tubulin levels in patients with advanced HCM. Increased levels of detyrosinated α-tubulin were also observed in paediatric DCM patients.

In contrast to the big changes seen in our human patient myocardium, tubulin changes in the various animal models of cardiovascular disease were modest. As observed in the

biopsies from NYHA class II-III HCM patients, the development of hypertrophy initiated by pressure overload, such as 3 week aortic banding (AoB) in pigs, or a genetic trigger, such as strongly reduced levels of cMyBP-C in homozygous *MYBPC3*$_{772G>A}$ mice, coincided with increased desmin levels. We observed a compensated, concentric hypertrophic in AoB-treated pigs which was characterized by a normal cardiac function and tubulin signature. In 18 months old pigs with a high body weight and disproportionately low stroke volume, we excluded that detyrosinated α-tubulin contributed to the reported diastolic disturbances because of an overall decreased tubulin signature.

Our comparison of sedentary wild-type mice to mice exposed to an 8-week voluntary wheel-running protocol revealed that exercise had no effect on the tubulin signature and desmin levels. The unchanged tubulin signature in 13 weeks old, heterozygous and homozygous *MYBPC3*$_{772G>A}$ differs from our previous study with older homozygous *MYBPC3* mice. We observed normal α-tubulin levels and increased levels of detyrosinated α-tubulin and desmin in 20 to 28 weeks old homozygous *MYBPC3*$_{2373insG}$ mice, and an increase in α-tubulin and a tendency to increased detyrosination of α-tubulin in 55 to 59 weeks old homozygous *MYBPC3*$_{772G>A}$ mice (**chapter 6**). Furthermore, contractile function was normalized by pharmacological inhibition of detyrosination of α-tubulin in isolated cardiomyocytes.

Our data indicate that the tubulin signature, including total, acetylated and detyrosinated α-tubulin, is increased most at the time of myectomy compared to healthy controls and an altered tubulin signature coincides with diastolic dysfunction. We provide proof that lowering detyrosination of α-tubulin may be a potential novel treatment strategy in patients with sarcomere mutation-positive HCM to improve contractile function and emphasize the need for genotype-specific treatment strategies in HCM. Further experiments are warranted to determine the effect of this treatment strategy in advanced HCM and paediatric DCM.

HCM underlies a complex pathomechanisms and animal models only partially recapitulate the tubulin remodelling. We showed that an aged mouse model with the Dutch founder mutation *MYBPC3*$_{2373insG}$ is mimicking the altered tubulin signature best. This emphasizes the need to establish better model systems to precisely elucidate the effect (compensation or consequence) on contractility, microtubule dynamics and stability of the observed tubulin signature in HCM patients and to test potential drugs re-writing the tubulin signature.

DROSOPHILA MELANOGASTER – A MODEL SYSTEM TO STUDY INHERITED CARDIOMYOPATHIES

In the third part of this thesis, we investigated whether *Drosophila melanogaster* is a model system to study inherited CMs. In **chapter 10**, we described and provided explanations for our unsuccessful attempt to make CRISPR/Cas9 edited *wupA*-mutant strains. *WupA* is the orthologue for the human *TNNI3* gene encoding Troponin I. TnI has a central role during early development and the gene locus within the haplolethal region 16F in *Drosophila melanogaster*.[45-47] Our genome editing approach causing reduced numbers of TnI isoforms or complete depletion of TnI had probably detrimental consequences for sarcomere morphogenesis because under TnI depletion Z discs fail to form.[48] We advise to

select a genome editing approach which does not lead to depletion of TnI isoforms.

In **chapter 11**, we studied two CRISPR/Cas9 edited *Mhc*-mutant strains to investigate the effects of HCM-causing variants located in either the head or the tail region of the protein. We provided a detailed characterization of the morphology of the heart tube. Initially, we planned to compare HCM- and DCM-causing mutations in *Drosophila melanogaster*, but had to deviate from the plan since the *wupA* mutants were not viable. *Drosophila melanogaster* is an interesting model to address histology-based research question because the heart tube consists of spirally oriented myofibrils covered by a ventral layer of longitudinal non-myocardial muscle cells running along the heart tube.[49] Moreover, the myofibrils display a clear striation pattern and the sarcomeric proteins are similar to mammalian cardiomyocytes.[49,50] In comparison to hiPSC-CMs, the effect of high fat or high sugar diet on cardiac function of *Drosophila melanogaster* can easily be studied.[51,52] The short life-time and the high reproduction number provide the opportunity to analyse intergenerational inheritance pattern, such as the high fat diet-induced cardiac lipotoxicity.[53] Therefore, genome-edited *Drosophila melanogaster* may be an interesting and low cost *in vivo* model to address histology- or diet-based research questions.

FUTURE PERSPECTIVE

In this thesis, we studied the PQC and tubulin signature in inherited CMs. So far, advances in elucidating PQC in the heart are relatively limited.[34] The aspect that both systems, PQC and microtubule network, are of a highly dynamic nature needs to be implemented in future model system to further elucidate the pathomechanisms of inherited CMs. Fluorescent tracking along the disease progression in simple, and complex cell-based systems and building a strong histopathological library of human tissue biopsies will provide valuable spatial and temporal data.[54] In addition, as observed at different part of this thesis, the PQC system is not a system which stands alone, but interacts with the microtubule network and metabolism, and both expression and regulation show sex-dependent differences. An improved and coordinated understanding of consequences and compensatory mechanisms when one system is derailed is warranted.

Interestingly, each component of the PQC system, including HSPs, ubiquitin-proteasome system and autophagy, is inherent dichotomy: each is capable of beneficial changes, and each is capable of destructive changes.[34] The ongoing puzzle is to determine whether quantitative differences (too much or too little) or qualitative distinctions are causative for the dichotomy.[34] Therefore, it is of utmost importance to determine the range of physiological concentration in health and disease for key PQC players and find new analytical tools to measure the individual capabilities.

Using the most adequate model system recapitulating the respective hallmarks of inherited CMs and taking sex- and genotype-based differences into account will be paramount to test potential drugs modulating the PQC and tubulin signature to find new personalized treatment strategies.

REFERENCES

1. Elliott P, Andersson B, Arbustini E, Bilinska Z, Cecchi F, Charron P, et al. Classification of the cardiomyopathies: a position statement from the European Society Of Cardiology Working Group on Myocardial and Pericardial Diseases. *Eur Heart J*. 2008;29(2):270-6.
2. Arbustini E, Narula N, Dec GW, Reddy KS, Greenberg B, Kushwaha S, et al. The MOGE(S) classification for a phenotype-genotype nomenclature of cardiomyopathy: endorsed by the World Heart Federation. *J Am Coll Cardiol*. 2013;62(22):2046-72.
3. Seferovic PM, Polovina M, Bauersachs J, Arad M, Gal TB, Lund LH, et al. Heart failure in cardiomyopathies: a position paper from the Heart Failure Association of the European Society of Cardiology. *Eur J Heart Fail*. 2019;21(5):553-76.
4. Levine A, Gupta CA, Gass A. Advanced Heart Failure Management and Transplantation. *Cardiol Clin*. 2019;37(1):105-11.
5. Chen B, Retzlaff M, Roos T, Frydman J. Cellular strategies of protein quality control. *Cold Spring Harb Perspect Biol*. 2011;3(8):a004374.
6. Robison P, Prosser BL. Microtubule mechanics in the working myocyte. *J Physiol*. 2017;595(12):3931-7.
7. Sontag EM, Vonk WIM, Frydman J. Sorting out the trash: the spatial nature of eukaryotic protein quality control. *Curr Opin Cell Biol*. 2014;26:139-46.
8. Humburg P, Maugeri N, Lee W, Mohr B, Knight JC. Characterisation of the global transcriptional response to heat shock and the impact of individual genetic variation. *Genome Med*. 2016;8(1):87.
9. Hoes MF, Bomer N, van der Meer P. Concise Review: The Current State of Human In Vitro Cardiac Disease Modeling: A Focus on Gene Editing and Tissue Engineering. *Stem Cells Transl Med*. 2019;8(1):66-74.
10. Buikema JW, Wu SM. Untangling the Biology of Genetic Cardiomyopathies with Pluripotent Stem Cell Disease Models. *Curr Cardiol Rep*. 2017;19(4):30.
11. Marcu IC, Illaste A, Heuking P, Jaconi ME, Ullrich ND. Functional Characterization and Comparison of Intercellular Communication in Stem Cell-Derived Cardiomyocytes. *Stem Cells*. 2015;33(7):2208-18.
12. Wells SP, Waddell HM, Sim CB, Lim SY, Bernasochi GB, Pavlovic D, et al. Cardiomyocyte functional screening: interrogating comparative electrophysiology of high-throughput model cell systems. *Am J Physiol Cell Physiol*. 2019;317(6):C1256-C67.
13. Ojala M, Prajapati C, Polonen RP, Rajala K, Pekkanen-Mattila M, Rasku J, et al. Mutation-Specific Phenotypes in hiPSC-Derived Cardiomyocytes Carrying Either Myosin-Binding Protein C Or alpha-Tropomyosin Mutation for Hypertrophic Cardiomyopathy. *Stem Cells Int*. 2016;2016:1684792.
14. Sparrow AJ, Sievert K, Patel S, Chang YF, Broyles CN, Brook FA, et al. Measurement of Myofilament-Localized Calcium Dynamics in Adult Cardiomyocytes and the Effect of Hypertrophic Cardiomyopathy Mutations. *Circ Res*. 2019;124(8):1228-39.
15. Sewanan LR, Campbell SG. Modelling sarcomeric cardiomyopathies with human cardiomyocytes derived from induced pluripotent stem cells. *J Physiol*. 2020;598(14):2909-22.
16. Buikema JW, Lee S, Goodyer WR, Maas RG, Chirikian O, Li G, et al. Wnt Activation and Reduced Cell-Cell Contact Synergistically Induce Massive Expansion of Functional Human iPSC-Derived Cardiomyocytes. *Cell Stem Cell*. 2020;27(1):50-63 e5.
17. Sontag EM, Samant RS, Frydman J. Mechanisms and Functions of Spatial Protein Quality Control. *Annu Rev Biochem*. 2017;86:97-122.
18. Lewis YE, Moskovitz A, Mutlak M, Heineke J, Caspi LH, Kehat I. Localization of transcripts, translation, and degradation for spatiotemporal sarcomere maintenance. *J Mol Cell Cardiol*. 2018;116:16-28.
19. Soltys BJ, Gupta RS. Immunoelectron microscopic localization of the 60-kDa heat shock chaperonin protein (Hsp60) in mammalian cells. *Exp Cell Res*. 1996;222(1):16-27.
20. Lin L, Kim SC, Wang Y, Gupta S, Davis B, Simon SI, et al. HSP60 in heart failure: abnormal distribution and role in cardiac myocyte apoptosis. *Am J Physiol Heart Circ Physiol*. 2007;293(4):H2238-47.
21. Parbhudayal RY, Garra AR, Gotte MJW, Michels M, Pei J, Harakalova M, et al. Variable cardiac myosin binding protein-C expression in the myofilaments due to MYBPC3 mutations in hypertrophic cardiomyopathy. *J Mol Cell Cardiol*. 2018;123:59-63.
22. Theis JL, Bos JM, Theis JD, Miller DV, Dearani JA, Schaff HV, et al. Expression patterns of cardiac myofilament proteins: genomic and protein analysis of surgical myectomy tissue from patients with obstructive hypertrophic cardiomyopathy. *Circ Heart Fail*. 2009;2(4):325-33.
23. Kraft T, Montag J. Altered force generation and cell-to-cell contractile imbalance in hypertrophic cardiomyopathy. *Pflugers Arch*. 2019;471(5):719-33.
24. Kraft T, Montag J, Radocaj A, Brenner B. Hypertrophic Cardiomyopathy: Cell-to-Cell Imbalance in Gene Expression and Contraction Force as Trigger for Disease Phenotype Development. *Circ Res*. 2016;119(9):992-5.
25. Sanbe A, Daicho T, Mizutani R, Endo T, Miyauchi N, Yamauchi J, et al. Protective effect of geranylgeranylacetone via enhancement of HSPB8 induction in desmin-related cardiomyopathy. *PLoS One*. 2009;4(4):e5351.
26. Sanbe A, Yamauchi J, Miyamoto Y, Fujiwara Y, Murabe M, Tanoue A. Interruption of CryAB-amyloid oligomer formation by HSP22. *J Biol Chem*. 2007;282(1):555-63.
27. Coats CJ, Heywood WE, Virasami A, Ashrafi N, Syrris P, Dos Remedios C, et al. Proteomic Analysis of the Myocardium in Hypertrophic Obstructive Cardiomyopathy. *Circ Genom Precis Med*. 2018;11(12):e001974.

28. Crilley JG, Boehm EA, Blair E, Rajagopalan B, Blamire AM, Styles P, et al. Hypertrophic cardiomyopathy due to sarcomeric gene mutations is characterized by impaired energy metabolism irrespective of the degree of hypertrophy. *J Am Coll Cardiol*. 2003;41(10):1776-82.
29. Witjas-Paalberends ER, Guclu A, Germans T, Knaapen P, Harms HJ, Vermeer AM, et al. Gene-specific increase in the energetic cost of contraction in hypertrophic cardiomyopathy caused by thick filament mutations. *Cardiovasc Res*. 2014;103(2):248-57.
30. Hill BG, Shiva S, Ballinger S, Zhang J, Darley-Usmar VM. Bioenergetics and translational metabolism: implications for genetics, physiology and precision medicine. *Biol Chem*. 2019;401(1):3-29.
31. Leviner DB, Hochhauser E, Arad M. Inherited cardiomyopathies–Novel therapies. *Pharmacol Ther*. 2015;155:36-48.
32. Fumagalli C, De Gregorio MG, Zampieri M, Fedele E, Tomberli A, Chiriatti C, et al. Targeted Medical Therapies for Hypertrophic Cardiomyopathy. *Curr Cardiol Rep*. 2020;22(2):10.
33. Catic A. Cellular Metabolism and Aging. *Prog Mol Biol Transl Sci*. 2018;155:85-107.
34. Wang ZV, Hill JA. Protein quality control and metabolism: bidirectional control in the heart. *Cell Metab*. 2015;21(2):215-26.
35. Chang J, Knowlton AA, Xu F, Wasser JS. Activation of the heat shock response: relationship to energy metabolites. A (31)P NMR study in rat hearts. *Am J Physiol Heart Circ Physiol*. 2001;280(1):H426-33.
36. Nijenkamp L, Bollen IAE, van Velzen HG, Regan JA, van Slegtenhorst M, Niessen HWM, et al. Sex Differences at the Time of Myectomy in Hypertrophic Cardiomyopathy. *Circ Heart Fail*. 2018;11(6):e004133.
37. van Driel B, Nijenkamp L, Huurman R, Michels M, van der Velden J. Sex differences in hypertrophic cardiomyopathy: new insights. *Curr Opin Cardiol*. 2019;34(3):254-9.
38. Lakdawala NK, Olivotto I, Day SM, Han L, Ashley EA, Michels M, et al. Associations Between Female Sex, Sarcomere Variants and Clinical Outcomes in Hypertrophic Cardiomyopathy. *Circ Genom Precis Med*. 2020.
39. Blenck CL, Harvey PA, Reckelhoff JF, Leinwand LA. The Importance of Biological Sex and Estrogen in Rodent Models of Cardiovascular Health and Disease. *Circ Res*. 2016;118(8):1294-312.
40. Birch CL, Behunin SM, Lopez-Pier MA, Danilo C, Lipovka Y, Saripalli C, et al. Sex dimorphisms of crossbridge cycling kinetics in transgenic hypertrophic cardiomyopathy mice. *Am J Physiol Heart Circ Physiol*. 2016;311(1):H125-36.
41. Chen C, Hu LX, Dong T, Wang GQ, Wang LH, Zhou XP, et al. Apoptosis and autophagy contribute to gender difference in cardiac ischemia-reperfusion induced injury in rats. *Life Sci*. 2013;93(7):265-70.
42. Le TY, Ashton AW, Mardini M, Stanton PG, Funder JW, Handelsman DJ, et al. Role of androgens in sex differences in cardiac damage during myocardial infarction. *Endocrinology*. 2014;155(2):568-75.
43. Jenkins EC, Shah N, Gomez M, Casalena G, Zhao D, Kenny TC, et al. Proteasome mapping reveals sexual dimorphism in tissue-specific sensitivity to protein aggregations. *EMBO Rep*. 2020;21(4):e48978.
44. Janke C, Magiera MM. The tubulin code and its role in controlling microtubule properties and functions. *Nat Rev Mol Cell Biol*. 2020;21(6):307-26.
45. Sahota VK, Grau BF, Mansilla A, Ferrus A. Troponin I and Tropomyosin regulate chromosomal stability and cell polarity. *J Cell Sci*. 2009;122(Pt 15):2623-31.
46. Casas-Tinto S, Ferrus A. Troponin-I mediates the localization of selected apico-basal cell polarity signaling proteins. *J Cell Sci*. 2019;132(8).
47. Prado A, Canal I, Ferrus A. The haplolethal region at the 16F gene cluster of Drosophila melanogaster: structure and function. *Genetics*. 1999;151(1):163-75.
48. Marin MC, Rodriguez JR, Ferrus A. Transcription of Drosophila troponin I gene is regulated by two conserved, functionally identical, synergistic elements. *Mol Biol Cell*. 2004;15(3):1185-96.
49. Taghli-Lamallem O, Plantie E, Jagla K. Drosophila in the Heart of Understanding Cardiac Diseases: Modeling Channelopathies and Cardiomyopathies in the Fruitfly. *J Cardiovasc Dev Dis*. 2016;3(1).
50. Choma MA, Suter MJ, Vakoc BJ, Bouma BE, Tearney GJ. Physiological homology between Drosophila melanogaster and vertebrate cardiovascular systems. *Dis Model Mech*. 2011;4(3):411-20.
51. Diop SB, Birse RT, Bodmer R. High Fat Diet Feeding and High Throughput Triacylglyceride Assay in Drosophila Melanogaster. *J Vis Exp*. 2017(127).
52. Na J, Musselman LP, Pendse J, Baranski TJ, Bodmer R, Ocorr K, et al. A Drosophila model of high sugar diet-induced cardiomyopathy. *PLoS Genet*. 2013;9(1):e1003175.
53. Guida MC, Birse RT, Dall'Agnese A, Toto PC, Diop SB, Mai A, et al. Intergenerational inheritance of high fat diet-induced cardiac lipotoxicity in Drosophila. *Nat Commun*. 2019;10(1):193.
54. Macario AJ, de Macario EC. Molecular mechanisms in chaperonopathies: clues to understanding the histopathological abnormalities and developing novel therapies. *J Pathol*. 2020;250(1):9-18.

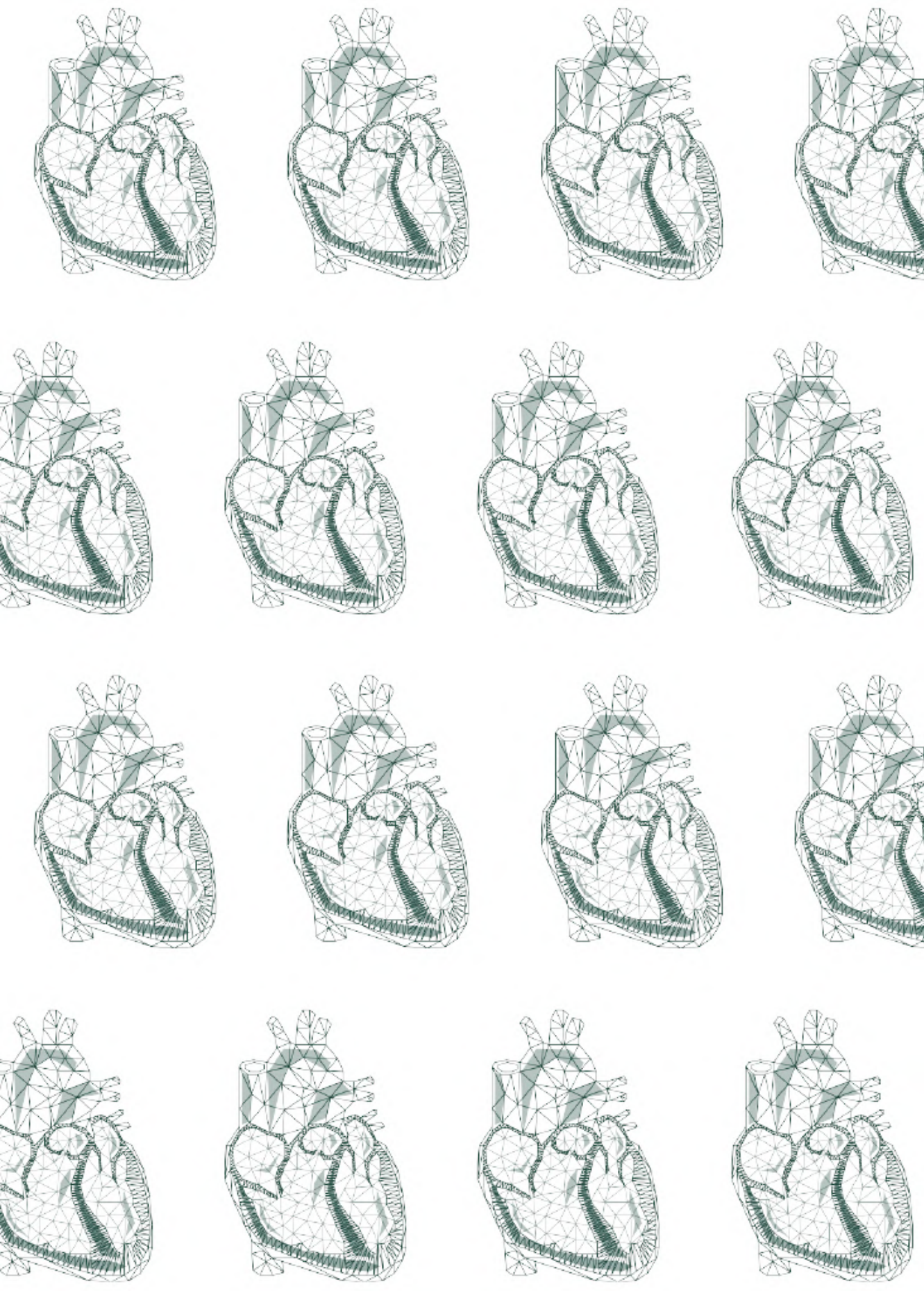

APPENDIX

GERMAN SUMMARY/DEUTSCHE ZUSAMMENFASSUNG

In dieser Doktorarbeit geht es um Kardiomyopathien. Das sind Erkrankungen des Herzmuskels (Myokardium), bei denen sich die Struktur des Muskelgewebes verändert und die Leistungsfähigkeit verloren geht. Das beeinträchtigte Herz kann nicht mehr genügend Blut durch den Kreislauf befördern und es entsteht eine Herzschwäche (Herzinsuffizienz). Man unterscheidet drei Hauptformen: dilatative (DCM), hypertrophe (HCM) und restriktive (RCM) Kardiomyopathie.

Bei der DCM dilatiert und verdünnt sich die Wand der linken Herzkammer. Dadurch ist die Kontraktion des Herzmuskels verringert und weniger Blut wird gepumpt.

Bei der HCM kommt es zu einer Verdickung des Herzmuskels in der linken Herzkammer. Die Verdickung tritt am häufigsten am Septum auf und kann eine Verengung verursachen, die den Blutfluss vom linken Ventrikel zur Aorta verringern oder blockieren kann. Die Ventrikel müssen stärker pumpen, um die Verengung oder Blockade zu überwinden. Hinzu kommt, dass sich der Herzmuskel schlechter entspannen kann, was die Füllung des Herzens mit Blut einschränkt.

Bei der RCM, die sehr selten ist, wird vermehrt Bindegewebe in den Herzmuskel eingelagert, dadurch versteift die linke Herzkammer. Die Starrheit des Myokardiums erschwert die Füllung mit Blut durch großen Widerstand, wodurch sich die Ventrikel nicht genügend füllen können und zu wenig Blut in den Kreislauf gepumpt wird.

Alle drei Kardiomyopathien können genetisch bedingt sein, was bedeutet, dass das Krankheitsbild durch eine erbliche Veranlagung (Mutation in der DNA) verursacht werden kann. In dieser Arbeit haben wir genetisch bedingte Fälle untersucht und uns auf Mutationen fokussiert, die den Herzmuskelapparat betreffen. Interessanterweise können Mutationen im gleichen Gen sowohl DCM, HCM als auch RCM verursachen, wie wir in Kapitel 2 anhand des Gens *TPM1* zeigen. Hinzu kommt, dass der Krankheitsverlauf individuell sehr unterschiedlich ist, auch bei Patienten mit der genetisch identischen Variante. Unsere Daten in Kapitel 2 veranschaulichen diese klinische Heterogenität und implizieren, dass die Pathophysiologie von vererbbaren Kardiomyopathien komplexer ist als das simple Vorhandensein einer Genvariante. Daher ist es von größter Bedeutung, zusätzliche Krankheitsauslöser, sogenannte Trigger, zu identifizieren, um den zugrunde liegenden Pathomechanismus besser zu verstehen. Wir haben zelluläre, genetische und klinische Daten aus gut erforschten Patientenkohorten und verschiedene Modellsystemen für Kardiomyopathien verwendet, um mögliche Trigger zu untersuchen. In dieser Arbeit konzentrierten wir uns auf das Proteinqualitätskontrollsystem (PQC) und das Mikrotubuli-Netzwerk.

Das PQC System ist ein zellulärer Schutzmechanismus, der für die Aufrechterhaltung eines funktionierenden Proteoms verantwortlich ist. Hierbei werden defekte oder mutierte Proteine von Hitzeschockproteinen (HSPs) erkannt und falls eine Reparatur nicht möglich ist, wird dieses abgebaut.

Mikrotubuli sind kleine, röhrenförmige Proteinkomplexe, die aus α- und β-Tubulin aufgebaut sind. Sie bilden die Grundlage für das Cytoskelett und geben damit der Zelle eine gewisse mechanische Stabilität. Es ist bekannt, dass sich das Mikrotubuli-Netzwerk bei verschiedenen Krankheiten umbaut.

Bisher ist die Anzahl an Studien, die die Rolle der PQC bei genetisch bedingten Kardiomyopathien untersucht haben, begrenzt. In Kapitel 3 geben wir deshalb einen Überblick über die strukturellen Veränderungen und wie sich das PQC System anpasst. Hierbei beobachteten wir, dass die Entgleisung des PQC Systems entweder direkt durch die Mutation oder sekundär in Folge von zellulären Veränderungen durch die Mutation verursacht sein kann.

In Kapitel 4 wird der Fokus auf zwei Genvarianten des kleinen Hitzeschockproteins HSPB5 verlagert, die beide DCM verursachen. In einem ersten Schritt haben wir die beiden HSPB5-Varianten in verschiedenen Zellsystemen überexprimiert, um den Funktionsverlust, wie zum Beispiel die Bildung von Aggregaten, zu studieren. In einem zweiten Schritt demonstrierten wir, dass das Einfügen einer zusätzlichen Mutation die Proteinaggregation verringert und zur Funktionswiederherstellung führt. Die potenzielle therapeutische Wirkung dieser zusätzlichen Mutation muss nun in komplexeren Modellen in weiteren Studien untersucht werden.

Weil die HSPs für das PQC System wichtig sind, stellt die pharmakologische Modulation der HSP-Spiegeln eine interessante Behandlungsmöglichkeit für altersbedingte Proteinfehlfaltungserkrankungen dar. Wir haben in Kapitel 5 gezeigt, dass eine orale Einnahme von Geranlylgeranylaceton (GGA) kurz vor einer Herzoperation die Expression von bestimmten HSPs im Herzvorhof von Patienten erhöht.

In Kapitel 6 wurde das Proteom von HCM-Patienten mit gesunden Kontrollproben verglichen. Unsere Analyse ergab, dass in den Patientenproben weniger Proteine exprimiert werden, die für die zelluläre Energiegewinnung wichtig sind. Des Weiteren wiesen Patienten mit einer Genmutation im Vergleich zu Patienten ohne Mutation eine stark erhöhte Menge an α-Tubulin auf, insbesondere von der detyrosinierten Form. Wir zeigten in einem Mausmodell mit einer häufigen HCM Mutation, dass eine pharmakologische Verringerung der detyrosinierten Tubulin-Form ein vielversprechender neuer Therapieansatz darstellt, da sich die Funktion der Herzmuskelzellen verbesserte.

In derselben HCM-Patientengruppe haben wir die Proteinspiegel wichtiger PQC Bausteine, wie zum Beispiel stabilisierende HSPs, HSPs mit der Kapazität Proteine zu falten und diverse Proteinabbaumarker, sowie Bestandteile des Mikrotubuli-Netzwerkes bestimmt (Kapitel 7). Hier war die Überlegung, dass die Genmutationen oft den Muskelapparat betreffen und diese Proteine einen großen Bestandteil von Herzmuskelzellen ausmachen. Eine große Anzahl an beschädigten Proteinen könnte zu einer Beeinträchtigung des PQC Systems führen und möglicherweise erklären, weshalb Patienten mit einer Genmutation in einem früheren Alter erkranken und an einem schlimmeren Krankheitsverlauf leiden.

Darüber hinaus beobachteten wir interindividuelle Unterschiede in der Kapazität des PQC und entgleisten Anpassungen an Stressauslöser, was zur klinischen Heterogenität beitragen könnte. Übereinstimmend mit Kapitel 6 war α-Tubulin, sowie auch dessen acetylierte Form, besonders erhöht in Patienten mit einer Genmutation.

Auch geschlechtsspezifische Unterschiede prägen das klinische Erscheinungsbild und tragen möglicherweise zur phänotypischen Heterogenität von HCM-Patienten bei. In Kapitel 8 analysierten wir Geschlechtsunterschiede auf Proteinebene in HCM-Patientengewebe und demonstrierten, dass Frauen mehr α-Tubulin sowie auch höhere Mengen an HSPs haben.

In Kapitel 9 befassten wir uns mit dem Mikrotubuli-Netzwerk in verschiedenen Maus- und Schweinmodellen für Hypertrophie und/oder Herzinsuffizienz. Im Gegensatz zu den deutlichen Mikrotubuli-Veränderungen, die wir in den Patientenproben detektiert haben, waren die Veränderungen in den verschiedenen Tiermodellen minimaler. Darüber hinaus untersuchten wir, ob das Mikrotubuli-Netzwerk auch in anderen vererbbaren oder erworbenen Herzerkrankungen, wie DCM und ischämische Herzerkrankungen, umgebaut wird. Unsere Daten zeigten, dass die Tubulin-Signatur, einschließlich gesamtes, acetyliertes und detyrosiniertes α-Tubulin, im Vergleich zu gesunden Kontrollen und den anderen Herzerkrankungen zum Zeitpunkt der Septummyektomie von HCM-Patienten am stärksten erhöht ist.

Im letzten Teil dieser Doktorarbeit wurden Fruchtfliegen (*Drosophila melanogaster*) als ein Modellsystem für vererbbare Kardiomyopathien untersucht. Mittels der Genschere CRISPR-Cas9 wurde versucht, verschiedene klinisch relevante Mutationen in das Erbgut einzufügen. In Kapitel 10 fokussierten wir uns auf zwei Mutationen in dem Gen *TNNI3* (*wupA* in *Drosophila melanogaster*), wobei eine Variante DCM und die andere HCM beim Menschen verursacht. Unser Ansatz war nicht erfolgreich und daher liefern wir an dieser Stelle verschiedene Erklärungen dafür. In Kapitel 11 wurden zwei verschiedene Mutationen ins *Mhc* Gen eingeführt, beide führen zu HCM im Menschen, jedoch befinden sich die Varianten an ganz unterschiedlichen Stellen des Mhc Proteins. Die *Mhc*-mutierten Fruchtfliegen verglichen wir mit der Kontrollgruppe (w^{1118}) und zeigten, dass morphologisch und molekularbiologisch keine Unterschiede bestehen.

In dieser Doktorarbeit wurden die PQC und Mikrotubuli-Signatur in vererbbaren Kardiomyopathien untersucht. Potenzielle Anknüpfstellen wurden aufgezeigt und es wird auf die Implementierung dynamischer Modellsysteme in zukünftigen Studien appelliert, um den Einfluss des PQC Systems und des Umbaus des Mikrotubuli-Netzwerkes auf den Pathomechanismus in Kardiomyopathien besser zu verstehen.

CURRICULUM VITAE

Larissa M. Dorsch was born in Bad Friedrichshall, Germany, in 1992. After graduating from secondary school (Justinus-Kerner-Gymnasium, Weinsberg, Germany) in 2011, she started her bachelor of science degree in Molecular Medicine at Ulm University, Ulm, Germany. She performed internships in the Department of Neuropsychology at University and Rehabilitation Clinics Ulm, Germany, supervised by Prof. Dorothée Lulé and in the Department of Physiology of the VUmc, Amsterdam, the Netherlands, supervised by Dr. Vasco Sequeira and Prof. Jolanda van der Velden. During her bachelor thesis in the group of Prof. Steffen Just, she studied the loss of Talin2a in the *in vivo* model zebrafish in the Department of Molecular Cardiology at Ulm University and received her bachelor's degree in 2014.

Driven by a fascination for tumour cells, she joined a master program in Biomedical Sciences at Philipps University of Marburg, Germany and specialized in tumour biology. During this time, she performed internships in the Institute of Molecular Biology and Tumour Research supervised by Prof. Alexander Brehm, in the Department of Medical Cell Biology supervised by Prof. Wulf Hildebrandt and in the Institute of Pathology supervised by Dr. Ansgar Schmidt and Prof. Roland Moll at Philipps University of Marburg, Germany. The master thesis was conducted in the Moll lab entitled: Analysis of the responsible interaction domains between Plakophilin 3 (PKP3) and Peptidyl-Prolyl Cis-Trans Isomerase NIMA-interacting 1 (PIN1).

In 2016, she received her master's degree and started her PhD under the supervision of Prof. Jolanda van der Velden, Prof. Bianca Brundel and Dr. Diederik Kuster in the Department of Physiology in Amsterdam, the Netherlands. Larissa worked within the national CVON-DOSIS consortium and focused on the role of protein quality control and tubulin remodelling in inherited cardiomyopathies. The results of the PhD research project are presented in this thesis. She collaborated with Dr. Paul van der Zwaag at the UMC Groningen, Prof. Dirk Duncker at the Erasmus MC in Rotterdam and the group of Prof. Folkert Asselbergs at the UMC Utrecht.

Since June 2021, Larissa has worked as a Medical-Marketing-Sales Trainee at Consumer Healthcare Sanofi in Frankfurt am Main.

LIST OF PUBLICATIONS

Dorsch LM, Sorop O, Vink A, Michels M, dos Remedios CG, Dalinghaus M, Carrier L, Duncker DJGM, Kuster DWD, van der Velden J. Tubulin signature and desmin levels in pig and mouse models for cardiomyopathies and human heart failure samples. *Pilot study.*

Dorsch LM, Espinosa González P, Kuster DWD, van der Velden J. Molecular biological and morphological characterization of CRISPR/Cas9-edited *Drosophila melanogaster* strains with *Mhc* variants R402Q and S1376M. *Manuscript in preparation.*

Vonk JJ*, **Dorsch LM***, Woods CN*, Freilich R*, van der Velden J, Brundel BJJM, Gestwicki JE, Klevit RE, Kampinga HH. Functional rescue of disease-causing HSPB5 mutants by interfering with interactions of the C-terminal tail and the hydrophobic β4-β8 groove in the α-crystallin domain. *Manuscript in preparation.*

Dorsch LM, Brundel BJJM, Kuster DWD, van der Velden J. Scarless CRISPR/Cas9 editing of haplolethal region 16F in *Drosophila melanogaster* results in lethality *Manuscript in revision.*

Pei J, Schuldt M, Nagyova E, Gu Z, El Bouhaddani S, Yiangou L, Jansen M, Calis JJA, **Dorsch LM**, Blok CS, van den Dungen NAM, Lansu N, Boukens BJ, Efimov IR, Michels M, Verhaar MC, de Weger R, Vink A, van Steenbeek FG, Baas AF, Davis RP, Uh HW, Kuster DWD, Cheng C, Mokry M, van der Velden J, Asselbergs FW, Harakalova M. Multi-omics integration identifies key upstream regulators of pathomechanisms in hypertrophic cardiomyopathy due to truncating MYBPC3 mutations. *Clin Epigenetics. 2021;13(1):61.* doi: 10.1186/s13148-021-01043-3.

Schuldt M, **Dorsch LM**, Knol JC, Pham TV, Schelfhorst T, Piersma SR, Dos Remedios C, Michels M, Jimenez CR, Kuster DWD, van der Velden J. Sex-Related Differences in Protein Expression in Sarcomere Mutation-Positive Hypertrophic Cardiomyopathy. *Front Cardiovasc Med. 2021;8:612215.* doi: 10.3389/fcvm.2021.612215.

Dorsch LM, Kuster DWD, Jongbloed JDH, Boven LG, van Spaendonck-Zwarts KY, Suurmeijer AJH, Vink A, du Marchie Sarvaas GJ, van den Berg MP, van der Velden J, Brundel BJJM, van der Zwaag PA. The effect of tropomyosin variants on cardiomyocyte function and structure that underlie different clinical cardiomyopathy phenotypes. *Int J Cardiol. 2021;323:251-258.* doi: 10.1016/j.ijcard.2020.08.101.

Schuldt M, Pei J, Harakalova M, **Dorsch LM**, Schlossarek S, Mokry M, Knol JC, Pham TV, Schelfhorst T, Piersma SR, Dos Remedios C, Dalinghaus M, Michels M, Asselbergs FW, Moutin MJ, Carrier L, Jimenez CR, van der Velden J, Kuster DWD. Proteomic and Functional Studies Reveal Detyrosinated Tubulin as Treatment Target in Sarcomere Mutation-Induced Hypertrophic Cardiomyopathy. *Circ Heart Fail. 2021;14(1):e007022.* doi: 10.1161/CIRCHEARTFAILURE.120.007022.

de Boer RA, Nijenkamp LLAM, Silljé HHW, Eijgenraam TR, Parbhudayal R, van Driel B, Huurman R, Michels M, Pei J, Harakalova M, van Lint FHM, Jansen M, Baas AF, Asselbergs FW, van Tintelen JP, Brundel BJJM, **Dorsch LM**, Schuldt M, Kuster DWD, van der Velden J; DOSIS consortium. Strength of patient cohorts and biobanks for cardiomyopathy research. *Neth Heart J. 2020;28(Suppl 1):50-56.* doi: 10.1007/s12471-020-01456-4.

Buikema JW, Lee S, Goodyer WR, Maas RG, Chirikian O, Li G, Miao Y, Paige SL, Lee D, Wu H, Paik DT, Rhee S, Tian L, Galdos FX, Puluca N, Beyersdorf B, Hu J, Beck A, Venkamatran S, Swami S, Wijnker P, Schuldt M, **Dorsch LM**, van Mil A, Red- Horse K, Wu JY, Geisen C, Hesse M, Serpooshan V, Jovinge S, Fleischmann BK, Doevendans PA, van der Velden J, Garcia KC, Wu JC, Sluijter JPG, Wu SM. Wnt Activation and Reduced Cell-Cell Contact Synergistically Induce Massive Expansion of Functional Human iPSC-Derived Cardiomyocytes. *Cell Stem Cell. 2020;27(1):50-63.e5.* doi: 10.1016/j.stem.2020.06.001.

van Marion DMS, **Dorsch LM**, Hoogstra-Berends F, Kakuchaya T, Bockeria L, de Groot NMS, Brundel BJJM. Oral geranylgeranylacetone treatment increases heat shock protein expression in human atrial tissue. *Heart Rhythm. 2020;17(1):115-122.* doi: 10.1016/j.hrthm.2019.07.010.

Dorsch LM*, Schuldt M*, dos Remedios CG, Schinkel AFL, de Jong PL, Michels M, Kuster DWD, Brundel BJJM, van der Velden J. Protein Quality Control Activation and Microtubule Remodeling in Hypertrophic Cardiomyopathy. *Cells. 2019;8(7):741.* doi: 10.3390/cells8070741.

Dorsch LM, Schuldt M, Knežević D, Wiersma M, Kuster DWD, van der Velden J, Brundel BJJM. Untying the knot: protein quality control in inherited cardiomyopathies. *Pflugers Arch. 2019;471(5):795-806.* doi: 10.1007/s00424-018-2194-0.

ACKNOWLEDGEMENTS

Time flies
But don't let it fly by
Spread your wings
And fly with it
- Ashlee Edens -

I would like to say thank you to everyone who directly or indirectly supported and helped me to fly through my PhD time.

Dear Jolanda, I highly appreciate that I had this amazing opportunity to do my PhD on the DOSIS project in your research team. Thank you for believing in me and for all the support. It was great to start into each week with the Monday morning meeting and a warm laugh in your office. Thank you so much for helping me equip my scientific toolbox with good tools and acquire the necessary skills. I am glad for having had plenty of possibilities for scientific exchange at summer schools, workshops and conferences. Thank you for all the scientific discussions, feedback on manuscripts/abstracts and overall supervision. I will always admire your determination and enthusiasm for research about cardiomyopathies.

Dear Bianca, I am really grateful for the opportunity to have started my PhD in the Physiology department. Thank you for introducing me to the fascinating protein quality control research field. It was interesting to see how much has already been investigated about atrial fibrillation and I enjoyed to catch up a bit about cardiomyopathies.

Dear Diederik, I really liked the fact that I could just walk by your office whenever I had any questions. Now and then, answering the questions ended in long scientific discussions. I really appreciate that you provided good constructive feedback for manuscripts from which I could learn a lot. The creative invitation emails for the Friday afternoon meeting were a highlight each Friday morning and I missed it a lot when the meetings became digital and the invitation was shortened to "zoom/teams call starting in 15 min".

Dear members of the reading committee: Coen, Dirk, Bert, Natasja, Paul and Herman, thank you for your time and effort to critically evaluate my thesis.

It was so great to be surrounded by so many familiar faces when I started with my PhD. Thanks Vasco, Paul, Max, Denielli, Joana, Robert, Nina, Barbara, Ruud and Aimée for the fun time and help during my summer internship in 2013 and my PhD. Vasco, you were such an inspiring supervisor during my internship and I wish you all the best for your scientific career. Thanks Paul, for sharing your EHT knowledge and the fun conversations we had. I am still surprised that your EHTs survived when I only refreshed the medium once a week. Oh Max, du warst das wandelnde elab und konntest bei jeder Frage weiterhelfen. Vielen Dank auch für den ganzen Spaß im Proteinlab. Denielli, your birthday barbecue was one of the best I ever ate. Ruud, thank you for being such a constant in the protein lab and taking care of this place so well. Aimée, I am still fascinated how quickly you were able to solve any bureaucratic problem. By the way, your sense of humor was the best!

A big thank you also to Jessica, Sjoukje and Eva for taking care of administrative affairs. Isabelle, thank you for all your support regarding the PhD programme.

To all my roomies of 12W28, I really enjoyed the vibe in our office and spending time with you. Thank you for all the nice conversations, complaining together, lots of laughter and last, but not least the klaagmuur post-it notes on the door. Denise, thank you for showing me how to plan and perform Western Blots in high-throughput. I still remember our language mixture of half-Dutch-half-German when we were talking to each other. Thank you Martijn for being a strong believer that I was living in the office and playing straight along this role for my whole PhD time. Eva, we started exactly the same day with our PhD. Thank you for always being there when I needed to share something (funny). Marloes, we both had the habit to be productive, when our roomies had gone home. Thank you for making this time more fun. Elisa, you made the office more colourful and always shared good tips at which places the best Italian food is served in Amsterdam. Kennedy, you were a great host of many dinner parties at your place. Imagine how much weight we would have gained if Corona had not stopped us. Thanks for saying to me "you are so smart" - I loved to answer to this phrase. Hua, you were always working very hard and I am already looking forward to visit you in your home country. Hey Guys, Ricardo and his chairs were the latest addition to our office. It was all the time fun to see the amounts of your favourite vegetable/fruit on your desk and the reaction of the people entering the office.

My dear Xu, aka People and Cull Culture Twin, you got me familiar with the lab and stayed as a very good friend. I still remember our cell culturing times talking, joking and laughing about empty bottle weather forecast, cell culture room nanny and the skateboard to slide the flasks within the cell culture hood. It was my pleasure to make you laugh, especially until your eyes started to fill with tears because of all the laughter. You were open to each adventure and even visited me in Germany to experience the harvest time with my family. Your tractor driving skills are excellent and my mom is still amazed how much meat you can eat. I enjoyed hanging out with you and seeing your excitement about good food. It is so nice that you end each zoom call by repeating the German words you have learned, of course these are the most important ones. I cannot wait to visit you soon.

Happy flies, happy life – thanks to everyone involved in implementing this. Zubayda and Max, you both mastered your task of cooking the (delicious) smelling fly food. Zubayda, it was hilarious working with you in the lab and I really enjoyed that you put me on your cake list. Menne and Emmy, it was great that I could ask you whenever I was struggling with the MultiCell set-up. Thanks Valentijn for your endless patience while measuring the fly hearts. I know it felt more like a physiological experiment in which the study participants will never figure out what the actual topic has been. Pedro, aka Staining Guy, thank you so much for making the fly project literally more colourful. I enjoyed our working environment so much, with all the discussions about research and life and sharing the same kind of humour. I am glad I could make you so happy by renting the OV fiets in Rotterdam.

Maike, Eva, Laura, Pedro and Tatjana, you were the best cappuccino buddies I could ever imagine. I liked how quickly we rephrased – "cappuccino today?" – into – "when will we have our cappuccino today?". Thank you so much for making this a special moment of a regular work day in which we laughed and joked, had nice conversations or just shared stuff which needed to be said. Pedro, I am still so sorry for not asking you in the beginning, I will never forget your disappointed look with your coffee mug in your hands. I guess we quickly learned from our mistake.

Dear climbing crew, Maike, Stefan, Eva, Pedro, Edgar, Rowan, Phat and Wout, thank you for all the fun times while fighting against gravity and for pushing me, to at least try whether I can grab one higher hold. Stefan, I know it took you quite some years to infect me with the bouldering fever. It was hilarious to watch how you could add some kind of awkwardness to almost each situation. Here, I would also like to officially apologize for tricking you with the box in the box in our office as stored cookies. Edgar, I enjoyed the scientific brainstorming sessions we had now and then and I will never forget the Bestätigungsgespräch moment on the hallway, it was really too funny.

Edgar and Xue, thanks for adding me to the TPO organizing committee in 2019. Who would have guessed that we will set a new record in the escape house?

Michiel, thanks for running the many Western blots for me and I wish you all the best for your retirement. Stan, thank you for working so independently, I am glad you did your internship with me. Sila, thank you for continuing the tubulin project, I am already looking forward to publishing the outcomes.

To all the other former and current colleagues: Phat, Sun, Josine, Mark, Louise, Ilse, Aref, Birgit, Kim, Rahana, Beau, Elza, Rafeeh, Qianliang, Yeszamin, Leon, Sylvia, Michi, Jin, Luciënne, Marit, Deli, Stan, Anoek, Nicole, Roselique, Diewertje, Veerle, Anke, Noelia, Rio, Philippa, Manon, Jisca, Fabienne, Vanessa, Igor, Chris, Pan, Liza, Xue, Aida, Zeineb, Jeroen, Natalija, Albert, Karlijn, Duncan, Jan, Dop, Reinier, Ed, Peter, Victor and Coen - thank you for the scientific input, the "gezelligheid" and the nice lunch breaks, borrels, Monday coffees and other moments.

I would like to thank all the co-authors of the publications in this thesis for the productive collaboration. Especially, I would like to thank Jan and Paul for the clinical and genetic expertise in the Tropomyosin project. Jiayi and Magdalena, thank you for your knowledge in omics data and the brainstorming in the Utrecht – Amsterdam meetings. Jan-Willem and Renee, thanks for the collaborative opportunity to make EHTs out of your expanded cardiomyocytes. Oana and Dirk, thanks for the plenty of pig samples.

A big thank you to all the members of the DOSIS consortium, I fully enjoyed to be part of this team! It was so great to witness how ideas became actual manuscripts. Thanks for the plenty opportunities to present my work and the nice meeting and discussion atmosphere.

To all the members of the Harmonie Orkest Amstelveen and Groot Excelsior Orkest Amsterdam, thank you for the music, the fun during the repetitions and nice concerts all over the Netherlands. Special thanks to the koper sections: Michel, Trijntje, Dick, Durk, Lisa, Eefke, Martijn, Ron, Annemiek and Kim.

Liebe Molmeds, Christina, Tabitha, Martina und Anja, es hat mich sehr gefreut, dass ihr euch immer für mich Zeit genommen habt. Danke für die spaßigen Stunden/Tage in München, Amsterdam und Salzburg. Tabitha, vielen Dank für die Gestaltung meines Coverlayouts. Christina, mit dir kann man einfach gut Impressionen gewinnen, wo auch immer wir gerade sind. Ich habe mich immer sehr auf unsere Skypegepräche gefreut. Es tut einfach gut, wenn Sätze zu Ende zu gelacht werden.

Felix, es ist einfach immer wieder schön, mit dir zu telefonieren. Cool, dass ich bei meiner Weihnachtsmärktetour auch in Regensburg vorbeischauen konnte.

Martin, dein herzhaftes Lachen ist einfach ansteckend und auf dich ist immer Verlass in Bezug auf gutes Unterhaltungsmaterial in Form von Musik, Videos oder Podcasts. Wann löffeln wir wieder Monte mit Caro am Rhein?

Liebe Caro, es fühlt sich bei dir einfach so an, als würden wir immer noch zusammen wohnen. Vielen Dank, dass du mit mir auf Moop Mama Konzerten getanzt hast und so viel Böhmi-Content mit mir geteilt hast. Ich freue mich schon auf die Zeit, wenn wir uns wieder öfters sehen können.

Tausend Dank an Maike, Laura und Tatjana, dass wir die gleiche Begeisterung für German-Trash-TV Abende geteilt haben, ich habe es gerne mit meiner gmx-Belesenheit abgerundet. Wie schön, dass wir immer genau wussten, wer welchen Kochschritt übernimmt und, dass es auf jeden Fall etwas mit geschmolzenem Käse sein muss. Last, but not least, bei der Frage nach einem Likörchen hört man sich einfach nicht nein sagen. Laura, mega, wie du dich über gutes Essen oder gute Likörkreationen freuen konntest. Mega auch, dass ich immer auf einen Absacker in der Kinkerstraat vorbeikommen durfte. Tatjana, uns verbindet nicht nur die gleiche Heimat, sondern auch die gleiche Podcast-Liebe. Schön, dass du mir immer wieder ein Lachen ins Gesicht werfen kannst. Ich freue mich schon auf Reunions im Ländle.

Liebe Maike, meine Amsterdam Sister, ich bin so froh, dass ich nicht nur eine Kollegin für dich bin, sondern auch eine Freundin, die sowas mit Science macht. Es war nicceeee, dass wir beide am gleichen Großprojekt gearbeitet habe. Vielen Dank für die schönen Traditionen und lustige Momente, wie zum Beispiel Submission-Dinner, Museums-Shops, immer wieder die gleichen Sätze vor deinem Backofen, ein sehr treuer Wegbegleiter übrigens, und natürlich das spontane Koffer-workout in Nizza. Danke, dass du bei jedem Wellengang für mich da warst. Es war so schön, mit einer Nachbesprechung und einem Cappuccino spezial ins Wochenende zu starten. Ich vermisse jetzt schon unsere Koch- und Netflixsessions. Vielen Dank auch an dieser Stelle für das Geschirrspülen. Zum Schluss

bleibt nur noch zu sagen – Stößchen auf uns!

Ein großes Dankeschön auch an meine Familie, besonders meine Eltern und Brüdern, für die Unterstützung während meines PhDs. Ich habe mich über jedes Foto oder Video von unserem Hund oder unseren Katzen gefreut. Vielen Dank für eure Besuche, Anrufe und alles andere!

Amsterdam Cardiovascular Sciences